

Institute of Geography and Earth Sciences
University of Wales, Aberystwyth

LABORATORY INVESTIGATIONS OF THE RATES, PROCESSES
AND CONTROLS OF SOLUTE ACQUISITION IN SUBGLACIAL
ENVIRONMENTS

Graham Ralph Pugh

Thesis submitted for the Degree of Doctor of Philosophy
May 1999

Laboratory investigations of the rates, processes and controls of solute acquisition in subglacial environments

Pugh, Graham Ralph

University of Wales, Aberystwyth

Candidate for the Degree of Ph.D.

Summary of thesis

In order to fully exploit the potential of meltwater quality variations in studies of subglacial hydrology and hydrochemistry, the process, rates and controls on solute acquisition need to be better constrained.

To further our understanding of rock-water interaction in glacial environments, geochemical models of solute acquisition have been developed. These are based on a suite of laboratory experiments, which have been parameterised by geochemical and mineralogical investigations at *Haut Glacier d'Arolla*, Switzerland.

Solute acquisition may be explained using a two-stage dissolution model. Firstly, rapid solute acquisition is accompanied by the net consumption of CO₂, controlled primarily by reactive mineralogy and surface area. Additional dissolution is driven by sulphide oxidation during this initial stage, which terminates as a result of proton exhaustion. Subsequently, solute acquisition during Stage 2 is slower, and is predominantly controlled by the rate of CO₂-drawdown, and therefore effectively halted without atmospheric access. This differs from previous studies (e.g. Fairchild *et al.*, 1994) which suggested that sulphide oxidation was a major control in Stage 2. Sulphide oxidation was strongly dependent on reactive surface area, and was severely restricted during Stage 2 by the formation of a chemical barrier on pyrite surfaces. Dilution events temporarily restored Stage 1 conditions.

The experimental results may be applied to data of bulk meltwater quality draining *Haut Glacier d'Arolla* in order to estimate subglacial lithological provenance. Carbonates, sulphides, olivine, pyroxene and amphibole are identified as the dominant sources of solutes. This is corroborated using PHREEQC inverse modelling techniques.

A number of elements are identified as potential indicators of solute provenance. However, laboratory investigations suggest that dissolution behaviour of many trace elements in glacial hydrochemical regimes is complex. It is clear that inferences of source mineralogy based on the trace element chemistry of the aqueous phase should be treated with caution.

DECLARATION

This work has not previously been accepted in substance for any degree and is not being concurrently submitted in candidature for any degree.

Signed(candidate)

Date

STATEMENT 1

This thesis is the result of my own investigations, except where otherwise stated.

Other sources are acknowledged by footnotes giving explicit references. A bibliography is appended.

Signed(candidate)

Date

STATEMENT 2

I hereby give consent for my thesis, if accepted, to be available for photocopying and for inter-library loan, and for the title and summary to be made available to outside organisations.

Signed(candidate)

Date

ACKNOWLEDGEMENTS

Firstly I would like to thank my thesis supervisors Dr. Giles Brown and Dr. Ron Fuge for their advice and support. Also, Dr. Bill Perkins and Mrs. Lorraine Hill, who provided invaluable advice and assistance with rock and solution analyses.

Thanks also to Andrew Seagren who shared meltwater sampling duties and undertook particle size analysis on my behalf, Catie who provided assistance with laboratory experiments, and the various technicians in the Department of Geography and Earth Sciences and the Soil Science Unit who provided additional help and resources..

The University of Wales provided funding for the project, and additional funding for fieldwork expenses and laboratory equipment.

A special thankyou to Louise, Mum, Dad and Grannie for much love and support.

To Nick, and Veronica, who should have still been around to see this.

NOTES ON NOMENCLATURE USED IN THIS THESIS

SI units and their derivatives are used throughout the study (refer to: National Institute of Science and Technology, web site).

Concentrations are represented by the following abbreviations:

M \equiv mol/L

ppm (rock) \equiv mg/kg (rock) \equiv mg/L (solution)

ppb (rock) \equiv ng/g (rock) \equiv ng/mL (solution)

neq/mL \equiv μ eq/L (microequivalent units per litre)

Throughout the document, the term $p(\text{CO}_2)$ refers to the partial pressure of carbon dioxide in the gaseous phase with which solutions are in equilibrium. The equilibrium values range between $10^{-3.5}$ and approximately $10^{-3.6}$ between altitudes of zero and 2000m respectively (Fairchild *et al.*, 1994). Values of $\log p(\text{CO}_2)$ are often used.

Experimental nomenclature is derived from the rock identifying number described in Section 3.3.1, and the geochemical condition under which the experiment was undertaken. Hence, an experiment involving rock 1 under closed system conditions is termed '1(c)', and another experiment involving a mixture of rock 5 and pyrite, reopened to the atmosphere, is termed '5P(r)'. For experiments involving pyrite and/or calcite, the letters P and C infer that 0.2g/L sediment was added unless the subscript 0.1 is appended, inferring that 0.1g/L of either pyrite ($\text{P}_{0.1}$) or calcite ($\text{C}_{0.1}$) was added. All the other experiments (1-9, M) involve 4g/L sediment.

Frequently, numerous experiments are referred to together in the text. To avoid lengthy lists the nomenclature is abridged, thus '1-5/1P/5P/9P(c)' refers to each of experiments 1(c), 2(c), 3(c), 4(c), 5(c), 1P(c), 5P(c) and 9P(c), and '2(c)/(r)' refers to experiments 2(c) and 2(r). The full list of laboratory experiments is presented in Table 2.4.

TABLE OF CONTENTS

SUMMARY	ii
DECLARATION AND STATEMENTS	iii
ACKNOWLEDGEMENTS	iv
NOTES ON NOMENCLATURE USED IN THIS THESIS	v
TABLE OF CONTENTS	vi
INDEX OF FIGURES	xv
1. INTRODUCTION AND REVIEW OF LITERATURE	1
1.1 INTRODUCTION	1
1.2 BACKGROUND TO STUDIES OF WATER QUALITY IN GLACIAL ENVIRONMENTS	2
a) Chemical investigations of bulk meltwater chemistry	
b) Early chemical models of glacier hydrology	
c) The role of glacial chemical denudation in climate change	
1.3 MODELS OF GLACIER HYDROLOGY AND HYDROCHEMISTRY	5
1.3.1 Formation of the distributed drainage system	5
1.3.2 Processes of chemical weathering in the distributed system	6
1.3.2.1 Acid hydrolysis	6
a) Organic -derived acidity	
b) Atmosphere-derived acidity	
c) Carbon dioxide-derived acidity	
d) Sulphide oxidation-derived acidity	
1.3.2.2 Hydrolysis	11
a) Hydrolysis of carbonate minerals	
b) Hydrolysis of sulphate minerals	
1.3.2.3 Coupled sulphide oxidation and carbonate dissolution	13
1.3.3 Formation of and processes of solute acquisition within the channelised drainage system	14
a) Formation	
b) Solute acquisition	
c) Mixing of quickflow and delayed flow meltwaters	
1.4 LABORATORY INVESTIGATIONS OF SOLUTE ACQUISITION	17
1.4.1 Laboratory investigations of glacial chemical weathering	17
a) Suspended sediment concentration	
b) Particle size	
c) Proton availability	
d) Repeated wetting of pre-reacted sediment	
e) Restriction of access to atmospheric gases	
f) Summary	
1.4.2 Experimental investigations of pyrite oxidation	20

a) Oxidation by oxygen	
b) Oxidation by ferric iron	
c) Inhibition of oxidation rate with time	
1.4.3 Experimental investigations of carbonate dissolution	24
1.4.4 Rates of silicate and aluminosilicate dissolution	28
1.4.5 Summary	30
1.5 THE USE OF MINOR AND TRACE ELEMENT ANALYSES AS AN AID TO INVESTIGATIONS OF SOLUTE PROVENANCE	30
1.5.1 Overview of major element solute provenance	33
1.5.2 Overview of minor and trace element solute provenance	36
a) Lithogenic Provenance	
b) Mobility of the trace element	
c) Speciation, ion pairing and complexation	
d) Oxidation state	
e) Equilibrium	
f) Sorption	
g) Cation exchange	
1.5.3 Rock and aqueous geochemistry of specific major, minor and trace elements	41
1.5.3.1 Alkali metals	44
a) Rock & mineral affinities	
b) Dissolution and precipitation characteristics	
1.5.3.2 Alkaline Earth Metals	45
a) Rock & mineral affinities	
b) Dissolution and precipitation characteristics	
1.5.3.3 Group III Elements	48
a) Rock & mineral affinities	
b) Dissolution and precipitation characteristics	
1.5.3.4 Group IV and V Elements	49
a) Rock & mineral affinities	
b) Dissolution characteristics	
1.5.3.5 Group IIIB Transition Metals	51
a) Rock & mineral affinities	
1.5.3.6 Iron and Iron-Group Metals	52
a) Rock & mineral affinities	
b) Dissolution characteristics	
1.5.3.7 Other metals	56
a) Zinc and cadmium	
b) Zirconium	
c) Molybdenum & Tungsten	
d) Silver and gold	
e) Rhenium & Platinum-group metals	
f) Mercury	
1.5.3.8 Non-metals	59
1.5.3.9 Summary of abundance, occurrence and soluble properties of the elements	60
1.6 CONCLUSION	62
2. METHODS AND TECHNIQUES	64
2.1 INTRODUCTION	64

2.2 FIELD AND LABORATORY SAMPLING TECHNIQUES	64
2.2.1 Rock sampling for detailed mineralogical analysis and laboratory leaching experiments	64
a) Morainic- and side-rocks	
b) Subglacial sediment	
2.2.2 Meltwater sampling for chemical analysis	65
a) Bulk meltwater	
b) Snout samples	
c) Supraglacial meltwaters	
d) Groundwater	
2.3 LABORATORY EXPERIMENTS	69
2.3.1 Experimental materials	69
2.3.1.1 Rocks/sediment	69
a) “End-member” investigations of sulphide oxidation and carbonate dissolution	
b) Morainic rocks	
c) Preparation of rocks and sediment for experimental use	
d) Calculation of specific surface area	
2.3.1.2 Water	72
2.3.2 Temperature control	72
2.3.3 Duration of water:rock contact	74
2.3.4 Access to atmospheric gases	75
2.3.5 Experimental set up	75
2.3.6 Sampling procedure	75
2.3.7 Summary of experiments undertaken	78
2.4 ANALYTICAL TECHNIQUES	78
2.4.1 Discharge measurement	78
2.4.2 Measurement of pH	78
2.4.2.1 Investigation of continuous pH measurement during laboratory dissolution experiments	79
2.4.3 Determination of dissolved oxygen concentration	81
2.4.4 Determinations of alkalinity, partial pressure of carbon dioxide (pCO ₂) and calcite saturation indices (SI(calcite))	82
2.4.5 Determination of bulk rock composition by ICPMS and AA	85
2.4.5.1 Rock digestion	85
2.4.5.2 Atomic absorption spectroscopy	86
2.4.5.3 Inductively-Coupled Plasma Mass Spectrometry	87
2.4.6 Determination of minor and trace elements in solution	88
2.4.7 Determination of major ionic composition of meltwaters and experimental solutions by ion-exchange chromatography	88
2.4.7.1 Anion determination	90
a) Equipment and eluent	
b) Calibration standards	
2.4.7.2 Cation determination	90
a) Equipment and eluent	
b) Calibration standards	
2.4.7.3 Dionex quality control	91
a) Calibration	
b) “Blank” determination regime	
c) Repeat standard reproducibility	
d) Contamination monitoring	

e) Repeat experiment reproducibility	
2.5 PHREEQC GEOCHEMICAL MODELLING	95
2.5.1 Observations of trace metal speciation using PHREEQC Interactive	95
2.5.2 Mixing modelling using PHREEQC Interactive	95
2.5.3 Dissolution modelling using PHREEQC Interactive	95
2.5.4 Inverse modelling using PHREEQC Interactive	96
2.6 CONCLUSION	97
3. FIELD PARAMETERISATION	98
3.1 INTRODUCTION	98
3.2 GEOLOGY OF MORAINIC AND ADJACENT ROCKS AT <i>HAUT GLACIER D'AROLLA</i>	99
3.2.1 Existing literature	99
3.2.2 Field observations	102
3.3 PETROLOGY OF MORAINIC ROCK	104
3.3.1 Bulk analysed samples	105
3.3.2 Other rock samples	108
3.3.3 Summary of petrological investigations	113
3.4 MORAINIC ROCK COMPOSITION: BULK ANALYSIS	114
3.4.1 Element abundances in moraine rocks: an overview	114
3.4.2 Interpretation of the relationships between major and trace elements in the morainic rocks of <i>Haut Glacier d'Arolla</i>	118
a) Elements associating with pyrite	
b) Elements associating with magnesium	
c) Potassium & Rubidium	
d) Elements associating with calcium	
e) Nickel, Arsenic, Tellurium, Antimony, Cobalt	
f) Elements with apparent sodium affinity	
g) Zirconium & Tin	
h) Rare Earth elements	
i) Other elements	
3.4.3 Summary	129
3.5 MELTWATER ANALYSIS	130
3.5.1 Bulk meltwaters	130
3.5.1.1 Discharge	130
3.5.1.2 pH & dissolved oxygen	131
3.5.1.3 Major ions	133
a) Calcium and sulphate	
b) Bicarbonate	
c) Relationship between sulphate and dissolved oxygen	
d) pCO ₂ and SI(calcite)	
3.5.2 Supraglacial melt and groundwater	139
3.5.2.1 Chemical variability between portal meltwater streams	141
3.5.3 Discussion of meltwater analysis	142

3.6 CONCLUSION	144
4. LABORATORY SIMULATIONS OF SUBGLACIAL SOLUTE ACQUISITION: RESULTS AND INITIAL INTERPRETATION	146
4.1 INTRODUCTION	146
4.1.1 Experiments using “end-member” components	147
4.1.2 Investigations using morainic rock samples	147
4.2 SUMMARY OF RESULTS OF EXPERIMENTS INVOLVING MORAINIC ROCKS	149
4.2.1 Mean experimental concentrations of dissolved elements	149
4.2.2 Solubility	149
4.3 DETAILED ANALYSIS OF INDIVIDUAL SPECIES	153
4.3.1 Acidity	153
a) Closed system	
b) Open system	
4.3.2 Dissolved oxygen	154
4.3.3 Major cations	155
4.3.3.1 Calcium	155
a) Open system, end member experiments	
b) Closed system experiments	
c) Reopening closed system	
d) Influence of sulphide oxidation	
e) Experiments 50% diluted with deionised water after 24h	
4.3.3.2 Magnesium	160
a) Morainic rock experiments	
b) Reopening a closed system	
c) 50% dilution	
d) Influence of sulphide oxidation	
e) Note on variation between results obtained from HPIC and ICPMS analysis	
4.3.3.3 Sodium	164
a) Morainic rock experiments	
b) Reopening closed system experiments to the atmosphere	
c) Influence of sulphide oxidation	
d) Reopening closed system experiments to the atmosphere, and diluting 50% with deionised water	
4.3.3.4 Potassium	166
a) Morainic rock experiments	
b) Reopening closed system experiments to the atmosphere, and diluting 50% with deionised water	
c) Influence of sulphide oxidation	
4.3.4 Major anions	168
4.3.4.1 Bicarbonate	169
a) Effects of sulphide oxidation	
4.3.4.2 Sulphate	170
a) Morainic rock experiments	
4.3.4.3 Chlorine	171

4.3.4.4 Nitrate	172
4.3.5 Trace elements	173
4.3.5.1 Strontium	174
4.3.5.2 Other trace elements strongly affected by carbonate dissolution	174
a) Zinc	
b) Bismuth	
c) Caesium	
d) Thorium	
e) Titanium	
4.3.5.3 Barium	180
4.3.5.4 Iron, aluminium and nickel	181
a) Iron	
b) Aluminium	
c) Nickel	
4.3.5.5 Lead	183
4.3.5.6 Rare Earth Elements	183
4.3.5.7 Trace elements with dominantly provenance-controlled dissolution characteristics	186
a) Uranium	
b) Rubidium	
c) Tungsten and rhenium	
d) Molybdenum	
e) Cobalt	
4.4 CONCLUSION	192
5. RATES AND CONTROLS OF SOLUTE ACQUISITION IN LABORATORY SIMULATIONS OF GLACIAL ENVIRONMENTS	194
5.1 INTRODUCTION	194
5.2 OVERVIEW OF CONTROLS ON SOLUTE ACQUISITION OF CATIONS	194
a) Relationships between ionic radii and solubility	
b) Major and trace element speciation modelling using PHREEQC	
c) Summary	
5.3 PROCESSES, RATES AND CONTROLS OF CALCIUM ACQUISITION	199
5.3.1 Investigations of controls on acquisition of calcium from “pure” calcite	200
5.3.1.1 Relationship between calcium acquisition and time	200
a) Open system dissolution	
b) Closed-system dissolution	
5.3.1.2 Relationship between calcium acquisition and sulphide oxidation	204
a) Open system pyrite/calcite dissolution	
b) Closed system pyrite/calcite dissolution	
5.3.1.3 Relationship between calcium acquisition and pCO ₂	206
a) Open system	
b) Closed system	
5.3.1.4 Relationship between calcium acquisition and SI(calcite)	209
a) Open system “end-member” experiments	
b) Closed system: end member experiments	

5.3.1.5 Comparison with equilibrium relationships between Ca^{2+} , pCO_2 , HCO_3^- , CO_3^{2-} , pH and temperature	210
5.3.1.6 Summary of controls on calcite dissolution	212
5.3.2 Investigations of controls on acquisition of calcium from various rocks collected from moraines at <i>Haut Glacier d’Arolla</i>	213
5.3.2.1 Relationship between calcium acquisition and time	213
a) Closed system experiments	
b) Experiments reopened to the atmosphere after 24h in a closed system	
c) Experiments diluted by 50% with deionised water, and subsequently reopened to the atmosphere after 24h in a closed system	
5.3.2.2 Relationship between calcium acquisition and sulphide oxidation	215
a) Experiments 2(c)/(r): closed/open system dissolution of morainic rock 2	
b) Effects of additional pyrite on morainic rock Ca^{2+} acquisition	
5.3.2.3 Relationship between calcium acquisition and pCO_2	218
5.3.2.4 Calcite supersaturation	220
5.3.2.5 Effect of morainic rock mineralogy on calcium acquisition	222
a) Rocks 1, 5 and 9 (carbonate-rich rocks)	
b) Other rocks (non-carbonate-rich)	
5.3.2.6 Summary of controls on calcium acquisition in morainic rock experiments	228
5.4 PROCESSES, RATES AND CONTROLS OF ACQUISITION OF OTHER SPECIES	229
5.4.1 Controls on sulphide oxidation	229
a) Pyrite content	
b) Dissolved oxygen	
c) Grain size & pyrite content of sediment	
d) Oxidation of the surface of pyrite grains	
5.4.2 Sodium acquisition	232
a) Relationship between sodium acquisition and time	
b) Relationship between sodium acquisition and pCO_2	
c) Effect of sulphide oxidation	
5.4.3 Potassium acquisition	234
a) Effect of pCO_2	
b) Effect of sulphide oxidation	
5.4.4 Magnesium acquisition	235
a) Effect of pCO_2	
b) Effects of sulphide oxidation	
5.4.5 Controls on dissolution of minor and trace elements in laboratory experiments	237
5.4.6 Appraisal of the use of trace elements in investigations of solute acquisition in subglacial environments	239
5.5 SUMMARY OF CONTROLS ON AND RATES OF SOLUTE ACQUISITION IN SIMULATED SUBGLACIAL CONDITIONS	240
5.5.1 Controls on solute acquisition	240
a) Calculated relationship between calcium acquisition, sulphide oxidation, carbonate equilibria, CO_2 -drawdown and rock provenance	
b) Other cations	
c) Rapid, “Stage 1” acquisition	
5.6 COMPARISON OF EXPERIMENTAL MODELS WITH PREVIOUS STUDIES OF MELTWATER QUALITY	246

5.6.1 Comparison with experiments involving open system dissolution of proglacial sediment from <i>Haut Glacier d’Arolla</i>	246
5.6.2 Two-stage carbonate dissolution (Fairchild <i>et al.</i> , 1994)	247
a) Coupled SO-CD in a carbonate system	
b) Aluminosilicate dissolution	
5.6.3 Comparison with modelled solute acquisition using PHREEQC	251
5.6.3.1 Equilibrium modelling	252
a) Pyrite/calcite mixtures	
b) Modelled dissolution of individual morainic rocks	
5.6.3.2 Inverse modelling of dissolution of experimental solutions	255
5.6.4 Comparison with kinetic models	257
5.7 CONCLUSION	258
6. APPLICATION OF EXPERIMENTAL AND GEOCHEMICAL MODELS TO HYDROGEOCHEMICAL DATA	260
6.1 INTRODUCTION	260
6.2 APPLICATION OF EXPERIMENTAL MODELS TO GLACIAL GEOCHEMICAL DATA	260
6.2.1 Introduction	260
6.2.2 Inference of geochemical parameters using experimental models of cation acquisition	262
6.2.2.1 Indication of the processes of calcium acquisition	262
6.2.2.2 Indications of provenance of sodium acquisition	265
6.2.2.3 Indication of potassium provenance using experimental equations	266
6.2.2.4 Magnesium	267
6.2.3 Discussion of the limitations and necessary assumptions	268
a) Limitations of experiments	
b) Assumptions and necessary simplifications	
c) Summary	
6.3 METHODS OF SIMULATING SUBGLACIAL WEATHERING USING GEOCHEMICAL MODELLING COMPUTER PACKAGES	271
a) Model 1: modelled dissolution of mixed sediment	
b) Model 2: modelled equilibrium mixing of individual solutions	
c) Model 3: inverse modelling of field data	
6.4 APPLICATION OF EXPERIMENTAL INVESTIGATIONS OF KEY INDICATOR SPECIES TO FIELD DATA	276
6.4.1 Comparison of modelled speciation between experimental simulations, bulk meltwater and average river data	277
6.4.2 Evaluation of key indicator species by comparison of experimental and bulk meltwater data from <i>Haut Glacier d’Arolla</i> .	277
a) Sulphate and uranium as indicators of sulphide oxidation	
b) Strontium and magnesium as indicators of carbonate dissolution	
c) Other potential indicators of sulphide oxidation	
d) Inter-elemental associations	
6.5 CONCLUSION	283

7. CONCLUSIONS	285
7.1 INTRODUCTION	285
7.2 ESTABLISHMENT OF A SET OF GEOCHEMICAL DATA ALLOWING PARAMETERISATION OF LABORATORY INVESTIGATIONS	286
7.2.1 Rock mineralogy and chemistry	286
7.2.2 Bulk meltwater chemistry	287
7.3 EXPERIMENTAL SIMULATIONS OF SUBGLACIAL SOLUTE ACQUISITION	287
7.3.1 Experimental models of solute acquisition in subglacial environments	288
i) Calcium	
ii) Sodium, potassium and magnesium	
7.3.2 Application of laboratory models to bulk meltwater data	289
7.3.3 Studies of trace element behaviour in experimental simulations	290
7.4 CRITIQUE OF THE EXPERIMENTAL MODELS	291
7.5 RECOMMENDATIONS FOR FURTHER WORK	293
7.5.1 Field parameterisation	293
7.5.2 Species analysis	293
7.5.3 Trace element analytical technique	294
7.5.4 Laboratory methods & techniques	295
7.6 CONCLUSION	297
BIBLIOGRAPHY	298
APPENDICES	308

INDEX OF FIGURES

Chapter 1

Figure 1.1 Schematic drawings of the distributed drainage system.	6
Figure 1.2 Relative concentrations of carbonate species at 0°C (using formulae from Garrels and Christ, 1965; adapted from Raiswell et al., 1980).	8
Figure 1.3 Variations in the concentrations of Ca^{2+} , HCO_3^- , and SO_4^{2-} over the diurnal cycle June 22-23 1989, early in the meltseason before a channelised drainage network has developed (after Brown et al., 1994a).	13
Figure 1.4 Ca^{2+} concentration versus time during open system dissolution experiments using 4g/L of uncrushed 63-125 μm sediment from the proglacial area of Haut Glacier d'Arolla and sediment of the same initial size distribution crushed to <63 μm (after Brown et al., 1996b)	19
Figure 1.5 Linear regression plots of rate data for the aqueous oxidation of pyrite by dissolved oxygen (after Williamson and Rimstidt, 1994,; Figure 2)	21
Figure 1.6 Log rate of calcite dissolution as a function of pH in acids at 25°C (after Morse, 1983, Figure 2)	23
Figure 1.7 Influence of pCO_2 on the rate of dissolution of calcite at constant pH (5.6-5.7) (Wollast, 1990, Figure 2).	26
Figure 1.8 Hydrated sodium ion in aqueous solution (cf. Stumm and Morgan, 1996, Figure 1.6).	38
Figure 1.9 Computed curves for adsorption of selected metals on SiO_2 (after Drever, 1982)	41
Figure 1.10 Generalised affinities of some trace elements in rocks..	60

Chapter 2

Figure 2.1 Systematic map of the meltwater stream portals at the snout of the Haut Glacier d'Arolla, showing some of the meltwater and sediment sampling sites..	68
Figure 2.2 Grain size distribution of TEMA-crushed mixed moraine sediment (rock M); and cumulative particle size distribution.	72
Figure 2.3 Temperature of stirred deionised water using an AC magnetic stirrer..	74
Figure 2.4 Observed pH buffer measurements prior to and subsequent to immersion in solutions containing ferrous sulphide and/or precipitated calcium carbonate.	80
Figure 2.5 Relative concentrations of carbonate species at 0°C (after Equation 2.5), assuming equilibrium with atmospheric carbon dioxide	82
Figure 2.6 Comparison of titration alkalinity with charge balance error calculations	84
Figure 2.7 Contamination of blank samples, excluding initial blank determinations	92

Chapter 3

Figure 3.1 Schematic diagram of the glacial hydrochemical network	99
Figure 3.2 Haut Glacier d'Arolla, based on the 1:200000 Geotechnische Karte der Schweiz, Sheet 3 (after Brown, 1991, Figure 5.3).	101
Figure 3.3 Proportions of minerals in moraine samples of the Haut Glacier d'Arolla (adapted from Brown, 1991)	104
Figure 3.4 Concentrations of major and trace elements in morainic rock samples (rocks 1-9) and pyrite and calcite.	116
Figure 3.5. Relative abundances of major and trace elements in morainic rock samples (Rocks 1-9).	117
Figure 3.6. Relative mean abundances of elements in moraine rock samples	117
Figure 3.7 Relative abundances of elements with affinity for pyrite	119
Figure 3.8 Relative abundances of Mg, V, Ti, Sc, Cr, Th, Cs, Ga and total REE in morainic rocks.	121
Figure 3.9. Relative abundances of K, Rb and Tl in morainic rocks.	122
Figure 3.10 Relative abundances of Ca and Sr in morainic rocks.	123
Figure 3.11 Relative abundances of Ni, Co, As, Sb and Te in morainic rocks.	124

Figure 3.12	Relative abundances of Na, W and Re in morainic rocks.	125
Figure 3.13	Relative abundances of Zr & Sn in morainic rocks.	126
Figure 3.14	Absolute and relative abundances of REE in morainic rocks	127
Figure 3.15	Relative abundances of the REE in moraine samples using chondrite-normalised data (Taylor and McLennan, 1985) to account for abundance variations between odd and even atomic numbers (McLennan, 1989).	128
Figure 3.16	Relative abundances of Cd, In, Br, I and Mo.	129
Figure 3.17	Bulk meltwater discharge from Haut Glacier d'Arolla for the 1995 meltseason	130
Figure 3.18	Bulk meltwater discharge draining Haut Glacier d'Arolla, 28 July to 26 August 1995	131
Figure 3.19	Seasonal trends of pH and DO ₂ concentration in meltwaters draining Haut Glacier d'Arolla.	131
Figure 3.20	pH and O ₂ (aq) values in bulk meltwaters draining Haut Glacier d'Arolla over three 1995 diurnal cycles	132
Figure 3.21	O ₂ (aq) - discharge relationship in bulk meltwaters draining Haut Glacier d'Arolla, 28 July-26 August 1995.	132
Figure 3.22a	Late-season trend of Ca ²⁺ and SO ₄ ²⁻ in bulk meltwaters draining Haut Glacier d'Arolla, 1995.	133
Figure 3.23	Ca ²⁺ -, SO ₄ ²⁻ - and HCO ₃ ⁻ -discharge relationships in bulk meltwaters draining Haut Glacier d'Arolla, 1995.	135
Figure 3.24	SO ₄ ²⁻ /(SO ₄ ²⁻ +Ca ²⁺) - discharge relationship in bulk meltwaters draining Haut Glacier d'Arolla, 1995.	135
Figure 3.25	SO ₄ ²⁻ /(SO ₄ ²⁻ +HCO ₃ ⁻) - discharge relationship in bulk meltwaters draining Haut Glacier d'Arolla.	136
Figure 3.26	SO ₄ ²⁻ - O ₂ (aq) relationship in bulk meltwaters draining Haut Glacier d'Arolla.	137
Figure 3.27	Ratio of O ₂ (aq)/SO ₄ plotted versus discharge, from data of bulk meltwaters draining Haut Glacier d'Arolla.	137
Figure 3.28	log pCO ₂ and SI(calcite) values in bulk meltwaters draining Haut Glacier d'Arolla, 1995.	138
Figure 3.29	Seasonal trends for Na ⁺ , K ⁺ , Mg ²⁺ , Cl ⁻ & NO ₃ ⁻ concentrations in bulk meltwaters draining Haut Glacier d'Arolla.	139
Figure 3.30	Mean concentrations of major ions in meltwaters from supraglacial meltwater (n=5), groundwater and bulk meltwater concentration over entire field season (n=108).	140
Figure 3.31	Variations in concentrations of Ca ²⁺ and SO ₄ ²⁻ in meltwaters draining different glacier snout portals.	141

Chapter 4

Figure 4.1	(left) Mean concentrations of metals and major anions resulting from all open- and closed-system experiments from this study (all time increments). (right) Difference between concentration after 1h and 24h closed system dissolution, expressed as percentage of the difference in relation to the largest concentration.	150
Figure 4.2	Mean solute yield (M/mol) of major and trace elements from 24 hours closed system dissolution of experiments 1-9(c).	151
Figure 4.3	pH of laboratory experiments	153
Figure 4.4	pH variations in "end member" experiments C/P/PC/P _{0.1} C/PC _{0.1} (c) (closed system) and C/P/PC(o) (open system).	153
Figure 4.5	Dissolved oxygen concentrations (mg/L) in experiments 1/5/9/M/PC _{0.1} /PC/1P/5P/ 9P	155
Figure 4.6	Calcium concentrations from open system experiments C/P/PC(o), and closed system experiments C/P/PC/P _{0.1} C/PC _{0.1} (c)	155
Figure 4.7	Mean concentrations of Ca (ng/mL) in laboratory experiments	156
Figure 4.8	Ca ²⁺ acquisition from rocks 1-9 after 24 hours closed system dissolution, plotted versus the corresponding Ca content of each rock.	157
Figure 4.9	Ca ²⁺ yield in closed system dissolution of rocks 1-9, after 24 hours dissolution.	157
Figure 4.10	Closed system Ca ²⁺ concentrations in experiments 1/5/9/1P/5P/9P(c), continuing through to open system acquisition after 24h (1440 min) (1/5/9/1P/5P/9P(r)).	159
Figure 4.11	Effects of 50% dilution of experiments with atmosphere-equilibrated deionised water on Ca ²⁺ concentration.	159

Figure 4.12 Concentrations of Mg (ng/mL) in laboratory experiments	160
Figure 4.13 Comparison of Mg ²⁺ concentrations in solution after 24 hours' dissolution with corresponding rock Mg content	160
Figure 4.14 Comparison of mean Mg ²⁺ and Ca ²⁺ concentrations in dissolution experiments under all time scales and conditions.	161
Figure 4.15 Comparison of Mg ²⁺ concentrations in solution after 24 hours' dissolution with corresponding rock Fe content	162
Figure 4.16 Closed system Mg ²⁺ concentrations in experiments 1/5/9/1P/5P/9P(c), continuing through to open system acquisition after 24 hours (1440 minutes) (1/5/9/1P/5P/9P(r))	162
Figure 4.17 Effects of 50% dilution of experiments with atmosphere-equilibrated deionised water on Mg ²⁺ concentration	163
Figure 4.18 Comparison between observed concentrations of Mg ²⁺ (ng/mL) after 24h of experiments 1-9(c) obtained from HPIC and ICPMS analyses	164
Figure 4.19 Concentration of Na in laboratory experiments	164
Figure 4.20 Comparison of Na ⁺ concentrations in solution after 24 hours' dissolution with corresponding rock Na content	165
Figure 4.21 Closed system Na ⁺ concentrations in experiments 1/5/9/1P/5P/9P(c), continuing through to open system acquisition after 24 hours (1440 minutes) (1/5/9/1P/5P/9P(r))	165
Figure 4.22 Effects of 50% dilution of experiments with atmosphere-equilibrated deionised water on Na ⁺ concentration	166
Figure 4.23 Concentrations of K (ng/mL) in laboratory experiments	167
Figure 4.24 Comparison of K ⁺ molar concentrations in solution after 24 hours' dissolution with corresponding rock K content	167
Figure 4.25 Relationship between potassium solute yield and Ca rock content, after 24h dissolution	167
Figure 4.26 Effects of 50% dilution of experiments 1/5/9(r) with atmosphere-equilibrated deionised water on K ⁺ concentration (experiments 1/5/9(rd))	168
Figure 4.27 Effects of pyrite in experiments 1P/5P/9P(c)&(r) on K ⁺ concentration, compared with pyrite absent experiments 1/5/9(c)&(r)	169
Figure 4.28 Concentrations of HCO ₃ (ng/mL) in laboratory experiments	169
Figure 4.29 HCO ₃ /Ca ratios of laboratory experiments	169
Figure 4.30 SO ₄ ²⁻ acquisition in end member experiments C/P/PC/P _{0.1} C/PC _{0.1} (c) (closed system) and C/P/PC(o) (open system).	170
Figure 4.31 Concentrations of SO ₄ ²⁻ (ng/mL) in laboratory experiments	171
Figure 4.32 Concentrations in SO ₄ ²⁻ from closed system experiments 1/2/5/9/1P/5P/9P(c) and in subsequent reopened experiments 1/2/5/9/1P/ 5P/9P(r).	171
Figure 4.33 Concentrations of Cl ⁻ (ng/mL) in laboratory experiments	172
Figure 4.34 Mean concentrations of NO ₃ (ng/mL) in laboratory experiments	173
Figure 4.35 Mean concentrations of Sr (ng/mL) in laboratory experiments	174
Figure 4.36 Mean calcium (left) and strontium (right) concentrations after 24h closed system dissolution, plotted against rock calcium content	174
Figure 4.37 Sr(aq)/Ca(aq) ratios (ng/ng) in laboratory experiments	175
Figure 4.38 Sr(aq) versus Ca(aq) during closed and open system dissolution experiments	175
Figure 4.39 Mean concentrations of Zn (ng/mL) in laboratory experiments	176
Figure 4.40 Comparison of mean Zn ²⁺ and Ca ²⁺ concentrations in dissolution experiments under all time scales and conditions.	177
Figure 4.41 Mean concentrations of Bi (ng/mL) in laboratory experiments	177
Figure 4.42 Mean Bi concentration from experiments 1-9/P/C for all time increments and conditions, plotted versus (left) the corresponding Ca content of each rock and (right) the mean Ca ²⁺ concentration.	178
Figure 4.43 Mean concentrations of Cs (ng/mL) in laboratory experiments	179
Figure 4.44 Mean Cs concentration from experiments 1-9/P/C for all time increments and conditions, plotted versus the corresponding Ca content of each rock.	179
Figure 4.45 Mean concentrations of Th (ng/mL) in laboratory experiments	179
Figure 4.46 Mean concentrations of Ti in laboratory experiments	180
Figure 4.47 Mean concentrations of Ba (ng/mL) in laboratory experiments	181
Figure 4.48 Mean Ba concentration from experiments 1-9/P/C for all time increments and conditions, plotted versus the corresponding Ba content of each rock.	181
Figure 4.49 Mean concentrations of Fe in laboratory experiments	182

Figure 4.50	Mean concentrations of Al (ng/mL) in laboratory experiments, at 24 hours.	182
Figure 4.51	Mean concentrations of Ni (ng/mL) in laboratory experiments	183
Figure 4.52	Mean concentrations of Pb (ng/mL) in laboratory experiments	183
Figure 4.53	Mean concentrations of total REE, and La, Lu and Y (ng/mL) in laboratory experiments	184
Figure 4.54	Relative mean concentrations of REE in experiments 1-9	185
Figure 4.55	Ratios of mean concentrations of REE in morainic rocks and pyrite to overall mean REE.	185
Figure 4.56	Mean concentrations of U (ng/mL) in laboratory experiments	186
Figure 4.57	Mean concentrations of U (ng/mL) in experiments 1P/5P/9P(c)/(r)	187
Figure 4.58	Mean concentrations of U ^{total} versus mean SO ₄ ²⁻ concentrations in laboratory experiments	187
Figure 4.59	Mean concentrations of Rb (ng/mL) in laboratory experiments	187
Figure 4.60	Mean Rb/K ratios in laboratory experiments	188
Figure 4.61	Mean Rb concentration from dissolution experiments (nos. labelled) for all time increments and conditions, plotted versus the corresponding Ca ²⁺ concentration.	188
Figure 4.62	Mean concentrations of W in laboratory experiments	188
Figure 4.63	Mean concentrations of Re (ng/mL) in laboratory experiments, at 24 hours.	189
Figure 4.64	Mean Re concentration from dissolution experiments for all time increments and conditions, plotted versus the corresponding Ca ²⁺ concentration.	190
Figure 4.65	Mean W concentration from dissolution experiments (nos. labelled) for all time increments and conditions, plotted versus the corresponding Gd concentration.	190
Figure 4.66	Mean concentrations of Mo (ng/mL) in laboratory experiments	190
Figure 4.67	Mean Mo concentration from experiments 1-9/P/C for all time increments and conditions, plotted versus the corresponding Ca content of each rock.	191
Figure 4.68	Mean concentrations of Co (ng/mL) in laboratory experiments	191

Chapter 5

Figure 5.1	Mean yield of major and trace elements at (left) 1h, (middle) 4h and (right) 24h, classified by valency, and plotted versus ionic radius	195
Figure 5.2	Graphical representation of dissolution rate parameters of proglacial sediment derived from Haut Glacier d'Arolla in deionised water, 0.0-3.1°C, atmospheric CO ₂ pressure (Brown et al., 1994), and open system acquisition of calcium from "pure" calcite in experiment C(o) and from a calcite-pyrite mixture in experiment PC(o).	201
Figure 5.3	Calcium acquisition from the dissolution of 0.2g/L "pure" calcite under open access to the atmosphere (experiment C(o)) up to one hour	201
Figure 5.4	Regression lines for Ca ²⁺ acquisition from closed system experiments C/PC/P _{0.1} C/PC _{0.1} (c)	203
Figure 5.5	Relationship between Ca ²⁺ and pCO ₂ in open system experiments C(o) (0.2g/L calcite) and PC(o) (0.2g/L pyrite plus 0.2g/L calcite).	204
Figure 5.6	Relationship between Ca ²⁺ and HCO ₃ ⁻ in closed system experiments C(c) (0.2g/L calcite), P _{0.1} C(c) (0.2g/L calcite plus 0.1g/L pyrite) and PC(c) (0.2g/L calcite plus 0.2g/L pyrite).	205
Figure 5.7	Relationship between pH and pCO ₂ in closed system experiments C(c) (0.2g/L calcite), P _{0.1} C(c) (0.2g/L calcite plus 0.1g/L pyrite) and PC(c) (0.2g/L calcite plus 0.2g/L pyrite).	205
Figure 5.8	Trends of calculated values of log(pCO ₂) in open system experiments C/PC(o), and closed system experiments C/PC/P _{0.1} C/PC _{0.1} (c).	206
Figure 5.9	pCO ₂ versus time in experiments C(o) and PC(o).	207
Figure 5.10	The relationship between calcium concentrations and pCO ₂ in experiment C(o). The equilibrium relationship between Ca ²⁺ and log(pCO ₂) is shown in red, and the progression of the Ca ²⁺ -log(pCO ₂) relationship is shown in black.	207
Figure 5.11	Trends of calculated values of SI(calcite) in open system experiments C/PC(o), and closed system experiments C/PC/P _{0.1} C/PC _{0.1} (c).	209
Figure 5.12	Trends of [Ca ²⁺][HCO ₃ ⁻]/[H ⁺] ratios in closed system experiments C/P _{0.1} C/PC(c).	210
Figure 5.13	Calculated equilibrium concentrations of Ca ²⁺ concentration at given log (pCO ₂) values and temperature. (lines are based on equations in Garrels and Christ, 1965)	211

Figure 5.14 The relationship between calcium concentrations and pCO ₂ in experiment C(c), compared with the equilibrium relationship at 10°C (equilibrium lines are based on equations in Garrels and Christ, 1965)	211
Figure 5.15 Rates of Ca ²⁺ acquisition in experiments 1/5/9(r), reopened to the atmosphere after 24 hours under a closed system.	213
Figure 5.16 Ca ²⁺ acquisition in open system experiments 1/5/9(rd)	215
Figure 5.17 Calculated log pCO ₂ values in open system experiments 1/5/9(rd)	215
Figure 5.18 Concentrations of SO ₄ ²⁻ and Ca ²⁺ in experiments 2(c) (closed system) and 2(r) (reopened to the atmosphere after 24 hours).	216
Figure 5.19 Calculated variations in pCO ₂ in experiments 1/5/9(r), and pyrite-added experiments 1P/5P/9P(r)	217
Figure 5.20 Relationship between mean ΔCa _{SOCD} (concentration of Ca ²⁺ in experiment containing pyrite minus concentration of Ca in corresponding experiment not containing pyrite) and SO ₄ ²⁻ concentrations (experiments 1/5/9(c))	218
Figure 5.21 Calculated trends of log(pCO ₂) in experiments 1/5/9(r), reopened to the atmosphere after 24 hours under a closed system.	219
Figure 5.22 Variation of Ca ²⁺ acquisition with pCO ₂ in experiments 1/5/9(c)/(r)	219
Figure 5.23 SI(calcite) values for Experiments 1(c), 5(c) and 9(c).	221
Figure 5.24 Calculated values of SI(calcite) in laboratory experiments	221
Figure 5.25 Plot of power laws describing the variation of Ca ²⁺ acquisition with pCO ₂ in experiments 1/5/9(c)/(r)	222
Figure 5.26 Mean HCO ₃ ⁻ /Ca ²⁺ ratio plotted vs. (left) time, and (right) log p(CO ₂) (calculated equilibrium lines for 10° and 25°C are based on equations in Garrels and Christ, 1965)	223
Figure 5.27 Relationship between non-Ca rock metal content and HCO ₃ ⁻ /Ca ²⁺ ratio, after 24 hours closed system dissolution (experiments 1-9(c))	224
Figure 5.28 Relationship between pCO ₂ and Ca ²⁺ for closed and open system morainic rock experiments 1/3-9(c); 1/2/5/9(r)	225
Figure 5.29 Relationship between ΔCa ²⁺ _{MIN} and the pH of solution after 60minutes in experiments 1-9/P/C/PC(c).	226
Figure 5.30 Ca ²⁺ concentration of experiments 1-9(c) after 24h, plotted versus original rock Ca wt%. Labels represent corresponding rock Ca/Sr ratios. Individual points are plotted for samples at 60, 240 and 1440min.	227
Figure 5.31 O ₂ (aq) and SO ₄ ²⁻ concentrations vs. time during a closed dissolution experiment using 3g/L calcite/pyrite-deionised water solution (based on Willis et al., 1995, Figure 38).	231
Figure 5.32 Relationship between concentrations of (a) Na ⁺ , (b) K ⁺ and (c) Mg ²⁺ and pCO ₂ from experiments 1/5/9(c)&(r).	233
Figure 5.33 Modelled calcium concentrations in experimental solutions with preset values of log(pCO ₂) and mineralogical parameter ΔCa ²⁺ _{MIN} (axis 'C') and (left) zero SO ₄ ²⁻ , (right) 200neq/mL SO ₄ ²⁻ , (top) factors M and D akin to rock 9 (low extreme of both); (bottom) factors M and D akin to rock 3 (high extreme of both)	244
Figure 5.34 Relationship between experimental and modelled concentrations of Ca ²⁺	245
Figure 5.35 Plot of Ca ²⁺ versus pCO ₂ for experiments involving pyrite and calcite, with experiment from Brown (1994) involving 4 g/L proglacial sediment also plotted	247
Figure 5.36 Plot of concentration of Ca ²⁺ versus HCO ₃ ⁻ for experiments 1-9/M/C/P(c) and 1/2/5/9/M(r)	248
Figure 5.37 Plot of concentration of Ca ²⁺ versus HCO ₃ ⁻ for experiments 1-9/M/C/P(c) and 1/2/5/9/M(r), focussed on experiments with lower concentrations	251

Chapter 6

Figure 6.1 Calculated relationships between Ca ²⁺ and pCO ₂ using Equation 5.13, with the relationship at minimum, mean and maximum Ca ²⁺ concentrations for meltseasons 1990-1996.	263
Figure 6.2 Calculated relationships between Ca ²⁺ and pCO ₂ using Equation 5.13, with 10:00 and 17:00 field data from the 1995 sampling period, and the 1996 diurnal cycle data, superimposed.	264
Figure 6.3 Concentrations of SO ₄ ²⁻ in bulk meltwater draining <i>Haut Glacier d'Arolla</i> between 09:00, 17 August and 10:00, 18 August, 1996	279

Figure 6.4 Concentrations of U^{total} , SO_4^{2-} and Ca^{2+} in bulk meltwater draining <i>Haut Glacier d'Arolla</i> between 09:00, 17 August and 10:00, 18 August, 1996.	279
Figure 6.5 Concentrations of U^{total} in bulk meltwater draining <i>Haut Glacier d'Arolla</i> between 09:00, 17 August and 10:00, 18 August, 1996, plotted versus SO_4^{2-} and Ca^{2+} .	280
Figure 6.6 Concentrations and flux of calcium, magnesium and strontium in bulk meltwater draining <i>Haut Glacier d'Arolla</i> between 09:00, 17 August and 10:00, 18 August, 1996	281
Figure 6.7 Concentrations of Ba^{2+} in bulk meltwater draining <i>Haut Glacier d'Arolla</i> between 09:00, X August and 10:00, Y August, 1996.	282
Figure 6.8 Concentrations of Pb^{2+} , Cu^{total} and Zn^{2+} in bulk meltwater draining <i>Haut Glacier d'Arolla</i> between 09:00, X August and 10:00, Y August, 1996.	282
Figure 6.9 Concentrations of Ni^{2+} , Cr^{total} and Ti^{total} in bulk meltwater draining <i>Haut Glacier d'Arolla</i> between 09:00, X August and 10:00, Y August, 1996.	283
Figure 6.10 Relationship between Ni^{2+} , Cr^{total} and Ti^{total} in bulk meltwater draining <i>Haut Glacier d'Arolla</i> between 09:00, X August and 10:00, Y August, 1996.	283

1. INTRODUCTION AND REVIEW OF LITERATURE

1.1 INTRODUCTION

Studies of glacier meltwater quality have shown that chemical denudation rates in glacial environments are high in spite of the low temperature regime, and investigations of the fundamental subglacial chemical weathering reactions have suggested that reactions involving sulphides and carbonates provide much of the solute, despite their minor abundance (Rainwater and Guy, 1961; Keller and Reesman, 1963). Enhanced rates of chemical denudation in glacierized catchments therefore have important implications for CO₂-drawdown and associated CO₂-regulated greenhouse warming on a global scale over glacial-interglacial cycles (Sharp, 1995). Despite this, the role of glaciated catchments as buffers of atmospheric levels of carbon dioxide are often ignored in many studies of global CO₂ flux variations (e.g. Post *et al.*, 1990).

This thesis attempts to further the understanding of the relative roles of atmospheric gases and lithology as controls on the rates and processes of solute acquisition in subglacial environments, with the aim of facilitating the deduction of variations in hydrological parameters such as the residence time of subglacial waters, reactive sediment availability, and solute provenance, from field observations of variations in subglacial water chemistry. Thus, an improvement in understanding of the role of chemical denudation in glacial environments as a CO₂-buffer may be facilitated.

The foundation for the study is provided by a suite of laboratory simulation experiments designed with the benefit of a multi-phase framework of solid, liquid and gaseous geochemical parameters. The specific aims of this project are:

1. To isolate the major processes of solute acquisition in subglacial environments within alpine glaciers.
2. To establish the rates and relative importance of individual controls on solute acquisition in a range of chemical conditions pertinent to subglacial chemical weathering.
3. To evaluate the role of minor and trace elements in subglacial weathering, with a view to the identification of key indicators of major solute acquisition processes.

Parameterisation was derived solely from the investigation of the geology and geochemistry of the *Haut Glacier d'Arolla* basin in the Canton of Valais in south-west Switzerland, but the implications of the research will be important in the interpretation of glacial hydrochemistry generally.

This review chapter aims to provide the rationale for the laboratory-based investigations that are described in this thesis. Numerous investigations into the processes involved in glacial chemical weathering are reviewed, and these are related to laboratory investigations of the geochemistry of natural waters in general, to further the understanding of the rates and controls on subglacial geochemical processes. Finally, a review of literature concerned with the inference of solute provenance in subglacial environments is combined with information about trace element geochemistry in natural waters, so that an understanding of possible indicator species of solute provenance and hydrological routing can be gained.

1.2 BACKGROUND TO STUDIES OF WATER QUALITY IN GLACIAL ENVIRONMENTS

Initially, it was assumed that the rate of chemical weathering in glacial environments would be slower than in most other weathering environments on Earth, and would be insignificant in comparison to physical processes operating in the Alpine environment (Peltier, 1950). However, early studies of Alpine hydrology and water quality reported a significant dissolved load in sub-alpine and glacial meltwater streams (Rainwater and Guy, 1961; Keller and Reesman, 1963; Feth *et al.*, 1964) (Table 1.1), and showed that as glacial ice originates as naturally distilled water which only contains material picked up from the atmosphere, the dissolved load must be dominantly rock-derived (Keller and Reesman, 1963).

Sugden & John (1976) termed temperate glaciers to be 'warm-based'. Although the temperature at the base of the glacier is approximately 0°C (Reynolds Jr. and Johnson, 1972) (up to 1.5°C suggested by Sugden & John (1976)), the term refers to the occurrence of pressure melting of ice at the glacier bed, due to overburden pressure, frictional heat released by ice movement, meltwater flow (Röthlisberger, 1972), geothermal heat (Sugden and John, 1976) and the influx of heat by supraglacial meltwaters (Röthlisberger, 1972). The presence of water at the ice-rock interface facilitates movement of the ice, driven by the accumulation of snow in the upper area of a glacier and melting/evaporation in the lower reaches (Tangborn, 1966). Even this simplistic explanation demonstrated that the grinding of moving ice on rock demonstrated that there is constant production and renewal of fresh rock surfaces in the presence of water, which will lead to accelerated rates of chemical reaction (Reynolds Jr. and Johnson, 1972).

Table 1.1 Some chemical characteristics of glacial meltwater compared to the world river water average. Units are neq/mL

Component	Mean river water ¹	Mean freshwater ²	Bulk meltwater ³	Bulk meltwater ⁴
HCO ₃ ⁻	960	160	7.2-61	180-460
SO ₄ ²⁻	230	44	19-71	20-340
Cl ⁻	220	37	28-580	0.9-6.7
NO ₃ ⁻	16	N/A	3.2-4.8	0-36
Ca ²⁺	750	420	45-550	140-470
Mg ²⁺	340	180	16-255	15-52
Na ⁺	270	90	52-540	5-36
K ⁺	59	10	8-33	3.3-19

¹ Global river water average (Henderson, 1976).

² "Mean" freshwater (from Gorham, 1961; Church, 1974).

³ Bulk meltwater ranges for the Lewis River, draining the Lewis Glacier, an outlet of the Barnes Ice Cap on Baffin Island, Northwest Territories, Canada (Church, 1974).

⁴ Bulk meltwater ranges are for the field seasons 1989 & 1990 at the *Haut Glacier d'Arolla*, Valais, Switzerland (Brown and Fuge, 1998a).

a) Chemical investigations of bulk meltwater chemistry

Early studies concerned with water quality and chemical denudation rates investigated the major-element chemistry of bulk meltwaters. The major constituents of bulk meltwaters draining glaciers on Baffin Island, Canada were found to be Ca²⁺, Mg²⁺, HCO₃⁻ and SO₄²⁻ (Church, 1974). Other studies have shown that these species dominate the solute load in many catchments despite a dominantly igneous and/or metamorphic bedrock lithology (Reynolds Jr. and Johnson, 1972; Holland, 1978; Raiswell, 1984; Drever and Hurcomb, 1986). The dominance of Ca²⁺ and HCO₃⁻ suggest that carbonate dissolution, carbonation, and perhaps simple dissolution of gypsum are major sources of solute in the internal hydrological system of many glaciers (Tranter *et al.*, 1993; Brown *et al.*, 1996b; Tranter *et al.*, 1996). The relatively high SO₄²⁻ and total Fe values may be due to the oxidation of pyrite (Reynolds Jr. and Johnson, 1972; Tranter *et al.*, 1993), which is often ubiquitously distributed in trace quantities in Alpine glacial environments (Fairchild *et al.*, 1994).

b) Early chemical models of glacier hydrology

Inferences about the internal hydrology using water quality rely on the analysis of bulk meltwater quality, due to the inaccessibility of the glacier interior. Stable isotope analysis of meltwaters in the Rofenache drainage basin, Austria (Behrens *et al.*, 1971) and at Austre Okstindbreen, Nordland, Norway (Theakstone and Knudsen, 1996) gave indications of the contributions to runoff of ice melt, snow melt and subglacial water. Zeman & Slaymaker (1975) suggested that different hydrological pathways may yield different quantities and different characteristics of major cationic solute load, with lithogenic influences controlling

“baseflow” solute acquisition, and atmospheric influences controlling glacier and snowmelt composition. These observations, and measurements of electrical conductivity of bulk meltwater draining glaciers over a meltseason (Behrens *et al.*, 1971; Collins, 1977; Collins, 1978; Collins, 1979a; Collins, 1979b) showed diurnal variations that are inversely related to discharge, which were interpreted as being driven by a two-component hydrological system. These results were interpreted as showing conservative mixing between a concentrated (high EC) meltwater component and a dilute (low EC) component, with bulk meltwater being dominated by dilute meltwaters at peak discharge (generally during the day when solar radiation is highest) and by concentrated meltwaters during periods of recession flow (generally at night or during periods of snowfall) (Collins, 1979a; Collins, 1979b). The dilute component was interpreted to be meltwater that flowed quickly through an internal, efficient network of channels. The concentrated component was interpreted to be meltwater that was inefficiently drained and was in contact with bedrock and sediment for longer periods of time (Collins, 1979a; Collins, 1979b).

Although the two-component conservative mixing model continues to be used (Collins, 1981; Collins, 1983; Gurnell and Fenn, 1984; Fenn, 1987; Collins, 1989; Tranter and Raiswell, 1991; Leece, 1993; Collins, 1995), more recent developments in the understanding of the nature of glacier drainage systems (e.g. Nienow *et al.*, 1996a; Nienow *et al.*, 1996b), and of the different chemical weathering processes operating in such systems (e.g. Tranter *et al.*, 1993) have showed that the assumptions involved make the use of such chemical mixing models unreliable (Brown and Tranter, 1990; Sharp, 1991; Sharp, 1995). As a result, more recent studies have begun to investigate individual ion chemistries, solute provenance and the rates, processes and controls of subglacial chemical weathering. These studies are necessary if interactions in meltwater quality are to be effectively utilised in hydrological investigations (Sharp, 1991).

c) *The role of glacial chemical denudation in climate change*

CO₂ is a greenhouse gas, and therefore any change in its concentration in the atmosphere due to changes in its rate of uptake by weathering affects its ability to absorb infrared radiation and heat the earth’s surface (Berner, 1995). Glacial environments remove CO₂ from the atmosphere due to enhanced weathering rates caused by the continual production of fresh weathering surfaces produced by grinding of rock by ice movement (Berner, 1995). Additionally, the apparent domination of carbonation-derived acid hydrolysis reactions in glacial environments (Tranter *et al.*, 1996), consuming CO₂ and producing bicarbonate

(Tranter *et al.*, 1993; Krauskopf and Bird, 1995), has important implications for the role of glacial chemical weathering in the global carbon cycle (Sharp, 1991).

The role of sulphide oxidation in glacial environments is also important in the global cycles of oxygen and sulphur (Raiswell *et al.*, 1980; Francois and Gerard, 1986; Sharp, 1991). Oxygen is consumed by pyrite oxidation, which is enhanced in many glacial environments compared to global averages (Tranter *et al.*, 1996), and sulphate is released into the hydrosphere.

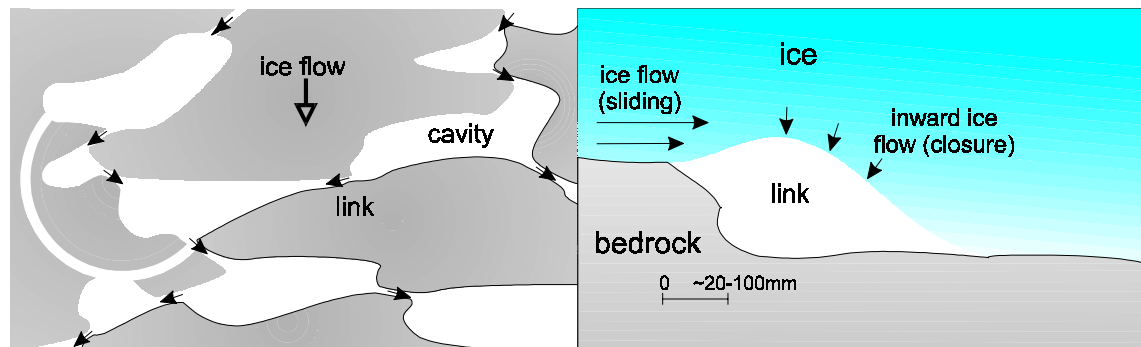
1.3 MODELS OF GLACIER HYDROLOGY AND HYDROCHEMISTRY

1.3.1 Formation of the distributed drainage system

Regelation, or pressure melting of ice, occurs on the stoss side of bedrock obstacles where pressure is locally increased. The meltwater generated by this process flows around the bump to the lee side, where the pressure is lower. Due to the lower pressure, the meltwater re-freezes on the lee side, and heat is transferred back through the obstacle to promote further melting (Weertman, 1957). Regelation aids basal sliding, a major contributor to the down-valley motion of a glacier (Sugden and John, 1976). The meltwater produced by pressure melting on the stoss side of a hummock may acquire solute from the available rock surface and freshly ground sediment. Additionally, re-freezing in the lower pressure regime may cause reprecipitation on rock surfaces on the lee side (Hallet, 1976). Partial re-freezing is likely to occur, with the result that the meltwater would become concentrated with solute acquired on pressure melting (Hallet, 1976). However, if ice flow is sufficiently rapid, a series of meltwater-filled cavities may form at the glacier bed (Walder, 1986).

Theoretical analyses of glacier hydrology have shown that water flow in subglacial cavities may occur if they are in close proximity (Walder, 1986) (Figure 1.1), or linked by a film of water (Weertman, 1972), permeable sediments (Shoemaker, 1986; Hooke, 1989) or very small-scale conduits (Walder and Fowler, 1994). If this occurs an inefficient subglacial hydrological network may develop. This has been termed the *distributed* drainage system through which flows *delayed flow* meltwaters (cf. Tranter *et al.*, 1993). The distributed system may not only be fed by pressure-melting, as snowmelt is likely to be a major contributor to the many parts of the system (Tranter *et al.*, 1993).

Figure 1.1 Schematic drawings of the distributed drainage system. Left: a linked-cavity drainage network. Ice is in contact with bed in shaded areas (modified from Hooke, 1989, Figure 4). Right: cross-section of a link between two cavities (modified from Hooke, 1989, Figure 5).



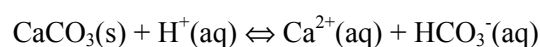
Due to the inefficiency of the distributed drainage system, meltwaters may remain in contact with sediment for relatively long periods of time. This means the potential for solute acquisition is increased (Tranter *et al.*, 1993; Brown *et al.*, 1994b). As the ablation season progresses, fine, reactive sediment is progressively removed from the system, and the ‘reaction potential’ may be reduced (Hooke *et al.*, 1985). However, the reactive surface area will be maintained to some extent by the continual generation of fresh sediment by physical abrasion of rock and sediment by basal sliding, especially in areas of enhanced sliding, where a sub-centimetre-thick layer of water separates basal ice from bedrock, or where the ice is in contact with soft deformable sediment so that friction and effective bed roughness are reduced (Reynolds Jr. and Johnson, 1972; Sugden and John, 1976; Sharp, 1995).

1.3.2 Processes of chemical weathering in the distributed system

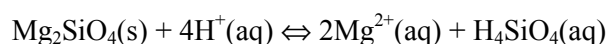
1.3.2.1 Acid hydrolysis

The most important mechanism of chemical weathering of minerals is by acid hydrolysis, where a metal cation is released into solution by a certain amount of hydrogen ions (protons), producing either a completely, or partially soluble anionic component (Raiswell, 1984). This process is common to carbonates, silicates and aluminosilicates (e.g. Equation 1.1, Equation 1.2, Equation 1.3).

Equation 1.1 Acid hydrolysis of calcite (Raiswell, 1984)



Equation 1.2 Acid hydrolysis of forsterite (Raiswell, 1984)



Equation 1.3 Acid hydrolysis of albite (Stollenwerk, 1994)



The extent of supply of protons by acids is therefore an important control on the chemical weathering of minerals (Nordstrom and Munoz, 1985). The anionic components of meltwaters can indicate the acid source(s) used in the dissolution of rock and sediment (Raiswell, 1984). Sources of acids in the natural environment include carbon dioxide from the atmosphere, oxidation of graphite and organic carbon, and from biogenic respiration, sulphide oxidation, organic acids, and pollutant gases, e.g. SO₂.

a) Organic -derived acidity

Organic material may be deposited, or be living (e.g. algae, ice worms) on the glacier surface (Goodman, 1971; Thomas, 1972; Wharton and Vinyard, 1983), served by a mineral source of particles dissolved in moisture present on or near the snow surface (Kol, 1942). However, the contribution of organic acids resulting from decay of such material to snow, and subsequently to the glacial water system, is likely to be very small (Raiswell, 1984). Therefore, organic acids are unlikely to be a significant source of acidity in glacial environments, in contrast to, say, solute acquisition in soils (Reynolds Jr. and Johnson, 1972; Raiswell, 1984). In addition, the modification of the surface properties and reactivity of grains by adsorbed organic compounds (Hunter and Liss, 1982) is likely to be much less extensive in glacial environments.

b) Atmosphere-derived acidity

Protons may also be derived directly from the dissolution of acid that has been scavenged from the atmosphere by snow, ice or dust deposited on the surface of the glacier (Odén and Ahl, 1970; cited in Zeman and Slaymaker, 1975; Barrie, 1991; Cadle, 1991). Acidic gases, e.g. SO₂ and NO₂, can be absorbed by precipitation and aerosol particles, and form acids, e.g. sulphuric and nitric (Winkler, 1980). Formation of the snowpack can trap atmospheric gases within pore spaces (Zeman and Slaymaker, 1975), and gas exchange can continue as air may be pumped through the snow by surface winds (Colbeck, 1989).

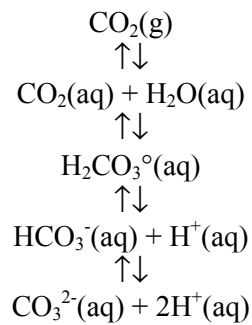
Since delayed flow meltwaters are largely fed by snowmelt (Brown *et al.*, 1994a), solute acquisition in these waters may be enhanced by the initial flush of protons that were stored over the winter, as fractionation of ions into the snowmelt occurs (Johannessen and Henriksen, 1978; Tranter, 1991; Fountain, 1996). This source of protons diminishes in significance as the ablation season progresses, and the snowpack is progressively leached (Fountain, 1996). However, long-term storage of atmospheric ions (e.g. NO₃⁻) may occur, as

meltwater may be ‘ponded’ beneath the glacier in subglacial sediment pore spaces, for example (Stone and Clarke, 1996).

c) Carbon dioxide-derived acidity

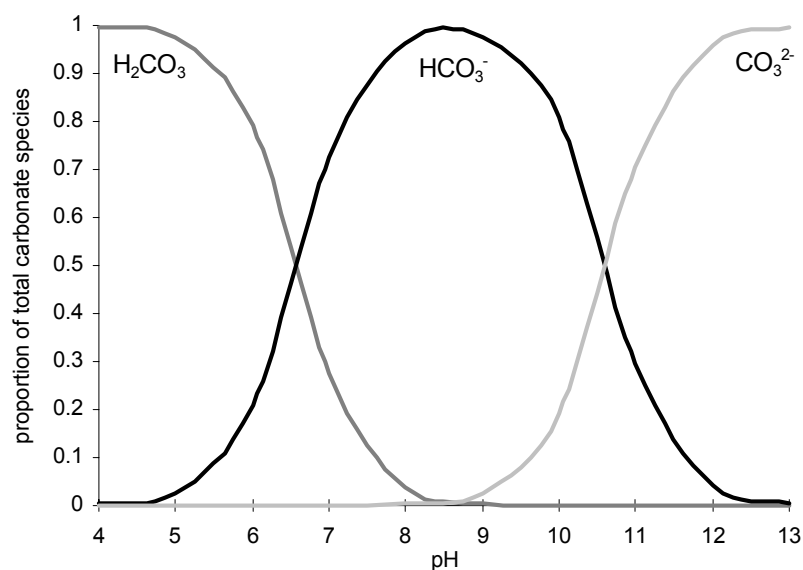
Aqueous protons may also be derived from carbonation reactions, which involve the dissolution and combination of atmospheric CO₂ with water to form carbonate species (Brownlow, 1979; Stumm and Morgan, 1996) (Equation 1.4).

Equation 1.4 Carbonate equilibria transformations in natural waters (see text and Figure 1.2).



At 0°C, 1 bar pressure and open access to atmospheric CO₂, the equilibria between carbonate species varies with pH as shown in Figure 1.2.

Figure 1.2 Relative concentrations of carbonate species at 0°C (using formulae from Garrels and Christ, 1965; adapted from Raiswell et al., 1980). At this temperature, the point of equilibrium between H₂CO₃ and (HCO₃⁻ + H⁺) (Equation 4) is at pH 6.58. At 25°C this is at 6.35 (Garrels and Christ, 1965). This shows the effect of temperature on carbonate speciation.



The extent of proton production by carbonation is dependent on the extent of drawdown of atmospheric CO₂, which itself is dependent on atmospheric access, temperature and pressure (Garrels *et al.*, 1960; Brownlow, 1979; Gill, 1996), and also the proportion of carbonate species, which also varies with pH, temperature and pressure (Garrels and Christ, 1965; Morse, 1983; Gill, 1996). In subglacial environments, variations in temperature are minimal due to the contact of ice and water (Reynolds Jr. and Johnson, 1972), although variations in pressure may be sufficient to have some influence. However, in general, the access to CO₂(g) is likely to be the most significant control on carbonation reactions.

Due to the closed, pressurised nature thought to characterise the distributed system, it may be the case that little or no atmospheric input of CO₂ (or indeed other atmospheric gases, e.g. O₂) into the system occurs. Furthermore, there is not likely to be a significant biogenic input of carbon dioxide into the distributed system (Raiswell, 1984). Access to CO₂(g) is generally restricted to that which may be already in solution, from snowmelt percolating through the ice into the distributed system, from bubbles trapped in basal ice (Tranter *et al.*, 1996), or through oxidation of inorganic elemental carbon (graphite), which is often associated with metapelites such as schists and gneisses (Brown *et al.*, 1996b). In the presence of reactive sediment, proton consumption is rapid, and it is likely that these sources of CO₂ will be quickly exhausted. Meltwaters under these conditions exhibit low p(CO₂), “closed system” characteristics (Garrels and Christ, 1965; Raiswell, 1984; Raiswell and Thomas, 1984; Thomas and Raiswell, 1984; Tranter *et al.*, 1993).

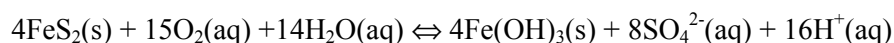
d) Sulphide oxidation-derived acidity

The rate and extent of sulphide oxidation is affected by many factors, including dissolved oxygen concentration (or oxidising potential, *E_h*), the reactive surface area of the sulphide mineral, the solubility of the mineral, dissolved ferric iron concentration, pH, temperature and the presence of bacteria (van Breeman, 1972; Lawson, 1982; Nordstrom, 1982; McKibben and Barnes, 1986; Moses *et al.*, 1987; Nicholson *et al.*, 1988; Hering and Stumm, 1990). Although the effects of temperature and pH on rates of pyrite oxidation are important, in glacial environments the temperature variation is slight, and carbonate buffering keeps the pH relatively constant (Nicholson *et al.*, 1988), so these factors become less important than other factors such as access to reactive rock/sediment, residence times and availability of atmospheric gases (Raiswell and Thomas, 1984; Tranter *et al.*, 1993; Brown *et al.*, 1994a). A suitable oxidising agent is required in solutions to drive the oxidation process.

(i) Aerobic sulphide oxidation:

The oxidation of sulphides by oxygen is an effective proton producing process (Raiswell, 1984; Chillrud *et al.*, 1994). In the case of ferrous sulphide (pyrite), four moles of acidity are produced by the oxidation of one mole of pyrite (Stumm and Morgan, 1996) (e.g. Equation 1.5).

Equation 1.5 Oxidation of pyrite by oxygen

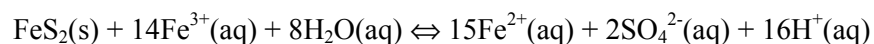


However, meltwater input to the hydrological system may not be in equilibrium with atmospheric O₂ levels. Measurements have shown that freshly melted snow at the *Haut Glacier d'Arolla* is 55-58% saturated, and glacier ice only 34-38% saturated with respect to atmospheric O₂ (Brown *et al.*, 1994a; Seagren, 1995). These data show that the levels of O₂(aq) in meltwaters involved in chemical weathering may diminish as the meltseason progresses, as the proportion of icemelt to snowmelt increases, reducing the surface residence times of the meltwater (Ferguson, 1973; Stenborg, 1973), and increasing ablation rates due to the lower albedo of ice compared to snow (Röthlisberger and Lang, 1987). Furthermore, in distributed systems of glaciers, dissolved oxygen concentration may become diminished, as access to atmospheric oxygen is restricted in the same way as CO₂, retarding the oxidation of sulphides by oxygen.

(ii) Oxidation by ferric iron:

Sulphide oxidation by Fe³⁺ can take place either simultaneously with oxidation by dissolved oxygen, or in its absence (Toran and Harris, 1990; Williamson and Rimstidt, 1994) (e.g. Equation 1.6).

Equation 1.6 Oxidation of pyrite in connection with ferric iron reduction



Ferric iron is abundant in the solid phase, mainly associated with clay minerals, oxides and glauconite peloids (Bierens de Haan *et al.*, 1994). In buffered solutions, however, Fe³⁺ is highly insoluble, and is virtually absent in most circumneutral or alkaline waters (Stone and Morgan, 1990; Bierens de Haan *et al.*, 1994). Therefore, Fe³⁺ in solution is unlikely to have a major role in oxidising pyrite in glacial environments, since pH is generally neutral to alkaline in such waters, but it is possible that Fe³⁺ in the solid phase may still have a rate-accelerating influence on the process (Bierens de Haan *et al.*, 1994).

(iii) Oxidation by nitrate:

Dissolved nitrate (NO_3^-) may be present in subglacial environments from acidic snowmelt, and provides the potential to oxidise pyrite in the absence of oxygen (e.g. Equation 1.7).

Equation 1.7 Oxidation of pyrite accompanying nitrate reduction



Equation 1.7 shows that this process produces relatively fewer protons in comparison to aerobic oxidation, and therefore would be less effective in driving acid hydrolysis reactions in the subglacial environment. The process may be a significant oxidising agent in $\text{O}_2(\text{aq})$ -depleted areas, although to date there is no direct evidence of this, and observed depletions of NO_3^- in glacial meltwaters may alternatively be due to microbiological activity (Tranter *et al.*, 1994).

(iv) Catalysis of sulphide oxidation by oxidising bacteria:

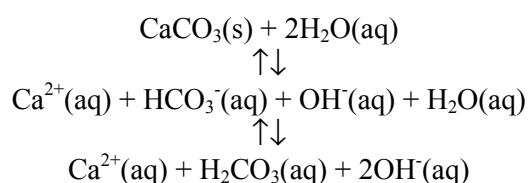
The role of bacteria in pyrite oxidation is not thought to be major in glacial environments (Bierens de Haan, 1991), as the activity of the main pyrite oxidation catalysing bacteria (*Thiobacillus ferrooxidans*) is severely diminished at circumneutral to alkaline waters which typically characterise glacial catchments (Lundgren and Silver, 1980), due to a lower energy-availability at such pH ranges (Lees *et al.*, 1969; Nicholson *et al.*, 1988). However, it has been suggested that microenvironments with large pH gradients could occur within the distributed system, whereupon microbial catalysis of pyrite could occur. This has been observed in concrete weathering, which is generally a highly alkaline environment (Fairchild *et al.*, 1994), and more recently has been shown to occur in a carbonate-rich glacial catchment (Fairchild *et al.*, 1999).

1.3.2.2 Hydrolysis

a) Hydrolysis of carbonate minerals

Carbonate weathering may occur in the absence of protons by simple hydrolysis with water molecules, supplying calcium and bicarbonate ions into solution. In waters with negligible gas phase present, the number of total dissolved carbonate molecules is always the same as the number of calcium ions in solution (Garrels and Christ, 1965). The solution becomes alkaline because of the release of hydroxide ions (Equation 1.8).

Equation 1.8 Calcite hydrolysis reactions in natural waters



This the only form of carbonate dissolution that could occur in a true “closed system” environment. In reality, this process rarely happens in isolation, as such a restricted composition is almost never encountered (Garrels and Christ, 1965), and glacial meltwaters entering the subglacial environment will have appreciable, if not atmospheric equilibrium levels of pCO_2 (see above).

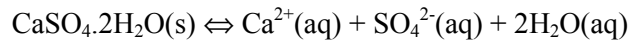
Since it is thought that the distributed system approaches a closed system with respect to CO_2 (Raiswell, 1984; Raiswell and Thomas, 1984; Thomas and Raiswell, 1984; Tranter *et al.*, 1993), the thermodynamics of the reaction of pure water in equilibrium with atmospheric CO_2 with a calcite-bearing mineral in a closed system (i.e. where no additional input of atmospheric CO_2 can occur) are relevant here. This would equate to snowmelt from the glacier surface percolating down through the glacier (without further reaction) before reaching the ice-bedrock interface and coming into contact with reactive calcite. Hence, the dissolved carbonate species present in the snowmelt produced by carbonation reactions during any contact time with the atmosphere prior to rock-water contact (Equation 1.4) are augmented by carbonate from calcite hydrolysis (Equation 1.8). Calculations by Garrels & Christ (1965) show that the difference in equilibrium concentrations of calcium and carbonate species between the above scenario and those resulting from simple hydrolysis of calcite is minimal; in fact the increase in solubility of calcite is only about 10% over that in pure water. This suggests that the influence of snowpack-sourced CO_2 on the magnitude of carbonate dissolution is less significant than the effects of hydrolysis and CO_2 already present in the distributed system, particularly as it is likely that snowpack-derived meltwater is undersaturated with respect to $\text{CO}_2(\text{g})$, since O_2 is generally undersaturated (Brown *et al.*, 1994b).

b) Hydrolysis of sulphate minerals

Gypsum can occur in igneous and metamorphic geologies, in mineral veins where sulphuric acid produced by the oxidation of pyrite has reacted with calcareous wall rocks (Hamilton *et al.*, 1974). Gypsum can also be a secondary product of sulphide oxidation by percolating groundwaters, or a replacement product of pyrite in some calcareous muds or clays (Clark, 1979). Therefore secondary gypsum may be significant in subglacial calcareous

environments where sulphide oxidation is occurring. The main process of sulphate dissolution is by simple hydrolysis.

Equation 1.9 Hydrolysis of gypsum

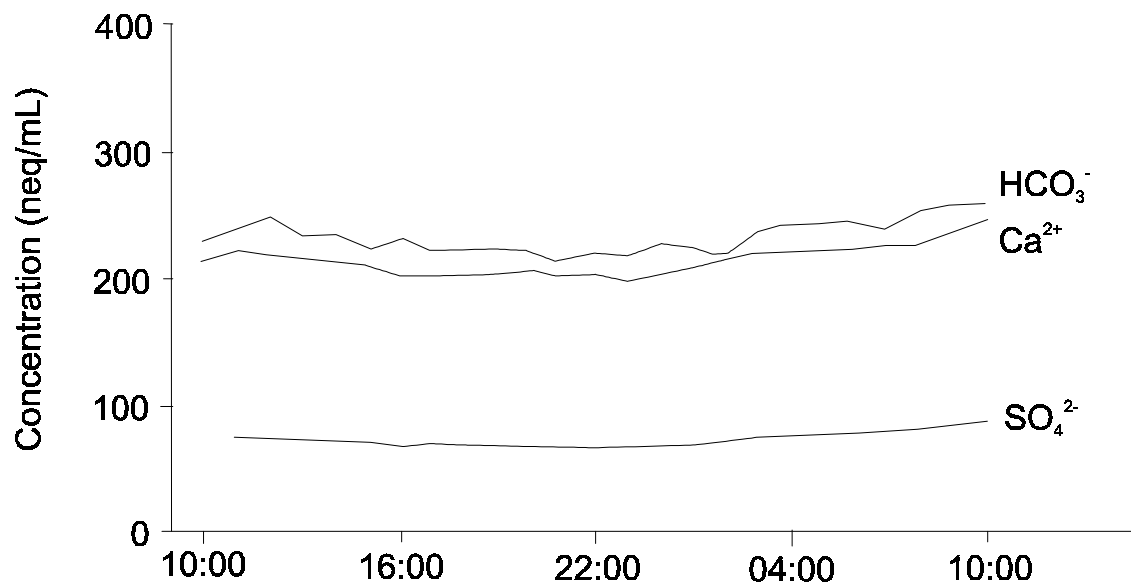


Little attention has been given to this mineral as a source of sulphate in glacial meltwaters. Sulphur isotope data have suggested that evaporites are unlikely to be the source of SO_4^{2-} in glacial meltwaters except in areas of exceptional catchment geology (Chillrud *et al.*, 1994). However, it remains possible that some calcium and sulphate in delayed flow meltwaters may have been produced from the dissolution of gypsum or anhydrite.

1.3.2.3 Coupled sulphide oxidation and carbonate dissolution

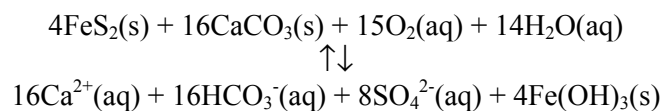
High observed concentrations of Ca^{2+} , HCO_3^- , and SO_4^{2-} in early season bulk meltwaters that are believed to be predominantly delayed flow (Brown *et al.*, 1996b) (Figure 1.3) have led to the suggestion that sulphide oxidation is providing the bulk of acidity to drive carbonate dissolution in delayed flow meltwaters, and that this combined process is a major control on the composition of delayed flow meltwaters (Tranter and Raiswell, 1991; Tranter *et al.*, 1993; Brown *et al.*, 1994a; Brown *et al.*, 1996a; Brown *et al.*, 1996b).

*Figure 1.3 Variations in the concentrations of Ca^{2+} , HCO_3^- , and SO_4^{2-} over the diurnal cycle June 22-23 1989, early in the meltseason before a channelised drainage network has developed (after Brown *et al.*, 1994a).*



The association between sulphide oxidation and carbonate dissolution can be considered as a coupled reaction (Equation 1.10, after Tranter *et al.*, 1993).

Equation 1.10 Calcite dissolution driven by protons released into solution by oxygen-driven pyrite oxidation



Ratios of $\text{SO}_4^{2-}/\text{HCO}_3^-$ in borehole meltwater samples drilled in situ from the distributed system, which show an approximate 1:1 relationship in equivalence units, were interpreted as showing that the coupled sulphide oxidation/carbonate dissolution reaction is important (Lamb *et al.*, 1995). However, in reality, this reaction cannot fully describe the process of solute acquisition, as simple hydrolysis of carbonates is neglected, and CO_2 cannot be ignored in the presence of sulphides.

1.3.3 Formation of and processes of solute acquisition within the channelised drainage system

a) Formation

Internal deformation of an Alpine glacier is achieved by inter-granular slip and recrystallization, and is a function of hydrostatic overburden pressure and shear stress (Sugden and John, 1976). This ‘creep’ is not an efficient process, and results in the formation of tensional crevasses. Where crevasses are exposed, below the snowline on a glacier surface, the volume of supraglacial meltwater draining into crevasses may be sufficient to propagate the cracks further down into the glacier, eventually reaching the ice-bedrock interface (Röthlisberger, 1972). The volume of icemelt that the glacier has to accommodate during the ablation season leads to internal hydrological reorganization, and seasonal evolution of the subglacial hydrological network. This system may develop into an efficient channelised system which rapidly transports meltwater down-glacier, and develops at the expense of the distributed system.

Meltwater rapidly transported through a channelised system has been termed ‘quickflow’ meltwater, due to the short residence times within the glacier (Hooke, 1989; Sharp *et al.*, 1993). The rapid draining of this meltwater means that variations in bulk discharge patterns are closely matched to diurnal variations in solar radiation levels, with a delay of only a few hours (Rainwater and Guy, 1961; Brown, 1991).

Dye tracing experiments have shown that over the meltseason, the channelised network progressively consumes parts of the distributed network as it extends headwards, following the retreat of the seasonal snowline (Brown *et al.*, 1996a), so the ratio of contributions to bulk meltwater between the distributed and channelised components decreases (Seagren, 1999). In addition, re-freezing and pressure-closing of the channels during the winter means the system is unlikely to retain a constant structure from year to year. This has been shown by dye-tracing studies (Willis *et al.*, 1990; Hock and Hooke, 1993; Nienow *et al.*, 1996a; Nienow *et al.*, 1996b).

b) Solute acquisition

Quickflow meltwaters travel mainly through ice-walled conduits, with contact with rock and sediment restricted to that frozen into the ice. Solute acquisition is therefore restricted to carbonation and limited acid hydrolysis of any reactive sediment encountered (Brown *et al.*, 1994a). As a result, these waters remain relatively dilute until they come into contact with the ice/bedrock interface.

c) Mixing of quickflow and delayed flow meltwaters

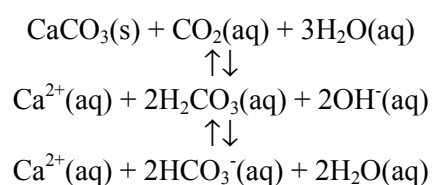
It is thought that the distributed network is widely spread across the ice-bedrock interface in areas away from the channelised network. In particular, many components of the distributed network may be situated beneath snow-covered areas of the glacier, which is up-glacier of parts of the channelised network, in which case delayed flow meltwaters are likely to drain into channels occupied by quickflow meltwaters (Humphrey *et al.*, 1986; Nienow *et al.*, 1996a; Nienow *et al.*, 1996b). In addition, measurements of borehole water pressures at the *Haut Glacier d'Arolla* showed fluctuations in water pressure through areas of basal sediment up to around 70m away from a subglacial meltwater channel, which has been termed a "Variable Pressure Axis (VPA)" (Hubbard *et al.*, 1995). These investigations suggest that delayed flow waters could also be infiltrated if, at peak flow, quickflow waters are forced under pressure into the surrounding sediment. These waters may return into the channelised network when the pressure reduces after peak flow (Brown and Tranter, 1990; Hubbard *et al.*, 1995).

It is suggested, therefore, that when quickflow waters reach the ice-bedrock interface, they begin to mix with delayed flow waters (Sharp *et al.*, 1993). In these basal arterial channels, the dilute quickflow waters encounter, and acquire sufficient power to mobilise, high suspended sediment concentrations, and it has been demonstrated that a significant amount of solute may be acquired from the weathering of basal and suspended sediments in the post-

mixing environment (Raiswell, 1984; Raiswell and Thomas, 1984; Thomas and Raiswell, 1984; Tranter *et al.*, 1993; Brown *et al.*, 1994a). The extent of these so-called “post-mixing reactions” depends on the suspended sediment concentration in the bulk meltwaters, its nature, and the contact time of these waters with the suspended sediment (Brown *et al.*, 1994a). Progressive winnowing of sediments over a meltseason, in channels and through the VPA, and the extent and nature of each hydrological network will affect suspended sediment concentrations in the bulk meltwater, which in turn affects the extent of post-mixing reactions (Brown *et al.*, 1994a; Hubbard *et al.*, 1995; Willis *et al.*, 1995).

Channels that develop through the meltseason are generally not filled, except at periods of peak flow (Raiswell and Thomas, 1984; Stone and Clarke, 1996). In partially filled channels, quickflow meltwaters generally have access to atmospheric gases. Solute acquisition is achieved predominantly by rapid exchange reactions between base cations on the surface of rock and sediment at the glacier bed and protons in solution derived mainly from carbonation reactions (see above) (Equation 1.11) (Tranter *et al.*, 1993). The carbonate dissolution reaction is therefore a combination of Equation 1.4 (carbonation) and Equation 1.1 (acid hydrolysis of calcite)

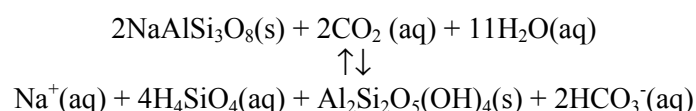
Equation 1.11 Carbonation-driven acid hydrolysis of calcite in natural waters.



It can be seen that the protons released by carbonation are consumed by acid hydrolysis (Krauskopf and Bird, 1995). The rate of diffusion of $\text{CO}_2(\text{g})$ into solution is generally slower than proton removal by surface-exchange, so pCO_2 can drop in these waters and restrict the rate of acid hydrolysis (Garrels and Christ, 1965; Tranter *et al.*, 1993). The stoichiometry of carbonation-driven carbonate dissolution produces a 2:1 molar ratio of $\text{HCO}_3^-/\text{Ca}^{2+}$, which is a 1:1 charge-equivalent ratio. This is distinct from the 1:2 charge-equivalent ratio of the coupled sulphide oxidation and carbonate dissolution reaction., and the 1:2 charge-equivalent ratio of the simple calcite hydrolysis reaction.

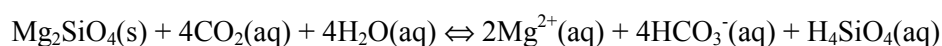
Carbonation-driven silicate dissolution also produces bicarbonate, such as albite dissolution (Equation 1.12). The molar ratio of HCO_3^- to Na^+ products is 1:1, (also 1:1 in equivalent units). The dissolution of albite (or any other aluminosilicate) in a calcite solution waters therefore increases the ratio of HCO_3^- to Ca^{2+} above 1:1 equivalent units.

Equation 1.12 Carbonation-driven acid hydrolysis of albite (Na-end-member of plagioclase solid solution series)



Carbonation-driven dissolution of forsterite (Equation 1.13) requires four moles of aqueous CO_2 to dissolve each mole of silicate, as more protons are required to mobilise the silicate tetrahedra into its soluble form. However, the resultant ratio of solution $\text{HCO}_3^-/\text{Mg}^{2+}$ is the same as that from magnesite (MgCO_3) dissolution, so Mg provenance cannot be discerned using these ratios.

Equation 1.13 Carbonation-driven acid hydrolysis of forsterite (Mg end-member olivine)



The dissolution of aluminosilicates may be further retarded by the production of a surface film of alumina tetrahedra which prevents further reaction (Keller and Reesman, 1963; Stumm and Morgan, 1996).

1.4 LABORATORY INVESTIGATIONS OF SOLUTE ACQUISITION

It is clear that solute acquisition within a glacier depends on hydrologic, hydraulic, minerallic, and gaseous controls. Although field and theoretical investigations have brought forward the understanding of the likely processes of solute acquisition, quantitative determinations of the rates, controls and magnitudes of solute acquisition are necessary in such a closed-box system as a glacier hydrological network. This section reviews literature relating to laboratory simulations of glacial environments, and the determination of rates of pyrite oxidation, and carbonate and aluminosilicate dissolution, with reference to parameters relevant to the glacial environment.

1.4.1 Laboratory investigations of glacial chemical weathering

Laboratory work as far back as 1924 indicated that rock-forming silicates react rapidly with water at near-freezing temperatures (Tamm, 1924; cited in Reynolds Jr. and Johnson, 1972). Reynolds Jr. & Johnson (1972) conducted experiments with crushed bedrock of different types from the catchment of the South Cascade Glacier, to compare field data with composite laboratory data. This study showed that dissolution of the main rock types of the catchment

(diorites and schists) could satisfactorily explain the observed dominance of Ca^{2+} in bulk meltwater despite the low abundance of calcite in the catchment. Mass-balance calculations using data and mineralogical evidence from the same glacier also determined that trace amounts of calcite provided the principle source of solute in bulk meltwater (Drever and Hurcomb, 1986). More recent experiments have focussed on the individual variables that may affect the magnitudes of weathering of sediment in glacial environments. These include concentration of suspended sediment, particle size distribution, proton availability, rewetting and access to atmospheric gases. The extent of research of these variables are detailed below.

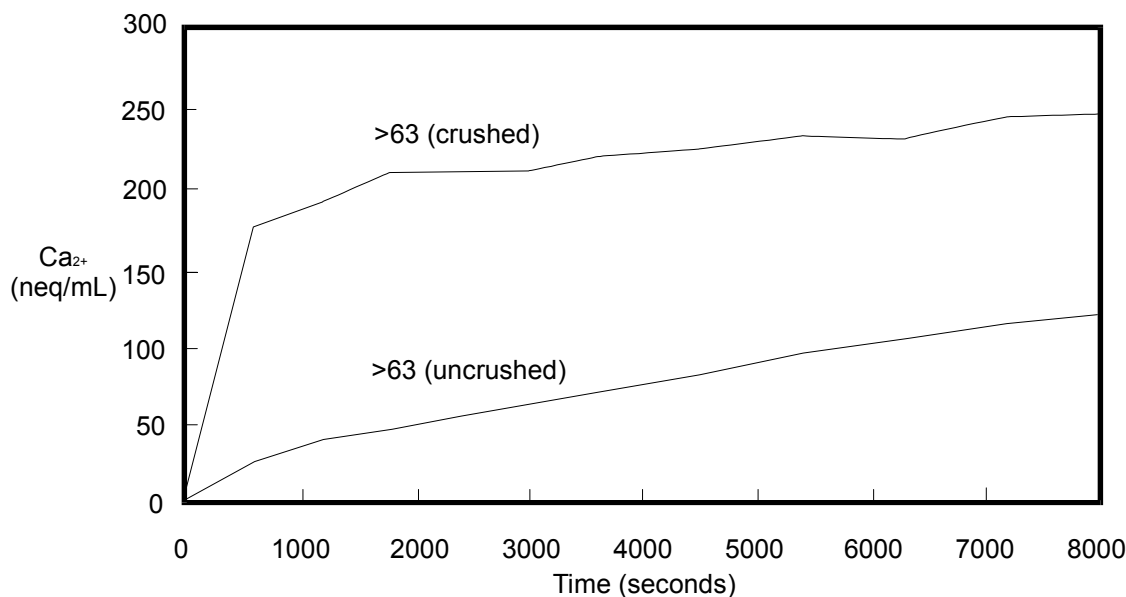
a) Suspended sediment concentration

Experimental investigations of the dissolution of different concentrations of proglacial sediment from the *Haut Glacier d'Arolla* were carried out in free access to the atmosphere (Brown *et al.*, 1996b). The experiments were designed to show the extent of weathering of suspended sediment in bulk meltwaters, a process neglected in the early conservative mixing models (e.g. Collins, 1977, etc.). These experiments showed considerable solute acquisition, and also showed Ca^{2+} to be the dominant cation, and an approximately 1:1 (charge-equivalent) relationship between Ca^{2+} and HCO_3^- , which is the relationship expected for open system carbonation of calcite (Equation 1.11). The rate of sulphate production in the same experiments was very slow after a short initial period of rapid dissolution which was attributed to slow sulphide oxidation on the mineral surfaces during sample storage and subsequent rapid release during the early stages of the experiments. This supported theories that sulphide oxidation is a slow process that would only contribute significantly to the solute load of waters that had long residence times at the glacier bed, or came into contact with sediment that had been isolated from meltwater channels for long periods of time (Tranter *et al.*, 1993). The results showed that carbonation-driven acid hydrolysis of carbonates was the dominant process in bulk meltwaters.

b) Particle size

The use of different size fractions in these experiments showed enhanced solute acquisition in the finer fractions, and in particular, very rapid release of ions from the finest (<63 μm) particle sizes (Brown *et al.*, 1996b). This suggested that the number of reactive sites, which increases with decreasing grain sizes, and possible size-fraction sorting of mineralogy, directly affects the rate of chemical weathering (Tranter *et al.*, 1993). This was further corroborated by the comparison of solute acquisition from uncrushed proglacial sediment

Figure 1.4 Ca^{2+} concentration versus time during open system dissolution experiments using 4g/L of uncrushed 63-125 μm sediment from the proglacial area of Haut Glacier d'Arolla and sediment of the same initial size distribution crushed to <63 μm (after Brown *et al.*, 1996b)



(size fraction 63-125 μm) and sediment of the same initial size fraction that was crushed to <63 μm (see Figure 1.4). This showed that fresh, unreacted mineral surfaces are initially very reactive, especially when crushed to micro-particle size as suggested in Tranter & others (1993).

c) Proton availability

A modification of the experiments investigating particle size effects, involving pre-acidified fluids to increase the availability of protons, showed enhanced solute acquisition in comparison to non-acidified experiments, suggesting that proton availability was a further controlling factor in the rate of dissolution (Brown *et al.*, 1996b). This may equate to the mixing of delayed flow meltwaters, which may have acidity derived from sulphide oxidation, with alkaline quickflow waters (Brown *et al.*, 1994a).

d) Repeated wetting of pre-reacted sediment

Experiments involving the repeated wetting of the same sample of sediment from Haut Glacier d'Arolla showed continued solute acquisition upon the second wetting of the sample (Brown *et al.*, 1996b). However, although the second wetting gave only partially diminished levels of Ca^{2+} and HCO_3^- in comparison with the initial wetting, there was no SO_4^{2-} released into solution with the second wetting. This showed that carbonation-derived protons are a limiting factor in the acquisition of solute from suspended sediment.

e) Restriction of access to atmospheric gases

Very few experiments have been carried out in environments designed to simulate the closed system characteristics of the distributed system of the glacial hydrological network. However, simple dissolution experiments on CaCO_3 rock flour from Robertson Glacier, Alberta, Canada, in a sealed vessel, showed rapid initial Ca^{2+} release, followed by limited additional acquisition after around 20 minutes (Willis *et al.*, 1995). This showed that initial weathering occurred by simple calcite hydrolysis with some additional carbonation-derived acid hydrolysis, and that once the proton supply was exhausted, weathering ceased as the supply was not renewed.

Sealed experiments using a 3g/L calcite-pyrite mixture showed rapid initial release of Ca^{2+} and SO_4^{2-} (within 1 hour), followed by slower release of SO_4^{2-} up to 24 hours, by which time dissolved oxygen levels had dropped from 10 to 1mg/L, after which time they remained constant (Willis *et al.*, 1995). These showed that pyrite oxidation becomes limited by the availability of dissolved oxygen in a closed system after about 24 hours at such concentrations. Similar dissolutions in a 0.03mM HNO_3 solution showed no significant differences (Willis *et al.*, 1995). This suggested that NO_3^- reduction in anaerobic conditions is not a likely oxygen source for continued pyrite oxidation in the absence of bacterial populations (Equation 1.7).

f) Summary

The experiments using proglacial sediment and calcite and pyrite under open and closed systems have begun to address the role of gas availability in subglacial weathering, and have confirmed that the composition of meltwaters in the distributed system is controlled by sediment mineralogy, proton availability, and continued access to atmospheric gases (Willis *et al.*, 1995). However, this method of experimentation is still in its infancy, and has yet to address the extent of the coupled sulphide oxidation and carbonate dissolution reaction, or to quantify the rates of solute acquisition.

1.4.2 Experimental investigations of pyrite oxidation

This section details research investigating the rates and controls on pyrite oxidation by the different oxidising agents that have been suggested as potential oxidants in delayed flow meltwaters.

a) Oxidation by oxygen

The prevalence of surface-controlled dissolution of pyrite at low temperatures is evidenced by an activation energy (E_a) of around 39-88kJ/mole (Lowson, 1982), higher than that expected of diffusion-controlled reactions; which are generally less than 30kJ/mole (Lasaga, 1984; Hering and Stumm, 1990; Moses and Herman, 1991). In waters with a pH of up to 7, virtually all oxygen consumed by the product SO_4^{2-} is water-derived dissolved oxygen (Reedy & others, 1991).

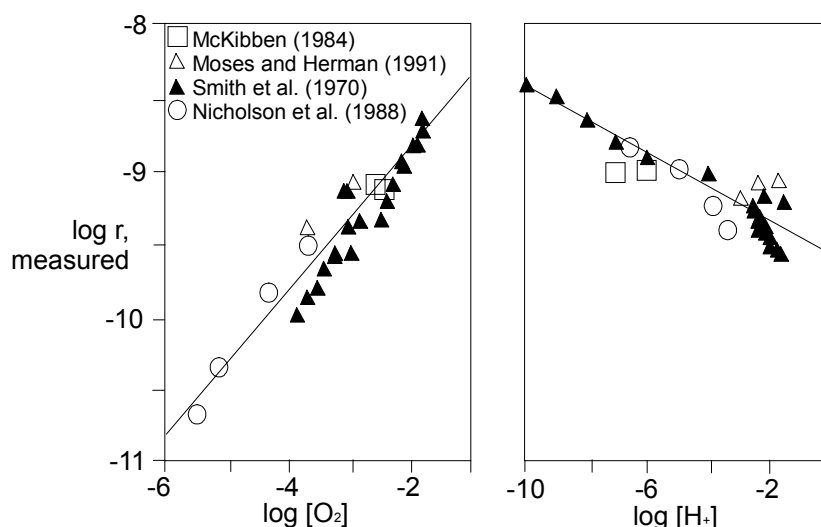
The majority of surface and near-surface waters which are carbonate-buffered have pH values in the range of 7 to 8 (Nicholson *et al.*, 1988), which means that any influence of pH on the oxidation rate of pyrite is negated in the presence of significant carbonate in solution (Smith *et al.*, 1968). The pyrite dissolution rate shows a non-linear dependence on $\text{O}_2(\text{aq})$ concentration (Nicholson *et al.*, 1988).

Williamson & Rimstidt (1994) give a rate law for the oxidation of pyrite by dissolved oxygen (Equation 1.14), which is a development of experiments showing a square root dependence on dissolved oxygen concentrations and a virtual independence of pH variations (McKibben and Barnes, 1986). The rate is illustrated in Figure 1.5.

Equation 1.14 Rate law for the oxidation of pyrite by oxygen, where r = rate of pyrite destruction in mol/m/s, $[\text{O}_2(\text{aq})]$ is the molarity of dissolved oxygen and $[\text{H}^+(\text{aq})]$ is molarity of $\text{H}^+(\text{aq})$, i.e. $10^{-\text{pH}}$ (after Williamson and Rimstidt, 1994)

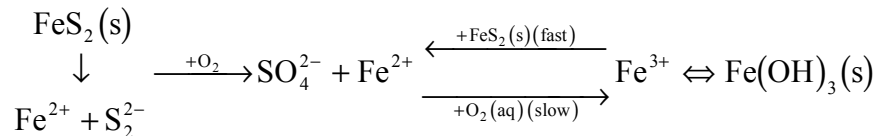
$$r = 10^{-8.19(\pm 0.10)} \frac{[\text{O}_2(\text{aq})]^{0.5(\pm 0.04)}}{[\text{H}^+(\text{aq})]^{0.11(\pm 0.01)}}$$

Figure 1.5 Linear regression plots of rate data for the aqueous oxidation of pyrite by dissolved oxygen (after Williamson and Rimstidt, 1994, : Figure 2)



The rate relationship with oxygen suggests that the process of pyrite oxidation in unbuffered systems is complicated, with the oxidation of Fe²⁺ to Fe³⁺ and subsequent decomposition of oxidation products with equilibrium adsorption of O₂ on the pyrite surface being the likely rate-limiting step in a multistage process (Equation 1.15) (Nicholson *et al.*, 1988; Stumm and Morgan, 1996).

Equation 1.15 The multistage processes involved in pyrite oxidation (after Stumm and Morgan, 1981)



Investigations showed that the reaction between pyrite and O₂(aq) was independent of concentrations of SO₄²⁻ and Cl⁻, and ionic strength (I) (Williamson and Rimstidt, 1994). However, these experiments do not report variations with temperature.

Experiments by Nicholson & others (1988) showed that there is an approximate tripling of the oxidation rate with a 10°C rise in temperature, which is an approximate Arrhenius variation. They gave the rate of pyrite oxidation as in Equation 1.16:

*Equation 1.16 Rate law for oxidation of pyrite, where w is a coefficient relating to the mole ratio of SO₄²⁻ to O₂ in Equation 1.5, S is the surface area (m²), C is the concentration of oxygen in the gas phase (mol/m³), R is the gas constant (kJ/mol/K), T is the absolute temperature (K), K is the oxygen absorption constant for pyrite and A is the pre-exponential factor in the Arrhenius equation (after Nicholson *et al.*, 1988)*

$$r = \frac{wSKCA \left(\frac{-E_a}{RT} \right)}{1 + KC}$$

Since K and A are constants (1.36m³/mol and 3.34x10⁻¹⁴ mol/m²/s respectively), the oxidation rate can be determined when the surface area, concentration of oxygen and temperature are known (Nicholson *et al.*, 1988).

Certain experiments have suggested that major differences in oxidation rates exist between pyrite samples from different locations (Nordstrom, 1982). For instance, crushed museum grade pyrite was shown to be “relatively inert” in comparison to some sedimentary pyrites, which oxidise rapidly. It was concluded that sedimentary pyrite has greater available surface areas due to framboidal textures and microcrystallinity (Carrucio *et al.*, 1981). More recent experiments have variously shown maximum variations of 46% (Wiersma and Rimstidt, 1984) and 25% (Nicholson *et al.*, 1988) from the mean rate shown above. It was not established whether variations in the trace metal concentrations within the pyrite, or in

adjacent, unobserved mineral phases (e.g. chalcopyrite), were responsible for the observed variations in rate.

b) Oxidation by ferric iron

Another potential oxidising agent is ferric iron (Fe^{3+}) in solution. Fe^{3+} , often present as ferric oxyhydroxide, has low solubility, particularly in neutral to alkaline solutions (Nicholson *et al.*, 1988), but experiments have shown that pyrite oxidation is at least as fast in Fe^{3+} -saturated solutions as dissolved oxygen-saturated solutions at pH values around 7 (Moses *et al.*, 1987), and at pH 2 the Fe^{3+} -driven rate is two magnitudes higher than the $\text{O}_2(\text{aq})$ -fuelled rate. There is no significant dependence on pH in the presence of $\text{O}_2(\text{aq})$ (the concentration of $\text{O}_2(\text{aq})$ does not affect this statement). However, in the absence of $\text{O}_2(\text{aq})$ the influence of pH is marked (McKibben and Barnes, 1986; Hering and Stumm, 1990; Williamson and Rimstidt, 1994). The rate law for pyrite oxidation by ferric iron in the presence of $\text{O}_2(\text{aq})$ was described as shown in Equation 1.17 (after Williamson and Rimstidt, 1994). In the absence of $\text{O}_2(\text{aq})$, the rate law was as in Equation 1.18 (after Williamson and Rimstidt, 1994).

Equation 1.17 Rate law for the oxidation of pyrite by ferric iron in the presence of oxygen, where r = rate of pyrite destruction in mol/m/s, $[\text{Fe}^{3+}(\text{aq})]$, $[\text{Fe}^{2+}(\text{aq})]$ and $[\text{H}^+(\text{aq})]$ are the molarities of ferric iron, ferrous iron and aqueous protons respectively (after Williamson and Rimstidt, 1994)

$$r = 10^{-8.58(\pm 0.15)} \frac{[\text{Fe}^{3+}(\text{aq})]^{0.30(\pm 0.02)}}{[\text{Fe}^{2+}(\text{aq})]^{0.47(\pm 0.03)} [\text{H}^+(\text{aq})]^{0.32(\pm 0.04)}}$$

Equation 1.18 Rate law for the oxidation of pyrite by ferric iron in the absence of oxygen, where r = rate of pyrite destruction in mol/m/s, $[\text{Fe}^{3+}(\text{aq})]$ and $[\text{Fe}^{2+}(\text{aq})]$ are the molarities of ferric and ferrous iron respectively (after Williamson and Rimstidt, 1994)

$$r = 10^{-6.07(\pm 0.57)} \frac{[\text{Fe}^{3+}(\text{aq})]^{0.93(\pm 0.07)}}{[\text{Fe}^{2+}(\text{aq})]^{0.40(\pm 0.06)}}$$

Equations 16 & 17 show a fractional-order (i.e. non-linear) dependence on $[\text{Fe}^{3+}]$ (McKibben and Barnes, 1986; Moses *et al.*, 1987), and an inverse correlation between $[\text{Fe}^{2+}]$ and rate. Therefore the ratio of $\text{Fe}^{3+}/\text{Fe}^{2+}$ in solution is very significant in determining the rate of oxidation by ferric iron. When $\text{Fe}^{3+}/\text{Fe}^{2+}$ is high, the rate seems to be virtually independent of $\text{O}_2(\text{aq})$ concentrations, as long as some $\text{O}_2(\text{aq})$ is present (McKibben and Barnes, 1986; Moses *et al.*, 1987; Moses and Herman, 1991), but when $\text{Fe}^{3+}/\text{Fe}^{2+}$ is lower, the rate is faster in anaerobic conditions (Williamson and Rimstidt, 1994). Equation 6 shows that ferrous iron

is produced by the oxidation of pyrite by ferric iron, so the rate will be dependent to a large extent on removal of the products, as Fe^{2+} will quickly inhibit further reaction if it is not removed (McKibben and Barnes, 1986).

The rate of sulphide oxidation in mixed $\text{O}_2(\text{aq})$ and Fe^{3+} oxidation systems in delayed flow meltwaters, and the relative importance of each oxidant, is therefore complicated and has not been evaluated, either in a rate law, by field observations or by laboratory experiments to date. Furthermore, no comprehensive cation analysis has been carried out on glacial meltwaters to date, and iron concentrations have not been reported in any studies of glacial meltwaters. Concentrations, and therefore the roles of dissolved Fe^{3+} and other potential oxidants remain unknown. Closed-system dissolution experiments in the presence of these potential oxidants may lead to a much better determination of the rates of, and controls on sulphide oxidation in closed-system glacial weathering environments.

It should be emphasised that the units for r , the rate of pyrite destruction, in the above laws are moles per square metre per second, so that the rate of sulphide oxidation is not only dependant on concentration of oxidant, but is also affected by the reactive surface area of sulphide mineral and time of contact between the sulphide mineral and the solution (Stumm and Morgan, 1996).

c) Inhibition of oxidation rate with time

Experiments investigating pyrite oxidation rate (Williamson and Rimstidt, 1994) revealed a slowing in rate of oxidation by both oxygen and ferric iron over time, which could not be attributed to the consumption of the respective oxidants. Additionally, the re-reaction of pre-reacted pyrite grains subsequent to washing with water, concentrated HNO_3 or EDTA failed to reproduce original rates of reaction, indicating that a change in surface properties of the pyrite, rather than solution effects, are responsible for the reduction in rate over time. Polishing of surfaces, however, was reported to alter the rate (Williamson and Rimstidt, 1994).

1.4.3 Experimental investigations of carbonate dissolution

Other than evaporite minerals such as gypsum and halite, calcite is one of the most soluble and rapidly weathering rock-forming minerals found in nature (Stumm and Morgan, 1996). In glacial environments, significant dissolution of calcite was observed within ten seconds of contact between a meltwater stream and a band of marble (Delthier, 1977, cited in Drever and Hurcomb, 1986). However, in the natural environment, the rate of dissolution of carbonate minerals is generally less than would be expected for diffusion-controlled reactions, that is to

say reactions limited by the transport of the reacting species between the bulk of the solution and the surface of the mineral through a stagnant boundary layer (Wollast, 1990). It is assumed, therefore, that the chemical reaction on the mineral surface itself is the rate-determining step. This reaction occurs at weakened crystal bonds on the surface, and interactions of reactants at these specific sites allow the detachment of surface ions into the solution (Wollast, 1990). The rate of surface reaction can be related to that of decomposition of an activated surface complex. The formation of the activated complex depends to a great extent on the properties of the mineral surface. The reaction rate of calcium carbonate dissolution depends on the concentration of each reacting species of the reactions involved in the formation of the activated surface complexes (Wollast, 1990) (see Equation 1.11).

Experimental investigations of the influence of the concentration of each of the reactants on the rate of dissolution of calcite showed that the rate of dissolution is proportional to the activity of H^+ below a pH of around 4.5 to 5 (Wentzler, 1971; Berner and Morse, 1974; Plummer *et al.*, 1978; Sjöberg, 1978; cited in Morse, 1983), and is independent of pH above this value (Figure 1.6) (Plummer *et al.*, 1978; Sjöberg, 1978; Busenberg and Plummer, 1986).

Figure 1.6 Log rate of calcite dissolution as a function of pH in acids at 25°C. All data are far from equilibrium and independent of $p(CO_2)$. The slope is -0.95 and rate may be assumed, within the uncertainties of the data, to be first order in all. Above pH 5, the rate is independent of pH (Wollast, 1990). (after Morse, 1983, Figure 2)

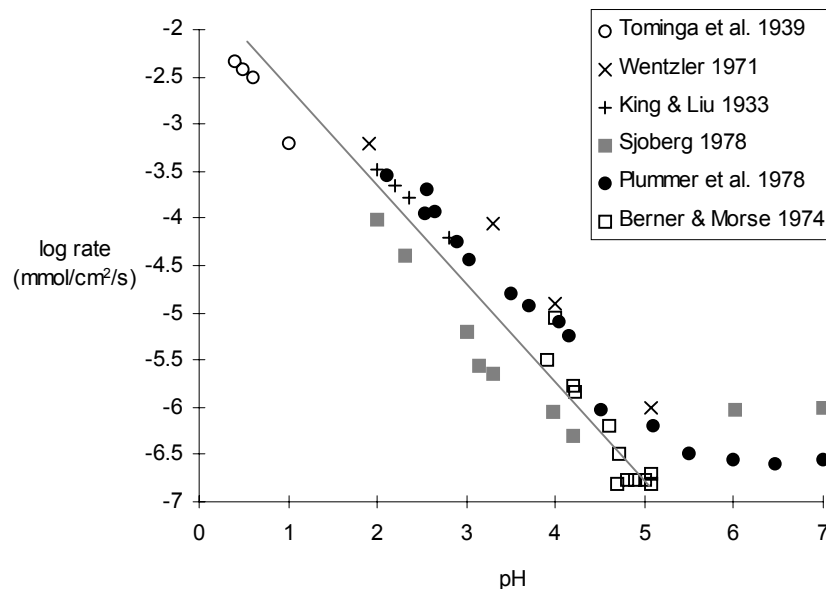


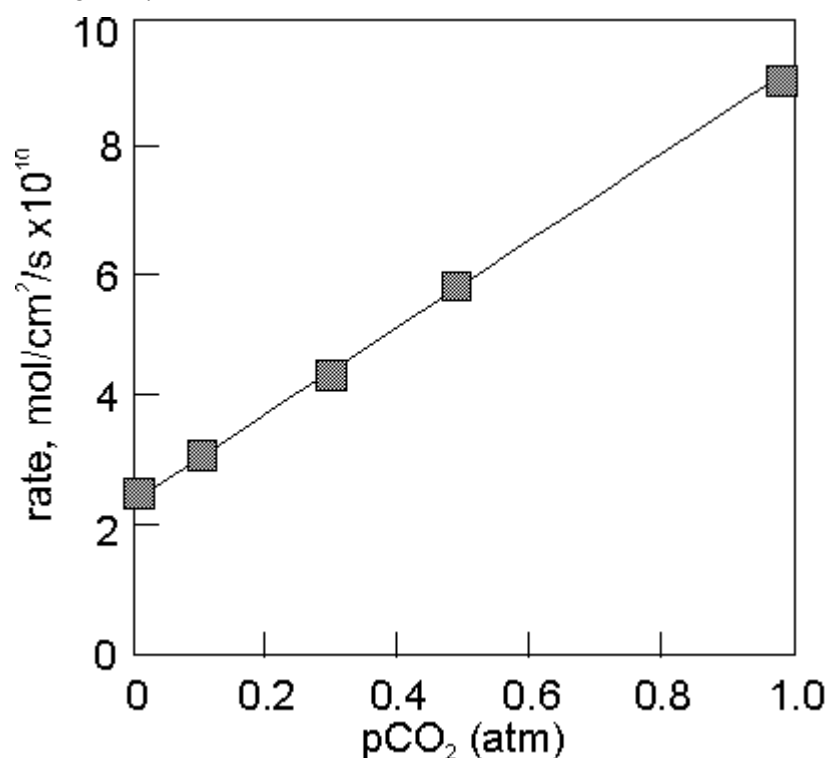
Figure 1.6 shows that under acidic conditions, acid hydrolysis is dominant (Equation 1.1), whereas under alkaline processes, simple hydrolysis is dominant (Equation 1.8).

Studies have also shown that the rate dependence on the concentration of H_2CO_3 is also first-order, corresponding to Equation 1.4 (Figure 1.7) (Busenberg and Plummer, 1986). The overall rate of dissolution shown by these experiments depends, therefore, on the protonation of the surface ($k_1 \cdot a_{\text{H}^+}$), the carbonation of the surface ($k_2 \cdot a_{\text{H}_2\text{CO}_3}$), and the hydration of surface sites of the calcite minerals to form an activated complex that then rapidly decomposes ($k_3 \cdot a_{\text{H}_2\text{O}}$) (Plummer *et al.*, 1978; Busenberg and Plummer, 1986; Chou *et al.*, 1989; Wollast, 1990) (Equation 1.19). All these constants are temperature- and time-dependent, and k_2 is also effectively dependent on pCO_2 (Morse, 1983). r_d is the reaction rate in $\text{mol}/\text{cm}^2/\text{s}$.

Equation 1.19 Overall experimental rate law for dissolution of calcite (the 'Plummer-Wigley-Parkhurst' (PWP) model), where k =individual rate constants, and a =activity (see text) (cf. Wollast, 1990)

$$r_d = k_1 a_{\text{H}^+} + k_2 a_{\text{H}_2\text{CO}_3} + k_3 a_{\text{H}_2\text{O}} - k_4 a_{\text{Ca}^{2+}} a_{\text{CO}_3^{2-}}$$

Figure 1.7 Influence of pCO_2 on the rate of dissolution of calcite at constant pH (5.6-5.7) (Wollast, 1990, Figure 2).



The fourth term of Equation 1.19 (k_4) describes the backward reaction rate, and is also pCO_2 -dependent (Morse, 1983; Chou *et al.*, 1989). Close saturation with respect to calcite, the backward precipitation reaction becomes significant - at equilibrium, this rate must be equal to the dissolution rate (Wollast, 1990). This can explain why the observed rates of reaction are often less than the calculated rate according to the forward rate constant. The backward rate can therefore be estimated by subtracting the observed rate from the calculated rate.

Experiments by Chou *et al.* (1989) showed that this method gives close approximations of the observed backward precipitation rate.

Table 1.2 Experimental determinations of rate constants of dissolution and precipitation of calcite (after Wollast, 1990).

Type of calcite	log k ₁	log k ₂	log k ₃	log k ₄	Reference
Powder	-4.29	-7.47	-9.93	-	Plummer <i>et al.</i> (1978)
Single crystal	-5.06	-7.32	-9.93	-	Busenberg & Plummer (1986)
Powder	-4.05	-	-10.19	-1.73	Chou <i>et al.</i> (1989)

According to Equation 18, k_3 , corresponding to the simple hydration of the calcite surface and the detachment of Ca^{2+} and CO_3^{2-} ions, is the dominant term, except in low pH, high pCO_2 or almost-saturated conditions, where the activities of H^+ , H_2CO_3 and Ca^{2+} and HCO_3^- respectively become more influential (Plummer *et al.*, 1978; Morse, 1983; Wollast, 1990). The glacial environment is not likely to encounter a pH less than 5, except perhaps in isolated extreme cases where water is stagnated in contact with pyrite for long periods of time. In addition, since water is in excess in solution, it can be assumed that its activity is 1. Therefore, a reasonable approximation of the overall dissolution rate in a glacial environment is shown in Equation 1.20.

Equation 1.20 Rate law for calcite dissolution where $\text{pH} \geq 5$, and activity of water $\cong 1$

$$r_d = k_3 - k_4 a_{\text{Ca}^{2+}} a_{\text{HCO}_3^-}$$

Since the rate is time-, surface area- and temperature-dependent, variations in the rate may occur in the glacial hydrological system depending on reactive surface area, and may occur in the laboratory if temperature control is not vigilant. The rate will also be modified by variations in the ionic strength, concentration of dissolved carbonate and proton load in the meltwater reacting with calcite, as these will affect the activities of calcium and bicarbonate ions, which in turn have an effect on the rate of backward reaction. Additionally, components which adsorb on mineral surfaces may severely inhibit reaction (and precipitation) rates (Morse, 1983). For instance, it has been demonstrated that carbonate minerals are strongly influenced by certain dissolved ions, such as magnesium and phosphate, and in solutions with a high $\text{Mg}^{2+}/\text{Ca}^{2+}$ ratios, aragonite may precipitate out of solution in preference to calcite (Morse, 1983).

Recent developments have shown the potential importance of mass transfer as a factor that may slow the rate somewhat. This is of most importance in areas where the reactive surface area/water ratio is very high and CO_2 -demand is therefore at a premium, with dissolution

limited by the rate of CO₂ conversion to H₂CO₃ (hydration) (Dreybodt *et al.*, 1996). The modification is shown in Equation 1.21.

*Equation 1.21 The Buhmann-Dreybodt (B-D) model of Ca²⁺ dissolution rate (Dreybodt *et al.*, 1996), where V is the solution volume, A is the reactive surface area, CO_2 is in moles and R is the dissolution rate of Ca²⁺ from the surface of calcite in moles/cm²/s.*

$$V \frac{d(CO_2)}{dt} = AR$$

These conditions could prevail in parts of the distributed glacial drainage network, such as the VPA, flow through sediment pore spaces and film between glacier ice and bedrock. Variations between calculations of rate by the PWP and B-D models may be of an order of magnitude (Fairchild *et al.*, 1999).

1.4.4 Rates of silicate and aluminosilicate dissolution

Silicates and aluminosilicates generally weather at much lower rates than carbonates (Table 1.3).

Table 1.3 Relative rates of dissolution of different minerals in laboratory experiments at pH 5 far from equilibrium (taken from Drever and Clow, 1995)

Mineral	Subtype	Rate(mineral)/Rate(albite)
Quartz		0.02
Mica	Muscovite	0.22
	Biotite	0.6
K-feldspar	Microcline	0.6
Plagioclase	Albite	1
	Oligoclase	1
	Andesine	7
	Bytownite	15
Orthopyroxene	Enstatite	57
Clinopyroxene	Diopside	85
	Forsterite	250
Olivine		250
Dolomite		360000
Calcite		6000000

The dissolution of many silicate and aluminosilicate minerals is a complicated processes, with the reaction products consisting of both dissolved species and an aluminosilicate residue (Raiswell *et al.*, 1980). The equilibrium in many hydrolysis and acid hydrolysis reactions involving silicate minerals lies towards the reactants. From the reaction for acid hydrolysis of albite (Equation 1.3), the equilibrium product is as shown in Equation 1.22.

Equation 1.22 Equilibrium constant for acid hydrolysis of albite. Pure phases are assumed to have a concentration of one (Raiswell *et al.*, 1980)

$$K_{\text{eq}} = \frac{[\text{Na}^+]^2 [\text{H}_4\text{SiO}_4]^4}{[\text{H}^+]^2} = 10^{-15.9}$$

The low value of the equilibrium constant, which is similar in magnitude to many other aluminosilicates and silicates, shows that equilibrium is quickly reached by small increases in the concentrations of the aqueous products or in pH (Raiswell, 1984). Therefore, the rate and magnitude of reaction of silicates and aluminosilicates is strongly dependent on water flow rate, as the reaction products are removed, and a fresh source of protons is supplied more quickly with faster flow rates (Raiswell *et al.*, 1980).

The mechanism by which aluminosilicate dissolution occurs has been demonstrated to consist of mineral hydrolysis via surface complexes formed by the adsorption and desorption of protons and ligands from solution, with framework bonds being destroyed by the decomposition of the activated surface complexes (Oxburgh *et al.*, 1994). The rate of dissolution of feldspars in the pH range 3-7 may be described as a combination of surface complex reaction and the Arrhenius equation (Equation 1.23). At circumneutral pH, dissolution rate is effectively independent of surface charge (C_H^s), with reaction rates varying according to the anorthite content of the feldspar. This is due to an increase in the density of neutral alumina sites with anorthite content (Oxburgh *et al.*, 1994).

Equation 1.23 Feldspar dissolution rate in the pH range 3-7, where C_H^s is the concentration of protonated surface sites, x_a is the mole fraction of these that are activated, A is the Arrhenius pre-exponential factor, and E_a is the activation energy for the reaction. The reaction order n is dependent on mineral composition, increasing with anorthite content (Oxburgh *et al.*, 1994).

$$R_d = x_a A \exp\left(\frac{E_a}{kT}\right) (C_H^s)^n$$

More simplistically, feldspar dissolution rates increase with decreasing pH below pH 4-5, are independent of pH between pH 4-5 and pH 8, and increase above pH 8 due to the increased solubility of Al^{3+} (Drever and Stillings, 1997). The influence of saturation indices (“chemical affinity”) on dissolution rates is not well defined, with a theoretical influence in rate of feldspar dissolution occurring above -1.43, but reports of reduction occurring at a saturation index of -5 (at 80°C, pH 8.8) (Drever and Clow, 1995). Reductions in dissolution rate have also been attributed to the progressive removal of high-energy lattice defects, and the deposition of secondary material, such as Al- and Fe-oxides, on the mineral surface,

decreasing contact between the mineral and solution - a 'protective' secondary layer (Drever and Clow, 1995).

Laboratory-based studies investigating the alteration of silicate minerals (Busenberg and Clemency, 1976) noted an initial period of nonstoichiometric release of excess calcium, occurring when fresh mineral surfaces contact the solution, but lasting for periods of hours to days (Drever and Hurcomb, 1986). This factor was thought to be a reason for high Ca^{2+} and low silica concentrations in solutions from short-term leaching experiments involving the dissolution of ground-up silicate-dominant rocks from the South Cascade Glacier area (Reynolds Jr. and Johnson, 1972).

1.4.5 Summary

It can be seen that dissolution rates have been established for numerous minerals in a range of conditions, but these conditions are usually at or above room temperature, and often at artificial partial pressures of carbon dioxide and pH ranges outside that of most glacier catchments. Weathering rates of minerals in different lithologies may vary by up to a factor of 20 (Drever and Clow, 1995). It is important that catchment lithology and mineralogy are therefore properly constrained if the processes of chemical weathering beneath a glacier, and their rates, are to be evaluated.

1.5 THE USE OF MINOR AND TRACE ELEMENT ANALYSES AS AN AID TO INVESTIGATIONS OF SOLUTE PROVENANCE

The importance of solute provenance with respect to solute acquisition in glacial environments is now widely recognised (Raiswell, 1984; Tranter *et al.*, 1993; Drever and Clow, 1995; Brown *et al.*, 1996a; Brown *et al.*, 1996b). The review so far has shown how different minerals have distinct dissolution processes, rates, controls and interactions. Therefore, it is essential to be able to isolate the mineral-specific solute acquisition processes, to understand the overall chemical weathering regime in the glacial hydrological system (Sharp, 1995; Brown and Fuge, 1998a; Brown and Fuge, 1998b).

Dissolved solute species may be derived from a number of sources, which may be conveniently divided into atmospheric and lithogenic sources (Brown *et al.*, 1996a). Atmospheric sources include those derived from sea-salt, acid aerosol and dissolution of atmospheric CO_2 , whereas the lithogenic component is derived from the reactive mineralogy of the catchment, dominated by carbonates, sulphides, aluminosilicates and perhaps sulphates

(Reynolds Jr. and Johnson, 1972; Church, 1974; Holland, 1978; Raiswell, 1984; Drever and Hurcomb, 1986; Tranter *et al.*, 1993; Brown *et al.*, 1996a; Tranter *et al.*, 1996).

1.5.1 Overview of major element solute provenance

Major elements and ions in solution are often characterised by having more than one source (Goldschmidt and Muir, 1958). As an example, Ca^{2+} in solution may theoretically have dissolved from carbonate, sulphate, silicate, aluminosilicate, phosphate, borate or oxide minerals (Clark, 1979), each of which has different dissolution characteristics.

Hydrochemical cationic analysis of meltwaters draining the Miller Creek Basin, British Columbia (Zeman and Slaymaker, 1975) suggested that the relative contributions from atmospheric and lithogenic sources could be calculated if the concentrations of the major cations plus chloride and silica are known.

Variations of the ratio between SO_4^{2-} and HCO_3^- in bulk meltwater draining the *Haut Glacier d'Arolla* have been used to infer changes in the importance of different mechanisms of carbonate dissolution over a meltseason (Brown *et al.*, 1996b). A ratio of $\text{HCO}_3^-/(\text{SO}_4^{2-} + \text{HCO}_3^-)$ approaching unity suggests that the dominant reactions are pure hydrolysis and acid hydrolysis utilising protons derived from atmospheric CO_2 (Equation 1.11). A lower ratio, approaching 0.5, may suggest that the coupled reaction of sulphide oxidation and carbonate dissolution is the dominant process of solute acquisition (Equation 1.10) (Brown *et al.*, 1996b). However, observations are dependent on the assumption that there is no significant dissolution of sulphate minerals such as gypsum, and/or contributions of each anion from atmospheric sources, which would affect interpretations of the extent of both sulphide oxidation and carbonate dissolution.

Table 1.4 describes many of the calculations that were carried out in order to infer solute provenance by Brown & others (1996b), using data of major elemental analyses undertaken on samples of bulk meltwater draining *Haut Glacier d'Arolla*. These gave approximations of solute provenance, from which it was inferred that there is an increase in carbonation-driven acid hydrolysis reactions over a meltseason. It was therefore concluded that drainage structure and reactive mineral abundance within the catchment are key controls on the magnitude of chemical weathering in the subglacial environment (Brown *et al.*, 1996b). However, it can be seen that in coming to these conclusions, many assumptions about provenance have been made, which are difficult to test in the field, including:

Table 1.4 Solute provenance calculations based on major ion analysis (after Brown *et al.*, 1996b)

Species	Provenance	Calculation
NO ₃ ⁻	snowpack	100%
Cl ⁻	sea salt	100%
Na ⁺	sea salt	Mean seawater Cl ⁻ :Na ⁺ ratio†
	A-D	$Na^+_{total} - Na^+_{sea-salt}$
K ⁺	sea salt	Mean seawater Cl ⁻ :K ⁺ ratio†
	A-D	$K^+_{total} - K^+_{sea-salt}$
SO ₄ ²⁻	sea salt	Mean seawater Cl ⁻ :SO ₄ ²⁻ ratio†
	snowpack	Ratio of mean Cl ⁻ to SO ₄ ²⁻ concentrations measured in winter snowpack
	S-O	$SO_4^{2-}_{total} - SO_4^{2-}_{sea-salt} - SO_4^{2-}_{snowpack}$
Mg ²⁺	sea salt	Mean seawater Cl ⁻ :Mg ²⁺ ratio†
	S-O/C-D	$2 * SO_4^{2-}_{S-O}$
	carbonate hydrolysis	$Mg^{2+}_{total} - Mg^{2+}_{S-O/C-D}$
HCO ₃ ⁻	A-D	$Na^+_{A-D} + K^+_{A-D}$
	S-O/C-D	$SO_4^{2-}_{S-O}$
	C-D derived from acid aerosol stored in snowpack	$NO_3^- + (2 * SO_4^{2-}_{snowpack})$
	Atmospheric carbonation	$HCO_3^-_{total} - HCO_3^-_{S-O/C-D} - HCO_3^-_{A-D} - HCO_3^-_{A-A/C-D}$
	carbonation derived from other CO ₂ sources	$HCO_3^-_{total} - HCO_3^-_{atmos-carb}$

- *All Cl⁻ is derived from sea salt.* Although chlorine is obviously found predominantly in salts, Cl⁻ is also present in rocks at a crustal average of 314mg/kg (Goldschmidt and Muir, 1958), and so it is possible that significant amounts of Cl⁻ may be derived from lithogenic sources. This has knock-on effects on the calculations of sodium, potassium, calcium, magnesium, bicarbonate and sulphate provenance. Chlorine may also be present in fluid inclusions within glacier ice, and in other areas of long-term storage of meltwater.
- *All Ca²⁺ and Mg²⁺ has a carbonate provenance.* This assumption was made from an observed close relationship between Ca²⁺ and Mg²⁺ in bulk meltwaters (Brown *et al.*, 1996b). However, it is possible that Ca²⁺ may be derived from sulphate minerals (Tranter *et al.*, 1993), which would not be evident in proglacial sediment due to their relatively high solubility (see Table 4). Ca²⁺ may also be derived from aluminosilicate minerals, although studies by Brown (1991) suggest that Ca-bearing aluminosilicate minerals (such as plagioclase) are not abundant in the *Haut Glacier d'Arolla* catchment (Table 1.5). Mg²⁺ has many alternate sources. Table 1.5 shows that Mg-bearing minerals such as biotite, chlorite and amphiboles are present in significant amounts in rock and sediment at *Haut Glacier d'Arolla* (Brown, 1991), and may contribute significant amounts of Mg²⁺ to the solute (Brown and Fuge, 1998a; Brown and Fuge, 1998b). Therefore, the importance

of carbonate dissolution may be exaggerated slightly, and the significance of aluminosilicate and sulphate dissolution negated somewhat.

- *All Na⁺ and K⁺ is derived from aluminosilicate dissolution or sea salt.* It is of note that Na⁺ may be present in carbonate minerals at levels up to 1%, although this is probably mainly a feature of marine carbonates (Veizer, 1983). Turekian & Wedepohl (1961) state that K⁺ has an average level of 2700mg/kg in carbonates, although the level is likely to be much lower in non-marine and vein calcites (Veizer, 1983).

These assumptions are necessary using field data, as it is impossible to physically isolate each chemical weathering process, and unfortunately they can only show trends rather than describe actual rates and rate-limiting species/conditions.

Table 1.5 Mineral composition of fine material from the medial moraines of the Haut Glacier d'Arolla (data from Brown, 1991)

		Range (%)	Mean (%)
Carbonates	Calcite	0.00 - 11.45	2.54
Silicates	Quartz	27.53 - 66.75	53.51
	Sphene	0.00 - 3.04	0.38
Micas	Muscovite	11.39 - 26.51	16.24
	Biotite	0.00 - 10.93	2.68
	Misc. micas	1.69 - 10.53	5.58
Other aluminosilicates	Total feldspars	0.23 - 4.50	1.96
	Total amphiboles	1.00 - 13.76	5.67
	Epidote/Zoisite	0.63 - 8.17	3.38
	Chlorite	1.17 - 9.22	5.37
Other minerals	(non-opaque)	0.00 - 2.95	0.76
	(opaque)	0.82 - 4.96	1.92
Total		99.56 - 100.40	99.99

The mineralogy of rocks from the catchment of *Haut Glacier d'Arolla* is discussed in more detail in Chapter 3.

1.5.2 Overview of minor and trace element solute provenance

A trace element is ostensibly any element that has an average crustal rock abundance of less than 0.01%, or 100mg/kg, with minor elements considered to be those between 1% and 0.01% (Battey, 1981). By this rule, the major elements constitute O, Na, Mg, Al, Si, K, Ca and Fe, and the minor elements constitute H, C, F, P, S, Cl, Ti, V, Cr, Sr, Zr and Ba[‡]. Trace elements occasionally form minerals in which they are a major constituent, but more

[‡] Henceforth in this study, elements are categorised into major cations (Ca²⁺, Mg²⁺, Na⁺, K⁺, Si⁴⁺) and anions (Cl⁻, NO₃⁻, HCO₃⁻, CO₃²⁻, SO₄²⁻) with no distinction made between minor and trace elements (all other analysed elements). These categories are made to aid comparison with previous studies of glacial geochemistry that have made similar distinctions (e.g. Brown and Fuge, 1998a; Brown and Fuge, 1998b; Ruffles, 1999; Seagren, 1999).

frequently a trace element occurs as an “intruder” in the minerals formed by the major elements (Broecker and Oversby, 1971).

Table 1.6 Some common geochemical associations of elements, including Goldschmidt's geochemical classification of the elements (Goldschmidt and Muir, 1958; with specific associations taken from Krauskopf, 1979).

Group	Association
<i>Plutonic rocks</i>	
General association (lithophile elements)	Si-Al-Fe-Mg-Ca-K-Ti-Mn-Zr-Th-U-B-Be-Li-Sr-Ba-V-Cr-Sn-Ga-Ta-W-REE
Specific associations	
Felsic igneous rocks	Si-K-Na
Alkaline igneous rocks	Al-Na-Zr-Ti-REE
Mafic igneous rocks	Fe-Mg-Ti
Ultramafic rocks	Mg-Fe-Cr-Ni-Co
Some pegmatitic differentiates	Li-Be-B
Some contact metamorphic deposits	Mo-W-Sn
Potash feldspars	K-Ba-Pb
Many other potash minerals	K-Na-Rb-Cs-Tl
Ferromagnesian minerals	Fe-Mg-Mn-Cu-Zn-Co-Ni
<i>Sulphide ores</i>	
General associations (chalcophile elements)	S-Cu-Zn-Pb-Fe-Ag-Au-Hg-Cd-In-As-Sb-Bi-Ni-Co-Mo-Pt
Specific associations	
Limestone replacement	Zn-Pb-Ba-Sr
Complex base metal	Fe-Zn-Pb-Ag-Cu-Sb-Bi
Simple precious metal	Ag-Au-As
Complex precious metal	Ag-Au-As-Sb-Zn-Cu-Pb-Hg
Ores associated with mafic igneous rocks	Fe-Ni-Co-Pt
Porphyry copper	Fe-Cu-Mo-Re
Fumarolic deposits	Hg-Sb-As
<i>Sedimentary rocks</i>	
Iron oxides	Fe-As-Co-Ni
Manganese oxides	Mn-As-Ba-Co-Mo-Ni-V-Zn
Phosphorite	(P)-Ag-Mo-Pb-U
Black shales	Al-Ag-As-Au-Bi-Cd-Mo-Ni-Pb-Sb-V-Zn

Table 1.6 shows the affinities of trace elements to major elements and mineral types (Goldschmidt and Muir, 1958; Krauskopf and Bird, 1995; Gill, 1996). This shows simply that some trace elements are favoured in sulphide minerals and some are favoured in other minerals, e.g. carbonates, aluminosilicates, halides, sulphates, oxides etc. This can be particularly useful in iron-rich environments, where iron (III) oxides and ferromagnesian silicates and aluminosilicates may harbour different trace metals to iron (II) sulphides (Krauskopf and Bird, 1995).

Substitution of elements in minerals can occur to some extent at random; by interstitial substitution between planes; substitution into defective parts of the lattice; or by adsorption caused by residual ionic charges (Veizer, 1983). The abundance of major elements in magmatic or sedimentary fluids means that this default substitution can account for

significant quantities of the element in minerals that are not necessarily favourable to incorporation of those elements.

The low abundances of trace elements means that “default” incorporation into minerals is insignificant. Significant substitution for a major element may only occur if the ionic radii do not differ by more than around 15%, and if the ionic charge is either the same or one unit apart. The covalent bonds formed by the trace element must be similar in character for substitution to be extensive (Krauskopf and Bird, 1995). Therefore, it is a feature of some trace elements that they may replace a major element in one mineral, but the substitution is not favoured in another mineral due to a structural difference, despite consisting of the same major cation (Brownlow, 1979). In glacial environments particularly, where the complicating factors of biological activity and pollution are relatively uninfluential, trace elements can be useful indicators of solute provenance due to their association with particular major elements.

Table 1.7 Average abundances of metals and submetals in various rock types and streams, (data extracted from Battey, 1981; Drever, 1982)

mg/kg	Granite	Basalt	Shale	Sandstone	Limestone	Streams (ng/mL)
Na	3.48(ox%)					5150
K	4.11(ox%)					1300
Mg	0.88(ox%)					3350
Ca	1.99(ox%)					13400
Fe	20000	86500	47200	9800	4000	40
Li	30	10	60			
Be	5	0.5	3			
B	15	5	100			
S	270	250	220			2100 (SO ₄)
Sc	10	30	13	1	1	0.004
Ti	m	m		m	400	10
V	50	250	130	20	20	1
Cr	10	170	90	35	11	1
Mn	450	1500	850	50	1100	8
Co	4	48	19	0.3	0.1	0.2
Ni	10	130	68	2	20	2
Cu	20	87	45	2	4	7
Zn	50	105	95	16	20	30
Ga	17	17	19	12	4	0.1
As	2	2	13	1	1	2
Br	4	4	4	1	6	20
Rb	150	130	140	60	3	1
Sr	250	465	300	20	600	60
Y	40	25	35	10	4	0.07
REE	0.5-70	1.0-80	1.0-80	0.05-15	0.05-8	0.001-0.1
Zr	150	140	160	220	20	0
Mo	1	1.5	2.6	0.2	0.4	0.5
Ag	0.04	0.1	0.07	0	0	0.3
Cd	0.13	0.2	0.3	0	0.03	0
Sb	0.2	0.1	1	0.4	0.3	1
I	0.5	0.5	2	1	1	7
Cs	3	1	6	6	6	0.03
Ba	600	330	580	0	10	50
W	1.7	0.7	1.8	1.6	0.6	0.03
Au	0.002	0.002	0.005	0.006	0.006	0.002
Hg	0.03	0.01	0.4	0.03	0.04	0.07
Tl	1.5	0.2	1.4	0.8	0	0
Pb	17	6	20	7	9	1
Th	14	2.7	12	5.5	2	0.1
U	3	1	4	2	2	0.1

It is the variations in these associations across different mineral and geochemical phases that can make trace elements useful as indicators of element provenance (Brown and Fuge, 1998b). Table 1.7 shows the variations in abundance of elements across the spectrum of igneous and sedimentary rocks.

The extent of dissolution of trace elements during chemical weathering depends on numerous factors and is regulated by various processes.

a) Lithogenic Provenance

Table 1.8 shows common trace element associations with major rock-forming minerals.

Table 1.8 "Selected elements found in small amounts in common rock-forming minerals of igneous rocks, and relative stability of the minerals. The groupings are generalizations; for example, only the allanite variety of epidote contains abundant REE, and only some varieties of muscovite will have Rb and Li in the quantities indicated". Original source of table unknown, taken from Leeds University Department of Earth Sciences handout (1993).

Stability	Mineral	X %	0.X %	0.0X %	0.00X% and less
Easily weathered	olivine amphibole pyroxene biotite plagioclase	Ti F K	Ni Mn	Ca Al Cr Ti P Co	Zn V Cu Sc
			Ti K Mn Cl Rb	Zn Cr V Sr Ni	Ba Cu P Co Ga Pb Li B
			Ti Na Mn K	Cr V Ni Cl Sr	P Cu Co Zn Li Rb Ba
			Ca Na Ba Mn Rb	Cl Zn V Cr Li Ni	Cu Sn Sr Co P Pb Ga
Moderately stable	epidote sphene apatite garnet K-feldspar muscovite	REE Mn Cr Na	Sr	Ba Rb Ti Mn	P Ga V Zn Ni Pb Cu Li
			Mn Ti	Th Sn	V Nb Zn Be U
			REE Nb Sn Sr	Mn Ta V Cr	Ba
			Sr REE Mn	U Pb	As Cr V
			Ti REE	Ga	
			Ca Ba Sr	Rb Ti	Pb Ga V Zn Ni Cu Li
Stable	tourmaline magnetite zircon quartz	Ti Al Cr Hf	Ti Na Fe Ba Rb Li	Cr Mn V Cs Ga	Zn Sn Cu B Nb
			Ti Li Mn	Cr Ga Sn Cu V	Rb
			Mn V	Zn Cu Sn Ni	Co Pb Mo
			REE Th	Ti Mn P	Be U Sn Nb
					Fe Mg Al Ti Na B Ga Ge Mn Zn

The trace metal content of the mineral in which the element occurs has a primary control on the amount that may be released into solution, and the mineral type may determine the intensity of chemical weathering, depending on the stability of the mineral in the given environment and the reactivity of surface sites. Many trace elements do not substitute readily into the structure of feldspars or ferromagnesian minerals, and during rock-forming processes may be concentrated in, for example, chemically resistant accessory minerals such as zircon, apatite or sphene, or as sulphides, which weather rapidly in oxygenated water. The resistant minerals generally remain unaltered unless weathering is very intense, and so their alteration never causes high trace element concentrations in waters; intense weathering is usually associated with large amounts of water, so dilution prevents high concentrations (Drever, 1982). Many of the occurrences of higher concentrations of trace elements are in sulphides, for example copper, zinc, molybdenum, silver, lead etc. Since sulphides weather rapidly, sulphide deposits can lead to locally high concentrations of dissolved trace metals (Drever,

1982). The Fournet/Schütz series describes the affinity for sulphur of sulphide-forming metals (highest - lowest affinity): Mn>Cu>Ni>Co>Fe>Sn>Zn>Pb>Sb>Ag (Rankama and Sahama, 1950).

b) Mobility of the trace element

Elements that are strongly partitioned into seawater, such as Na, Mg, Ca, U and Rb, are readily mobilised by weathering processes. These are of limited use in discerning provenance of particulates and sedimentary rocks. Elements with very low solubilities in natural waters, such as Ti, Sc, Th and REE, are likely to be transferred dominantly into terrigenous sediments (restites), and therefore display a more accurate record of provenance (McLennan, 1989). The aqueous geochemistry of the low solubility elements is, however, not well suited for provenance determinations (McLennan, 1989). Table 1.9 shows the range of mobilities of selected elements, characterised by the ratio of concentrations in seawater to concentrations in the upper continental crust.

Table 1.9 Relative mobilities of the elements in the secondary environment Original source of table unknown, taken from Leeds University Department of Earth Sciences handout (1993)

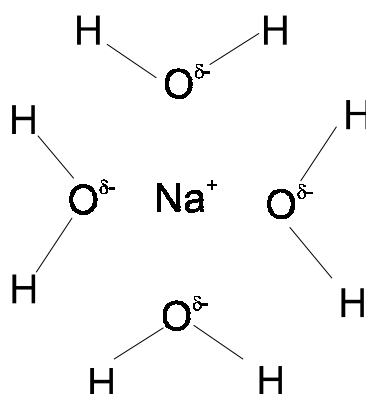
Relative mobilities	Environmental Conditions			
	Oxidizing	Acid	Neutral to alkaline	Reducing
Very high	Cl I Br S B	Cl I Br S B	Cl I Br S B Mn V U Re	Cl I Br
High	Mn V U Re Ca Na Mg Sr Zn	Mn V U Re Ca Na Mg Sr Zn Cu Co Ni Hg Ag Au	Ca Na Mg Sr	Ca Na Mg Sr
Medium	Cu Co Ni Hg Ag Au As Cd	As Cd	As Cd	
Low	Si P K Pb Li Rb Ba Be Bi Sb Ga Cs Tl	Si P K Pb Li Rb Ba Be Bi Sb Ga Cs Tl Fe Mn	Si P K Pb Li Rb Ba Be Bi Sb Ga Cs Tl Fe Mn	Si P K Fe Mn
Very low to immobile	Al Ti Sn Te W Sb Pt Cr Zr Th REE Fe Mn	Al Ti Sn Te W Sb Pt Cr Zr Th REE	Al Ti Sn Te W Sb Pt Cr Zr Th REE Zn Cu Co Ni Hg Ag Au	Al Ti Sn Te W Sb Pt Cr Zr Th REE S B Mn V U Re Zn Cu Co Ni Hg Ag Au As Cd Pb Li Rb Ba Be Bi Sb Ga Cs Tl

c) Speciation, ion pairing and complexation

The chemical form in which the element is present in solution may affect their behaviour. Ions are never actually “free” in solution, despite the often-used terminology “free ions”. Species exist in water in *solvated* form, where water molecules form ion-dipole bonds with a

dissolved metal ion (or molecule), as shown in the example of sodium in Figure 1.8. The energy (and therefore strength) of the ion-dipole bonds is higher with higher charge and lower ionic radius (Stumm and Morgan, 1996). The strength of these bonds affects the ability of an ion to stay in solution or be sorbed or precipitated.

Figure 1.8 Hydrated sodium ion in aqueous solution (cf. Stumm and Morgan, 1996, Figure 1.6).



Ions and molecules of opposite charge in solution may also become bonded. Ion pair (ionic bonding) and complex (covalent bonding) formation can be very important with some species, for example Al^{III} as $\text{Al}(\text{OH})_2^+$ and $\text{Al}(\text{OH})_4^-$ (Drever, 1982), U^{VI} as $\text{UO}_2(\text{CO}_3)_3^{4-}$ in $\text{pH} > 8$, oxidising conditions (Langmuir, 1978). Obviously, solutions with higher ionic strength have greater ability to host complexes due to the higher numbers of charged species. The Garrels-Thompson Model of Seawater Chemistry (Garrels and Christ, 1965) shows that in seawater, 91% of CO_3^{2-} , 31% of HCO_3^- and 46% of SO_4^{2-} is bound in complexes, dominantly with highly mobile elements such as Mg^{2+} and Na^+ (see below). These complexes are somewhat less prevalent in low ionic strength (fresh) waters, however. Anomalously high concentrations of trace elements in solution may often be related to the presence of stable complexes (Hering and Morel, 1990). However, a significant amount of metal complexation can be attributed to metal interactions with organic (humic) substances. Cu^{II} is almost completely complexed with humic substances in surface waters, Zn may be 42-95% organically complexed, and Al 39-42% complexed. In contrast, Mn^{II} and Cd show negligible organic complexation (Hering and Morel, 1990). No attempt is made to deal with organic complexes in this study. A summary of the extent of inorganic complexation in selected major and trace elements is given in Table 1.10 (Stumm and Morgan, 1996).

Table 1.10 Major inorganic species in freshwaters (adapted from Stumm and Morgan, 1996, Table 6.5), showing ionic radii, co-ordination numbers and electronegativity (Battey, 1981)

Element	Ionic radius (nm)	Co-ordination no.	Electro-negativity	Major Species	Freshwater $[M^+]/M_t$
Hydrolysed, anionic					
B ^{III}	0.023	3/4	2.0	H ₃ BO ₃ , B(OH) ₄ ⁻	
V ^V	0.059	6	1.6	HVO ₄ ²⁻ , H ₂ VO ₄	
Cr ^{VI}	0.052	6	1.6	CrO ₄ ²⁻	
As ^V	0.058	6	2.0	HAsO ₄ ²⁻	
Mo ^{VI}	0.062	6	1.8	MoO ₄ ²⁻	
Si ^{IV}	0.042	4/6	1.8	H ₄ SiO ₄	
Predominantly free aquo-ions					
Li	0.068	6	1.0	Li ⁺	1.00
Na	0.097	6/8	0.9	Na ⁺	1.00
Mg	0.066	6	1.2	Mg ²⁺	0.94
K	0.133	8/12	0.8	K ⁺	1.00
Ca	0.099	6/8	1.0	Ca ²⁺	0.94
Sr	0.112	8	1.0	Sr ²⁺	0.94
Cs	0.167	12	0.7	Cs ⁺	1.00
Ba	0.134	8/12	0.9	Ba ²⁺	0.95
Complexation with OH⁻ / CO₃²⁻ / HCO₃⁻ / Cl⁻					
Be ^{III}	0.035	4	1.5	BeOH ⁺ , Be(OH) ₂ ^o	1.5×10 ⁻³
Al ^{III}	0.051	4/6	1.5	Al(OH) ₃ (s), Al(OH) ₂ ⁺ , Al(OH) ₄ ⁻	1×10 ⁻⁹
Ti ^{IV}	0.068	6	1.5	TiO ₂ (s), Ti(OH) ₄ ^o	
Mn ^{IV}	0.060	6	1.5	MnO ₂ (s)	
Fe ^{III}	0.064	6	1.8	Fe(OH) ₃ (s), Fe(OH) ₂ ⁺ , Fe(OH) ₄ ⁻	2×10 ⁻¹¹
Co ^{II}	0.072	6	1.8	Co ²⁺ , CoCO ₃ ^o	0.5
Ni ^{II}	0.069	6	1.8	Ni ²⁺ , NiCO ₃ ^o	0.4
Cu ^{II}	0.072	6	1.9	CuCO ₃ ^o , Cu(OH) ₂ ^o	0.01
Zn ^{II}	0.074	6	1.6	Zn ²⁺ , ZnCO ₃ ^o	0.4
Ag ^I	0.089	6	1.9	Ag ⁺ , AgCl ^o	0.6
Cd ^{II}	0.097	6	1.7	Cd ²⁺ , CdCO ₃ ^o	0.5
REE ^{III}	0.114-0.085	6/8?	1.2	REECO ₃ ⁺ , REE(CO ₃) ₂ ⁻	8×10 ⁻³
Hg ^{II}	0.110	6/8?	1.9	Hg(OH) ₂ ^o	1×10 ⁻¹⁰
Tl ^I / Tl ^{III}	0.147 / 0.095	12/8?	1.8	Tl ⁺ , Tl(OH) ₃ , Tl(OH) ₄ ⁻	2×10 ⁻²¹ (Tl ^{III})
Pb ^{II}	0.120	8	1.8	PbCO ₃ ^o	0.05
Bi ^{III}	0.096	6	1.9	Bi(OH) ₃ ^o	7×10 ⁻¹⁶
Th ^{IV}	0.102	8	1.3	Th(OH) ₄ ^o	
U ^{VI}	0.080	6	1.7	UO ₂ (CO ₃) ₂ ²⁻ , UO ₂ (CO ₃) ₃ ⁴⁻	1×10 ⁻⁷ (UO ₂ ²⁺)

d) Oxidation state

The oxidation state of a fluid affects the speciation and therefore solubility of species, e.g. U solubility is strongly affected by oxidation state (soluble under oxidising conditions, insoluble at nonextreme pH & reducing conditions).

e) Equilibrium

Equilibrium with respect to a solid phase containing the element as a major component affects trace metal dissolution. For instance, dissolved aluminium concentration in rivers corresponds well to equilibrium with kaolinite, and dissolved Fe corresponds to equilibrium with amorphous Fe(OH)₃. The solubility of phases containing the element as a major

constituent (commonly an oxide/hydroxide, carbonate, or sulphide) provides upper limits to the activities and concentrations of specific elements (Drever, 1982).

f) Sorption

The concentrations of trace elements in natural waters are often much lower than would be expected on the basis of either equilibrium solubility calculations or of supply to the water from various sources. These discrepancies are commonly caused by adsorption of the element on to a solid phase, or coprecipitation with a newly-forming precipitate. The two processes are sometimes grouped together and termed sorption (Drever, 1982). Mixing a dilute solution containing trace metals with solid phases usually results in a decrease in concentration of the metals due to sorption or cation exchange (see below) (Leckie and James, 1974). Adsorption occurs by exchange with surface-associated metal cations, and is a relatively rapid process, taking seconds to hours (Zachara *et al.*, 1993).

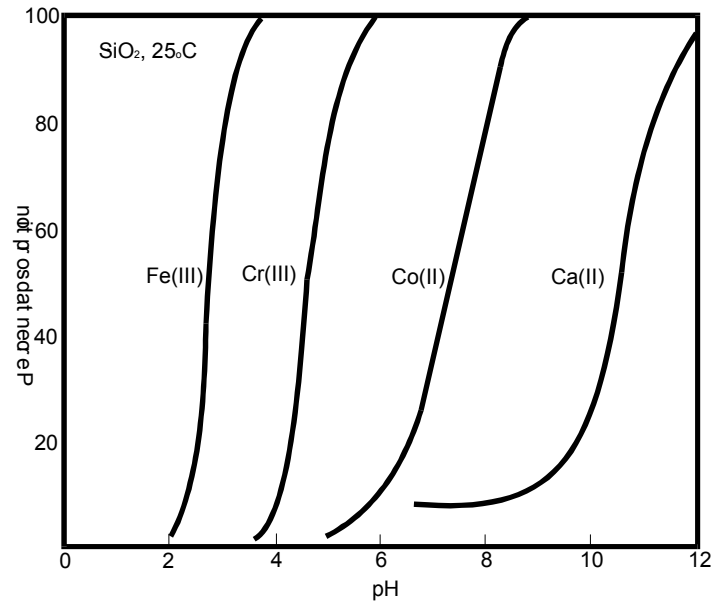
Iron and manganese oxides are the most important sorbates in nature (Drever, 1982). However, CaCO₃ may dominate as a sorbent over oxides and silicates in calcareous, high pH waters, depending on the mutual number of surface sites (Zachara *et al.*, 1993). Generally, elements present in solution as cationic species are more likely to be adsorbed than those present as anionic species (except phosphate anions). Co, Ni, Cu, Zn, Pb, Ag and Cd are strongly adsorbed by iron and manganese oxides, and Cd, Zn, Mn, Co and Ni may be strongly adsorbed (15-100%) onto calcite, with Ba and Sr often 3-10% adsorbed.

The adsorption behaviour of hydrolyzable metal ions at the solid-water interface is strongly pH dependent. At low pH there is essentially no sorption, and at high pH all cations are strongly sorbed. Over a narrow range of pH, which is different for individual ions, but often less than 1 unit, there is a transition from the former to the latter (Leckie and James, 1974). Examples are shown in Figure 1.9.

g) Cation exchange

Cation exchange reactions involving clay minerals can also maintain the concentrations of trace elements at low levels. This can become a significant factor in some cases, because the exchanger can be highly selective for a particular ion, so that it is removed from solution even when it is present in very low concentrations. However, in oxidising environments, adsorption by iron and manganese oxides appears to be generally much more important (Drever, 1982).

Figure 1.9 Computed curves for adsorption of selected metals on SiO₂ (after Drever, 1982)



1.5.3 Rock and aqueous geochemistry of specific major, minor and trace elements

Section 1.5.2 shows that during interpretation of data of trace element concentrations in natural waters, not only does the solid-phase trace element content of rocks in contact with the waters need to be determined, but also a knowledge of the mineralogy of the rocks and the behaviour of the elements in response to weathering and dissolution. The geochemistry of elements in rocks is well known, but the dissolution characteristics are often less definitely defined.

This section describes the geochemistry of the elements in terms of mutual affinities, common host minerals and weathering characteristics. The chemical formulas of minerals mentioned in this section are listed in Table 1.9.

Table 1.11 Chemical formulas and occurrences of minerals referred to in Section 1.6, with listing of some commonly substituting trace elements (after Battey, 1981).

Type	Mineral	variations	chemical formula	occurrence	common substitutions	abbrev ^o .
FRAMEWORK SILICATES	Quartz		SiO ₂	i,a,s,cm,rm	Ge	-
	Feldspars	Microcline	K{AlSi ₃ O ₈ }	a,a-p	Tl,Rb,Cs,Sr,CEE,Pb	kf
		Orthoclase	(K,Na){AlSi ₃ O ₈ }	a,cm,rm	Tl,Rb,Cs,Sr,Ba,CEE,Pb	kf
		Adularia	K{AlSi ₃ O ₈ }	i-h,a-h	Tl,Rb,Cs,Pb	kf
		Albite	Na{Al ₂ Si ₂ O ₈ }	a-p,a-h,rm		nf
		Plagioclase	(Na,Ca){Al ₂ Si ₂ O ₈ }	ub,b,i,a,rm	Tl,Sr,Eu	cf
		Anorthite	Ca{Al ₂ Si ₂ O ₈ }	cm	Sr,Eu	cf
	Feldspathoids	Leucite	K{AlSi ₂ O ₆ }	a		le
		Nepheline	Na{AlSiO ₄ }	a	Be	ne
	CHAIN SILICATES	Amphibole	Tremolite-Actinolite	Ca ₂ (Mg,Fe ²⁺) ₅ {Si ₈ O ₂₂ }(OH,F) ₂	rm	
Hornblende			(Na,K) ₀₋₁ Ca ₂ (Mg,Fe ²⁺ ,Al,Fe ³⁺ ,Mn,Ti) ₅ {(Al,Si) ₈ O ₂₂ }(O,OH,F) ₂	i,a,rm	B,Sc,V,Cr,Mn,YEE,Zr	am
Clinopyroxene		Diopside-Augite-Hedenbergite	Ca(Mg,Fe ²⁺) ₂ AlFe ³⁺ Ti{(Si,Al) ₂ O ₆ }	ub,b,i,cm,rm	Li,Sc,Ti,V,Cr,Mn,Cu,YEE,Zr	px
		Aegerine	NaFe ³⁺ {Si ₂ O ₆ }	i,a	Zr	px
Orthopyroxene		Enstatite-Hypersthene-Ferrosilite	(Mg,Fe){SiO ₃ }	ub,b,i,cm,rm	Li,Sc,Ti,Ni,YEE,Zr	px
ISLAND SILICATES	Olivine	Forsterite	Mg ₂ {SiO ₄ } (Mg end-member)	ub,b,rm		ol
		Fayalite	Fe ₂ {SiO ₄ } (Fe end-member)	i,a	Co,Ni	ol
		Monticellite	CaMg{SiO ₄ }	cm		ol
		Sphene	CaTi{SiO ₄ }(O,OH,Cl,F)	a,pl	REE,Zr,Sn	sp
	Zircon	Zr{SiO ₄ }	a,pl	U,Th,REE	zr	
	Topaz	Al ₂ {SiO ₄ }(OH,F) ₂	a-p	Ge	-	
	Garnet	(Mg,Fe ²⁺ ,Mn ²⁺ ,Ca) ₃ (Al,Cr,Fe ³⁺) ₂ {SiO ₄ } ₃	i-h,a-h,rm	Ti,Ge,YEE	gt	
	RING SILICATES	Tourmaline	(Na,Ca)(Li,Mg,Al) ₃ (Al,Fe,Mn) ₆ (OH) ₄ (BO ₃) ₃ {Si ₆ O ₁₈ }	a-p	Cu,Ga,Tl	to
Cordierite		Al ₃ (Mg,Fe ²⁺) ₂ {Si ₅ AlO ₁₈ }	cm		cd	
Beryl		Be ₃ Al ₂ {Si ₆ O ₁₈ }	a-p	Li	-	
COUPLET SILICATES	Epidote	Ca ₂ (Al,Fe ³⁺)Al ₂ {SiO ₄ }{Si ₂ O ₇ }O(OH)	b-h,rm	Sr,CEE,Pb	ep	
	Zoisite	Ca ₂ AlAl ₂ {SiO ₄ }{Si ₂ O ₇ }O(OH)	rm	Sr,CEE	ep	
	Thalenite	Y ₂ {Si ₂ O ₇ }	a-p		-	
	Bazzite	unknown - Sc-silicate with REE, Na, Fe			-	
LAYER SILICATES	Mica	Muscovite	KAl ₂ {AlSi ₃ O ₁₀ }(OH) ₂	a,a-p,rm	Li,Mn,Ga,Tl,Rb,Cs,Ba	mu
		Biotite	K(Mg,Fe) ₃ {AlSi ₃ O ₁₀ }(OH,F) ₂	a,a-p,cm,rm	Li,B,Sc,Ti,V,Cr,Mn,Zn,Rb,Cs,Ba,Zr,Sn,Pb	bi
		Lepidolite	K(Li,Al) ₃ {AlSi ₃ O ₁₀ }(OH,F) ₂	a-p		lp
	Chlorite group	(Fe,Mg,Al) ₂₋₃ (OH) ₆ / (Mg,Fe,Al) ₂ {(Al,Si) ₄ O ₁₀ }(OH) ₂	i-h,a-h,s,rm	Ni,Ga	cl	
	Talc	Mg ₃ {Si ₄ O ₁₀ }(OH) ₂	ub-h		tc	
	Serpentine	Mg ₆ {Si ₄ O ₁₀ }(OH) ₂	rm		-	
	Clay minerals	Montmorillonite	0.33M ⁺ (Al,Mg) ₂ {Si ₄ O ₁₀ }(OH) ₂ .nH ₂ O	s	Be,Rb,Cs,Ba,Sn	-
		Illite	(K,H ₃ O)Al ₂ {(Al,Si) ₄ O ₁₀ }(OH) ₂	s	Ti,V,Cr,Rb,Cs,Ba,Sn	-
		Glauconite	(K,H ₃ O) ₂₋₃ (Mg,Fe ²⁺ ,Ca) ₁₋₃ (Al,Fe ³⁺) ₂ {Al ₂₋₃ Si ₁₃₋₁₄ O ₄₀ }(OH) ₈ }	s		-
Greenalite		Fe ⁹⁻²⁺ Fe ³⁺ {Si ₄ O ₁₁ }(OH) ₆ }.2H ₂ O	s		-	

Abbreviations: see next page

Table 1.11 (continued)

Type	Mineral	chemical formula	occurrence	common substitutions	abbrev ^o .
OXIDES	Haematite	Fe ₂ O ₃	s,rm		hm
	Magnetite	Fe ₂ O ₃ .FeO	ub,b,i,a,a-p,s,pl	Zn,Mn,Ni,V,Cr,Zn,Ga	mt
	Ilmenite	FeTiO ₃	b,pl	Mg,Mn,V,Zn	il
	Perovskite	CaTiO ₃	b-m,i-m	Ce,Y,La	-
	Rutile	TiO ₂	a-h,pl		-
	Chromite	FeCr ₂ O ₄	ub-m	Mg,Ga,Ag,Au	cr
	Cassiterite	SnO ₂	a-h,pl	Sc,In,W,Ag,U	cs
	Pitchblende	UO ₂	a-p	Th,REE,Y,Pb	-
PHOSPHATES	Apatite	Ca ₅ (PO ₄) ₃ (F,Cl,OH)	b,i,a,a-p	As,Bi,Sr,CEE,Pb	ap
	Monazite	CePO ₄	a-p	CEE	mo
	Xenotime	YPO ₄		YEE	xe
CARBONATES	Calcite	CaCO ₃ (trigonal)	b-h,i-h,a-h,s,cm	Mn,Fe,Zn,Sr,Eu,REE,Pb	ca
	Magnesian calcite	Ca _{0.8-1} Mg _{0-0.2} CO ₃ (trigonal)	s	REE	ca
	Dolomite	CaMg(CO ₃) ₂ (trigonal)	i-h,a-h,s	Fe,REE	do
	Magnesite	MgCO ₃ (trigonal)	ub-h,s		mg
	Siderite	FeCO ₃ (trigonal)	s	In	si
	Aragonite	CaCO ₃ (orthorhombic)	2,s	Ba,Sr,Pb,REE	ar
	Witherite	BaCO ₃ (orthorhombic)	2		-
	Strontianite	SrCO ₃ (orthorhombic)	2		-
	Cerussite	PbCO ₃ (orthorhombic)	2		ce
SULPHIDES	Pyrrhotite	Fe _{1-x} S (end member = <i>troilite</i>)	ub-m	Se,Zr,Se	pp
	Pentlandite	(Fe,Ni) ₉ S ₈	ub-m	Se	pp
	Pyrite	FeS ₂	ub-h,i-h,a-h,2,s	Co,Ni,Cd,As,Re,Se	py
	Arsenopyrite	FeAsS	i-h,a-h,s	Co,Sb	as
	Chalcopyrite	CuFeS ₂	i-h,a-h,s	Cd,Sn	cc
	Galena	PbS	i-h,a-h,s	Se,Te,Cd,Tl,Sb,Bi,Ag,Sn	ga
	Sphalerite	ZnS	a-h,s	Cd,Co,Ga,Ge,Sn	sr
	Bornite	Cu ₅ FeS ₄	2		-
	Cubanite	CuFe ₂ S ₈			-
Molybdenite	MoS ₂	a-h	W,Re,Ag,Au	mb	
SULPHATES	Gypsum	CaSO ₄ .2H ₂ O	s		gy
	Anhydrite	CaSO ₄	s		-
	Barite	BaSO ₄	i-h,a-h,s		br
FLUORIDES	Fluorite	CaF ₂	i-h,a-p,a-h	Sc,Sr,YEE,U	-
TUNGSTATES	Wolframite	(Fe,Mn)WO ₄	a-h	Mo,Sn	wf

Abbreviations: ub: ultrabasic; b: basic; i: intermediate; a: acid/alkaline; minerals without flags are rock forming minerals and as such are likely in magmatic, pegmatitic and hydrothermal form. Flags: -m: magmatic ore mineral; -p: pegmatitic ore mineral; -h: hydrothermal ore mineral. 2: secondary mineral; s: sedimentary mineral; cm: associated with contact metamorphism; rm: associated with regional metamorphism; pl: resistant mineral commonly found as a placer deposit. For explanations of the abbreviations REE, YEE and CEE, see Section 1.7.2.18.

1.5.3.1 Alkali metals

Lithium, sodium, potassium, rubidium and caesium, the Alkali Metals, form a chemically coherent group. They are strongly ionic, univalent, and form pronounced basic hydroxides (Volborth, 1969).

a) Rock & mineral affinities

The average Na/K ratio in igneous rocks is 1.09:1, although this is dependent on the rock type (Table 1.12). This is due to the larger ionic radius of K^+ and lower electronegativity, which makes potassium characteristic of late crystallates due to its readiness to become enriched in residual melts and solutions during magmatic differentiation.

Table 1.12 Na/K ratios in igneous rock types.

Material	Na:K
Gabbros:	2.55:1
Diorites:	1.43:1
Granodiorites:	1.20:1
Granites:	0.76:1

The bulk of Na and K in igneous rocks are found in *feldspars* (Rankama and Sahama, 1950). Although alkali feldspars as a whole show affinity for later crystallates, *K-feldspars* are later than *Na-feldspars*, hence the ratio progression. Sodium is more prevalent in alkali *amphiboles* and *pyroxenes* because of its smaller ionic radius with respect to potassium. This additional differentiation accentuates the ratio variation in igneous rock types. Na & K are also found in *micas*, with average (Na_2O+K_2O) contents of 11.79% in *muscovite* and 9.14% in *biotite*. Potassium is much more common in these than Na, and micas are also chiefly formed during the latter stages of crystallization (Rankama and Sahama, 1950).

Lithium is very reluctant to enter the structure of feldspars, despite being an alkali metal. Lithium generally appears in place of Al and Fe, or sometimes K and Mg, and occasionally Be, Ca, and Na and may be present in *muscovite* and *biotite* at levels up to 0.9% (Vlasov, 1966).

Rubidium and Caesium generally coexist with K in alkali feldspars and micas; there are no common independent Rb-bearing minerals, and Cs-minerals are also rare (Ahrens, 1964). Rubidium occurs at a K/Rb ratio of 84:1 on average in igneous rocks, and Cs at a K/Cs ratio of 3700:1 (Rankama and Sahama, 1950). The Rb content increases in later-developing minerals (especially pegmatites) (Krauskopf, 1979), as the ionic radii of Rb and Cs are even larger than that of K (Rankama and Sahama, 1950). Rb is not common in hydrothermal minerals, even if muscovite and/or microcline are present (Rankama and Sahama, 1950).

b) Dissolution and precipitation characteristics

During weathering, alkali feldspars and the feldspathoids *leucite* (K) and *nepheline* (Na) may be completely dissolved, with Na^+ & K^+ staying in solution whilst Al and SiO_2 react to form clay minerals. Some K may remain in the clay minerals formed by the weathering of mica (such as *illite*) (Rankama and Sahama, 1950). Potassium is also more prone to readsorption by clay minerals than Na, with the result that Na becomes more dominant as a dissolved species than it is in the rocks, and K is more dominant in pelitic sediments (Rankama and Sahama, 1950). Potassium may be present in carbonates up to 0.3% (Turekian and Wedepohl, 1961).

Table 1.13 Na/K ratios in waters and sediment

Material	$\text{Na}^+:\text{K}^+$
Dissolved solids in lake and river waters:	2.73:1
Dissolved solids in sea waters:	27.8:1
Pelitic sediments (shales)	0.36:1

Due to the even smaller ionic potential of Rb and Cs in comparison to K, weathering results in concentrations of Rb & Cs into clay minerals such as *illite* & *montmorillonite*. However, the K/Rb and K/Cs ratios in pelitic rocks (83:1 and 2000:1 respectively) are similar to those of the average igneous rocks, despite the seawater ratios being considerably enhanced (approximately 2000:1 and 200000:1 respectively) (Rankama and Sahama, 1950).

1.5.3.2 *Alkaline Earth Metals*

Beryllium, magnesium, calcium, strontium and barium form the Alkaline Earth Metals.

a) Rock & mineral affinities

Calcium is the most abundant of the alkaline earths, and in igneous rocks is mainly found in the following silicate minerals: *orthopyroxenes* (*diopside-hedenbergite* series), *clinopyroxenes* (*augite* series), *hornblende*, *actinolite*, *epidote/zoisite* and *plagioclase feldspars* (*anorthite*) (Rankama and Sahama, 1950). Calcium can exist in both the ferromagnesian and alkaline components of igneous rocks. The Ca content of pyroxenes and amphiboles may account for approximately one half of the total amount found in igneous rocks. Ca is, however, not common in micas (Rankama and Sahama, 1950). Calcium is also common in carbonate, sulphate, fluorite, phosphate and oxide minerals such as *calcite*, *aragonite*, *dolomite*, *gypsum*, *anhydrite*, *fluorite*, *apatite* and *perovskite*, with Ca uranites, arsenates, vanadates, molybdates and tungstates also encountered. These may be of igneous, hydrothermal, metamorphic or sedimentary origin (Battey, 1981).

The average content of magnesium in igneous rocks is around 2%. It is mostly confined to silicates, and is almost exclusively combined with oxygen. It is present in *olivines*, *garnets*, *cordierite*, *pyroxenes*, *amphiboles*, *micas*, *chlorites*, *talc* and magnesian clay minerals. Magnesium is almost totally confined to the early-crystallizing melanocratic constituents of igneous rocks (e.g. gabbros), earlier than Ca and alkali metals, and is almost always accompanied by Fe^{2+} , except in *cordierite*. The ionic radius of magnesium is, however, more structurally favourable than iron in most major rock-forming minerals, with the result that Mg is enriched in the mineral structures, whereas iron is enriched in the magmatic residue and later forming minerals with lower melting temperatures. Igneous metal oxide minerals are largely devoid of magnesium (Rankama and Sahama, 1950).

Strontium and barium are among the most abundant trace elements in nature, but rarely form independent minerals. Strontium is generally dispersed in calcium and potassium minerals (Rankama and Sahama, 1950). It is thought that 50-60% of Sr present in igneous rocks is confined to plagioclases, and 30-40% confined to *K-feldspars* (e.g. microcline), at levels of 0.1-1% (Rankama and Sahama, 1950; Vlasov, 1966). However, of the common silicate minerals, only *epidote* and *zoisite* have high levels of Sr (2.0, 2.5% resp.). Strontium in *Ca-plagioclases* is generally at <0.1-0.4%, and is generally low in *Ca-pyroxenes* and *amphiboles*, because at the earlier stages of crystallization, the Sr concentration is relatively low.

Barium does not replace Ca as readily as Sr due to the larger difference in ionic radii with respect to Ca (Ba 0.134nm, Sr 0.112nm, Ca 0.099nm). Whilst both Sr and Ba have an association with early crystallising K minerals such as *K-feldspars*, Ba is not common in *Ca-plagioclases* (Volborth, 1969; Krauskopf, 1979). *Muscovite* and *biotite*, specifically those that are early-forming, may also contain appreciable levels of Ba, replacing K, whereas Sr is not as common in micas due to the low Ca content. Generally, the Sr/Ba ratio is smaller in igneous rocks containing K-feldspar, so late forming granites are generally impoverished with respect to Sr, as the Sr content of the magma has already largely been crystallized (Rankama and Sahama, 1950).

In metamorphic rocks, Sr is associated with fissure and vein minerals. Sr may replace Ca in *aragonite*, *calcite* and *fluorite* of hydrothermal veins. These may be of higher Sr-content than sedimentary carbonates, although their content is lower than primary crystallized calcite. For instance, the rhombic *aragonite*, can support 5-6 times more Sr-substitution than the sedimentary equivalent. Barium content is very low in these minerals. However, Ba may occur in metalliferous hydrothermal mineral veins in the form of *barite*, *witherite*, etc. (Rankama and Sahama, 1950). Strontium may substitute for Ba^{2+} in these minerals, and for Pb^{2+} in some lead minerals, such as *cerussite* (up to 3% SrO).

Beryllium occurs in rocks only in very low abundances, and is dominantly present as Be^{2+} either replacing Si^{4+} in silicate tetrahedra, particularly in alkalic rocks low in silica (e.g. nepheline syenites), or in independent Be minerals in granite/nepheline pegmatites.

b) Dissolution and precipitation characteristics

During chemical weathering, Ca goes into solution as bicarbonate, but with some Ca retained in the weathering zone as sulphate or carbonate. Calcium is not readily adsorbed into clays and so remains largely in solution, or is precipitated as carbonates under saturation (Rankama and Sahama, 1950). The average Ca content of pelites (2.23wt%) is therefore relatively lower than in igneous rocks (3.63wt%).

Magnesium is mainly released into solution as soluble chloride or sulphate, or is carried undissolved or in partially decomposed Mg-clays in suspension. Mg may be enriched by metasomatic processes, replacing alkali metals and Ca. The resultant rocks are often enriched in sulphide-ore deposits. Magnesium is also contained within carbonate deposits such as *calcite*, *aragonite*, *magnesian calcite* and *dolomite*: marine calcites are likely to be relatively enriched in Mg, along with Sr, Na, Ba and U. *Dolomite* may also originate from igneous rocks rich in Mg (e.g. pyroxenites), in metasomatic reactions which involve the replacement of silica by CO_2 . Additionally, if Mg-bearing hydrothermal fluids come into contact with calcium carbonate, *dolomite* or *magnesite* may be formed (Rankama and Sahama, 1950). Mg, Ca, Mn, Br, Sr and Y are the only elements present at concentrations higher than that of shales containing dominantly aluminosilicate minerals (Turekian and Wedepohl, 1961).

The sulphates and carbonates of Sr and Ba are less soluble than the corresponding Ca salts. Barium is only sparingly soluble in distilled water, but its solubility increases in the presence of hydrochloric acid or alkali metal chlorides in solution.

All *calcite* contains a small amount of Sr (Broecker and Oversby, 1971), but the low temperatures of formation of sedimentary carbonates and sulphates do not favour the incorporation of Sr (Rankama and Sahama, 1950). Strontium is generally present in sedimentary *calcite* at less than 1%, but may be present in *aragonite*, which has a more favourable structure, at up to 4%. Anhydrite in evaporite deposits maybe particularly enriched in Sr (Goldschmidt and Muir, 1958). In *gypsum* the level is no higher than 0.35%. Gypsum is also structurally unfavourable for Ca substitution. However, strontium carbonates (*strontianite*) and sulphates (*celestite*) may coprecipitate with calcium and gypsum, so for the purposes of dissolution characteristics may be considered as of equal provenance (Broecker and Oversby, 1971). *Apatite* may include Sr levels as high as 13.7%.

Ba is more readily adsorbed into clays than Sr, with the result that the Sr/Ba ratio changes from 0.6:1 in igneous rocks to 260:1 in seawater. Therefore, Ba is much more abundant in pelitic non-carbonate sediment than Sr (possibly up to 200 times more concentrated), whereas in limestones there may be 2 to 3 times more Sr than Ba, and much of the Ba content may be in non-carbonate form.

During weathering, beryllium closely follows the course of aluminium, being enriched in clays, bauxites etc. It is not common in carbonates or quartzites (Rankama and Sahama, 1950)

1.5.3.3 Group III Elements

The Group III elements consist of boron, aluminium, gallium, indium and thallium.

a) Rock & mineral affinities

Aluminium, the most abundant Group III metal, commonly substitutes for Si^{4+} in the silicate structure, which creates an ionic imbalance by which other cations become bonded to the silicate tetrahedra. Aluminium is therefore widespread in aluminosilicate minerals such as *amphiboles*, *pyroxenes*, *micas*, etc.

Gallium is fairly closely related to aluminium, iron and zinc. It is rather enhanced in some *muscovites* and *chlorites* due to a Ga^{3+} - Al^{3+} exchange, but also displays sulphophile characteristics, and may be present in early-forming hydrothermal ore deposits (in *magnetite* and *chromite*) but in general the concentration in all these minerals is rather low (<10mg/kg) (Vlasov, 1966). Gallium is also accommodated in the structure of *sphalerite*. Gallium may reach concentrations of 70-80mg/kg in acidic igneous rocks.

Indium has a less strongly oxyphile character than Ga, and may substitute for Fe^{2+} in sulphides associated with granites (Rankama and Sahama, 1950). It has also been found in *cassiterite* and *siderite*. Indium is in very low abundances in all cases, and reached a maximum of approximately 2mg/kg in igneous rocks.

Thallium appears to associate with K, Rb and Cs as Tl^+ , and with Fe^{3+} and Ca^{2+} as Tl^{3+} . As such it may be present in *K-feldspars*, *plagioclase*, *micas*, *tourmaline* etc., but has also been reported in *galena* (Vlasov, 1966). Variations in each of these minerals is great, however, and percentages of Tl in these are generally very low and inconsistent. Tl only attains concentrations of 1-3mg/kg in acidic igneous rocks.

The small ionic radius of boron (0.023nm) results in the bulk being enriched in residual magmas even during the last stages of crystallization (Battey, 1981), so may be present in

late-forming minerals in granite such as *tourmaline* (9-11% B). However, some minerals containing hydroxyl groups, such as *biotite* and *amphiboles*, may incorporate B into their structure; these may crystallize in earlier forming basic igneous rocks. B may also replace Si in silicate tetrahedra, although the difference in ionic radius keeps the degree of substitution limited.

b) Dissolution and precipitation characteristics

Aluminium is insoluble in solutions of natural pH, with the result that aluminosilicate minerals are often partially weathered, leaving much of the aluminium and silicate in the solid phase as clays such as *kaolinite*, *illite*, *montmorillonite*, etc.

Gallium follows Al into clay during weathering, whereas indium follows iron and manganese into sedimentary iron deposits, or occasionally deposits in marine carbonates. Thallium may also be sorbed into clays. However, there is little evidence of significant enrichment of these three elements in the sedimentary environment (Rankama and Sahama, 1950).

Boron is more abundant in sedimentary rocks, because it is relatively highly concentrated in seawater. As such, B can be an indicator of the origin of metamorphic rocks, that is to say, whether they were igneous or sedimentary (Rankama and Sahama, 1950).

1.5.3.4 Group IV and V Elements

Germanium, tin and lead constitute Group IV metals, and arsenic, antimony and bismuth form Group V elements.

a) Rock & mineral affinities

Germanium closely resembles gallium in terms of modes of occurrence. Ge^{4+} may replace Si^{4+} in silicates, due to similar ionic radii (0.053nm and 0.042nm respectively). This is most common in *topaz* and *garnet*, which have relatively weaker Si-O bonds, but actually may occur in *quartz*, especially that of a hydrothermal origin. Ge may also accompany Sn in hydrothermal *sphalerite*.

Tin may occur in sulphides such as *sphalerite*, *galena* and *chalcopyrite*, and is generally enriched in late-forming igneous rocks. Sn^{4+} may substitute for Fe^{2+} , Sc^{3+} and Ti^{4+} and Sn^{2+} may replace Ca^{2+} in silicate rocks. Thus, in late-forming fractions, Sn may be found in *sphene*, *wolframite* and *biotite*. The most tin-rich mineral is *cassiterite*, which is also preferentially formed in late-crystallites and hydrothermal veins.

A considerable portion of lead in igneous rocks is present in sulphides, particularly *galena* (Volborth, 1969; Krauskopf, 1979; Battey, 1981). However, much of the Pb content may mirror the occurrences of Sr. With an ionic radius of 0.120nm, Pb^{2+} partially replaces Ca^{2+} in minerals such as *apatite*, *aragonite*, *epidote* and *biotite*, and also replaces K^+ (radius 0.133nm) particularly in *K-feldspars*. Therefore Pb is rather enriched in acidic igneous rocks (Rankama and Sahama, 1950). Pb may concentrate in hydrothermal veins, where it may substitute for Ca^{2+} in *calcite*.

Arsenic and antimony readily combine with S, Se and Te forming sulphosalts, arsenides and antimonides with heavy metals, preferentially Cu, Fe, Ni and Co. They are also found in their native state in mineral veins. Arsenic may be present in notable amounts in *pyrite*, where it replaces sulphur (the accessory mineral *arsenopyrite* represents the end-member of this replacement), but also in *apatite*, where it replaces phosphorus, and in silicates. Bismuth is also sometimes found in *apatite*, as the radius of Bi^{3+} (0.096nm) is close to that of Ca^{2+} (0.099nm). All three elements are generally enriched in late magmatic crystallates, and particularly hydrothermal mineralization (Battey, 1981). They are found in *galena*, particularly Sb which may be present at up to 1%.

b) Dissolution characteristics

Germamium is readily extracted from minerals during weathering, and is transported as stable soluble salts. It is commonly precipitated in sedimentary iron ores, but is also present in shales.

Cassiterite is very resistant to chemical weathering, and so tends to remain in resistate sediments, and silicate- and sulphide-bound tin is sorbed into Al-rich clay sediments. Its content is low in sedimentary iron ores.

Lead is often preferentially extracted from rocks and sediment during weathering. *Galena* is oxidised to lead sulphate, a process which is enhanced by the presence of *pyrite*, which yields Fe-sulphate and acts as an oxidising agent. $PbSO_4$ is not particularly soluble. In the presence of carbon dioxide and bicarbonate, Pb bicarbonate may be formed, which is rather more soluble, but subject to adsorption onto silicates (Stumm and Bilinski, 1972). Lead may therefore be deposited in carbonate sediments, but generally only up to levels of tens of mg/kg. A secondary Pb-Zn sulphide deposit association is common (Battey, 1981).

Upon weathering, arsenic, antimony and bismuth are mainly sorbed on iron hydroxide, and may concentrate in sedimentary iron ores. Arsenic is particularly enriched in sedimentary *pyrite*. Metamorphic reactions tend to remove As from Fe-rich sediments, however.

Sandstones and shales generally only contain around 1mg/kg Sb & Bi (Rankama and Sahama, 1950).

1.5.3.5 Group IIIB Transition Metals

Group III transition metals include scandium, yttrium, lanthanum and the lanthanides, actinium and the actinides. Yttrium, lanthanum and the lanthanides are commonly referred to as rare-earth elements (REE). The only naturally occurring actinides are thorium and uranium.

a) Rock & mineral affinities

Scandium most commonly substitutes for Fe^{2+} or Mg^{2+} , predominantly in *pyroxenes*, *hornblende* and *biotite* from early crystallates, but also in biotites of late-forming granite pegmatites (Rankama and Sahama, 1950; Vlasov, 1966). The simultaneous occurrence of Al^{3+} in these minerals provides for the required valence compensation during the Fe-Sc or Mg-Sc replacement. Therefore Sc is lower in olivine. Scandium is seldom encountered in hydrothermal deposits, but may accompany W and Sn in minerals such as *cassiterite* and *wolframite*, particularly where Fe^{2+} , Mg^{2+} and Mn^{2+} are present. These minerals may be found to coexist with *pyrite* (Rankama and Sahama, 1950). Although there is negligible Sc substitution in calcites of any origin, *bazzite*, another Sc-bearing mineral, may coexist with calcite, as was found in Alpine veins in Italy and Switzerland (Vlasov, 1966, Table 99).

The rare-earth elements are all strongly lithophile, and this character increases with increasing ionic radius (i.e. in the order Lu-La, as ionic radius decreases with increasing atomic number). Due to slight differences in their chemical properties, Y and La-Lu are often categorized into two sub-groups; light REE or cerium-earth elements (CEE): La, Ce, Pr, Nd, Pm, Sm, Eu; and heavy REE or yttrium-earth elements (YEE): Gd, Tb, Dy, Ho, Er, Tm, Yb, Lu, Y (Rankama and Sahama, 1950; Ahrens, 1964). Europium is sometimes included with YEE. The CEE are generally more abundant, especially La, Ce & Nd, and Y is the most common YEE (Ahrens, 1964). Due to their relatively large ionic size in comparison to Sc, which otherwise has similar chemical properties, REE^{3+} rarely replace Fe^{2+} and Mg^{2+} in mineral structures, and so are often enriched in granites and syenites, but also in residual crystallates of basic rocks. There is no common mineral-forming element that is geochemically similar to REE^{3+} . Ca^{2+} and Na^+ are closest, but charge imbalances exist. Any substitution is generally for Ca^{2+} (McLennan, 1989).

In certain minerals, for instance *apatite*, *monazite* and members of the *epidote-zoisite* group, the CEE predominate, whereas others, such as *garnet*, *fluorite* and *xenotime* are dominated by

YEE. These minerals (with the exception of *apatite*) are particularly associated with granites and granitic pegmatites. In *sphene*, the dominance of CEE or YEE is determined by the silica content of the parent magma, granite pegmatite sphenes are YEE dominant, whereas nepheline-syenite pegmatite has CEE-dominant sphene (Rankama and Sahama, 1950).

YEE-Ca isomorphism is more common than with CEE, as YEE, with ionic radii of (0.098-0.085nm) substitutes for Ca^{2+} (0.099nm) in 6-fold coordinated sites more readily than the CEE (0.114-0.100nm). Divalent Eu^{2+} , which has an ionic radius (0.098nm) similar to Sr^{2+} (0.112nm), may occupy Ca sites in greater abundance, including some *Ca-plagioclases* (Krauskopf, 1979), as the electrical charge can be neutralised more conventionally (Rankama and Sahama, 1950). Since many REE remain in the residual melt until the latter stages of crystallization, YEE may also be present in hydrothermal *calcites* at up to 0.56%. CEE may substitute for K^+ (0.133nm) in *K-feldspars*, especially La^{3+} , although this is again limited by electro-neutrality problems (Ahrens, 1964). Partial melting may also cause an enrichment in CEE, especially in garnets, amphiboles and pyroxenes (McLennan, 1989).

Thorium is a strongly oxyphile element, and is strongly concentrated in acidic rocks during magmatic differentiation, so may show similar occurrences to Zr, REE and U. Thorium may often be incorporated into *zircon*, and may also substitute for REE (particularly CEE) in many minerals, due to the similar ionic radii (Th^{4+} has radius 0.102nm). Since it is radioactive, the daughter atom ^{208}Pb accumulates in Th-bearing minerals, although specialised analysis is necessary to discern this from other lead isotopes.

Uranium does not form sulphides, but may form hydrous U-sulphates in rocks, which are often associated with pyrite and especially its oxidising products. During magmatic differentiation, U becomes strongly concentrated in acidic rocks; granites (Battey, 1981). Like the REE, U becomes concentrated in the residual fluids, as the ionic radius of U^{4+} (0.097) is too large (given the valency) to be incorporated into common rock-forming minerals. U may accompany Zr and Th in zircon, and REE in their minerals, and Ti in pegmatites. U is most abundant in hydrothermal mineralization; U occurs in tin veins and *pitchblende* associated with Co, Ni, Bi and As sulphides, and in late-forming *fluorite* (Rankama and Sahama, 1950).

b) Dissolution characteristics

Scandium forms relatively insoluble hydroxides, but $\text{Sc}(\text{OH})_3$ is precipitated at pH 6.1, compared with pH 5.5 for $\text{Fe}(\text{OH})_3$. However, when in solution in natural waters, it generally is only present in complexes or in a sorbed state. Scandium may be found at enhanced levels

in sedimentary *iron oxides* (up to 0.01%) and other iron deposits. Metamorphic rocks also frequently show enhanced levels of Sc, especially metapelites with a clay origin.

Rare-earth elements are quite strongly sorbed by clays, but some may remain in solution. Speciation is dependent on pH: at $\text{pH} \geq 8$ many REE complex with OH^- , forming $\text{REE}(\text{OH})_3$ complexes. Some REE have a $\text{REE}_2(\text{CO}_3)_3$ stability field at around $\text{pH} = 9$. At $\text{pH} < 8$, REE tend to remain as free ions (McLennan, 1989). REE may be collected by carbonate sediments: such as sedimentary calcites. Europium is again often enriched in these sediments due to the presence of Eu^{2+} , although under oxidising conditions Eu^{2+} is largely oxidised to Eu^{3+} , whereupon it follows the trends of the other REE more closely (Rankama and Sahama, 1950). Generally, REE are not easily fractionated during dissolution reactions, and hence may provide an index of average provenance compositions (McLennan, 1989).

Thorium behaves similarly to REE upon weathering, and may precipitate with Fe- and Mn-hydroxides. Therefore, Th is generally more concentrated in pelitic sediments and shales than arenaceous rocks or limestones (Rankama and Sahama, 1950).

Uranium compounds are readily sorbed into Fe-, Al- and Mn-hydroxides, although some may remain in solution to be deposited in marine evaporites.

1.5.3.6 Iron and Iron-Group Metals

Iron-group metals include titanium, vanadium, chromium, manganese, cobalt and nickel. These have similar properties to iron, and often have similar occurrences (Volborth, 1969).

a) Rock & mineral affinities

Iron is present in the earliest products of magmatic differentiation, as iron oxides (often Ti-rich), and iron monosulphides (*pyrrhotite-pentlandite*), which form in conjunction with Ni & Cu ores. Percentages are highest in early-crystallizing magmas, decreasing in latter stage products (Table 1.14). The decrease in content with increasing acidity is not as pronounced as Mg, and hence the Fe/Mg ratio increases with increasing acidity. This is explained by the fact that although Fe^{2+} decreases sharply as crystallization progresses, the change in Fe^{3+} content decreases less sharply. Fe^{2+} generally accompanies Mg^{2+} , due to similar ionic radii (0.074nm and 0.066nm respectively), whereas Fe^{3+} tends to substitute for Al^{3+} (0.064 and 0.051nm respectively). It can be seen, however, that the difference between Fe^{3+} and Al^{3+} is rather large, and so substitution is largely confined to minerals where Al is present outside the aluminosilicate complex such as *hornblende*, *augite*, *muscovite* etc., and not in feldspars. Fe^{2+} is present in many other silicate minerals, such as *fayalite* (the iron end member of *olivine*), *pyroxenes*, *amphiboles* and ferromagnesian *micas*. Other iron oxides include

haematite, *magnetite* and *ilmenite*, and iron sulphides include *pyrrhotite* and *pyrite*. Of the opaque minerals in common igneous rocks, the most common are, in order, magnetite, ilmenite, pyrrhotite, followed by other sulphides. Haematite is not common as a primary mineral, as it requires a higher oxidising environment than exists in most silicate melts, but may occur as a secondary alteration product. Iron sulphides, sulphates and *siderite* commonly occur in hydrothermal mineralizations (Rankama and Sahama, 1950).

Table 1.14 Iron distribution in igneous rocks (Rankama and Sahama, 1950)

Material	wt% Fe
Hornblendite (ultrabasic):	11.76
Gabbro:	8.84
Diorite:	5.63
Granodiorite:	3.28
Granite:	2.48

Titanium is dominantly tetravalent, and has similar chemical properties to thorium. It is strongly oxyphile, and may occur as *ilmenite* (most common), *rutile* (rarer), *sphene* and *perovskite*. *Ilmenite* is a very common accessory mineral in igneous rocks, along with iron oxides such as *magnetite*. Ti^{3+} (radius 0.076nm) is also present in pyroxenes (e.g. *augite*), *garnets*, *amphiboles* and *micas*, replacing Al^{3+} (0.051nm), Fe^{3+} (0.064nm) and occasionally Mg^{2+} (0.066nm). Smaller amounts of Ti^{4+} may substitute for Si^{4+} in the silicate tetrahedra in some silicates and aluminosilicates, such as *hypersthene* (orthopyroxene) and *biotite*, due to the same valence state (Volborth, 1969), although the difference in ionic size between Ti^{4+} (0.068nm) and Si^{4+} (0.042nm) keeps this limited (Rankama and Sahama, 1950). It can be seen by the common mineralogy that Ti is most abundant in the early products of crystallization (Battey, 1981).

Vanadium may be enriched in iron oxides which are also Ti-enriched, such as *ilmenite*, and also enters readily into the crystal structure of *magnetite*. V^{4+} (radius 0.063nm) readily substitutes for Ti^{4+} (0.068nm), Fe^{3+} (0.064nm) and Al^{3+} (0.051nm). Vanadium is often associated with Fe in silicate minerals associated with gabbros, dolerites and basalts, such as *pyroxenes*, *amphiboles* and *micas* (Krauskopf, 1979), but are generally not present in feldspars. No stability field for a V-sulphide compounds exists in natural environments (Krauskopf, 1979).

Chromium commonly associates with Fe^{III} , so may be found in iron oxides etc. (Krauskopf, 1979, p.473-480). In igneous rocks, Cr is concentrated in early differentiates, which are also enriched in Fe, Mg and Ti. *Chromite* is generally the first mineral to crystallize from a calc-alkaline magma. Igneous iron ores are often Cr-enriched, as Cr is readily incorporated into

the structure of *magnetite*. It is not present in significant quantities in sulphide minerals. Cr^{3+} behaves similarly to Ti^{3+} in silicate minerals, and replaces Fe^{3+} and Al^{3+} , but is too large to substitute for Si^{4+} in the silicate tetrahedra. Consequently, Cr is relatively abundant in *hornblende*, *augite* and *biotite*.

Manganese resembles iron in many respects, as far as its occurrence in nature is concerned. The Mn^{2+} state is the most stable in silicate minerals, so may associate with Fe^{2+} , Mg^{2+} , Zn^{2+} or Ca^{2+} (Volborth, 1969), but the occurrence of Mn in igneous rocks generally mirrors that of Fe^{2+} (Table 1.15). Dark silicate minerals containing hydroxide (OH) groups contain the most Mn, such as *biotite* and *hornblende*, but Mn may also occasionally be present in *augite*, *muscovite*, *tourmaline* and others. In oxides, Mn is more common in the Mn^{4+} or Mn^{3+} states. Mn^{3+} is also present in some hydrothermal minerals, which can replace Fe^{3+} , Al^{3+} and Cr^{3+} . Mn may be found in *sphalerite* and *apatite* (in granite pegmatites), but is rare in pyrite and pyrrhotite.

Table 1.15 Manganese distribution and ratio with FeO in igneous rocks (Rankama and Sahama, 1950)

Rock	MnO%	FeO%	MnO:FeO
Gabbro	0.15	8.6	0.017
Diorite	0.09	6.0	0.015
Granite	0.05	2.9	0.018

Nickel is concentrated in ferromagnesian rocks. A strong affinity of Ni to S in terrestrial rocks has been demonstrated. An Ni-As-Sb combination is typical. Cobalt also shows this affinity, but is more lithophile (Volborth, 1969). The first crystallization of igneous magma produces *pentlandite* which is usually intergrown with *pyrrhotite* (Battey, 1981). Contrastingly, Co tends to stay in the melt fraction, and is relatively more common in hydrothermal mineralization than Ni. Cobalt is therefore considerably more common than Ni in *pyrite*, substituting for Fe, and may also be accommodated in the structure of *sphalerite*. Much of the Co and Ni content of igneous rocks is in silicate minerals, however. In these minerals, Ni and Co are strongly enriched in the ultrabasic rocks, although Co is relatively more prevalent in silicic rocks (Table 1.16). Nickel may be mainly hosted by *olivine* and *hypersthene*, with much lower amounts in *augite*, *amphibole* and *biotite*. Feldspars do not host Ni. Metalliferous veins containing Co and Ni often contain arsenic; these are associated with basic rocks (Rankama and Sahama, 1950).

Table 1.16 Cobalt and nickel distribution and ratio in igneous rocks (Rankama and Sahama, 1950)

Material	Co (mg/kg)	Ni (mg/kg)	Co:Ni
Peridotite	237	3160	0.08

Gabbro	79	158	0.50
Diorite	32	40	0.80
Granite	8	2.4	3.33

Copper has one of the highest affinities for sulphur among metals (see Section 1.5.2a), hence the majority of copper is found in sulphides and sulphosalts in rocks. Copper is chiefly present as *chalcopyrite* in igneous rocks, although Cu-Fe sulphides such as *bornite* and *cubanite* may form in the last stages of crystallization, in the interstices between other minerals (Battey, 1981). The mode of occurrence in igneous rocks is listed below:

Table 1.17 Copper distribution in igneous rocks (Rankama and Sahama, 1950)

Material	Cu (mg/kg)
Basic igneous rocks:	149
Intermediate igneous rocks:	38
Acidic igneous rocks	16

Cu²⁺ may also replace Fe²⁺ in silicate minerals if there is a low S content of melts, as their respective ionic radii are very similar (0.072nm and 0.074nm respectively). Cu may therefore be found in minerals such as *augite* and *tourmaline*. However, this mode of occurrence is relatively rare and unimportant (Rankama and Sahama, 1950).

b) Dissolution characteristics

Magnetite and ilmenite are relatively resistant to chemical weathering. Iron is not stable in weathering solutions, and is converted to ferric hydroxide by the action of carbon dioxide and water. Most is deposited as sedimentary iron ores or occasionally as iron silicates such as *glauconite* and *greenalite* (only in marine environments) (Rankama and Sahama, 1950). Non-marine sedimentary calcites are likely to be enriched in Fe, Zn, Co and Cu, due to the composition of the fluid from which they were precipitated.

During weathering, Ti from ferromagnesian minerals is largely sorbed in a combined Fe-Al “hydroxide” precipitate. Minerals such as ilmenite, sphene and rutile are particularly resistant to chemical weathering, and may remain unchanged in weathering residue. In highly metamorphosed schists of sedimentary origin, sphene is not generally abundant, and Ti is largely present in the form of oxides (Rankama and Sahama, 1950). Titanium is often assumed to be immobile in geochemical studies, and is used as a normalising element to compare the mobility of other elements (McLennan, 1989).

Vanadium is generally incorporated upon weathering into clay minerals, although the V⁵⁺ ion is relatively mobile, and may form Pb, Cu, Zn and U vanadates, especially in higher pH

waters associated with calcitic/dolomitic limestones. Vanadium is generally more abundant in sedimentary rocks that contain iron oxides.

In sedimentary rocks, chromium often follows Fe^{3+} & Al because of the similarity of the chemistry of these 3 elements. Hence, little Cr remains in weathering solutions, and some Al-rich clays, bauxite, shales, schists and different types of iron ores may be relatively rich in Cr.

Manganese is more soluble than Fe, particularly in carbonate-bearing waters, and may reach a ratio of 5:1 with respect to Fe, despite its lower abundance in source rocks. Manganese may therefore become enriched in carbonate sediments in comparison to Fe, where it replaces Ca. It is also common in pelitic sediments associated with Fe, however. Metamorphic processes may enhance Mn levels in silicates, as MnO and MnCO_3 are readily converted.

Nickel largely remains in the solid phase of weathering products, but is actually much more stable in solution than Fe and Mn. Ni-hydrosilicate minerals may be formed, which are often in *chlorite*-form. Cobalt remains in weathering solutions as bicarbonate or hydroxide colloids, and appears to coexist with sedimentary iron ores (Rankama and Sahama, 1950). Sedimentary Co and Ni sulphides are commonly formed in reducing environments.

During weathering of chalcopyrite, copper is brought into solution as copper sulphate, which is relatively stable in soluble form, and will only deposit as sulphides once conditions allow. Some Cu is also sorbed into clays, and may therefore be found in many types of sedimentary rocks, although it is more common in pelitic sediments than limestones and sandstones (Rankama and Sahama, 1950; Battey, 1981).

1.5.3.7 Other metals

a) Zinc and cadmium

Although zinc is relatively abundant in the upper lithosphere, *sphalerite* is relatively scarce (Rankama and Sahama, 1950). Cadmium is an invariable accessory of Zn, and in natural conditions is also associated with Zn and Fe^{2+} . Zn and Cd tend to be concentrated in the late hydrothermal sulphide phase of crystallization, because the affinity of Zn and Cd for S is lower than Ni, Cu and Fe (Volborth, 1969). Silicate rocks may contain Zn^{2+} , which replaces Fe^{2+} and Mg^{2+} - this is most common in *biotite*. Zinc is more common in the later forming ferromagnesian minerals, and so the Zn content of igneous rocks is higher in intermediate and acidic rocks, despite there being no appreciable levels of Zn in feldspars. Zn may also replace Fe^{2+} and Mg^{2+} in *magnetite* and *ilmenite*.

Cadmium may be present in *sphalerite* (0.01-5.0%), *chalcopyrite*, *galena* and *pyrite* (0.0001-0.02%). The relatively common appearance of sphalerite and pyrite in many deposits may indicate that Zn and Cd are useful indicators of sulphide mineral provenance (Vlasov, 1966). The average Zn/Cd ratio of igneous rocks is approximately 530:1, but in hydrothermal *sphalerite* the ratio is often considerably lower, indicating a tendency for Cd to become enriched in residual melts with respect to Zn (Rankama and Sahama, 1950).

Zinc and cadmium go readily into solution as sulphate and chlorides, and are quite mobile. They are generally precipitated in sulphur-bearing muds once a reducing environment is encountered, sometimes accompanying lead. Zinc and, to a lesser extent, cadmium may also be deposited in carbonate sediments (Rankama and Sahama, 1950).

b) Zirconium

Zirconium exists only as, or within, oxides or silicates, particularly melanocratic Fe-minerals (*pyroxenes*, *amphiboles* and to a lesser extent, *micas*), exclusively present as Zr^{4+} . However, Zr is more common in alkali (sodic) versions of those Fe-minerals, e.g. *hornblende* may contain 0.116%, but alkali hornblende has contained 0.045-0.53%. The distribution in igneous rocks is shown in Table 1.18. Zirconium is also generally enhanced in other iron-bearing granitoid minerals, e.g. *aegerine* and *sphene*. It forms a relatively common independent orthosilicate, *zircon*, which is thought to contain most of the igneous content of Zr (Rankama and Sahama, 1950; Vlasov, 1966).

Zircon is very stable against mechanical and chemical weathering, so Zr remains largely undissolved. Some Zr from other minerals does dissolve, but is readily removed by sorption processes. Rocks of a precipitatory origin are therefore depleted with respect to Zr.

Table 1.18 Zirconium distribution in igneous rocks (Rankama and Sahama, 1950)

Material	Zr (mg/kg)
Gabbros:	140
Diorites:	280
Granites:	460

c) Molybdenum & Tungsten

Molybdenum and tungsten are generally concentrated in the last differentiates of magmatic crystallization. Tungsten generally stays in the residuum later than molybdenum, which usually crystallizes as *molybdenite*. Tungsten may coexist with Sn in *cassiterite*. Additionally, the ionic radii of W^{4+} and Mo^{4+} are equal (0.062nm), and so can replace each other in many minerals. It would appear from the literature that these elements exist mainly

in the form of *molybdenite* or various molybdates and tungstates, such as *wolframite* (Rankama and Sahama, 1950). No significant incorporation into silicates is reported. Also, no particular association of molybdenite with other sulphide minerals is noted.

d) *Silver and gold*

The manner of occurrence of silver and gold resembles that of Cu, with Ag mostly combined with S or Se, and Au is either in a native state or accompanies Se & Te. Native Ag is often a secondary product. Ag and Au may be found in early-forming *chromites*, but are more common in late-forming and hydrothermal formations (Battey, 1981), and may be found in *cassiterite* and *molybdenite* (Rankama and Sahama, 1950). *Galena* may contain up to 2% Ag. Gold may also be found in hydrothermal quartz veins, whereas Ag is more associated with carbonate veins. The quantities of Ag and Au in igneous rocks are very low, however (often sub-parts-per-billion).

Silver is a relatively insoluble metal and upon weathering is rapidly reprecipitated or sorbed into clays. Gold is inert, and is generally reduced to its native state, remaining in the residue (Rankama and Sahama, 1950).

e) *Rhenium & Platinum-group metals*

Rhenium is chemically related to molybdenum, and is one of the least abundant elements. It is strongly associated with sulphides such as *molybdenite* and to a lesser extent *pyrite*. Its overall abundance in igneous rocks is about 1ng/g. Hydrothermal rocks are similarly low in Re. Only molybdenites contain vaguely significant amounts of Re (less than 0.25%) (Rankama and Sahama, 1950; Vlasov, 1966).

Platinum group metals (Os, Ru, Rh, Pa, Ir, Pt) are very rare metals which show mainly siderophile qualities, but are often present in their native state. They may be present in ultrabasic *chromites*, formed during the first stages of magmatic crystallization (Battey, 1981), but are almost completely absent from any rocks formed after the initial stage. Hydrothermal tin ores such as *cassiterite* may contain platinum metals, or may remain in the last melt phase and crystallize in their native state in quartz veins (Rankama and Sahama, 1950).

f) *Mercury*

Mercury is present in very low levels throughout the igneous fractionating sequence and hydrothermal sulphide deposits. Enrichment generally occurs in the secondary environment, particularly in shales, as it is strongly sorbed. Mercury may be present in spring water only

up to tenths of ng/g, and the average in rain water is 2ng/g, so any traces of mercury found in river water may be significantly of an atmospheric source (Rankama and Sahama, 1950).

1.5.3.8 Non-metals

Chlorine (Cl) is nearly always present in igneous rocks of the main stage of crystallization. It is an essential part of *apatite*, especially in basic rocks, and is a common constituent of *sphene*. It is present in igneous rocks typically at levels of 200-500mg/kg, often substituting for (OH) groups in silicate minerals. Bromium and iodine are characteristically dispersed elements in igneous rocks, present in small quantities throughout the magmatic differentiation sequence. Bromium is present only at levels up to 3mg/kg, and iodine is only present at sub-mg/kg levels in igneous rocks.

1.5.3.9 Summary of abundance, occurrence and soluble properties of the elements

Table 1.19 summarises the affinities and dissolution characteristics of the major and trace elements in nature. The complicated nature of the occurrence of these elements is clearly illustrated, indicating that interpretation of trace element data is not a straightforward process. Many elements may give a loose impression of solute provenance if there are distinct rock types in the catchment, for instance, there are distinct differences in the trace geochemistry of iron sulphides from iron silicates, and some elements may indicate a dominantly hydrothermal provenance. Figure 1.10 shows a ballpark representation of the affinities of some trace elements, according to Table 1.19.

Figure 1.10 Generalised affinities of some trace elements in rocks. Other trace elements may show less distinct affinities or more complicated relationships.

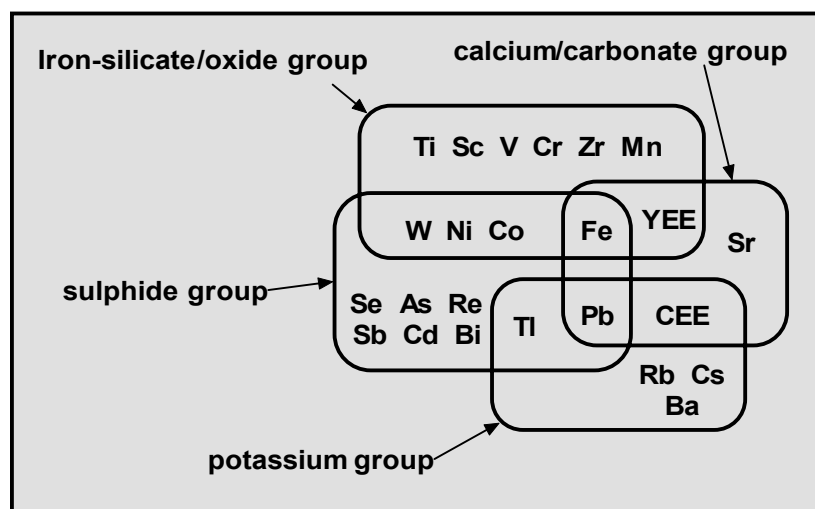


Table 1.19 Summary of elemental affinities for stage of crystal fractionation of igneous rocks, other elements, minerals, sedimentary deposition environment and relative solubility in natural waters (data extracted from Rankama and Sahama, 1950; Turekian and Wedepohl, 1961; Battey, 1981; Drever, 1982).

mg/kg	Igneous affinity	Element affinity	Mineral affinity	Sediment affinity	Solubility
Li	a+h	~Al	mu bi px to	Al-clay	low-mo
Na	a	~K	kf mu bi le	clay	mod
K	i-a	~Na	nf am px mu bi ne	mobile	high
Rb	a+h	K	kf bi mu lp	Al-clay	low-mo
Cs	a+h	Rb K	kf bi mu lp	Al-clay	low-mo
Be	a+h	~Si	ne	Al-clay	low
Mg	ub-b	Fe ~Ca	ol gt cd px am bi cl do tc ca mg	Mg-clay m.c.	mod-hig
Ca	b-a+h		px am ep cf ca do gy ap	m.c.	high
Sr	i-a+h	Ca ~K	cf kf ca ar ap ±ce	m.c.	mod-hig
Ba	a+h	K	bi mu br ±ar	clay / m.c.	mod
Sc	b-i+h	Fe Mg	px am bi ±cs wf	Fe-OH / Al-clay	low
Y	YEE: i-a+h	~K Ca	gt xe sp px am ca	clay / m.c.	low-mo
REE	CEE: a+h	~K	ap mz ep sp kf	clay / m.c.	low-mo
	Eu ²⁺ : i-a+h	~Ca YEE	cf ca at xe sp px am	clay / m.c.	mod
Th	a+h	~Zr ~CEE ~U	zr mo ep sp kf	Fe/Mn-OH	low
U	a+h	~Zr ~REE	zr cs ±ar	Fe/Mn-OH	low-mo
B	a+h	~Si	to ±bi am	clay / m.c.	mod
Ga	a	Al	mu cl	Al-clay	low
In	a+h	Fe ²⁺	py cs si	Fe-OH / m.c.	low-mo
Tl	a+h	K Rb ~Ca	kf cf mu to	Al-clay	low
Sn	a+h	S	sr ga cc cs sp wf ±bi	res / Al-clay	low
Pb	a+h	~Sr ~Ca	ga ap ar ep bi kf ca	m.c. / S-mud	low-mo
As	h	S ~P	py ap as	Fe-OH	low
Sb	h	S	ap	Fe-OH	low
Bi	h	S ~Ca	ap		
Ti	ub-b	Fe ³⁺ Al	il sp px gt am bi	Fe-OH / Al-clay	low
V	ub-b	Ti Fe ³⁺	il mt px am bi	Fe-OH	low
Cr	ub-b	Fe ³⁺	cr mt am px bi	Fe-OH / Al-clay	low
Mn	ub-i+h	Fe	bi am ±px mu to sr ap	Fe-OH / m.c.	low-mo
Fe	ub-i+h	Mg ~Al	pp mu ol px am hm mt il py si	Fe-OH / Al-clay / FeS	low-mo
Co	ub-b+h	Ni S Mg ~Fe	pp py ±ol px am bi	Fe-OH / FeS	low
Ni	ub-b	Mg Fe S	pp py pl ±px am bi	Fe-OH / FeS	low
Cu	ub-b+h	Fe ²⁺	cc ±px to	clay	mod
Zn	a+h	Fe	bi mt il sr	S-Pb mud / m.c.	mod
Zr	b+h	Fe	px am sp zr	clay	low
Mo	a+h	-	mb		
Ag	h	-	ga n(c)	clay	low
Cd	a+h	S	sp cc ga py	S-mud	low-mo
W	a+h	-	cs wf	res	low
Pt	ub+h	-	cr cs n(q)	res	low
Au	ub+h	-	cr n(q)	res	low
Hg	disp.	-	-	clay	low
S	ub-a+h	-	pp py as cc ga sr mb gy br	mobile / S-mud	mod
Br	disp.	-	-	mobile	high
I	disp.	-	-	mobile	high

Abbreviations:

Igneous affinities: ub: ultrabasic rocks b: basic i: intermediate a: acid h: hydrothermal veins/very late pegmatitic rocks. This is a sequence of magmatic crystallization, hence b-a+h means the element is found in minerals in basic, intermediate and acid rocks as well as in hydrothermal veins. For more details, see the individual element descriptions in the previous section.

For mineral abbreviations, see Table 1.9. These are not exhaustive, more detail is provided in the text of Section 1.6.

Sedimentary affinities: res: belongs to a resistant mineral, so may be found in resistate sediments (Al-)clay: is sorbed into clay (associated with Al) Fe-OH: is deposited with sedimentary iron oxides/hydroxides m.c.: precipitated as marine carbonates S-mud: precipitated in sulphurous muds, often containing heavy metals mobile: tends to stay in solution, concentrates in seawater. These descriptions are given more comprehensively in the previous section.

Metasomatism, however, complicates matters as it may alter the mineralogy of a rock and change the occurrence of trace metals. Hence, general statements about trace element solute provenance without thorough examination of the catchment geology may lead to inaccurate predictions of meltwater geochemistry. Additionally, the effect of differentiation of elements upon weathering between the dissolved and undissolved phases must be carefully considered, as trace chemistry of solute directly dissolved from a certain rock type may display totally different proportions of major and trace elements to the bulk rock chemistry.

1.6 CONCLUSION

Geochemical studies of meltwater quality indicated that solute acquisition is substantial in subglacial environments, and early chemical models of glacier hydrology gave indications of a heterogeneous subglacial drainage system. More detailed investigations of meltwater quality gave indications of kinetic, sedimentological, hydrological and mineralogical controls on solute acquisition, relating specifically to proton availability, access to atmospheric gases, solute provenance, meltwater residence times and drainage dynamics.

Laboratory investigations of solute acquisition have begun to isolate the controls on solute acquisition, allowing quantification of the rates and controls on the processes of acquisition in isolation. More detailed laboratory investigations of these processes in isolation and in combination may facilitate a greater understanding of subglacial chemical weathering mechanisms.

A novel approach to the understanding of subglacial solute acquisition is using minor and trace metal analysis. It is clear that certain minor and trace elements have close associations with major cations that are abundant in subglacial meltwater. However, problems with interpretation arise from the differences in the mobility of the associated elements in solution. This can result in low observed correlations between major elements and their associated trace metals (Brown and Fuge, 1998b). Similarly, since major elements in solution may have more than one provenance, attempting to detect key indicator species of dissolution and oxidation processes by interpreting correlations between trace metals and the major elements with which they are expected to substitute (Brown and Fuge, 1998b) is likely to be equivocal. A possible improvement in the interpretation of solute provenance utilising trace metal analysis would occur if mineral- or rock-specific major and trace element analyses of the dominant rock types in the catchment of the glacier are carried out, so that a direct connection between observed trace metal concentrations in rock and solution can be made. To date this has not been carried out in glacial literature. This could aid in the identification of key indicator species of subglacial chemical weathering processes, allowing the

conclusions made from laboratory investigations to be better related to field observations of variations in subglacial meltwater chemistry.

2. METHODS AND TECHNIQUES

2.1 INTRODUCTION

To further the understanding of the relative influence, rates and magnitude of the processes of solute acquisition in a subglacial environment, the individual processes, or variables, must be constrained (Brown *et al.*, 1996b). This is impossible in the field due to the inaccessibility of the *in situ* environment, where only isolated snapshots via borehole sampling can be collected (Sharp and Richards, 1996). Therefore, simulation of the subglacial environment is necessary to enumerate the variables. In this chapter, the techniques field sampling and analysis, and determination of bulk rock chemistry are described. Experimental methods, analytical techniques, and the methods of use of geochemical modelling packages, are also detailed.

2.2 FIELD AND LABORATORY SAMPLING TECHNIQUES

The data acquisition of this project was predominantly laboratory based, with parameters determined by data gathered from a period of field sampling. Much of the field sampling techniques are well established after work by various authors (e.g. Brown and Tranter, 1990; Brown, 1991; Tranter *et al.*, 1993; Brown *et al.*, 1994a; Brown *et al.*, 1994b; Lamb *et al.*, 1995; Seagren, 1995; Sharp, 1995). Some of the equipment and sampling techniques employed were similar for both field and laboratory sampling and analysis. Section 2.2.1 describes the procedures of rock and sediment sampling, Section 2.2.2 outlines the techniques of field meltwater collection, and laboratory sampling techniques are described in Section 2.2.3.

2.2.1 Rock sampling for detailed mineralogical analysis and laboratory leaching experiments

Previous studies of glacial meltwater quality have suggested that the controls on solute acquisition are sedimentological and mineralogical, as well as kinetic and hydrological (Chapter 1). To evaluate these controls, a knowledge of the geology of the catchment is required, and laboratory studies specifically require the mineralogy and chemistry of the rock and sediment samples to be known. To this end, observations of geology were made at *Haut Glacier d'Arolla* (Chapter 3), and samples of morainic rock and sediment were collected for petrologic and chemical analysis.

Rocks and sediment chosen from the catchment were immediately placed in plastic sample bags which were labelled with the location.

a) Morainic- and side-rocks

Systematic descriptions of the geology of morainic and side-scrée material were carried out on *Haut Glacier d'Arolla* and Glacier des Bouquetins during the period 28 July to 26 August 1995, with an emphasis on the spatial variations observed across the glacier, in particular with respect to sulphide minerals (Section 3.3). Specimens of numerous rock types were collected manually from the moraines for preparation into thin-sections enabling petrographic descriptions and quantitative bulk mineralogical analysis by AAS and ICPMS and to fuel laboratory experiments investigating variations in the dissolution characteristics with rock type (see Chapter 4).

b) Subglacial sediment

Direct access to subglacial sediment is severely restricted. During the 1995 field season a number of attempts were made to gather such sediment in ice-caves at various locations under the glacier. Sediment was collected in an ice-cave at the eastern margin of the snout, which extended some 150m under marginal ice at the side of the glacier (Figure 2.1). The meltstream within the cave appeared to come from snowmelt above the east side of the glacier, so may not be representative of a subglacial channel travelling down-glacier from the upper reaches. The sediment appeared to contain coarse (sand- to pebble-sized) fragments of a wide mixture of rocks seen on the surface moraines, and was therefore thought to be useful as a “mixed moraine sediment” amalgam for use in laboratory dissolution experiments (“rock M”).

2.2.2 Meltwater sampling for chemical analysis

Bulk meltwater quality sampling at *Haut Glacier d'Arolla* has been undertaken since 1989 (e.g. Brown and Tranter, 1990; Brown, 1991; Lamb *et al.*, 1995; Lamb, 1997), and the techniques for sampling meltwater; and determining pH and dissolved oxygen concentrations ($O_2(aq)$) are now well established.

To speed up the process of sample filtration and pH and $O_2(aq)$ analysis, a ‘field laboratory’ tent was set up adjacent to the bulk meltwater sampling site, within which all filtration, pH and $O_2(aq)$ measurement procedures were carried out. This meant that processing of bulk meltwater samples was undertaken within minutes of collection from the proglacial channel.

Processing of samples collected from the glacier snout and the main area of supraglacial meltwater collection began within five minutes of collection.

Filtered supraglacial meltwater was used in lieu of deionised water at the field site for washing of containers, as it was impractical to transport the required amount of deionised water up to the analysis site.

The collection of water samples for subsequent chemical analysis employed the same method for all meltwater types. A 500mL polythene screw-cap bottle was rinsed out in the meltstream three times at the sampling site, and the sample was taken, returned to the laboratory tent. Using 250mL Nalgene polysulphone vacuum filter apparatus and a 0.45 μ m Whatman cellulose filter membrane, the complete unit was immediately flushed through with 15-30mL of the meltwater sample three times, prior to 150mL of the sample being filtered as rapidly as possible to dryness. The process of filtration took around 5-25 minutes, depending on the concentration of suspended sediment in the sample. Filter membranes were handled with plastic tweezers to avoid contamination. Each sample utilised a new filter membrane, which was discarded once filtration of the sample had been completed.

Around 40mL of the filtrate was used for pH analysis, and the remainder was decanted into 30mL polypropylene sample bottles, which had been pre-rinsed three times with small amounts of filtrate. Two bottles of each sample were taken to allow sufficient quantities for both anion and cation determinations.

a) *Bulk meltwater*

To give a picture of seasonal trends, sampling was undertaken twice a day, at the approximate time of maximum and minimum bulk discharge. This is designed to show the maximum diurnal range in solute concentration.

Ablation season discharge records from the meltstream draining the *Haut Glacier d'Arolla* during the 1989 and 1990 meltseason showed that the average minimum rate of discharge (Q_{\min}) occurs around 10:00 local time, and that the maximum rate (Q_{\max}) occurs at around 17:00, with deviations of up to 2 hours at Q_{\min} , and up to 3 hours at Q_{\max} (Brown, 1991). During August, these deviations were generally no more than one hour. The discrepancy between the measured Q_{\min}/Q_{\max} and the actual values recovered later from Grande Dixence SA records, was generally $<0.25\text{m}^3\cdot\text{s}^{-1}$ at Q_{\max} and $<0.05\text{m}^3\cdot\text{s}^{-1}$ at Q_{\min} (Brown, 1991). In the light of these results, 10:00 and 17:00 were again adopted as the sampling times of bulk meltwater for the 1995 field season. Sampling was undertaken during the period starting 17:00, 28 July 1995 (Julian Day 209) and ending 10:00, 28 August, 1995 (Julian Day 240), a

period of 31 days. A complete set of Q_{\min} and Q_{\max} meltwater samples were taken over this period, with the exception of 17:00, 1 August and 10:00, 2 August, providing a virtually unbroken record of maximum and minimum bulk discharge samples for the latter part of the melt season.

In addition to the twice-daily sampling for seasonal trends, short-term trends were investigated over three diurnal sampling cycles, approximately ten days apart, on 5-6 August, 15-16 August and 24-25 August, 1995. A total of 19 samples were collected during each 24 hour period, hourly between 10:00 and 19:00, and then bi-hourly between 21:00 and 09:00, with the next 10:00 collected as normal. Sampling was more intensive during the day than overnight because the time between Q_{\min} and Q_{\max} is only approximately 7 hours, whereas the time between Q_{\max} and Q_{\min} is 17 hours, and chemical and physical properties of the meltwater have been shown to adjust at accordingly similar rates to discharge (Brown, 1991).

Sampling was undertaken at a fixed point in the meltstream approximately 400m downstream from the glacier snout. At the glacier snout there were at least two main portals, which have different catchments within the glacier. This has previously been demonstrated by dye-tracing experiments (Nienow *et al.*, 1996b). Sampling a little way from the snout allowed waters draining from the portals to be sufficiently mixed, providing a bulk sample of meltwater quality draining the whole glacier. The specific site was chosen because it was downstream of the point where braided channels rejoined to form a single channel, whilst as close as possible to the snout to reduce the potential for downglacier chemical evolution.

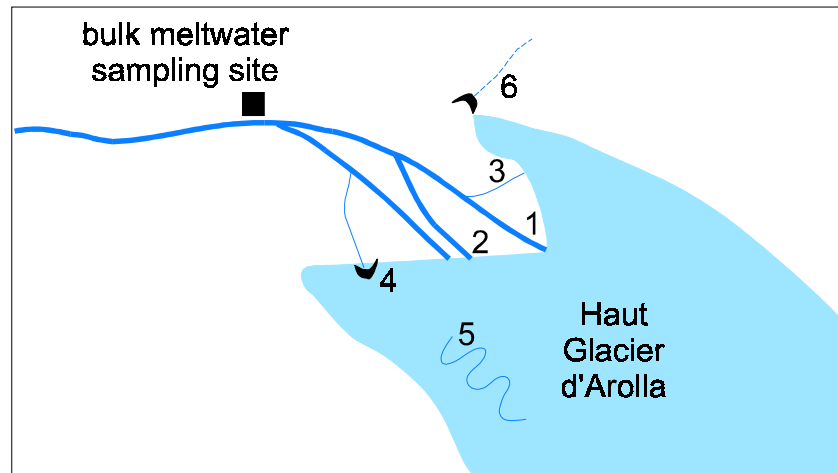
b) Snout samples

Observations of meltwaters draining the snout of *Haut Glacier d'Arolla* often showed distinct colour variations in the suspended sediment load between the two main portals. This may reflect differences in the suspended sediment mineralogy of the two waters. To investigate whether these apparent differences in sediment characteristics had any effect on the dissolved load, a number of samples were collected from each portal over the field season. These included samples from the Eastern Main Portal on 4, 8, 21 and 22 August, the Western Main Portal on 8, 21 and 22 August, a small channel on the eastern side on 4, 8 and 21 August and a subglacial ice-cavern beneath the western side of the glacier base on 8 August (see Figure 2.1).

c) Supraglacial meltwaters

A small number of supraglacial meltwaters were collected throughout the field season, to give an indication of the chemistry of the most dilute component of the glacial hydrological

Figure 2.1: Systematic map of the meltwater stream portals at the snout of the Haut Glacier d'Arolla, showing some of the meltwater and sediment sampling sites. Those numbered are: 1 - the Eastern Main Portal; 2 - the Western Main Portal; 3 - the small isolated Eastern channel; 4 - subglacial ice-cavern on Western side; 5 - one of the main supraglacial channels; 6 - the Eastern ice cave from which the "mixed moraine" sediment was collected (see Section 2.2.1b).



system. These were mainly collected from at or near the glacier terminus, to minimise the time between sample collection and filtration and pH/O₂ (aq) analysis (see Figure 2.1).

d) Groundwater

Groundwater input is thought to be a possible factor in the alteration of the chemical properties of meltwater in channelized flow near the toe of a glacier (Raiswell, 1984), but its identification and sampling is difficult. The geology of the catchment of the *Haut Glacier d'Arolla* is dominantly igneous and metamorphic, so the bedrock is largely impermeable and, therefore, groundwater may not be an important component of the hydrological system in this catchment. However, small water discharges were observed seeping from a rock exposure above the main glacier but below the Glacier des Bouquetins; a small, virtually extinct tributary glacier above the east side of the lower reaches of the *Haut Glacier d'Arolla* (see Figure 3.2). Although this water is likely to be meltwater from the Glacier des Bouquetins, which is only tens of metres above, it does show the potential for a certain amount of permeation through fissures in the rock, and so was sampled as a separate, albeit small, component of the hydroglacial system.

Sampling was difficult due to the very small volumes of water seeping from the rock. Two areas of the exposure had sufficient flow to enable the collection of the groundwater as it emerged from the rock and collected in small cracks. This was done using a 10mL sterilised

syringe in conjunction with a 50mm × 1.1mm Monoject sterile needle and a 0.45mm Whatman cellulose nitrate filter membrane which fits inside a plastic filter unit that is placed between the syringe and the needle. Approximately 30mL of sample was collected as quickly as possible and placed into a pre-rinsed polypropylene sample bottle. There was a delay of around an hour between the collection of this sample and its filtration and pH measurement due to the distance of the sampling site from the laboratory tent.

2.3 LABORATORY EXPERIMENTS

Comparisons between laboratory- and field-acquired data are not always favourable, with orders of magnitude of difference in acquisition rates sometimes occurring (Schnoor, 1990). To reduce the chance of discrepancies caused by apparatus, sampling procedures and analysis, these aspects of experimental technique were kept as similar as possible to the field techniques.

This section describes the materials, conditions and procedures employed in the various laboratory experiments undertaken.

2.3.1 Experimental materials

2.3.1.1 Rocks/sediment

Different sediment types were required for experiments investigating sulphide oxidation and carbonate dissolution, and those investigating solute provenance:

a) “End-member” investigations of sulphide oxidation and carbonate dissolution

To isolate the rates, controls and magnitude of solute acquisition by the coupling of sulphide oxidation and carbonate dissolution reactions, a series of experiments involving pure, end-member calcite and pyrite were envisaged. Initially, preliminary tests were carried out using precipitated calcium carbonate (PCC) and manufactured ferrous sulphide, but the PCC was found to block the filter membranes upon sample collection, and the TEMA-crushed ferrous sulphide was found to badly contaminate laboratory ware and leave bottles and filter units permanently stained. Following these experiments, therefore, it was decided to use mineralic calcite and pyrite, which compromised the “pure” nature of these experiments to a small extent. Calcite vein material collected from moraine of the *Haut Glacier d’Arolla* was selected. Pyrite, when present, was generally disseminated through the morainic rocks of the Haut Glacier, or was present in very small clusters, and would have been very difficult to extricate from the surrounding “gangue”. Instead, pyrite from an unknown source was gained

from the rock stores of the Institute of Earth Studies at the University of Wales, Aberystwyth. A full bulk analysis of the calcite and pyrite samples was carried out (see Section 3.7).

Nicholson *et al.* (1988) undertook trace element analyses of six samples from different locations, and measured oxidation rates from each variety (Table 2.1). Whilst these experiments did not involve either pyrite from *Haut Glacier d'Arolla*, or the pyrite used in the experiments in this study, it gives an indication of the variations in trace element content and oxidation rate that may be expected between random samples. No relation between rate and any particular element were found. It can be seen the variations in rate between samples of different origin are relatively small, although there may be greater variations with sedimentary pyrites (Carrucio *et al.*, 1981). These variations indicate that some caution must nevertheless be taken in the interpretation of trace element variations due to pyrite, when samples from different sources are being compared, and that possible variations in oxidation rate may also result.

*Table 2.1 Summary of selected analyses of elements in pyrite specimens from five different worldwide locations. These were mainly aggregates of euhedral crystals or relatively pure massive specimens; one sample was a flotation concentrate from uranium tailings. Units are in ng/mL, except Fe (wt%). Oxidation rates (r) are in mol/h/g ($\times 10^{-8}$). Data from Nicholson *et al.*, (1988)*

Species	Al	Ba	Ca	Co	Cu	Fe %	Mg	Mn	Ni	Pb	Si	Sr	Th	Ti	V	Zn	Zr	r
mean	183	2	183	106	513	56	198	16	66	203	56	2	28	22	10	852	10	7.04
std dev	204	3	41	227	420	2	340	6	105	381	68	2	46	30	1	1590	6	0.72

b) Morainic rocks

Although pyrite oxidation and carbonate dissolution have been previously described as the major processes of solute acquisition in subglacial environments, an evaluation of these processes cannot be fully satisfied using pyrite and calcite alone, as these minerals are only minor mineralogic components of the catchment geology underlying *Haut Glacier d'Arolla*. Experiments involving common morainic rock and sediment types collected from the glacier were also undertaken so that more realistic simulations of subglacial dissolution could be obtained. Detailed bulk analysis of these rocks was undertaken, and each was also subjected to numerous laboratory experiments. Tying in the analysis with geological observations and dissolution experiments allowed the dominant reactive minerals in the Arolla catchment to be constrained, and controls affecting dissolution behaviour to be identified.

c) Preparation of rocks and sediment for experimental use

Early experiments involving pyrite and calcite (experiments P/C/P_{0.1}C/PC_{0.1}/PC/4P/4C/4PC(c) and P/C/PC(o)) used pyrite and calcite that was hand-crushed using a mortar and pestle. No grain-size analysis is available for this sediment, but observations suggest a grain size distribution in the range <63.5µm to 1mm in diameter.

For subsequent experiments (experiments 1-9/M(c)/(r)/(rd)), morainic rock samples were crushed individually in a TEMA mill, prior to ICPMS and AA bulk analysis (Section 2.4.5). Later experiments involving pyrite (Experiments 1P/5P/9P(c)/(r)) also used TEMA-crushed pyrite. The powders were stored in sealed polyethene bags.

Weighing was carried out to a precision of $\geq \pm 0.5\%$ on an electronic balance accurate to 0.0001g, using small plastic vials which were washed three times in Milli-Q 18MΩ water between each use.

d) Calculation of specific surface area

The post-crushing grain size distribution of the mixed moraine sediment (rock M) was determined using a Micromeretics SediGraph model 5100 Particle Size Analyser, using the parameters shown in Table 2.2. A detailed evaluation of this technique is available in Seagren (1999).

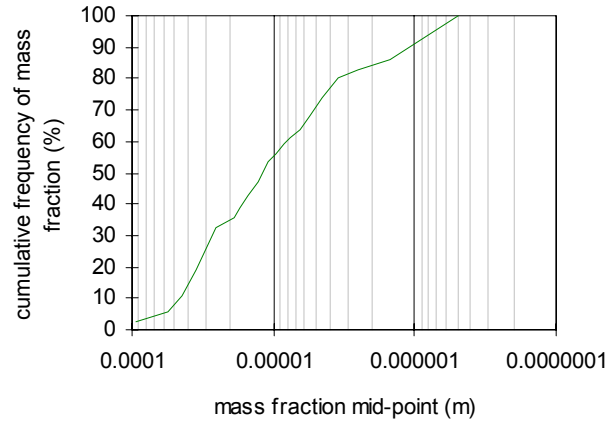
Table 2.2 Sedigraph Particle Size Analysis Parameters

Liquid type	Calgon 0.05% (density: 1.00g/cm ³ ; viscosity: 0.80cp)
Analysis type	30.0°C
Run time	3 minutes
Sample density	2.67 g/cm ³
Reynolds number	1.03

Figure 2.2 shows the cumulative grain size distribution and the percentages of each size interval in terms of both mass and grain size, indicating that the modal grain size of the analysed sediment is a diameter of 20-30µm, and the median grain size by mass is around 11µm. However, surface area calculations show that the finest particles contribute the bulk of the total surface area, so that the median grain size in terms of number of particles is at below 4µm. Indeed, 14% of particles were nominally less than 1µm in diameter (Figure 2.2), and these particles are likely to provide the bulk of the surface area in TEMA-crushed sediment. This has a major effect on the dissolution behaviour of sediment, as microparticles show rapid dissolution rates compared to larger particles (Holdren and Berner, 1979).

Figure 2.2 Grain size distribution of TEMA-crushed mixed moraine sediment (rock M); and cumulative particle size distribution. Median values do not include sizes below 1 μm ;

Median diameter by mass (μm)	11.04
Median diameter by surf.area (μm)	3.88



Specific surface area (SSA) is calculated from grain diameter and mass fraction data, assuming that all particles are spherical with a density of 2.67g/cm³ (Equation 2.1).

Equation 2.1 Equation for the calculation of specific surface area (SSA), where f = frequency in wt% within each grain size interval, ρ = density (2670000g/m³), and m = mid-point of each grain-size interval.

$$SSA = \frac{\sum \left[\left(\frac{f/\rho}{4/3\pi(m/2)^3} \right) 4\pi(m/2)^2 \right]}{100}$$

The SSA of the analysed sample was calculated as 0.87m²/g. This is within the range of SSAs of suspended sediment collected from meltwater draining *Haut Glacier d'Arolla* during the 1996 meltseason of 0.87-1.12m²/g (Seagren, 1999).

2.3.1.2 Water

Analysis of samples of supraglacial meltwater collected from the *Haut Glacier d'Arolla* has generally shown a very low ionic strength (Table 2.3), with the exception of those from the early meltseason, which may contain atmospheric acid input (Brown *et al.*, 1996a). In the laboratory, the analogy of supraglacial meltwater was made by using distilled, deionised water obtained from a Milli-Q device to a standard of 18M Ω . Although this is purer than supraglacial meltwater, its use allowed the isolation of processes involved in the chemical

Table 2.3 Range of concentrations of supraglacial and deionised water analyses (Brown, 1991)

Species	Snowpack	Supraglacial meltwater		Milli-Q deionised water (this study)
	(1989)	(1989)	(1995)	
Ca ²⁺	0 - 17	3.1 - 170	47 - 512	0 - 13
Mg ²⁺	0 - 3.3	0.4 - 2.4	1.4 - 94	0
Na ⁺	0 - 10	0.4 - 6	1.5 - 27	0 - 6.2
K ⁺	0 - 7.9	0 - 3	1.3 - 10.5	0 - 1.5
HCO ₃ ⁻	n/a	2 - 210	38 - 415	n/a
SO ₄ ²⁻	0.2 - 25	1 - 15	8.9 - 459	0 - 3.5
NO ₃ ⁻	1.3 - 11	0.7 - 2.3	0 - 1.8	0 - 1.9
Cl ⁻	n/a	0 - 3.7	0.6 - 9.5	0 - 2.2
pH	4.8 - 6.4	6 - 8.1	6.8 - 7.4	n/a

evolution of meltwaters in response to the dissolution and oxidation of bedrock minerals in the absence of acid and aerosol input.

2.3.2 Temperature control

The Arrhenius equation (Equation 2.2) shows that dissolution rate constants are strongly dependant on temperature:

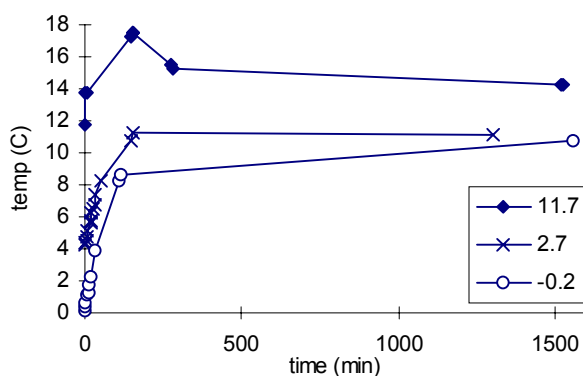
Equation 2.2 Arrhenius' equation of pre-exponential rate of dissolution, where k is the rate constant; A is the frequency constant, E_a is the activation energy, R is the gas constant and T is the temperature in Kelvin.

$$k = A \exp\left(\frac{-E_a}{RT}\right)$$

The effect of heat on a chemical reaction is that the rate of reaction is approximately doubled for every 10°C increase in temperature (Underwood and Webster, 1975; Raiswell *et al.*, 1980). Since the temperature of the main meltwater channels remained within a small range of approximately 1 to 4°C, laboratory experiments conducted at room temperature may be expected to have a much faster reaction rate than the rates encountered in the field. The apparent importance of residence times on the processes likely to cause the chemical signature of the bulk meltwaters is described in Chapters 1 and 2. Therefore the rates of solute acquisition in subglacial environments are an important control on the magnitude and nature of acquisition. For laboratory experiments to effectively investigate the effects of residence times, therefore, the temperature must be kept as close as possible to those encountered in the field. This was attempted by conducting experiments within a standard 210 litre refrigerator (type Hotpoint RF50). Certain experiments were also conducted at room temperature to evaluate the effect of temperature on solute acquisition.

The initial use of AC-powered magnetic stirrers (type Gallenkamp SS590), was found to cause the temperature within the refrigerator cabinet to rise well above 10°C, due to their internal transformer (Figure 2.3). Nine-volt battery-powered magnetic stirrers (type Stuart Scientific SM7) were subsequently used, but these were prone to stopping if left in refrigerated conditions for more than a few hours, presumably due to a loss of battery effectiveness at lower temperatures. A more successful solution was found by converting the battery-powered stirrers, so that they could be powered by external DC adapters, situated outside the refrigerator with the power cable threaded between the body of the refrigerator and the door seal, with insignificant disruption to the seal.

Figure 2.3 Temperature of stirred deionised water using an AC magnetic stirrer. Initial temperatures of each experiment prior to stirring are shown in the legend, in °C.



As a result of these adaptations, the ambient temperature in the refrigerator was reduced somewhat, to a mean of $7.3^{\circ}\text{C} \pm 1.5^{\circ}\text{C}$, still higher than glacial environments, but the lowest possible with the equipment used. The temperature is taken into account when calculating carbonate speciation, pCO_2 and $\text{SI}(\text{calcite})$.

2.3.3 Duration of water-rock contact

Dye-tracing experiments at *Haut Glacier d'Arolla* showed that distributed meltwater may stay resident in the subglacial drainage system for up to 24 hours, although the quickflow component has a shorter residence time, as little as 2 hours (Nienow *et al.*, 1996a). To establish rates of acquisition, long residence times had to be considered. Therefore the majority of experiments were run for 24 hours or above. Rapid and short-term chemical evolution also had to be considered, especially in the case of closed-system environments, where atmospheric gases may be used up quickly. Therefore, sampling of experiments at short intervals over the first few hours was also necessary.

For closed and open system experiments, standard time intervals of sampling were therefore used. All experiments had samples taken at 1, 4 and 24 hours rock-water contact. This gave an indication of the levels of acquisition at both short and long “residence” times. Further detail was gained by taking additional samples at the following time intervals in many experiments: 5, 10, 20, 40 minutes; 2, 8, 16, 18, 48 hours. Experiments involving the reopening of a closed system at 24 hours, and those that were also diluted at this point, had additional samples taken at 24.5, 25, 26 and 28 hours under open system conditions.

2.3.4 Access to atmospheric gases

The 1995 field results in Chapter 4 suggest that subglacial meltwater retained access to carbon dioxide and oxygen, although previous studies had suggested that distributed meltwaters may become closed with respect to these gases (Tranter *et al.*, 1993). Laboratory experiments were therefore designed under both closed and open atmospheric conditions to examine the variation in rates in an open and closed system.

Experiments involving the reopening of a closed system were carried out to simulate the evolution of meltwaters as they emerge from the distributed network into the channelised system, where access to the atmosphere may be regained, and flow velocity is greater, so that the residence time in this part of the hydrological pathway is restricted to a few hours (Nienow *et al.*, 1996a). Other experiments involving 50% dilution with deionised water and open access to the atmosphere, after 24 hours of closed system dissolution, were designed to simulate the evolution of bulk meltwater after the distributed flow and quickflow meltwater components mix.

2.3.5 Experimental set up

1000mL Nalgene HDPE wide-necked bottles were used to contain the experiments. One litre of deionised water was measured and placed in the HDPE bottle. The bottle was sealed, and allowed to cool in the refrigerator until the water had reached the ambient temperature of the refrigerator (Section 2.3.2). At this point the bottle was placed on the magnetic stirrer, opened, and a stirrer paddle added. Long, flat-based (triangular prism-shaped) stirrer paddles were utilised to ensure the maximum possible sediment agitation. The water was stirred with the top open for approximately 60 minutes, in an attempt to equilibrate the solution with respect to atmospheric gases.

After this time, the appropriate crushed sediment was poured into the bottle. In experiments investigating open access to atmospheric gases, the top was left open, whereas in experiments

investigating a closed system environment, the top was sealed. Around 25cm³ of air-filled space is left in the bottle after sealing as the bottles are slightly larger than one litre.

2.3.6 Sampling procedure

The methods used for sampling were designed to be similar to those used in the field, particularly with regard to the apparatus used and the method of storage. 250mL Nalgene polysulphone vacuum filter apparatus was again used with 0.45µm Whatman cellulose filter membranes, and prewashing with small amounts of sample was carried out three times prior to sample filtration. Similar amounts of sample were collected, and storage was in two 30mL sample bottles, which were placed in a refrigerator.

With experiments undertaken with open access to atmospheric gases, sampling for each time interval was carried out from the same solution, with the remaining unfiltered solution replaced onto the magnetic stirrer. At each time interval the bottle top was replaced immediately prior to sampling, to allow thorough shaking of the bottle, ensuring the homogeneity of the solution. In the case of closed system experiments, the only satisfactory method of maintaining a system closed to atmospheric input was to run entirely separate experiments for each time interval of sampling. After the specified time of the experiment, the stirrer was stopped and the bottle removed from the refrigerator, and again shaken to ensure homogeneity. Hereafter, the sampling method was exactly as carried out in the field. pH and dissolved oxygen measurements were also made using the same apparatus and procedure as in the field. In some experiments, titration alkalinity was also determined (see Section 2.4.4).

Experiments involving reopening of a closed system

Experimental and sampling techniques were identical to those described above, except that after a sample has been taken after 24 hours in a sealed environment, the bottle is replaced in the refrigerator and stirred, with the bottle top left off. Further samples were taken after a further 30 minutes, 1 hour, 2 hours and 4 hours, with the remaining unfiltered solution put back in the refrigerator after each sample. In these experiments, around 120mL was filtered rather than 150mL, due to the premium of solution available. It was important to replace the solution in the refrigerator as soon as possible to minimise temperature increase and maximise stirring time.

2.3.7 Summary of experiments undertaken

The sequence of experiments undertaken was somewhat adaptive as results were considered and design setbacks were overcome. The experiments are summarised in Table 2.4.

Table 2.4 Laboratory experiments undertaken, where the following abbreviations are used: Rock 1-9: crushed morainic rocks; Rock C: crushed morainic calcite; Rock P: crushed pyrite; Rock M: crushed mixed moraine sediment; FeS: ferrous sulphide; PCC: precipitated calcium carbonate; EMS: Eastern moraine sediment.

Experiment No.	No. of replicates	Total samples	Open/closed system	Description	Trace analyses
<i>i</i>	2	4	open	4g/L uncrushed EMS	
<i>ii</i>	1	0 (pH)	open	pH test using 15g/L PCC	
<i>iii</i>	1	9	open	5g/L FeS	
<i>iv</i>	1	2	open	8g/L EMS	
<i>v</i>	1	1	open	8g/L proglacial silt	
<i>vi</i>	1	5	open	1g/L FeS	
<i>vii</i>	1	6	open	1g/L PCC	
<i>viii</i>	1	6	open	0.5g/L FS + 0.5g/L PCC	
<i>ix</i>	1	6	closed	0.6g/L EMS	
<i>x</i>	1	4	closed	2g/L EMS	
<i>xi</i>	1	5	closed	8g/L EMS	
C(c)	2	9	closed	0.2g/L Rock C	3
C(o)	2	14	open	0.2g/L Rock C	
P(c)	2	9	closed	0.2g/L Rock P	2
P(o)	1	8	open	0.2g/L Rock P	
PC(o)	2	10	open	0.2g/L Rock C + 0.2g/L Rock P	4
PC(c)	2	13	closed	0.2g/L Rock C + 0.2g/L Rock P	
PC _{0.1} (c)	2	13	closed	0.1g/L Rock C + 0.2g/L Rock P	2
P _{0.1} C(c)	2	13	closed	0.2g/L Rock C + 0.1g/L Rock P	3
1(c)	4	8	closed	4g/L Rock 1 - opened 24-28 h	8
1(r)	2	8	reopened		8
2(c)	2	4	closed	4g/L Rock 2 - opened 24-28 h	4
2(r)	1	4	reopened		4
3(c)	2	4	closed	4g/L Rock 3	4
4(c)	3	7	closed	4g/L Rock 4	7
5(c)	4	9	closed	4g/L Rock 5 - opened 24-28 h	9
5(r)	1	4	reopened		4
6(c)	2	4	closed	4g/L Rock 6	4
7(c)	2	4	closed	4g/L Rock 7	4
8(c)	2	4	closed	4g/L Rock 8	4
9(c)	5	9	closed	4g/L Rock 9 - opened 24-28 h	9
9(r)	3	9	reopened		9
M(c)	4	7	closed	4g/L Rock M - opened 24-28 h	7
M(r)	3	12	reopened		12
4P(c)	1	3	closed	4g/L Rock 4 + 0.2g/L Rock P	3
4C(c)	1	3	closed	4g/L Rock 4 + 0.2g/L Rock C	3
4PC(c)	1	3	closed	4g/L Rock 4 + 0.2g/L Rock P + 0.2g/L Rock C	3
1P(c)	1	3	closed	4g/L Rock 1 + 0.5g/L Rock P	3
1P(r)	1	4	reopened		4
5P(c)	1	3	closed	4g/L Rock 5 + 0.5g/L Rock P	3
5P(r)	1	4	reopened		4
9P(c)	1	3	closed	4g/L Rock 9 + 0.5g/L Rock P	3
9P(r)	1	4	reopened		4
1(rd)	1	5	reopened	4g/L Rock 1 50% diluted @ 24 h	5
5(rd)	1	5	reopened	4g/L Rock 5 50% diluted @ 24 h	5
9(rd)	1	5	reopened	4g/L Rock 9 50% diluted @ 24 h	5
M(rd)	1	5	reopened	4g/L Rock M 50% diluted @ 24 h	5
Total:	80	284			161

2.4 ANALYTICAL TECHNIQUES

2.4.1 Discharge measurement

Discharge of meltwater from *Haut Glacier d'Arolla* is continually measured by Grand Dixence SA at a gauging station approximately one kilometre from the glacier snout and 600m from the field sampling tent. Hourly discharge data for the entire 1995 meltseason was made available (Figure 4.2.1).

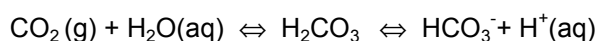
2.4.2 Measurement of pH

Analysis of pH utilised an Orion model 290A portable pH/ISE meter, with a Ross combination pH electrode and automatic temperature compensator (ATC). Some of the laboratory analyses utilised a Corning benchtop pH meter (Model 220), connected to a Corning General Purpose Combination Electrode (Cat. No. 476530), with manual temperature adjustment. No significant difference in precision using either meter or electrode was found. Calibration of the electrodes were carried out according to the instructions of the meter (Orion Research Incorporated, 1991a), using Orion Pure Water™ low ionic strength pH “a” and “b” buffer solutions of pH 6.98 and 4.10 at 20°C respectively, which have been shown to be more accurate than standard BDH buffer powder solutions (Brown, 1991). Around 40mL of each buffer solution was placed into separate 50mL polythene beakers. Buffers were replaced when the slope between them on the pH meter fell outside the 97-103% range (generally every 2-3 days). A mercury thermometer was used to set the temperature of the Corning benchtop pH meter when used.

The electrode and ATC probe were rinsed thoroughly with either deionised water (in the laboratory), or filtered supraglacial meltwater (in the field), between each buffer and sample. The filtered analyte was placed into a separate 50mL beaker, which was pre-rinsed three times with small amounts of the same analyte. Orion Pure Water™ pHisa ionic strength adjuster was added to each sample. This solution is recommended for use in low ionic strength solutions, as it increases the ionic strength of the solution without altering the pH. This has the effect of increasing the accuracy of the pH measurement, as higher ionic strength solutions improve electrode performance (Orion Research Incorporated, 1991a). 0.4mL (1% vol/vol) was added using a 1mL graduated syringe (Orion Research Incorporated, 1991a).

The electrode and ATC probe were placed in the sample and agitated for 30 seconds, and then left in the beaker for a further 90 seconds before a reading was taken. The reading tended to drift, but instances of a “ready” reading were recorded in addition to readings at 2 minutes. The direction of drift after 2 minutes was also recorded to give a crude idea of the $p(\text{CO}_2)$ of the solution. A high $p(\text{CO}_2)$ would tend to move the reaction to the right, causing pH to decrease, whereas a low $p(\text{CO}_2)$ would tend to consume H^+ ions, increasing the pH (Equation 2.3).

Equation 2.3 Equilibrium reactions between $\text{CO}_2(\text{g})$ and bicarbonate species.



Although replicates were not carried out during the 1995 field season, replicate analyses during the 1989 field season using the same technique gave precision figures of ± 0.16 pH units on average (Brown, 1991). The accuracy is ± 0.1 pH units (Brown *et al.*, 1994a).

Due to the pH measuring equipment being permanently set up in the laboratory tent close to the sampling sites, field analysis of pH from all sites (except the “groundwater” sampling site) was therefore generally completed within 30 minutes of sample collection, including the time for filtration, and within 20 minutes for bulk meltwater samples. This small delay could not be avoided, and was similar to the time for pH analysis in the laboratory

2.4.2.1 Investigation of continuous pH measurement during laboratory dissolution experiments

Continuous pH analysis is useful in laboratory experiments as an indicator of the chemical evolution of solutions between samples for chemical analysis. This was thought to be especially useful in the initial period of rapid acquisition after sediment addition (Brown *et al.*, 1996b). However, the recommended method of use of the Ross combination pH electrode involves measurement of filtered sample. Experiments were therefore undertaken to test the accuracy of *in situ* pH measurement, of unfiltered waters. This was carried out with open system dissolution of precipitated calcium carbonate powder (PCC) and TEMA-crushed artificial ferrous sulphide (Fe-S_x). The pH electrode and ATC were left in the solution as dissolution progressed, and were periodically removed from the solution, rinsed, and placed in a pH 7.01 buffer.

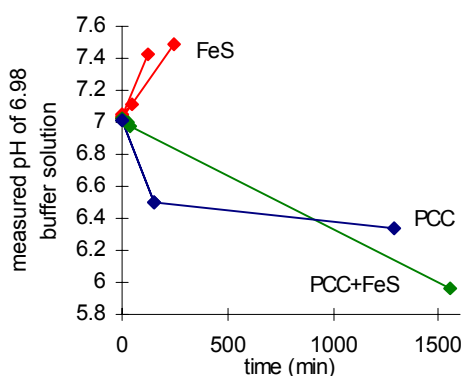
Table 2.5 and Figure 2.4 show that the readings obtained by the Ross combination electrode are affected considerably by being left in an unfiltered solution. Further observations showed that leaving the electrode in the buffer solution for around 15-20 minutes was sufficient for

the reading to return to around 7.01. The direction of reading drift is reverse to the ambient pH of the solution, and so is particularly affected in the high pH solutions created by the dissolution of carbonate sediment.

Table 2.5 Observed pH buffer measurements prior to and subsequent to immersion in solutions containing ferrous sulphide and/or precipitated calcium carbonate

Sediment concentration and type	Time in solution (minutes)	measured pH of 7.01 buffer
5g/L Fe-S _x	0	7.041
	125	7.424
5g/L Fe-S _x	0	7.030
	242	7.486
1g/L Fe-S _x	0	7.051
	50	7.113
1g/L PCC	0	7.012
	147	6.494
1g/L PCC	0	7.010
	1283	6.339
0.5g/L Fe-S _x + 0.5g/L PCC	0	6.974
	1437	5.957

Figure 2.4 Observed pH buffer measurements prior to and subsequent to immersion in solutions containing ferrous sulphide and/or precipitated calcium carbonate. For details of individual experiments see Table 2.5.



Further problems encountered with this method of pH measurement was that it was difficult to obtain a stable reading due to the solution being agitated by magnetic stirring, and that pHisa ionic strength adjuster could not be added to the solution as it would affect subsequent sediment dissolution and artificially increase K⁺ and Cl⁻ concentrations. Additional logistical problems were encountered attempting to recreate these experiments under a closed system environment, as it was difficult to adapt a closed vessel to fit the electrode within a hole in the cap, requiring a sealant that was airproof and non-contaminant, and a method of sample withdrawal whilst maintaining isolation from the atmosphere. .

Due to the difficulties described above, it was decided not to undertake further continuous pH measurement, and restrict measurement to that of post-filtered analyte at fixed time intervals.

2.4.3 Determination of dissolved oxygen concentration

Measurement was carried out using an Orion model 97-08 O₂ electrode connected to an Orion model 290A pH/ISE meter. The manufacturer's specifications state an accuracy of $\pm 2\%$. Comparison with the standard wet-chemistry technique of O₂(aq) determination (Winkler titration) have shown closely matched results (generally within 5%) (Brown *et al.*, 1994b).

The electrode consists of silver electrodes in an electrolyte solution, which is separated from the sample across a gas-permeable membrane. O₂(aq) in the sample diffuses through the membrane and the silver cathode reduces the oxygen to (OH)⁻ ions, with electrons produced on the anode. The resultant current is converted to a voltage and interpreted by the pH meter, giving a O₂(aq) value in parts per million (Orion Research Incorporated, 1991b).

Calibration of the electrode is necessary to compensate for altitudinal and atmospheric pressure effects. 2500m was chosen as the approximate altitude of the field site, and 100m was chosen as the altitude of the laboratory, both according to local mapping, and calibration was carried out according to the instruction manual (Orion Research Incorporated, 1991b). The electrode was suspended in a bottle sealed from the atmosphere, with water in the bottle up to a level a little below the electrode tip, for half an hour, allowing equilibration between the electrode and a water-saturated atmosphere. The second calibration point of zero is electronically derived, allowing a calibration curve to be achieved.

The time between sample collection and measurement has to be as short as possible, as oxygen rapidly diffuses from the atmosphere into meltwaters which are under-saturated with respect to the atmosphere. Filtration of samples is not required in the measurement of dissolved oxygen concentration, however, meaning that measurement could take place soon after sample collection. The sample was placed in a 50mL beaker, on top of a portable battery-operated magnetic stirrer. The electrode was held in the sample for two minutes, above the base of the beaker, allowing the magnet built in to the electrode casing to spin freely. During the two minutes, the O₂(aq) concentration reading often fell to a minimum, and then started to rise again. The minimum value, and the value after two minutes were recorded.

The operation of the electrode was monitored periodically by measuring the $O_2(aq)$ of a prepared 5% $Na_2SO_3(aq)$ solution. The solution consumes all $O_2(aq)$ within the water, and so the meter should read $<0.3ppm$ during normal operation.

2.4.4 Determinations of alkalinity, partial pressure of carbon dioxide (pCO_2) and calcite saturation indices (SI(calcite))

Samples of certain laboratory experiments were measured for titration alkalinity, post-filtration. 25mL of analyte were titrated with 1mM HCl to a pH 4.5 end-point identified by a mixed BDH indicator solution, which turns from blue to grey at pH 4.5 and grey to orange at pH 4.4. The total alkalinity is calculated using Equation 2.4. A total of 84 determinations were carried out.

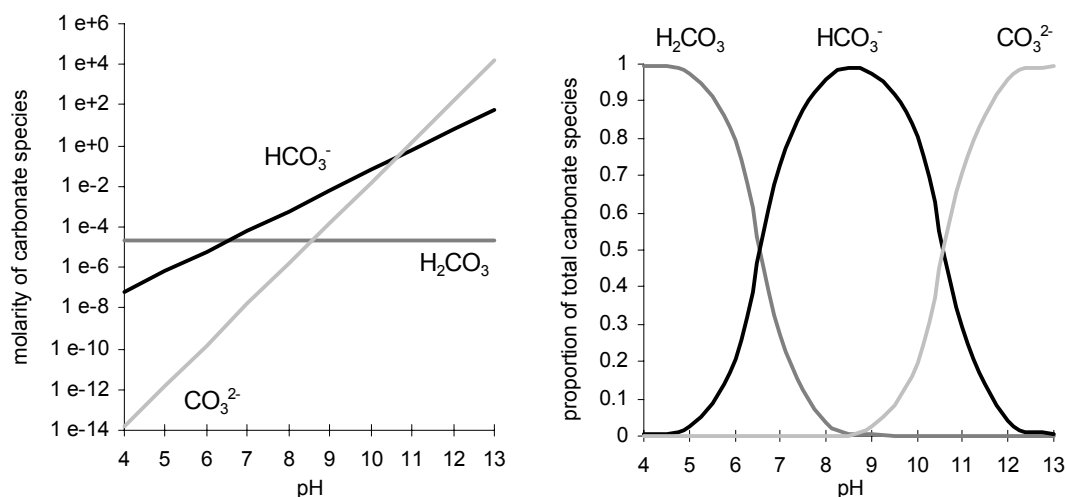
Equation 2.4 Determination of total alkalinity by titration

$$\text{Total alkalinity (neq/mL)} = 1000 \times \text{vol. (1mM HCl) (mL)} \div \text{vol. (sample) (mL)}$$

In all experiments, alkalinity was assumed to account for the charge balance errors between the total anionic equivalent units (i.e. the sum of the ionic concentrations of SO_4^{2-} , NO_3^- and Cl^-), and the total cationic equivalent units (the sum of the ionic concentration of Na^+ , K^+ , Mg^{2+} and Ca^{2+}). Ionic concentrations are determined by high performance ion-exchange chromatography (see Section 2.4.7).

Bicarbonate has often been used as an approximation of the total alkalinity in meltwater solutions and associated laboratory experiments (e.g. Brown, 1991). The accuracy of this

Figure 2.5 Relative concentrations of carbonate species at $0^\circ C$ (after Equation 2.5), assuming equilibrium with atmospheric carbon dioxide ($pCO_2 = 10^{-3.5}$ bar).



assumption depends on the pH of the solution (Figure 2.5). At pH=8.3 (and 25°C), 97.8% of all carbonate species is HCO_3^- , but at a lower pH, H_2CO_3 becomes more abundant, and at higher pH values, CO_3^{2-} is more stable, and calcium carbonate complexes also contribute to the total alkalinity (Table 2.6) (Christie, 1995). Therefore, at the low and high extremes of pH measured in the field in 1989 (6.81, 9.23 respectively), HCO_3^- accounts for 72% and 92% of the total alkalinity respectively. Interpretations involving ratios of species to HCO_3^- may therefore become affected by carbonate speciation at extreme pH.

Table 2.6 Percentage distribution of carbonate at pH 6, 9 and 12, at 25°C in a solution with calcite (after Christie, 1995) .

Species	% total carbonate		
	pH 6	pH 9	pH 12
CO_3^{2-}	0	5	71
$\text{H}_2\text{CO}_3^\circ$	32	0	0
HCO_3^-	68	90	1
CaCO_3°	0	5	28

To ensure the accuracy of bicarbonate values, HCO_3^- was calculated from the alkalinity determinations using carbonate equilibria constants (Equation 2.5), given that:

$$[\text{total alkalinity}] = [\text{H}_2\text{CO}_3] + [\text{HCO}_3^-] + [\text{CO}_3^{2-}] \text{ (all values in mol/L).}$$

Similar corrections were made to titration alkalinity determinations in Tranter *et al.* (1997).

Equation 2.5 Carbonate equilibria (after Garrels and Christ, 1965).

$$K_{(\text{CO}_2)} = \frac{[\text{H}_2\text{CO}_3]}{p\text{CO}_2} \quad K_{(\text{H}_2\text{CO}_3)} = \frac{[\text{H}^+][\text{HCO}_3^-]}{[\text{H}_2\text{CO}_3]}$$

$$K_{(\text{CO}_3^{2-})} = \frac{[\text{H}^+][\text{CO}_3^{2-}]}{[\text{HCO}_3^-]} \quad K_{(\text{CaCO}_3)} = [\text{Ca}^{2+}][\text{CO}_3^{2-}]$$

Equation 2.6 Derived equations for the calculation of $p\text{CO}_2$, SI(calcite) and equilibrium values of Ca^{2+} in a pH-buffered carbonate system.

$$p\text{CO}_2 = \frac{[\text{H}^+][\text{HCO}_3^-]}{K_{(\text{CO}_2)}K_{(\text{H}_2\text{CO}_3)}}$$

$$\text{SI}(\text{calcite}) = \log\left(\frac{\text{IAP}}{K_{(\text{CaCO}_3)}}\right) = \log\left(\frac{[\text{Ca}^{2+}][\text{CO}_3^{2-}]}{K_{(\text{CaCO}_3)}}\right) = \log\left(\frac{[\text{Ca}^{2+}][\text{HCO}_3^-]K_{(\text{CO}_3^{2-})}}{[\text{H}^+]K_{(\text{CaCO}_3)}}\right)$$

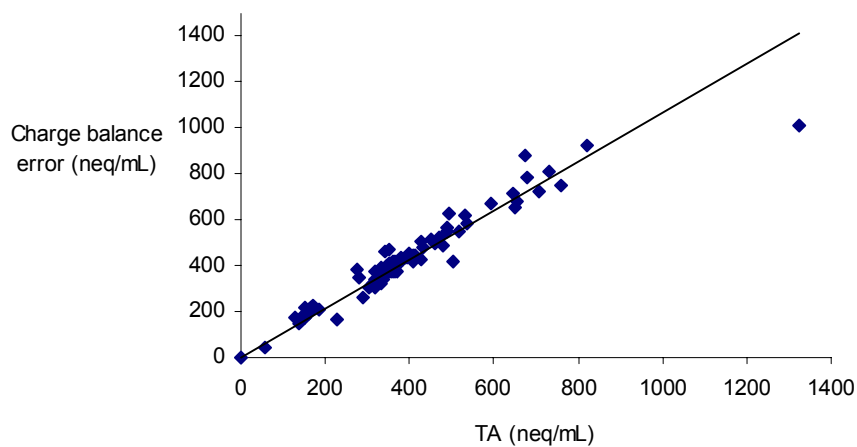
Table 2.7 Equilibrium constants for use in Equation 2.5 and Equation 2.6 (after Garrels and Christ, 1965).

Temp (°C)	pK ₁	pK ₂	pK _s	pK(CO ₂)
	-log K(H ₂ CO ₃)	-logK(CO ₃ ²⁻)	-logK(CaCO ₃)	-logK(CO ₂)
0	6.58	10.62	8.02	1.12
5	6.52	10.56	8.09	1.19
10	6.47	10.49	8.15	1.26
15	6.42	10.43	8.22	1.33
20	6.38	10.38	8.28	1.40
25	6.35	10.33	8.34	1.47

$$[\text{Ca}^{2+}] = \frac{K_{(\text{CaCO}_3)} [\text{H}^+]^2}{K_{(\text{CO}_3^{2-})} K_{(\text{CO}_2)} K_{(\text{H}_2\text{CO}_3)} p\text{CO}_2}$$

The calculated HCO₃⁻ values by titration alkalinity and charge balance errors were compared for 84 samples of various rock dissolution experiments (Figure 2.6). There is a good correlation between the values obtained via titration alkalinity and charge balance error. It is of note, however, that the slope of the relationship is slightly greater than one charge balance error unit per unit titration alkalinity (Equation 2.7). The discrepancy is within the statistical boundaries of error: the mean difference between the data sets is 9.1% ±10.1%. However, any systematic difference may be due to carbonate speciation (neutral species such as H₂CO₃^o and CaCO₃^o will not affect charge balance calculations but will affect titration alkalinity determinations), or may be due to the presence of unanalysed anions in solution such as F⁻ and PO₄³⁻.

Figure 2.6 Comparison of titration alkalinity with charge balance error calculations (n=84)



Equation 2.7 Observed relationship between bicarbonate determinations derived from charge balance error calculations and total alkalinity titrations ($r^2 = 0.89$)

$$\text{HCO}_3^- \text{ (by charge balance error)} = 1.07 \times \text{HCO}_3^- \text{ (by titration alkalinity)}$$

2.4.5 Determination of bulk rock composition by ICPMS and AA

Bulk rock chemical analysis of the material used in dissolution experiments, in addition to petrological descriptions of mineralogy, isolate the variability in solute provenance in the interpretation of dissolution results. This section describes the process of rock digestion and analysis undertaken on morainic samples.

2.4.5.1 Rock digestion

Samples of morainic rocks 1-9, a sample of “pure” morainic calcite from *Haut Glacier d’Arolla* (identified as “rock C” forthwith), and a “standard” sample of pyrite mineral (“rock P”) were selected for bulk chemical analysis. Mineralogical investigations of rocks 1-9 by petrography are described in Chapter 3.

Samples of rock to be analysed by AAS or ICPMS were prepared by total digestion in acids. Eleven rock and sediment samples were each crushed using a tungsten TEMA mill for 30 seconds, and 5g of each was measured out to an accuracy of within $\pm 0.0005\text{g}$. A blank sample was also prepared in the same method to check for contamination through the digestion process, identified as “Digest Blank”.

Each sample was placed in a 60mL PTFE beaker and treated with 5mL cold concentrated hydrochloric acid (HCl) overnight to digest carbonate material. 15mL cold hydrofluoric acid (HF) with 4mL perchloric acid (HClO₄) was then added and left for 24 hours to digest the remaining minerals. Subsequently the solution was evaporated to near dryness. Many of the samples retained undigested material by this point, so repeated treatments of HF and HClO₄ were undertaken. Some samples, namely rocks 1, 2, 5 & 7, persisted in having a black residue present, which may be tourmaline, kyanite/sillimanite, pyrrhotite, zircon or a titanium mineral such as anatase. To attempt to digest this material, 15mL concentrated HNO₃ plus 1mL concentrated H₂O₂ was added, with the samples heated slightly after 30 minutes, and left for a week. The heat was then increased until evaporation to dryness occurred. Some residue still persisted after this time.

20mL of MQ water and 5mL HNO₃ was added to each beaker and warmed. Then, the samples were individually filtered through Whatman No. 1 filter paper and made up to 100mL with water. The weight of the dried filter papers and beakers was recorded

afterwards to give an estimation of the weight percentage of undigested residue. These results are presented in Table 2.8.

Table 2.8 Digestion statistics of morainic rock samples.

Sample no.	Colour after 1 HF treatment	Colour after 2 HF treatments	Beaker residue (g)	Filter residue (g)	Total (%)
Rock 1	black	black	-0.0013	0.0746	14.67
Rock 2	black	black	0.0066	0.0480	10.92
Rock 3	white	clear	0.0050	0.1045	9.56
Rock 4	clear	clear	0.0073	0.0731	16.08
Rock 5	black	black	0.0108	0.0847	19.11
Rock 6	clear	clear	0.0161	0.0379	10.80
Rock 7	black	black	0.0063	0.0900	19.24
Rock 8	clear	clear	0.0049	0.0570	12.38
Rock 9	grey	grey	0.0035	0.1004	20.77
Rock P	yellow	clear	0.0073	0.0825	17.98
Rock C	clear	clear	0.0057	0.1334	27.78
Digest Blank	clear	clear	0.0121	0.0573	-

An average filter paper weight was obtained by weighing out six dry papers (mean weight: 1.5044g; Standard deviation: 2.7%). The large standard deviation was unexpected, and compromised the accuracy of these investigations to a small extent. Weighing the actual papers used for filtration prior to use would obviously have been preferable. Since the blank sample retained a residual weight of 0.694g, an equivalent of around 12% in the other samples, any percentage residues below 12% were rejected as error due to filter paper variation. As can be seen, residue percentages did not bear a close resemblance to the discolouration of the samples.

2.4.5.2 Atomic absorption spectroscopy

This method of analysis involves the vapourization of a liquid sample, so that non-excited atoms in the sample absorb electromagnetic radiation at characteristic wavelengths. The energy normally comes from a hollow cathode lamp. A different lamp is normally required for each element analysed, although some combination multi-element lamps exist. A particular signal is generated in response to the presence of that element. The instrument only reports changes in intensity, so calibration using three or more standards is required, which is too high to analyse minor, trace and highly adsorbed elements effectively in solution, but sufficient for major elements and bulk rock digest analysis.

Analysis for iron, calcium, magnesium, sodium and potassium was undertaken using atomic absorption spectrophotometry. Three lamps were used, one for Na and K, one for Fe and one for Ca and Mg. The digested samples, acidified with 5% HNO₃, were measured against five levels of standard solution (metal chloride solutions), at 0, 1, 3, 5 and 10mg/L. In many cases additional dilutions of the digestions had to be carried out. The detection limits of AA by

normal use is 10^{-6} to 10^{-7} M. The precision of this method is reported as $\pm 5\%$ (Brown *et al.*, 1994a). Results were adjusted into neq/mL; these are presented in Section 3.7.

2.4.5.3 Inductively-Coupled Plasma Mass Spectrometry

ICPMS is used to determine a large selection of minor and trace elements in a completely dissolved or digested sample without the need for multiple runs for different elements (Jarvis *et al.*, 1992; McLaren, 1992). The ICPMS was tuned to Indium (mass 115) until a response of above 10^6 hz was reached. An internal standard was utilised, which enables the correction for short- and long-term fluctuations in signal without the need for frequent quality control sample runs (Jarvis *et al.*, 1992). A 100ng/L ^{103}Rh internal standard was chosen, which is advantageous due to its central position in the mass range, its low concentration in most samples, its level of ionisation (~94%) and because it is monoisotopic (Jarvis *et al.*, 1992).

All digested samples were prepared by adding 5.9mL of Milli-Q deionised water and 0.1mL of rhodium internal standard to 4mL of sample, to make a 10mL analyte, immediately prior to analysis. These were prepared in polyester test tubes using automatic volumetric pipettes. To mix the solution, each tube was capped with a cut-square of unused clingfilm and shaken by hand.

A pre-prepared “all element” standard, containing 100ng/L of the elements listed in Table 2.9 was analysed before and after the sample run to monitor instrument drift. Each sample was analysed twice, with the average result calculated by the instrument computer. Between each sample, the instrument was flushed with a wash solution consisting of deionised water with 5% HNO_3 to prevent cross-contamination. All analysis runs lasted for between 30 and 45 seconds. The raw data was processed by correcting for instrument response of standards and samples, and converted to parts per billion.

*Table 2.9a Elements standardised by “all elements” standard during ICPMS analysis, in order of atomic number. * indicates elements that were analysed in 24 hour initial dissolution experiments only. ¹ indicates elements that were sometimes unstandardised.*

Li*	Mg*	Al*	Sc	V ¹	Cr ¹	Co	Ni	Cu	Zn
As	Rb	Sr	Y	Zr*	Mo	Cd	In	Sn	Sb
Te*	Cs	Ba	La	Ce	Pr	Nd	Sm	Eu	Gd
Tb	Dy	Ho	Er	Tm	Yb	Lu	Re*	Hg	Tl
Pb	Bi	Th	U						

Table 2.9b Elements analysed unstandardised or with unsatisfactory standardisation during ICPMS analysis.

Be	B	Ca	Ti	Mn	Fe	Ga	Br	Ag	I
W	Pt	Au							

The mean variation between all-element standards for both standardised and unstandardised elements within single runs is 11%, with a median deviation of 7%.

2.4.6 Determination of minor and trace elements in solution

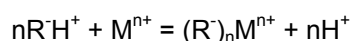
Numerous selected laboratory dissolution samples were analysed for a suite of minor and trace elements using ICPMS. The analysis required 9.7mL of each filtered laboratory sample, which was acidified using 0.2mL (2%) of concentrated nitric acid and 0.1mL (1%) rhodium reference spike solution. Set up of the instrument was carried out as described in Section 2.4.5.3. Calibration was carried out using a pre-prepared “all-element” standard, which contained 100ng/L concentrations of elements described in Table 2.9. This standard was run prior to and at the end of each suite of samples run (generally around 60-90 samples), to monitor instrument drift. Deviations were as for bulk rock analysis.

Table 2.10 illustrates that levels of certain species often do not exceed those of the “blank” determinations. These values must be taken sceptically, especially relationships between various values that do not exceed blank determinations. However, systematic variations can often be distinguished from contamination “noise”, so each case is treated individually, rather than to dismiss all sub-blank level determinations.

2.4.7 Determination of major ionic composition of meltwaters and experimental solutions by ion-exchange chromatography

Analyses for the major cations Ca^{2+} , Mg^{2+} , Na^+ and K^+ , and the major anions Cl^- , NO_3^- and SO_4^{2-} were carried out on a Dionex DX100 high performance ion-exchange chromatograph with separate anion and cation columns. Separation of species by ion exchange chromatography is achieved by the selective exchange of ions between a mobile phase and a stationary phase which has a higher and varying affinity for the ions to be separated (Equation 2.8) (Fifield, 1995).

Equation 2.8 Generalised ion exchange reaction for the cationic system, where R represents the stationary phase matrix, a styrene-divinyl benzene copolymer (Fifield, 1995)



The solution is then analysed for electrical conductivity over a period of minutes. Each ionic species has a sub-constant delay of release from the column under a constant flow rate, so that each species is identified by the release delay time (Fifield, 1995).

Eluents, pump rates, run length and calibration standards are different for anion and cation determination.

2.4.7.1 Anion determination

a) Equipment and eluent

Anion-exchange was achieved using an IonPac[®] AS4A-SC 4×250mm analytical column, composed of polyethylvinylbenzene/divinylbenzene aggregated with anion exchange latex. A precautionary guard column (IonPac[®] CG12A 4×50mm) was also used. A carbonate/bicarbonate eluent is used, which is less susceptible to CO₂(g) contamination than hydroxide eluent systems (DIONEX Corporation, 1992). Peaks are optimised by an anion self-regenerating suppressor (ASRS-Ultra 4mm).

Table 2.11 Anion-exchange chromatography operating parameters

Eluent type and strength:	0.1908g/L (1.8mM) sodium carbonate (Na ₂ CO ₃) + 0.1428g/L (1.7mM) sodium bicarbonate (NaHCO ₃)
Background conductivity	15-18 μS
Flow rate	1.5 mL/min
Injection loop volume	10 μL
Run time per sample:	9-10 min

b) Calibration standards

Three-level calibration standard solutions were used, generally at the following levels:

Table 2.12 Typical anion calibration standard levels

Anion	Level 1 (mg/L)	Level 2 (mg/L)	Level 3 (mg/L)
Cl	0.1	0.5	1.0
NO ₃	0.1	0.5	1.0
SO ₄	2.0	10.0	20.0

These were prepared using Analar salts KCl, KNO₃ and K₂SO₄ to make a stock solution of 100mg/L Cl⁻, 100mg/L NO₃⁻ and 2000mg/L SO₄²⁻, which was then diluted 1000, 200 and 100 times to make the three levels of standard.

2.4.7.2 Cation determination

a) Equipment and eluent

Cation-exchange was achieved using an IonPac[®] CS12A 4×250mm analytical column, which is designed specifically for the analysis of alkali metals, alkaline earth metals, and ammonium. A precautionary guard column (IonPac[®] CG12A 4×50mm) was also used. The stationary phase, consisting of weak phosphonic and carboxylic acids, has a high selectivity for hydronium ion, and utilises a low ionic strength eluent to isocratically elute mono- and

divalent cations relatively quickly (DIONEX Corporation, 1994b). Performance is improved by a cation self-regenerating suppressor (CSRS-I), which removes the eluent and hydronium ions after separation, so that conductivity analysis takes place in an electroneutralised solution (DIONEX Corporation, 1994a).

Table 2.13 Cation-exchange chromatography operating parameters

Eluent type and strength:	1.7mL/L methanesulphonic acid (CH ₄ O ₃ S)
Background conductivity	1.2-1.8 µS
Flow rate	1.0 mL/min
Injection loop volume	10 µL
Run time per sample:	13-15 min

The eluent was made directly from the concentrated acid without a stock solution. Suppression was carried out using self-regenerated eluent. Cations require a slower pump rate than anions to optimise peak separation, hence 1.0mL/min was used.

b) Calibration standards

Cation standards were generally prepared at the levels described in Table 2.14, depending on expected sample concentration.

Table 2.14 Typical cation calibration standard levels

Cation	Level 1 (mg/L)	Level 2 (mg/L)	Level 3 (mg/L)
Na ⁺	0.1	0.5	1.0
K ⁺	0.1	0.5	1.0
Mg ²⁺	0.1	0.5	1.0
Ca ²⁺	1.0 or 2.0	5.0 or 10.0	10.0 or 20.0

The standards were prepared using 1000mg/L Spectrosol solutions of NaSO₄, KSO₄, MgCO₃ and CaSO₄, to make a stock solution of 10mg/L Mg, Na and K, and 100mg/L Ca. This was diluted 100, 20 and 10 times to make up the calibration standards.

2.4.7.3 Dionex quality control

a) Calibration

Calibration standards were run prior and separately to the samples, to allow quality control of the standards to take place. The Dionex software package calculates the correlation coefficient of the calibration standards, and r² values less than 0.99 with a forced-zero linear regression were rejected. Blanks were also run prior to and subsequent to the standard run to check for contamination of deionised water, sample vials or the internal system of the Dionex

DX100. If the standard run provided satisfactory results, the standard schedule was run. The data was frequently checked for correct optimisation of the traces. Any samples falling outside the calibration range for any ion were rejected and re-run after dilution.

b) “Blank” determination regime

At least two “blank” samples were run at the beginning of each set of determinations. This acted as a confirmation that the system was uncontaminated, and was especially important after the changeover between columns to prevent contamination from the incompatible eluents or acidified samples affecting sample results. Blanks were also run at regular intervals between samples to ensure no contamination build-up was occurring. Figure 2.7 shows the extent of contamination blank determinations, excluding initial and post-column changeover samples, and shows that contamination is generally negligible in at least 99% of samples. Two blanks out of 75 were highly contaminated with K⁺, however. This has an effect on the interpretation of spurious experimental results, as potentially up to 3% of samples may have been contaminated with K⁺ prior to or during analysis.

Figure 2.7 Contamination of blank samples, excluding initial blank determinations. n=60 (anions), n=76 (cations). Results are sorted in order of concentration of each species, highest last.

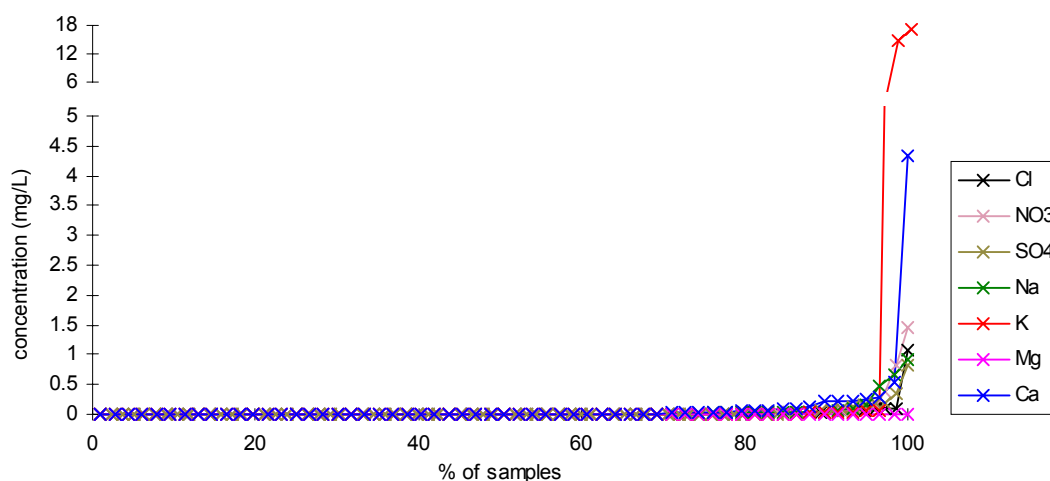


Table 2.15 Mean and standard deviations of anion and cation blank determinations by ion chromatography. n = 75 (anions), 57 (cations)

ion	Cl ⁻	NO ₃ ⁻	SO ₄ ²⁻	Na ⁺	K ⁺	Mg ²⁺	Ca ²⁺
mean	0.03	0.04	0.03	0.05	0.55	0.00	0.12
s.d.	0.13	0.20	0.11	0.16	2.93	0.00	0.57

c) Repeat standard reproducibility

Standards were frequently run between samples to check for reproducibility of analysis in long runs. Typically, a standard and a blank (deionised water) were run as samples with every 10 experimental or field samples. Table 2.16 shows the extent of deviation of the observed concentrations of standards run as blanks from the concentration of the same standard when run as a calibration level standard. It can be seen that the highest concentrated species (Ca^{2+} , SO_4^{2-}) show less deviation than the others.

Table 2.16 Accuracy of ion chromatography: percentage of standard determinations within 5% and 10% of calibration levels, and standard deviations from mean.

	% $\pm 5\%$	% $\pm 10\%$	standard deviation
Cl^-	83%	100%	0.07
NO_3^-	67%	88%	0.28
SO_4^{2-}	100%	100%	0.01
Na^+	96%	100%	0.05
K^+	84%	100%	0.07
Mg^{2+}	84%	96%	0.21
Ca^{2+}	100%	100%	0.03

d) Contamination monitoring

Numerous tests were carried out on vial cleanliness, between-sample contamination and water quality. These are summarised in Table 2.17. The tests showed that acid washing pre-used vials was preferable, although contamination was rare, and that Milli-Q stored in carbuoys should be replaced frequently. This was generally done after 2 days.

Changing columns produced contamination of the initial subsequent blank analysis with residual eluent from the alternate column. This peak coincided with Cl^- during anion

Table 2.17 Ion chromatography contamination monitoring tests .

Vial quality regime:	Contamination level
New, pre-cleaned vials and caps, Milli-Q water injected through filter cap	none
New, pre-cleaned vials and caps	none
New, uncleaned vials and caps	none
Pre-used, acid-washed and 3x Milli-Q vials and caps	none
Pre-used, 3x Milli-Q washed vials and caps	none-low
Water quality:	
Milli-Q water obtained directly from deioniser	none
Milli-Q water obtained from storage in carbuoy for 1 day	none
Milli-Q water obtained from storage in carbuoy for 7 days	none-low
Milli-Q water obtained from storage in wash bottle for 1 day	none
Milli-Q water obtained from storage in wash bottle for 7 days	low
Tap water	significant
Cross-contamination:	
Post-level 3 standard	none
Post-high concentration sample (off-scale)	low
Initial blank post-column change	high
Second blank post-column change	none

determination, but was prior to Na⁺ during cation determination. However, the second blank was never contaminated with eluent. Nevertheless, three blanks were run immediately post-column changes to reduce contamination risk.

Unusually high sample concentrations that produced off-scale results were shown to slightly contaminate the subsequent sample in some cases. To remove this effect, any samples that followed an off-scale result of any ion were re-analysed along with the diluted high-concentration sample.

e) *Repeat experiment reproducibility*

Ion chemistry reproducibility of repeat experiments is dependent on the homogeneity of material and the strictness of control of conditions. Condition controls employed, and remaining possible causes of experimental error, are summarised in Table 2.18.

Table 2.18(a) *Experimental quality controls*

Water Temperature	(see "Contamination monitoring" above) Water pre-chilled for at least 60 minutes. Steps taken to keep refrigerator ambient temperature as low as possible. Range 7°C ±3°C
Gas content of water	All water used in experiments pre-stirred under open-system conditions for 15 minutes prior to sediment addition

Table 2.18(b) *Possible compromises of reproducibility:*

Temperature Homogeneity	(see Table 2.18a) Experiments 7-14 used hand-crushed, rather than TEMA crushed sediment. Small quantities of relatively large grains are likely to produce more random errors than finer, mixed grains.
Gas content of water	Atmospheric conditions may effect the solution gas content

Reproducibility of experiments can not be determined by the simple comparison of individual results, because this assumes that time is the major determining factor in the magnitude of dissolution. The presentation and discussion of results in Chapter 4 therefore generally deals with each repeat individually, and variations are generally explained chemically rather than statistically.

2.5 PHREEQC GEOCHEMICAL MODELLING

2.5.1 Observations of trace metal speciation using PHREEQC

Interactive

PHREEQC Interactive (PhreeqI) is a graphical user interface for the geochemical water chemistry computer modelling package PHREEQC (Parkhurst, 1995; Charlton *et al.*, 1997), with the capability of using the MINTEQA2 speciation database within the same package (Allison *et al.*, 1990), which has an extended dataset involving more trace elements in comparison to the PHREEQE and WATEQ4F databases (Parkhurst *et al.*, 1980; Ball and Nordstrom, 1991).

Speciation modelling of various freshwaters and laboratory water samples were undertaken, using the MINTEQA2 database through the PhreeqI modelling package. This was carried out in order to understand the influence of speciation of elements on their chemical properties and affinities in the hydrological environment.

The following elements were available for speciation analysis using the MINTEQA2 database (elements with * are unavailable in the PHREEQC and WATEQ4F databases):

Ag*	Al	As*	B	Ba	Be*	Br	C	Ca	Cd	Cl
Cr*	Cu	Fe	Hg*	I*	K	Li	Mg	Mn	N	Na
Ni*	Pb	Rb*	S	Sb*	Sr	Tl*	U*	V*	Zn	

Speciation modelling was carried out on data from 24-hour duration closed-system dissolution experiments involving morainic rocks. An initial log p(CO₂) of -3.5, representing atmospheric equilibrium, was assumed. An example of the input file is shown in PHREEQC Input File 2.1 (see Appendix 1).

2.5.2 Mixing modelling using PHREEQC Interactive

The PHREEQC program also allows the modelling of theoretical mixing of waters, using the MIX command. This was used to test the chemistry of theoretical mixes between laboratory experiments. An example input file is shown in PHREEQC Input File 2.2 (see Appendix 1).

2.5.3 Dissolution modelling using PHREEQC Interactive

Dissolution modelling using thermodynamic data is also possible using PHREEQC, and was used to calculate equilibrium concentrations of the major elements in contact with the amounts of minerals. The “end member” experiments were simulated by modelling simple reaction between pure water and calcite and pyrite, as shown in PHREEQC Input File 2.3

(see Appendix 1). Morainic rock experiments were also simulated using the mineral proportions determined by petrological analysis (Chapter 3).

2.5.4 Inverse modelling using PHREEQC Interactive

Inverse modelling represents the reaction of an initial solution with minerals and gases to produce a second solution. The model calculates the amount of gases and minerals produced or consumed from the difference in concentrations between the two solutions (Parkhurst, 1995). However, there are a number of limitations to the application of this model.

1. The model requires the potential reactive minerals to be defined. Some knowledge of the reactive geology of the rock in contact with the fluid is therefore required. Since the model does not use thermodynamic data (i.e. log K values), phases additional to those already in the PHREEQC, MINTEQA2 or WATEQF databases can be added. These phases must be added in the form of a balanced reaction, however, as shown in PHREEQC Input File 2.4 (see Appendix). Solid solution minerals must be given an exact formula. In this study such data was not available, so an uncertainty exists.
2. The known solution chemistries must include all phases present in the minerals, and vice versa. Hence, minor phases within minerals can not easily be incorporated within the model without knowing the stoichiometry of the minor phases within each mineral. Also, if aluminosilicate minerals are involved in the model, solution Si and Al data must be entered. This data was not available in most of the experimental and field results of this study, but was overcome by entering a value from similar studies of meltwater chemistry and adding a 100% uncertainty proviso.
3. Attempts at inverse modelling between pure water and evolved water were not successful, so modelling the behaviour of laboratory experiments from time=0 was not possible. Generally, very small concentrations of elements cause problems for the model, and uncertainty allowances have to be high for successful calculations of most models at typical glacial concentrations.
4. The inverse model often produces multiple scenarios that can satisfy the evolution between the initial and final concentrations. Definite mineralogies cannot be ascertained in these circumstances, although it is a useful interpretative tool when bedrock geology is known.

An example of an input file for inverse modelling is presented in Appendix A, PHREEQC Input File A-4.

2.6 CONCLUSION

The suite of laboratory experiments encompasses many variables in the subglacial weathering system, with the main aims of investigating the importance of sulphide oxidation and carbonate dissolution, and solute provenance in the *Haut Glacier d'Arolla* catchment in particular. Many different rock types from the Glacier catchment are involved in the dissolution experiments under various conditions of access to atmospheric gases, acidity, residence times and specific mineral reactivity. All experiments are constrained by parameters obtained from field sampling and analysis as described in Section 2.5, and influenced by the geological investigations set out in Chapter 2. For the first time, data from field studies, laboratory experimentation and computer modelling involving both major and trace elements is combined giving a broad-ranged approach to the study of the geochemistry of glacial meltwater.

3. FIELD PARAMETERISATION

3.1 INTRODUCTION

Previous studies of glacial meltwater quality have suggested that the controls on solute acquisition are sedimentological, mineralogical, kinetic and hydrological (Chapter 1). Therefore, solute acquisition depends on the interaction of the solid, aqueous and gaseous phases (Table 3.1). Figure 3.1 shows the complexity of the hydrochemical system of an alpine glacier, with the following phase components

Table 3.1 Factors influencing the final composition of water draining a glacier, divided into phase components

Solid phase components:	morainic rock, snow, ice, bedrock, subglacial sediment, suspended sediment, dry deposits (aerosol)
Aqueous components:	precipitation, siderock runoff, supraglacial meltwater, groundwater, various components of delayed flow, englacial and subglacial quickflow, bulk meltwater, proglacial meltwater
Gas phase components:	atmospheric O ₂ , CO ₂ , SO ₂ , etc.
Other factors:	temperature, pressure, albedo, season (extent of evolution of hydrological network)

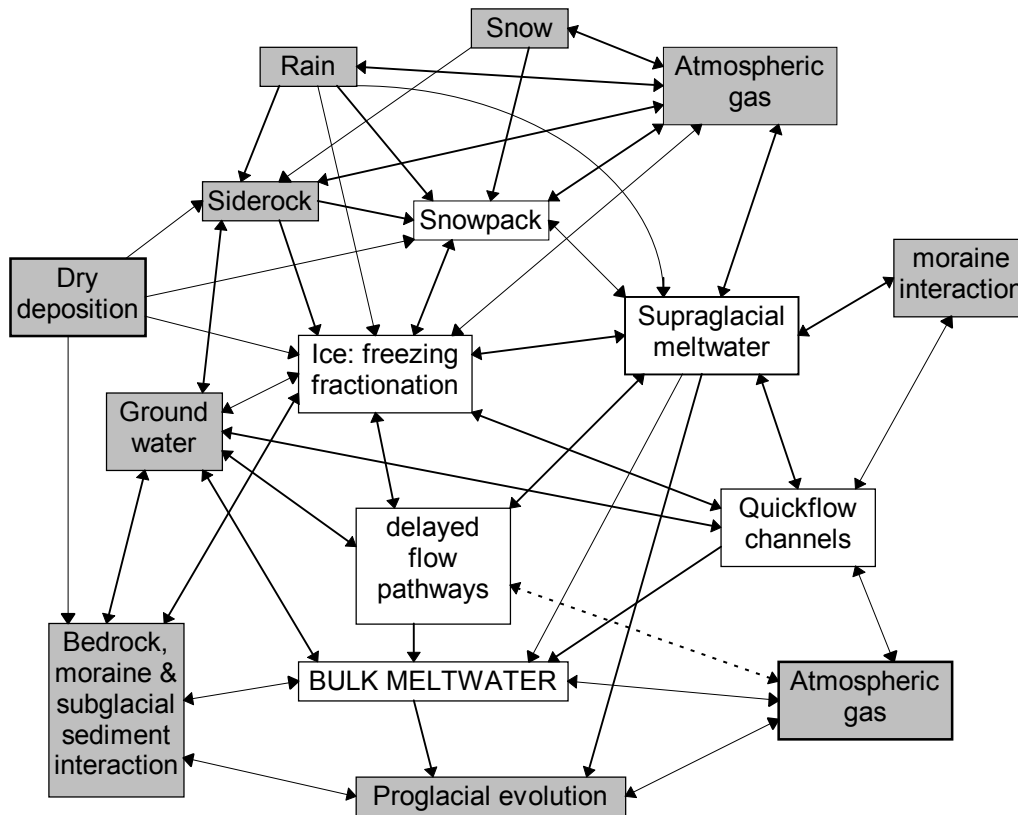
The complexity of the processes of solute acquisition in subglacial environments makes the correct parameterisation of laboratory simulation experiments paramount. Sediment type (mineralogy, grain size), rock:water ratios, residence times, access to atmospheric gases, temperature, diffusion rates, pH etc. must be equivalent to field data in order to have confidence in the applicability of laboratory results.

Steps were taken in this study to parameterise laboratory experiments for the following variables:

- a) sediment variability (geology and sedimentology of the catchment)
- b) solid phase chemistry (mineralogy and bulk chemistry of rock and sediment samples)
- c) the input solution properties (i.e. supraglacial meltwater quality, groundwater input)
- d) the output solution properties (i.e. bulk meltwater)
- e) gas phase dynamics

Field investigations of these variables were carried out in the latter part of the 1995 meltseason, period 28 July-26 August.

Figure 3.1 Schematic diagram of the glacial hydrochemical network. Each box represents a discrete solid, liquid or gaseous phase that may influence the meltwater output from an alpine glacier. Influences external to the glacier are shaded.



3.2 GEOLOGY OF MORAINIC AND ADJACENT ROCKS AT HAUT GLACIER D'AROLLA

Observations of geology were made at *Haut Glacier d'Arolla* to constrain spatial variations, and samples of morainic rock and sediment were collected for detailed chemical and petrological analysis.

3.2.1 Existing literature

There is little in the way of geological literature specific to the *Haut Glacier d'Arolla* catchment. The catchment is situated within the Arolla series of the Dent Blanche nappe, which consists of Arolla Granites, Arolla Gneisses and associated hornblende-biotite tonalites, hornblende-biotite-quartz diorites and gabbros (Brown, 1991). Brown's thesis identified the mineralogical composition of the major geological units based on thin section studies of fine (<5mm diameter) morainic material. The study noted considerable variations in the quantities of major minerals such as quartz, micas and calcite, but did not expand on

this. From the minerals identified and from mass-balance calculations following assumptions made by Holland (1978), it was suggested the potential sources of major cations in glacial meltwater were as shown in Table 3.2.

*Table 3.2 The potential major sources of major cations in glacial meltwater. * dolomite was not observed in morainic samples of Haut Glacier d’Arolla. † estimates of proportion of calcium and magnesium derived from the solution of carbonates in river waters (suggested by Holland, 1978).*

Calcium:	calcite/dolomite* (64-84%)†, epidote, hornblende, tremolite-actinolite, zoisite
Magnesium:	calcite/dolomite* (20-60%)†, olivine, pyroxene, hornblende, biotite, tremolite-actinolite, chlorite, magnesite
Sodium:	feldspars, micas, seasalt aerosol, halite fluid inclusions, concentrated films on grain surfaces
Potassium:	feldspars, micas

It was noted that sulphate minerals such as gypsum were absent in the fine material analysed (Brown, 1991). Therefore all dissolved sulphate in meltwater was assumed to be derived from the oxidation of pyrite. Bicarbonate dissolved in meltwater was assumed to be derived from either carbonation, carbonate dissolution or silicate/aluminosilicate dissolution (Table 3.3).

Table 3.3 The provenance of major dissolved species in glacial meltwaters

Dry deposition, salt dissemination in rocks, groundwater	1%
Sulphide deposits and disseminations	11%
Carbonate material	28%
Silicates	60%

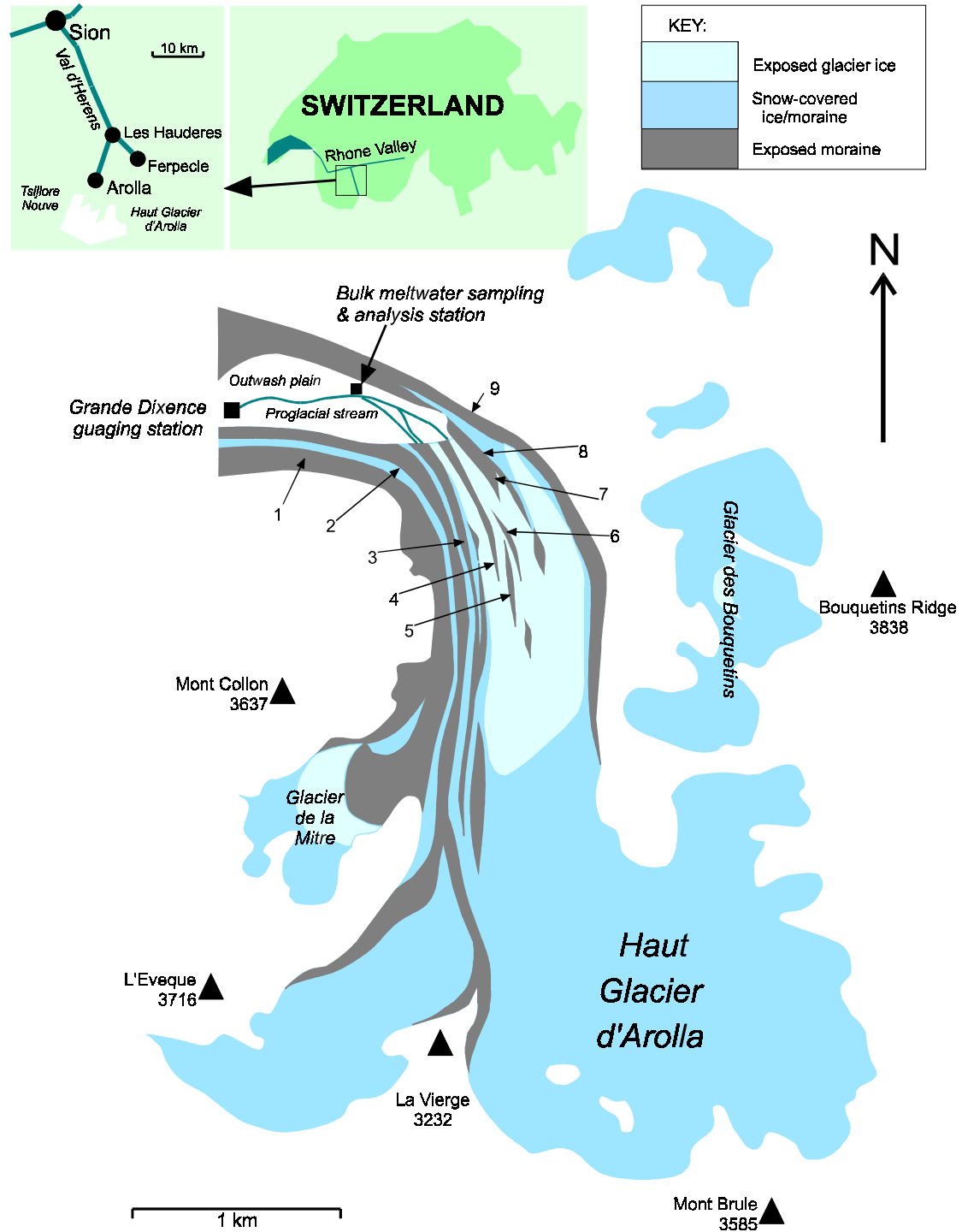
Details of the methods used in apportioning provenance assumptions to major ion concentrations is detailed in Table 1.3 (Chapter 1).

Spatial variations

A study of debris supply to the medial moraines of the *Haut Glacier d’Arolla* (Gomez and Small, 1985; Small, 1987) included some incidental geological observations, describing the lithology of the eastern moraine as “schists and gneisses, comparable to exposures on the western face of the Pointe Barnes-Pointe de la Grande Arete ridge”, and described the western moraine as “derived from the rapidly weathered schists on the flanks of La Vierge”. Small (1987) also described a debris band derived from basal ice and associated sediment from the Glacier de la Mitre on the western flanks of the *Haut Glacier d’Arolla* (Brown, 1991) identified schistose granite around the accumulation zone, chloritic schist and gneiss to the south-east of the catchment, amphibolites, chloritic schist and diorite/gabbro flanking

Mont Collon and amphibolites to the north-east, adjacent to the lower glacier. The major geological units in the glacier basin are shown in Figure 3.2.

Figure 3.2 Haut Glacier d'Arolla, based on the 1:200000 Geotechnische Karte der Schweiz, Sheet 3 (after Brown, 1991, Figure 5.3). Moraines are labelled according to the numbers assigned in Section 3.2.2, and their positions are based on the author's observations.



3.2.2 Field observations

Brief field observations of the types of rock present in each moraine across the lower glacier were made, traversing the glacier from west to east. This was carried out without mineral identification tools (dilute acid, streak plate, etc.), so the geological references could not be specific. For instance, the presence of marble-rich rocks (see Section 3) was misidentified as metapelitic material. Nonetheless, significant variations across the glacier were identified.

It can be seen that there is considerable spatial variation in rock type, and in particular the incidence of veining and abundance of oxide and sulphide minerals. The catchment as a whole is dominated by granites, metagranites, gabbros, marbles, many of which show schistose and gneissose metamorphism. Finer metapelites are less common but present particularly in the central and eastern moraines. Small (1987) suggested four main sediment accumulation zones on *Haut Glacier d'Arolla*:

1. Supraglacial lateral moraine material falling from Mont Collon (equivalent to part of moraine 1)
2. Medial moraine material from the intersection between *Haut Glacier d'Arolla* and Glacier de la Mitre, which is partially overwhelmed by the supraglacial lateral moraine (equivalent to part of moraine 1).
3. Medial moraine material from La Vierge, partially supraglacial and partially englacial in origin (equivalent to part of moraine 2 and moraine 3).
4. Medial moraine material of an englacial origin that forms sub-parallel ridges emerging 1km from the snout, formed by rock fall from the headwall in the main accumulation zone between La Vierge and Pointe Barnes and compressed into parallel longitudinal structures (equivalent to moraines 4-8).

The most pyritic rocks appear to be on the eastern and western lateral moraines with a provenance from Mont Collon and in particular the Bouquetins Ridge, with less pyrite present in the moraines with origins in the L'Eveque-La Vierge-Mont Brule area. Vein material is also more common in the lateral moraines. Pyrite is present in the calcite veins but also disseminated through some of the coarser metapelites.

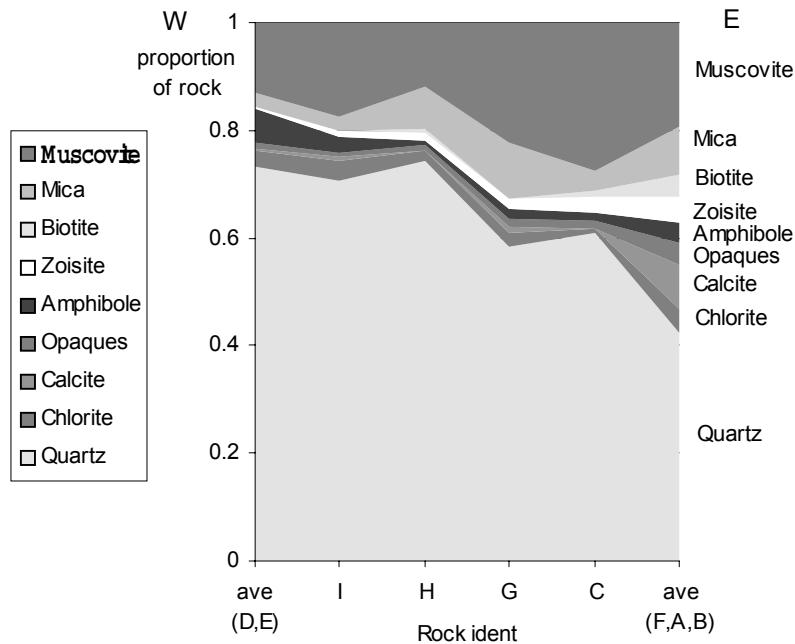
Table 3.4 Field observations of moraines on Haut Glacier d’Arolla. Moraine numbers are represented on Figure 3.2. The petrology of numbered rock types is described in Section 3.3.1.

Moraine	Description
1	<ul style="list-style-type: none"> Material from the col containing Glacier de la Mitre plus direct rockfall from Mont Collon Abundance of iron-stained, pyrite-rich, medium-grained rock (rock 4) consistent with red colouration of eastern face of Mont Collon Pyrite also present in vein material (dominantly quartz and calcite) (rock 8, rock 9) Other rock types: granite; coarse gabbros (rock 2); migmatite
2	<ul style="list-style-type: none"> Predominantly coarse metagranite with large plagioclase porphyroblasts (rock 6) - green colouration (attributable to amphibole or chlorite) suggests greenschist or amphibolite facies metamorphism (MacKenzie and Adams, 1993). Often muscovite-rich, some biotite-rich. Other rock types: medium-grained metagranite with large biotite grains; granite (rock 13) (some with xenoliths of the finer mafic material) Little evidence of iron staining except for a small amount on greenschist material on the east face of the moraine
3	<ul style="list-style-type: none"> Main rock types: greenschists; coarse plagioclase metagranites; granites Other rock types: finer metagranites with pink feldspar (rich in quartz veining) (rock 14) Metagranites often feature flat fracture plains and/or veins of a maroon-red mineral with polished appearance (possibly haematite) - more often on the finer examples, also occasionally on greenschists. Likely to be secondary, as flat surfaces are not rock-type specific, and do not follow the often highly convoluted banding between quartz- and mica-dominant layers of the finer-grained rocks Iron staining on rocks only a minor feature in this moraine - brown and red colouration of rocks due mainly to high biotite content of many granites and dark red veining on the other rock types
4	<ul style="list-style-type: none"> Minor moraine mainly composed of fine-medium grained, green metamorphic rocks - quartz veining common (rock 10) and disseminated pyrite made evident by oxidation products Thin band of highly iron-stained boulders along centre of the moraine - often quite rich in pyrite, mainly within fine veins Eastern side of moraine similar to Moraine 3 with examples of red vein-coated grey-green metaquartzite
5	<ul style="list-style-type: none"> Sparsely scattered moraine with some iron stained rocks of various types (source of the iron staining is unknown - no unweathered oxide minerals are visible) Dominant rock types: fairly coarse-banded gneiss with feldspar and mica layering (rock 17); darker, finer metapelite with quartz veining (rock 1).
6	<ul style="list-style-type: none"> Finely-scattered moraine dominated by coarse metagranite with plagioclase porphyroblasts similar to more western moraines, but highly fractured into flat surfaces, often with black metallic surfaces (rock 14).
7	<ul style="list-style-type: none"> Western face of southern section consists predominantly of highly fractured metagranite as Moraine 6 Eastern face also contains iron stained, quartz veined banded metapelite (rock 5) Northern section dominated by finer metamorphosed rock with quartz-rich layers intermixed with chlorite-dominated layers (rock 11)
8	<ul style="list-style-type: none"> Contains distinctly iron-stained material, with red-brown appearance both on the glacier surface and beyond the glacier snout in the proglacial moraine Dominant rock type: banded quartz/mica gneiss with pyrite often disseminated through the mica layers (rock 17) - fairly richly calcite veined, containing quartz and iron oxides Also significant amounts of metapelite (rock 5) - some display larger pyrite grains, often distorted by pressure into elongated (flattened) shapes.
9	<ul style="list-style-type: none"> Lateral moraine, contains same rock types as moraine 8, no distinction between moraines 8 and 9 in proglacial region.

Figure 3.3 shows that by rearranging the data of mineral proportions in the morainic sediment (Brown, 1991, Table 5.2) into transverse positioning of each moraine across the glacier, it becomes clear that the samples of the eastern moraines showed quartz levels that were generally lower than within the western moraine samples. Many other minerals showed the

opposite trend, with micas, zoisite, calcite, sphene and opaque minerals tending to be more concentrated in the eastern moraine materials. The difficulties of obtaining morainic sediment that shows a “representative” lithology for each moraine must be emphasised at this point.

Figure 3.3 Proportions of minerals in moraine samples of the Haut Glacier d’Arolla (adapted from Brown, 1991). Samples D and E are from Moraine 3, I from 4, H from 5, G from 6, C from 7 and F, A and B from Moraines 8 and 9.



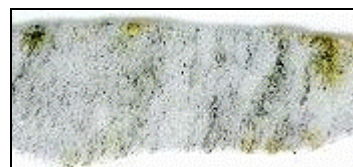
The observations of spatial variations of sulphide minerals across the glacier suggests that the extent of sulphide oxidation may be spatially variable in the subglacial hydrological network. Therefore, seasonal evolution of the hydrological network may not only affect the processes of solute acquisition due to alterations in residence times, access to atmospheric gases and rock/water ratios, but may also affect the nature of the rock which the meltwater encounters.

3.3 PETROLOGY OF MORAINIC ROCK

Examples of many of the rock types used for analysis (Chapters 2, 4), and some other rock types, were prepared in thin section for petrological analysis. Descriptions of rock 1-9, and seven other rocks, are presented here, including observations from hand specimen and thin section.

3.3.1 Bulk analysed samples

The following rock types were analysed in thin section, with bulk elemental analysis of digested samples also undertaken (Section 3.4). Thin section scans are shown above each description.



Rock 1: diopside marble

The rock displays a somewhat banded texture, giving an appearance resembling that of schistose rocks. On closer inspection this banding is only displayed by some alignment of opaque minerals and their oxidation products. The dominant observed mineralogy is as follows:

65%	Calcite	wide crystal size distribution. Crystals overgrow other minerals.
5%	Diopside (clinopyroxene)	broken porphyroblasts, some rather altered and embayed.
3%	Amphibole	smaller matrix crystals, sometimes elongate but with little orientation.
2%	Olivine	small crystals with irregular fracturing.
1%	Quartz	small granular crystals, mostly in patches (vein material), but also small amounts disseminated throughout the section.
<1%	K-feldspar	simple twinning and perthitic structures displayed. One crystal only.
2%	Opaque mineral	widely disseminated. A slight brown-red glow of some generally anhedral crystals in thin section indicates that these are possibly ilmenite or oxidised product of pyrite (haematite). Black streak indicates pyrite presence. Also a separate specimen of apparently the same rock type (not sectioned) contains very large pyrite crystals.
25%	Glaucophane/muscovite alteration zones	these zones are quite widely spread throughout the section. These zones contain relatively higher proportions of opaque minerals and haematite.



Rock 2: serpentinitised olivine gabbro

The rock is dark grey in colour, though with lighter grey crystals evident. This colour is due to a high ferromagnesian and opaque content, and due to the degree of serpentinisation. A loosely banded structure is displayed, particularly evident in the feldspars. Grain sizes are generally large, with plagioclase and olivine crystals up to 3mm in diameter. Weathered surfaces of the hand specimens show areas of iron oxidation, including deep red (haematite) and ochre yellow (limonite - hydrated iron oxide) areas. The composition is as follows:

40%	Plagioclase	rather irregular lamellar twinning. Mostly contain somewhat oriented hairline fractures that are infilled with an opaque mineral.
20%	Olivine	highly altered along irregular fractures to serpentine and an opaque mineral. In many cases the porphyroblasts are almost entirely serpentinised.
15-20%	Amphibole	both primary and secondary mineralisation is evident, as some has clearly grown around the porphyroblasts. Difficult to discern from clinopyroxene.
15-20%	Diopside	generally more highly serpentinised, and with less regular fractures than the amphibole, and with lower interference colours than the olivine. As with the olivine, some examples are very highly serpentinised.
<5%	K-feldspar	evidence of straining and fracturing creates irregular extinction.
<1%	Opaque mineral	oxidised, displaying deep red oxidised “haloes” in some cases.



Rock 3: quartz vein

The rock has an off-white, massive appearance, with orange-brown staining along the lines of all fractures, however small. Some grey staining is also evident. The overall mineralogy is as follows:

>99%	Quartz	dominated by small, interlocking crystals, although occasional crystals may reach up to around 0.5mm diameter.
<1%	Amphibole	secondary mineralization in fractures. Brown-green appearance, inclined extinction, 2nd order interference colours and approximately 50-60 cleavage where two are present.
<<1%	Calcite	a very small amount present, adjacent to opaque minerals in fractures.
<1%	Opaque minerals	mineralization along fractures, accompanied by “green” alteration of adjacent quartz, although this does not generally affect interference colours or structures. A very small amount of opaque microcrystals are disseminated through the unfractured sections of the section. In hand specimen, the form of the opaque grains on fracture surfaces is sometimes almost square (flat), suggesting pyrite mineralogy, although these grains seem to be almost totally oxidised to haematite.



Rock 4: Diorite

This rock is coarse grained, with a distinctly black and white appearance. However, many areas, weathered or freshly cut, show red oxidised discolouration. The rock is particularly identifiable on exposed surfaces, where the stubby black shiny crystals of pyroxene are most prominent. Deposits of what appears to be reprecipitated calcium carbonate are present in patches. The dominant mineralogy observed via thin section is:

70%	Plagioclase	medium to large crystals, which are about 25% altered, giving a somewhat mottled appearance in both plane and crossed polars. Carlsbad and lamellar twinning are both displayed.
10-20%	Diopside	low 2nd order interference colours, one good cleavage, light brown in plane polarised light. Lack of second cleavage makes it difficult to discern diopside from amphibole, although some crystals have extinction angles too high to be amphibole.
10-20%	Amphibole	also pale brown under plane polars; some examples show twinning, and lower extinction angles than pyroxene. A second type of amphibole, with much deeper brown colouration, is present as secondary (or late) mineralization: some of this shows a second cleavage. This mineral is present as the alteration product of clinopyroxene, and as an exsolution product between plagioclase and pyroxene crystals, representing about 20% of the total amphibole present.
<1%	Calcite?	present as some secondary, fine grained crystallization, which makes identification difficult, but the interference colours tentatively suggest calcite.
<1%	Orthopyroxene?	rounded, high relief “grains” with bright interference colours and straight extinction. Alteration has resulted in internal mottling.
1%	Opaque mineral	some grains are actually a translucent, deep red colour in thin section, suggesting that these are iron oxide (perhaps ilmenite, or haematite). Percolating oxidation staining spreads out from these grains. Some grains are up to 0.5mm in diameter, whilst some are narrow and elongated.

Rock 5: marble

No thin section was prepared for this rock, although the hand specimen suggests that it is similar to rock 1. However, rather more mica and amphibole/pyroxene is present in this rock. A high calcite content is confirmed by the overall softness of the rock.



Rock 6: metagranite mylonite

The rock displays a banded structure that could be described as cataclastic in thin section. The K-feldspar porphyroblasts are clearly relic phenocrysts from granitic material, and deformation metamorphism results in the spread of elongated mica crystals around the porphyroblasts. The rock sample showed haematite surface fractures, indicated by a deep red streak and a hardness between that of steel and quartz. This was not present in the thin section, however. Minerals present included:

45%	K-feldspar	present both as porphyroblasts and as smaller matrix grains. The somewhat patchy extinction and twinning patterns in thin section are perhaps more characteristic of cordierite, but the pink colour of the blasts in hand specimen suggests that these are K-feldspar. Carlsbad twinning is evident. Occasional evidence of a rhombic cleavage suggests that the variety adularia may be present. Maximum size of around 2mm by 1.5mm.
40%	Quartz	dominates the matrix. Some grains are elongated in the pressure direction (indicated by the mica foliation).
15%	Mica	very aligned, some is concentrated in distinct layers, although this is not exclusive. Colour varies from pale brown to white, so both biotite and muscovite may be present.
<1%	Calcite	not widely distributed, this appears to be secondary mineralization.
<<1%	Rutile/haematite?	deep red grains with very high relief.

Rock 7: graphitic shale

The rock has a very greasy, graphitic texture and readily deposits graphite. The streak is also graphitic, but the rock is not purely graphite, as some minerals cut into, and are therefore harder than, calcite (pencil graphite does not do this). This rock was not suitable for preparation into thin section. The presence of this rock in the catchment is rare and highly localised (location of origin unknown).

Rock 8: quartz vein

This rock was not sectioned, as it is very similar to rock 3. The rock is often orange-brown stained due to oxidisation, and pyrite is visible, and has a black streak. Some calcite is also present, identifiable by hardness. A small amount of wallrock material, which went through to bulk rock analysis, contains dominantly pyroxene or amphibole, and rather resembles rock 2.

Rock 9: calcite vein

This rock is a fairly pure calcite vein, with small amounts of quartz present. A small section of wallrock was left on the sample, which consists of feldspar and pyroxene or amphibole, with some mica/chlorite also present.

3.3.2 Other rock samples

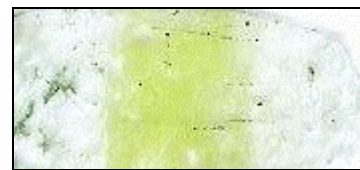
These rock descriptions are included to show that the rocks chosen for analysis are by no means an entire representation of the catchment geology, which is very diverse.



Rock 10: Fault zone metagranite?

The rock contains massive white/colourless bodies of quartz and chlorite-rich sections. Grains often appear rather brecciated, with the spaces between grains infilled with a fine matrix, which could suggest a sedimentary origin, but the feldspar presence suggests otherwise. Hence, the brecciated appearance may be due to high physical pressure upon a microgranite. Alternatively this may be an intrusive sill or dyke. Mineral descriptions are:

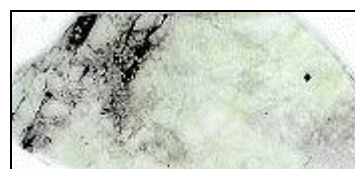
45%	Quartz	generally rather small crystals with uneven extinction patterns. Very small grains are present around the pyrite (see below).
40%	Feldspar	small crystals of plagioclase, with very fine lamellar twinning, and larger K-feldspar and plagioclase phenocrysts/porphyroblasts. Very fine lamellar twinning in the plagioclase is only visible at high magnifications. The phenocrysts generally have rather rough edges, and have fine inclusions along fractures that are mainly filled with quartz and the fine matrix material (see below). Some fine grained microcline is present around the pyrite.
10%	Chlorite	fine grained matrix material. Foliated. Occasionally associated with decaying plagioclase. Green in plane polarised light and in hand specimen. Bright interference colours and straight extinction.
<<1%	Rutile/Fe-tourmaline?	pleochroic, light-dark brown, very high relief. Pseudo-hexagonal. Some zoning. Small and not common, hence difficulty in identification. Usually associated with secondary mineralogy.
5%	Opaque mineral (pyrite?)	large isolated patch of crystals covering an area of about a square centimetre. The mineral is about the same hardness as steel, has a metallic lustre and has a black streak. Although it does not have the “foolsgold” appearance of some pyrites found in the catchment, this example is harder than galena, has the wrong streak colour for sphalerite or chalcopyrite, and has similar streak and hardness properties to more obvious pyrite crystals tested.



Rock 11: Layered chloritic metagranite/pegmatite?

This rock has two distinct textures; the first resembles the more chloritic sections of rock 10, although with a larger, pegmatitic grain size, whereas a central band varies between grass green and quartz-rich (colourless). There is a suggestion of a platy alignment of chlorite in the “pegmatite” layer, which is transected at about 40° by the grass-green, finer grained layer. There are uneven boundaries between the two layers that strongly indicate this transection angle. Minerals are as follows:

40% (coarse layer) 30% (fine layer)	Quartz	large grains in the coarse layer; small, sometimes aligned grains in the fine layer.
50% (coarse layer) 10% (fine layer)	K-feldspar	large and very large, sometimes poikilitic crystals with chlorite and quartz inclusions.
10% (coarse layer) 60% (fine layer)	Chlorite	secondary mineralization between quartz and feldspar grains, sometimes covering large areas. In the central band this mineral dominates, with no sign of a ghost mineralogy. This gives an intrusive appearance. Often associated with fine grained quartz.



Rock 12: highly altered metaquartzite

This rock is dominated by quartz, but is highly mineralized by calcite, pyrite and haematite, which is very distinctive, appearing to form a matrix between brecciated fragments of quartzite which also contain chlorite, giving them a green appearance. This feature is less obvious when observed through the microscope, where the haematite appears to occupy a network of veins. Weathered surfaces of the hand specimen show characteristic orange-brown oxidation staining. Mineral relationships are described below:

80%	Quartz	generally small grained.
3%	Calcite	patches in various sections of the section, and has the largest grain size of the minerals in the section. Mainly associated with the haematite veining.
12%	Chlorite/biotite?	green-brown in plane polarised light, with variations between these two colours, some may be biotite. Both have high relief and second order interference colours, somewhat masked by the strong pleochroism.
<<1%	Pyrite	a small number of crystals present on the slide, one of which displays a good parallelogram form.
<<1%	Amphibole?	fine grained with high relief and bright interference colours, but show one cleavage and inclined extinction, in contrast to the chlorite with straight extinction.
up to 5%	Haematite	difficult to quantify in thin section as some is ultrafine grained, with grains only distinguishable at 400 times magnification, appearing as staining at 40 times magnification. Widely spread through the slide, larger grains (or aggregates) may show opaque quantities, whereas more isolated and smaller grains are translucent, deep red. The streak is deep red from this mineral.



Rock 13: granite

This coarse rock is dominantly siliceous and does not show the foliation or degree of alteration found in the metagranites examined above. However, feldspars are highly altered throughout the specimen. Mineral proportions are as follows:

30%	Quartz	
20-25%	Unaltered K-feldspar	has the appearance of microcline, although the presence of rhombic sections may suggest adularia.
40%	Alteration product of K-feldspar	very fine grained, bright interference colours. No banding.
5-10%	Biotite	hand specimen clearly shows large brown biotite layers.



Rock 14: haematite-infiltrated metagranite

This rock has similar appearance to rock 12, but contains significantly higher amounts of K-feldspar, which are observed in hand specimen as pink porphyroblasts. The sample is very heavily brecciated by haematite, which forms the coating of two flat surfaces on the rock sample. The haematite on this surface often portrays a metallic lustre and iron grey colour, though is dull red elsewhere. However, a dull red streak is obtained from areas of both lustre type showing that it is likely that it is all haematite, rather than graphite or galena, both of which it resembles in places. The mineralogy is as follows, although some of the matrix is too fine to distinguish mineralogy:

40-50%	Quartz	remnants of larger crystals are present, but most appear rather “smashed” into smaller fragments.
40-50%	K-feldspar	remnants of larger crystals are present, but also mainly fragmented appearance. K-feldspar consists of both microcline and sanidine (perhaps adularia).
2%	Calcite	generally small grains, associated with haematite-filled fractures.
~5%	Haematite	appearance as in rock 12.

Rock 15: metagranite

Another variety of metagranite, the mineralogy of this sample is similar to previous examples, but the appearance throughout the sample (weathered and freshly-cut surfaces) is particularly rusty-orange in colour. However, the overall texture is less altered than many of the metagranites examined here. The mineralogy is approximately 50% strained quartz and 50% microcline, with an accessory mineral that is pale brown, with very high relief and intermediate interference colours (pink to black). This may be zircon. Iron oxides, perhaps ilmenite, are also disseminated through the slide.



Rock 16: metadiorite

This rock shows a fairly similar texture to rock 6 in thin section, with some mica banding and a similar crystal size distribution. However, the appearance in hand-specimen is more felsic, with light green, colourless and orange-pink minerals dominant. The texture could not be described as cataclastic, as deformation is of a lower degree to rock 6. The dominance of feldspar over quartz in the sample makes the composition more dioritic than granitic.

Mineralogy is as follows:

~70%	K-feldspar	a strong 80-85° cleavage is displayed on some porphyroblasts. Both cross-hatch twinning and perthitic texture are displayed in the section, although the porphyroblasts are dominantly microcline. Some simple twinned K-feldspar (sanidine/adularia) is also evident.
10-15%	Plagioclase	small grains only, showing lamellar albite twinning.
10-15%	Quartz	again, only present in the matrix.
3-5%	Chlorite/biotite	high relief, slightly pleochroic (brown/green), bright interference colours, ~60° cleavage in basal sections; hence difficult to categorically define as chlorite over amphibole. However, straight extinction is displayed.
2-5%	Opaque mineral	sometimes present in strained cracks, associated with chlorite. Some cracks contain voids. Occasional red glow in thin section suggests these are iron oxide.

Rock 17: Felsic schist

This common rock type was not sectioned or analysed, but is quite distinctive in hand specimen as a strongly foliated rock, with quartz-rich layers of between 0.5 and 2mm separated by chlorite/mica-rich layers that are generally much thinner. Some examples of this rock type show significantly folding, whereas others are not. Both layers contain some evidence of oxidation, and finely-disseminated iron oxides are visible with a hand lens. Although approximate, the rock is likely to be 70-80% quartz ± feldspar, 20-30% mica/chlorite.

3.3.3 Summary of petrological investigations

The analysed and other rocks that have been described petrologically above are summarised in Table 3.5.

Table 3.5 Summary of petrology of moraine rock samples from Haut Glacier d'Arolla.

Sample	Rock type	Qz	Fsp	APO	Cc	Op/Ox	Oth.	Moraine #s
Rock 1	diopside marble	1	<1	10	65	2	25	5 7 8 9
Rock 2	serpentinised olivine gabbro	-	~45	~55	-	<1	-	1
Rock 3	quartz vein	>99	-	<1	t	<1	-	all
Rock 4	diorite	-	70	30	<1	1	-	1
Rock 5	marble	carbonate-rich mineralogy						7 8 9
Rock 6	metagranite	40	45	-	<1	t	15	2
Rock 7	graphitic shale	unknown mineralogy						-
Rock 8	quartz vein	>95% quartz, + pyrite + calcite						1
Rock 9	calcite vein	>90% calcite						all
Rock 10	metagranite	45	40	10	-	5	-	4
Rock 11	metagranite	~35	~30	-	-	-	~35	7
Rock 12	metaquartzite	80	-	t	3	<5	12	GdB
Rock 13	granite	30	~23	-	-	-	~47	2
Rock 14	metagranite	~45	~45	-	2	~5	-	3 4 6
Rock 15	metagranite	~50	~50	-	-	t	-	
Rock 16	metadiorite	~12	>80	-	-	~4	~4	
Rock 17	felsic schist	>70	P	-	-	<1	>20	5 8 9

Abbreviations: Qz: quartz; Fsp: total feldspar; APO: total amphibole+pyroxene+olivine; Cc: calcite; Op/Ox: total opaque/oxide minerals; Oth.: other minerals, i.e. mica, chlorite and non-opaque alteration products (e.g. serpentine, kaolinite). Values are approximate percentages present in thin sections, so are only rough guidelines. 't' means trace amounts (<<1%) were observed. Where thin sections were not prepared, 'P' means that significant amounts of the relevant mineral were present. Moraine #s refers to the moraines where each rock type may be found, but is not exclusive, as a comprehensive moraine survey was not carried out. GdB means 'Glacier des Bouquetins'.

The analysis of unreacted morainic rocks presented here gives a new insight into the reactive chemistry at *Haut Glacier d'Arolla*. Although at first glance the geology of the *Haut Glacier d'Arolla* catchment appears to be dominated by regionally metamorphosed granites, diorites and gabbros, this section shows that the small-scale geology is very varied, including an abundance of hydrothermal mineralization, sulphide mineralogy of up to ore-grades, metamorphosed carbonate sediments, and abundant secondary products of metamorphism, diagenesis, mineralization and oxidation. These are often the most reactive parts of rocks, and as such may be dissolved more readily than the major constituents.

Previous studies had analysed and utilised proglacial sediment that had passed through the subglacial network and was therefore at least partially weathered, and therefore depleted in the most reactive mineralogy. Table 3.6 shows how the 1989 sediment is relatively depleted in mobile elements, such as Ca & Na, and reactive minerals, such as feldspar, pyroxenes and carbonates. Contrastingly, it is relatively enhanced in insoluble elements such as Mg & Fe, weathering-resistant minerals such as amphiboles, quartz, sphene etc., and weathering

products (sheet silicates/clays). The proglacial sediment is clearly a weathering product, causing systematic errors in determination of provenance and mineral reactivity.

Table 3.6 Comparison of mean mineral and metal content of proglacial sediment collected in 1989 (Brown, 1991) and morainic rocks collected in 1995 (this study). 1989 metal content is derived from mineralogical observations. 1995 metal content determined from analysis of digested rock samples (see Section 3.4).

Mineral / element	Mean & error of occurrence (1989 proglacial sediment) (%)	Mean & error of occurrence (1995 morainic rocks) (%)
Quartz	54±14	37±31
Feldspar	2±2	31±25
Pyroxene	2±3	8±20
Amphibole	3±2	3±6
Olivine	-	2±6
Layer silicates/clays	30±15	12±16
Carbonate	3±4	6±19
Opagues/oxides/restite	6±7	2±2
Ca	4.7±4.8	9.3±10.3
Na	0.2±0.1	3.5±7.5
K	4.1±1.2	2.2±1.7
Mg	5.2±2.7	0.6±0.6
Fe	5.7±3.2	1.4±1.3

It is possible that much of the solute acquisition in meltwaters draining this catchment may be affected by the accessory, vein and secondary minerals, as well as feldspar. In the inefficient hydrological pathways that are thought to exist in the subglacial distributed meltwater flow environment, these extremes of geology are potentially important contributors to total dissolved load of meltwaters, if medium to long term reservioring of metlwaters at the ice-bedrock interface takes place.

3.4 MORAINIC ROCK COMPOSITION: BULK ANALYSIS

The methods of rock digestion and analytical techniques are described in Chapter 2: the rock digestion procedure is explained Section 2.4.5.1; the analysis technique for Na, K, Mg, Ca and Fe by atomic absorption spectrometry is detailed in Section 2.4.5.2 and the method of analysis for other species by ICPMS is described in Section 2.4.5.3. The results of ICPMS and AA analyses of moraine samples described in Section 3.3 are summarised in Table 3.7.

3.4.1 Element abundances in moraine rocks: an overview

Figure 3.4 shows the concentrations of the analysed components in the morainic rock samples, pyrite and calcite. Distinct chemistries of the rock types can be discerned: rocks 1, 5 and 9 are highly calcic, with rocks 1 & 5 containing around 5% other cations, with Fe the

second most abundant analysed cation. Rock 8 shows a similar trend, but contains only 8% analysed material suggesting a dominance of silica.

Table 3.7 Standardised bulk analyses of moraine samples from Haut Glacier d'Arolla. Major elements (Na, K, Mg, Ca, Fe) were determined by atomic absorption; all other elements were determined by ICPMS. Results are expressed to 3 significant figures.

Rock:	1	2	3	4	5	6	7	8	9	P	C
Element	ppm										
Na	8000	14300	21600	23300	2730	31600	888	5020	2190	188	260
K	11500	22000	50100	38600	9580	22500	39800	4580	690	0	0
Mg	7700	15100	239	2560	5910	4150	15400	2160	1010	53	0
Ca	215000	32000	835	1380	200000	8510	55800	61400	265000	907	360000
Fe	16000	38000	0	6000	16000	9000	33000	3600	3600	444000	0
Co	22.6	13.7	23.6	19.3	12.2	13.9	13.8	18	7.95	0.15	5.42
Ni	53.5	66.3	5.5	10.2	62.5	21.5	123	18.3	40.3	33.8	34.5
Cu	17.4	25.2	4.54	7.35	24.3	6.38	40.3	10.8	7.76	301	3.94
Zn	61.4	131	17.6	42.3	62.8	39.2	142	104	11.7	688	3.62
Rb	59.9	116	157	197	45.3	99.5	186	19.1	6.06	0	8.22
Sr	2570	809	17.5	28.9	3540	79.6	1350	409	2500	5.78	2860
Ba	404	837	247	250	229	351	1290	134	23.6	2.06	2.61
Pb	6.15	10.2	9.66	4.9	9.1	2.42	23	30	5.25	1870	3.76
U	3.37	1.84	0.86	3.26	3.68	1.72	2.21	0.21	0.25	11.3	0.01
Total %	28.4	17.2	7.47	8.21	26.6	8.95	20.2	8.48	28.3	83.8	36.6
Element	unstandardised analysis result										
Ti	165	367	12.5	39.5	190	73.5	618	45.6	108	3.88	77.9
Fe	22100	47200	1810	9140	27200	12600	51900	7010	6770	390000	2350

Rocks 3 and 4 are dominated by sodium and potassium, but again may be dominantly silica. Rock 6 is dominantly sodium, but contains slightly more calcium, iron and magnesium than rocks 3 and 4. Rocks 2 and 7 contain all major cations in significant amounts, although sodium is nearly absent from rock 7. A maximum of 27% of the total rock content of the moraine samples is analysed using ICPMS and AA techniques (Figure 3.5). The unanalysed chemistry of the rocks is likely to consist predominantly of silicate, aluminium, carbonate and sulphur (as sulphide), with other minor constituents not analysed including sulphate, hydroxide, fluoride, phosphate, chloride, elemental carbon and water. On average, only 0.2% of the rocks consist of analysed trace elements (Figure 3.5). However, a wide range of mineralogy is represented by these samples, so that rocks dominated by minerals of all the major cations are investigated. This is especially useful in determining the provenance of trace elements in the Arolla catchment.

Figure 3.4 Concentrations of major and trace elements in morainic rock samples (rocks 1-9), and pyrite and calcite.

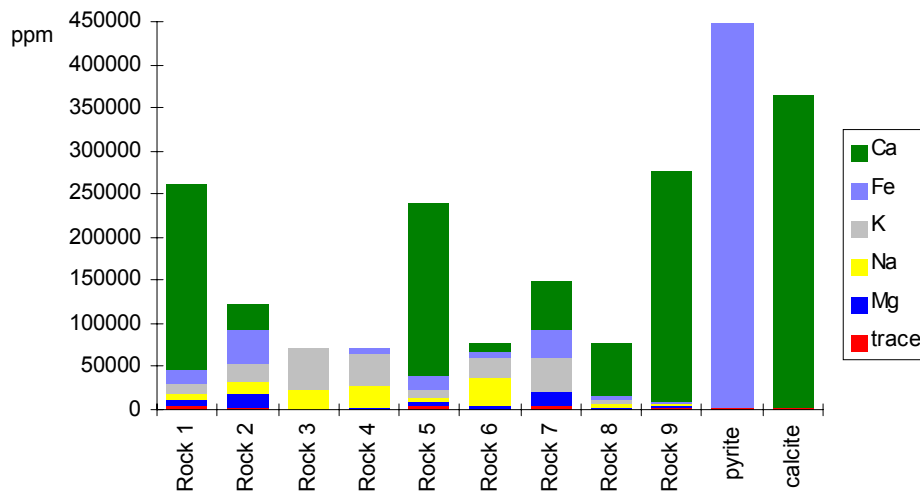


Table 3.8 and Figure 3.6 show the mean abundances of major and trace elements in the sampled moraine material, pyrite and calcite. These show that the most abundant elements other than Ca, Mg, Na, K and Fe in the morainic rocks are Sr, Ba, Ti, Zn, and Rb. The Rare-Earth element cerium (not shown), was more abundant than copper, cobalt, nickel, lead and uranium. Sodium, potassium, magnesium, nickel, cobalt, rubidium and barium are most concentrated in morainic rocks, whereas iron, copper, zinc, lead and uranium are more concentrated in pyrite, and calcium and strontium are most concentrated in calcite.

Figure 3.5. Relative abundances of major and trace elements in morainic rock samples (Rocks 1-9).

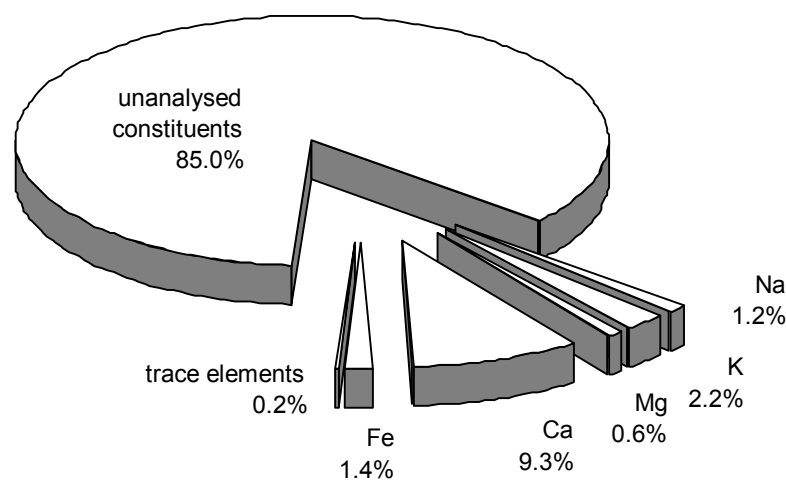


Figure 3.6. Relative mean abundances of elements in moraine rock samples, pyrite and calcite.

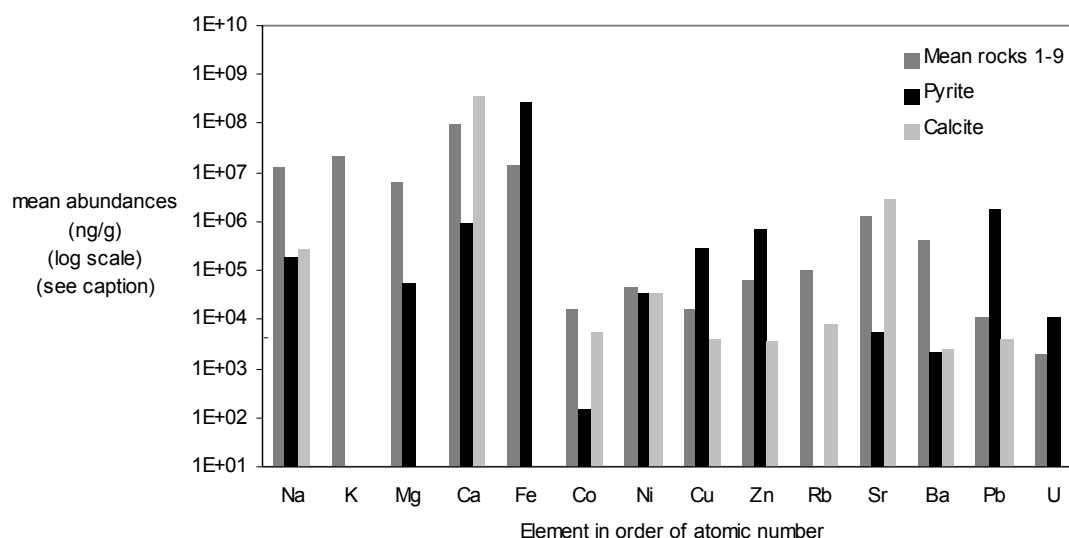


Table 3.8. Mean values for individual elements (mg/kg) in Rocks 1-9, and overall mean (also including pyrite and calcite), rounded to 3 significant figures.

(mg/kg)	Na	K	Mg	Ca	Fe	Ti	Co	Ni	Cu	Zn	Rb	Sr	Ba	Pb	U
Mean moraine	12200	22200	6020	93300	13900	180	16.1	44.6	16	67.9	98.3	1260	418	11.2	1.93
Overall mean	10000	18100	4930	109000	35300	155	13.7	42.7	40.8	118	81.1	1290	342	180	261

Table 3.9 shows that there is little correlation between the major elements in the samples analysed, except for iron and magnesium which are closely correlated. Calcium and magnesium clearly have at least partially different rock sources, in contrast to many studies which assume a carbonate source for both. This may be a reasonable assumption in carbonate catchments [e.g. Fairchild, 1994 #51], but is not the case at *Haut Glacier d'Arolla* [Brown, 1998 #110].

It would appear that in these samples calcium is largely mutually exclusive to sodium and potassium. The most siliceous rocks generally display the lowest total cation content (Figure 3.4), and these rocks generally display the highest relative sodium content. It may be coincidental, therefore, that the rocks in these experiments show a general mutual exclusiveness of sodium and calcium, because there are a number of carbonate-rich rocks analysed here, which generally have low sodium content. However, if these rocks are representative of the overall provenance of the catchment of *Haut Glacier d'Arolla*, then the use of ratios between sodium and calcium may be a useful indicator of lithogenic provenance variations.

Table 3.9. Correlation matrix between incidence of major elements in morainic rocks of the Haut Glacier d'Arolla. With 11 samples and therefore 9 degrees of freedom, the $P < 0.05$ level of confidence of a significant correlation is approximately 0.60.

Element:	Fe	Na	K	Ca
Na	-0.38	-	-	-
K	-0.01	0.40	-	-
Ca	0.10	-0.63	-0.63	-
Mg	0.99	-0.45	-0.03	0.10

3.4.2 Interpretation of the relationships between major and trace elements in the morainic rocks of Haut Glacier d'Arolla

Table 3.10 shows the main correlations between the major elements and trace elements. Whilst this shows at first glance which elements are most abundant in the rocks rich in each of the major elements, it does not begin to describe the mineralogical provenance of the trace elements. The following section describes in detail the relationships between selected analysed elements based on the theoretical associations described in Section 1.5 and summarised in Table 1.18.

Table 3.10. Correlations between major elements and selected trace metals in morainic rocks of the Haut Glacier d'Arolla. Only correlations over the significance level of 0.60 are shown.

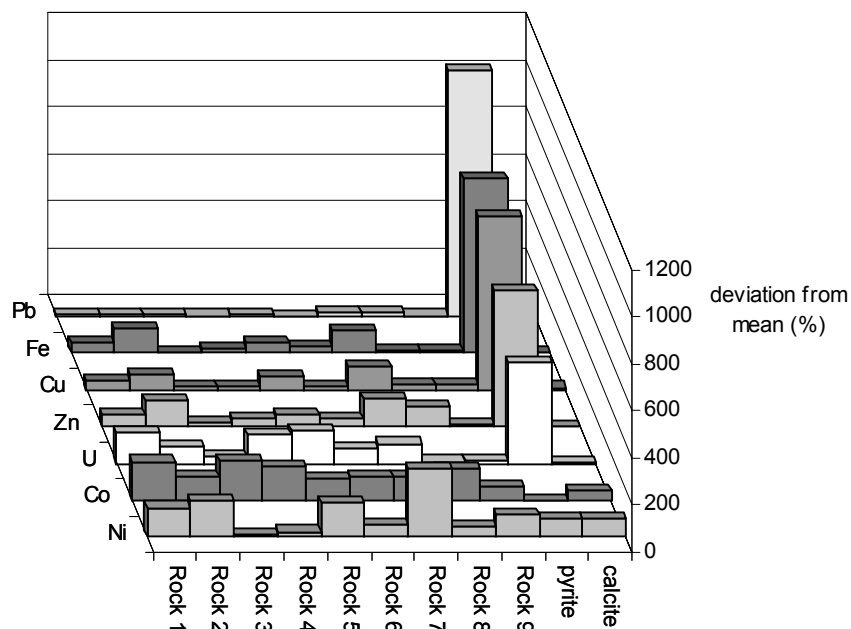
Major element	Trace element	Correlation
Fe	Ti	0.90
	Cu	0.82
	Ni	0.89
	Zn	0.82
	Ba	0.87
Mg	Ti	0.94
	Cu	0.91
	Ni	0.93
	Zn	0.88
	Ba	0.91
Ca	Sr	0.93
Na	no significant correlations	-
K	Rb	0.92

a) Elements associating with pyrite

The relative abundances of elements with relatively enhanced concentrations in the pyrite sample, compared with their abundances in the other samples (Figure 3.7), gives a measure of the affinity of each element to the sulphide phase. Iron shows an expected affinity for pyrite, although lead is relatively depleted in the other rocks even compared to iron. This shows that lead is exhibiting a greater affinity for sulphur than iron in these samples. The relative

affinity for pyrite is progressively diminished in copper, zinc and uranium, although their abundance is much higher in pyrite than in any of the morainic samples.

Figure 3.7 Relative abundances of lead, iron, copper, zinc, uranium, cobalt and nickel, expressed as % deviation from overall mean (see Table 3.8).



In the moraine samples, there are distinct variations in the abundances of these elements. Iron, zinc and copper show the largest concentrations in rocks 7 and 2, although they also show significantly high values in 1 and 5. Zinc and iron may exist in oxides such as magnetite and ilmenite, and iron and copper may exist in ferromagnesian minerals such as pyroxene (Table 1.18). The slightly enhanced levels in iron, zinc, lead and uranium also suggest that rock 5 contains a certain amount of sulphide minerals such as pyrite, galena, sphalerite. The rock description included fine veining, so it is probable that hydrothermal or secondary mineralization has occurred: pyrite that has formed in the higher temperatures of primary magmatic crystallization is less accommodating to trace elements than hydrothermal pyrite/marcasite, and sphalerite is less common in rocks crystallized at high temperatures (Clark, 1979). Pyrite, galena and sphalerite are often found as replacement bodies in limestones and dolomites (Clark, 1979).

b) Nickel and cobalt

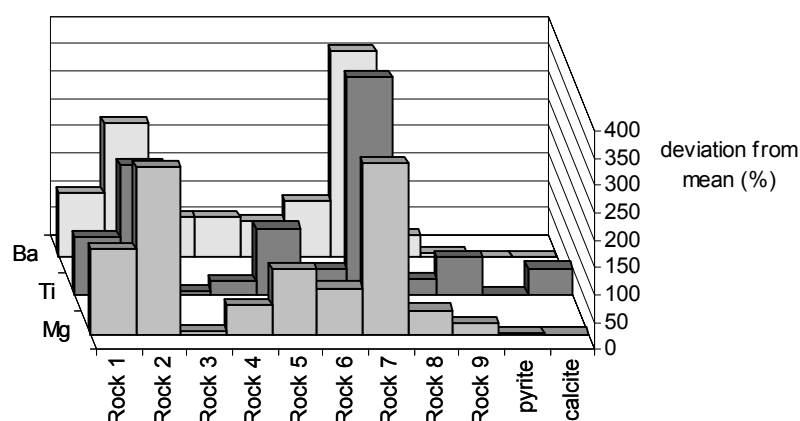
Nickel and cobalt were not enhanced in pyrite (Figure 3.7), in contrast to the suggestions of Brown & Fuge [1998 #110], and nickel in fact had a closer distribution in the morainic rocks to that of magnesium than iron or other elements enhanced in pyrite (see below). Cobalt and nickel are only likely to associate with pyrite (in pyrrotite, for example) that

forms specifically at the beginning of magma cooling events, but not with hydrothermal and secondary pyrites. These elements are often more likely to be present in silicates (see Section 1.5.3e).

c) *Magnesium, titanium and barium*

Magnesium and titanium show very similar occurrences: both are most common in rocks 2 and 7, but are not present in significant amounts in pyrite (Figure 3.8). Both elements commonly associate with, or substitute for iron in silicates and oxides, but not in sulphides (see Table 1.18). These are probably indicators of the presence of pyroxenes, amphiboles,

Figure 3.8 Relative abundances of Mg, Ti and Ba in morainic rocks, expressed as % deviation from Mean 1.



biotite, and/or oxide minerals such as ilmenite and magnetite. Magnesium is slightly less abundant in rock 7 relative titanium, suggesting that titaniferous iron oxides are present in this rock, as magnesium would not be significantly present in these minerals. Contrastingly, magnesium and iron are relatively more abundant in rocks 1 and 2. This suggests that in the minerals in rock 7 are more accommodating to the minor elements than those in rocks 1 and 2. Although there are significant amounts of magnesium in carbonate-rich rocks 1 and 5, there is very little in calcite and Rock 9 (calcite-rich). This emphasises the fact that magnesium should not be grouped with calcium and strontium are a dominantly carbonate-derived element in the *Haut Glacier d'Arolla* catchment.

Barium shows high values in rocks 2 and 7, similar to magnesium, iron and titanium. Barium usually associates with potassium in muscovite, biotite etc., but concentrates in aluminosilicate clays upon weathering (Table 1.18). The coexistence of barium reflects the petrological observations of rocks 2 and 7 as metamorphic rocks of pelitic origin. As with

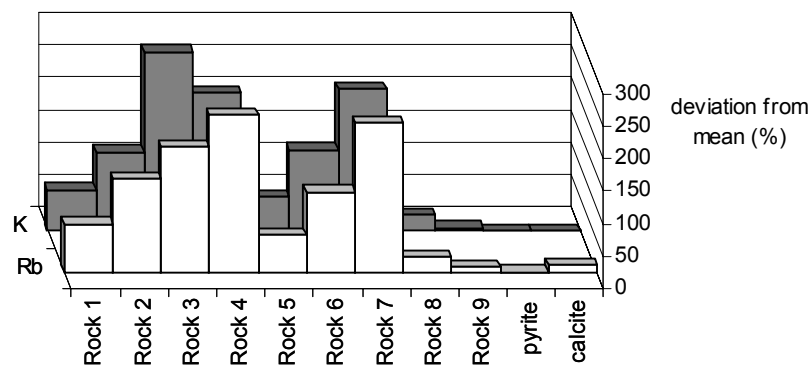
magnesium, it is clear that barium is not dominantly carbonate-derived, in contrast to the suggestions of Brown & Fuge [, 1998 #110].

It can be seen that titanium content is slightly increased in rocks 9 (dominantly calcite) and C (“pure” calcite) in comparison to magnesium and iron. There may be some accessory apatite, sphene, rutile or other mineral associated with calcite that would accommodate titanium.

d) Potassium & Rubidium

Potassium and rubidium are relatively abundant in rock 7, as in all elements described above (Figure 3.9). However, potassium and rubidium are most abundant in rocks 3 and 4. These rocks are samples of quartz vein material and metagranite. Granites are normally rich in K-feldspar, and rubidium commonly substitutes for potassium (Table 1.18). Potassium appears to be particularly enhanced in the quartz vein material, suggesting that the rock also contained significant K-feldspar. The other quartz vein, rock 8, shows no significant potassium or rubidium presence. Significant quantities of potassium and rubidium are present in rocks 1/2/5/6. These probably contain various quantities of biotite, muscovite and K-feldspar.

Figure 3.9. Relative abundances of K and Rb in morainic rocks, expressed as % deviation from Mean 1.



e) Calcium and strontium

Calcium is most abundant in calcite and rock 9 (also mainly calcite), but is also significantly concentrated in rocks 1 & 5 (Figure 3.10). Some calcium is present in rocks 2, 7 & 8, but in lower quantities. Strontium shows similar trend of occurrence, but is relatively enriched in

rocks 1/2/3/5/7, and slightly depleted in rocks 9 and calcite, as indicated by Ca/Sr ratios (Figure 3.11). This suggests that the calcite structure is a little less favourable to strontium incorporation than calcium-bearing silicate minerals such as plagioclase, epidote/zoisite, apatite etc., and may also indicate a slight tendency to incorporate into potassium minerals. Hence, rock C (calcite) displays a Sr/Ca ratio of 0.0002, whereas rock 3, the rock highest in potassium, has a Ca/Sr ratio of 0.0021. Nevertheless, strontium is overall very closely correlated to calcium ($r^2=0.93$).

Figure 3.10 Relative abundances of Ca and Sr in morainic rocks, expressed as % deviation from Mean 1.

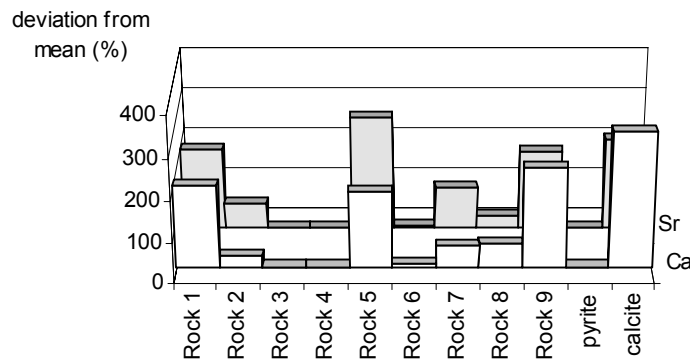


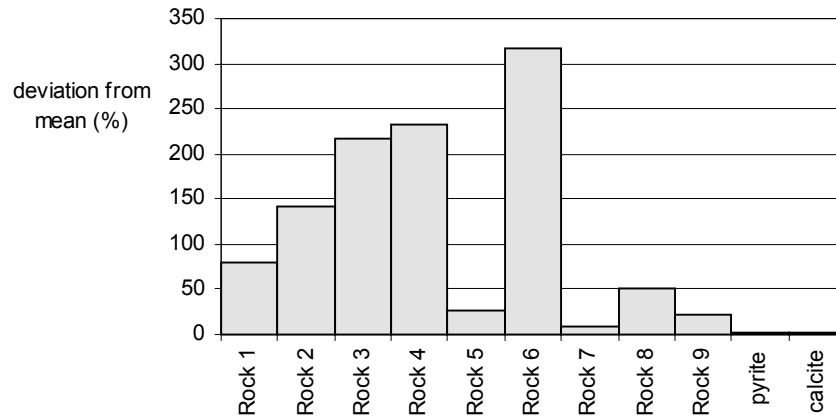
Table 3.11 Ca/Sr ratios in morainic rocks, pyrite and calcite.

Rock	1	2	3	4	5	6	7	8	9	P	C
Ca/Sr	84	40	48	48	57	110	41	150	110	160	130

f) Sodium

Table 3.9 shows that there is a weak correlation ($r=0.404$) between sodium and potassium in morainic rocks from *Haut Glacier d'Arolla*. This is due to the relatively higher concentrations of both elements in rocks 3 and 4, and low concentrations in pyrite & calcite (Figure 3.11). The major differences between the two are found in rocks 6 & 7; whilst potassium is found in relatively high quantities in rock 7, sodium is absent, and whilst potassium has a moderately low concentration in rock 6 compared with other rock types, sodium is particularly enriched. The absence of sodium in rock 7 further suggests a dominantly clay-mineral assemblage, as sodium is not greatly sorbed onto clay minerals. The high sodium content in rock 6 could be for a number of reasons, such as a high albitic content, or a sodium-rich mineral being present in the vein material. A possible candidate is tourmaline, although since the sodium content of tourmaline is not high, this would indicate that sodium is relatively sparse in the common mineralogy of the other rock types.

Figure 3.11 Relative abundances of sodium in morainic rocks, expressed as % deviation from Mean 1.



3.4.3 Summary

This section has aimed to fully describe the ranges in trace element chemistry that are found in the rocks of the moraine of *Haut Glacier d'Arolla*, and the likely mineral sources where identifiable. It is clear that general assumptions of provenance are unsatisfactory if trace elements are to be used as indicators of processes of solute acquisition in subglacial environments. Although mineral-specific major and trace element analysis was not possible directly in this study, isolating rock types has furthered the understanding of trace element distribution in the catchment geology.

3.5 MELTWATER ANALYSIS

This section presents and discusses the results of a one-month period of meltwater sampling at *Haut Glacier d'Arolla* between 28 July and 28 August 1995. Sampling and analysis techniques are discussed in Chapter 2. The collection of field data is essential to determine the conditions of laboratory dissolution experiments in terms of temperature, pH range and saturation levels of O₂ and CO₂, and to constrain the ranges of concentration of dissolved species in meltwater, and the limits of overall ionic strength for laboratory experiments.

3.5.1 Bulk meltwaters

3.5.1.1 Discharge

Discharge for the period 28 April to 14 September 1995 is shown in Figure 3.17. The period of field sampling encompassed the latter part of the melting season, over which time the two-day mean discharge decreased from approximately 4.3 to 2.2 m³/s (Figure 3.18). Variations at a diurnal time scale are very large in many instances: discharge approached an order of magnitude greater at peak flow than at recession flow at certain times during the field season, such as 15-16 August when discharge dropped from around 5.5 m³/s at 16:00h (15 August) to 0.6 m³/s at 07:00h (16 August). The extreme limits were around 6.6 m³/s on 6 August, and 0.5 m³/s on 18 August.

Figure 3.14 Bulk meltwater discharge draining Haut Glacier d'Arolla, 28 July to 26 August 1995. The 2-day moving average is shown in black.

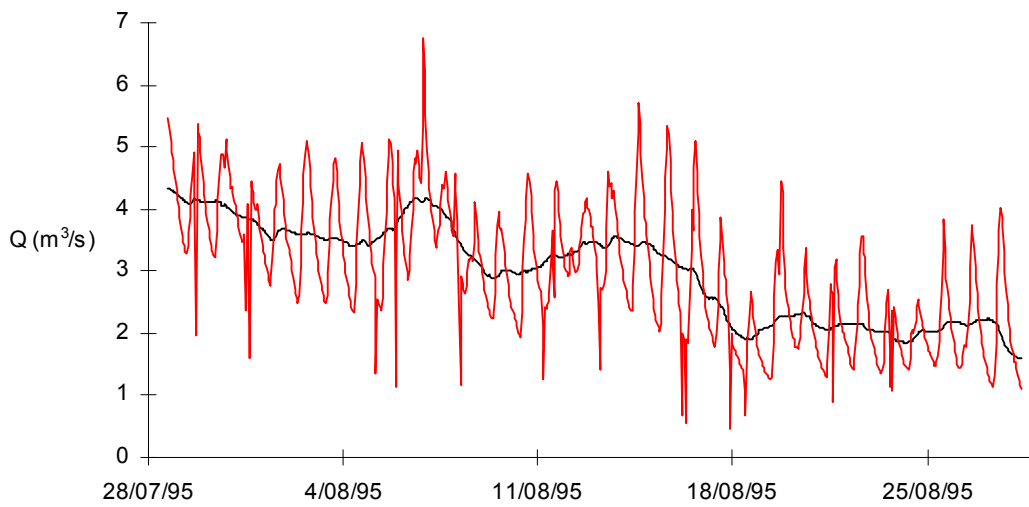
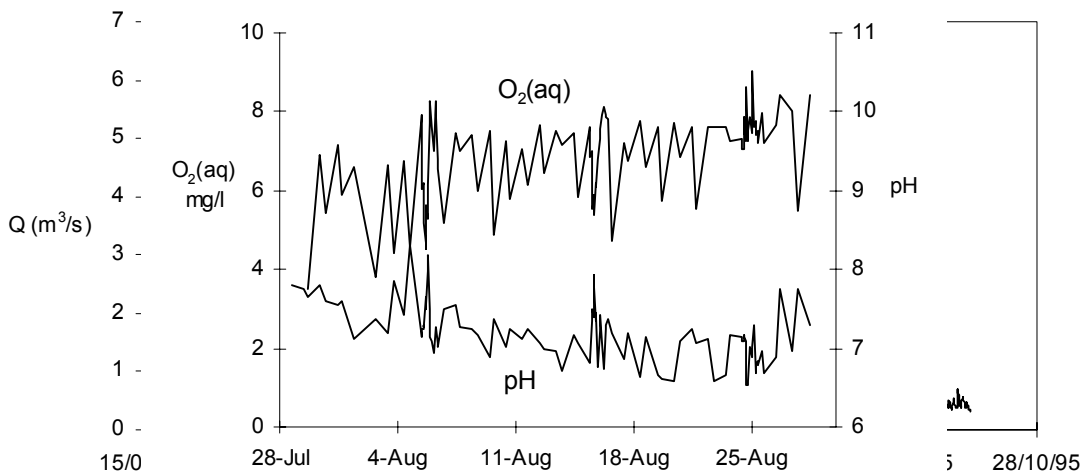


Figure 3.13 Seasonal trends of pH and DO₂ concentration in meltwaters draining Haut Glacier d'Arolla, 1995. The period of field sampling is shown between the two vertical dashed lines.



3.5.1.2 pH & dissolved oxygen

pH decreased significantly over the sampling period (Table 3.14, Figure 3.19), in line with the decrease in discharge (Figure 3.19). Figure 3.20 shows the pH values over 3 diurnal cycles, 10:00-10:00h, 5-6, 15-16 and 24-25 August 1995. pH is shown to show a diurnal variation. Table 3.14 shows that the relationship between pH and discharge over the sampling period is statistically positive, although the degree of scatter limits any confidence in quantifying the relationship.

Dissolved oxygen concentration displayed an inverse relationship with discharge over the sampling period (Figure 3.19, Figure 3.21, Table 3.14), and in each of the measured diurnal cycles (Figure 3.15), with a mean increase from 5.8 to 8.0 mg/L over the sampling period.

Figure 3.15 pH and O₂(aq) values in bulk meltwaters draining Haut Glacier d'Arolla over three 1995 diurnal cycles. Discharge is also shown for comparison.

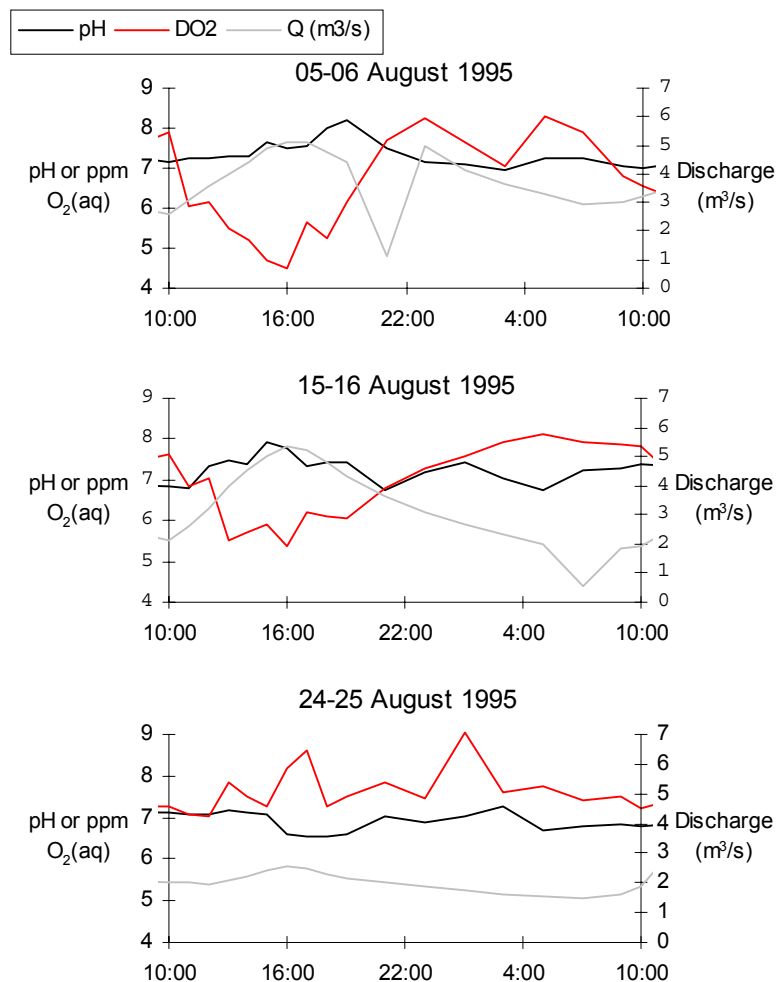
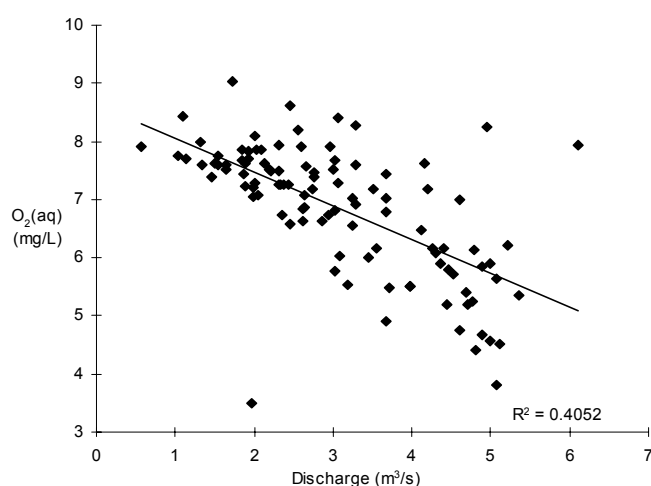


Figure 3.16 $O_2(aq)$ - discharge relationship in bulk meltwaters draining Haut Glacier d'Arolla, 28 July-26 August 1995.



3.5.1.3 Major ions

a) Calcium and sulphate

The mean concentration of Ca^{2+} and SO_4^{2-} increased significantly over the period of study (Figure 3.22). The mean daily concentrations of Ca^{2+} and SO_4^{2-} also increased between each of the sampled diurnal cycles. Both Ca^{2+} and SO_4^{2-} showed a corresponding decrease in concentration with increasing discharge. However, the degree of scatter again casts doubt upon the slope and intercepts of the relationships: the “best fit” was logarithmic trends (Figure 3.24).

The ratio of $SO_4^{2-}/(SO_4^{2-}+Ca^{2+})$ roughly indicates the amount of calcium dissolution that may be attributed to protons released by sulphide oxidation. According to Equation 3.1, a 1:2 molar (or molar equivalent) ratio of SO_4^{2-}/Ca^{2+} (i.e. $SO_4^{2-}/(SO_4^{2-}+Ca^{2+})=0.333$) would be expected if this was the only process of Ca^{2+} acquisition, whereas a ratio tending to zero would indicate that all Ca^{2+} dissolution was due to other processes such as hydrolysis and/or carbonation. A $SO_4^{2-}/(SO_4^{2-}+Ca^{2+})$ greater than 0.333 means that surplus SO_4^{2-} is present in solution assuming a sulphide mineral provenance.

$\text{SO}_4^{2-}/(\text{SO}_4^{2-}+\text{Ca}^{2+})$ showed a significantly negative relationship with discharge (Figure 3.19), suggesting that sulphide oxidation becomes less important as a proton source with increasing discharge.

Figure 3.17a Late-season trend of Ca^{2+} and SO_4^{2-} in bulk meltwaters draining Haut Glacier d'Arolla, 1995.

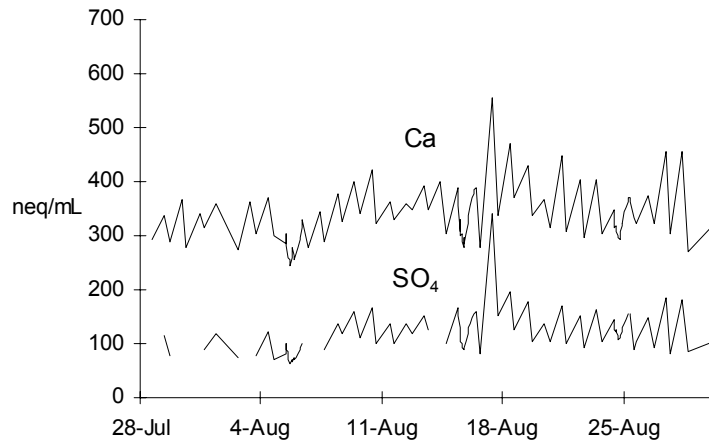
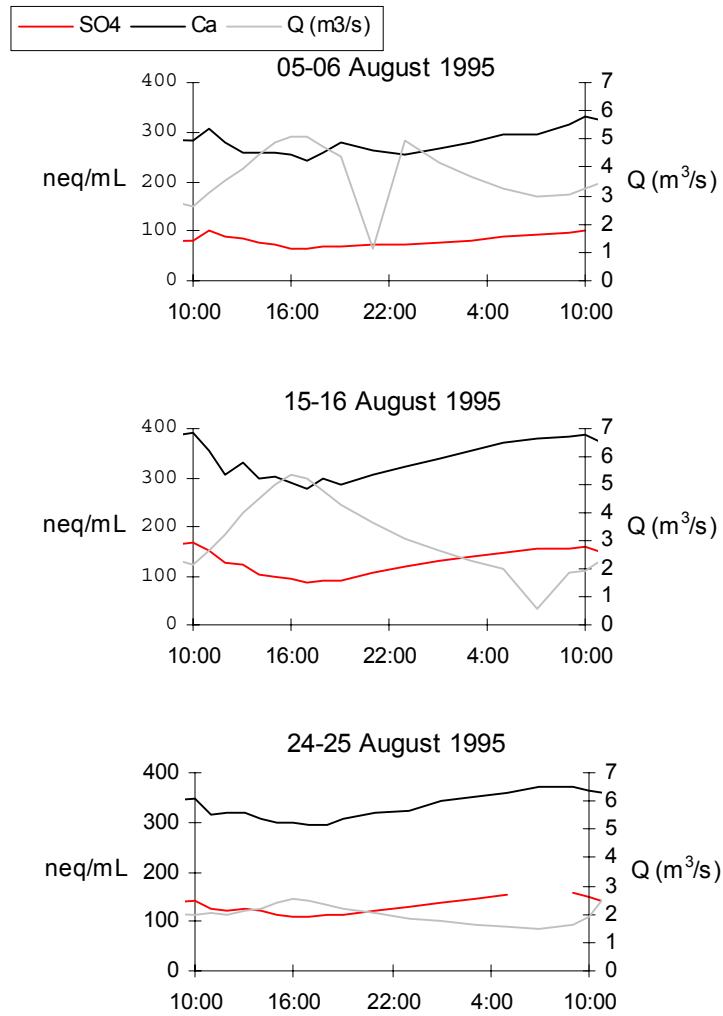


Figure 3.22b Diurnal trends of Ca^{2+} and SO_4^{2-} in bulk meltwaters draining Haut Glacier d'Arolla, 1995.



Equation 3.1 Coupled sulphide oxidation and carbonate dissolution

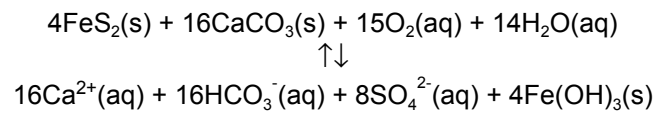


Figure 3.18 Ca^{2+} -, SO_4^{2-} - and HCO_3^- -discharge relationships in bulk meltwaters draining Haut Glacier d'Arrolla, 1995.

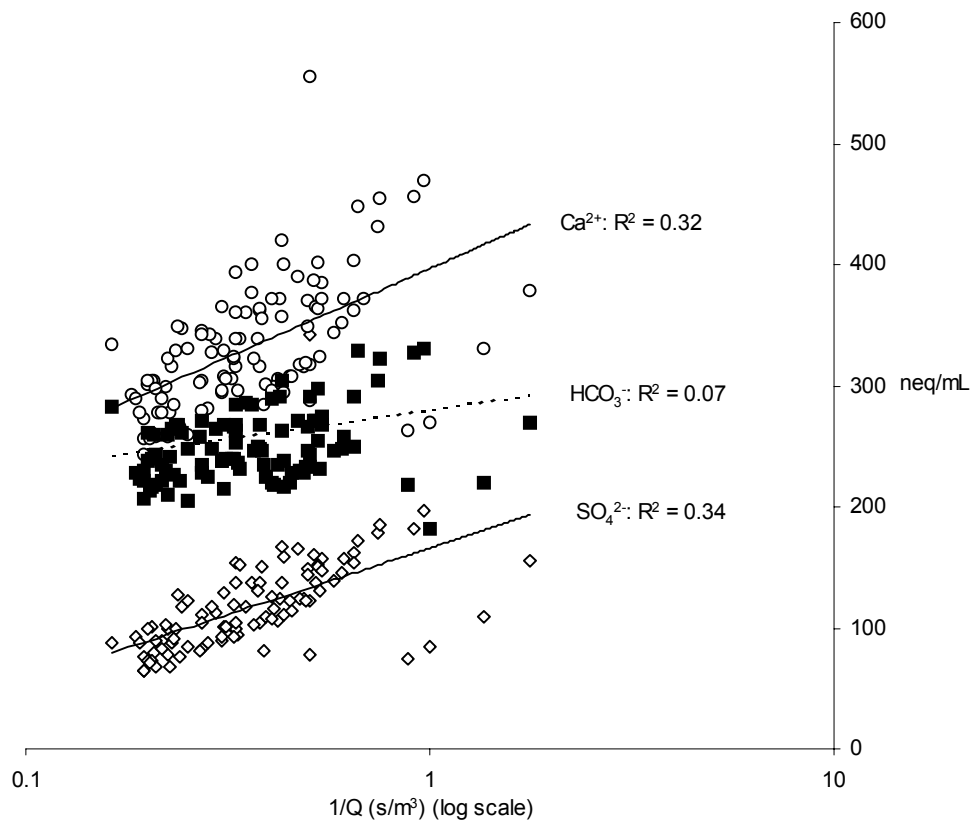
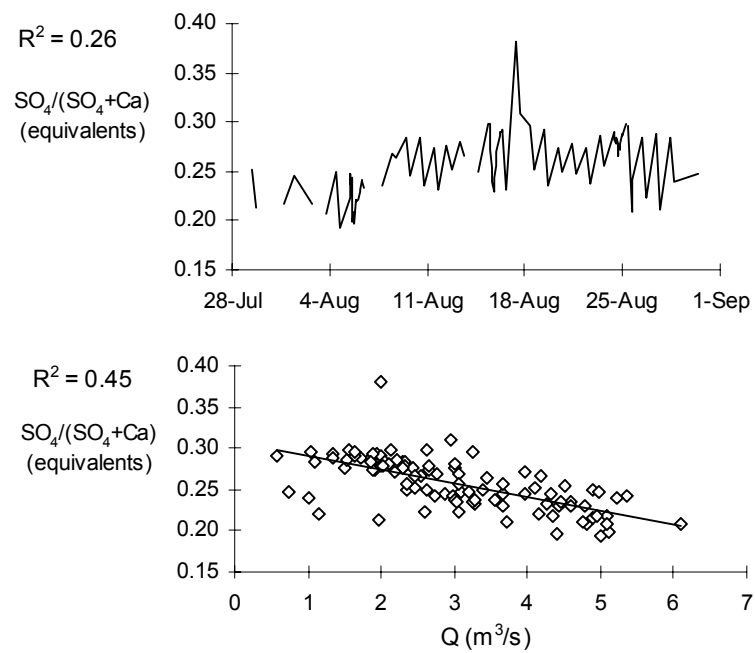


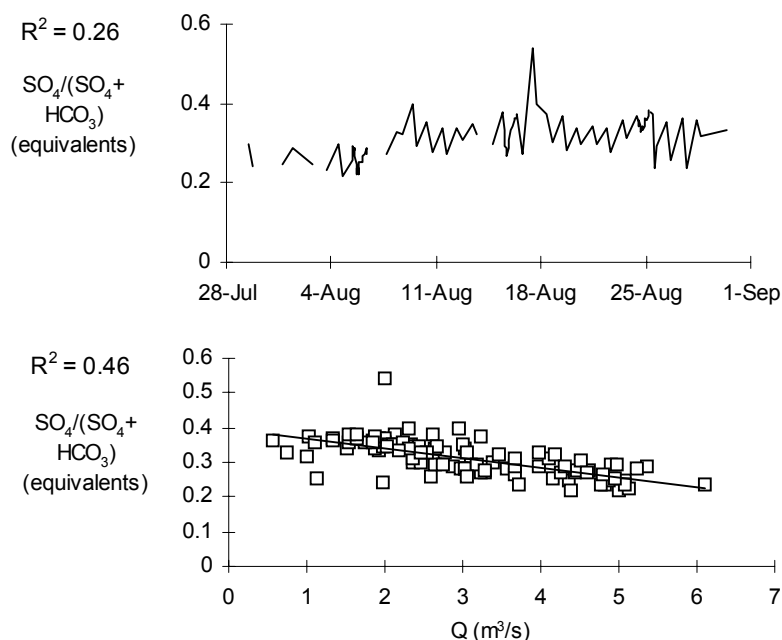
Figure 3.19 $\text{SO}_4^{2-}/(\text{SO}_4^{2-} + \text{Ca}^{2+})$ - discharge relationship in bulk meltwaters draining Haut Glacier d'Arrolla, 1995.



b) Bicarbonate

The nature of the relationship between HCO_3^- in solution and discharge is again difficult to discern due to the higher degree of scatter (Figure 3.23), although the relationship is statistically negative. However, there is a significant decrease in ratio of $\text{SO}_4^{2-}/(\text{SO}_4^{2-} + \text{HCO}_3^-)$, from around 0.4 at the lowest values of discharge to around 0.25 during highest discharge levels (Figure 3.20). This suggests that variation in HCO_3^- concentration with discharge is not as great as that of SO_4^{2-} . This is to be expected given the opportunity for carbonation reactions to occur in waters with access to atmospheric CO_2 , without the need for long residence times in contact with reactive sediment, the likely dominant source of SO_4^{2-} in late-season meltwaters (Brown *et al.*, 1996a).

Figure 3.20 $\text{SO}_4^{2-}/(\text{SO}_4^{2-} + \text{HCO}_3^-)$ - discharge relationship in bulk meltwaters draining Haut Glacier d'Arolla, 1995.



c) Relationship between sulphate and dissolved oxygen

The relationship between SO_4^{2-} and $\text{O}_2(\text{aq})$ is positive ($r^2=0.23$, $n=99$) (Table 3.14, Figure 3.21). At face value this seems at odds with the fact that $\text{O}_2(\text{aq})$ is used up in the production of SO_4^{2-} by sulphide oxidation. It is evident, however, that both show negative relationships with discharge, and that the ratio of $\text{O}_2(\text{aq})/\text{SO}_4^{2-}$ significantly increases with discharge ($r^2=0.16$, $n=96$) (Figure 3.22). Therefore, it would seem that oxygen is indeed relatively depleted in low discharge meltwaters, where SO_4^{2-} is most concentrated, but that other factors influence the concentration of $\text{O}_2(\text{aq})$. Such factors could include the fact that snowmelt is undersaturated in $\text{O}_2(\text{aq})$ (Brown *et al.*, 1994b), and waters with a longer residence time

within the glacier have greater opportunity to equilibrate with the atmosphere (assuming sufficient access to the atmosphere in the subglacial environment). This is in agreement with Seagren (1995), which stated that within-channel processes and chemical controls are of relatively minor importance. This also suggests that the system may not in fact become closed with respect to oxygen, so other oxidising agents such as iron, nitrates and elemental carbon may not be significant enhancers of sulphide oxidation rate.

Figure 3.21 SO_4^{2-} - $O_2(aq)$ relationship in bulk meltwaters draining Haut Glacier d'Arolla, 1995.

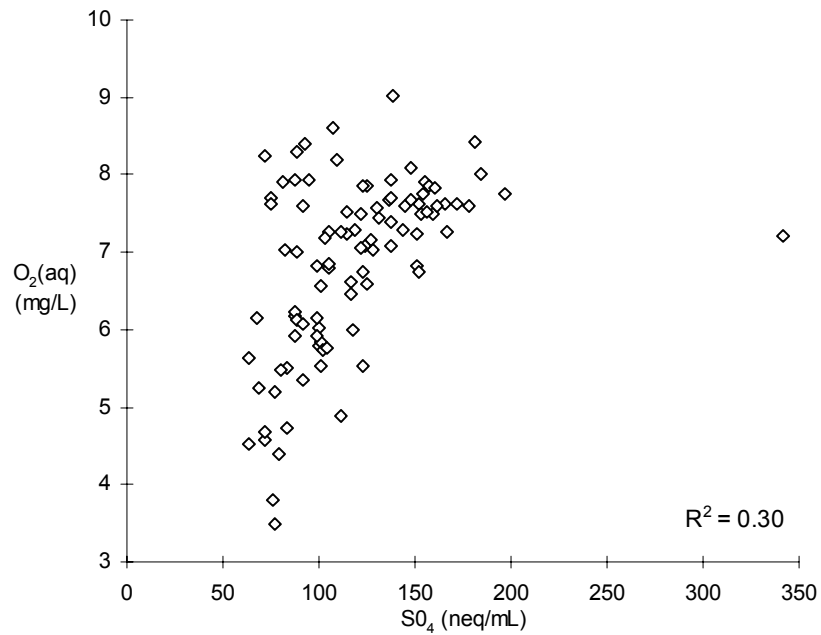
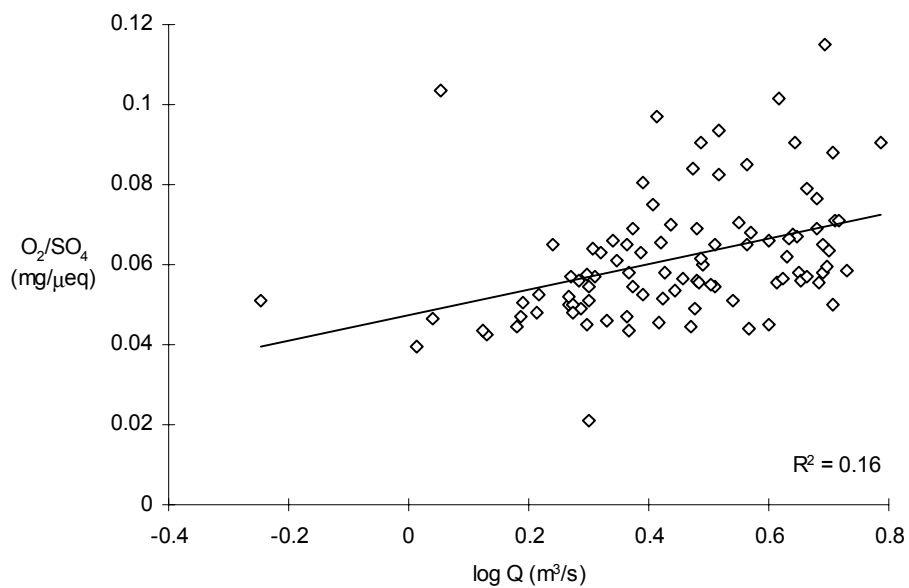


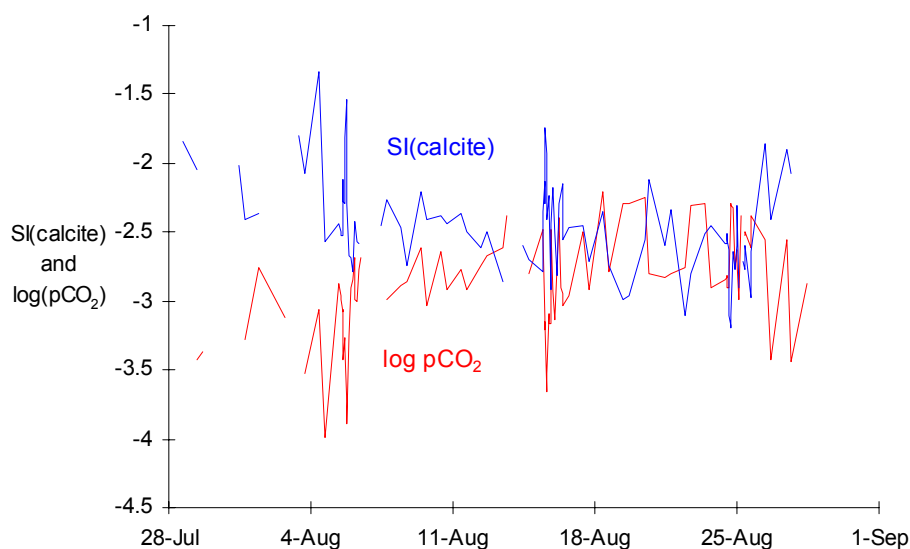
Figure 3.22 Ratio of $O_2(aq)/SO_4$ plotted versus discharge, from data of bulk meltwaters draining Haut Glacier d'Arolla, 1995.



d) $p\text{CO}_2$ and $SI(\text{calcite})$

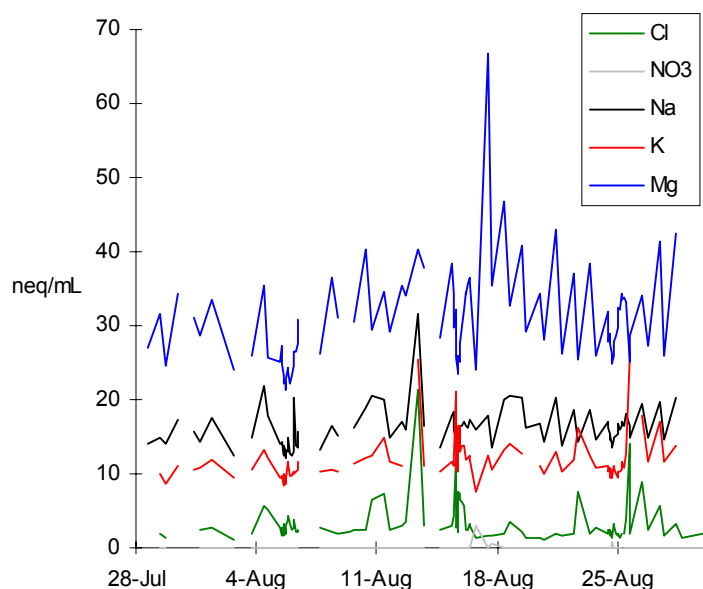
$p\text{CO}_2$ increased towards the end of the meltseason, reaching values in excess of the expected atmospheric levels (up to log values of -2.5) (Figure 3.23). Similarly, $SI(\text{calcite})$ decreased as the meltseason progressed, despite slight increases in meltwater Ca^{2+} concentration during this period. These relations are a result of the decreasing pH as the meltseason progresses (Figure 3.19), which in turn increases the solubility of calcite, providing additional acidity to drive carbonate dissolution (Garrels and Christ, 1965).

Figure 3.23 $\log p\text{CO}_2$ and $SI(\text{calcite})$ values in bulk meltwaters draining Haut Glacier d'Arolla, 1995.



The levels of the other major ions in solution are shown in Figure 3.24. Mg^{2+} showed a close correlation with Ca^{2+} , and Na^+ and K^+ were also generally inversely related to discharge. Cl^- normally varied with Na , but there were a small number of spikes where the concentration during the day was much higher than average. The spikes are also seen in the Na^+ and K^+ traces, but are less significant because the base level is higher. This may be due to a salt influx due to a precipitation event, or due to contamination by pH buffers or electrode fluid, which contain KCl , although this should not be possible as pH analysis took place after filtration and sample bottling. Unfortunately no meteorological data is available.

Figure 3.24 Seasonal trends for Na^+ , K^+ , Mg^{2+} , Cl^- & NO_3^- concentrations in bulk meltwaters draining Haut Glacier d'Arolla, 1995.



3.5.2 Supraglacial melt and groundwater

The sampling of supraglacial meltwaters and groundwater allows parameterisation of input meltwater composition into the subglacial environment (Sharp, 1991). Table 3.12 shows considerable variation in the chemistry of supraglacial meltwaters sampled between 31 July and 21 August 1995. The two samples labelled “SUPE” were collected from the same site on the surface of the Haut Glacier, and yet still show considerable variation in composition between each day. The high concentrations of ionic species in some of the samples show that dissolution of morainic rocks can occur on the surface of the glacier as well as at the ice-rock interface. However, it must be noted that these samples were taken from supraglacial channels towards the snout of the glacier, where the majority of moraine is exposed (Figure 3.2). Further up the glacier, and above the snowline, there is little exposed moraine, and so solute acquisition would be much more restricted. It is suggested that these values represent

Table 3.12 Sampled supraglacial meltwater quality from Haut Glacier d'Arolla, 1995 (* 1989 data taken from Brown, 1991).

ID	date/time	Cl	NO ₃	SO ₄	Na	K	Mg	Ca	HCO ₃	DO ₂	pH	pCO ₂	SI _{calcite}	
	(1995)	neq/mL									mg/L			
SUPE	31/07 13:00	1.6	<	4.9	1.5	1.3	1.4	47	43	5.1	6.78	-3.3	-4.5	
SUPE	08/08 12:15	3.5	<	60	22	5.6	81	440	470	7.9	7.21	-2.6	-2.0	
SUP1	21/08 15:00	0.4	<	23	13	11	38	410	430	5.7	6.97	-2.4	-2.4	
SUP2	21/08 15:00	2.8	<	250	27	7.0	91	490	340	6.3	7.35	-2.9	-2.9	
SUP3	21/08 15:00	5.8	1.1	220	27	7.3	94	510	390	6.5	7.16	-2.7	-2.7	
	Mean:	2.8	0.2	110	18	6.3	61	380	330	6.3	7.09	-2.7	-2.6	
-	1989 min*	0.0	0.7	1.0	0.4	0.0	0.4	3.1	2.0	n/a	6.0	n/a	n/a	
-	1989 max*	3.7	2.3	15	6.0	3.0	2.4	170	210	n/a	8.1	n/a	n/a	

the upper limit of concentrations for supraglacial inputs to the subglacial drainage network. Analysis of supraglacial meltwaters in 1989 (Brown, 1991) did not show concentrations as high as those presented here (Table 3.12) (see also Table 2.3.2).

Water sampled from fissures above *Haut Glacier d'Arolla*, beneath Glacier des Bouquetins (see Figure 2.3.2), showed concentrations of most major ionic species that are much lower than the bulk meltwater ionic concentrations (Table 3.13). Since these waters are probably the result of snow and ice melt in the col containing the Glacier des Bouquetins, it follows that the short residence time in contact with the rock means that solute acquisition is more restricted than in the case of the bulk meltwater draining *Haut Glacier d'Arolla*. However, Na^+ and Cl^- concentrations are a little enhanced in these waters compared to the bulk mean. (Figure 3.25). This may be as a result of evolution within fissures of the rock, where salt may be deposited, or may be due to the fact that the higher altitude of the Glacier des Bouquetins results in a delayed snow meltseason, so that the winter accumulation of aerosol salts has not been flushed from the snow at this stage. This suggests that winter accumulations in high altitude snowpacks may influence meltwater chemistry throughout the meltseason to some extent, although in this case the volume of is likely to be small

Figure 3.25 Mean concentrations of major ions in meltwaters from supraglacial meltwater (n=5), groundwater and bulk meltwater concentration over entire 1995 field season (n=108).

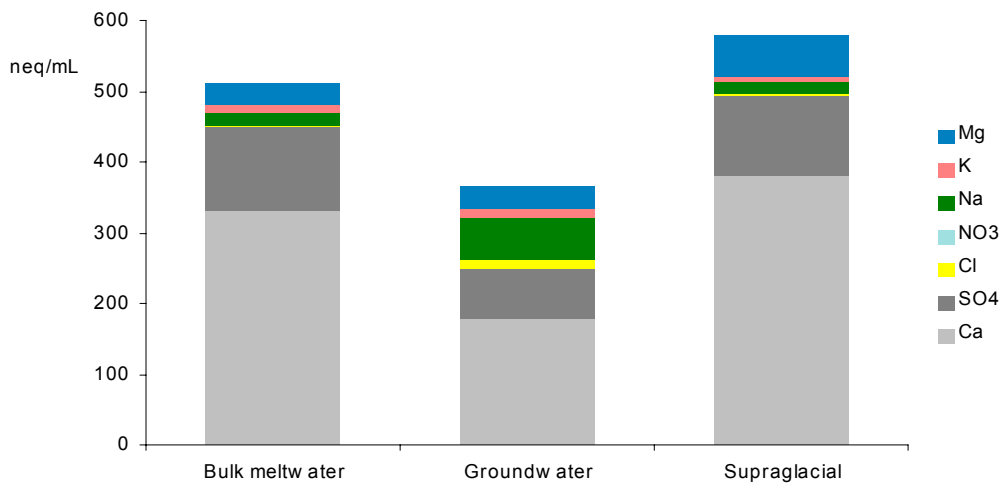


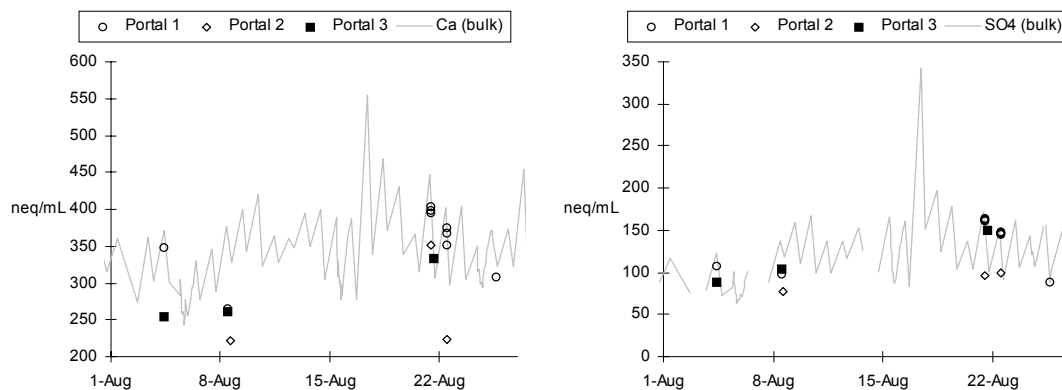
Table 3.13 Sampled groundwater quality from rock seepage beneath Glacier des Bouquetins, 1995.

date	Cl	NO ₃	SO ₄	Na	K	Mg	Ca	HCO ₃
(1995)	neq/mL							
11/08/95 13:30	7.4	<	47	40	6.8	30	180	160
17/08/95 14:00	25	<	66	70	22	32	170	140
17/08/95 14:00	12	4.5	90	65	12	33	170	110
17/08/95 17:00	3.8	<	86	57	8.7	34	180	130
Mean:	20	1.8	72	58	12	32	180	140

3.5.2.1 Chemical variability between portal meltwater streams

Figure 3.26 shows the concentrations of SO_4^{2-} and Ca^{2+} in meltwater collected from the different portals of the snout, as shown in Figure 2.2.2. It can be seen that significant variation existed between the portals, suggesting that they were draining different catchments within the glacier (consistent with Nienow *et al.*, 1996a; Nienow *et al.*, 1996b). Portal 1, the “Eastern Main Portal,” was consistently the most concentrated for both Ca^{2+} and SO_4^{2-} . This channel had a slightly brown-stained colouration, whereas the channel draining Portal 2, the “Western Main Portal,” was of a lighter colour. Portal 3 drained only a small amount of meltwater, and may in fact have been the surfacing of a side-channel that was observed in an ice-cave at the eastern margin of the glacier snout. The channel had a visible, “milky” sediment load at the beginning of August, but was much clearer on the 21st August. Nevertheless, the channel remained more concentrated in SO_4^{2-} than Portal 2, and had a similar Ca^{2+} concentration.

Figure 3.26 Variations in concentrations of (left) Ca^{2+} and (right) SO_4^{2-} in meltwaters draining different glacier snout portals of Haut Glacier d’Arolla, 1995.



The differences in ionic concentration between the main eastern and western portals may be due to lateral variations in sub-ice lithology, or may be due to different subglacial drainage network characteristics. These data are not sufficient to show whether SO_4^{2-} is relatively more depleted in the western drainage network than Ca^{2+} , or visa versa. Much of the larger supraglacial channels are situated on the western side of the glacier surface, and so the lower ionic strength of the western side may simply be a factor of dilution by supraglacial meltwaters entering the glacier through crevasses and moulins close to the glacier snout.

Portal 1 (eastern) meltwaters, apart from the 8th August sample, have SO_4^{2-} and Ca^{2+} concentrations very similar to the bulk meltwater values (Figure 3.26), showing that the dominant meltwater channel is also the most solute rich. Therefore, minor drainage channels are not necessarily less evolved or contain higher proportions of delayed flow meltwater.

3.5.3 Discussion of meltwater analysis

Table 3.14 shows the summarised field results, which represent the parameters by which the laboratory experiments have been set. Volume weighted means are calculated using Equation 3.2.

Table 3.14 Summary of field parameters, 28 July-26 August 1995. "Correlation" means Pearson's Product-Moment Correlation Coefficient (r). ✓ = significant correlation with discharge (Q) and time (T). Critical r values are 0.20 (whole data set: n=100) and 0.38 (10:00 and 17:00 data sets: n=25). Scatter from volume-weighted mean (VWM) values are calculated to the 95% confidence level.

	VWM	Min	Max	Correlation with Q	Q	T	VWM (10:00)	Q	T	VWM (17:00)	Q	T
Q (m ³ /s)	3.1±0.2	0.47	6.8				2.1±0.3			3.7±0.4		
pH	7.3±1.8	6.5	8.3	+0.52	✓	✓	7.0±2.0	✓	✓	7.2±3.0		✓
O ₂ (aq) (mg/L)	6.3±1.3	3.5	9.3	-0.64	✓	✓	6.8±1.7	✓	✓	6.8±1.7	✓	✓
Ca ²⁺ (neq/mL)	320±60	260	560	-0.59	✓	✓	380±90	✓		310±120		
SO ₄ ²⁻ (neq/mL)	97±20	64	340	-0.62	✓	✓	150±40			96±37		
HCO ₃ ⁻ (neq/mL)	220±58	180	330	-0.34	✓	✓	280±70			250±100		
Mg ²⁺ (neq/mL)	27±6	22	67	-0.57	✓	✓	35±9			28±10		
K ⁺ (neq/mL)	10±4	8	26	0.00		✓	12±5			10±5		
Na ⁺ (neq/mL)	14±4	12	32	-0.42	✓	✓	18±6			15±6		
Cl ⁻ (neq/mL)	3.2±2.4	0.1	21	+0.19			4.1±4.6			2.6±2.5		
NO ₃ ⁻ (neq/mL)	0.05±0.27	0	2.9	+0.11			0			0.2±1.0		
log pCO ₂	-2.7±0.9	-4.0	-2.2	-0.53	✓	✓	-2.7±0.9	✓	✓	-3.0±1.5	✓	✓
SI _{calcite}	-2.2±0.6	-3.2	-1.3	+0.33	✓	✓	-2.4±0.6			-2.4±0.9		✓
SO ₄ ²⁻ /(SO ₄ ²⁻ +Ca ²⁺)	0.22±0.05	0.32	0.53	-0.67	✓	✓	0.27±0.07			0.24±0.09		
SO ₄ ²⁻ /(SO ₄ ²⁻ +HCO ₃ ⁻)	0.27±0.06	0.40	0.98	-0.68	✓	✓	0.34±0.08			0.28±0.10	✓	✓

Equation 3.2 Calculation of volume-weighted means, where X_{bulk} = concentration of the individual ionic species in bulk meltwater; Q_{bulk} = bulk discharge at the time of sampling.

$$\text{volume weighted mean (VWM)} = \frac{\sum(X_{\text{bulk}} * Q_{\text{bulk}})}{\sum Q_{\text{bulk}}}$$

The domination of SO₄²⁻, Ca²⁺ and HCO₃⁻ ions in the field results is consistent with previous studies at *Haut Glacier d'Arolla* (Table 3.15) (Brown, 1991; Tranter and Raiswell, 1991; Tranter *et al.*, 1993, etc.; Brown *et al.*, 1994a; Lamb *et al.*, 1995; Lamb, 1997). The range of concentrations is also encompassed by the selection of data from other glaciers shown in Table 3.16, although not unexpectedly, Na⁺ and Cl⁻ data is considerably lower than in meltwater draining coastal glaciers in Baffin Island (Church, 1974). The dominance of Ca²⁺ and HCO₃⁻ in meltwaters in these studies led to suggestions that carbonation and carbonate dissolution are major chemical processes of solute acquisition of many Alpine glaciers including the Haut Glacier (Tranter *et al.*, 1993; Brown *et al.*, 1996b; Tranter *et al.*, 1996), with the extent of sulphide oxidation attributed to widely disseminated pyrite in many Alpine glacial environments (Reynolds Jr. and Johnson, 1972; Tranter *et al.*, 1993; Fairchild *et al.*, 1994; Fairchild *et al.*, 1999).

Table 3.15 Comparison of bulk meltwater compositions at Haut Glacier d'Arolla for recent years (data from 1. Brown, 1991; 3. Lamb, 1997, 4. this study; 2. Tranter *et al.*, 1997). Data is in neq/mL, except Q (m³/s) and pH.

	1989 ¹ vwm	1990 ¹ vwm	1992 ²	1993 ³ vwm	1994 ³ vwm	1995 ⁴ vwm
JD	152-243	152-243	232-265	130-256	198-246	209-238
Q	0.4-6.5	0.4-7.2		0.08-5.7 2.2	1.2-6.5 3.5	0.6-6.1 3.1
Ca	160-470 230	140-410 170	250-560	250-900 340	280-540 320	256-555 320
Mg	15-49 24	18-52 23	26-110	25-87 36	19-54 27	22-67 27
Na	5.1-36 11	5.2-27 8.6	11-55	12-41 18	7.6-30 11	12-32 14
K	5.4-18 9	3.3-19 6.9	8.6-36	8.5-37 12	7.6-22 22	8-36 10
HCO ₃	180-370 230	200-460 250	220-360	180-580 290	250-400 280	180-330 220
SO ₄	30-240 54	20-340 50	46-220	61-282 120	58-300 100	64-340 97
pH	6.8-8.2 8.0	6.5-9.1 7.0	7.0-8.9	n/a ~7.0	n/a ~6.5	6.5-8.3 7.1

Table 3.16 Comparison of 1995 data for Haut Glacier d'Arolla with other glaciers (* Keller and Reesman, 1963; data from Church, 1974; ** Fairchild *et al.*, 1999). Data in neq/mL except SiO₂ (nM/mL) and pH. SiO₂ data for Haut Glacier d'Arolla is for 1993 & 1994 meltseasons (Lamb, 1997).

	Haut Glacier d'Arolla 1995	Lewis River, Baffin Island 1963-4	N/S Rivers, Ekalugad Fiord, Baffin Island 1967	Maktak River, Maktak Fiord, Baffin Island 1972 (mean)	Trient, Switzerland (mean)*	Tsanfleuron Glacier 1994 (diurnal cycle, upper stn.)**
Ca	260-560	45-550	30-350	80	264	530-790
Mg	22-67	16-255	25-120	33	310	61-150
Na	12-32	52-540	35-39	110	9	n/a
K	8-36	8-33	13-28	92	13	n/a
HCO ₃	180-330	7.2-61	0-5.0	55	n/a	508-701
SO ₄	64-340	19-71	29-200	77	n/a	52-300
Cl	1.0-21	28-580	11-17	28	n/a	n/a
SiO ₂	8-34	3.4-20	12-45	85	25	n/a
pH	6.5-8.3	5.7-6.0	5.2-6.1	6.7	6.9	6.9-8.2

The trends in major ion concentration over the period of study appear to be closely related to discharge. (Brown *et al.*, 1996a) suggested that seasonal variations in major ion concentration may be attributed to evolution of the hydrological network as the meltseason progresses, although the role of discharge is not discussed. Nevertheless, discharge relationships generally yielded higher correlations than temporal relationships in this study, and may therefore be considered to be more influential than the effects of seasonal evolution over this length of period of study.

Tranter *et al.*, (1993) described a quickflow network dominated by carbonation and carbonate dissolution reactions, and a delayed flow network dominated by coupled sulphide oxidation and carbonate dissolution reactions. Dye tracing studies at the Haut Glacier showed that quick flow waters contribute significantly to the overall composition of peak flow bulk meltwaters, whereas delayed flow meltwaters may form a larger constituent of the bulk meltwater at minimum flow (Nienow *et al.*, 1996a; Nienow *et al.*, 1996b). It is shown that all the major ions (except bicarbonate) and dissolved oxygen show a negative relationship with discharge. It therefore follows that the delayed flow component is more concentrated in major ions than the quickflow component.

Previous studies have suggested that sources of sulphide are likely to be exhausted prior to mixing of delayed and quickflow components, so that post-mixing evolution is not likely to enhance the concentration of sulphate in bulk meltwaters (Tranter *et al.*, 1993). Contrastingly, carbonate and aluminosilicate dissolution from subglacial and suspended sediment may enhance Ca^{2+} and concentration in post-mixing waters. Therefore the Ca^{2+} and HCO_3^- traces were less depleted than the SO_4^{2-} during peak flow conditions, when the influence of the quickflow component was highest. This resulted in relatively lower $\text{SO}_4^{2-}/(\text{SO}_4^{2-}+\text{Ca}^{2+})$ and $\text{SO}_4^{2-}/(\text{SO}_4^{2-}+\text{HCO}_3^-)$ ratios during peak flow conditions.

The relationship between pH and SO_4^{2-} was significantly negative ($r^2=0.20$, $n=99$), with waters with the lowest sulphate content showing pH values in the range 7.0 to 8.5, and waters with the highest SO_4^{2-} concentrations showing a pH range of 6.6 to 7.3. This suggests that the acidity being produced by sulphide oxidation was being partially buffered by carbonate dissolution, although this may be masked by the influence of suspended sediment variations with discharge (Tranter and Raiswell, 1991). The $\text{SO}_4^{2-}/\text{Ca}^{2+}$ relationship fails to describe a complete coupling of sulphide oxidation and carbonate dissolution, since the $\text{SO}_4^{2-}/\text{Ca}^{2+}$ ratio increases during the periods of maximum SO_4^{2-} concentration.

Calcium and sulphate were significantly correlated with a linear relationship ($r^2=0.86$, $n=99$), but with an intercept of $\text{Ca}^{2+} = 180$, and a slope of $\text{Ca}^{2+} = 1.3 \times \text{SO}_4^{2-}$. A completely coupled reaction would produce a slope of $\text{Ca}^{2+} = 2 \times \text{SO}_4^{2-}$, indicating that only a fraction of the total acidity produced by sulphide oxidation was used to enhance carbonate dissolution.

The calculated values for $\text{p}(\text{CO}_2)$ generally remained within the range ± 1 of atmospheric levels (3.5) in the 1995 data, but were statistically related positively to Ca^{2+} ($r^2=0.22$, $n=96$) and HCO_3^- ($r^2=0.08$, $n=96$). It is not, however, possible to show that CO_2 drawdown was a limiting factor for carbonate dissolution during the period of field sampling. pCO_2 values showed a significantly positive relationship with SO_4^{2-} concentration, however, suggesting that protons supplied by SO_4^{2-} may reduce the extent of carbonation reactions.

3.6 CONCLUSION

Inferences of processes occurring within the the hydrological network have hitherto relied on crude mass-balance calculations (e.g. Brown *et al.*, 1996a), with estimations of mineralogy based on petrological investigations of post-reacted proglacial sediment (Brown, 1991). Petrological investigations of freshly-crushed rocks sampled from medial moraines on *Haut Glacier d'Arolla* have revealed a higher proportion of reactive minerals, including calcite,

than previously identified, which has important implications for previous interpretations of weathering processes within the glacier's drainage system.

Multi-elemental analysis of a selection of digested samples of morainic rocks is undertaken, allowing direct comparisons between the rock content and resultant concentration of dissolved species in dissolution experiments involving the same rocks. Analysis of both major and trace elements was undertaken, to widen the scope of water quality investigations from those hitherto undertaken.

A period of field sampling of bulk meltwater and other glacial meltwaters draining *Haut Glacier d'Arolla* in the latter part of the 1995 melt season was undertaken, and the results are presented and interpreted here. This study, complementing previous studies at the catchment, enabled parameterisation of laboratory experiments in terms of the ranges of water quality data that laboratory experiments should encompass. This places a greater relevance of the laboratory dissolution experiments presented in this study than previous laboratory-based studies of chemical weathering processes thought to prevail in a glacial hydrological network, which generally represented chemical and/or physical conditions dissimilar to those in a glacial environment.

The combination of petrological evidence, bulk rock analysis, and meltwater sampling, produces the most complete and integrated dataset to date, providing a good basis for the parameterised study of solute acquisition in subglacial environments presented in subsequent chapters.

4. LABORATORY SIMULATIONS OF SUBGLACIAL SOLUTE ACQUISITION: RESULTS AND INITIAL INTERPRETATION

4.1 INTRODUCTION

Previous studies of water quality variability in glacial meltwaters have indicated the presence of a heterogeneous subglacial drainage system, and the primary controls on solute acquisition in subglacial environments have been identified as reaction kinetics, sediment availability, particle size distribution and surface morphology, mineralogy and hydrology (Chapter 1). Specifically, proton availability, access to atmospheric gases, reactive chemistry, meltwater residence times and drainage dynamics have been isolated as key controls on the rates, processes and magnitude of solute acquisition in these environments (Raiswell and Thomas, 1984; Brown, 1991; Sharp, 1991; Brown *et al.*, 1994b; Brown *et al.*, 1996b).

Detailed chemical analysis of bulk meltwater composition has suggested that certain key chemical indicator species may be identified, which may indicate the contribution of different meltwater flow components to the overall composition of waters draining from a glacier (Brown *et al.*, 1996b). Studies investigating the major ion chemistry of meltwaters (Brown, 1991; Sharp, 1995; Brown *et al.*, 1996b) suggested that the principal processes of solute acquisition are carbonation reactions in quickflow meltwaters and coupled sulphide oxidation and carbonate dissolution in delayed flow meltwaters (Tranter *et al.*, 1993; Brown *et al.*, 1994a). This interpretation is based on the concentrations and stoichiometric ratios of Ca^{2+} , HCO_3^- , and SO_4^{2-} in meltwater draining *Haut Glacier d'Arolla* (Tranter and Raiswell, 1991) (Tranter *et al.*, 1993; Brown *et al.*, 1994a; Lamb *et al.*, 1995; Brown *et al.*, 1996a; Brown *et al.*, 1996b) (Sections 1.3, 1.4).

However, investigations of water-rock interaction in glacial environments (Sections 1.5.1 and 3.5), whilst confirming the importance of sediment mineralogy, proton availability and access to atmospheric gases in determining the composition of meltwaters, have not quantified the role of the theoretical coupled sulphide oxidation and carbonate dissolution reaction in the delayed flow component, or the rates of solute acquisition in subglacial environments.

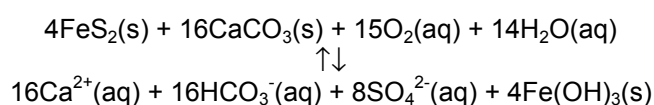
This chapter presents data from a suite of laboratory dissolution experiments which were conducted to investigate the processes of subglacial solute acquisition, including the roles of sulphide oxidation, carbonate and aluminosilicate dissolution in conditions approximating those in the distributed system. Many of the samples from the experiments were also analysed for trace elements (experiments with trace element analysis data sets are listed in

Table 2.4.5). Comparisons are made between the metal content of the rocks and the concentrations in solution to analyse the dissolution behaviour of individual species. By comparing the dissolution behaviour of trace and major elements with associated rock provenance, the role of interaction between ionic species is obtained. Particular species are identified that are likely to be key diagnostic indicators of chemical weathering processes in the subglacial environment.

4.1.1 Experiments using “end-member” components

“Coupled sulphide oxidation and carbonate dissolution” (Equation 4.1) (Tranter *et al.*, 1993) describes the process where protons released by the oxidation of sulphide minerals such as pyrite, sphalerite and galena by oxidants such as oxygen, nitrate, phosphate and oxidising bacteria (e.g. *Thiobacillus Ferrooxidans*), are consumed by the dissolution of carbonate minerals such as calcite, dolomite, aragonite etc. This process has been suggested to account for much of the solute acquisition in delayed flow meltwater (Tranter *et al.*, 1993; Lamb *et al.*, 1995; Brown *et al.*, 1996b) (Section 1.3.2.3).

Equation 4.1 Coupled sulphide oxidation and carbonate dissolution



To directly investigate the importance of and controls on this specific process, laboratory investigation of pyrite and calcite dissolution as “end-member” components of the process were carried out. These also act as a comparison with subsequent experiments involving morainic rock samples, so that the coupled process may be evaluated. The bulk rock composition of the pyrite and calcite used in these experiments is fully described in Section 3.4.. The results are summarised in Table 4.1.

4.1.2 Investigations using morainic rock samples

Laboratory dissolution experiments were also carried out on crushed moraine rock samples derived from *Haut Glacier d’Arolla*, to further investigate the controls on solute acquisition using sediment parameters pertinent to a fieldsite where detailed records of water quality exist. This permits comparison with the end-member experiments, to evaluate the role of coupled sulphide oxidation and carbonate dissolution in the overall pattern of solute acquisition in subglacial environments (see Section 2.3.1 for more details).

Table 4.2 summarises the results of closed and reopened dissolution experiments, and those where additional dilution was carried out. Experiments involving the addition of pyrite are also displayed.

Table 4.1 Mean results of laboratory dissolution experiments involving pure calcite and pyrite, after 24 hours closed system dissolution. Units are neq/mL.

Conditions	24 hours closed system					24 hours open system			
	Exp. No.	C(c)	P(c)	PC(c)	PC _{0.1} (c)	P _{0.1} C(c)	C(o)	P(o)	PC(o)
pyrite (g/L)	-	0.2	0.2	0.2	0.2	0.1	-	0.2	0.2
calcite (g/L)	0.2	-	0.2	0.1	0.2	0.2	0.2	-	0.2
Na ⁺ (neq/mL)	0.9	1.0	1.2	0.9	1.3	7.2	7.0	5.3	
K ⁺ (neq/mL)	1.1	0.6	0.6	1.4	0.8	16	12	13	
Mg ²⁺ (neq/mL)	<	0.6	0.7	0.7	0.5	<	1.5	0.7	
Ca ²⁺ (neq/mL)	240	33	230	230	260	730	26	680	
SO ₄ ²⁻ (neq/mL)	0	25	27	29	12	6.6	23	23	
HCO ₃ ⁻ (neq/mL)	240	10	200	200	240	720	15	670	
pH	9.9	6.3	8.9	9.7	9.7	8.6	5.2	8.6	
SI(calcite)	-0.12	-5.1	-1.0	-0.3	-0.1	-0.3	-6.7	-0.37	
log p(CO ₂)	-5.6	-3.7	-4.7	-5.4	-5.4	-3.9	-2.2	-3.8	
SO ₄ ²⁻ / (SO ₄ ²⁻ +HCO ₃ ⁻)	0.00	0.55	0.12	0.13	0.05	0.01	0.66	0.03	

Table 4.2 Mean results of laboratory dissolution experiments involving morainic rocks. Units are neq/mL.

Description of conditions	24 hours closed system										24 hours closed system, 4 hours open system					24 hours closed system, 50% dilution, 4 hours open system				0.2g/L pyrite added, 24 hours closed system						Pyrite added, 24 hours closed, 4 hours open			
	Exp. No.	1(c)	2(c)	3(c)	4(c)	5(c)	6(c)	7(c)	8(c)	9(c)	M(c)	1(r)	2(r)	5(r)	9(r)	M(r)	1(rd)	5(rd)	9(rd)	M(rd)	1P(c)	4P(c)	4C(c)	4PC(c)	5P(c)	9P(c)	1P(r)	5P(r)	9P(r)
Rock #	1	2	3	4	5	6	7	8	9	M	1	2	5	9	M	1	5	9	M	1+P	4+P	4+C	4+P+C	5+P	9+P	1+P	5+P	9+P	
Major mineral	Cc	FeMg	Qz	Pl	Cc	Kfsp	?	Qz	Cc	?																			
n	3	2	2	3	3	2	2	2	4	3	2	1	1	3	3	1	1	1	1	1	1	1	1	1	1	1	1	1	1
Na ⁺ (neq/mL)	6.4	6.1	36	20	4.9	19	2.5	3.8	4.6	8.4	13	12	10	11	19	8.2	7.3	11	21	7.8	35	29	27	8.7	7.1	28	16	14	
K ⁺ (neq/mL)	46	45	45	40	35	21	69	5.7	4.7	10	63	52	22	4.5	14	36	24	3.2	14	61	48	41	40	62	44	71	68	49	
Mg ²⁺ (neq/mL)	17	17	<	4.1	13	6.1	3.7	1.9	9.5	12	25	54	22	9.5	16	15	13	7.4	14	29	8.9	7.0	6.8	26	28	32	28	31	
Ca ²⁺ (neq/mL)	320	87	77	200	340	300	250	300	300	140	850	110	690	720	170	600	640	700	170	550	230	210	220	480	540	860	780	920	
Cl ⁻ (neq/mL)	4.2	13	32	20	3.9	13	28	80	3.1	7.4	6.5	11	2.4	15	8.7	3.9	2.1	2.1	5.0	4.5	78	13	5.6	4.8	1.2	13	7.1	4.0	
NO ₃ ⁻ (neq/mL)	<	11	10	3.1	14	40	18	5.8	0.7	0.4	2.1	1.1	1.1	2.6	0.2	<	0.9	<	<	<	1.9	1.7	<	<	<	2.5	1.1	0.94	
SO ₄ ²⁻ (neq/mL)	1.4	200	29	11	9.9	1.1	14	5.8	4.6	<	1.9	192	9.2	5.7	0.6	<	5.0	4.3	1.2	170	49	<	36	150	170	190	150	200	
HCO ₃ ⁻ (neq/mL)	390	-	87	240	360	290	260	220	310	170	950	26	750	630	210	660	680	710	210	480	190	270	250	420	440	790	730	820	
pH	9.1	7.4	7.9	9.8	9.2	9.4	9.3	9.6	9.2	8.6	7.4	7.1	7.5	7.8	6.9	7.5	7.7	7.4	6.7	8.3	9.9	10.1	10.2	8.6	8.4	7.6	7.7	7.5	
SI(calcite)	0.3	-	-2.2	0.3	0.2	0.4	0.1	0.3	0.1	-1.1	-0.7	-3.6	-0.9	-0.7	-2.6	-1.2	-0.9	-1.2	-3.0	-0.6	+0.2	+0.6	+0.6	-0.4	-0.5	-0.9	-0.8	-0.9	
log p(CO ₂)	-5.0	-	-4.4	-5.7	-4.9	-5.2	-5.2	-5.5	-5.0	-4.7	-2.8	-4.1	-2.9	-3.2	-3.2	-2.8	-3.0	-2.6	-2.5	-3.7	-5.7	-5.8	-5.9	-4.1	-3.9	-2.8	-3.0	-2.7	
SO ₄ ²⁻ / (SO ₄ ²⁻ +HCO ₃ ⁻)																	0.01	0.01	0.01	0.26	0.20	-	0.13	0.27	0.28	0.20	0.17	0.2	

4.2 SUMMARY OF RESULTS OF EXPERIMENTS INVOLVING MORAINIC ROCKS

4.2.1 Mean experimental concentrations of dissolved elements

The mean concentrations and standard deviations of a suite of metals and major anions for all experimental data are shown in Figure 4.1. The figure also indicates that different elements display different dissolution curves, i.e. some elements were more concentrated at 1 hour than at 24 hours, whereas some show continued acquisition over the longer time scale. These patterns are significant in the interpretation of bulk meltwater trace element data, as elements that do not remain in solution for long periods of time may not be transported from the distributed system into bulk meltwater and proglacial stream. This is mainly due to adsorption and coprecipitation onto particulates (see Section 1.5). Therefore their presence in proglacial meltwater samples may indicate reactions taking place in the bulk meltwaters. More soluble elements may remain in solution from the distributed system to the proglacial stream. Increased yields with time under closed system conditions may be due to surface exchange reactions with saturated cations, e.g. calcium in a solution supersaturated with respect to calcite

4.2.2 Solubility

An important factor in the dissolution character of elements is variations in solubility, or yield of individual species from solid to solution that are due to the host mineralogy (Drever, 1982). The extremes of this variable are (a) a metal with a high element trace content in a mineral with a very low yield will show low concentrations in solution; and (b) a metal that is barely present in a mineral, but has a very high yield may show relatively higher concentrations in solution. This variation adds a further complication to the interpretation of meltwater chemistry, and these experiments are therefore essential to be able to account for observed variations. Figure 4.2 shows the mean elemental solute yields from closed system dissolution experiments involving morainic rocks. The 1 hour and 24 hour means for each rock type are shown in Table 4.3.

Figure 4.1 (left) Mean concentrations of metals and major anions resulting from all open- and closed-system experiments from this study (all time increments). (right) Difference between concentration after 1h and 24h closed system dissolution, expressed as percentage of the difference in relation to the largest concentration.

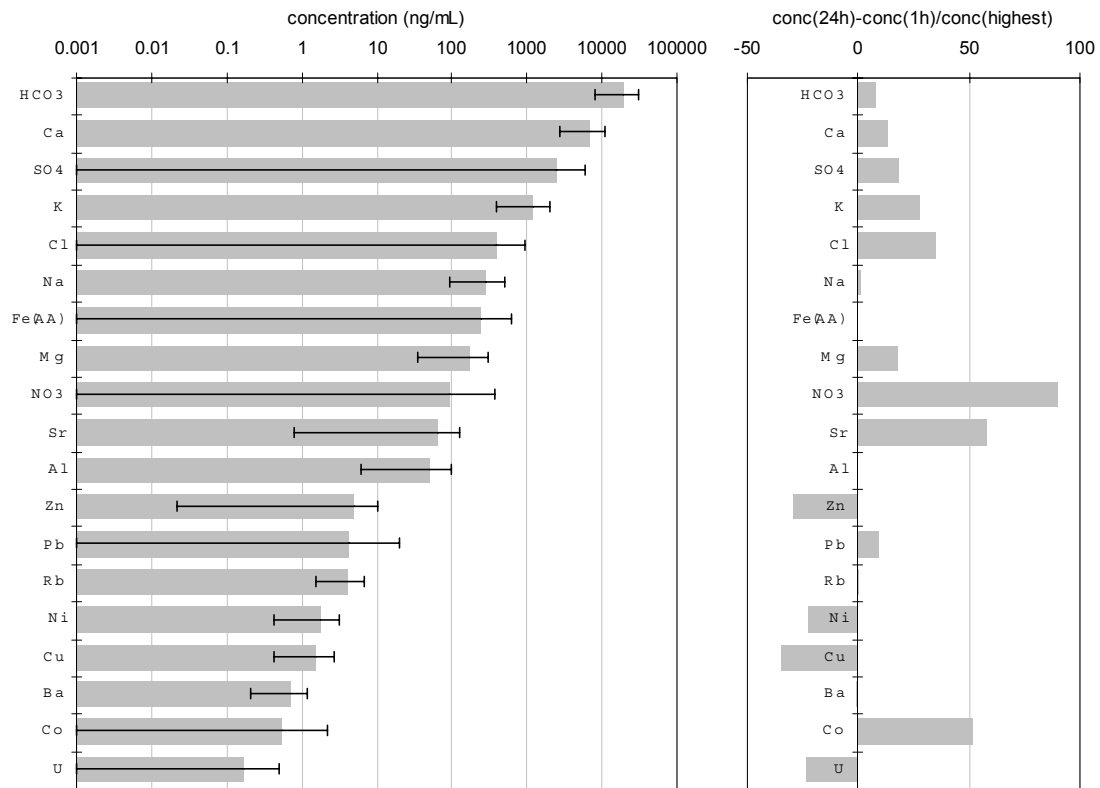


Figure 4.2 Mean solute yield (M/mol) of major and trace elements from 24 hours closed system dissolution of experiments 1-9(c).

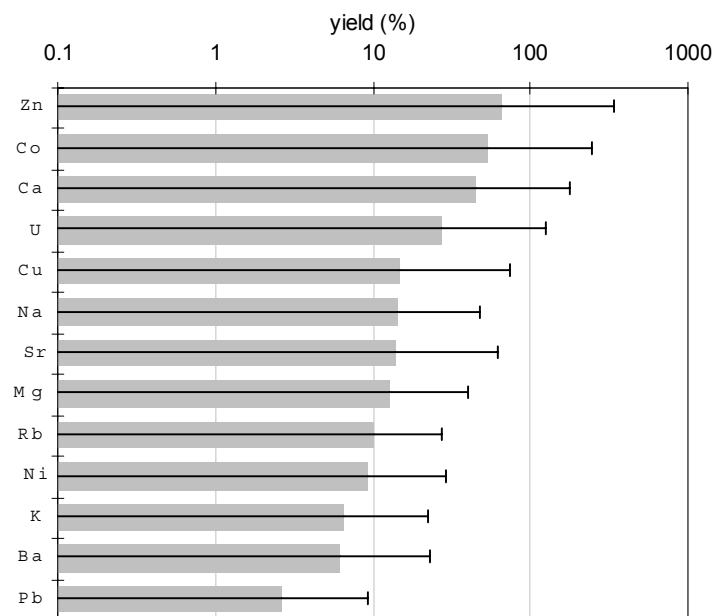


Table 4.3 Mean solute yields of major and trace elements at 1 and 24 hours (%) in laboratory experiments.

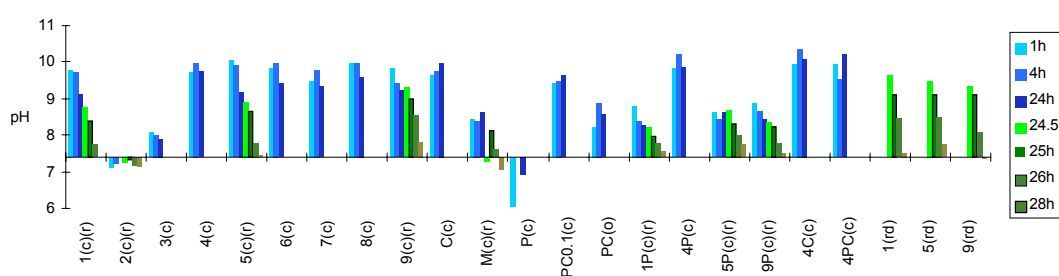
Rock	1(c) 1(c)	2(c) 2(c)	3(c) 3(c)	4(c) 4(c)	5(c) 5(c)	6(c) 6(c)	7(c) 7(c)	8(c) 8(c)	9(c) 9(c)	C(c) C(c)	P(c) P(c)
Time	1h 24h	1h 24h	1h 24h	1h 24h	24h 1h	1h 24h	1h 24h	1h 24h	24h 1h	1h 24h	1h 24h
Na	0.56 0.46	0.37 0.24	0.69 0.95	0.61 0.49	1.02 1.56	0.68 0.34	2.14 1.62	0.89 0.43	1.20 0.58	28.7 48.2	66.7 42.8
K	3.85 3.91	1.89 2.00	0.50 0.88	0.83 1.00	3.56 2.68	1.39 0.92	1.10 1.69	1.84 1.22	6.72 2.84		
Mg	0.40 0.68	0.57 0.70	3.45	0.72 0.49	0.64 0.46	1.03 0.45	0.15 0.07	0.32 0.27	2.85 1.60		75.7 56.2
Ca	0.80 0.75	1.41 1.36	29.4 46.0	68.7 73.8	0.84 0.89	17.7 17.8	2.07 2.20	2.50 2.43	0.57 0.58	5.12 6.61	>100 >100
Fe		0.66				1.67					
Co	0.21 0.09	0.31 0.08	4.06 17.2	0.69 0.44	0.20 1.07	1.01 0.15	0.76 0.11	0.81 0.10	0.34 0.31	23.7 60.9	>100 >100
Ni	0.36 0.23	0.61 0.11	3.41 1.00	4.73 3.52	0.30 0.34	4.59 0.86	0.81 0.12	4.55 1.40	0.59 0.61	74.1 78.8	21.8 4.07
Cu	1.51 1.50	0.64 0.08	2.94	2.92 2.37	0.66 1.86	3.45 0.08	0.60 0.03	2.30 0.48	5.98 4.01	>100 >100	8.24 1.31
Zn	0.86 1.88	0.09 0.28	2.71	1.60	1.06 1.64	1.97 1.96	0.21 0.12	0.11 0.20	5.40 16.1	1210	31.2 9.48
Rb	1.50 1.74	1.56 0.61	0.30 0.38	0.80 0.86	1.74 2.54	1.40 0.70	0.97 0.52	3.45 1.30	15.8 5.96	21.9 44.7	
Sr	0.44 2.87	0.29 0.22	4.46 3.39	6.73 6.62	1.08 0.41	3.31 3.26	0.19 0.15	2.83 5.96	1.57 0.50	2.57 3.04	>100 >100
Ba	0.04 0.03	0.04 0.01	0.07 0.07	0.06 0.06	0.05 0.07	0.03 0.03	0.03 0.01	0.10 0.06	0.51 0.21	35.0 65.2	70.5
Pb	1.10 6.29	83.0	5.19 0.01	8.86 6.17	0.19 0.21	63.4 1.34	2.75	10.0 0.04	1.11 10.2	>100	4.10 1.28
U	0.12 0.17			0.05 0.20	0.17 0.32		0.28		3.22 0.76	>100	2.26 18.0

4.3 DETAILED ANALYSIS OF INDIVIDUAL SPECIES

4.3.1 Acidity

Values of pH in “end member” and morainic rock experiments are summarised in Figure 4.3.

Figure 4.3 pH of laboratory experiments. The horizontal axis represents the average initial pH of the deionised water prior to sediment introduction. In this and all similar figures, experiments labelled (c) were run under closed system conditions up to 24h only, (o) labels indicate open system experiments up to 24h only, and those labelled (c) (r) were run under closed system conditions until 24 hours and then continued under open system conditions between 24 and 28 hours. Those labelled (rd) were 50% diluted by deionised water after 24 hours closed system dissolution, with dissolution continuing under open system conditions until 28 hours.



a) Closed system

Figure 4.4 shows the pH variations in the closed system experiments P/C/PC/P_{0.1}C/PC_{0.1}(c) involving calcite and pyrite. In experiment C(c), rapid pure calcite dissolution raised the pH from its initial value of approximately 7.4 to around 9.7 within one hour, after which pH rose very slowly to reach around 9.9 after 24 hours. This small rise is linked to the continued low-scale carbonate dissolution driven by protons derived from carbonation reactions which also caused the rapid drop in pCO₂.

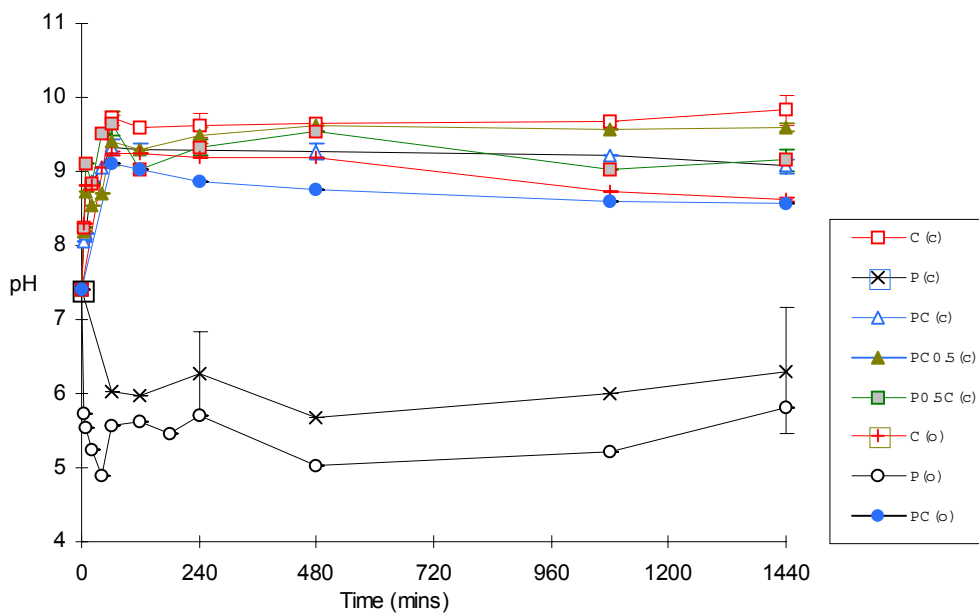
A pH drop of around 1-1.5 units occurred in experiment P(c), which involved the oxidation of 0.2g/L pyrite in the absence of calcite (Figure 4.4). The variation between the duplicates of experiment P(c) is explained if referral is made to Figure 4.6, which shows that significant accessory Ca²⁺ was acquired in one duplicate.

Comparing experiments C(c) and PC(c), the variation in pH in carbonate-buffered solutions with or without pyrite was small after 1 hour (0.3 units). However, the trends then deviated, and a gradual decline in pH occurred with time in experiment PC(c). This trend indicates that the protons produced by sulphide oxidation in these experiments were not completely buffered by carbonate dissolution, but shows that the sulphide source of protons must be partially utilised to explain the continued acquisition of Ca²⁺ in solution despite the slightly increasing pCO₂.

b) Open system

pH variations in open system experiments C/P/PC/P_{0.1}C(o) followed similar trends to that under

Figure 4.4 pH variations in “end member” experiments C/P/PC/P_{0.1}C/PC_{0.1}(c) (closed system) and C/P/PC(o) (open system).

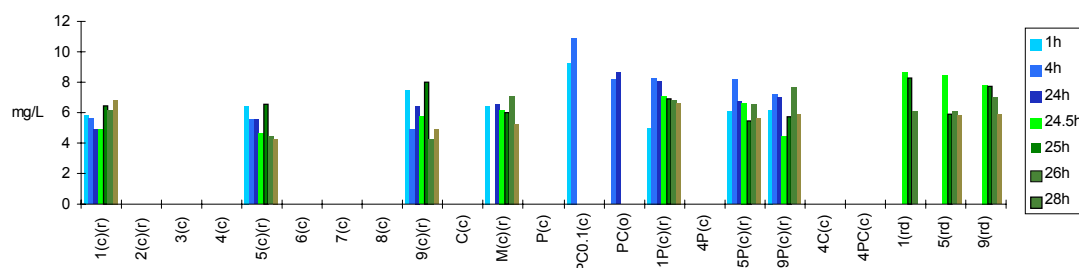


a closed system, rising initially to above 9, linked to carbonate dissolution using up protons (Figure 4.4). The slight downward trend after 1 hour can be attributed to the moving equilibrium between Ca^{2+} , carbonate species and pCO_2 (this is examined in more detail in Section 5.2.3.4) (Garrels and Christ, 1965).

4.3.2 Dissolved oxygen

There is no evidence of dissolved oxygen levels in any experiments (Figure 4.5) decreasing to the levels observed in the field, which reached levels as low as 3mg/L (Figure 3.19), compared to the saturation value at 3000m of 10mg/L (Brown *et al.*, 1994b), or in previous closed system experiments involving pyrite and calcite (Willis *et al.*, 1995), where levels dropped to 1mg/L after 24 hours. However, these previous experiments involved an unrealistically high pyrite/calcite concentration, (3g/L total) (see Section 1.5.1). There is also no apparent recovery of O_2 levels in reopened experiments. If the data presented here is correct, then pyrite oxidation in these experiments was not controlled by the availability of dissolved oxygen. It is possible that the dissolution of pyrite is inhibited by the formation of surface oxidised layers that form an insoluble casing for the sulphide grains (Williamson and Rimstidt, 1994).

Figure 4.5 Dissolved oxygen concentrations (mg/L) in experiments 1/5/9/M/PC_{0.1}/PC/1P/5P/9P. At sea level, the oxygen saturation level is at approximately 15mg/L.



4.3.3 Major cations

4.3.3.1 Calcium

a) Open system, end member experiments

Figure 4.6 shows the acquisition of Ca^{2+} during open-system conditions for experiments C(o), P(o), PC(o) and $\text{P}_{0.1}\text{C}(\text{o})$. Experiments containing calcite underwent a period of rapid acquisition lasting approximately one hour. After this period, acquisition continued at an approximately linear rate to 24h (experiments C(o) and PC(o)) and to 48h (experiment $\text{P}_{0.1}\text{C}(\text{o})$). The Ca^{2+} concentration reached around 650-750 neq/mL after 24 hours, a yield of 6.6% Ca^{2+} from 0.2g/L calcite. Approximately 30-40 neq/mL Ca^{2+} was obtained from the dissolution of pyrite, indicating that the specimen used was not 100% pure FeS_2 .

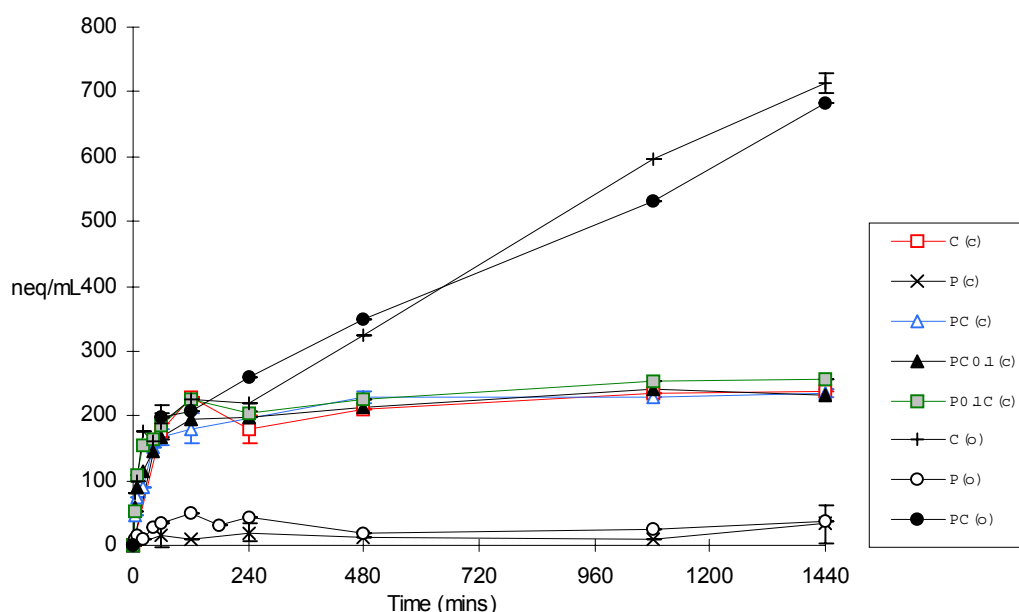
b) Closed system experiments

Dissolution of calcite and calcite/pyrite mixtures under closed system conditions was rapid in the initial hour of the experiments, as was the case with open conditions. After this point, however, dissolution rate slowed dramatically, with very little additional acquisition between 1 and 24 hours (experiments C/PC/ $\text{P}_{0.1}\text{C}$ / $\text{PC}_{0.1}(\text{c})$). There was no additional acquisition up to 48h from experiment PC(c). Ca^{2+} acquisition after 24 hours reached 230-250 neq/mL (Table 4.2).

Experiment PC(c) involved the dissolution of 0.2g/L pyrite plus 0.2g/L calcite, whereas experiment $\text{PC}_{0.1}(\text{c})$ involved 0.2g/L pyrite plus 0.1g/L calcite. However, the similarity in Ca^{2+} concentration after 24 hours of experiments PC/ $\text{PC}_{0.1}(\text{c})$ show that there was apparently little variation as a result of halving the amount of calcite added to the experiment.

In closed system experiments involving morainic rock samples, Ca^{2+} concentrations for rocks

Figure 4.6 Calcium concentrations from open system experiments C/P/PC(o), and closed system experiments C/P/PC/ $\text{P}_{0.1}\text{C}$ / $\text{PC}_{0.1}(\text{c})$.



1, 5, 6, 8 and 9 (experiments 1/5/6/8/9(c)) levelled out in a small range of concentrations, around 250-300neq/mL (Table 4.2, Figure 4.7). Calcium is present at over 20 wt% in rocks 1, 5 and 9 (Table 3.7a), hence calcite was likely to be present in excess amounts in these experiments (i.e. more than sufficient thermodynamically for saturation to occur). Ca is present at 6 wt% in rock 8, but rock 6 contains only 0.85 wt% Ca. When compared with the lower Ca^{2+} concentrations after 24h dissolution from rocks 2 and 7 (experiments 2/7(c)), which contain 3 and 6 wt% respectively (Table 3.7a), it can be seen that the release of calcium into solution was not only a function of Ca content of the rock, but also depended on the mineralogy of the sediment. It is likely that the Ca in rock 2 is largely bound in minerals which are more resistant to chemical weathering, such as feldspar, amphiboles and pyroxenes, which have lower solubilities than calcite. In contrast, the more felsic rocks such as rocks 4 and 6, and rocks containing trace calcite (e.g. rock 3 & 8) produced higher Ca yield percentages (Figure 4.8).

Figure 4.7 Mean concentrations of Ca (ng/mL) in laboratory experiments.

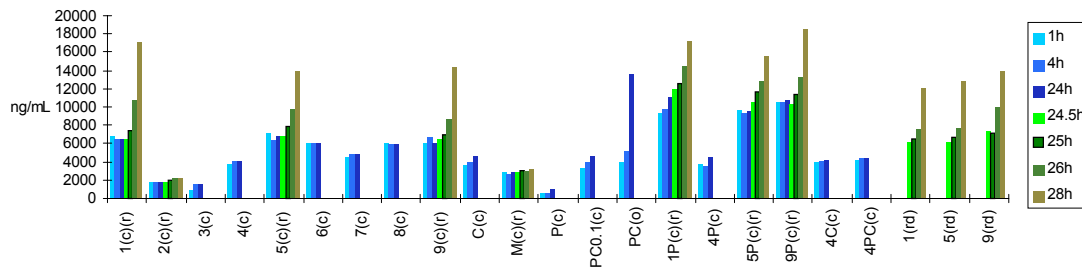


Figure 4.8 Ca^{2+} acquisition from rocks 1-9 after 24 hours closed system dissolution, plotted versus the corresponding Ca content of each rock.

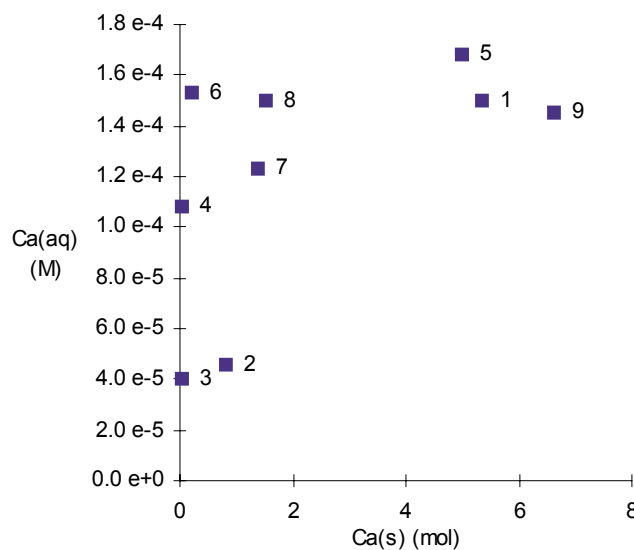
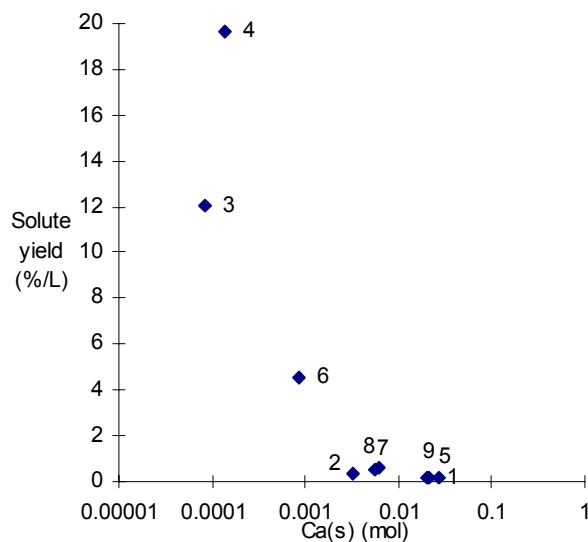


Figure 4.9 shows the solute yield of Ca^{2+} after 24 hours in a closed system environment. The complete dissolution (100% solute yield) of Ca^{2+} from 0.2g/L calcite would produce 10000

neq/mL. Table 4.1 shows that just 240 neq/mL (4.8mg/L) was produced under closed system conditions after 24 hours. This is a 2.4% solute yield.

Figure 4.9 Ca^{2+} yield in closed system dissolution of rocks 1-9, after 24 hours' dissolution.



c) Reopening closed system

Experiments 1/2/5/9/M(c) were continued after 24 hours dissolution for a further 4h under open system conditions, forming experiments 1/2/5/9/M(r).

The extent of Ca^{2+} acquisition between 1 and 24 hours was close to zero in all closed system experiments (Table 4.2; Figure 4.10). However, concentrations of Ca^{2+} increase rapidly upon reopening, albeit at varying rates of acquisition (these variations are discussed in detail in Chapter 5). The range of increase after 4h open system dissolution of rocks 1, 5 and 9 is 200-270%. The same was not true of mixed sediment M and rock 2, which showed increases of 20% and 30% respectively (Table 4.2).

A separate run of experiment 9(c) was continued to 48h under closed system conditions (Figure 4.10), showing that without reopening the system to the atmosphere, no significant further acquisition occurs.

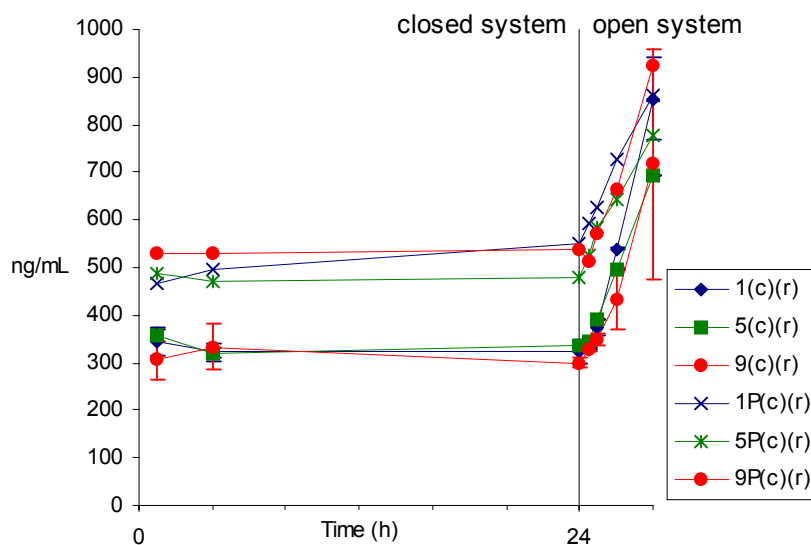
In experiments 1P/5P/9P(r) (with pyrite added to rocks 1, 5 and 9 respectively), the increase in Ca^{2+} concentrations after the 4 hour period of open system acquisition is 160-170%, suggesting that the influence of pyrite oxidation is less under open system conditions than closed system conditions.

d) Influence of sulphide oxidation

In the “end-member” experiments, significant variations existed between experiments C/PC/P_{0.1}C/PC_{0.1}(c) during the first 8 hours. Beyond this time Ca²⁺ concentrations in these experiments reached a similar level (within 7% after 24 hours) (Figure 4.6). The same is true of the open system C/PC/P_{0.1}C(o) (Figure 4.6). Only experiments P(c)/(o), with no calcite added, produced lower values. There was no significant variation in rate or magnitude as a result of the presence of pyrite, suggesting that the level of proton supply produced by the addition of 0.2g/L pyrite with this grain size distribution is not sufficient to drive significant further dissolution.

In contrast to the “end member” experiments, the amount of Ca²⁺ produced in experiments involving calcium-rich morainic rocks and added pyrite (experiments 1P/5P/9P(c)) is considerably higher under closed system conditions than in similar experiments without pyrite added (experiments 1/5/9(c)) (Table 4.2, Figure 4.10). The concentration of Ca²⁺ after 24 hours from experiments 1P/5P/9P(c) was 170%, 140% and 180% higher respectively than the corresponding experiments without pyrite. The amount of SO₄²⁻ produced in experiments 1P/5P/9P(c) was considerably higher than in experiments C/P/PC/P_{0.1}C/PC_{0.1}(c) (see Section 4.4.2). Calcium production was clearly increased as a result of the magnitude of pyrite oxidation that occurred to produce the observed levels of SO₄²⁻.

Figure 4.10. Closed system Ca²⁺ concentrations in experiments 1/5/9/1P/5P/ 9P(c), continuing through to open system acquisition after 24h (1440 min) (1/5/9/1P/5P/9P(r)). Error bars are shown for experiments 1(c)/(r) and 9(c)/(r), which had repeat runs. Zero concentration is assumed at time=0.



e) Experiments 50% diluted with deionised water after 24h

Separate runs of experiments 1/5/9(c) were continued beyond 24 hours under open system conditions, after being diluted by 50% at this point with atmosphere-equilibrated deionised water. Open system dissolution continued for a subsequent 4 hour period. Table 4.2, Figure 4.10 and Figure 4.11 show that the pattern of the increase in concentration of Ca^{2+} after reopening the system to the atmosphere was virtually the same whether dilution had occurred or not: experiments 1/5/9(rd) showed increases of 190-230% compared with 200-270% from the corresponding undiluted experiments. A mean 20% increase in Ca^{2+} concentration from mixed sediment M was observed (experiment M(rd)), identical to the figure obtained without dilution (Table 4.2).

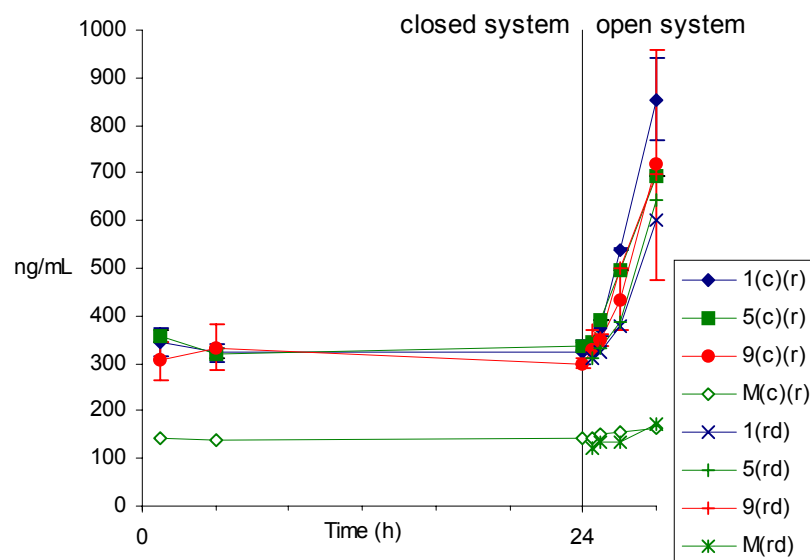
4.3.3.2 Magnesium

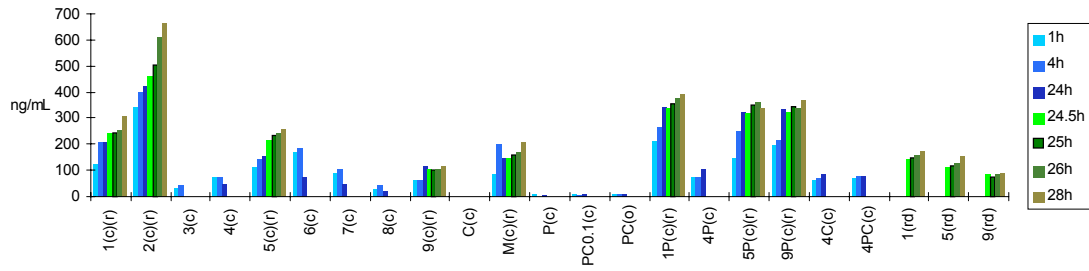
a) Morainic rock experiments

The concentrations of magnesium obtained in solutions resulting from “end-member” and morainic rock dissolution experiments are illustrated in Figure 4.12. Closed system concentrations do not exceed 420ng/mL (35neq/mL) in any experiment, and Mg was not found in solutions of pure calcite (experiment C(c)).

Figure 4.12 Concentrations of Mg (ng/mL) in laboratory experiments.

Figure 4.11 Effects of 50% dilution of experiments with atmosphere-equilibrated deionised water on Ca^{2+} concentration. Experiments were under closed system conditions up to 1440 min. Dilution occurred immediately after the 1440 min sample was taken, after which the experiment was continued under open conditions. Error bars are shown for experiments 1(c)/(r) and 9(c)/(r), which had repeat runs. Zero concentration is assumed at time=0.



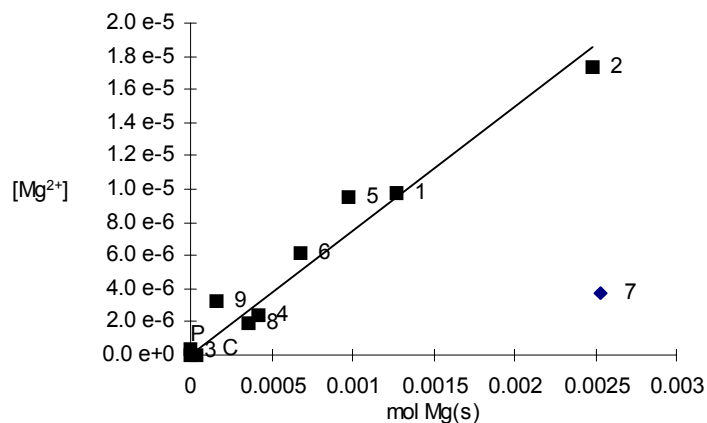


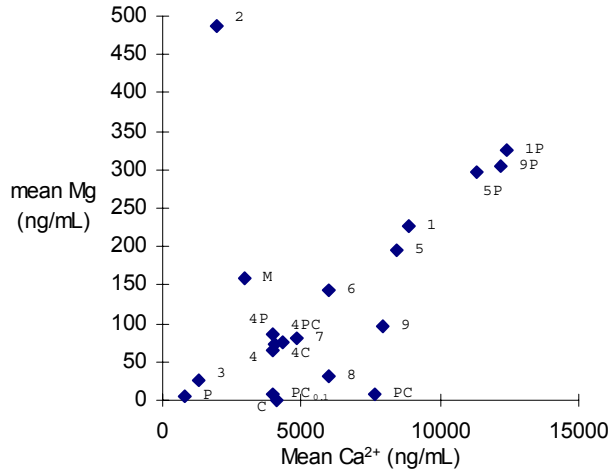
Magnesium concentrations in solution after 24 hours were closely related to the original rock Mg content (Figure 4.13). The exception was rock 7, which produced an unusually low Mg yield, but is in any case a very atypical catchment rock. In bulk meltwaters, Mg is often assumed to be dissolved from carbonate rocks, due to the highly coincident abundances of Ca^{2+} and Mg^{2+} (Brown *et al.*, 1996b). These experiments show that an alternative source of Mg present in rock 2 (olivine gabbro) provides the highest concentration of Mg, although Mg also dissolves significantly from carbonate-rich diopside marbles (rocks 1 and 5).

The plot of mean Mg^{2+} and Ca^{2+} concentrations (Figure 4.14) suggests that Mg^{2+} provenance is linked to Ca^{2+} provenance in experiments dissolving rocks 1, 3, 4, 5, 6, 7 and P. The similar ratio in all experiments suggests a similar calcium/magnesium mineral provenance that is likely to be carbonate (dolomite or magnesian calcite). Experiments 8/9/C produced lower Mg/Ca ratios, suggesting a purer calcite provenance. However, experiment 2 showed a much higher Mg/Ca ratio suggesting a non-carbonate magnesium provenance. The Mg/Ca ratio of experiment M suggests that the mixed sediment contained some grains of the type of rock 2.

Figure 4.14 Comparison of mean Mg^{2+} and Ca^{2+} concentrations in dissolution experiments under all time scales and conditions.

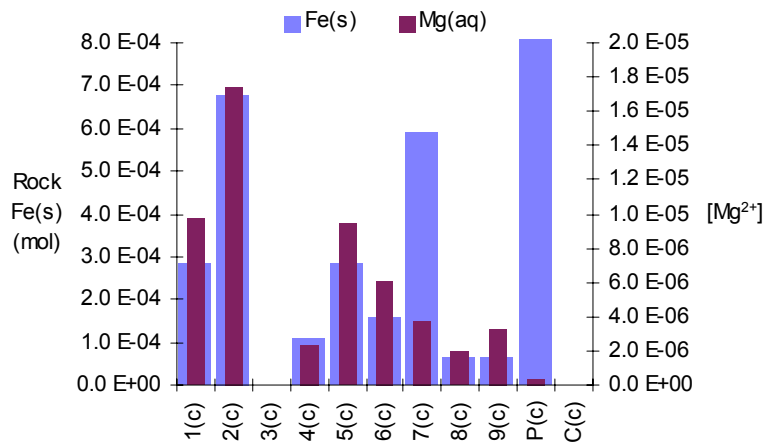
Figure 4.13 Comparison of Mg^{2+} concentrations in solution after 24 hours' dissolution with corresponding rock Mg content. Regression statistics: $[\text{Mg}^{2+}] = 0.0075(\text{Mg}(s))$; $r^2 = 0.95$ (rock 7 was excluded from the regression calculations).





Mg concentrations in closed system experiments were also closely related to rock Fe content, except with experiments 7(c) and P(c) (Figure 4.15). This is linked to the fact that Fe and Mg were closely coincident in the morainic rocks studied ($r^2=0.99$, $n=9$) (Table 3.4, Chapter 3), although Mg was not significantly present in pyrite (Table 3.2, Chapter 3). The mutually high concentrations of Mg^{2+} and SO_4^{2-} produced from the dissolution of rock 2, therefore, may be due to a mineral assemblage including both Fe-Mg silicates (such as pyroxenes, biotite, amphiboles and/or secondary oxides) and pyrite or a sulphate mineral (see below).

Figure 4.15 Comparison of Mg^{2+} concentrations in solution after 24 hours' dissolution with corresponding rock Fe content. The rock Fe(s) content of pyrite is above the scale, at 0.0047 mol.

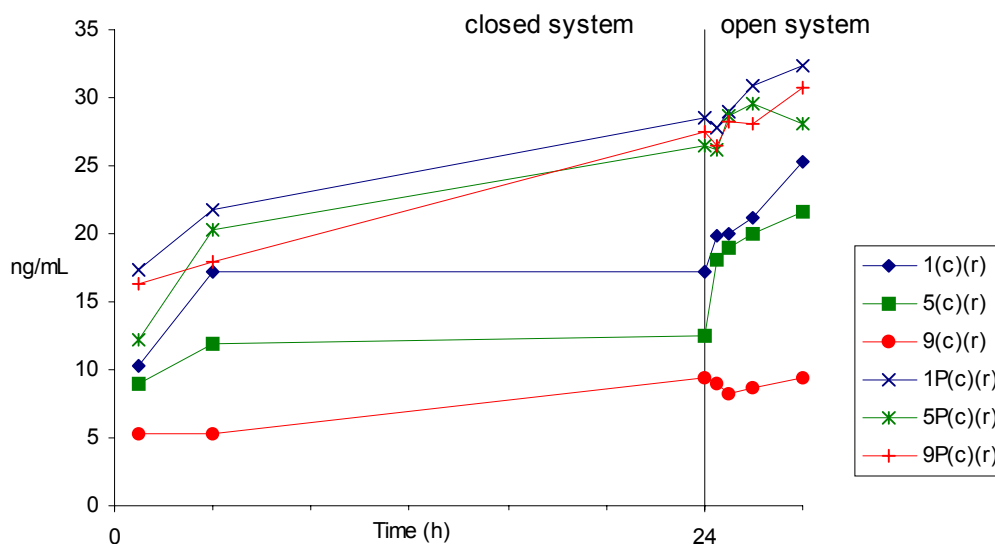


b) Reopening a closed system

The concentration of Mg^{2+} generally increased in experiments that were reopened after 24 hours of closed system dissolution. Experiments 1/2/5(r) showed significant increases in Mg^{2+} concentration over the period of dissolution with open access to the atmosphere,

between 24 and 28 hours (Figure 4.16). These increases were between 50 & 70%. In contrast, no increase occurred in experiment 9(r).

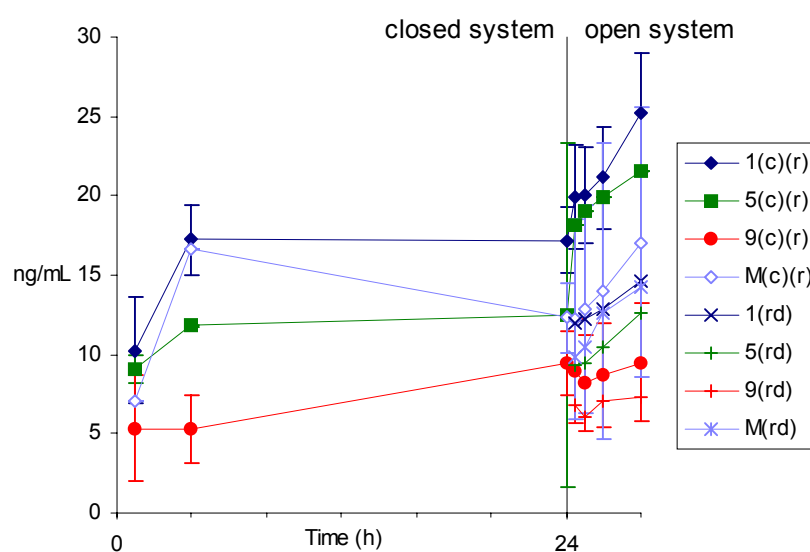
Figure 4.16 Closed system Mg^{2+} concentrations in experiments 1/5/9/1P/5P/9P(c), continuing through to open system acquisition after 24 hours (1440 minutes) (1/5/9/1P/5P/9P(r)). Error bars are shown for experiments 1(c)/(r) and 9(c)/(r), which had repeat runs. Zero concentration is assumed at time=0.



c) 50% dilution

The recovery of Mg^{2+} concentrations in solution after 50% dilution with deionised water is slow despite open system conditions (Figure 4.17). The effects of dilution are therefore distinct from those of Ca^{2+} , which quickly recovered to pre-diluted concentrations (see Section 4.3.3.1).

Figure 4.17 Effects of 50% dilution of experiments with atmosphere-equilibrated deionised water on Mg^{2+} concentration. Experiments were under closed system conditions up to 24h. Dilution occurred immediately after the 24h sample was taken, after which the experiment was continued under open conditions.



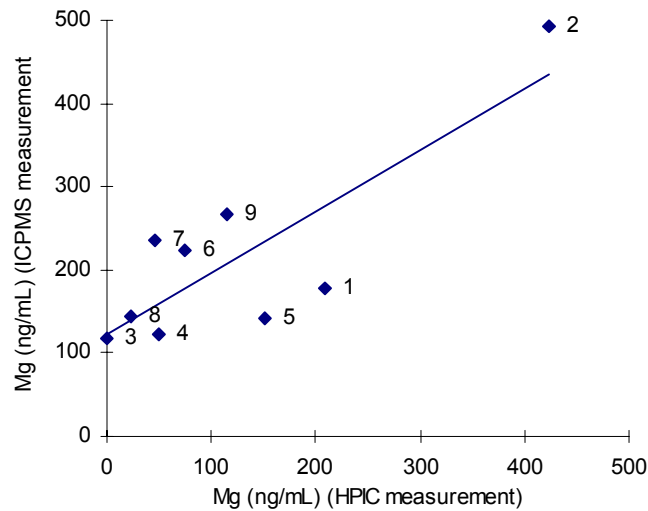
d) Influence of sulphide oxidation

The concentrations of Mg^{2+} in experiments 1P/5P/9P(c) together with pyrite were 170%, 200% and 290% higher than the corresponding experiments without pyrite (Figure 4.16): the presence of pyrite clearly had a significant effect on the acquisition of Mg^{2+} . Protons produced by pyrite oxidation in experiment 2(c) are likely to have driven the dissolution of magnesium-bearing minerals, giving a similar yield of Mg to that of experiments 1/5/9(c).

e) Note on variation between results obtained from HPIC and ICPMS analysis

ICPMS analysis of experiments 1-9(c) showed apparently higher observed concentrations in rocks 2 and 7 in comparison to analysis by ion chromatography (Figure 4.18). This difference highlights a problem of analysis of filtered solutions by ICPMS. Since solutions were filtered through 0.45 μ m filter membranes, particles finer than this may be present in the filtrate. These particles may be analysed by ICPMS, with particle metal content included in the total analysed concentration. However, solutions undergo further filtration in the analytical process by HPIC, and particles may not influence the analyses to the same extent (although further dissolution could occur during the storage of samples prior to analysis). It is therefore probable that the HPIC results are a more accurate reflection of true Mg^{2+} ionic concentration than the ICPMS analyses. This problem is likely to affect highly insoluble and adsorbable species, which undergo the bulk of transport in the particulate phase.

Figure 4.18 Comparison between observed concentrations of Mg^{2+} (ng/mL) after 24h of experiments 1-9(c) obtained from HPIC and ICPMS analyses. The linear regression statistics are: $Mg(ICP) = 0.74Mg(HPIC) + 120$; $r^2 = 0.68$.

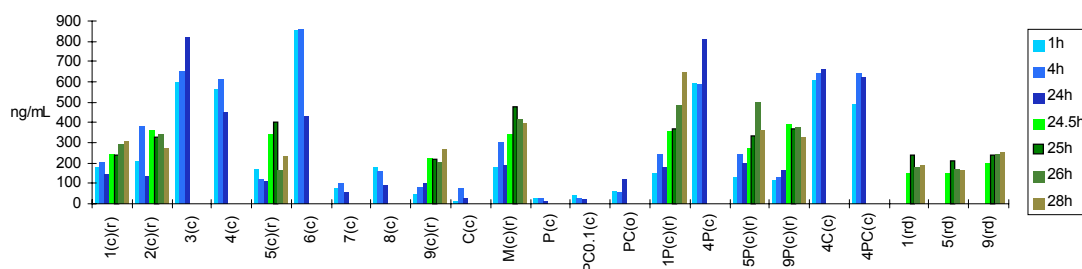


4.3.3.3 Sodium

a) Morainic rock experiments

Sodium dissolution reached highest concentrations from experiments 3/4/6(c) (Figure 4.19). The concentrations of Na^+ after 24 hours was closely related to rock sodium content (Figure 4.20). Although sodium is particularly soluble in water, and can reach parts-per-thousand concentrations before saturation levels are reached. Equation 1.20 shows that albite hydrolysis is likely to depend dominantly on the activity of the silicate weathering product.

Figure 4.19 Concentration of Na, in laboratory experiments.



It is of note that the rock-water ratio for both sodium and magnesium in experiments 1-9/P/C(c) are very similar:

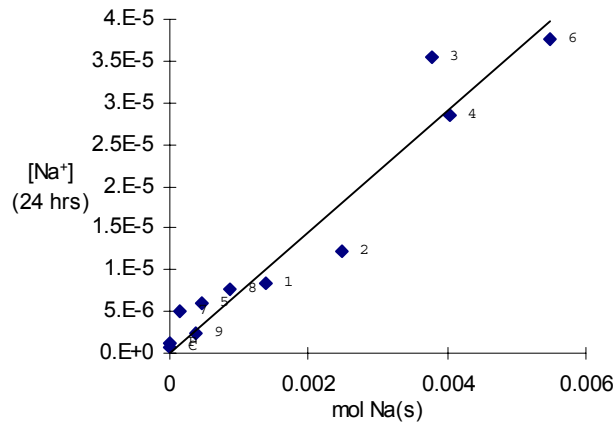
$$[Mg^{2+}] = 0.0075(Mg(s))$$

$$[Na^+] = 0.0073(Na(s))$$

This suggests that the dissolution of both elements is related to the surface area of the crushed sediment. Although surface area variations were not implicitly investigated in this

study, it is apparent that quantification of this parameter would be common for all elements for which good correlations between rock content and dissolved concentration were obtained.

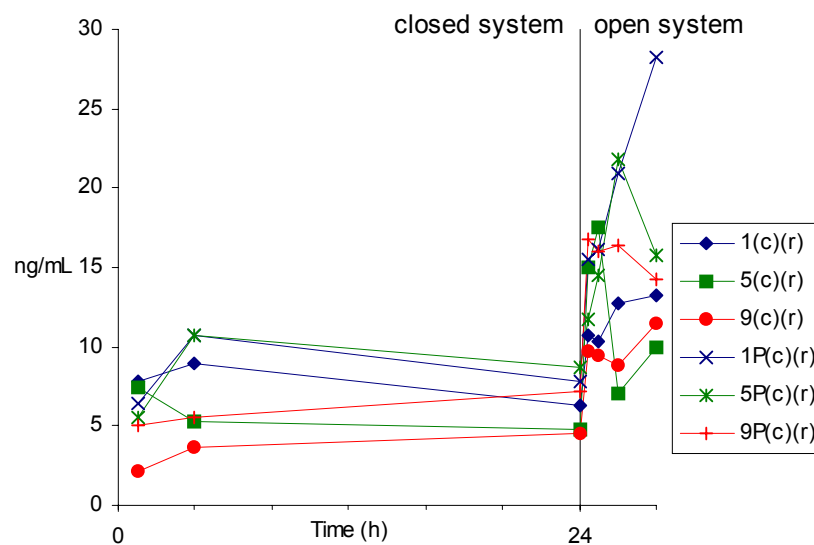
Figure 4.20 Comparison of Na^+ concentrations in solution after 24 hours' dissolution with corresponding rock Na content. Linear regression statistics: $[\text{Na}^+] = 0.0073(\text{Na(s)})$; $r^2 = 0.93$.



b) Reopening closed system experiments to the atmosphere

The relationship between rock-water contact time and sodium acquisition was not continued under reopened experiments, as demonstrated by the relationship between sodium yield and time in experiments 1/5/9(r) and 1P/5P/9P(r) (Figure 4.21) (note these experiments were low in both sodium rock content and Na^+ concentration). Each of these experiments showed rapid increases in acquisition in the first hour after reopening the experiments at 24h,

Figure 4.21 Closed system Na^+ concentrations in experiments 1/5/9/1P/5P/9P(c), continuing through to open system acquisition after 24 hours (1440 minutes) (1/5/9/1P/5P/9P(r)). Error bars are shown for experiments 1(c)(r) and 9(c)(r), which had repeat runs. Zero concentration is assumed at time=0.



followed by either a reduction in the rate of acquisition or an episode of reprecipitation. However, it would appear that the concentration between 2 and 4h of reopened dissolution may be more closely linked to residence time, and in all reopened morainic rock experiments (1/2/5/9/M(r)), the increase in concentration between the end of the period of closed system acquisition (24h), and subsequent to the further 4h period of open system acquisition, was consistently around double ($114\% \pm 16\%$).

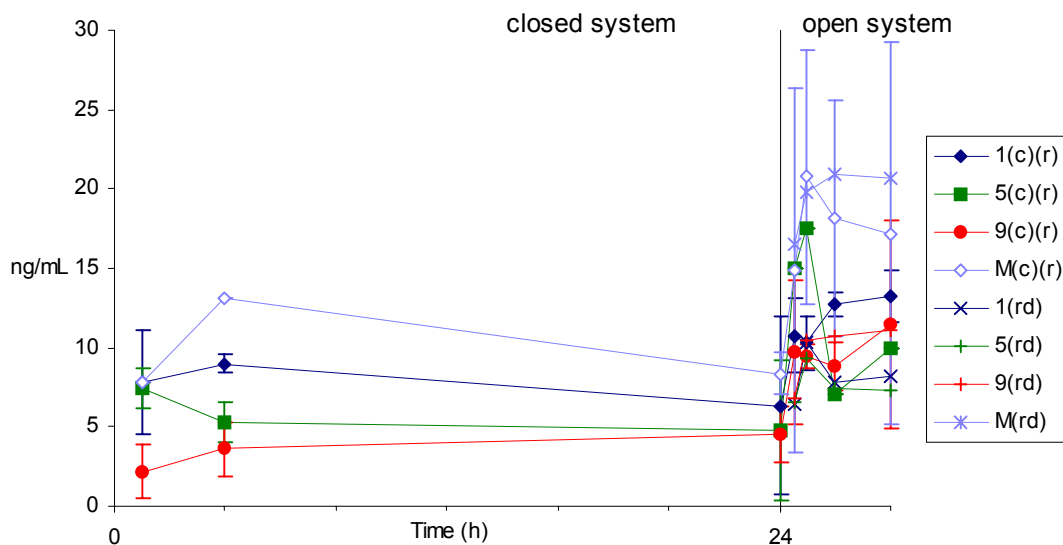
c) Influence of sulphide oxidation

The concentrations of Na^+ in experiments dissolving rocks 1, 4, 5 and 9 together with pyrite are respectively 120%, 180%, 180% and 150% higher than the corresponding experiments without pyrite, after 24 hours closed system dissolution (Figure 4.19). The presence of pyrite therefore also had a significant effect on the acquisition of Na^+ . Unlike Mg^{2+} , however, the influence of pyrite appeared to remain as great upon opening the system.

d) Reopening closed system experiments to the atmosphere, and diluting 50% with deionised water

In experiments 1/5/9(rd), 50% dilution with deionised water after 24 hours closed system dissolution resulted in a near doubling in Na^+ concentration between the time of dilution and 1 hour hence, with little further acquisition after this time (Figure 4.22). There is also an 250% increase in experiment M(rd) (mixed sediment) at this point. These results were

Figure 4.22 Effects of 50% dilution of experiments with atmosphere-equilibrated deionised water on Na^+ concentration. Experiments were under closed system conditions up to 24h. Dilution occurred immediately after the 24h sample was taken, after which the experiment was continued under open conditions.



broadly similar to those of experiments 1/5/9(r) where dilution did not take place. There was no evidence of salt contamination during the dilution process, as Cl^- concentrations were not systematically increased after dilution.

4.3.3.4 Potassium

a) Morainic rock experiments

Figure 4.23 Concentrations of K (ng/mL) in laboratory experiments.

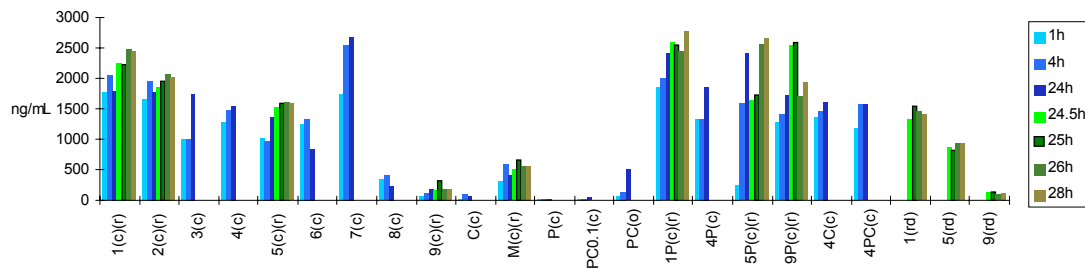


Figure 4.24 Comparison of K^+ molar concentrations in solution after 24 hours' dissolution with corresponding rock K content. Linear regression $[\text{K}^+] = 0.013\text{K}(\text{s})$; $r^2 = 0.21$

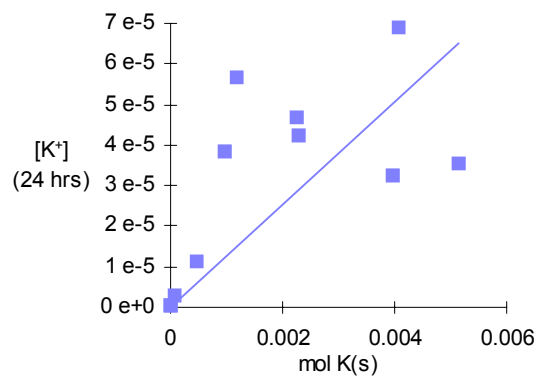
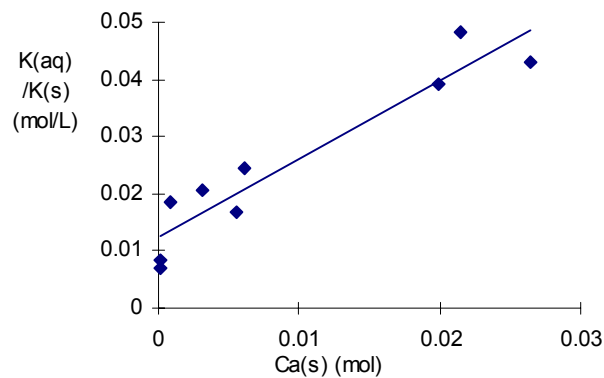


Figure 4.25 Relationship between potassium solute yield and Ca rock content, after 24h dissolution. Linear regression statistics: $[\text{K}^+]/\text{K}(\text{s}) = 1.37\text{Ca}^{2+}(\text{s}) + 0.01$; $r^2 = 0.90$



The concentrations of potassium resulting from “end-member” and morainic rock experiments are illustrated in Figure 4.23. Acquisition is less closely linked to original rock content than the other major ions, according to Figure 4.24. The mean relationship between rock content and dissolved concentration is also significantly higher than that of sodium and magnesium, which were thought to be related to surface area. Therefore, it is apparent that another control affected potassium acquisition.

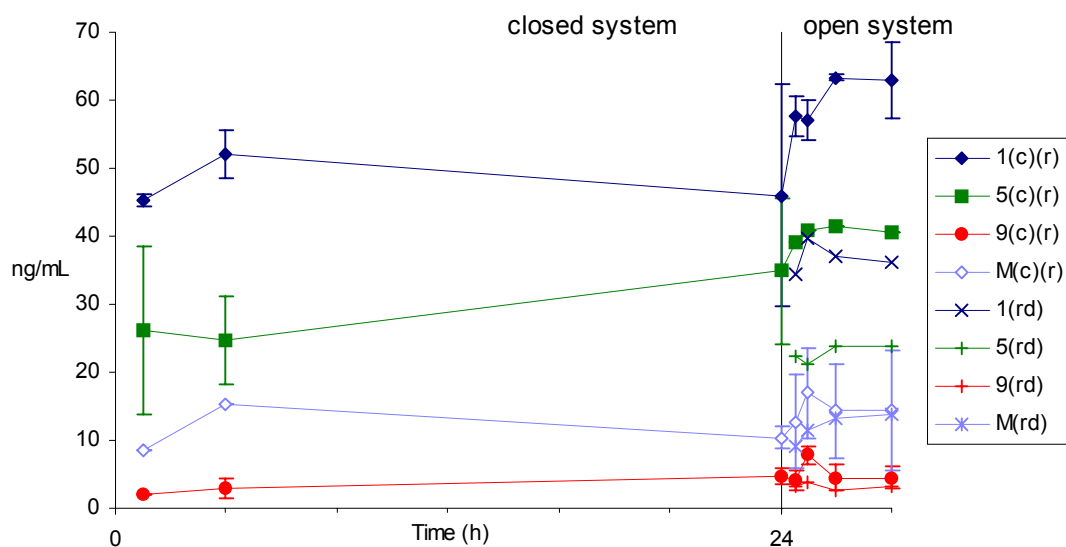
Figure 4.25 shows that the solute yield of K ($K^+(aq)/K(s)$) increases in rocks with a higher Ca content ($r=0.62$, $n=9$). This suggests that the carbonate-driven CO_2 -drawdown and proton production has a residual effect on the dissolution of potassium. Alternatively, there may be less opportunity for adsorption of K^+ from the carbonate-rich solutions, as these are often low-Fe experiments, or would support more Fe- CO_3 complexing, with the result that fewer iron oxides and hydroxides are precipitated, which are the main adsorbers of most solutions (Rankama and Sahama, 1950).

Reopening experiments involving rocks 1, 5, 9 and M to the atmosphere had little effect on the concentration of K^+ in solution (Table 4.2), with the concentration after 4 hours between 60 and 140% of the closed system concentration after 24 hours.

b) Reopening closed system experiments to the atmosphere, and diluting 50% with deionised water

Potassium concentrations in experiments 1/5/9(rd) did not recover quickly subsequent to 50%

Figure 4.26 Effects of 50% dilution of experiments 1/5/9(r) with atmosphere-equilibrated deionised water on K^+ concentration (experiments 1/5/9(rd)). Experiments were under closed system conditions up to 24h. Dilution occurred immediately after the 24h sample was taken, after which the experiment was continued under open conditions.



dilution with deionised water, and after 4 further hours remained at 68-80% of the concentrations prior to dilution (Figure 4.26).

c) Influence of sulphide oxidation

The concentration of K^+ in solutions with rocks 1 and 5 with pyrite (experiments 1P/5P(c)) after 24 hours were 130% and 180% greater respectively than those without pyrite (Figure 4.27). The presence of pyrite had an even greater effect on the concentration of K^+ produced from rock 9, which was ten times higher than without pyrite. These effects continued in open system conditions. However, there was no relationship between K^+ and SO_4^{2-} in other experiments ($r=0.3$, $n=11$), and negligible K content in pyrite.

4.3.4 Major anions

4.3.4.1 Bicarbonate

Bicarbonate concentrations were derived from charge balance error calculations. These calculations were verified with frequent titration alkalinity determinations (see Section 2.4.4). Results are summarised in Figure 4.28.

Figure 4.27 Effects of pyrite in experiments 1P/5P/9P(c)&(r) on K^+ concentration, compared with pyrite absent experiments 1/5/9(c)/(r). Experiments were under closed system conditions up to 24h, after which the experiment was continued under open conditions.

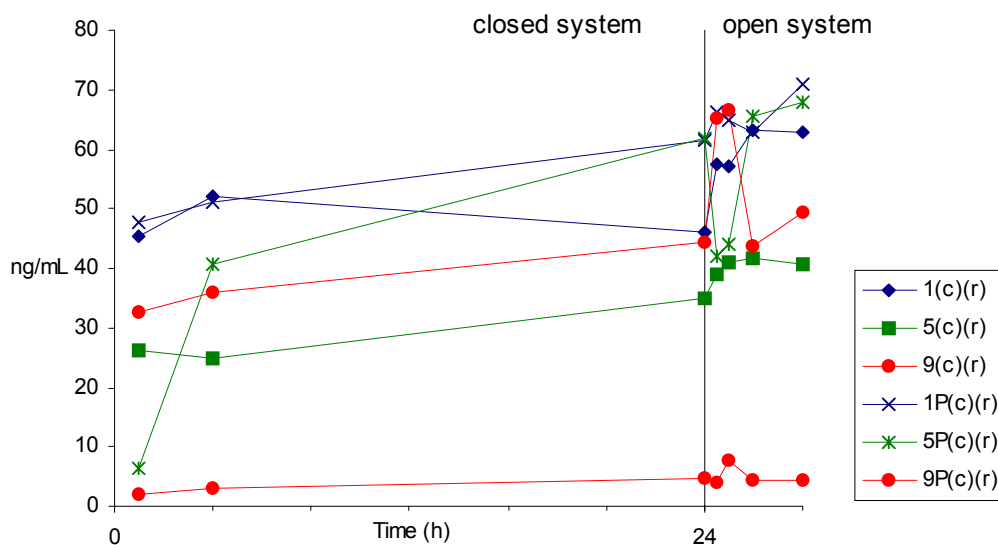
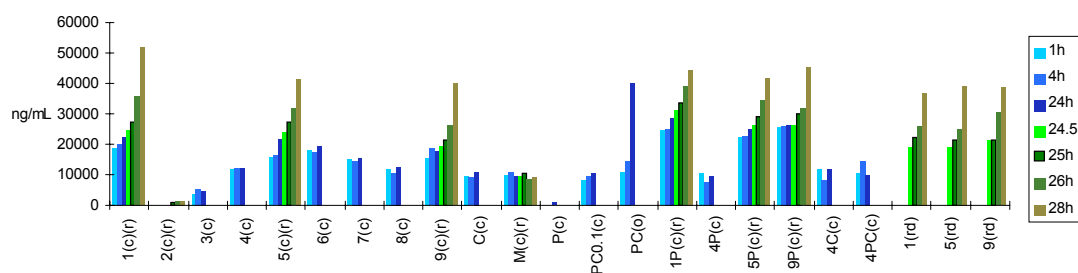
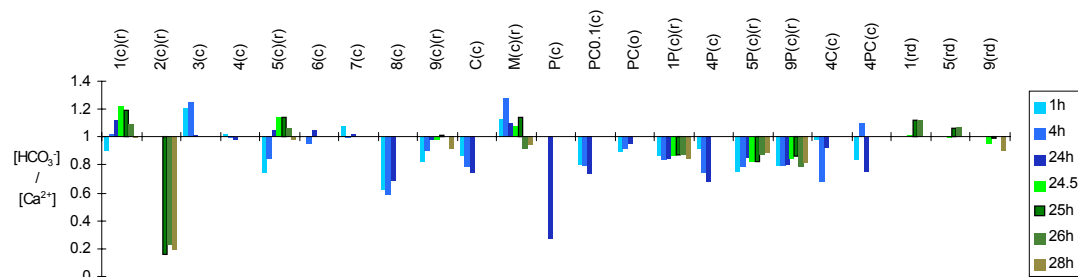


Figure 4.28 Concentrations of HCO_3^- (ng/mL) in laboratory experiments.



In all experiments, bicarbonate concentrations closely reflected Ca^{2+} levels in solution, but $\text{HCO}_3^-/\text{Ca}^{2+}$ charge equivalent ratios were higher in rocks with a metal content less dominated by calcium. Thus, experiments 1/5(c) (both involving diopside marble) displayed $\text{HCO}_3^-/\text{Ca}^{2+}$ ratios of 1.22 and 1.06 respectively, after 24 hours closed system dissolution, indicating a significant influence of aluminosilicate dissolution (Figure 4.29) whereas experiments 9/C(c) (both involving dominantly calcite vein material) had ratios of 1.03 and 0.99 respectively, indicating a dominance of carbonation-driven carbonate dissolution (see Section 1.3.3c for details on interpretation of $\text{HCO}_3^-/\text{Ca}^{2+}$ ratios).

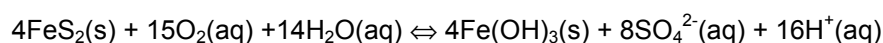
Figure 4.29 $\text{HCO}_3^-/\text{Ca}^{2+}$ ratios of laboratory experiments.



a) Effects of sulphide oxidation

Sulphide oxidation produces additional protons (Equation 4.2), reducing the requirement for CO_2 drawdown and subsequent conversion to HCO_3^- . Calcite dissolution driven by sulphide oxidation produces 1:2 equivalent ratios of $\text{HCO}_3^-/\text{Ca}^{2+}$.

Equation 4.2 Oxidation of pyrite by oxygen



Consistent with this theory, experiments 1P/5P/9P(c), involving pyrite and with high SO_4^{2-} concentrations, produced lower $\text{HCO}_3^-/\text{Ca}^{2+}$ ratios (in the range 0.81-0.89) than those without pyrite.

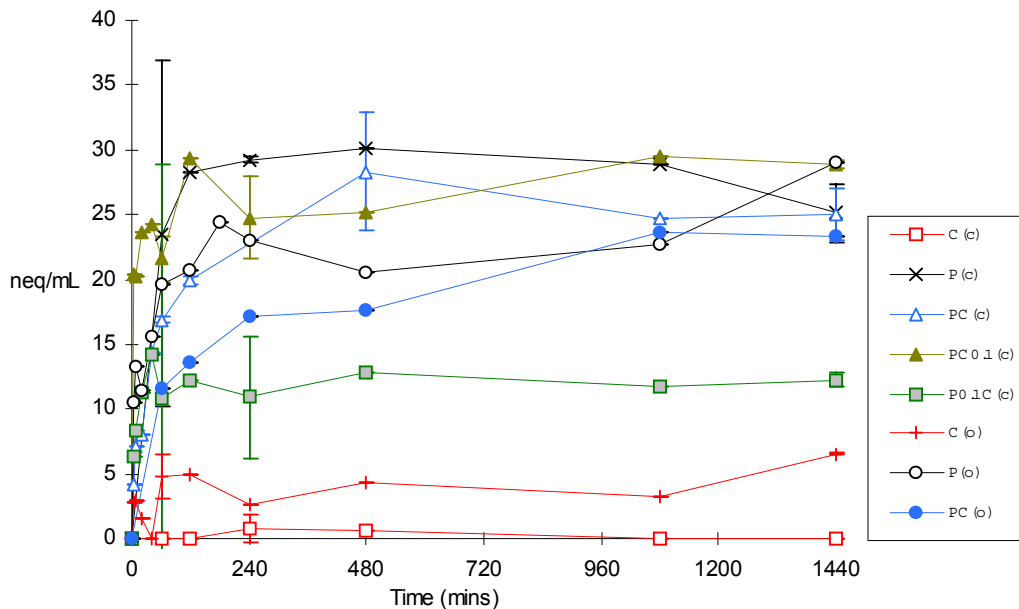
4.3.4.2 Sulphate

a) End-member experiments

A mean of just 25 neq/mL SO_4^{2-} (2.2 mg/L) was produced after 24 hours dissolution of 0.2 g/L pyrite, from a potential 2200 neq/mL available (assuming approximately 53% S content of pyrite). Thus, no more than 1.1% dissolution of the pyrite can have occurred, assuming uniform dissolution.

The mean yield of SO_4^{2-} from pyrite is not significantly increased under open system conditions, with just 23 neq/mL dissolved from 0.2 g/L pyrite after 24 hours (Table 4.2, Figure 4.30). The results are, however, very variable in these samples.

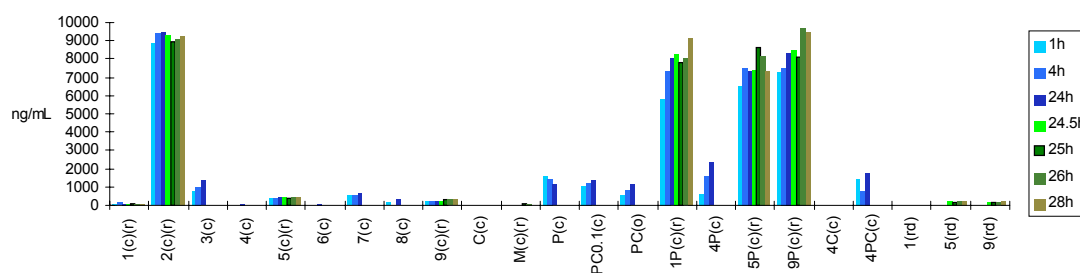
Figure 4.30 SO_4^{2-} acquisition in end member experiments C/P/PC/P_{0.1}C/PC_{0.1}(c) (closed system) and C/P/PC(o) (open system).



b) Morainic rock experiments

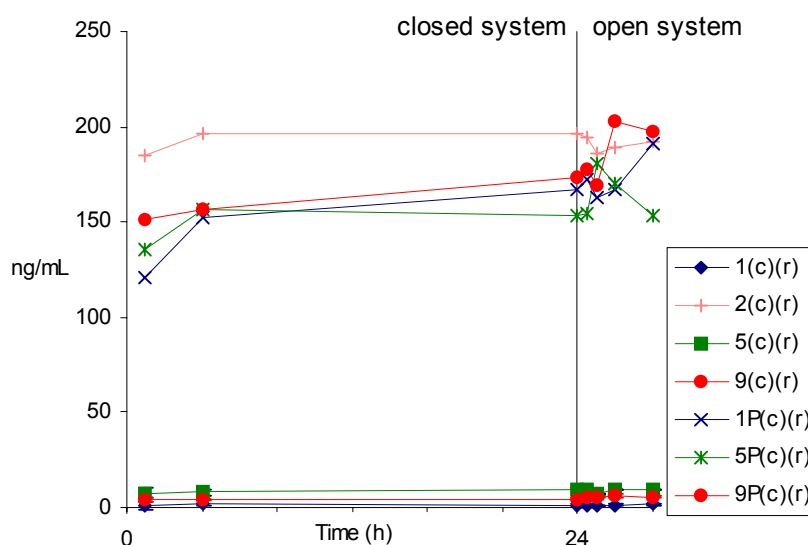
SO_4^{2-} acquisition in solutions resulting from experiment 2(c) reached 9000 ng/mL after 4h, with no additional subsequent acquisition. Experiments 1P/5P/9P(c)/(r) also reached concentrations in excess of 7500 ng/mL (Figure 4.31) at 24h. No other experiments resulted in concentrations in excess of 3000 ng/mL, and only experiments 3/4P/4PC(c) produced over 1000 ng/mL. The concentrations achieved in experiments 4P/4PC(c) were similar to experiments P/PC(c), showing that the morainic sediment had no discernable effect on pyrite oxidation.

Figure 4.31 Concentrations of SO_4^{2-} (ng/mL) in laboratory experiments.



Unlike in the “end-member” experiments described above, the pyrite used in experiments 1P/5P/9P(c)/(r) had been previously crushed in a TEMA mill. Given the small concentrations of SO_4^{2-} produced from experiments 1/5/9(c)/(r) (Figure 4.32), it is likely that the dominant source of SO_4^{2-} in experiments 1P/5P/9P(c)/(r) was pyrite. Therefore, the increased surface area produced by TEMA-crushing (as opposed to hand-crushing with a mortar and pestle) is responsible for an almost factor-of-ten increase in sulphide oxidation.

Figure 4.32 Concentrations in SO_4^{2-} from closed system experiments 1/2/5/9/1P/5P/9P(c) and in subsequent reopened experiments 1/2/5/9/1P/5P/9P(r).



The dissolution of rock 2 under closed systems (experiment 2(c)) produced concentrations of SO_4^{2-} of 200 ng/mL, in excess of the concentrations in experiments 1P/5P/9P(c) involving TEMA-crushed, pure pyrite. Petrological observations suggested that pyrite may be present in rock 2, but not at equivalent levels to produce the same magnitude of aqueous SO_4^{2-} as 0.2g/L pure pyrite. (around 5% total rock content). However, pyrite present in rock 2 may have a different form to the pyrite used, which may have affected the reactive surface area. Variations in surface area may also occur as an artefact of the crushing process.

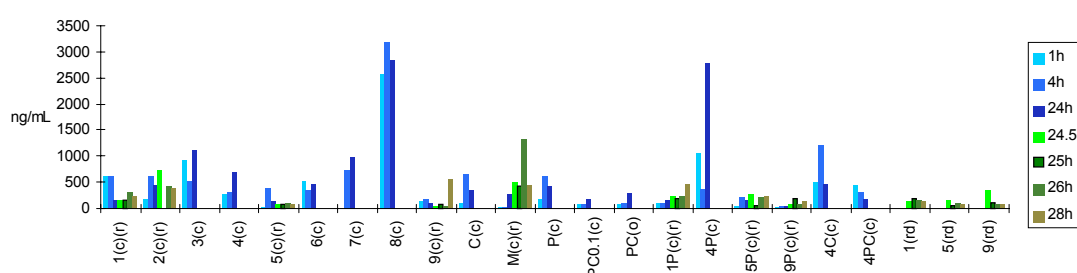
The possibility that gypsum or anhydrite may be present in small amounts in rock 2 can not be discounted. The presence of hydrothermal mineralization was suggested by petrological investigations. Anhydrite is often associated with hydrothermal mineralization, and secondary weathering of sulphurous hydrothermal minerals could produce gypsum (Clark, 1979). This would have important implications for investigations of the coupling of sulphide oxidation and carbonate dissolution based on solution SO_4^{2-} concentrations.

4.3.4.3 Chlorine

A relatively high Cl^- concentration resulted from experiment 8(c) (closed system dissolution of rock 8) in comparison to other dissolution experiments (Figure 4.33). Since this was not associated with an abnormally high sodium content, the likelihood of sample contamination by salt was unlikely, and the results also suggest that acid-contamination could explain this anomaly, as concentrations are consistent across the time intervals, and high values were not encountered in other samples that were analysed at the same time. The average chlorine content of crustal rocks is 314mg/kg (Goldschmidt and Muir, 1958), and so it is possible that the rock either contains significant Cl^- , or that salt had deposited on the rock sample in the field. All samples were bagged on site and hand-contamination could not affect the results to the tune of 60neq/mL, given that the samples were not handled after crushing and homogenizing.

There is little evidence of an influence of access to atmospheric gas in the results shown, and Cl^- values did not appear to recover from 50% dilution with deionised water.

Figure 4.33 Concentrations of Cl^- (ng/mL) in laboratory experiments.



4.3.4.4 Nitrate

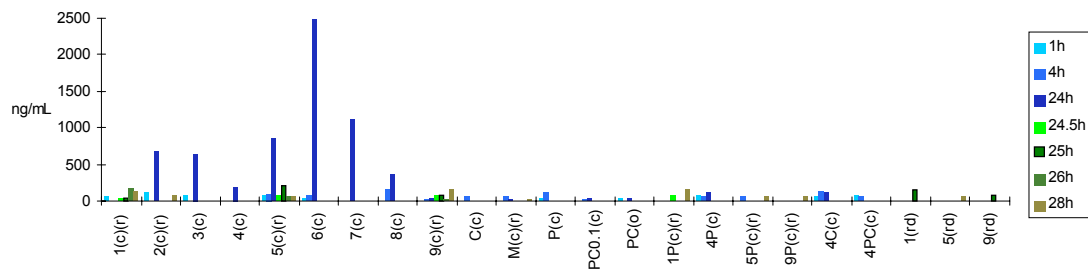
The high concentrations of nitrate in experiments 2-8(c) (Figure 4.34) over 24 hours may have been due to contamination from acid-washed sample bottles, as repeat experiments did not show similar concentrations (Table 4.4). However, rock samples were not pre-washed, so the possibility of a bacterial presence on samples also exists. If the latter is true, this may

have implications for solute acquisition in closed system environments with high rock-water ratios (see Section 1.3.21). Other experiments showed very low concentrations of NO_3^- . The influence of NO_3^- in pyrite oxidation would appear negligible as no noticeable increases in SO_4^{2-} are associated with the high NO_3^- concentrations. This is unsurprising given that $\text{O}_2(\text{aq})$ concentrations did not appear to reach low enough levels to require other, less favourable oxidising agents (Section 4.3.2).

Table 4.4 Differences between NO_3^- concentrations from repeat experiments (closed system).

Experiment	Repeat 1	Repeat 2
1(c) (24h)	0.94	0.00
4(c) (24h)	1.47	4.76
5(c) (24h)	27.2	0.00
9(c) (24h)	1.26	0.00

Figure 4.34 Mean concentrations of NO_3^- (ng/mL) in laboratory experiments.

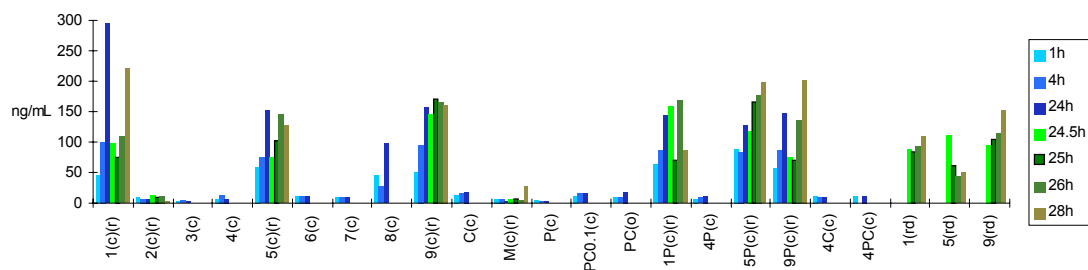


4.3.5 Trace elements

4.3.5.1 Strontium

Concentrations reach 150-300ng/mL after 24h dissolution from closed system experiments PC/1/5/9/1P/5P/9P(c), around 100ng/mL from experiment 8(c), but less than 20ng/mL from experiments involving other rocks (experiments 2/3/4/6/7/C/M/P/PC_{0.1}/4P/4C/4PC(c)) (Figure 4.35).

Figure 4.35 Mean concentrations of Sr (ng/mL) in laboratory experiments.



Strontium is closely associated with calcium in many rock types and minerals due to similar ionic radii and equal electronegativity and ionic charge, although Sr-Ca substitution is less favourable in calcite (Section 1.7.2.3) (Rankama and Sahama, 1950). This was reflected in

variations in bulk Ca/Sr ratios between rock types (see Table 3.12). However, the variations in yield into solution between different rock types are not as great as for calcium, with the result that Sr^{2+} concentrations in solution are more closely related to rock Ca content than Ca^{2+} concentrations (Table 4.3). Strontium concentrations in meltwaters may therefore quantify the solute provenance component of the Ca acquisition rate equation described in Chapter 4.

Figure 4.36 Mean calcium (left) and strontium (right) concentrations after 24h closed system dissolution, plotted against rock calcium content. The Sr/Ca(s) regression translates to $\text{Sr}^{2+}(\text{M}) = 0.061\text{Ca}(\text{s})$ (mol).

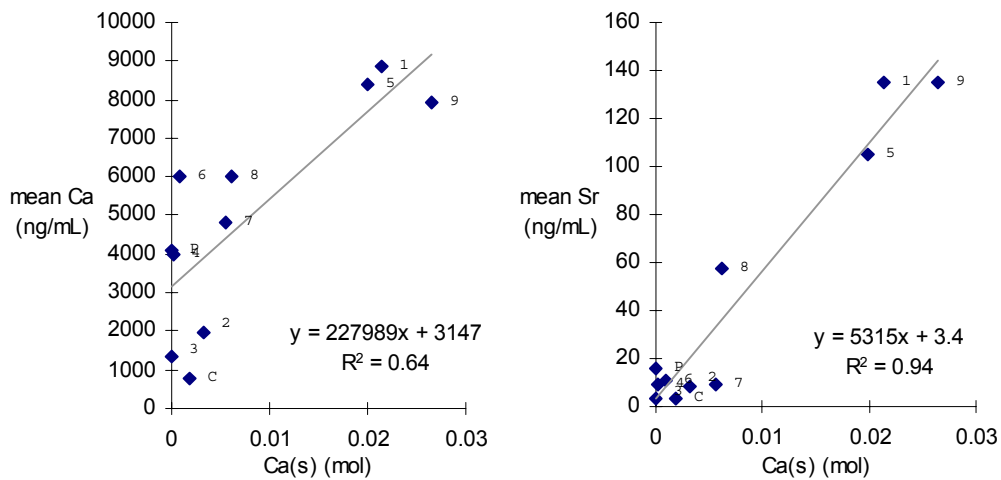
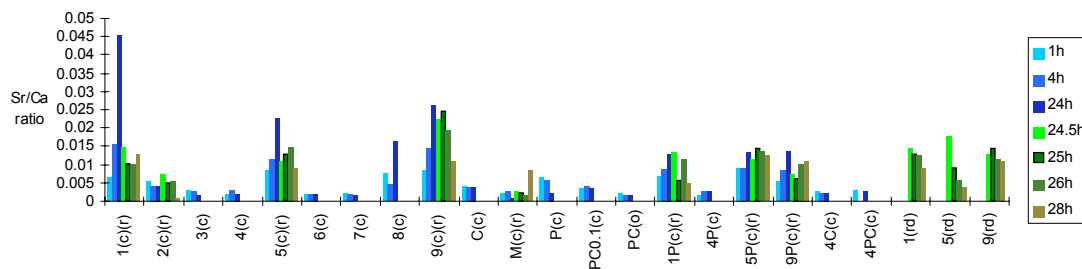


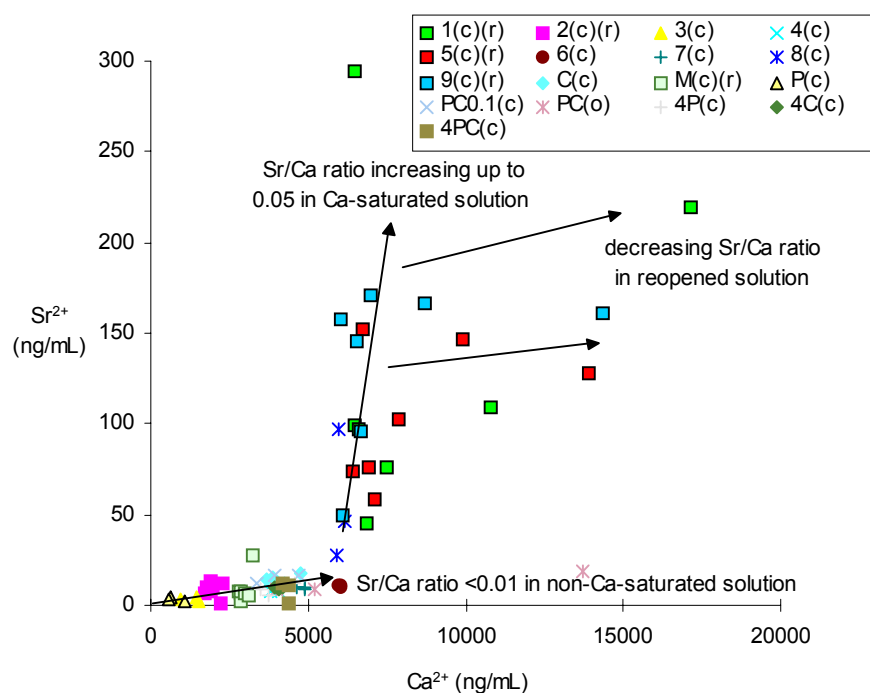
Figure 4.37 Sr(aq)/Ca(aq) ratios (ng/ng) in laboratory experiments.



Sr(aq)/Ca(aq) ratios showed a positive correlation with rock Ca content (Figure 4.37), although rock 6 deviated from this trend with an unusually high solute yield of Sr into solution (Table 4.3). This is the reverse of rock Sr/Ca ratios, which are generally lower in the high Ca rocks studied here (see Section 3.4.2.4). The reason for this is that Sr is actually more abundant in the Ca-rich rocks than the Ca-poor rocks in absolute terms (see Figure 3.9, Chapter 3), and whereas Ca dissolution levels are roughly similar in many experiments due to the saturation of Ca in a closed systems, Sr can continue to dissolve so that the Sr/Ca increases with time. This is shown clearly in Figure 4.38. It can be seen that once the closed

system experiments are reopened, the ratio decreased once more, as Ca levels rose more rapidly than Sr.

Figure 4.38 Sr(aq) versus Ca(aq) during closed and open system dissolution experiments. Arrows depict generalised trends for groups of experiments: in experiments 2/3/4/6/7/M/P/C/PC_{0.1}/PC/4P/4C/ 4PC the Sr/Ca ratio remains low (<0.01); in experiments 1/5/8/9 the ratio increases under a closed system due to continued Sr acquisition but approximately constant Ca concentration. The ratio decreases upon reopening in such experiments as Ca acquisition occurs at a faster rate than Sr acquisition.



4.3.5.2 Other trace elements strongly affected by carbonate dissolution

Although only strontium showed similar lithological provenance to calcium, many trace elements showed correlations with Ca²⁺(aq), or increased yields in Ca²⁺-rich solutions, suggesting that they were influenced by the process of carbonate dissolution. These include zinc, bismuth, caesium, thorium and titanium.

a) Zinc

Zn showed relatively high concentrations from experiment P(c), dissolving “pure” pyrite (Figure 4.39), with solute yields higher than the other common accessory metals of pyrite (Table 4.3), and much higher Zn(aq)/Ca(aq) ratios than in other experiments (Figure 4.40). However, as with many other metals, significant reprecipitation occurred between 1 and 24 hours. It is possible that the zinc dissolving from experiments involving pyrite may be due to accessory sphalerite within the pyrite. A high solute yield was obtained from calcite in the 24 hour samples. However, the presence of carbonate appears to have inhibited the

dissolution of zinc, as concentrations showed a progressive reduction between experiments P/PC_{0.1}/PC(c) involving pyrite and 0, 0.1 and 0.2 g/L calcite respectively (Figure 4.40). The progressive reduction in Zn concentration from experiments involving pyrite with increasing mass of non-sulphide material suggests active adsorption or coprecipitation processes occurring, associated with surface exchange reactions on carbonate material and/or production of insoluble Zn-silicate weathering products. Contrastingly, solute yields from morainic rock experiments were generally higher in experiments involving calcium-rich rocks, which may be linked to the relative stability of the ZnCO₃ complex. Reopening various experiments to the atmosphere did not significantly increase Zn concentrations in comparison with closed system levels.

Figure 4.39 Mean concentrations of Zn (ng/mL) in laboratory experiments.

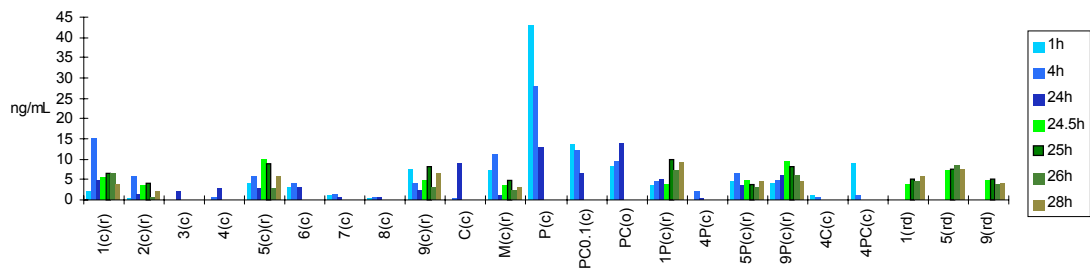
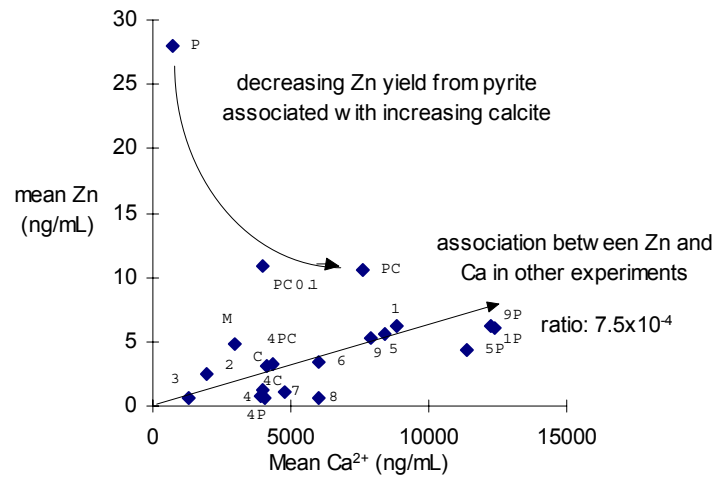


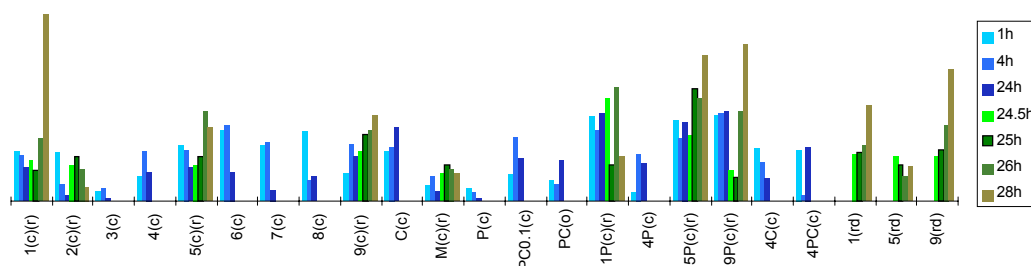
Figure 4.40 Comparison of mean Zn²⁺ and Ca²⁺ concentrations in dissolution experiments under all time scales and conditions.



b) Titanium

Titanium concentrations revealed a similar dissolution behaviour to Fe (see Section 4.3.5.4), but with a lower relative concentration in many solutions reacting with pyrite (Figure 4.41). Longer term solute yields of Ti were generally increased in experiments 1/5/9(c)/(r)/(rd) (weathering rocks 1, 5 and 9).

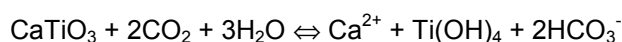
Figure 4.41 Mean concentrations of Ti in laboratory experiments. There are no units, as the analysis was unstandardised.



Titanium yields were further increased in experiments 1P/5P/9P(c)/(r) (reacting with mixtures of calcium-rich rocks and pyrite) in comparison with the corresponding experiments without pyrite. Ti does not commonly substitute for Ca in the structure of carbonate minerals, but may be present in apatite, which often shows common occurrences to sedimentary carbonates (Rankama and Sahama, 1950). Apatite could react with the weak sulphuric acid produced by pyrite dissolution. Other common titanium-bearing minerals (e.g. ilmenite, rutile, sphene) are resistant to chemical weathering.

Concentrations increased in open system dissolution of rocks 1, 5 and 9, compared to levels under a closed system, but not with rocks 2 or M. This further suggests an association with increased calcium dissolution, suggesting that titanium acquisition is dependent on carbonate dissolution, either due to increased ion exchange reactions or a codependence on CO₂ drawdown, as apatite dissolution is likely to be largely driven by acid hydrolysis in the same way as carbonate dissolution (Equation 4.3).

Equation 4.3 Apatite dissolution driven by carbonic acid hydrolysis.



4.3.5.3 Barium

Barium solute yields were very low in all experiments (Figure 4.42), producing concentrations well below a reported world stream average of 50 ng/mL (see Table 1.5), despite the theoretical association with K and Ca, and the above-average concentrations of these major elements in many of the experiments. The pattern of dissolution was fairly closely associated with rock abundances (Figure 4.48), but increased in open system experiments involving rocks 1, 5 and 9, approximately doubling the concentration of Ba in solution in 4 hours.

Figure 4.42 Mean concentrations of Ba (ng/mL) in laboratory experiments.

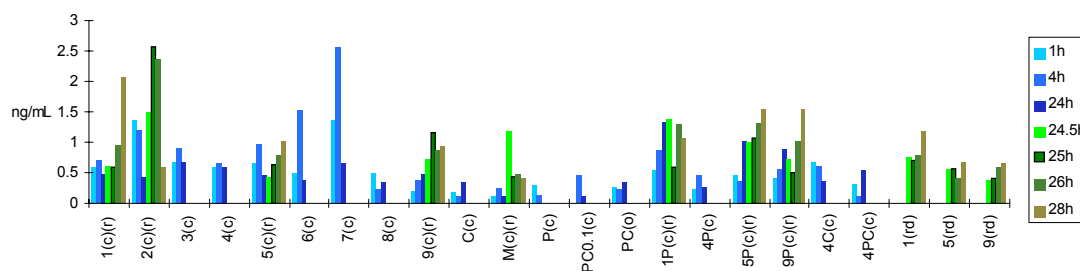
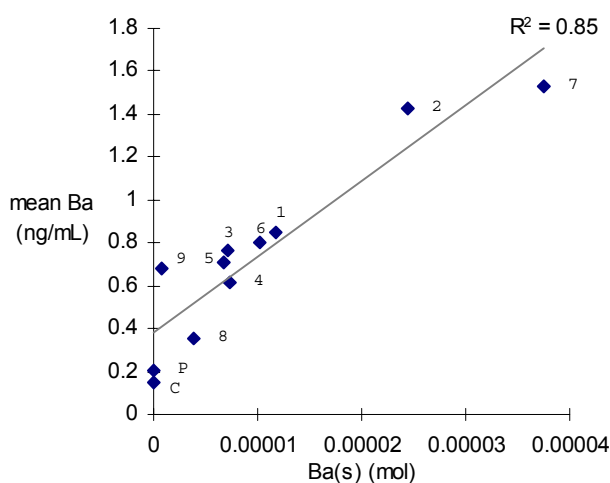


Figure 4.43 Mean Ba concentration from experiments 1-9/P/C for all time increments and conditions, plotted versus the corresponding Ba content of each rock.

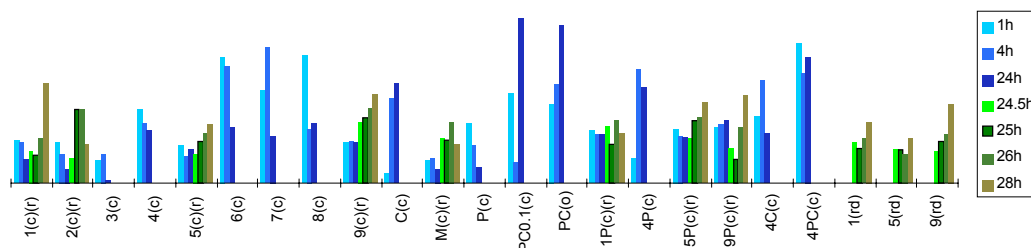


4.3.5.4 Iron, aluminium and nickel

a) Iron

Although Fe is most abundant in pyrite and rocks 2 and 7 (Figure 3.4.4), concentrations in solution were generally evenly distributed, reflecting the wide range of minerals that may weather to produce Fe (Figure 4.44). Concentrations were low: although the ICPMS results are unstandardised, analysis of weathering solutions of experiments 1-9(c) by atomic absorption with a detection limit of 500ng/mL only detected Fe in the 24h samples from experiments 1/6(c). This reflects the fact that Fe is relatively insoluble and tends to precipitate as ferric hydroxide. PHREEQC speciation modelling (see Section 5.4) confirmed that iron is almost exclusively present in hydroxide form, and also indicated that many iron minerals became strongly supersaturated in solution, for example haematite (Fe_2O_3), goethite (FeOOH) and amorphous $\text{Fe}(\text{OH})_3$, suggesting that precipitation would have been favoured.

Figure 4.44 Mean concentrations of Fe in laboratory experiments. There are no units, as the analysis was unstandardised.

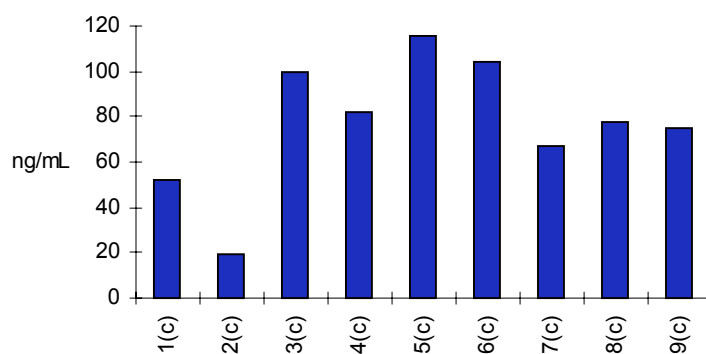


Concentration of Fe in solution appears to increase in many cases when systems are reopened, particularly with rocks 1, 5 and 9. This may be linked to the reduction in pH that occurs in these waters which changes the solubility of iron-bearing minerals, or due to the increase in pCO_2 providing additional protons to drive iron-silicate dissolution.

b) Aluminium

Only one data set was available for Al (Figure 4.45). The results do not seem to reflect the likely rock Al content, given the mineralogy suggested in Table 3.1. Aluminium is a very insoluble element at all but extreme pHs, however, and it may be that the apparent concentrations were due to the influence of microparticles that passed through the filtration process (personal communication with Dr. R. Fuge, 1998).

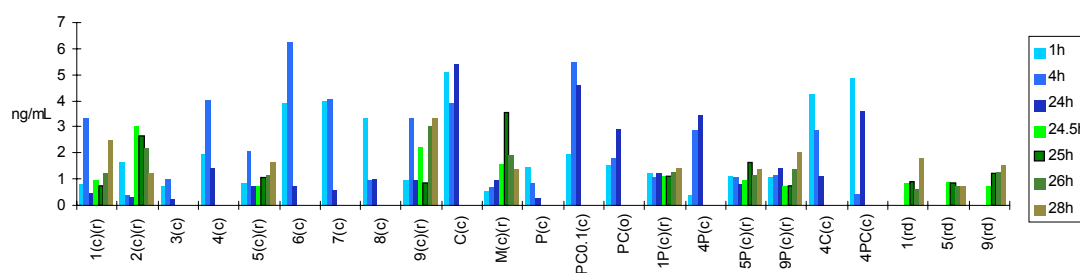
Figure 4.45 Mean concentrations of Al (ng/mL) in laboratory experiments, at 24 hours.



c) Nickel

Nickel tended to fall out of solution by adsorption or reprecipitation to some extent between 1 and 24 hours in many experiments (Figure 4.46). Nickel demonstrated a dissolution pattern similar to that of Fe, consistent with the affinity of Ni for Fe-bearing minerals such as pyrite, pyroxenes, amphiboles and biotite.

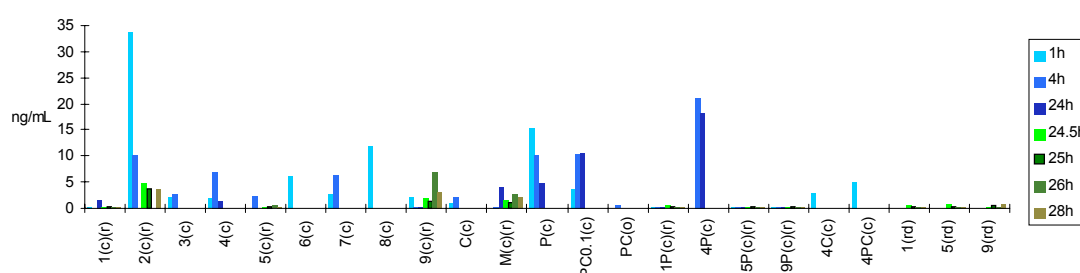
Figure 4.46 Mean concentrations of Ni (ng/mL) in laboratory experiments.



4.3.5.5 Lead

Lead concentrations in laboratory experiments are summarised in Figure 4.47. A low to moderate solute yield in all experiments, although the yield after 1 hour of dissolution of experiments 2/6(c) was somewhat higher (Table 4.3). Generally Pb showed a low solubility beyond 1 hour, reflected in the reduction in apparent solute yield at 24 hours. The uneven levels of Pb acquisition from experiments involving pyrite may suggest that Pb is unevenly distributed through the pyrite, and thus may be interpreted as being present as discrete accessory galena rather than substituting for Fe^{2+} within the pyrite structure. It is of note that experiments dissolving pyrite mixed with carbonate-rich sediment (experiments 1P/4PC/5P/9P(c), PC(o)) did not produce equivalent concentrations of Pb to experiments with pyrite alone, or with less carbonate (experiments P/PC_{0.1}/4P(c)). This may be due to an additional opportunity for adsorption, as PbCO_3 complexes are subjected to higher degrees of adsorption than free Pb^{2+} ions. This is discussed in Section 5.2.

Figure 4.47 Mean concentrations of Pb (ng/mL) in laboratory experiments.



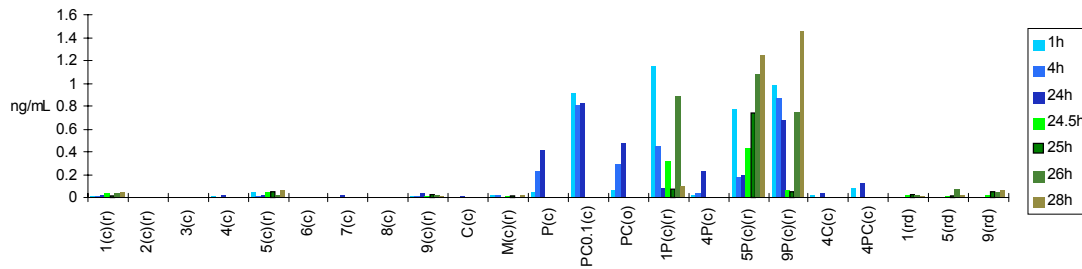
4.3.5.6 Trace elements with dominantly provenance-controlled dissolution characteristics

a) Uranium

Uranium showed a low yield into solution from moraine rocks, with concentrations under both closed and open system conditions often barely above the ICPMS detection limit of

0.002ng/mL (Figure 4.48). Only experiments involving pyrite produced uranium concentrations over 0.1ng/mL, and concentrations exceeded 1.0ng/mL in experiments 1P(c) (1 hour), 5P(r) (26 & 28 hours) and 9P(r) (28 hours). Concentrations in these experiments showed two peaks; firstly at one hour, and secondly in experiments 1P/5P/9P(r), where the system was reopened at 24 hours, with U concentrations showing a progressive increase over the period of open-system dissolution (24-28 hours) (Figure 4.49).

Figure 4.48 Mean concentrations of U (ng/mL) in laboratory experiments.



It is of note that uranium concentration was not directly linked to sulphate content. Experiments P/PC_{0.1}/PC(c) showed 1000U^{total}/SO₄²⁻ ratios of between 0.14-0.7 (Figure 4.58), whereas ratios of 0.05-0.09 were encountered in experiments 1P/5P/9P(c)/(r) and 4P/4PC(c). Experiments 2/3(c) and 2(r) did not produce any uranium, despite significant concentrations of SO₄²⁻.

Figure 4.49 Mean concentrations of U (ng/mL) in experiments 1P/5P/9P(c)/(r)

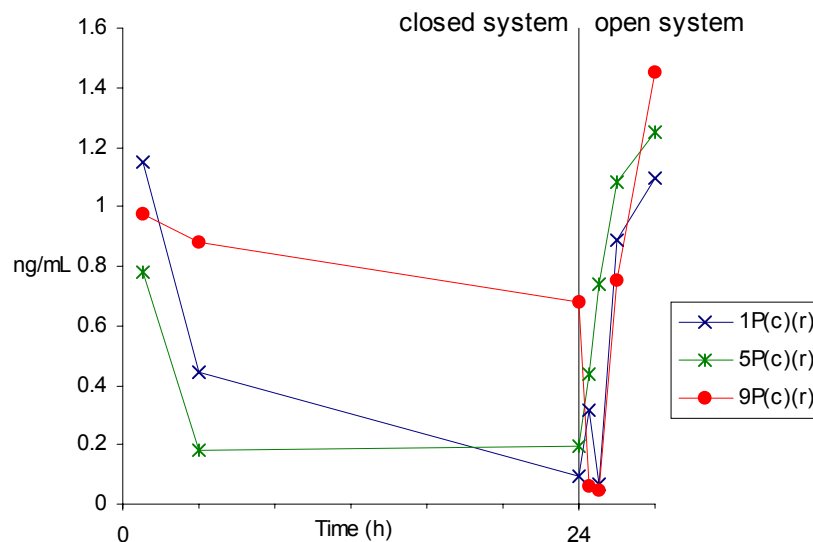
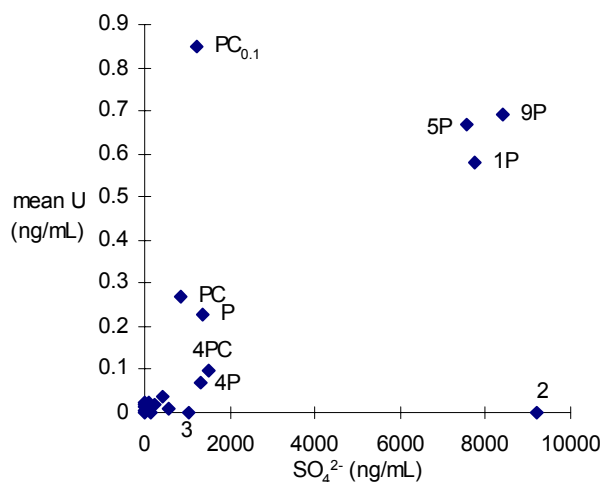


Figure 4.50 Mean concentrations of U^{total} versus mean SO_4^{2-} concentrations in laboratory experiments. Experimental nos. are labelled.



The controls on acquisition of uranium are demonstrated as (1) rock content, which is much higher in pyrite than in any of the morainic rocks (Section 3.4.2.1) and (2) carbonate content of the water. The former mainly controlled the short term solute yield of U. Section 1.7.7.8 indicated that U is dominantly present in solution as a charged uranyl-carbonate complex. These complexes are only stable in waters of high pH (Drever, 1982), although the uranyl biphosphate complex stable in circumneutral pH cannot be considered here due to lack of PO_4^{3-} data. Assuming phosphate levels are not significant in laboratory experiments or in glacial meltwaters draining *Haut Glacier d'Arolla*, pH may be the controlling factor on the long-term solute yield of U in solution.

It cannot be said with the data available here that U is an accessory metal of pyrite in the Arolla catchment, as experiments involving just morainic rocks did not produce significant uranium. This suggests either that the trace element chemistry of pyrite in rocks 2 and 3 is different to that of the pyrite 'P', or that a significant non-pyrite source of SO_4^{2-} is present in those rocks.

b) *Rubidium*

Rubidium concentrations reached a maximum of 10ng/mL in laboratory experiments, and under closed system conditions were highest from experiment 4(c) (Figure 4.51). Rb/K ratios were similar in many experiments, with the exception of experiment 3(c) which displayed a lower mean Rb/K ratio, and experiments 9/P/C(c) which produced a higher Rb/K ratio (Figure 4.52). The latter variation tentatively suggests that Rb/K ratios may be used to distinguish between some rocks of hydrothermal or sedimentary origin.

c) Cobalt

Figure 4.51 Mean concentrations of Rb (ng/mL) in laboratory experiments.

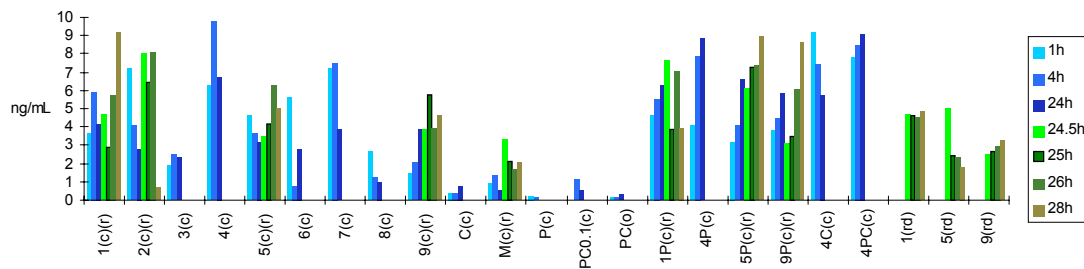


Figure 4.52 Mean Rb/K ratios in laboratory experiments.

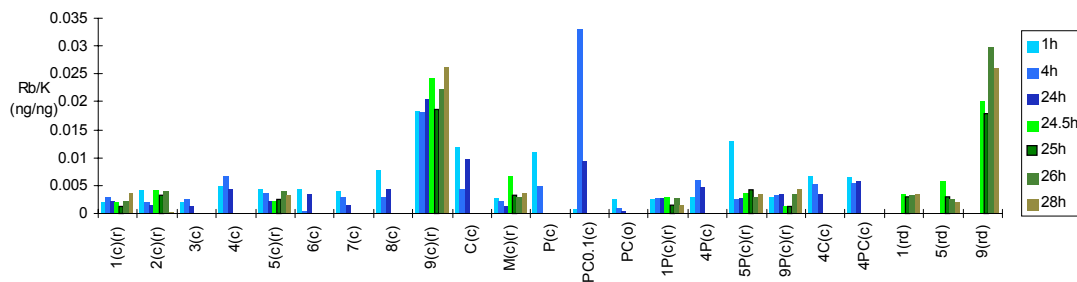
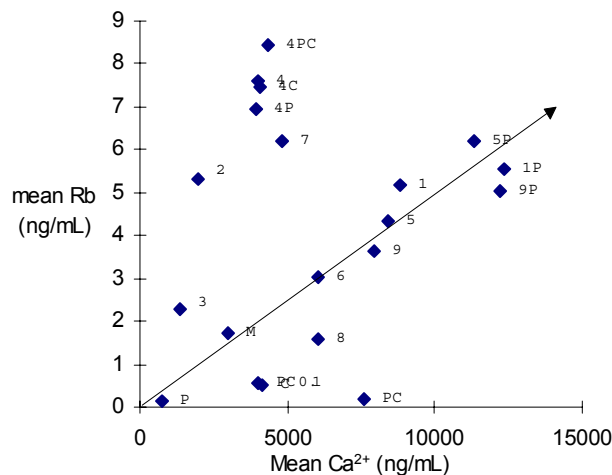
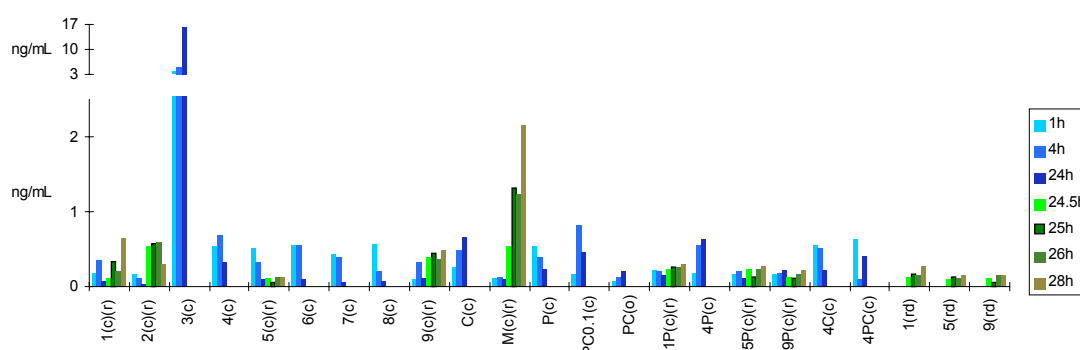


Figure 4.53 Mean Rb concentration from dissolution experiments (nos. labelled) for all time increments and conditions, plotted versus the corresponding Ca²⁺ concentration.



Cobalt reached particularly high concentrations from experiment 3(c), reaching 11.2 and 21.4ng/mL in the 24h repeats, compared to concentrations of less than 1 ng/mL in all other samples except from experiment M(r), which reached 2.5ng/mL after 28h (Figure 4.54). Cobalt is most abundant in rock 3, but the increased yield % also suggests that Co must be present in a particularly soluble mineral. Co may therefore be an indicator of the type of quartz vein exemplified by rock 3. The relatively high concentrations produced from experiment M(r) may indicate the presence of some minerals of similar provenance to those in rock 3.

Figure 4.54 Mean concentrations of Co (ng/mL) in laboratory experiments.



4.4 CONCLUSION

This chapter presents the results for a suite of laboratory experiments dissolving calcite and pyrite in quantities thought to represent the likely mineral-specific content of sediment in contact with meltwater within the hydrological network of *Haut Glacier d’Arolla*. The experiments were designed to constrain the role of the coupling of sulphide oxidation and acid hydrolysis of carbonate and silicate minerals thought to be a significant factor in delayed flow meltwaters (e.g. Tranter *et al.*, 1993). Further experiments were undertaken using powdered morainic rock samples for which bulk analysis is presented in Chapter 3.

The laboratory experiments carried out in this study indicate the dominance of Ca^{2+} and carbonate species in solutions produced by the dissolution of most morainic rock types present at *Haut Glacier d’Arolla*, with Ca^{2+} and $(\text{HCO}_3^- + \text{CO}_3^{2-})$ accounting for an average of 22% and 62% of total dissolved species by weight, respectively (44% and 41% respectively by equivalent units). Sulphate concentration resulting from the dissolution of morainic rocks was generally low, other than from altered olivine gabbro (rock 2), which yielded SO_4^{2-} concentration in excess of the mean field concentration.

The major fraction of the concentration of most species was due to rapid reactions immediately following rock-water contact. This emphasises the role of the production of

ultrafine particles by the movement of glaciers and attrition between basal sediments. Dissolution of calcite-rich morainic rocks in this period resulted in calcite supersaturation. Beyond the initial period of rapid acquisition, major cations were strongly influenced by rock content, but also by availability of atmospheric CO₂, demonstrating the dominance of carbonation-driven acid hydrolysis reactions. Supersaturation was not maintained in calcite-rich solutions, with the result that precipitation occurred.

Where sulphide oxidation was sufficient in experiments with pyrite added to morainic rock sediment, significant additional dissolution of the major cations resulted, indicating the importance of this process. Dilution of certain experiments reduced the concentration of cations, but calcium concentrations quickly recovered to levels found in equivalent, non-diluted experiments, suggesting that saturation of calcite is rapidly achieved in experiments dissolving marbles and calcites (rocks 1/5/9).

Trace elements were generally low in concentration, with iron, strontium, aluminium, boron (not shown), zinc and lead the six most concentrated elements of those calibrated against standards. Some elements showed solution concentrations that were closely linked to rock provenance (e.g. sodium and cobalt). However, many showed increased solute yields from experiments involving carbonate-rich sediment (e.g. zinc). This is attributed to cation exchange with calcium, which is supersaturated in the calcium-rich solutions.

This study has produced the broadest dataset of experimental results designed to simulate subglacial conditions, and is the first to look at minor and trace elements in detail. Additionally, these are the first experiments that have been carried out using rocks of known bulk chemistry. Therefore, new insights can be made into the processes, rates and controls on solute acquisition in subglacial environments, including the influences of CO₂-drawdown, carbonate equilibria, pH, dilution and, for the first time, solute provenance. The following chapters look in detail at the rates, processes and controls on acquisition of major, minor and trace elements in the laboratory experiments, and then discuss the applicability of the inferred laboratory controls to data of bulk meltwater draining *Haut Glacier d'Arolla*.

5. RATES AND CONTROLS OF SOLUTE ACQUISITION IN LABORATORY SIMULATIONS OF GLACIAL ENVIRONMENTS

5.1 INTRODUCTION

The dominance of dissolved Ca^{2+} and $(\text{HCO}_3^- + \text{CO}_3^{2-})$ in solutions produced by dissolution of rocks taken from supraglacial moraines at *Haut Glacier d'Arolla* under experimental conditions was indicated in Chapter 4. The aim of this study is to isolate the controls on dissolution of all abundant species through laboratory experiments, and to create a quantitative or semi-quantitative overall model of solute acquisition that can be applied to field data, in order to advance the understanding of the subglacial weathering regime and its role in removing CO_2 from the atmosphere. To achieve this, it is essential to analyse variations in solute acquisition rate and magnitude in more detail, with reference to potential controls on acquisition, including solute provenance, residence time, pCO_2 , pH, ionic strength and saturation indices.

5.2 PROCESSES, RATES AND CONTROLS OF CALCIUM ACQUISITION

The calcium content of the rocks used in laboratory experiments ranged from 0.02% to 27%, with a mean of 9.9% for rocks 1-9. This compares to a mean content of (Na+K+Mg+Fe) of 4.5% (see Section 3.4.1). Data for aluminium and silica were not available, but typical values for such rock types based on observed mineralogy would be around 25-30% Si and 1-3% Al. Therefore, calcium accounts for approximately 20-25% of mean total rock metal content (Table 5.1).

Although no analysis for dissolved silica concentrations were carried out in this study, field values for the 1994 meltseason at *Haut Glacier d'Arolla* of 8-34nM/mL should give a reasonable approximation of the expected range in laboratory experiments, given the similarity in concentrations of other dissolved species. Aluminium analysis in this study revealed no concentrations greater than 120ng/mL (4.4nM/mL). These compare with mean concentrations of major cations as shown in Table 5.1. This shows that solute acquisition of calcium is much greater than other major elements, and Ca^{2+} was the dominant cation in most laboratory experiments involving morainic rocks. The importance of understanding the processes involved in calcium acquisition to gain a knowledge of the overall controls on solute acquisition in subglacial environments is therefore evident.

Table 5.1 Comparison of mean rock content of rocks 1-9 and dissolved cation concentrations in corresponding experiments

	Mean rock %	Mean rock metal %	nM/mL	dissolved metal %
calcium	9.9	22	160	70
sodium	1.2	3	14	6
potassium	1.7	4	10	4
magnesium	0.6	1	14	6
iron	1.0	2	<5	<2
silicon	28	63	21	9
aluminium	2	5	4	2

High variations in solute yield of calcium between experiments using different rock types occurred (see Table 4.3), suggesting that controls other than mineralogy had a great influence on solute acquisition. The dissolution of carbonate minerals far from equilibrium is generally controlled by the rate of surface reaction (see Section 1.5.3), but it is clear from Chapter 4 that equilibrium processes affected the acquisition of Ca^{2+} , curtailing reaction under closed system conditions. This section investigates variations in calcium acquisition rate dependent on solute type, access to atmospheric gases, additional proton sources and dilution.

5.2.1 Investigations of controls on acquisition of calcium from “pure” calcite

5.2.1.1 Relationship between calcium acquisition and time

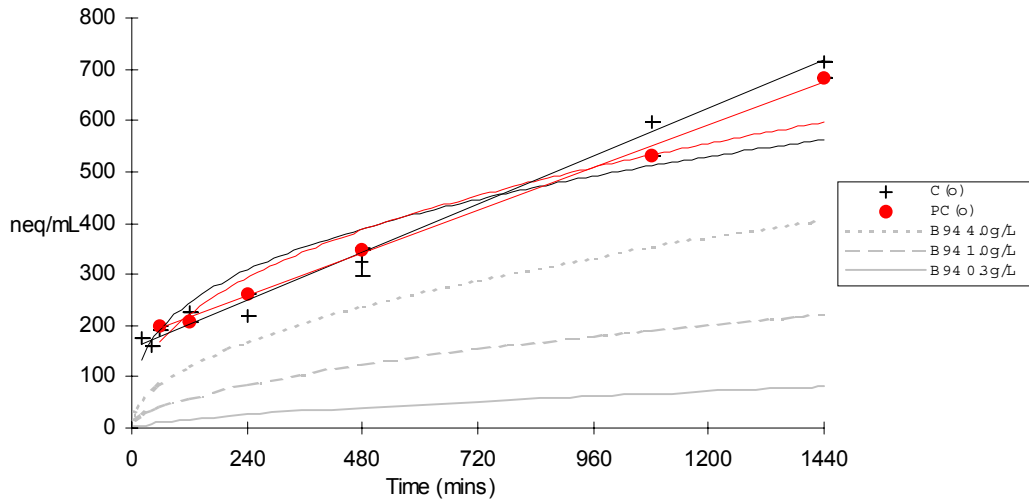
a) *Open system dissolution*

Previous laboratory studies of calcium acquisition by Brown *et al.* (1994) described power rates of acquisition dependent on sediment concentration and time, given a small temperature range and open atmospheric access (Table 5.2). The power curves were based on experimental open system dissolution of prewashed proglacial sediment over a period of 180min. Power rate laws were also established for calcium acquisition in experiments C(o) and PC(o). The curves are plotted over a 24h period in Figure 5.1, and are compared with linear regression best-fit lines through the same data.

Table 5.2 Dissolution rate parameters of proglacial sediment derived from Haut Glacier d’Arolla in deionised water, 0.0-3.1°C, atmospheric CO_2 pressure. t = time in seconds, T = time in minutes.

Sediment concentration	Dissolution rate parameter		
	neq/mL/s	neq/mL/min	neq/mL/min
0.3 g/L	$\text{Ca}^{2+} = 0.07t^{0.62}$	$\text{Ca}^{2+} = 0.89T^{0.62}$	
1.0 g/L	$\text{Ca}^{2+} = 0.54t^{0.53}$	$\text{Ca}^{2+} = 4.73T^{0.53}$	
4.0 g/L	$\text{Ca}^{2+} = 1.55t^{0.49}$	$\text{Ca}^{2+} = 11.5T^{0.49}$	
experiment C(o)		$\text{Ca}^{2+} = 33.3T^{0.40}; r^2=0.94$	$\text{Ca}^{2+} = 0.41T+140; r^2=0.99$
experiment PC(o)		$\text{Ca}^{2+} = 46.6T^{0.34}; r^2=0.94$	$\text{Ca}^{2+} = 0.35T+170; r^2=0.99$

Figure 5.1 Graphical representation of dissolution rate parameters of proglacial sediment derived from Haut Glacier d'Arolla in deionised water, 0.0-3.1°C, atmospheric CO₂ pressure (Brown *et al.*, 1994), and open system acquisition of calcium from “pure” calcite in experiment C(o) and from a calcite-pyrite mixture in experiment PC(o).



Although the regression statistics are significant, the figure and table show that the data beyond 20min for experiments C(o) and PC(o) are better represented by linear regression. However, the initial period of dissolution cannot be explained using the linear regression lines. This suggests a two-stage calcium acquisition profile similar to that described by Fairchild *et al.* (1994) for the acquisition of cations from carbonate:

1. Dissolution of carbonate in a “closing system” to a value of SI(calcite) greater than -2, kinetically controlled by the dissolution of CO₂(g). The term “closing system” was used to describe the situation where there is net removal of CO₂(g) due to the rate of removal due to carbonate dissolution being greater than the rate of CO₂ drawdown from the atmosphere. This stage was described as being independent of pyrite oxidation.
2. Introduction of CO₂ partly balanced by carbonate dissolution, or oxidation of available pyrite largely balanced by carbonate dissolution. The kinetic reason for the incomplete buffering of CO₂ drawdown in this stage, and therefore the solution remaining undersaturated with respect to calcite, was not established.

Figure 5.2 shows that for experiment C(o), the initial calcium acquisition followed an approximate relationship with log-time. The approximate relationship is described in Equation 5.1.

Equation 5.1 Initial dissolution rate in experiment C(o), where t is in seconds ($r^2 = 0.84$). The regression represents a lag in the start of dissolution of 46s.

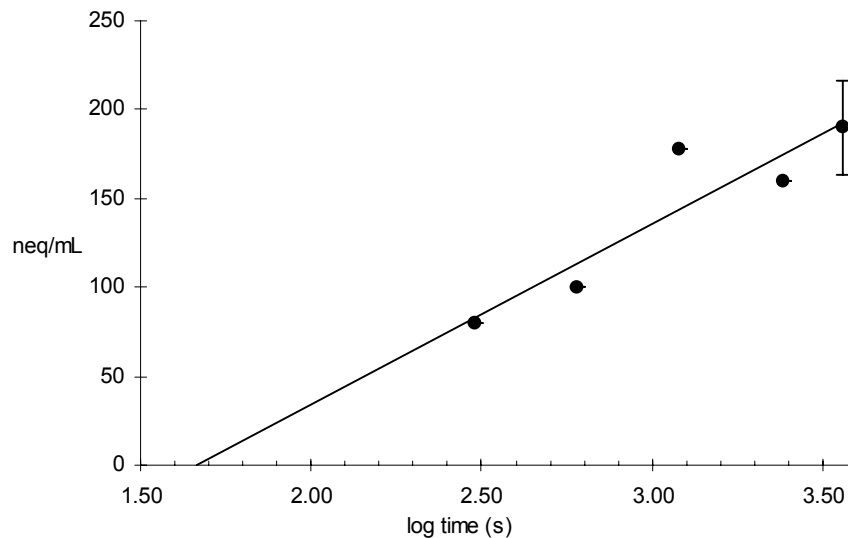
$$\text{Ca}^{2+} = 102 \text{ neq/mL}/\log(t) - 170$$

b) Closed-system dissolution

Calcium acquisition for closed system experiments C/PC/P_{0.1}C/PC_{0.1}(c) appeared to follow a two-stage process similar to that of open system experiments. All experiments fitted a regression line with log-time up to approximately one hour (Table 5.3, Figure 5.3). These regressions displayed an experimental lag of 70-140s. The magnitude of the equations is similar to that of open system experiment C(o) (see Table 5.3).

Data from 1h to 24h fitted regression lines with log time, forced through the abscissa at time=1s (log-time=0) (Table 5.3, Figure 5.3). These regression lines did not fit points representing concentrations at 5, 10, 20 or 40 minutes due to the apparent delay in initial acquisition described above. The post-one hour rate was lower than the linear rate of acquisition under open system conditions, and in fact equates to no greater than 30% additional calcium acquisition between one hour and 24 hours of dissolution in any experiments. The presence of pyrite in experiments PC/P_{0.1}C/PC_{0.1}(c) did not seem to

Figure 5.2 Calcium acquisition from the dissolution of 0.2g/L “pure” calcite under open access to the atmosphere (experiment C(o)) up to one hour. Data beyond one hour is neither plotted nor regarded in the calculation of the regression line.



significantly increase the slow calcium acquisition rates during this period (see Section 5.2.1.2).

Table 5.3 Log-linear rate laws for acquisition of calcium from experiments C/PC/P_{0.1}C/PC_{0.1}(c). *t* is in seconds.

Expt No.	0-1h			1-24h	
	Log-linear regression	x intercept (s)	r ²	Log-linear regression	r ²
C(c)	-	-	-	Ca ²⁺ =49(log t)	0.44
PC(c)	Ca ²⁺ =110(log t)	140	0.95	Ca ²⁺ =48(log t)	0.93
P _{0.1} C(c)	Ca ²⁺ =120(log t)	90	0.93	Ca ²⁺ =52(log t)	0.75
PC _{0.1} (c)	Ca ²⁺ =100(log t)	70	1.00	Ca ²⁺ =48(log t)	0.94
mean	Ca ²⁺ =110(log t)	100	-	Ca ²⁺ =49(log t)	-

The equations for the period 1-24h, whilst showing deviations from the observed experimental data from -2.3% to +4.4%, do not show systematic error (Table 5.4), due to the removal of pre-1 hour data from the regression. The mean error is less than 1%, well within the bounds of experimental error.

Figure 5.3 Regression lines for Ca²⁺ acquisition from closed system experiments C/PC/P_{0.1}C/PC_{0.1}(c). Linear regressions are plotted separate for data from 5-60min (300-3600s, 2.5-3.6 log s) and 60-1440min (3600-86400s, 3.6-4.9 log s). Regression statistics are shown in Table 5.3.

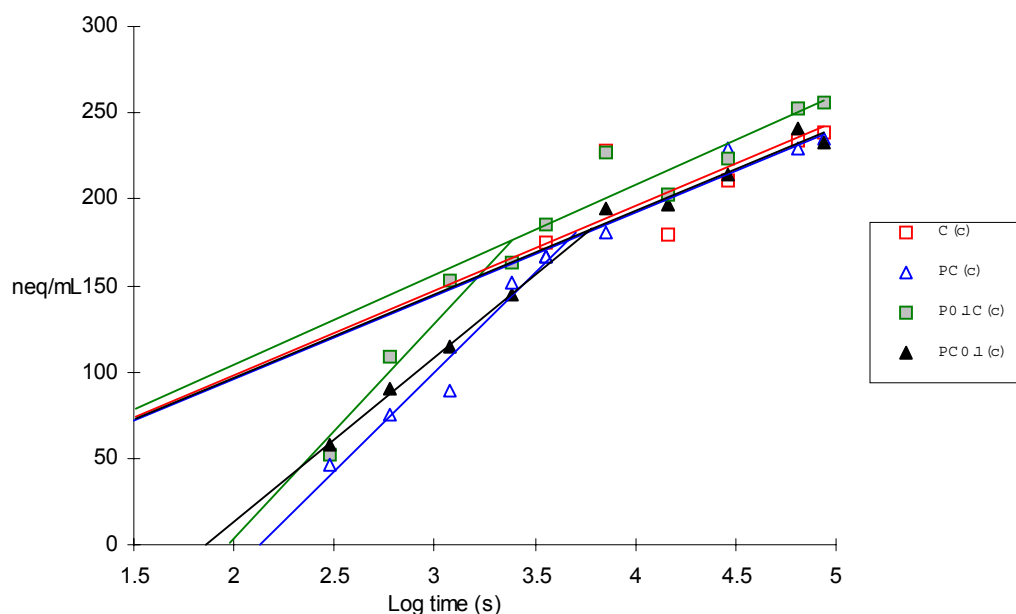


Table 5.4 Comparison of calculated and experimental Ca²⁺ concentrations after 1 and 24 hours dissolution. Calculated values use corrected rate laws (for 1-24 hours) in Table 5.3.

Experiment	calc. Ca ²⁺ (1hr)	obs. Ca ²⁺ (1hr)	error (%)	calc. Ca ²⁺ (24hr)	obs. Ca ²⁺ (24hr)	error (%)
C(c)	170	180	-2.3	240	240	0
PC(c)	170	170	+3.1	240	230	+4.4
P _{0.1} C(c)	170	170	+1.7	240	230	+0.9
PC _{0.1} (c)	180	190	-0.8	250	260	-1.6
mean	170	170	-0.6	240	240	0

Although the extent of Ca^{2+} acquisition in all closed system experiments was broadly similar, it is of note that the initial rate (0-1 hour) for Experiment $\text{PC}_{0.1}(\text{c})$ has a 17-20% lower slope than in experiments $\text{C/PC/P}_{0.1}\text{C}(\text{c})$. Whilst this observation cannot be said to be statistically significant, it may however suggest that the initial rate of acquisition is affected by calcite sediment concentration, whereas rate is not affected by surface area after this time.

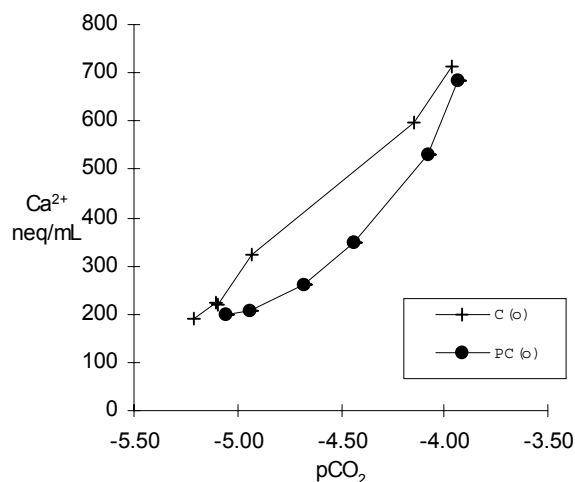
The change in rate of Ca^{2+} acquisition around 60min of acquisition could not be arbitrary. Fairchild *et al.* (1994) suggested that the change in magnitude occurs where pCO_2 becomes low enough as to halt the rapid calcite dissolution rates. This study shows that a small amount of dissolution continued beyond “Stage 1” into “Stage 2” even in a closed system, even in the absence of sulphide oxidation. This is further investigated below.

5.2.1.2 *Relationship between calcium acquisition and sulphide oxidation*

a) *Open system pyrite/calcite dissolution*

The additional protons produced by sulphide oxidation in open system experiment $\text{PC}(\text{o})$ (pyrite/calcite mixture) in comparison with experiment $\text{C}(\text{o})$ (calcite) did not significantly alter the concentration of Ca^{2+} during all stages of dissolution (see Figure 4.6). This is consistent with Fairchild *et al.* (1994), which stated that the second stage of open system dissolution under opening conditions is driven by *either* CO_2 drawdown *or* protons produced by pyrite oxidation. Therefore, the profile of the Ca^{2+} - pCO_2 relationship was altered by pyrite oxidation, with pCO_2 recovering towards atmospheric levels more rapidly in the presence of pyrite (experiment $\text{PC}(\text{o})$) than in its absence (experiment $\text{C}(\text{o})$) (Figure 5.4). It is clear that the process of coupled sulphide oxidation/carbonate dissolution occurred in experiment $\text{PC}(\text{o})$, but did not greatly effect the rate of calcite dissolution in open system conditions.

Figure 5.4 Relationship between Ca^{2+} and pCO_2 in open system experiments C(o) (0.2g/L calcite) and PC(o) (0.2g/L pyrite plus 0.2g/L calcite).



If protons formed by sulphide oxidation substitute for those provided by carbonation in nature, implications for estimations of CO_2 drawdown rates in glacial environments are apparent. The relationship between sulphide oxidation and CO_2 -drawdown is investigated further in subsequent sections.

b) Closed system pyrite/calcite dissolution

In a closed system, Stage 2 cation acquisition (Fairchild *et al.*, 1994) cannot be significantly fuelled by drawdown of CO_2 from the atmosphere. Therefore, any additional calcium acquisition in experiment PC(c) should in theory have been fuelled by pyrite oxidation. The extent of SO_4^{2-} acquisition is a direct indication of the supply of protons from pyrite, with the stoichiometry that the oxidation of 1 mole of pyrite produces 2 moles of sulphate and 4 moles of acidity. Therefore, 1neq/mL SO_4^{2-} is accompanied by 2neq/mL H^+ . According to theory (see Chapter 1, Section 1.3.2.3), in the presence of excess calcite, this can be buffered by the dissolution of calcite to produce 2neq/mL Ca^{2+} and 2neq/mL HCO_3^- (Tranter *et al.*, 1993). Therefore, 25neq/mL SO_4^{2-} acquisition should be buffered by the production of 50neq/mL Ca^{2+} . However, there is no evidence of the presence of pyrite significantly affecting the rates or extent of Ca^{2+} acquisition in these experiments. In fact, the experiments with the highest $\text{Ca}^{2+}(\text{aq})$ concentration after 24h were experiments C/P_{0.1}C(c), which had less pyrite added than experiments PC/PC_{0.1}(c).

However, pyrite oxidation in closed system “end member” experiments affected the relationship between Ca^{2+} and pCO_2 , pH and alkalinity. The ratio of HCO_3^- to Ca^{2+} is an indicator of the process of carbonate dissolution (Fairchild *et al.*, 1994): a 1:1 equivalent ratio (2:1 molar ratio) indicates carbonation-driven carbonate dissolution (see Equation 1.11),

whereas a 1:2 equivalent ratio (1:1 molar ratio) would result from an entirely coupled reaction with pyrite oxidation driving carbonate dissolution (see Equation 1.10). Consistent with the stoichiometry, experiment C(c) produced a $\text{HCO}_3^-/\text{Ca}^{2+}$ ratio of 0.99, whereas experiment $\text{P}_{0.1}\text{C}(\text{c})$ produced 0.94, and experiment $\text{PC}(\text{c})$ produced 0.89 (Figure 5.5).

Pyrite oxidation also affected pH and therefore pCO_2 in closed system “end-member” experiments, in the initial stage of acquisition up to 1h, in contrast to Fairchild *et al.* (1994), which stated that the initial stage is independent of pyrite oxidation. This is best illustrated by the values of pH and pCO_2 at their respective maxima, after 1 hour of dissolution (Figure 5.6). pH was higher in experiment $\text{P}_{0.1}\text{C}(\text{c})$ after 1 hour, and higher still in experiment $\text{PC}(\text{c})$, in comparison with experiment C(c). pCO_2 was correspondingly increased inversely to pH. Although this did not significantly affect Ca^{2+} concentrations, the effect of pyrite oxidation in the initial rapid stage of acquisition is clearly illustrated.

5.2.1.3 Relationship between calcium acquisition and pCO_2

a) *Open system*

The $\log(\text{pCO}_2)$ value for open system experiment C(o) (containing 0.2g/L calcite) rapidly decreased from atmospheric levels, assumed to be -3.5 (Fairchild *et al.*, 1994) to approximately -5.5 in the first hour (Figure 5.7). This equates to a 40% higher value of pCO_2 than the mean value for the equivalent closed system experiment C(c), suggesting that some

Figure 5.5 Relationship between Ca^{2+} and HCO_3^- in closed system experiments C(c) (0.2g/L calcite), $\text{P}_{0.1}\text{C}(\text{c})$ (0.2g/L calcite plus 0.1g/L pyrite) and $\text{PC}(\text{c})$ (0.2g/L calcite plus 0.2g/L pyrite).

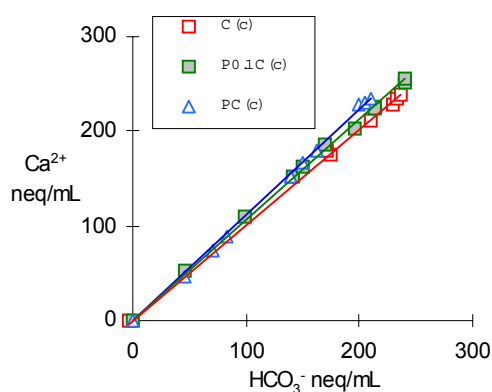
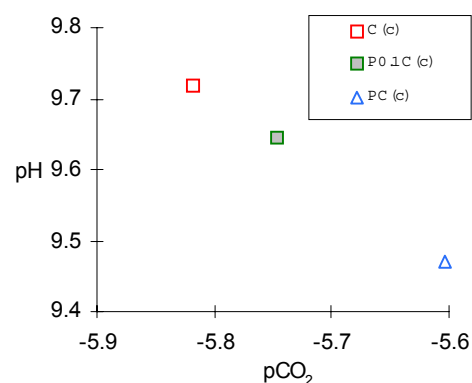
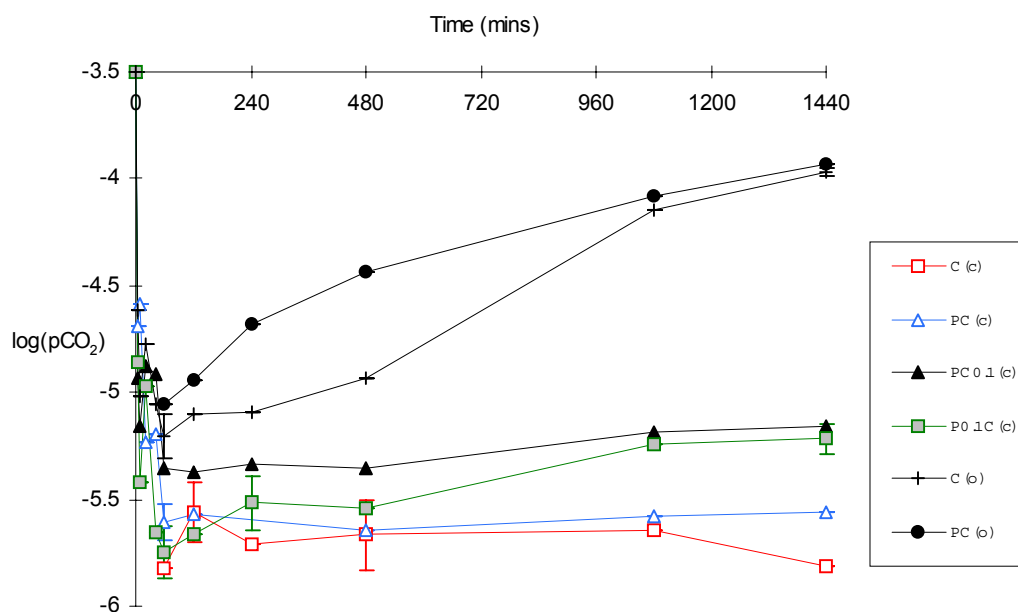


Figure 5.6 Relationship between pH and pCO_2 in closed system experiments C(c) (0.2g/L calcite), $\text{P}_{0.1}\text{C}(\text{c})$ (0.2g/L calcite plus 0.1g/L pyrite) and $\text{PC}(\text{c})$ (0.2g/L calcite plus 0.2g/L pyrite).



additional CO₂ may have been gained from the atmosphere in experiment C(o) that was not available in experiment C(c). Similarly, in experiment PC(o) (containing 0.2g/L calcite plus 0.2g/L pyrite), the pCO₂ value after 1 hour is around 55% higher than in the corresponding closed-system experiment PC(c).

Figure 5.7 Trends of calculated values of log(pCO₂) in open system experiments C/PC(o), and closed system experiments C/PC/P_{0.1}C/PC_{0.1}(c).



The pattern of variation in log(pCO₂) in experiment C(o) coincided with the step change in the magnitude of the rate of calcium acquisition, with the log(pCO₂) minimum marking the division between Stages 1 and 2. In experiment C(o), pCO₂ increased at a rate of approximately 10⁻⁸M/min up to 480min, and then at a rate of approximately 10⁻⁷M/min (Figure 5.8). The change in magnitude of the rate of pCO₂ increase at 480min coincided with Ca²⁺ and pCO₂ attaining a relationship equivalent to that of equilibrium (Figure 5.9). Prior to 480min, the pCO₂/Ca²⁺ ratio was higher than that of the carbonate equilibrium relationship. In experiment PC(o), pCO₂ rates recovered from 60min onwards, suggesting that protons produced by sulphide oxidation negated the requirement for protons from carbonation reactions. As neither open system experiment returned to atmospheric equilibrium values of pCO₂ within 24 hours, the effect of atmospheric equilibrium cannot be ascertained.

Figure 5.8 $p\text{CO}_2$ versus time in experiments C(o) and PC(o).

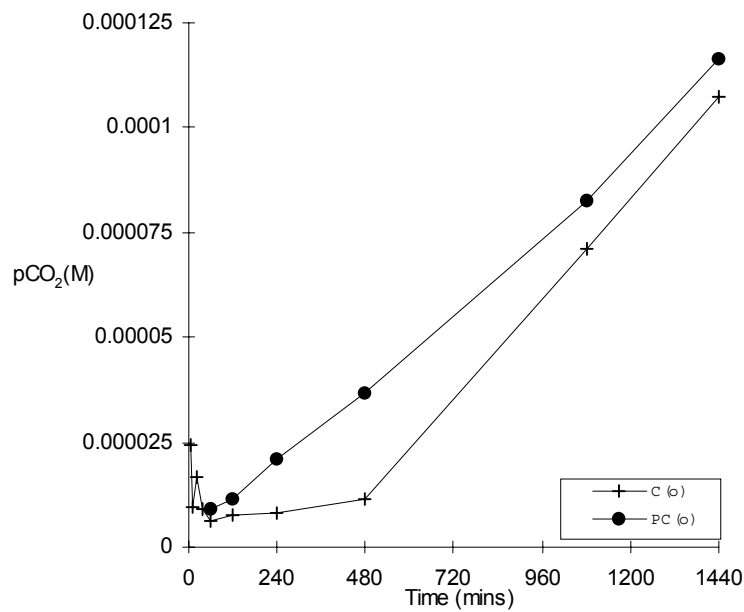
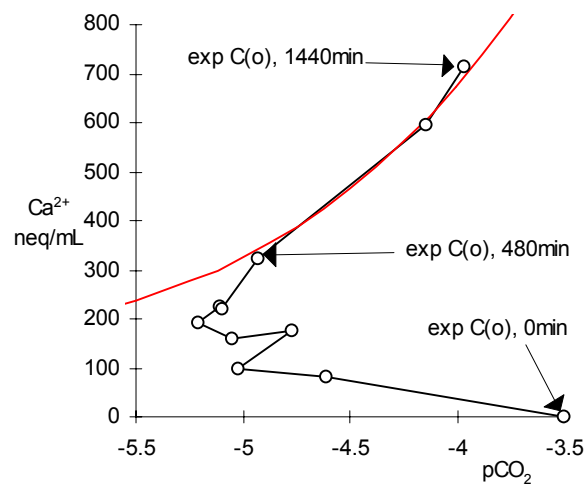


Figure 5.9 The relationship between calcium concentrations and $p\text{CO}_2$ in experiment C(o). The equilibrium relationship between Ca^{2+} and $\log(p\text{CO}_2)$ is shown in red, and the progression of the Ca^{2+} - $\log(p\text{CO}_2)$ relationship is shown in black.



The fact that $p\text{CO}_2$ values recover in the open system environment alongside continued calcite dissolution reflects the moving equilibrium levels of Ca^{2+} concentration with $p\text{CO}_2$. The rate of Ca^{2+} acquisition prior to equilibrium is controlled by the hydration of calcite surface sites, which is time-dependent (Wollast, 1990), but it would appear from these results that as $\text{Ca}^{2+}(\text{aq})$ approached equilibrium with $p\text{CO}_2$, acquisition rates were determined by the recovery of $p\text{CO}_2$ levels to those of the atmosphere. The results from morainic rock experiments allow the quantification of this relationship (see Section 5.3.2).

b) Closed system

As with open system experiment C(o), $\log(p\text{CO}_2)$ values in closed system experiments C/PC/P_{0.1}C/PC_{0.1}(c) rapidly decreased upon addition of the sediment (zero minutes), from atmospheric levels to between -5 and -5.5 (Figure 5.7). Unlike the open system experiments C/PC(o), however, no closed system experiments recovered to values of $\log(p\text{CO}_2)$ above -5 by 24h. There was a fairly clear distinction between the trends of each of the closed system experiments between 60 and 1440min, linked to the amount of pyrite present. In experiment C(c), which contained no pyrite, $\log(p\text{CO}_2)$ at 24h was -5.8; experiment P_{0.1}C(c), which contained 0.1g pyrite, had a value of $\log(p\text{CO}_2)$ at 24h of -5.6; and experiment PC(c), which contained 0.2g pyrite, had a value of $\log(p\text{CO}_2)$ at 24h of -5.1. Experiment PC_{0.1}(c), which also contained 0.2g pyrite, but unlike the other experiments only contained 0.1g calcite, also had a value of $\log(p\text{CO}_2)$ at 24h of -5.1, but also did not drop. Whilst the differences between each experiment are not great, they do appear to show an influence of pyrite oxidation on CO₂ content of the solution. This reflects the additional protons produced by sulphide oxidation, and is consistent with the processes of calcium acquisition suggested by Fairchild *et al.* (1994).

The slight recovery of pCO₂ levels in experiments PC/PC_{0.1}(c), in which pyrite oxidation was occurring, over the period between 1 and 24h, reflects the additional protons released into solution by pyrite oxidation. pCO₂ varies with both HCO₃⁻ and H⁺ concentrations (Equation 2.5), and so increases in pH also effect an increase in pCO₂.

The slight negative slope of experiment C(c) after the initial rapid drop (Figure 5.7) suggests that some carbonation of the remaining small percent of CO₂ in solution occurred.

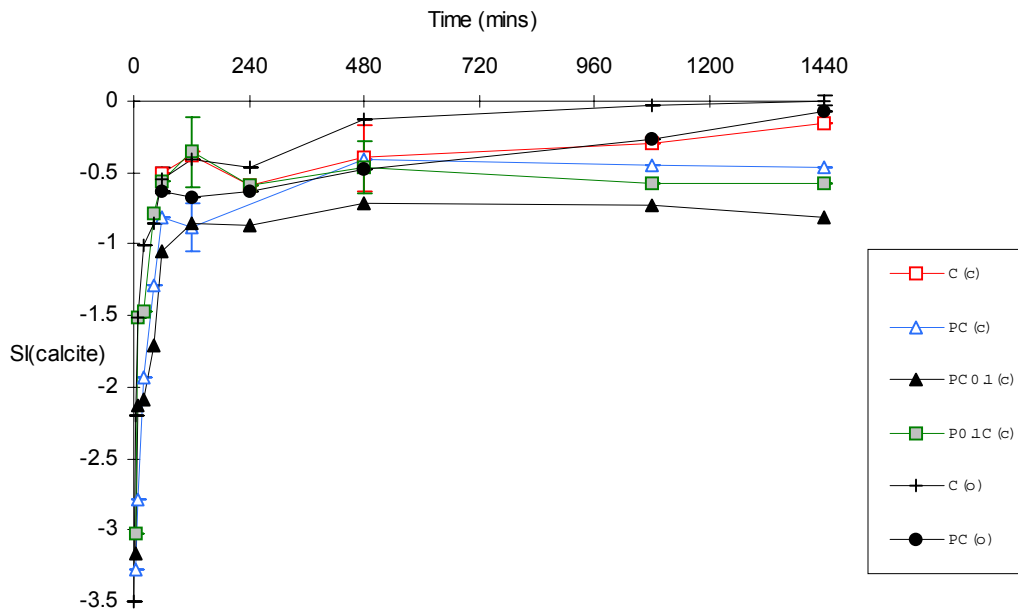
5.2.1.4 *Relationship between calcium acquisition and SI(calcite)*

a) Open system “end-member” experiments

SI(calcite) is the ratio between the ion activity product, i.e. the product of the molar concentrations of Ca²⁺ and CO₃²⁻, to the respective equilibrium value of the product at a given temperature (see Section 2.4.4). Under open system conditions, SI(calcite) values reached approximately -0.5 during the first 60min of dissolution of experiments C/PC(o) (Figure 5.10), and saturation was effectively reached by 480min in experiment C(o), corresponding to the attainment of equilibrium between Ca²⁺ and p(CO₂) by that time (Figure 5.9). Calcite saturation was also reached by 24h in experiment PC(o). The kinetic delay in the attainment of saturation is consistent with previous studies (e.g. Fairchild *et al.*, 1994). Observed rates

of reaction are often slower than the expected rates as saturation is approached, due to the backward precipitation rate becoming significant (Wollast, 1990).

Figure 5.10 Trends of calculated values of $SI(\text{calcite})$ in open system experiments $C/PC(o)$, and closed system experiments $C/PC/P_{0.1}C/PC_{0.1}(c)$.



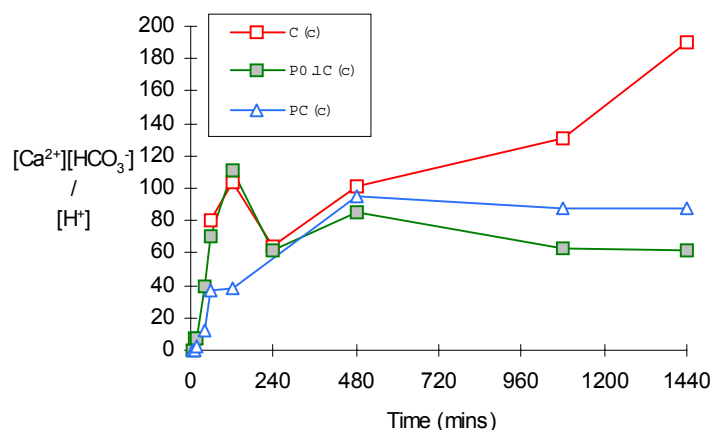
b) Closed system: end member experiments

Under closed system conditions, $SI(\text{calcite})$ in experiment $C(c)$ approached zero by 24h, delayed in comparison to open system experiments $C/PC(o)$ (Figure 5.10). However, $SI(\text{calcite})$ decreased in experiments $P_{0.1}C/PC/PC_{0.1}(c)$ between 4 and 24h dissolution. These trends should be taken into context, given some of the error bars between repeat experiments encountered (shown on Figure 5.10). However, it is clear that saturation was not approached in closed system experiments involving pyrite-calcite mixtures. Equation 5.2 indicates that the calculation of $SI(\text{calcite})$ depends on the ratio of $[Ca^{2+}][HCO_3^-]/[H^+]$. Therefore, an increase in acidity produced by pyrite oxidation, accompanied by a reduction in bicarbonate produced by carbonation-driven calcite dissolution, causes a reduction in the $[Ca^{2+}][HCO_3^-]/[H^+]$ ratio given a constant Ca^{2+} concentration. This is indicated in Figure 5.11, which shows that reduced ratios occurred in experiments $P_{0.1}C/PC(c)$ when compared to those in experiment $C(c)$, particularly after 24h.

Equation 5.2 Derivation of SI(calcite) calculation, based on Equation 2.5 (Chapter 2)

$$SI(\text{calcite}) = \log \left(\frac{[\text{Ca}^{2+}][\text{HCO}_3^-]K_{(\text{CO}_3^{2-})}}{[\text{H}^+]K_{(\text{CaCO}_3)}} \right)$$

Figure 5.11 Trends of $[\text{Ca}^{2+}][\text{HCO}_3^-]/[\text{H}^+]$ ratios in closed system experiments C/ $P_{0.1}$ C/PC(c).



5.2.1.5 Comparison with equilibrium relationships between Ca^{2+} , $p\text{CO}_2$, HCO_3^- , CO_3^{2-} , pH and temperature

Carbonate equilibria equations (see Section 2.4.4) in a calcite-buffered solution produce the relationships between Ca^{2+} , $p\text{CO}_2$, HCO_3^- , CO_3^{2-} , pH and temperature shown in Table 5.5. The equilibrium relationships between Ca^{2+} and $p\text{CO}_2$ at 0, 10 and 25°C are plotted on Figure 5.13.

Table 5.5 Equilibrium concentrations of Ca^{2+} , HCO_3^- , CO_3^{2-} and pH at different temperatures. h:c refers to the equilibrium $\text{HCO}_3^-/\text{Ca}^{2+}$ ratio.

log ($p\text{CO}_2$)	0 C				10 C				25 C			
	pH	HCO_3^- (neq/mL)	Ca^{2+} (neq/mL)	h:c	pH	HCO_3^- (neq/mL)	Ca^{2+} (neq/mL)	h:c	pH	HCO_3^- (neq/mL)	Ca^{2+} (neq/mL)	h:c
-6.0	10.06	230	300	0.78	9.99	180	240	0.76	9.93	130	180	0.72
-5.5	9.75	350	400	0.88	9.68	280	330	0.87	9.62	200	240	0.84
-5.0	9.42	530	560	0.94	9.36	420	450	0.93	9.30	300	330	0.92
-4.5	9.10	790	800	0.97	9.03	630	650	0.97	8.97	450	470	0.96
-4.0	8.77	1160	1180	0.99	8.70	930	940	0.98	8.64	660	680	0.98
-3.5	8.43	1710	1720	0.99	8.37	1370	1380	0.99	8.31	970	980	0.99
-3.0	8.10	2510	2520	1.00	8.03	2010	2020	1.00	7.98	1430	1440	1.00

Figure 5.12 Calculated equilibrium concentrations of Ca^{2+} concentration at given $\log(p\text{CO}_2)$ values and temperature. (lines are based on equations in Garrels and Christ, 1965)

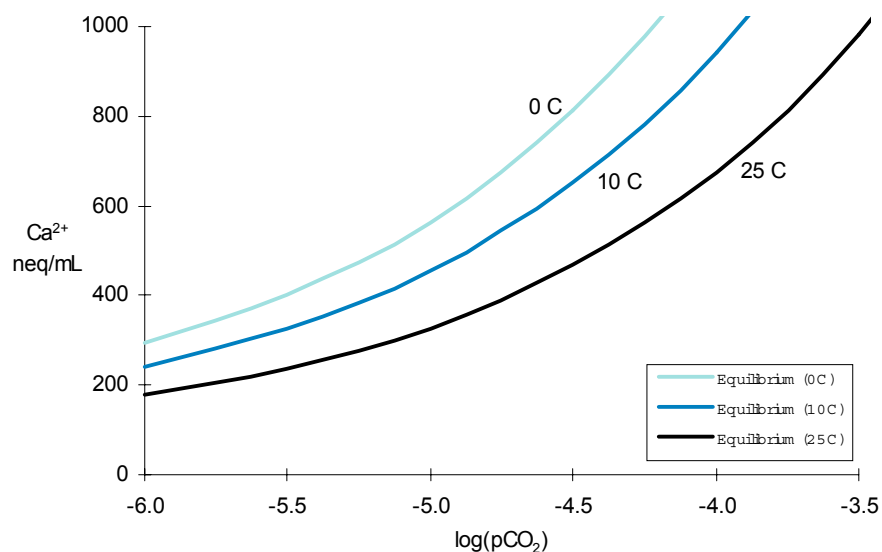
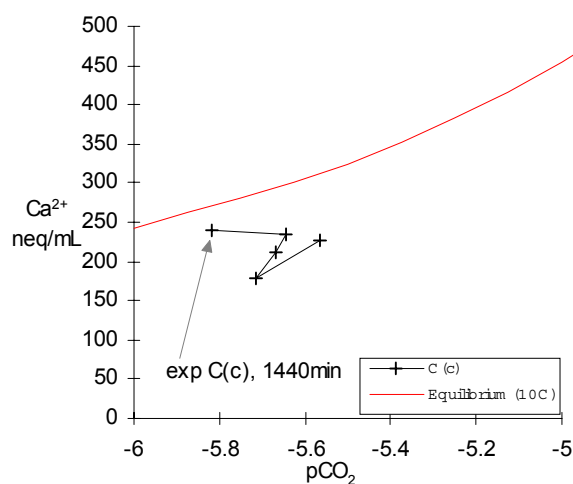


Figure 5.13 The relationship between calcium concentrations and $p\text{CO}_2$ in experiment C(c), compared with the equilibrium relationship at 10°C (equilibrium lines are based on equations in Garrels and Christ, 1965)



Open system experiment C(o) was carried out at room temperature, approximately 25°C, whereas closed system experiment C(c) was carried out under refrigerated conditions, at around 6-9°C (see Section 2.3.2). The relationship between Ca^{2+} and $p\text{CO}_2$ in experiment C(c) approached the 10°C equilibrium line by 24h (Figure 5.13), and the relationship in experiment C(o) closely followed the trend of the 25°C equilibrium line from 8-24h (Figure 5.9). These relationships suggest that calcite dissolution in open system experiments occurred in accordance with carbonate equilibria equations after a period of hours (Garrels and Christ, 1965), and that closed system experiments also approached equilibrium with

respect to carbonate species. Calcium acquisition under these conditions varied according to Equation 5.3.

Equation 5.3 Equilibrium concentration of calcium in solution with calcite (derived from equations in Garrels and Christ, 1965). Definitions and values of equilibrium constants (K) are presented in Equation 2.4 and Table 2.6 respectively.

$$\text{Ca}^{2+} = \frac{K_{\text{CaCO}_3} [\text{H}^+]^2}{K_{\text{CO}_3^{2-}} K_{\text{CO}_2} K_{\text{H}_2\text{CO}_3} p\text{CO}_2} \quad (\text{at } 25^\circ\text{C}) = 10^{9.81 - \log(p\text{CO}_2)} [\text{H}^+]^2$$

5.2.1.6 Summary of controls on calcite dissolution

Fairchild *et al.* (1994) suggested that initial (“Stage 1”) rapid dissolution of cations from carbonate minerals in water equilibrated with the atmosphere occurs at a rate faster than the rate of CO₂ drawdown into solution, so that the solution effectively becomes kinetically closed from the atmosphere. This occurred in both closed and open system experiments involving pyrite and calcite, but it was clear from the relationships between Ca²⁺ and HCO₃⁻, pH and pCO₂ that sulphide oxidation in experiments containing pyrite provided a small proportion of the protons used up in the initial stage, and reduced the magnitude of carbonation-driven calcite dissolution reactions in comparison to experiments without pyrite. This process change did not significantly affect the magnitude or rate of calcite dissolution in the initial rapid stage, as the extent of pyrite oxidation was small in comparison to the extent of carbonate dissolution.

“Stage 2” calcite dissolution (Fairchild *et al.*, 1994) was strongly dependent on access to pCO₂, and produced an apparently linear rate with time under open access to pCO₂, independent of pyrite oxidation. In open system experiment PC(o), pyrite oxidation allowed pCO₂ to increase more rapidly to near-atmospheric levels. Saturation of calcite occurred in open system experiments. In closed system experiment C(c) (dissolving calcite), saturation also occurred by 24h, but in experiments PC/P_{0.1}C(c) (dissolving pyrite/calcite mixtures), SI(calcite) remained below -0.5, due to lower bicarbonate concentrations and pH values. Pyrite oxidation did not affect the magnitude of calcium acquisition in closed system experiments, but did affect the pCO₂ of the solutions, suggesting that pyrite oxidation partially replaced carbonation as a proton source, rather than providing an additional source.

5.2.2 Investigations of controls on acquisition of calcium from various rocks collected from moraines at *Haut Glacier d’Arolla*

5.2.2.1 Relationship between calcium acquisition and time

a) Closed system experiments

Experiments involving morainic rocks were not sampled until 60min, but it was clear that rapid calcium acquisition took place in all experiments (1-9(c)) (Figure 4.7), and the second, post-rapid stage of acquisition referred to by Fairchild *et al.* (1994) had begun by 60min. Between 1 and 24h, the mean increase in Ca^{2+} under closed system conditions in experiments 1-9(c) was just 14%, and for calcite-rich experiments 1/5/9(c), the mean concentration of Ca^{2+} decreased by 15% between 1 and 24h.

b) Experiments reopened to the atmosphere after 24h in a closed system

Experiments showed an immediate response to renewed access to the atmosphere (see Section 4.3.3.1c). The action of reopening the experiments effectively begins the second stage of acquisition in an opening system described in open system “end-member” experiments (Section 5.2.2.1a) (Fairchild *et al.*, 1994). However, it is of note that significant variations in rate of Ca^{2+} acquisition occurred between repeat runs of experiments 1/9(r) (Figure 5.14). The variations in observed rates, expressed as linear regressions, are tabulated in Table 5.6. Whilst some repeat experiments closely fit linear regressions, others are more closely described by exponential and power curves (Figure 5.14). Linear regressions are compared here, to allow direct comparison between experiments and show the mean rate over the 4h period subsequent to reopening, rather than to describe the changes in rate within the 4h period.

Figure 5.14 Rates of Ca^{2+} acquisition in experiments 1/5/9(r), reopened to the atmosphere after 24 hours under a closed system.

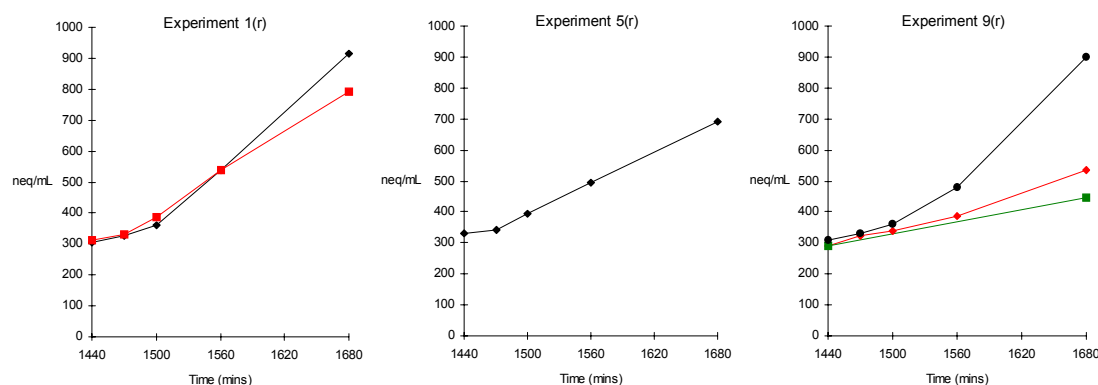


Table 5.6 Apparent rate of Ca^{2+} acquisition in Experiments 1/5/9(r), assuming linear rate with time. t is in minutes.

Experiment	Repeat	Regression	r^2	n
1(r)	1	$\text{Ca}^{2+}=2.6t$	0.97	5
1(r)	2	$\text{Ca}^{2+}=2.1t$	0.99	5
5(r)	-	$\text{Ca}^{2+}=1.6t$	0.99	5
9(r)	1	$\text{Ca}^{2+}=1.0t$	0.99	5
9(r)	2	$\text{Ca}^{2+}=2.5t$	0.95	5
9(r)	3	$\text{Ca}^{2+}=1.1t$	-	2

c) Experiments diluted by 50% with deionised water, and subsequently reopened to the atmosphere after 24h in a closed system

Experiments 1/5/9(c) (carbonate-rich rocks) and M(c) (mixed subglacial sediment) were repeated, but after 24h closed system dissolution, samples were diluted by 50% with 500ml deionised water that had been allowed to equilibrate with the atmosphere. The experiment was then continued under open conditions for a further 4h (see Section 4.3.3.1e). This was designed to simulate the mixing of delayed flow meltwaters, with long residence times and access to relatively large amounts of reactive sediment, with supraglacial meltwater or quickflow meltwaters with short residence times and relatively little contact with reactive sediment.

The results suggested that experiments with carbonate-rich rock types (experiments 1/5/9(rd)) underwent rapid calcium acquisition immediately upon dilution, recovering to concentrations found in the equivalent undiluted experiments (experiments 1/5/9(r)) within 30 minutes. Little overall deviation from the expected rate of acquisition without dilution was observed (Figure 5.17). However, pCO_2 recovery was delayed, and decreased slightly in experiments 1/5(rd) in the first half-hour after dilution, despite the system being open to the atmosphere at this point (Figure 5.17). This is consistent with rapid acid hydrolysis reactions occurring at this point, as occurred in the initial minutes of all experiments containing calcium-bearing minerals.

Figure 5.15 Ca^{2+} acquisition in open system experiments 1/5/9(rd). These experiments had undergone 24h of closed system dissolution, and were 50% diluted with atmosphere-equilibrated deionised water after 24h.

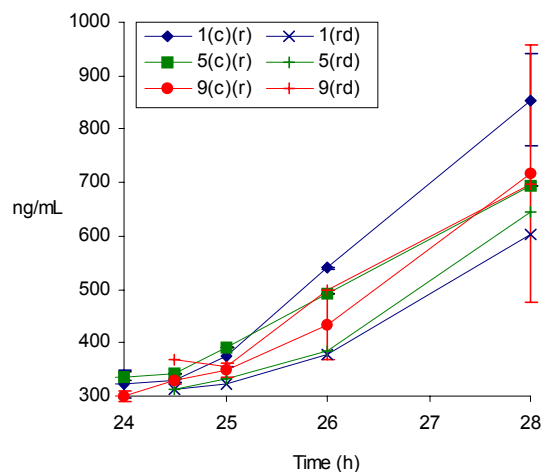
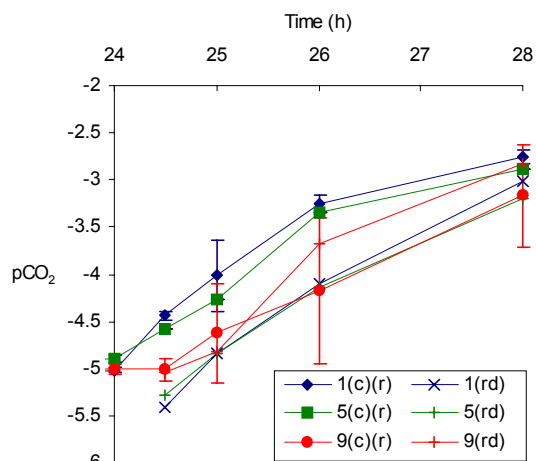


Figure 5.16 Calculated $\log p\text{CO}_2$ values in open system experiments 1/5/9(rd). These experiments had undergone 24h of closed system dissolution, and were 50% diluted with atmosphere-equilibrated deionised water after 24h.



5.2.2.2 Relationship between calcium acquisition and sulphide oxidation

a) Experiments 2(c)/(r): closed/open system dissolution of morainic rock 2

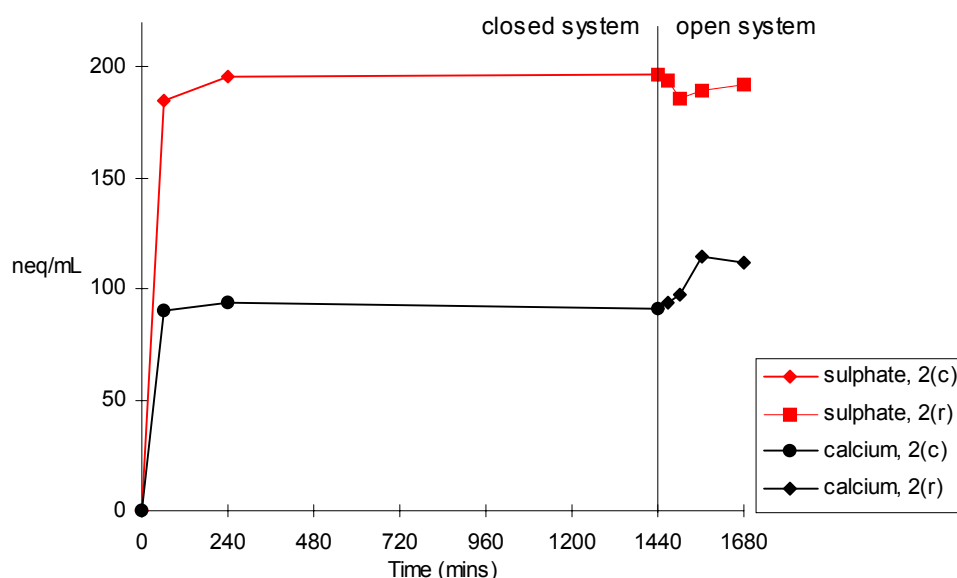
Experiment 2(c) involved the closed system dissolution of morainic rock 2 for 24h. The system was reopened after 24h (experiment 2(r)), with a further 4h dissolution. Rock 2 is the only rock that produced high concentrations of SO_4^{2-} . This experiment enabled the investigation of changes in SO_4^{2-} and Ca^{2+} concentrations upon reopening the system to the atmosphere.

Upon reopening the system to the atmosphere, a 25% increase in calcium concentration occurred (Figure 5.18), which was not reflected in an increase in dissolved concentration of SO_4^{2-} . It is therefore unlikely that the coupled process of sulphide oxidation and carbonate dissolution influenced Ca^{2+} concentrations in open system conditions, suggesting that carbonation-driven carbonate dissolution was the dominant process.

b) Effects of additional pyrite on morainic rock Ca^{2+} acquisition

Section 4.3.3.1d indicated that calcium concentrations in experiments 1P/5P/9P(c) (mixtures of calcium-rich morainic rocks and pyrite) were significantly increased under closed system conditions in comparison with corresponding experiments 1/5/9(c) (without pyrite). However, the difference in Ca^{2+} concentrations between experiments with and without pyrite

Figure 5.17 Concentrations of SO_4^{2-} and Ca^{2+} in experiments 2(c) (closed system) and 2(r) (reopened to the atmosphere after 24 hours).

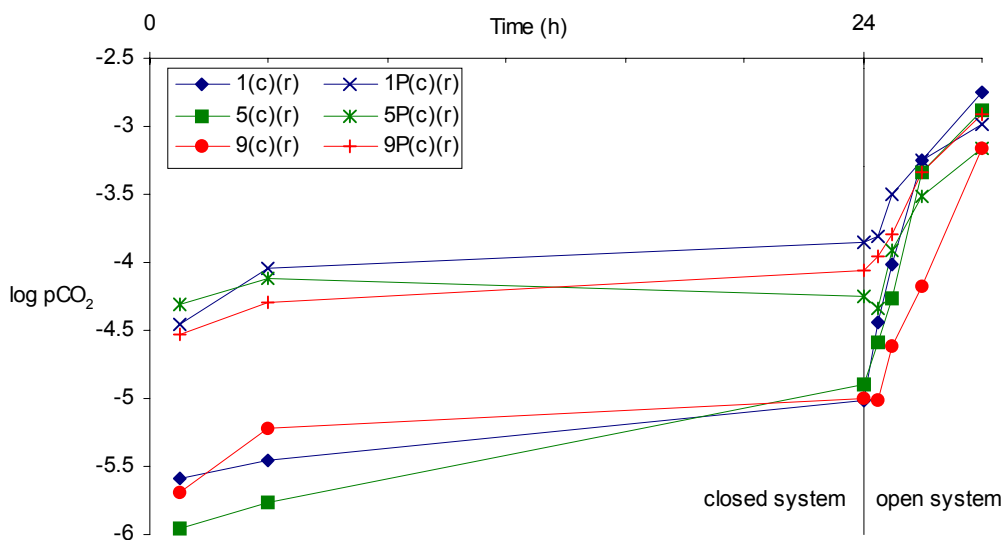


diminished under open access to the atmosphere (Figure 4.10). Similarly, values of $\log(\text{pCO}_2)$ were increased in experiments 1P/5P/9P(c) compared to experiments 1/5/9, with the differences reduced under open conditions (Figure 5.19).

1M SO_4^{2-} is associated with 2M H^+ during sulphide oxidation, which provides the acidity for 2M Ca^{2+} production. The dissolution of 1M $\text{CO}_2(\text{g})$ provides 1M H^+ , providing the acidity for 1M Ca^{2+} production (see Equation 1.10). The mean increase in pCO_2 under closed system conditions between experiments 1P/5P/9P(c) and corresponding experiments 1/5/9(c) was $10^{-4.19}\text{M} \pm 10^{-4.52}$. The corresponding increases in SO_4^{2-} and Ca^{2+} were $10^{-4.10}\text{M}$ and $10^{-3.99}\text{M} \pm 10^{-4.64}$ respectively. These observations are approximately consistent with stoichiometry, which suggests that $10^{-4.10}\text{M}$ SO_4^{2-} would be associated with approximately $10^{-3.79}\text{M}$ H^+ ($2 \times 10^{-4.10}\text{M}$), which would produce $10^{-4.10}\text{M}$ Ca^{2+} the equivalent of that produced by the the dissolution of $10^{-4.10}\text{M}$ CO_2 (see Equation 1.10 (sulphide oxidation-driven carbonate dissolution), Equation 1.11 (carbonation-driven carbonate dissolution)).

The extent of sulphide oxidation in experiments 1P/5P/9P(c) therefore reduced the extent of CO_2 -drawdown by approximately $10^{-4.19}\text{M}$ in comparison with experiments 1/5/9(c). This variation occurred within the first hour of dissolution, in the rapid initial phase, with little additional sulphide oxidation after this time. The fact that calcium does not continue to dissolve in experiments 1P/5P/9P(c) until pCO_2 is reduced to the levels in experiments 1/5/9(c) is likely to be due a modified equilibrium state between H^+ , $\text{CO}_2(\text{aq})$, Ca^{2+} and carbonate species.

Figure 5.18 Calculated variations in $p\text{CO}_2$ in experiments 1/5/9(r), and pyrite-added experiments 1P/5P/9P(r). Experiments were carried out under closed system conditions for 24h, then reopened to the atmosphere for a further 4h.



The additional Ca^{2+} produced by sulphide oxidation in experiments 1P/5P/9P(r) at any given time equated to approximately $1.13 \times \text{SO}_4^{2-}$ (neq/mL), with a corresponding $10^{-4.19}\text{M}$ increase in $p\text{CO}_2$. For a given value of $p\text{CO}_2$, the change in concentration of Ca^{2+} between experiments in the presence of pyrite and those in the absence of pyrite ($\Delta\text{Ca}_{\text{SOCD}}$) may be described by Equation 5.4.

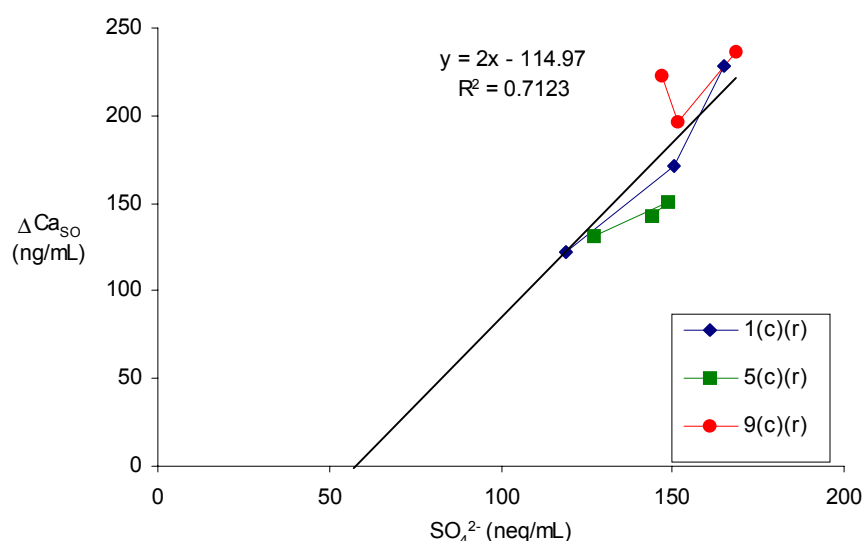
Equation 5.4 Relationship between mean $\Delta\text{Ca}_{\text{SOCD}}$ (concentration of Ca^{2+} in experiment containing pyrite minus concentration of Ca in corresponding experiment not containing pyrite) and SO_4^{2-} concentrations at any given value of $p\text{CO}_2$, based on experiments 1P/5P/9P(c) and corresponding experiments 1/5/9(c). Units are neq/mL.

$$\Delta\text{Ca}_{\text{SOCD}} = 0.78\text{SO}_4^{2-}.$$

However, these calculations were based on the mean concentration of SO_4^{2-} in experiments 1P/5P/9P(c). The effect of sulphide oxidation described in Equation 5.4 can only apply for calcium acquired via carbonate dissolution. Much of the calcium obtained from rocks 1, 5, 9 and C is likely to have come from carbonate minerals, which are abundant in these rocks. In contrast, no calcite was detected in rock 2, so the calcium obtained from rock 2 may have come from non-carbonate minerals, e.g. plagioclase, diopside (see Section 3.2.2). Therefore, Equation 5.4 cannot be valid for experiments 2(c)/(r). In these experiments, the total calcium concentration at any given time was around half the sulphate concentration. It is possible that a non-sulphide source of sulphate is present in rock 2.

Stoichiometrically, the coupled sulphide oxidation/carbonate dissolution reaction produces a solution $\text{Ca}^{2+}/\text{SO}_4^{2-}$ molar (or equivalent) ratio of 2:1 (see Equation 1.10). If a 2:1 regression is plotted between $\Delta\text{Ca}_{\text{SOCD}}$ and SO_4^{2-} concentrations of experiments 1P/5P/9P(c) at 1, 4 and 24h, the line crosses the abscissa at a SO_4^{2-} concentration of approximately 50neq/mL (Figure 5.19). The approximate nature of this trend must be emphasised, but it does infer that the effect of sulphide oxidation on Ca^{2+} concentrations would be insignificant in solutions with SO_4^{2-} concentrations lower than 50neq/mL. This is consistent with “end-member” experiments PC/PC_{0.1}(c) and morainic rock-pyrite mixture experiments 4P/4PC(c), none of which showed a significant increase in Ca^{2+} concentration in solutions with SO_4^{2-} concentrations of up to 35neq/mL (see Section 5.3.1.2).

Figure 5.19 Relationship between mean $\Delta\text{Ca}_{\text{SOCD}}$ (concentration of Ca^{2+} in experiment containing pyrite minus concentration of Ca in corresponding experiment not containing pyrite) and SO_4^{2-} concentrations (experiments 1/5/9(c)). Linear regression statistics: $\Delta\text{Ca}_{\text{SOCD}} = 2 \text{SO}_4^{2-} - 115$, $r^2 = 0.71$.

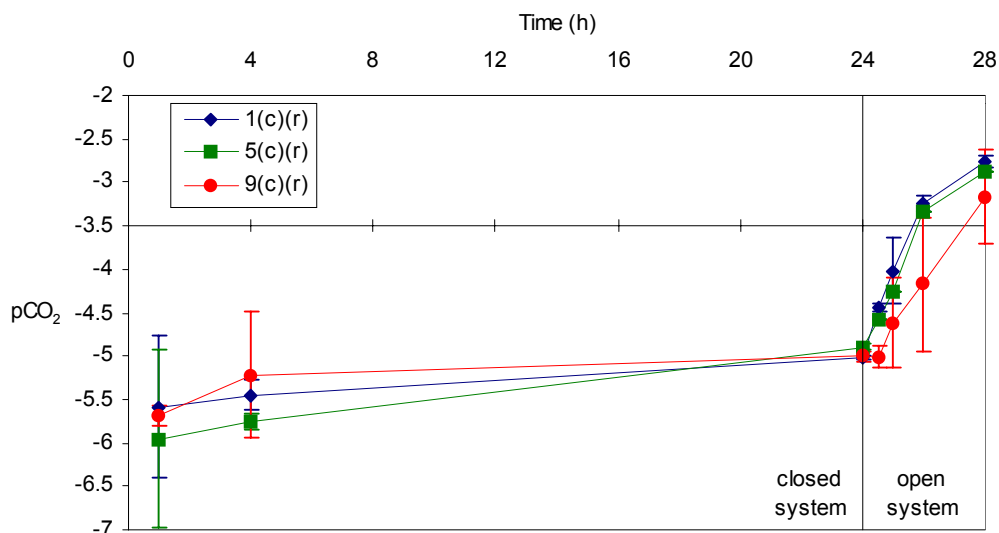


Stoichiometrically, 50neq/mL of SO_4^{2-} would be associated with the production of $10^{-4.6}\text{M}$ H^+ . Studies have shown that acidity producing greater than approximately $10^{-4.5}$ - 10^{-5}M H^+ is required to influence the rate of calcite acquisition (see Figure 1.7) (Wollast, 1990).

5.2.2.3 Relationship between calcium acquisition and $p\text{CO}_2$

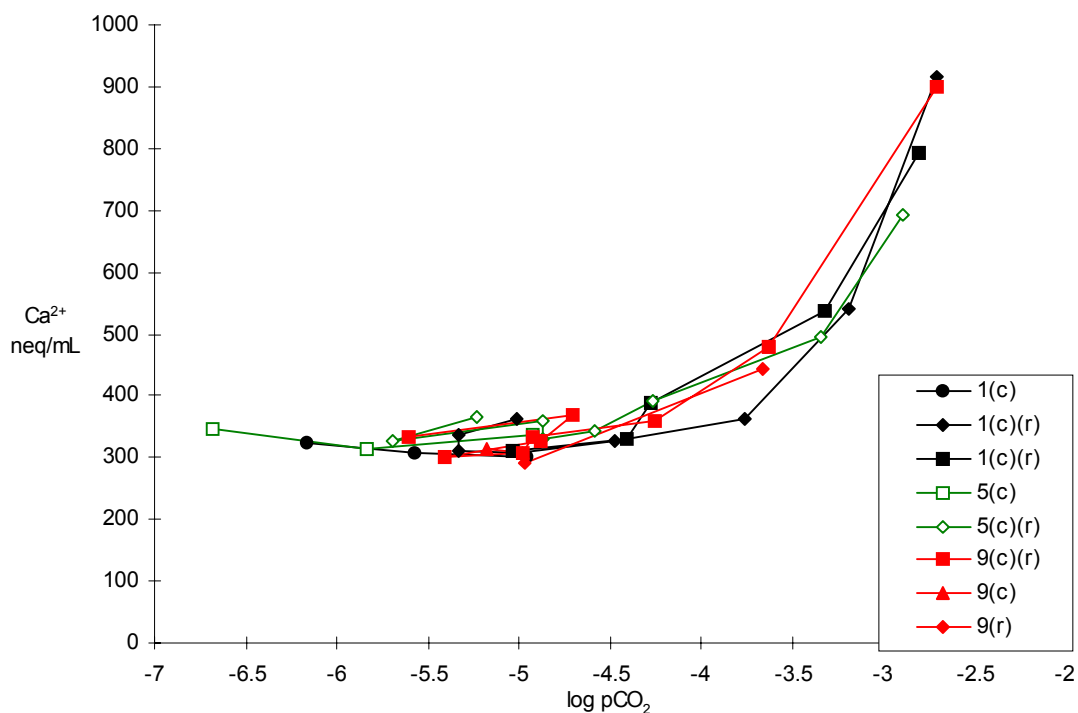
The 15% mean reduction in Ca^{2+} concentrations between 1 and 24h dissolution of closed system, calcite-rich experiments 1/5/9(c) was accompanied by an increase in $\log(p\text{CO}_2)$ in each experiment (Figure 5.21). Upon reopening, $\log(p\text{CO}_2)$ increased at varying rates with each experiment and repeat run (Figure 5.17) (see Section 5.2.2.4 for the reasons for the reduction in Ca^{2+} concentration).

Figure 5.20 Calculated trends of $\log(p\text{CO}_2)$ in experiments 1/5/9(r), reopened to the atmosphere after 24 hours under a closed system.



The variation of $p\text{CO}_2$ levels between repeat experiments is associated with the variations in Ca^{2+} (Figure 5.16), suggesting that Ca^{2+} concentrations in experiments 1/5/9(c)/(r) were governed by $p\text{CO}_2$ levels, as illustrated in Figure 5.22. This is consistent with the observations in “end-member” experiments which indicated CO_2 drawdown to be a major control on calcium acquisition from calcite.

Figure 5.21 Variation of Ca^{2+} acquisition with $p\text{CO}_2$ in experiments 1/5/9(c)/(r). Repeat runs of all experiments are shown individually.



Calcium concentrations in experiments 1/5/9(c)/(r) were also closely related to pH, as pH is very closely (inversely) related to $p\text{CO}_2$ in rocks that dominantly dissolve Ca^{2+} and HCO_3^- . However, in these experiments SO_4^{2-} concentrations did not reach 10neq/mL, and did not significantly increase when the experiments are reopened to the atmosphere (see Figure 4.26). This suggests that the extent of sulphide oxidation was insufficient to affect carbonate dissolution rates (see Section 5.2.2.2). It is likely that pH variations are controlled by the relationship between carbonate species, $\text{CO}_2(\text{g})$ and calcite.

The calculated power regression for 1/5/9(c)/(r) was calculated as shown in Equation 5.5. The calculated regression lines are plotted on Figure 5.24.

Equation 5.5 Calculated power regression for the relationship between Ca^{2+} and $p\text{CO}_2$ in experiments 1/5/9(c)/(r), for $SI(\text{calcite}) \leq 0$, (units in neq/mL/log($p\text{CO}_2$))

$$\text{Ca}^{2+} = 80000(\text{CO}_2) + \frac{2226}{-\log(p\text{CO}_2)} - 45$$

The values of $p\text{CO}_2$ may have varied in duplicate experiments for a number of reasons. Sampling for the 4 hours subsequent to reopening experiments 1/5/9(r) was carried out from the same solution (see Section 2.3.4), so that the total quantity of solution decreased with each time period. This process produced two possible means of increasing the rate of CO_2 drawdown:

- a) The exposed surface area to volume ratio of the solution was increased, and the distance from the surface to the unsuspending sediment at the base of the vessel.
- b) Shaking the bottle, a process necessary to ensure that the solution is homogeneous and that suspended sediment is evenly disseminated throughout the solution, may increase the potential for CO_2 drawdown by causing turbulent CO_2 incorporation.

Additionally, atmospheric concentrations of CO_2 are likely to vary with time of day, due to biotic activity (this has not been evaluated in this study).

The variations caused by laboratory procedural effects could reflect potential variations in exposed solution surface area and turbulence caused by flow pathways in subglacial environments.

5.2.2.4 Calcite supersaturation

Calcite saturation rapidly occurred in closed system experiments 1/5/9(c) (Figure 5.23). The reduction in Ca^{2+} concentration and recovery of $p\text{CO}_2$ between 1 and 24h may have occurred

in response to the early calcite supersaturation. Calcite supersaturation also occurred in other morainic rock experiments 4/6/8/4C/4PC(c) (Figure 4.7). Ca^{2+} levels also dropped significantly between 1 and 4 hours in these experiments, suggesting that reprecipitation of calcite occurred, as the supersaturated state is not stable. At 4 hours, all experiments (bar experiments 2/3/M(c)) were at $\text{SI}(\text{calcite}) \geq 0$ (Figure 5.24). After this time there was effectively no acquisition of Ca^{2+} from any rocks except rock 2, from which additional acquisition took place between 4 and 24 hours.

Figure 5.22 $\text{SI}(\text{calcite})$ values for Experiments 1(c), 5(c) and 9(c).

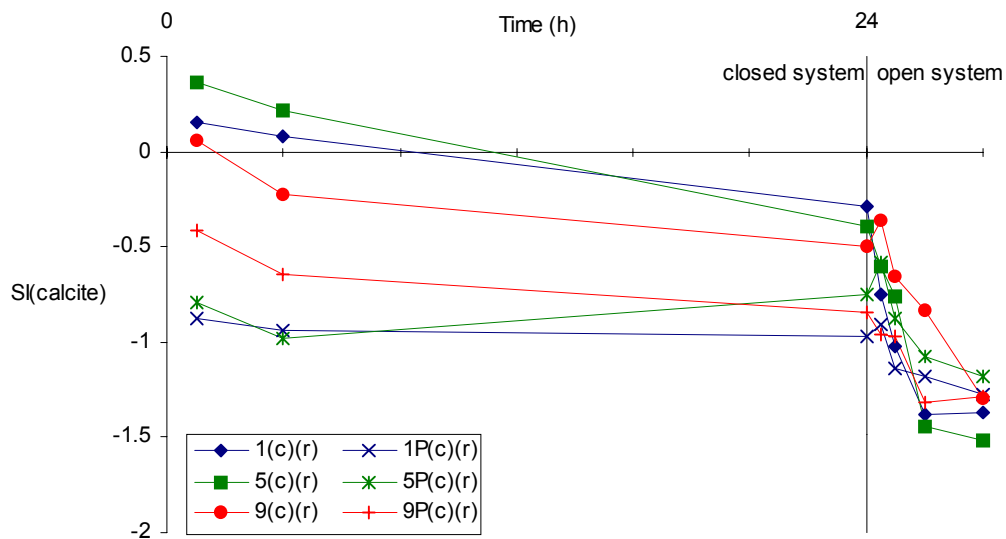
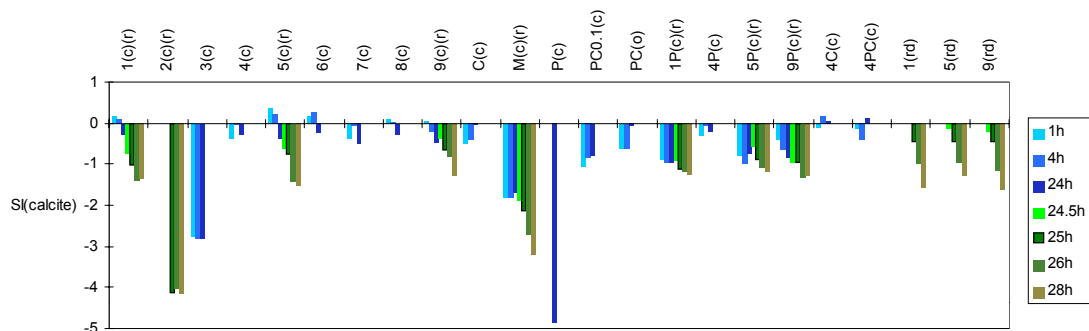


Figure 5.23 Calculated values of $\text{SI}(\text{calcite})$ in laboratory experiments, at 1, 4, 24, 24.5, 25, 26, 28 hours (where applicable). Experiments labelled (c) were run under closed system conditions, (o) labels indicate open system experiments, and those labelled (c) (r) were run under closed system conditions until 24 hours and then continued under open system conditions between 24 and 28 hours. Those labelled (rd) were 50% diluted by deionised water after 24 hours closed system dissolution, with dissolution continuing under open system conditions until 28 hours. See text for details.



The concentration of Ca^{2+} during supersaturation deviated from the calculated $\text{Ca}^{2+}/\text{pCO}_2$ relationship described in Equation 5.5. The increase in Ca^{2+} for a given value of pCO_2

resulting from the tendency for rapid initial calcium acquisition to form supersaturated solutions ($\Delta\text{Ca}_{\text{SAT}}^{2+}$) is described by Equation 5.6.

Equation 5.6 Relationship between mean $\Delta\text{Ca}_{\text{SAT}}^{2+}$ (concentration of Ca^{2+} in experiment containing pyrite minus concentration of Ca in corresponding experiment not containing pyrite) and SI(calcite) at a given value of $p\text{CO}_2$. Units are neq/mL.

$$\Delta\text{Ca}_{\text{SAT}}^{2+} = 10^{(\text{SI}(\text{calcite})+1.3)}$$

5.2.2.5 Effect of morainic rock mineralogy on calcium acquisition

a) Rocks 1, 5 and 9 (carbonate-rich rocks)

The combination of Equation 5.4, Equation 5.5 and Equation 5.6, which described the relationships between Ca^{2+} , $p\text{CO}_2$, SI(calcite) and SO_4^{2-} , produce the regressions plotted on Figure 5.24. These experiments were carried out at temperatures between 6 and 9°C, but it can be seen that the $\text{Ca}^{2+}/p\text{CO}_2$ relationship in these experiments deviated significantly from the equilibrium relationships at either 0 or 10°C. Temperature variations within these experiments were no more than 3°C (see Section 2.3.2), so therefore could not account for the non-equilibrium $\text{Ca}^{2+}/p\text{CO}_2$ relationship described by the figure.

Figure 5.24 Plot of power laws describing the variation of Ca^{2+} acquisition with $p\text{CO}_2$ in experiments 1/5/9(c)/(r). The equilibrium relationships between Ca^{2+} and $p\text{CO}_2$ at 0°C, 10°C and 25°C are also shown. The temperature of the plotted experiments ranged between 6 and 9°C

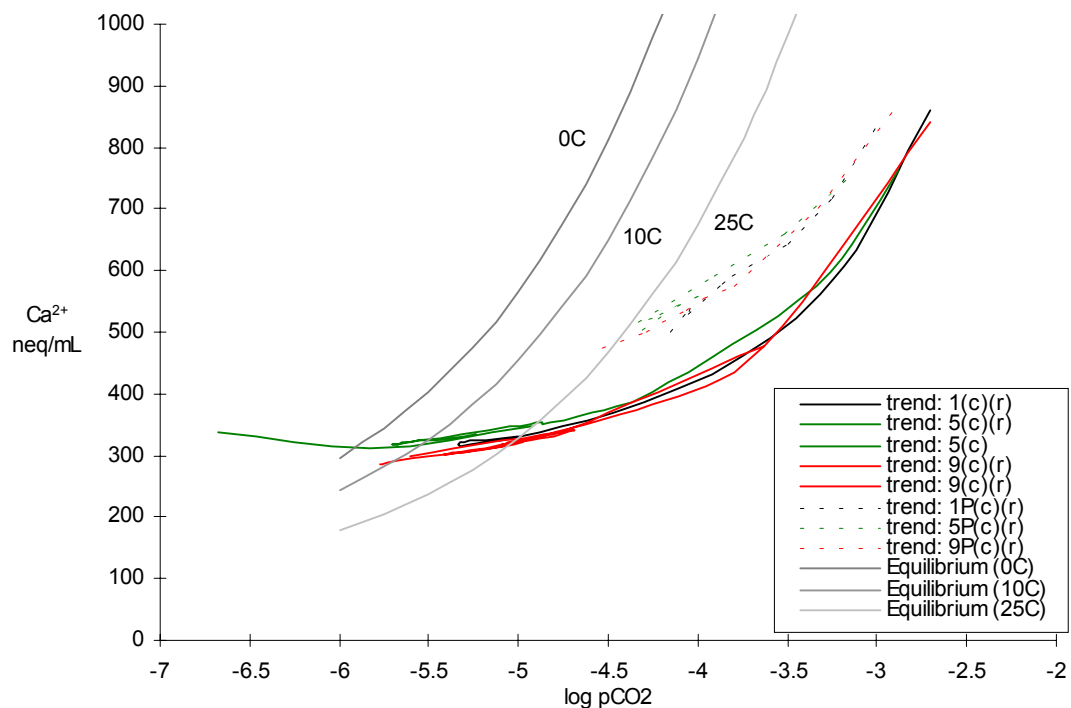
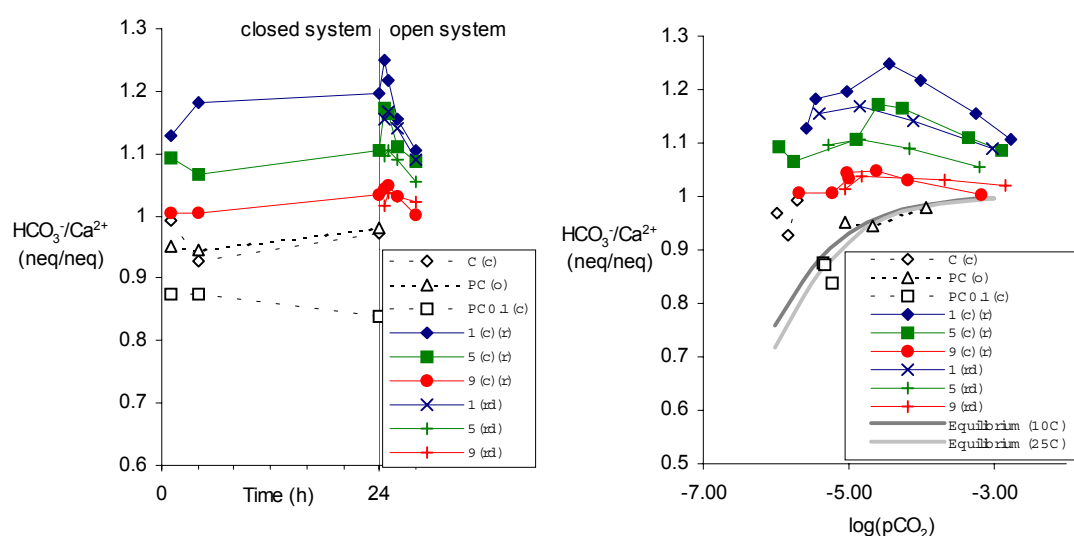


Table 5.6 shows that the equilibrium ratio between Ca^{2+} and HCO_3^- changes as pH decreases and pCO_2 increases (Garrels and Christ, 1965). At low pCO_2 /high pH conditions, the $\text{HCO}_3^-/\text{Ca}^{2+}$ ratio is below 0.8, due to the higher stability of CO_3^{2-} at high levels of pH. As pCO_2 increases, the ratio tends to 1. This trend is plotted on Figure 5.25, and it is apparent that “end-member” experiments C(o) and PC(o), which closely followed the equilibrium $\text{Ca}^{2+}/\text{pCO}_2$ relationship, also closely followed the $\text{HCO}_3^-/\text{Ca}^{2+}$ equilibrium relationship, except at the initial stages of acquisition, before equilibrium has been reached.

Figure 5.25 Mean $\text{HCO}_3^-/\text{Ca}^{2+}$ ratio plotted vs. (left) time, and (right) $\log \text{p}(\text{CO}_2)$ (calculated equilibrium lines for 10(and 25°C are based on equations in Garrels and Christ, 1965). For explanation of experimental nomenclature, see Figure 5.24.



In contrast to the experiments involving pure calcite, the ratios of $\text{HCO}_3^-/\text{Ca}^{2+}$ in experiments 1/5/9(c)/(r) were significantly above unity at low pCO_2 conditions, and further increased as closed system dissolution progressed (Figure 5.25). This may be due to carbonation reactions providing protons to dissolve aluminosilicate minerals containing other metal cations, as these reactions also produce carbonate species. Pure calcite dissolution produces 2 moles of HCO_3^- for each mole of Ca^{2+} , which is a 1:1 equivalent $\text{HCO}_3^-/\text{Ca}^{2+}$ ratio (reducing in low pCO_2 conditions, as described above) (Equation 4.2). However, if one mole of calcite and one mole of albite are dissolved from a mixed sediment, 4 moles of HCO_3^- are produced, giving a 2:1 equivalent ratio (again, pCO_2 -dependent) (Equation 5.7). Thus, a weak positive relationship existed between solution $\text{HCO}_3^-/\text{Ca}^{2+}$ ratio and non-calcium metal content of the morainic rocks used in experiments 1-9(c) (Figure 5.26). The additional metal cation dissolution and bicarbonate production also alters the relationship between Ca^{2+} and pCO_2 in solution, from 1:1 molar ratio in a pure calcite system to 1:3 in a mixed calcite-albite system.

Equation 5.7 Combined dissolution of calcite and albite driven by carbonation reactions.

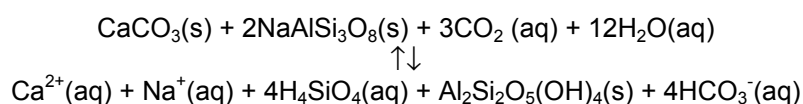
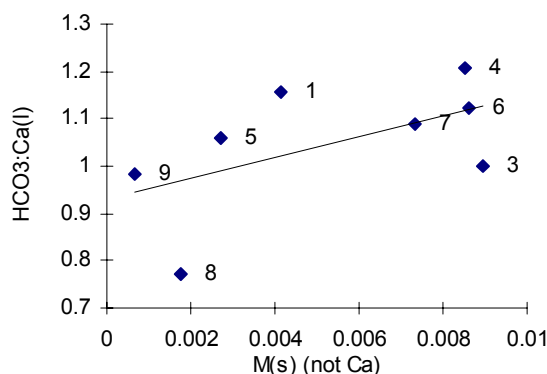


Figure 5.26 Relationship between non-Ca rock metal content and $\text{HCO}_3^-/\text{Ca}^{2+}$ ratio, after 24 hours closed system dissolution (experiments 1-9(c)).

Regression statistics: $\text{HCO}_3^-/\text{Ca}^{2+} = 22 (\text{M}(\text{s})-\text{Ca}(\text{s})) + 0.93$; $r^2 = 0.31$



As pCO_2 increased under open system conditions in experiments 1/5/9(r), Ca^{2+} became more dominant in solution in comparison to other cations, and therefore the $\text{HCO}_3^-/\text{Ca}^{2+}$ ratio tended towards 1:1 (Figure 5.25). The $\text{Ca}^{2+}/\text{pCO}_2$ relationship therefore also altered, with the magnitude of Ca^{2+} acquisition per unit increase in pCO_2 rising.

b) Other rocks (non-carbonate-rich)

Rocks 1, 5 and 9 each consist of in excess of 60% carbonates, so that acquisition of calcium is likely to be dominantly from carbonate dissolution reactions. The other rocks used in laboratory experiments only contained trace amounts of calcite, so that although the dissolution of even these amounts of calcite will produce significant amounts of calcium ions in solution, the importance of other sources of calcium are likely to become more significant. Figures 4.8 and 4.9 showed that the relationship between rock Ca content and solution concentration was not consistent across different rock types, suggesting that the variations in mineralogy influence rates and controls on calcium dissolution.

The relationship between pCO_2 and Ca^{2+} varied between morainic rock experiments (Figure 5.27). The variation is satisfied by introducing a mineralogical factor, $\Delta\text{Ca}^{2+}_{\text{MIN}}$. The values of $\Delta\text{Ca}^{2+}_{\text{MIN}}$ that correct for mineralogical variations are shown in Table 5.7. These were established by trial-and-error.

The mineralogical parameter ΔCa^{2+}_{MIN} predominantly affects the magnitude of short-term initial rapid Ca^{2+} acquisition. It is also effectively a degree of saturation, as for experiments involving relatively Ca-rich rocks, the value is 1, and the equilibrium variations described in the above parameters fully satisfy the Ca^{2+} variations encountered experimentally.

The variation in ΔCa^{2+}_{MIN} was found to be closely related to the pH of each solution under closed system conditions, and particularly the pH after 60 minutes of dissolution, as illustrated in Figure 5.28, and described in Equation 5.8.

Figure 5.27 Relationship between pCO_2 and Ca^{2+} for closed and open system morainic rock experiments 1/3-9(c); 1/2/5/9(r). Repeat runs for experiments 4(c), 1/5/9(c)/(r) are shown separately.

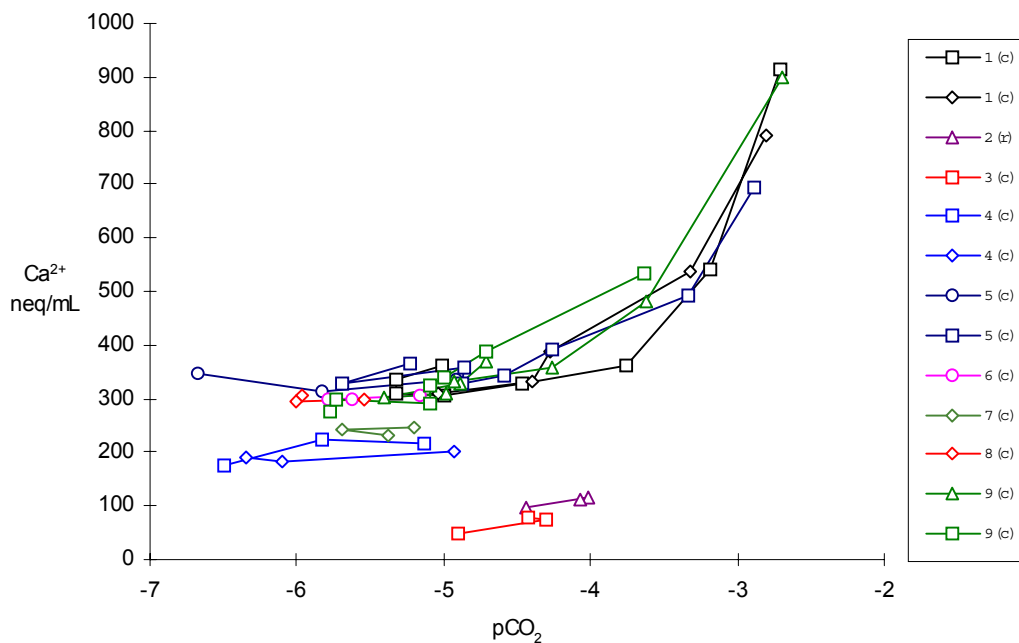


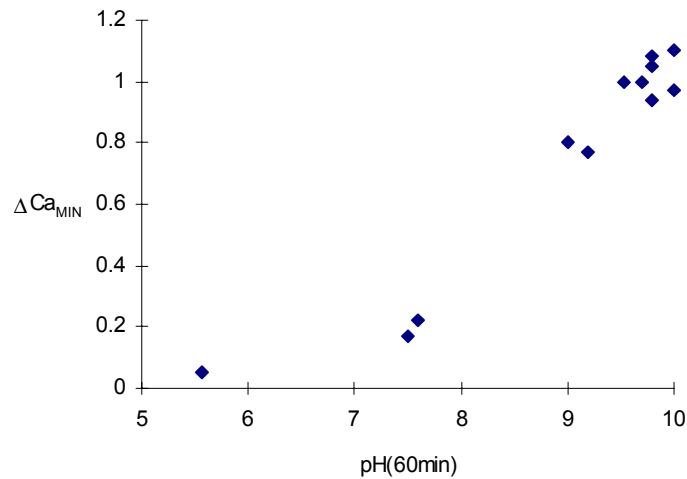
Table 5.7 Mineralogical factor ΔCa^{2+}_{MIN} for experiments 1-9/P/C/PC(c) (see text for details)

Experiment	Mineralogical factor C
1(c)/(r)	1.00
2(c)/(r)	0.22
3(c)	0.17
4(c)	0.80
5(c)/(r)	1.00
6(c)	0.94
7(c)	0.77
8(c)	0.97
9(c)/(r)	1.00
P(c)	0.05
C(c)	1.00
PC(c)	1.00

Equation 5.8 Relationship between mean ΔCa^{2+}_{MIN} (concentration of Ca^{2+} in experiment containing pyrite minus concentration of Ca in corresponding experiment not containing pyrite) and the pH of the solution after 60min dissolution at a given value of pCO_2 . Units are neq/mL.

$$\Delta Ca^{2+}_{MIN} = \frac{(pH_{60min} - 6.93)}{2.85}$$

Figure 5.28 Relationship between ΔCa^{2+}_{MIN} and the pH of solution after 60minutes in experiments 1-9/P/C/PC(c).



The pH at 60 minutes is a result of the extent of rapid dissolution of microfine particles, linked to the pCO_2 minima demarking the boundary between Stages 1 and 2 of the Ca^{2+} acquisition profile. This is kinetically controlled by the number of available surface sites on which hydration reactions can take place. However, using pH_{60min} as a parameter describing this variation does not directly relate to the number of surface sites, or to the different reaction stoichiometries between different minerals, and as such is merely an incidental parameter rather than an indication of the controlling factor of dissolution processes.

Determination of ΔCa^{2+}_{MIN} by calculating the degree of rock Ca in carbonate form

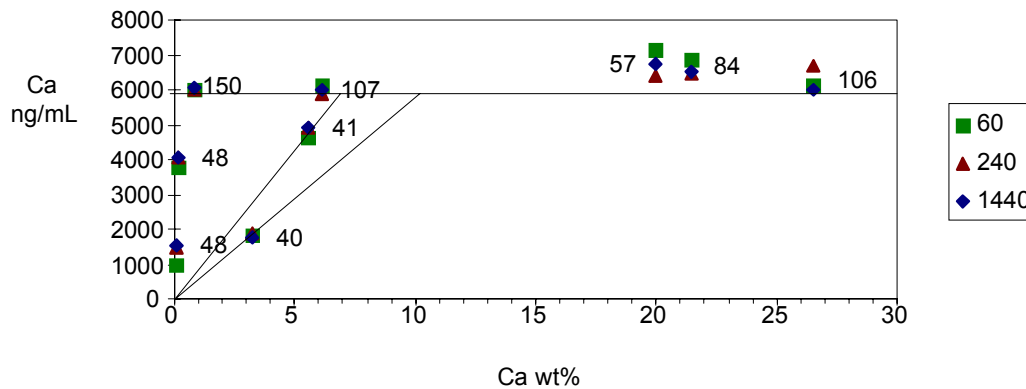
It is known that Sr is not favourably incorporated into the structure of calcite, and is more common in Ca- and K-silicates, such as feldspars (Rankama and Sahama, 1950) (see Section 1.6.3.2). It follows that the rock Ca/Sr ratio may indicate the degree to which Ca is present in carbonate minerals, with a relatively high Ca/Sr suggesting a carbonate provenance. Rock Ca/Sr ratios varied with rock type (Section 3.4.2.4), with the lowest Ca/Sr found ratios in Rocks 2, 3, 4 and 7. Figure 5.29 suggests that there was a relationship between rock Ca/Sr ratio and Ca^{2+} yield in laboratory experiments. In particular, experiment 6(c) (involving Rock 6), with a Ca/Sr ratio of 150:1, showed a high solute yield, and experiment 2(c) (involving Rock 2), with a Ca/Sr ratio of just 40:1, yielded a relatively low concentration of Ca^{2+} , despite a higher rock Ca content.

Lines were plotted through the origin and the points of rocks 2, 3, 4 and 7 (Figure 5.29), as with Figure 5.26. The points at which the plotted lines pass the $\Delta\text{Ca}^{2+}_{\text{MIN}}=1$ level produced the line described in Equation 5.9 ($r=-0.99$, $n=4$).

Equation 5.9 Determination of $\text{Ca}^{2+}_{\text{MIN}}$ using rock calcium and strontium concentrations. Calculated values above 1 merely show the potential levels of acquisition should equilibrium conditions allow further dissolution). The maximum Ca/Sr ratio that can be dealt with is 48.03, above which it is assumed that a null amount of Ca in the rock will yield Ca^{2+} to the $\Delta\text{Ca}^{2+}_{\text{MIN}}=1$ level. Units in wt%

$$\Delta\text{Ca}^{2+}_{\text{MIN}} = \frac{\text{Ca(s)}}{53.061 - 1.105\left(\frac{\text{Ca(s)}}{\text{Sr(s)}}\right)} \quad (0 < \Delta\text{Ca}^{2+}_{\text{MIN}} < 1)$$

Figure 5.29 Ca^{2+} concentration of experiments 1-9(c) after 24h, plotted versus original rock Ca wt%. Labels represent corresponding rock Ca/Sr ratios. Individual points are plotted for samples at 60, 240 and 1440min.



Equation 5.9 has the following limitations:

- the small number of points and the small range of Ca:Sr ratios involved in the calculation of this line are low, and as such, it cannot be stated whether further experiments would yield similar results.
- the accuracy of the equation is low at very low rock Ca^{2+} content: minute changes in ratio leads to large variations in calculated yield.
- Figure 4.13 shows that solution Ca/Sr ratios are unrelated to rock Ca/Sr ratios, nor are they closely related to rock Ca content. Therefore, interpretation of provenance cannot be made on the basis of solution Ca/Sr ratios, and provenance calculations cannot specify absolute Ca content or Ca/Sr ratios.

With the dataset available, no other suitable parameters such as chemical indicators in solution were found that could explain the variation in $\Delta\text{Ca}^{2+}_{\text{MIN}}$.

5.2.2.6 *Summary of controls on calcium acquisition in morainic rock experiments*

Calcium acquisition was very rapid in morainic rock experiments, with supersaturation being achieved within 60 minutes from experiments 1/5/9(c), which dissolved calcite-rich rock powder. Values of log pCO₂ reached -6 to -5 during this period. The effect of sulphide oxidation was most notable in this initial period, and showed little effect after this time. The additional calcium acquisition from calcite caused by sulphide oxidation may have been directly related to the stoichiometry of the coupled sulphide oxidation-carbonate dissolution reaction (Equation 1.10). The presence of sulphide also reduced the apparent extent of carbonation-driven carbonate dissolution, with values of log pCO₂ higher than in corresponding, sulphide-absent experiments.

The effect of sulphide oxidation on calcium acquisition from other minerals was not quantified, but experiment 2(c) showed that the relationship between calcite dissolution and sulphide oxidation was different to the relationship between sulphide oxidation and dissolution of other calcite-bearing minerals, as would be expected.

Oversaturation forced reprecipitation in closed system experiments beyond the initial rapid stage of acquisition. This was accompanied by an increase in log pCO₂. In non-supersaturated experiments, calcium acquisition was effectively curtailed under closed system conditions.

Calcium acquisition continued upon reopening experiments to the atmosphere. The rate of increase in Ca²⁺ concentration was approximately linked to the pCO₂ of the solution, but acquisition was not sufficient to prevent the recovery of pCO₂ values to levels above atmospheric equilibrium. Repeat experiments increased in calcium concentration at varying rates, but these variations were linked to variations in increase in pCO₂, suggesting that CO₂-drawdown is the dominant controlling factor on calcium acquisition. Experiment 2(r) indicated that increases in calcium concentration under open system conditions were not linked to further sulphide oxidation, which did not significantly occur when the experiment was reopened to the atmosphere.

5.3 PROCESSES, RATES AND CONTROLS OF ACQUISITION OF OTHER SPECIES

Although calcium and carbonate species dominated the solute load in many laboratory experiments, Section 5.3 shows that mineralogy (e.g. aluminosilicates, pyrite) had direct and indirect influential effects on the character of solute acquisition in the laboratory experiments

involving morainic rocks and/or pyrite. The effects of these species on calcium acquisition, carbonate equilibria and CO₂-drawdown have been described above. Therefore, it is important that the processes and controls on the acquisition of other cations are understood, to give an overall picture of the major controlling processes on solute acquisition in subglacial environments. Additionally, certain minor and trace elements may be associated with a certain mineralogy, and as such may better isolate the processes occurring in individual experiments. It is therefore necessary to identify the controls on acquisition of such species.

5.3.1 Controls on solute acquisition of cations: implications arising from major and trace element speciation modelling using PHREEQC

The adsorbability of trace elements is often dependent on their speciation. Many complexes are sorbed much more strongly than free metal ions, thought to be due to the reduction in reaction between the metal cation and the remaining aquo groups that keep the ion in solution (Stumm and Bilinski, 1972). This is the case for Pb(CO₃), which is much more strongly sorbed onto negatively charged silica than Pb²⁺, and so is more strongly sorbed at increasing pH, where the carbonate complex is more stable (Stumm and Bilinski, 1972). Lead therefore showed an initially enhanced solute yield, but was clearly reprecipitated as experiments progressed (see Table 4.3).

In contrast, anomalously high concentrations of trace elements in solution may often be related to the presence of stable complexes (Hering and Morel, 1990), although complexes are generally less prevalent in fresh waters, which are of lower ionic strength in comparison to seawater (Drever, 1982) (see Section 1.5.2). Chapter 4 indicated that the short- and long-term solubility of many minor and trace elements in laboratory simulation experiments appeared to be linked to the extent of carbonate dissolution. This may be due to surface exchange reactions due to calcite saturation (see above), but since carbonate complexes are often most stable in the circumneutral to alkaline pH ranges (e.g. copper in Stumm and Bilinski, 1972, Fig. 2) solubility of the trace elements may be governed by complexation with carbonate or other anions (see also Section 1.5.2). Carbonate complexes are generally much more soluble than hydroxide complexes in natural waters (Drever, 1982).

Table 5.1 shows the results of speciation modelling of mean data of closed system, 24 hour experiments 1-9/P/C/M(c), using the MINTEQA2 database through the PHREEQC Interactive

modelling package (see Section 2.5). An example of the input file is shown in Appendix 1 (PHREEQC Input File A-1). It is clear that certain elements preferentially form complexes in the chemical conditions of the experiments. Many elements are dominantly complexed, according to the speciation model. Many complexes are linked to the high pH of many of the laboratory solutions, which results in relatively high OH⁻ concentrations in solution. Therefore, relatively insoluble elements such as Al, Fe and Zn were mainly present in the form of hydroxides. Other elements complexed with carbonate ions, including Ni and Pb. These ions all reduced in concentration between 4 and 24h, demonstrating the tendency for sorption onto silicates described in Stumm & Bilinski (1972). Uranium also complexed with carbonate ions, but also formed uranyl (UO₂) species within the complex, which may effect the sorbability of uranium.

Table 5.1 Dominant speciation of major, minor and trace elements in average 24 hour laboratory experiments, according to PHREEQC modelling (see text for assumptions). 'Y_{24h}/Y_{max} %' is the solute yield % after 24h closed system dissolution divided by the maximum sampled solute yield over the period 1-24h inclusive. A 100% yield slope therefore shows that the peak concentration is after 24 hours, suggesting little adsorption or reprecipitation. A low percentage solute yield slope indicates that short-term concentrations are not maintained, with lower concentrations encountered after 24 hours. 'log M' refers to the log molalities of each species, '% species' refers to the proportion of the element present in the form of each species (complex/free ion). The dominant species in individual laboratory experiments is indicated by a ●; zero data/data not available indicated by a dash.

	Y _{24h} /Y _{max} %	log Y _{24h}	Dominant species	log M	% species	1	2	3	4	5	6	7	8	9	P	M	C		
Al	-	-	Al(OH) ₃	-6	39		●		●						-	-	-	-	
			Al(OH) ₄ ⁻	-6	61	●		●			●	●	●	●		-	-	-	-
Ba	75	-5.5	Ba ²⁺	-9	100	●	●	●	●	●	●	●	●	●	-	●	●	●	
C	100	-	HCO ₃ ⁻	-4	96	●	-	●	●	●	●	●	●	●	●	●	●	●	
Ca	100	-3.0	Ca ²⁺	-4	99	●	●	●	●	●	●	●	●	●	●	●	●	●	
Cl	100	-	Cl ⁻	-5	100	●	●	●	●	●	●	●	●	●	●	●	●	●	
Cu	50	-4.3	Cu(OH) ₂	-9	100	●	●	-	●	●	●	●	●	●	●	●	●	●	
Fe	-	~ -5.0	Fe(OH) ₄ ⁻	-6	88	●				●	●	●	●	●		●	●	●	
			Fe(OH) ₃	-7	11														
			Fe(OH) ₂ ⁺	-8	1		●	●	●							●			
K	100	-4.0	K ⁺	-5	100	●	●	●	●	●	●	●	●	●	●	●	●	●	
Mg	40	-4.7	Mg ²⁺	-5	99	●	●	-	●	●	●	●	●	●	●	●	●	-	
N	100	-	NO ₃ ⁻	-6	100	-	●	●	●	●	●	●	●	●	-	●	-	-	
Na	75	-4.5	Na ⁺	-5	100	●	●	●	●	●	●	●	●	●	●	●	●	●	
Ni	30	-4.5	NiCO ₃	-8	96	●		●	●	●	●	●	●	●		●	●	●	
			Ni ²⁺	-9	3		●										●		
Pb	8	-4.2	Pb ²⁺	-19			-									●			
			PbCO ₃	-9	79	●	-	●	●	●	●	●	-	●	●		●	●	●
			Pb(OH) ⁺	-9	15		-												
Rb	100	-4.0	Rb ⁺	-8	100	●	●	●	●	●	●	●	●	●	-	●	●		
S	100	-	SO ₄ ²⁻	-6	97	●	●	●	●	●	●	●	●	●	●	-	-	-	
Sr	100	-3.7	Sr ²⁺	-7	100	●	●	●	●	●	●	●	●	●	●	●	●	●	
U	100	-4.7	UO ₂ CO ₃	-12	1		-	-		-	-	-	-		●				
			UO ₂ (CO ₃) ₂ ²⁻	-11	64				●									●	
			UO ₂ (CO ₃) ₃ ⁴⁻	-11	34	●	-	-		●	-	●	-	●					●
Zn	60	-4.2	Zn ²⁺	-9	11		●	●	●							●			
			Zn(OH) ₂	-8	76	●					●	●	●	●	●		●	●	●
			ZnCO ₃	-9	9														

It is suggested that ions with an ionic radii closest to Ca^{2+} are likely to produce the most stable carbonate complexes, particularly if they also have the same valency. Ni and Pb dominantly formed carbonate complexes in the majority of conditions encountered in the laboratory experiments. Consistent with this theory, the mean yield of Pb (ir=0.120nm) was greater than that of Ni (ir=0.069nm).

Complexation appeared to influence the long-term solubility of elements. The average data suggests that free ions in solution appeared largely to remain in solution for up to 24 hours, with the average concentrations of free ionic species at 24 hours being 85% of the maximum value. Acidified species (e.g. C) show a similar pattern. This is likely to be due to the lower adsorption of these species (Stumm and Bilinski, 1972). Metals that the model suggested exist in solution dominantly as complexes tended to show a decrease in solution concentration after 1 or 4 hours, with concentrations of carbonate-complexing species showing concentrations at 24 hours 60% of the maximum observed levels, and hydroxy-complexes showing only 37% maximum levels at 24 hours, on average (Table 5.1). Again, this may be due to the sorption of these species onto negatively charged silica (Stumm and Bilinski, 1972).

a) Summary

It is clear that speciation has observable effects on the solubility and dissolution profile of trace elements. The modelling here is rather simplistic to make confident inferences of processes based trace element behaviour, and interpret trace element behaviour in meltwaters based on the same assumptions. The necessity for consideration of speciation and absorption processes in the role of trace elements in glacial meltwaters is, however, clearly illustrated.

5.3.2 Controls on sulphide oxidation

a) Pyrite content

The presence of pyrite in the sediment reacted during experiments 1-9(c) and 1/5/9(r) was the obvious and major control on sulphate concentration, indicating that sulphate concentration is a reliable tool as an indicator of sulphide oxidation from subglacial sediment.

Iron concentrations were generally higher in pyrite-added experiments 1P/5P/9P(c) than in pyrite-absent experiments 1/5/9(c), with a mean increase ($\Delta\text{Fe}^{\text{tot}}_{\text{PO}}$) of 16%. The mean $\Delta\text{Fe}^{\text{tot}}_{\text{PO}}$ between experiments 4/4C(c), and 4P/4PC(c) was 75%. However, the concentrations of iron resulting from experiments 1P/5P/9P(c) are no greater than the maximum iron

concentrations resulting from other experiments involving morainic rock without pyrite added, such as experiments 6/7(c). Therefore, although iron concentrations did increase in response to pyrite oxidation, the magnitude of change would not be sufficient to isolate the sulphide oxidation process in bulk meltwater, as iron was widely distributed throughout most of the morainic rocks used in the experiments, and did not appear to be preferentially eluted from sulphide minerals in comparison to other iron-bearing minerals.

b) Dissolved oxygen

Although Section 1.5.2 showed that pyrite oxidation showed dependence on dissolved oxygen (Nicholson *et al.*, 1988; Williamson and Rimstidt, 1994; Stumm and Morgan, 1996), observed O₂(aq) concentrations in the laboratory experiments did not show significantly lower levels in the presence of pyrite than in its absence (see Section 4.3.2 and Figure 4.5). Additionally, the experiments with significant SO₄²⁻ concentration that were reopened to the atmosphere after 24h closed system dissolution (experiments 2/1P/5P/9P(r)) showed either only small increases, or no increase at all upon reopening to the atmosphere (see Figure 4.27). This was unlike the increases in calcium concentration observed upon reopening the same experiments, due to renewed access to CO₂(g), and suggests that restriction of access to dissolved oxygen was a minor or insignificant control on sulphide oxidation processes. This is consistent with stoichiometric calculations of oxygen requirements using Equation 1.5 (pyrite oxidation by oxygen), which suggest that an O₂(aq) concentration of 10mg/L (10^{-3.51}M) would allow oxidation of pyrite sufficient to produce 375neq/mL (10^{3.73}M) SO₄²⁻, far in excess of any experiments in this study.

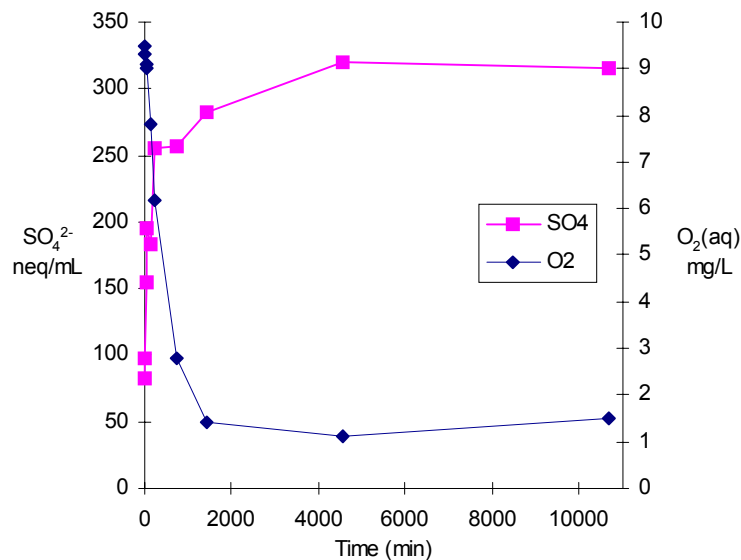
Further evaluation of the effect of varying dissolved oxygen concentrations on sulphide oxidation may be carried out using published oxidation rates. Equation 5.10 describes the rate law for pyrite oxidation by oxygen. Substituting typical initial experimental values of pH and O₂(aq) (7.4 and 10.0mg/L respectively) produces a rate of 930ng pyrite/min, given a surface area of 0.174m² (see Section 2.3.1). One hour of pyrite oxidation at this rate would produce 180neq/mL SO₄²⁻. This is consistent with the concentrations encountered after one hour of dissolution of experiments 1P/5P/9P(c). With the same pH, and an O₂(aq) concentration of 1mg/L, the rate law produces a rate of 290ng pyrite/min, which would produce 57 neq/mL SO₄²⁻ per hour. Pyrite oxidation experiments by Nicholson *et al.*(1988) encountered O₂(aq) concentrations of 0.02mg/L, with a pyrite oxidation rate of 36g pyrite/min, producing 7 neq/mL SO₄²⁻ per hour.

Equation 5.10 Rate law for the oxidation of pyrite by oxygen, where r = rate of pyrite destruction in mol/m/s, $[O_2(aq)]$ is the molarity of dissolved oxygen and $[H^+(aq)]$ is molarity of $H^+(aq)$, i.e. 10^{-pH} (after Williamson and Rimstidt, 1994)

$$r = 10^{-8.19(\pm 0.10)} \frac{[O_2(aq)]^{0.5(\pm 0.04)}}{[H^+(aq)]^{0.11(\pm 0.01)}}$$

Willis *et al.* (1995) suggested that $O_2(aq)$ becomes a limiter of pyrite oxidation at concentrations of 1-1.5mg/L. Closed system experiments of 3g/L mixed calcite/pyrite produced an increase in SO_4^{2-} concentration of approximately 30neq/mL between 20 and 180h, during which time the measured $O_2(aq)$ concentration remained between 1.1 and 1.6mg/L. For $O_2(aq)$ to be the limiting factor of pyrite oxidation, the concentration according to the rate law of Williamson & Rimstidt (1994) would have to have been around 0.0005mg/L. It is possible that an experimental delay in measuring $O_2(aq)$ concentration allowed time for a 1mg/L rise in concentration. However, $O_2(aq)$ did not appear to be reduced below 4mg/L in experiments 1P/5P/9P(c)/(r), and yet pyrite oxidation rates reduced to an equivalent magnitude to that of Willis *et al.* (1995). It is suggested, therefore, that other factors restricted the rate of pyrite oxidation.

Figure 5.30 $O_2(aq)$ and SO_4^{2-} concentrations vs. time during a closed dissolution experiment using 3g/L calcite/pyrite-deionised water solution (based on Willis *et al.*, 1995, Figure 38).



c) Grain size & pyrite content of sediment

The difference in grain size distribution between hand-crushed pyrite (using a mortar and pestle) and TEMA-crushed sediment was not analysed in this study, but the influence on

sulphide oxidation was clear when comparing SO_4^{2-} concentrations in experiments 1P/5P/9P(c) (containing 0.2g/L TEMA-crushed pyrite), with those of experiments P/PC/4P/4PC(c) (containing 0.2g/L hand-crushed pyrite) (see Figure 4.26). Thus, reactive surface area was likely to be a major factor in sulphide oxidation. TEMA-crushed laboratory sediment showed a similar specific surface area to those encountered in suspended sediment filtered from bulk meltwater draining *Haut Glacier d'Arolla* (Seagren, 1999) (see Section 2.3.1.1). This suggests that the influence of sulphide oxidation in meltwaters would be related more closely to experiments 1P/5P/9P(c)/(r) than experiments P/PC/4P/4PC(c).

It should also be reiterated that major differences in oxidation rates exist between pyrite samples from different locations (Carrucio *et al.*, 1981; Nordstrom, 1982; Nicholson *et al.*, 1988), which could have resulted in differences in rate and magnitude between experiments involving crushed pyrite of an unknown source (experiments P/PC/4P/4PC/1P/5P/9P(c), 1P/5P/9P(r)) and experiments involving morainic rock which contain indigenous pyrite.

d) Oxidation of the surface of pyrite grains

The majority of sulphate acquisition occurred within 1 or 2 hours of the mixing of sediment with deionised water, regardless of access to atmospheric oxygen, with little increase in sulphate concentration in experiments that were reopened to the atmosphere. Iron concentrations did increase upon reopening these experiments (1/5/9(r)), but these increases are not likely to have been due to additional pyrite oxidation, as the SO_4^{2-} concentration remained stable, suggesting that the additional iron came from carbonation-driven dissolution of carbonate and aluminosilicate minerals. This suggests that surface conditions stifle the rate subsequent to initial rapid acquisition. Section 1.4.2 details how pyrite oxidation rate has been shown to reduce with time due to the development of surface properties (Williamson and Rimstidt, 1994). However, the reduction in rate in such experiments was not as rapid as that experienced in this study. This may be due to products of dissolution reactions of other minerals further blocking the surface of the pyrite.

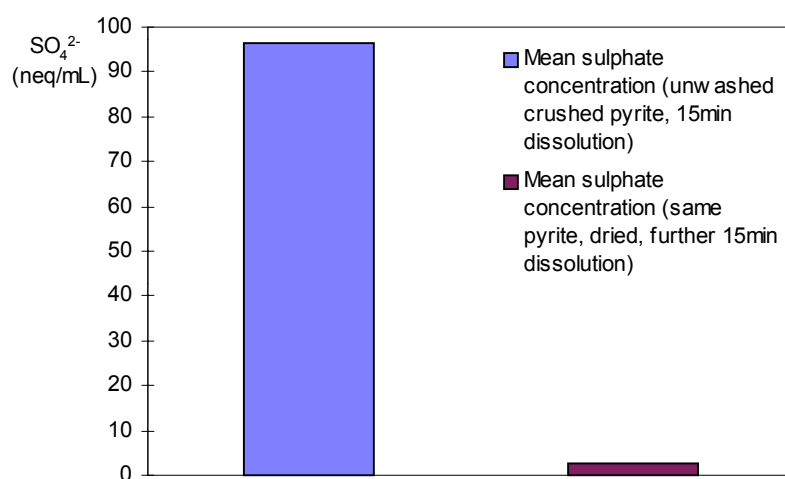
e) Production of highly reactive ultrafines or oxidation products during crushing

It is possible that the extent of initial pyrite oxidation in experiments 1P/5P/9P(c) was supplemented by oxidation products produced during the crushing process. This was tested by carrying out repeat experiments using 0.2g/L TEMA-crushed pyrite for 15 minutes, then filtering the undissolved pyrite sediment, drying it out and then repeating the experiment using the same sediment. The results (Figure 5.30) show that the rewetted experiment

produced only 3% of the SO_4^{2-} concentration produced from unreacted pyrite (2.68neq/mL compared to 96.4neq/mL). This may be explained by either of the following suggestions:

1. The crushing process caused oxidation of pyrite producing a sulphate by-product, which was quickly washed off once the pyrite came in contact with deionised water.
2. The crushing process produced ultrafine, highly reactive pyrite which was very rapidly dissolved in the first experiment. The filtration process may have removed much of the remaining ultrafine material, as it could either become lodged in the filter paper or passed through if grain size was $0.45\mu\text{m}$ or less. Therefore the second experiment would not involve ultrafines, and the sediment may have gained an unreactive surface film as prophesised above in Section 5.3.2d.

Figure 5.31 Mean concentration of sulphate produced from 15 minutes closed system dissolution of TEMA-crushed pyrite (2 repeats carried out for each). The left column represents dissolution of unwashed pyrite, and the right column represents redissolution of the same powder after drying.



It is not possible to state which of the above explanations is factual, but in any case, the physical grinding actions on pyrite encountered at the rock-ice margin beneath a glacier may produce similar conditions to those inside a TEMA mill, and either crushing by-products or ultrafine dissolution products would be incorporated into the dissolved load of subglacial meltwater. It may be stated, therefore, that a possible major control on sulphide oxidation, or more specifically sulphate acquisition, is the extent of physical weathering of pyrite at the ice-rock margin. This is unlikely to be a measureable control. If TEMA-crushing is considered to be at least as effective as the crushing processes at the base of a glacier, then the magnitudes of sulphate acquisition encountered in experiments 1P/5P/9P(c) may be offered as maxima for a given pyrite rock content.

5.3.3 Sodium acquisition

a) Relationship between sodium acquisition and time

After an initial rapid stage of acquisition similar to that of calcium, closed system experiments 1-9/P/C(c) showed small systematic increases with time, with the extent of Na acquisition after 24 hours rock-water contact an average 12% higher than that after 1 hour of contact. There was a strong correlation between Na(aq) and Na(s) at all time intervals: the mean relationships at 1, 4 and 24h time intervals of closed system experiments is shown in Table 5.9.

Table 5.2 Na solute yield from closed system experiments 1-9/P/C(c) at different time intervals. Units are in moles (s) and moles per litre (aq)

Time interval	Relationship	r	n
1 hour	$\text{Na}^+(\text{aq}) = 0.0064\text{Na}(\text{s})$	0.94	11
4 hours	$\text{Na}^+(\text{aq}) = 0.0069\text{Na}(\text{s})$	0.98	11
24 hours	$\text{Na}^+(\text{aq}) = 0.0073\text{Na}(\text{s})$	0.93	11

The magnitude of sodium acquisition for closed system experiments involving 1 hour or greater of rock-water contact was determined approximately by calculating the regression between the solid and aqueous sodium relationships from each time interval (Equation 5.11). This mean relationship was best described by logarithmic decay ($r^2=0.98$; $n=3$), consistent with previously published rate laws for sodium dissolution from glacial sediment (Brown *et al.*, 1994).

Equation 5.11 Approximate rate law for sodium acquisition from closed system experiments 1-9/P/C(c) beyond 1hour. Units: M (aq), mol (s), T is in minutes; $r^2=0.98$

$$\text{Na}^+(\text{aq}) = (0.0053 + 0.0006\log T)\text{Na}(\text{s})$$

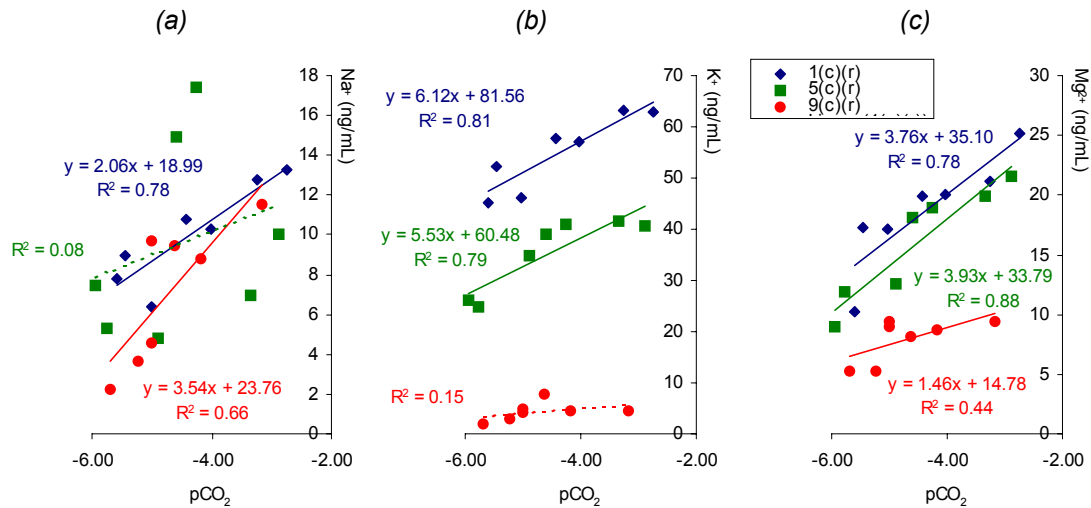
However, this relationship was altered in reopened experiments, and was very variable between experiments, (see Section 4.3.3.3). This suggests that dissolution was controlled by access to atmospheric gases.

b) Relationship between sodium acquisition and pCO₂

The variable rates of increase in sodium concentration in experiments under a closed system, and those that were reopened to the atmosphere (see above, and Figure 4.19), are to some extent characterised by a relationship with pCO₂ (Figure 5.32a) (which is virtually equivalent to a correlation with pH). The increases in concentration of sodium in experiment 1(r) were significantly correlated to increases in pCO₂, but experiments 5(r) and 9(r) did not show this

relationship due to the aforementioned rapid increases in sodium in the period immediately following reopening, which were not accompanied by rapid increases in pCO₂.

Figure 5.32 Relationship between concentrations of (a) Na⁺, (b) K⁺ and (c) Mg²⁺ and pCO₂ from experiments 1/5/9(c)&(r). Linear regression statistics are quoted on the plots.



The aforementioned doubling of sodium concentrations in reopened experiments 1/5/9/M(r) was accompanied by a mean increase in pCO₂ of 1.88±0.26. It may be reasonable to expect that the increases in sodium concentration are linked to the additional protons available in waters containing higher CO₂(g) concentrations, since the dissolution of aluminosilicate minerals is dominantly driven by acid hydrolysis. If this assumption is valid, and the mean 114% increase in Na⁺ concentration was linked to the pCO₂ increase, then Equation 5.11 may be modified to Equation 5.12. This relationship does not account for the rapid increase in concentration immediately subsequent to rock-water contact or system reopening.

Equation 5.12 Approximate rate law for sodium acquisition from experiments 1-9/P/C(c) beyond 1hour. Units: ng/mL (aq), ng/g (s), T is in minutes; r²=0.98

$$\text{Na}^+(\text{aq}) = \frac{(0.0053 + 0.0006\log T)\text{Na}(\text{s})}{3.951 + 0.599\log(\text{pCO}_2)}$$

c) Effect of sulphide oxidation

The increases in sodium acquisition associated with the extra protons provided by sulphide oxidation are quite varied, with the increases between 1P/5P/9P(c)/(r) and 1/5/9(c)/(r) averaging 59%±31%, or 1.9±0.5neq/mL (closed system) and 8±5neq/mL (open system) (see Section 4.3.3.3). These variations preclude a determination of the relationship between sodium acquisition and sulphide oxidation, but it is evident that a significant increase in

sodium-bearing aluminosilicate dissolution occurs in the presence of significant sulphide oxidation.

5.3.4 Potassium acquisition

Acquisition of K^+ was shown to be affected by both K and Ca provenance (Section 4.4.7). The apparent effect of Ca provenance is manifested due to higher potassium yields from rocks rich in calcite. This may be because adsorption of K^+ is more likely in solutions containing charged silica interfaces. Alternatively, potassium may be present in minerals that are more susceptible to chemical weathering in the calcite-rich rocks. The majority of K^+ is likely to be sourced from K-feldspar (less soluble) (Stumm and Morgan, 1996), and K-bearing micas (more soluble) (Drever and Hurcomb, 1986). However, potassium levels of up to 2700mg/kg have been reported (Turekian and Wedepohl, 1961). A time-dependence on this relationship is shown in Table 5.3.

Table 5.3 Potassium yield from closed system experiments involving morainic rocks 1-9, P and C at different time intervals. Units are moles (s) and moles per litre (aq)

Time interval	Relationship	r	n
1 hour	$K^+(aq) = [0.010 + 0.79Ca(s)]K(s)$	0.78	9
4 hours	$K^+(aq) = [0.013 + 0.80Ca(s)]K(s)$	0.76	9
24 hours	$K^+(aq) = [0.012 + 1.37Ca(s)]K(s)$	0.95	9

The approximate magnitude of K acquisition for closed system experiments involving 1 hour or greater of rock-water contact may therefore be determined using Equation 5.13.

Equation 5.13 Approximate rate law for potassium acquisition from closed system experiments 1-9/P/C(c) beyond 1hour. Units: ng/mL (aq), ng/g (s), T is time in hours, $r=1.0$

$$K^+(aq) = [0.012K(s) + 0.73Ca(s) + (0.020Ca(s) \cdot T)]$$

The rate varied under open system conditions (Section 4.3.3.4), increasing to a small extent in experiments 1/5/9(r), hence Equation 5.13 represents a baseline rate assuming no atmospheric input.

a) Effect of pCO_2

A significant correlation between K^+ and pCO_2 was observed from the reopened experiments 1(r) and 5(r) (Figure 5.32). However, the relationship was not significant in experiment 9(r), which released very low concentrations of K^+ into solution. The correlation between K^+ and pCO_2 suggests that carbonation reactions may be an important control on dissolution of the major potassium-bearing minerals found in rocks 1 and 5, with a rise of approximately

5.83neq/mL (or 8-9%) K⁺ per unit rise of log pCO₂ in each experiment (Figure 5.32). This relationship was not as important as the Ca²⁺/pCO₂ relationship described in Section 5.2.3.1, with rock K⁺ content accounting for the major differences in K⁺ concentration between individual samples. If the relationship between K⁺ concentration and pCO₂ is assumed to be constant for all rock types, then Equation 5.13 may be added to Equation 5.14

Equation 5.14 Approximate rate law for potassium acquisition from experiments 1-9/P/C(c) beyond 1hour. Units: ng/mL (aq), ng/g (s), T is time in hours.

$$K^+(aq) = [0.012K(s) + 0.73Ca(s) + (0.020Ca(s) \cdot T)] - (2.91 \times 10^{-5} - 5.83 \times 10^{-6} \log(pCO_2))$$

b) Effect of sulphide oxidation

The influence of pyrite was significant, but very variable, with K⁺ levels elevated by between 130 and 1000%, making quantification of the influence impossible.

5.3.5 Magnesium acquisition

The magnitude of Mg²⁺ acquisition in morainic rock experiments was shown to be closely related to rock provenance (Section 4.4.4). The relationships between solid and liquid phases at different time intervals is indicated in Table 5.4 (experiment 7(c) was not compatible with this relationship, however).

Table 5.4 Magnesium yield from closed system experiments involving morainic rocks 1-6, 8-9, P and C at different time intervals. Units are moles (s) and moles per litre (aq)

Time interval	Relationship	r	n
1 hour	Mg ²⁺ (aq) = 0.0056Mg(s)	0.95	10
4 hours	Mg ²⁺ (aq) = 0.0068Mg(s)	0.97	10
24 hours	Mg ²⁺ (aq) = 0.0075Mg(s)	0.98	10

The approximate magnitude of Mg acquisition for closed system experiments involving 1 hour or greater of rock-water contact may therefore be determined using Equation 5.15.

Equation 5.15 Approximate rate law for magnesium acquisition from closed system experiments 1-9/P/C(c) beyond 1hour. Units: ng/mL (aq), ng/g (s), T is in minutes, r=0.96

$$Mg^{2+}(aq) = (0.0033 + 0.0014\log T)Mg(s)$$

a) Effect of pCO₂

A significant correlation between Mg²⁺ and pCO₂ was observed from the reopened experiments 1(r) and 5(r) (Figure 5.32). A weaker correlation was also observed from experiment 9(r). The mean increase in Mg²⁺ concentration in these experiments was

9.3±0.6%. Therefore, the closed system relationship can be modified to account for pCO₂ values up to those in open system (Equation 5.16).

Equation 5.16 Approximate rate law for magnesium acquisition from experiments 1-9/P/C(c) beyond 1hour. Units: ng/mL (aq), ng/g (s), T is in minutes, r=0.96

$$\text{Mg}^{2+}(\text{aq}) = \frac{(0.0033 + 0.0014\log T)\text{Mg}(\text{s})}{2.08 + 0.216\log(\text{pCO}_2)}$$

b) Effects of sulphide oxidation

The extra protons produced by sulphide oxidation in experiments 1P/5P/9P(c) in comparison to pyrite-absent experiments 1/5/9(c) served to allow the dissolution of an additional 1.2×10⁻⁵, 1.7×10⁻⁵ and 1.9×10⁻⁵ M Mg²⁺ respectively (Figure 4.15). The rate of acquisition in experiments 1P/5P/9P(c) did not significantly alter with the reopening of the experiment to the atmosphere, in contrast to pyrite-absent experiments 1/5/9(r), suggesting that pyrite oxidation replaced CO₂-drawdown as the primary source of protons driving magnesium acquisition. However, the variable increase in Mg²⁺ concentration caused by pyrite addition (31±19neq/mL or 270±140% between experiments 1/5/9(c) and 1P/5P/9P(c) at 24h, and 12±7neq/mL or 60±46% between experiments 1/5/9(r) and 1P/5P/9P(r) at 28h) preclude determination of a quantified relationship between magnesium acquisition and pyrite acquisition that encompassed all rock types.

5.3.6 Controls on dissolution of minor and trace elements in laboratory experiments

The pattern of dissolution of all analysed elements and anionic species is summarised in Table 5.12. These elements may be grouped according to their dissolution characteristics (Table 5.7).

Many of the elements that showed increased yields in solutions with high bicarbonate concentration have similar ionic radii to Ca, and therefore may have been incorporated into calcite. Slight differences in ionic radii or charge may, however, have formed slight imperfections in the crystal structure of calcite, which may then be preferentially weathered when rock-water contact occurs (Morse, 1983). In contrast, other sources of these elements are likely to be minerals resistant to weathering such as zircon, sphene, rutile etc. Hence, in experiments not involving high quantities of calcium, solute yields of such trace elements may be expected to be lower.

Of the elements affected by carbonate dissolution listed, only U, Cu and Zn were analysable by PHREEQC due to the limited number of elements available in the PHREEQC and MINTEQA2 databases (see Section 2.4.5). Of these, only U was dominantly complexed by carbonate ions, although ZnCO_3° was significant. The monovalent cation K^+ was present as free-ions, and the bivalent cation Cu^{2+} was complexed with hydroxide, according to the model. It is therefore apparent that the increases in the solute yield of most elements in bicarbonate-rich waters was not a direct result of complexation with carbonate species. It is likely, however, that the increased surface-exchange activity in waters of higher ionic strength resulted in a higher rate of transfer of certain elements in solution, namely those that are present in carbonate minerals, and which are chemically conducive to become involved in the surface reactions dominated by Ca, CO_2 , HCO_3^- and H^+ .

Table 5.6 is a summary of potentially useful chemical indicators of various provenance.

Table 5.5 Summary of observations of major and trace metal behaviour in solution. Elements showing increased concentrations in solutions where carbonation-driven calcite dissolution is dominant are ticked under the column heading CO₂. Elements showing increased concentrations in solutions where sulphide oxidation is a major process are ticked under the column heading SO (with asterisk if increased concentrations mainly only occurred in experiments P, PC_{0.1}, 4P, 4PC). Long-term solubility is described as either low, medium or high (L,M,H), purely related to the difference in concentrations at 1/4h and 24h respectively. An asterisk () is added where long-term solubility is increased in experiments involving carbonate-rich Rocks 1, 5 and 9.*

Element	CO ₂	SO	Highest concentrations in the following closed system experiments	open system change	long-term solubility	50% dilution effect
Al			3, 5, 6 (>100ng/mL)	n/a	n/a	n/a
Ba		✓	2, 6, 7, 1P, 5P (>1ng/mL)	↑	M*	=
Ca	✓	✓	1, 5, 6, 7, 8, 9, PC, 1P, 5P, 9P (>5000ng/mL)	↑	M	=
Cl			3, 8, 4P, 4C (>1000ng/mL)	-	M	=
Co			3 (>3ng/mL)	-	L	↓
Cu	✓		1, 2, 5, 7, 9, M, C, P, PC _{0.1} , 1P, 5P, 9P (>1ng/mL)	-	L*	=
Fe		✓	4, 6, 7, 8, C, PC _{0.1} , PC, 4P, 4C, 4PC (n/a)	↑	L*	↓
K	✓	✓	1, 2, 3, 4, 5, 6, 7, 1P, 4P, 5P, 9P, 4C, 4PC (>1200ng/mL)	↑	H	↓
Mg		✓	2 (>400ng/mL); 1, 5, 6, M, 1P, 5P, 9P (>150ng/mL)	↑	H	↓
Na			3, 4, 6, 4P, 4C, 4PC (>500ng/mL)	↑	M	↑
Ni			1, 4, 6, 7, 8, 9, C, PC _{0.1} , PC, 4P, 4C, 4PC (>3.5ng/mL)	↑	L	↓
NO ₃			2, 3, 5, 6, 7 (>500ng/mL - 24h only)	-	H	↓
Pb		✓*	2, 4, 6, 7, 8, P, PC _{0.1} , 4P, 4PC (>5ng/mL)	-	L	↓
Rb		✓	1, 2, 4, 6, 7, 1P, 4P, 5P, 9P, 4C, 4PC (>5ng/mL)	↑	M	↓
SO ₄		✓	2, 1P, 5P, 9P (>6000ng/mL); 3, P, PC _{0.1} , PC, 4P, 4PC (>1000ng/mL)	-	H	↓
Sr			1, 5, 8, 9, 1P, 5P, 9P (>100ng/mL)	↑	H	↓
Ti	✓	✓	6, 8, C, 1P, 5P, 9P (n/a)	↑	L	=
U		✓	P, PC _{0.1} , PC, 1P, 4P, 5P, 9P (>0.2ng/mL)	↑	L	=
Zn	✓	✓*	1, 2, 5, 9, C, P, PC _{0.1} , PC, 1P, 5P, 9P, 4PC (>5ng/mL)	-	M	=

Table 5.6 Potential key indicator species and their use

Process	Potential key indicator
Sulphide oxidation	<ul style="list-style-type: none"> • Sufficiently identified by SO_4^{2-} concentrations, also particularly well identified by U. • Mg, Rb, Ba and Na dissolution was generally closely linked to provenance, but their dissolution was significantly enhanced when pyrite oxidation is sufficient. • Pb, Zn, Cl and Fe concentrations increased when pyrite oxidation was significant, but not if carbonate dissolution dominated water-rock interactions, where they may have been re-adsorbed during carbonate surface-exchange reactions. These elements are therefore likely to be more concentrated in more dilute waters, or those with low suspended sediment concentration.
Coupled SO-CD	<ul style="list-style-type: none"> • K and Ti showed increased yields in experiments dominated by carbonate dissolution, but showed further increased yield when both sulphide oxidation and carbonate dissolution reactions were significant.
Aluminosilicate dissolution	<ul style="list-style-type: none"> • Elements such as Na and Co are good indicators of provenance, as they are not significantly affected by carbonate dissolution.
Mode of rock formation	<ul style="list-style-type: none"> • Rb/K ratio may indicate mode of rock formation (low=sedimentary, high=hydrothermal) and therefore distinguish between different lithogenic provenances.
Hydrothermal provenance	<ul style="list-style-type: none"> • Cr may be a potential indicator of hydrothermal mineralogy (pyrite/quartz)
Residence time	<ul style="list-style-type: none"> • Ca/Sr ratio may indicate residence time, access to atmospheric gases, and also the ratio of calcite to other minerals (low Sr/Ca=low calcite, open system, high Sr/Ca=high calcite, closed system) • NO_3 may be a potential indicator of residence time variations, as it appeared to have slow release and high long-term solubility. A high risk of aerial contamination in the field exists, however.
Rock-specific indicators	<ul style="list-style-type: none"> • Co may indicate Rock 3 vein material (and distinguish from Rock 8 vein material) • Cl (and Re - not shown) may indicate Rock 8 vein material (and distinguish from Rock 3 vein material) • Mo (not shown) may indicate Rock 4 (diorite), and is unaffected by carbonate dissolution or pyrite oxidation

5.3.7 Appraisal of the use of trace elements in investigations of solute acquisition in subglacial environments

Prior to this study, no laboratory dissolution experiments aimed at furthering the understanding of subglacial processes had analysed for trace elements. Studies of trace element geochemistry of bulk meltwater draining *Haut Glacier d'Arolla* have to date been based on a very limited dataset, with existing assumptions of major element solute provenance simply assigned to trace elements, rather than using observations of trace elements themselves to identify solute provenance (Brown and Fuge, 1998a; Brown and Fuge, 1998b). The detailed analyses of a large range of trace elements presented here is directly related to rock provenance and, to some extent, mineralogy of the rocks. Therefore, the dissolution behaviour of the trace elements and their relationship to major element dissolution is discerned. The study has shown that many of the assumptions of provenance

arise due to a lack of knowledge of bedrock geochemistry and inter-species relationships in the aqueous environment.

Table 5.7 Effect of sulphide oxidation and carbonate dissolution on the concentration of minor and trace elements

Criteria	Elements/anions
Concentration increased by carbonate dissolution but not significantly affected by sulphide oxidation	Cu, Sr
Concentration increased by sulphide oxidation but not significantly affected by carbonate dissolution	Ba, Cr, Fe, Mg, Rb, SO ₄ , U
Concentration increased by sulphate oxidation, but not in experiments 1P/5P/9P	Cl, Zn, Pb
Concentration increased by both carbonate dissolution and sulphate oxidation	Ca, K, Ti
Concentration not significantly affected by either carbonate dissolution or sulphate oxidation	Na, Ni, Co, NO ₃
No specific associations found/not enough data	Al

5.4 SUMMARY OF CONTROLS ON AND RATES OF SOLUTE ACQUISITION IN SIMULATED SUBGLACIAL CONDITIONS

5.4.1 Controls on solute acquisition

The rates and controls on acquisition of major cations in laboratory simulations of subglacial environments have been constrained by parameters of provenance, pCO₂, saturation indices, ionic strength, carbonate equilibria, proton availability, temperature, and time. Numerous processes controlling the rate and magnitude of Ca²⁺ acquisition have been isolated and quantified. Rate laws of acquisition of other major cations have also been established. The behaviour of trace elements has been ascribed to various controlling factors. In this section, the models of major solute acquisition are summarised, and are then compared with thermodynamic theory and previous investigations of calcite dissolution.

Rapid surface-exchange reactions taking place immediately subsequent to addition of sediment contributed a large proportion of the total concentration of many elements. During this initial period, sodium and magnesium acquisition was closely linked to rock source. The acquisition of trace elements such as tin, molybdenum, cobalt and rhenium, in addition to chlorine, was also closely linked to rock content. Potassium acquisition linked to rock content, but relatively increased in magnitude in carbonate-rich waters. Many minor and trace elements were also affected in this way. Calcium acquisition was less directly linked to rock content due to the rapid attainment of saturated levels in all experiments bar those with extremely low calcium content.

By the end of the initial stage of rapid acquisition, CO₂ concentrations in most experiments had reached levels low enough to have effectively achieved “closed system” conditions, whereupon a step reduction in the rate of acquisition of all species occurred. Sulphide oxidation had a major effect on the magnitude of acquisition of many species in the initial stage, by providing additional protons into solution. The protons supplied by sulphide oxidation appeared to replace some of the protons otherwise produced by carbonation, with the result that levels of pCO₂ were significantly higher in experiments with pyrite added than in equivalent experiments without pyrite added.

In experiments where closed system conditions were maintained beyond the initial stage of acquisition, very slow dissolution of major cations occurred, related to time and small increases in levels of pCO₂.

In contrast, open system dissolution of 0.2g/L calcite followed the thermodynamic relationship between Ca²⁺ and pCO₂, and was controlled by the rate of CO₂-drawdown. The rate of open system dissolution of Ca²⁺ in morainic rock samples followed a modified relationship with pCO₂ due to calcium present in other minerals, and a proportion of carbonation reactions providing protons for the dissolution of other minerals.

Dilution of experiments 1/5/9(c) with 50% deionised water (experiments 1/5/9(rd)) caused rapid dissolution of calcite so that concentrations of calcium ions were equivalent to those in undiluted experiments within 30 minutes, suggesting that undiluted Ca²⁺ concentrations were in equilibrium with carbonate species, and were not being limited by kinetic controls. Other major elements did not recover to undiluted concentrations, but many minor and trace elements showed similar concentrations in equivalent undiluted and diluted experiments.

a) Calculated relationship between calcium acquisition, sulphide oxidation, carbonate equilibria, CO₂-drawdown and rock provenance

To enable the comparison between experiments run at room temperatures (experiments P/C/PC(o)) and refrigerated temperature (all other experiments), the effect of temperature on carbonate equilibrium must first be considered.

For the purposes of equilibrium calculations, it was assumed as an approximation that all experiments were at a fixed temperature of 10°C (actually varied between 6 and 9°C), except open system, “end-member” experiments C/P/PC(o) which were carried out in unrefrigerated conditions, and are assumed to have been at a constant 25°C (actually varied between 18 and 29°C). Therefore, to account for temperature differences, the relationships between pCO₂ and equilibrium calcium concentration at 10°C and 25°C were used to account for a

subtraction in rate of Ca^{2+} acquisition per unit pCO_2 ($\Delta\text{Ca}_{\text{TEMP}}^{2+} (T_{25}-T_{10})$). Table 5.8 shows the difference between equilibrium concentrations of Ca^{2+} at 0°C , 10°C and 25°C . The difference in equilibrium Ca^{2+} concentrations between 25°C and 10°C across the pCO_2 range experienced in these experiments remains at around 72%. The difference between the concentrations at field temperatures of around 0°C and experimental temperatures of around 10°C are approximately 125%. A temperature concentration factor can therefore be calculated over the 0 - 25°C range, which is presented in Equation 5.17.

Table 5.8 Variation in equilibrium Ca^{2+} concentrations with pCO_2 at 0°C , 10°C and 25°C [derived from Equation 5.3].

$\log(\text{pCO}_2)$	$\Delta\text{Ca}_{\text{TEMP}}^{2+} (T_{25}-T_{10})$ (neq/mL)	$\Delta\text{Ca}_{\text{TEMP}}^{2+} (T_{25}-T_{10})$ (%)	$\Delta\text{Ca}_{\text{TEMP}}^{2+} (T_0-T_{10})$ (neq/mL)	$\Delta\text{Ca}_{\text{TEMP}}^{2+} (T_0-T_{10})$ (%)
-6.0	-63	74.1	+54	122
-5.5	-88	72.9	+76	123
-5.0	-126	72.2	+110	124
-4.5	-184	71.8	+160	125
-4.0	-269	71.5	+234	125
-3.5	-394	71.4	+342	125
-3.0	-577	71.4	+502	125

Equation 5.17 Relationship between mean $\Delta\text{Ca}_{\text{MIN}}^{2+}$ (concentration of Ca^{2+} in experiment containing pyrite minus concentration of Ca in corresponding experiment not containing pyrite) and the solution temperature (T) at a given value of pCO_2 . Units for $\Delta\text{Ca}_{\text{MIN}}^{2+}$ are neq/mL; T is in $^\circ\text{C}$

$$\Delta\text{Ca}_{\text{TEMP}}^{2+} = 0.0002T^2 - 0.0274T + 1.25$$

Given this temperature correction, the individual controls of Ca^{2+} acquisition laws in laboratory simulation experiments may be combined to form a single overall law (Equation 5.18).

Equation 5.18 Calculated relationship between calcium acquisition, sulphide oxidation, carbonate equilibria, CO₂-drawdown and rock provenance during Stage 2 acquisition. Individual factors are described in Table 5.9.

$$\text{Ca}^{2+} = \Delta\text{Ca}_{\text{MIN}}^{2+} \times \Delta\text{Ca}_{\text{TEMP}}^{2+} \times \left[\Delta\text{Ca}_{\text{SO}}^{2+} + \Delta\text{Ca}_{\text{SAT}}^{2+} + A_{\text{CO}_2} + \left(10^{-M/E} B_{\text{CO}_2}\right) + D \log(\text{pCO}_2) + Y \right]$$

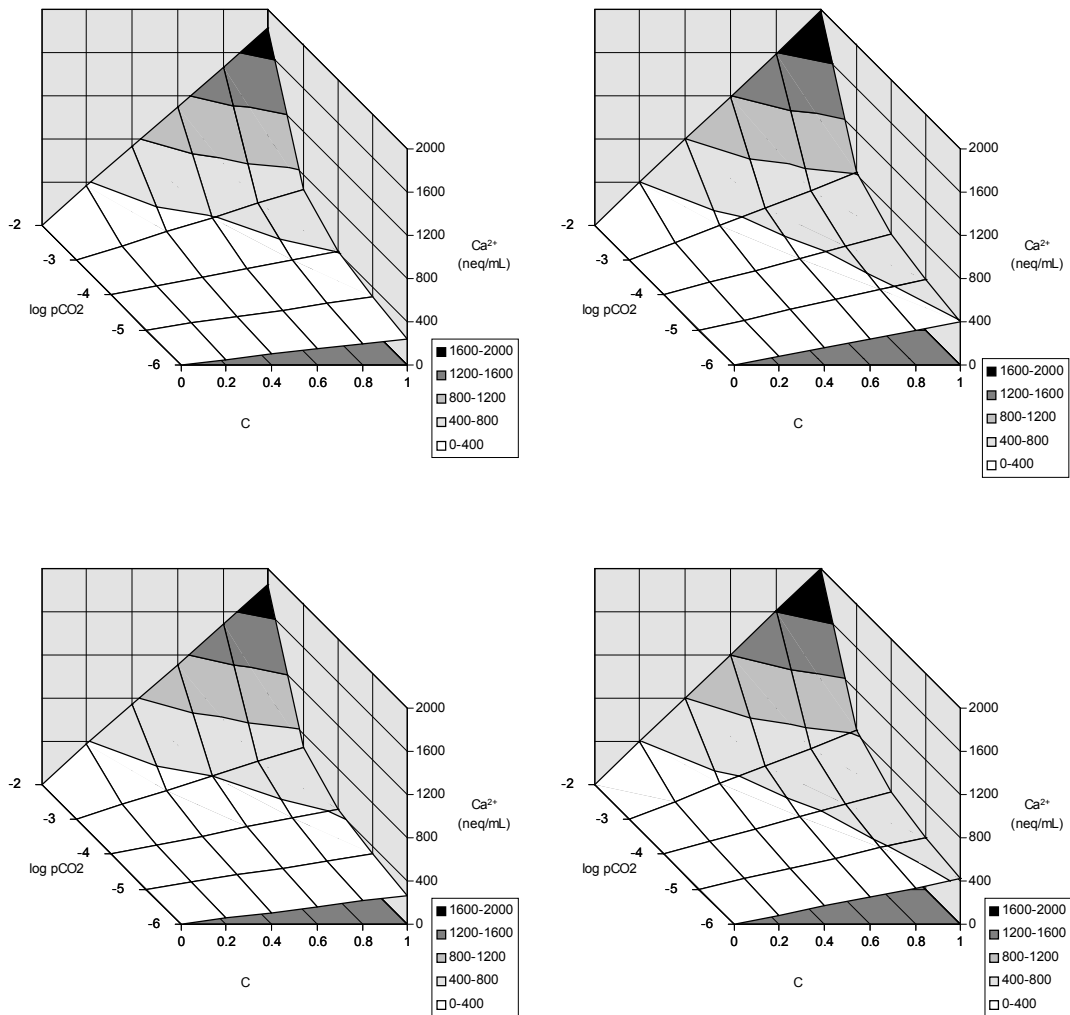
Table 5.9 Calculations of individual factors constituting the processes and controls on calcium acquisition in laboratory experiments

Calculation	Description
$\Delta\text{Ca}_{\text{MIN}}^{2+} = \frac{\text{Ca(s)}}{53.061 - 1.105 \left(\frac{\text{Ca(s)}}{\text{Sr(s)}} \right)}$	mineralogical factor (maximum value=1)
$\Delta\text{Ca}_{\text{TEMP}}^{2+} = 0.0002\text{T}^2 - 0.027\text{T} + 1.25$	temperature factor (T=temperature (°C), maximum range 0-25°C)
$\Delta\text{Ca}_{\text{SO}}^{2+} = 0.78(\text{SO}_4^{2-})$	sulphide oxidation factor
$\Delta\text{Ca}_{\text{SAT}}^{2+} = 10^{(\text{SI}(\text{calcite})+1.25)}$	calcite supersaturation factor
$A_{\text{CO}_2} = 80000 \times 10^{\log(\text{pCO}_2)}$	first pCO ₂ factor
$B_{\text{CO}_2} = -\frac{1626}{\log(\text{pCO}_2)}$	second pCO ₂ factor
$D = \frac{\text{Ca(s)}}{5(M - \text{Ca(s)})}$	carbonate/aluminosilicate dissolution proportion factor
$M = \text{Ca(s)} + \text{Mg(s)} + \text{Fe(s)} + \text{K(s)} + \text{Na(s)}$	M represents the influence of other metals on the ratio of HCO ₃ /Ca, which in turn affects the carbonate equilibria. The value of factor E is 2200000, determined by trial and error.
$Y = 45$	value determining the vertical position of the model curves, which is determined by Stage 1 dissolution magnitude.

The combined effects of the variation in rock factors D and M on the pCO₂/Ca²⁺ relationships produced by the calculations are illustrated in Figure 5.33. The graphs represent variations in Ca²⁺ concentrations over ranges of log(pCO₂) and mineralogical parameter ΔCa²⁺_{MIN}, at extreme concentrations of SO₄²⁻. It can be seen that the variation at particular values of pCO₂ and ΔCa²⁺_{MIN} between the low extremes of D and M (top graphs) and the high extremes (bottom graphs) is rather small, highlighting the fact that all factors in combination, particularly ΔCa²⁺_{MIN}, pCO₂ and concentration of SO₄²⁻, cause the wide variations in acquisition of Ca²⁺ found in laboratory experiments.

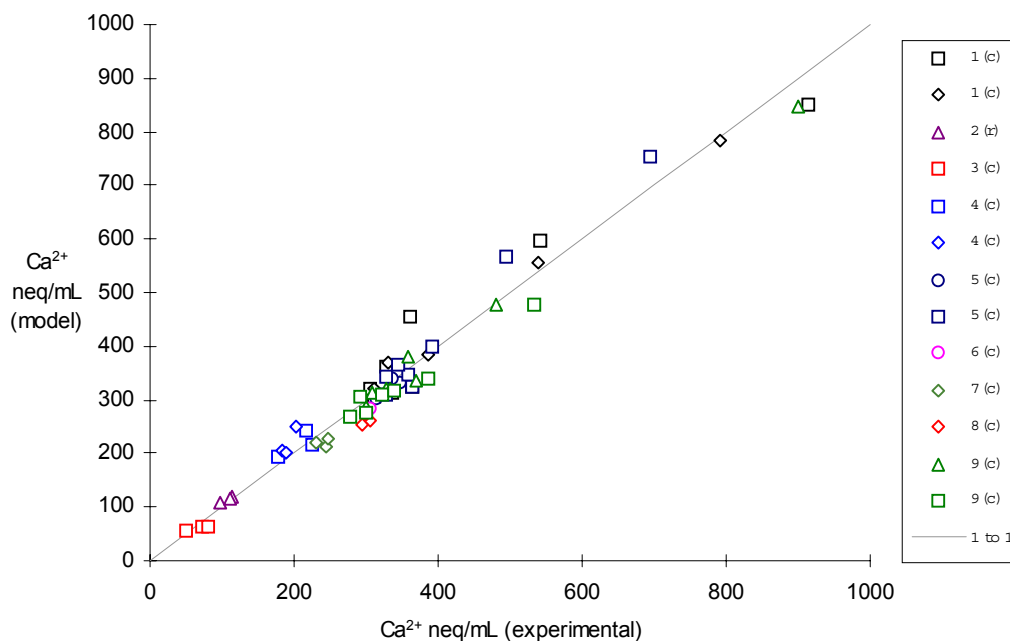
Figure 5.33 Modelled calcium concentrations in experimental solutions with preset values of log(pCO₂) and mineralogical parameter ΔCa²⁺_{MIN} (axis 'C') and (left) zero SO₄²⁻, (right)

200neq/mL SO_4^{2-} , (top) factors M and D akin to rock 9 (low extreme of both); (bottom) factors M and D akin to rock 3 (high extreme of both). $SI(\text{calcite})$ is fixed at zero throughout (model calculations are only affected where $SI(\text{calcite}) > 0$).



The relationship between the experimental and modelled concentrations of Ca^{2+} calculated from Equation 5.18 is shown in Figure 5.34, with morainic rock experiments showing an overall regression r^2 of 0.97, with a systematic underestimate of 1%.

Figure 5.34 Relationship between experimental and modelled concentrations of Ca^{2+} calculated from Equation 5.18. Overall regression statistics: $y = 0.99x$; $r^2=0.97$ ($n=61$).



b) Other cations

Other major cations were present in smaller concentrations to Ca^{2+} , and as such were less subject to equilibrium conditions. The dominant controls on these elements are shown to be provenance and time, with potassium also being affected by Ca provenance (Equations 12, 14 and 16; reprinted below).

Equation 5.12 Approximate rate law for sodium acquisition from closed system experiments 1-9/P/C(c) beyond 1hour. Units: ng/mL (aq), ng/g (s), T is in minutes

$$\text{Na}^+ (\text{aq}) = \frac{(0.0053 + 0.0006\log T)\text{Na}(\text{s})}{3.951 + 0.599 \log(\text{pCO}_2)}$$

Equation 5.14 Approximate rate law for potassium acquisition from closed system experiments 1-9/P/C(c) beyond 1hour. Units: ng/mL (aq), ng/g (s), T is in hours

$$\text{K}^+ (\text{aq}) = \left[0.012\text{K}(\text{s}) + 0.73\text{Ca}(\text{s}) + (0.020\text{Ca}(\text{s}) \cdot T)\right] - \left(2.91 \times 10^{-5} - 5.83 \times 10^{-6} \log(\text{pCO}_2)\right)$$

Equation 5.16 Approximate rate law for magnesium acquisition from closed system experiments 1-9/P/C(c) beyond 1hour. Units: ng/mL (aq), ng/g (s), T is in minutes

$$\text{Mg}^{2+} (\text{aq}) = \frac{(0.0033 + 0.0014\log T)\text{Mg}(\text{s})}{2.08 + 0.216\log(\text{pCO}_2)}$$

c) Rapid, “Stage 1” acquisition

The scope of the modelled rates shown in Equation 5.11-Equation 5.18 does not include determination of rate of acquisition in the period of initial rapid acquisition upon sediment addition or dilution. Fairchild *et al.* (1994) discounted the initial hour of acquisition as an experimental artefact, and used the chemistry at 60 minutes as the “starting fluid” for mixing models. In the laws for Na^+ , K^+ and Mg^{2+} described above, the concentration of each ion at 60 minutes was incorporated into the equations, giving apparent time=0 intercepts. In the law for Ca^{2+} acquisition, the $\text{pCO}_2/\text{Ca}^{2+}$ relationship described in Equation 5.18 was calculated assuming the curve for experiments 1/5/9(c) passed through a 60 minute Ca^{2+} concentration of 320neq/mL and a $\log(\text{pCO}_2)$ value of -5.5. Therefore, the models are inaccurate for calculation of water chemistry up to 60 min. The rate of acquisition of Ca^{2+} from pure calcite in the initial rapid stage was shown to be related to log time in both open and closing environments (Section 5.2.1.1). Experiments 1/5/9(rd) suggested the rate may have been more rapid in higher rock:water ratios, as little deviation from the calculated trend was shown in samples that were 50% diluted with deionised water and measured after 30 minutes.

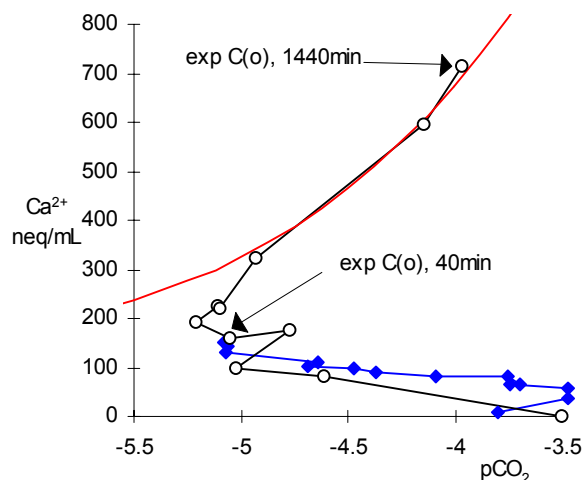
5.5 COMPARISON OF EXPERIMENTAL MODELS WITH PREVIOUS STUDIES OF MELTWATER QUALITY

5.5.1 Comparison with experiments involving open system dissolution of proglacial sediment from *Haut Glacier d’Arolla*

Open system experiments carried out by Brown *et al.*, (1994) using proglacial sediment yielded slower rates and lower concentrations of Ca^{2+} in comparison to studies presented here, despite similar rock-water ratios. The maximum yield of Ca^{2+} after 3 hours dissolution was 164 neq/mL from 4 g/L sediment. This is similar to experiments carried out in this study on “mixed” channel sediment, but lower than from all freshly crushed morainic rock other than rocks 2 and 3 (olivine gabbro and quartz vein respectively). This may reflect the use of proglacial sediment as the reactant, which has been through the subglacial system and eluted the most reactive products (see Section 3.3.3). This has the effect that equilibrium conditions are not met within the three hours duration of the experiment, so the effect of pCO_2 and carbonate equilibria is reduced and the relative importance of reactive surface area increased. This is illustrated in Figure 5.35, which shows the $\text{Ca}^{2+}/\text{pCO}_2$ relationship of open system

experiments involving 4 g/L proglacial sediment (Brown *et al.*, 1994) following a similar trend to the initial hour of dissolution of experiments involving calcite.

Figure 5.35 Plot of Ca^{2+} versus $p\text{CO}_2$ for experiments involving pyrite and calcite, with experiment from Brown (1994) involving 4 g/L proglacial sediment also plotted



The slower initial rates of Brown (1994) may reflect the technique of prewashing sediment utilised in the study. Whilst this technique removes the initial period of rapid acquisition from microfine particles, giving neat power regression cation acquisition curves, it produces the risk of preferential elution of the most reactive components of the sediment, prior to measurement. This is at odds with the subglacial system, where there is no opportunity for prewashing, and bulk meltwater chemistry would include dissolution products from all stages of reaction between meltwater and sediment.

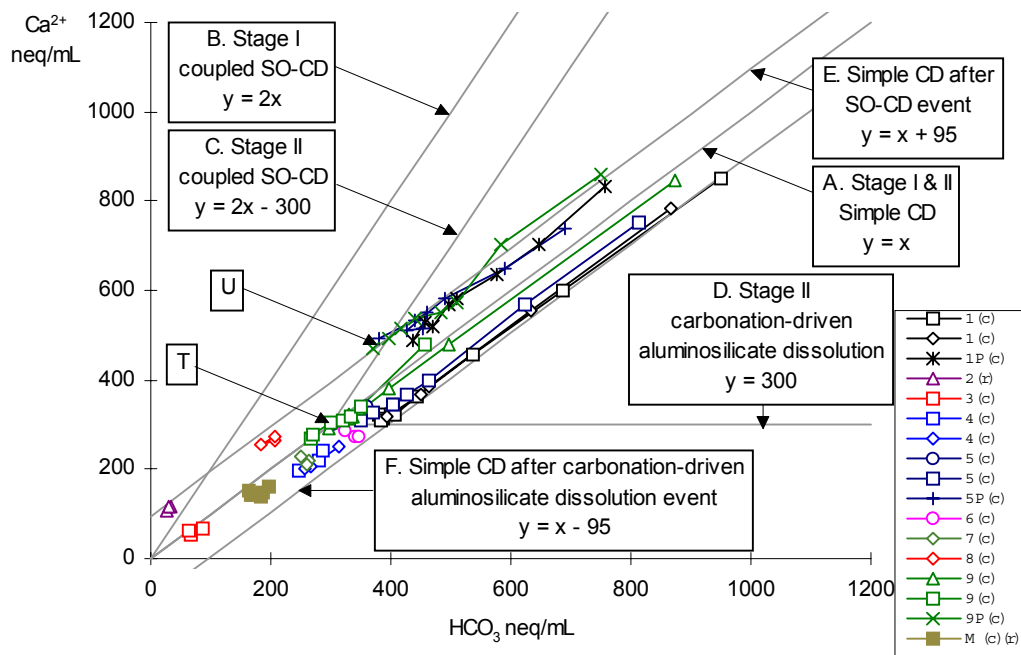
5.5.2 Two-stage carbonate dissolution (Fairchild *et al.*, 1994)

Fairchild *et al.* (1994) suggested that the processes of carbonate dissolution in carbonate terrains could be identified using plots of $(\text{Ca}+\text{Mg})$ versus alkalinity, as points on this diagram are not affected by the drawdown or degassing of CO_2 , and depend only on the relative amounts of carbonate dissolution and proton supply by pyrite oxidation. Simple dissolution of carbonate would progress along a 1:1 line, according to the reaction stoichiometry (see Equation 1.11). Meltwaters draining the North Tsanfleuron glacier plotted close to a 2:1 line that deviated from the 1:1 line at 400neq/mL. The authors suggested that sulphide oxidation did not effect the ratio in waters of a cationic concentration less than 400neq/mL, and that waters from the North Tsanfleuron glacier underwent a two-stage process of rapid, simple carbonate dissolution followed by coupled sulphide oxidation and carbonate dissolution (SO-CD), which has a 2:1 stoichiometrical relationship between $(\text{Ca}+\text{Mg})$ and alkalinity. All meltwaters draining glaciers in carbonate terrains were

suggested to lie between the 1:1 line of simple carbonate dissolution and the 2:1 line of SO-CD (Fairchild *et al.*, 1994).

The modelled relationships between Ca^{2+} and HCO_3^- in experiments 1-9/1P/5P/9P(c)/(r) are plotted on Figure 5.36 for comparison with the plot of Fairchild *et al.* (1994). The experiments encompassed dissolution from both carbonate and non-carbonate minerals, and so the use of (Ca+Mg) as a measure of carbonate dissolution was inappropriate.

Figure 5.36 Plot of concentration of Ca^{2+} versus HCO_3^- for experiments 1-9/M/C/P(c) and 1/2/5/9/M(r). Theoretical relationships are plotted grey and labelled individually (refer to text for details).



On Figure 5.36, line A represents simple carbonate dissolution. Line B represents a coupled SO-CD reaction for the duration of rock-water contact. Line C represents the Fairchild *et al.* model of coupled SO-CD in the second stage of acquisition following an initial stage of simple calcite dissolution, with the transformation between the two-stage process occurring at point T. Line D represents an extreme scenario where Ca^{2+} dissolution did not progress beyond Stage I simple dissolution (perhaps due to saturation), with carbonation reactions driving only aluminosilicate dissolution beyond point T (assuming no aluminosilicate Ca^{2+} content). Line E represents simple carbonate dissolution proceeding an initial rapid proton release event caused by sulphide oxidation. Finally, line F represents a period of carbonation-driven aluminosilicate dissolution preceding simple carbonate dissolution. Each scenario is discussed presently:

a) Coupled SO-CD in a carbonate system

The modelled relationships between Ca^{2+} and HCO_3^- in experiments 9(c)/(r) plotted close to line A, indicating simple carbonate dissolution (CD). The lowest concentration of experiment 9P(c) is close to line C, consistent with a progression from point T at stoichiometric proportions consistent with SO-CD. The sample of experiment 9(c) that plots at point T and the sample of experiment 9P(c) at point U represent the same duration of rock-water content, and indicate that the extent of calcite acquisition attributable to simple carbonate dissolution can be determined by following a 2:1 slope line down to the 1:1, $\text{Ca}^{2+} \equiv \text{HCO}_3^-$ line, as stated by Fairchild *et al.* (1994). However, it is evident that the influence of sulphide oxidation preceded 60 minutes, which suggests that the transformation between Stage I and II also preceded 60 minutes, and/or sulphide oxidation occurs during Stage I. Open system dissolution experiments using 4.0g/L of crushed mixed sediment from *Haut Glacier d'Arolla* conducted by Seagren (1999) suggested that the transition between Stages I and II, indicated by log pCO₂ minima, may occur as early as 15 minutes in such rock-water ratios. However, since concentrations of Ca^{2+} in closed system experiments 1/5/9(c) decreased beyond 60 minutes, there is every indication that concentrations of Ca^{2+} at the point of transformation between Stages I & II would be similar to those at 60min, regardless of the time at which the transformation occurred. It follows that sulphide oxidation must have therefore preceded the transformation. This is consistent with experiments C/PC_{0.1}/PC(c), which showed that in pure calcite/pyrite systems, the influence of sulphide oxidation was marked at the point of transformation (see Section 5.2.1.2). The reason for this was attributed to either chemical or physical processes during experimental sediment crushing (Section 5.3.2e), which it is assumed would also be produced during subglacial crushing.

The progression of experiment 9P(c)/(r) along line E indicates that beyond point U, dissolution was by carbonation-driven carbonate dissolution, unaffected by sulphide oxidation, as suggested in Section 5.2.2.2. This is in contrast to the Fairchild *et al.* model of coupled SO-CD in stage II. It was suggested in Section 5.2.2.2 that sulphide oxidation was curtailed by the formation of a surface barrier layer preventing surface reaction. Reaction may continue in fluids where reactive sulphide grains are continually being added to the meltwater: certainly, the concentrations of SO_4^{2-} in streams and pools from North Tsanfleuron (650±460 and 2100±2700neq/mL respectively) are considerably higher than those of any experiments undertaken here, suggesting either extremely high pyrite/water ratios, continual addition of fresh sulphide reactive surfaces, or evaporation-related increases in concentration. If the former is true, and sulphide oxidation was curtailed as quickly as in

experiments 1P/5P/9P(c), then it is possible that the individual points of the North Tsanfleuron samples actually represent a point on a line of simple carbonate dissolution similar to that of line E on Figure 5.36, but with a different intercept value on the calcium axis. The high standard deviations of SO_4^{2-} concentration of the sampled stream and pond waters would be consistent with this suggestion, although individual $\text{Ca}^{2+}/\text{SO}_4^{2-}$ relationships are not known. In either case, the suggestion that at least 400neq/mL carbonate dissolution must occur before pyrite oxidation (Fairchild *et al.*, 1994) must be treated with caution.

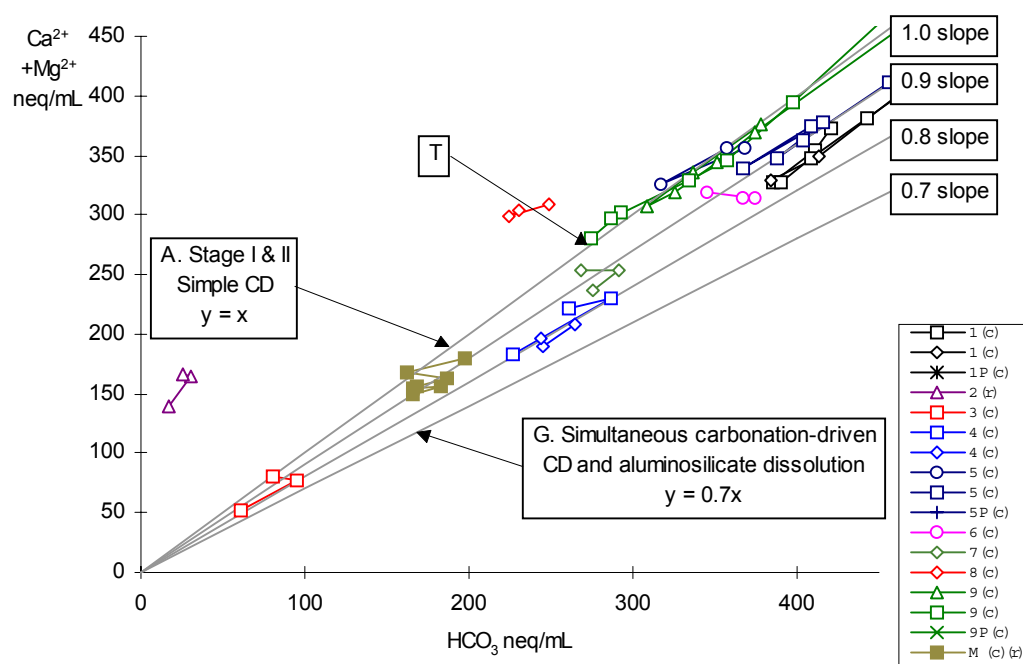
b) Aluminosilicate dissolution

Experiments 1/3/4/5/6/7/M(c) and 1/5/M(r) produced solution $\text{Ca}^{2+}/\text{HCO}_3^-$ relationships that plot below the 1:1, $\text{Ca}^{2+}=\text{HCO}_3^-$ line, due to the additional contribution of HCO_3^- by aluminosilicate dissolution (e.g. Equation 5.7). The position of experiment 8(c) on Figure 5.36 above the 1:1 is likely to be a result of the high Cl^- concentrations produced (see Section 4.3.4.3), which reduced the charge-balance-determined alkalinity. In experiments 1/5(c), sodium, potassium, magnesium and some other minor and trace elements increased in concentration slightly under closed system conditions (Equation 5.11-Equation 5.15) during Stage II, whereas calcium concentrations decreased or remained approximately constant during this time, due to saturation with respect to calcite (Sections 5.2-5.3). Therefore, the $\text{Ca}^{2+}/\text{HCO}_3^-$ ratio inevitably reduced in response to the relative increase in concentration of HCO_3^- produced by non-carbonate dissolution. Progressive dissolution under closed system therefore followed a path lying between lines A and D (Figure 5.36). The influence of aluminosilicate dissolution diminished upon reopening experiments 1/5(r) to the atmosphere, such that progressive dissolution beyond the point of reopening approximated to a 1:1, simple carbonate relationship as in experiment 9(r). Experiments 1P/5P(c) followed a similar trend, but starting from the altered $\text{Ca}^{2+}/\text{HCO}_3^-$ ratio produced by sulphide oxidation during Stage I (point U). Experiment 2(r) also lied along line E due to a comparable extent of pyrite oxidation between experiments 2/1P/5P/9P(c).

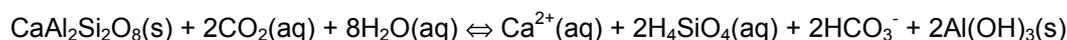
Experiments 3/4/6/7/M(c) displayed some variation in $\text{Ca}^{2+}:\text{HCO}_3^-$ ratio, but their 60 minute samples all lying close on slopes of $\text{Ca}^{2+} = 0.8\times$ to $0.9\times\text{HCO}_3^-$ (the 60 minute samples for experiment 1(c) also lay on this line (Figure 5.37). This indicates that 11-25% of HCO_3^- in these experiments was produced by carbonation-driven dissolution of non-carbonate minerals. The 24h samples often plotted closer to a slope of 1:1, but this is due to the and/or Cl^- in these samples (see Sections 4.3.4.3-4.3.4.4). Earlier discussions suggested contamination as a reason for the high increases in NO_3^- concentration in the 24h samples of experiments 1-9(c), which were not repeated in replicate samples of 1/4/5/9(c) (see Section

4.3.4.4). If these trends are then discounted, it shows that there was no preferential carbonate dissolution prior to aluminosilicate dissolution. Dissolution of anorthite (calcium-plagioclase), or the calcium phase of a plagioclase crystal containing both Na and Ca cations, would also produce a 1:1 (equivalent) $\text{Ca}^{2+}/\text{HCO}_3^-$ ratio (Equation 5.19), and would be less preferentially dissolved than calcite. Similarly, dissolution of forsterite produces a 1:1 $\text{Mg}^{2+}/\text{HCO}_3^-$ ratio (Equation 5.20). This suggests that non-carbonate minerals were a significant source of dissolution in experiments 3/4/7(c).

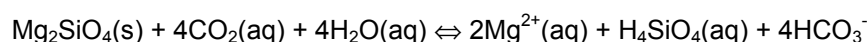
Figure 5.37 Plot of concentration of Ca^{2+} versus HCO_3^- for experiments 1-9/M/C/P(c) and 1/2/5/9/M(r), focussed on experiments with lower concentrations. Theoretical relationships are plotted grey and labelled individually (refer to text for details).



Equation 5.19 Acid hydrolysis of anorthite



Equation 5.20 Acid hydrolysis of forsterite



5.5.3 Comparison with modelled solute acquisition using PHREEQC

Equilibrium and inverse modelling provide contrasting methods of comparison with experimental results. The former utilises mineralogical details of rocks used in experiments (from petrological analyses presented in Section 3.3), and undertakes theoretical dissolution of the rock, or a user-defined mix of rocks, until as many minerals as possible are dissolved

to equilibrium (or to the saturation indices selected by the user). The latter evolves a solution from user-defined “input” and “output” chemistries by dissolving or precipitating minerals selected by the user.

5.5.3.1 Equilibrium modelling

Equilibrium modelling would ideally check the validity of the sediment composition suggested by the experimental modelling, but does not take into account kinetic controls or experimental factors such as rapid acquisition, formation of layers on mineral surfaces that restrict reaction, and so forth.

In addition to speciation modelling (Section b), PHREEQC equilibrium modelling was carried out using the petrological observations of mineralogy described in Chapter 3. The theoretical solution chemistry produced by modelling the dissolution of rocks of set mineralogy is compared with experimental observations. Modelling was carried out of pyrite/calcite dissolution (models P/C/PC(phreeq)) and morainic rock experiments (models 1/2(phreeq)).

a) *Pyrite/calcite mixtures*

Pyrite and calcite mixtures were simulated using the MINTEQA2 database, with input files as shown in Figure 2.11. Temperature was set to 5°C, initial pH was set to 7.4 (the experimental value), initial pCO₂ was set to 5×10⁻⁴M (atmospheric equilibrium value), and the water was pure and deionised. Repeated models were run with O₂(aq) levels of 0, 2, 4, 8 and 10 mg/kgw (Figure 2.11 shows the level at 10 mg/kgw), to simulate the degree of access to atmospheric O₂ (water saturated with respect to the atmosphere would have a O₂ concentration of approximately 14mg/L at sea level). An example input file is shown in Appendix A (PHREEQC Input File A-5). The results for models P(phreeq), C(phreeq) and PC(phreeq) are shown in Table 5.10.

Table 5.10 Output values of PHREEQC modelling of mixtures of pyrite and calcite. C(phreeq) = 0.2g/L calcite dissolution. P(phreeq) = 0.2g/L pyrite oxidation. PC(phreeq) = 0.2g/L pyrite oxidation + 0.2g/L calcite dissolution.

model ID	C(phreeq)	PC(phreeq)	P(phreeq)	PC(phreeq)
set O ₂ (aq) mg/L	Ca ²⁺ (neq/mL)	Ca ²⁺ (neq/mL)	SO ₄ ²⁻ (neq/mL)	SO ₄ ²⁻ (neq/mL)
0	210	210	-	<0.2
2	220	230	35	35
4	220	260	70	70
8	220	330	140	140
10	220	360	170	170

O₂(aq) concentrations strongly influence the extent of pyrite oxidation, which provides additional protons, increasing the equilibrium concentration of Ca²⁺ ions. The concentrations associated with 2mg/L O₂(aq) are closest to the concentrations of Ca²⁺ and SO₄²⁻ achieved in experiment PC(c) (the equivalent laboratory experiment). However, measured O₂(aq) remained at considerably higher levels throughout the experiment (see Chapter 4, Table 4.1). The discrepancy may be attributed to surface processes on pyrite, which form an insoluble oxidised “cap” on grain surfaces preventing reaction (Williamson and Rimstidt, 1994). This is consistent with the observations of dissolution behaviour of pyrite of different grain sizes (Section 5.3.2). Notwithstanding the discrepancy in O₂ concentration between modelled and experimental results, the production of 35neq/mL SO₄²⁻ in model PC(phreeq) is associated with a modelled increase in Ca²⁺ concentration of just 10neq/mL between models C(phreeq). This is consistent with experiment PC(c), and corroborates the discussion of the effects of sulphide oxidation presented in Section 5.2.1.2.

b) Modelled dissolution of individual morainic rocks

Modelled simulations of morainic rock dissolution required the input mineralogy to be quantified. The specific chemistry of solid-solution minerals such as plagioclase feldspar, pyroxenes, amphiboles and olivine were not determined in this study. Additionally, the databases of PHREEQC and MINTEQA2 have, by necessity, a finite database from which to model rock-water reactions. Therefore, certain assumptions and simplifications of observed mineralogy had to be made to run PHREEQC equilibrium modelling. Specifically,

1. *Observed olivine entered as forsterite.* In reality, olivine consists of solid solution variations between forsterite (Mg₂{SiO₄}) and fayalite (Fe₂{SiO₄}), but fayalite was not available in the MINTEQA2 database, so that the contribution of magnesium into solution from olivine is overestimated, and the contribution of iron from olivine is not accounted for.
2. *Observed amphibole entered as tremolite.* Amphibole has a wide range of cation chemistry, e.g. hornblende (a common amphibole) may contain Na, K, Ca, Mg, Fe²⁺, Fe³⁺, Al, Mn and Ti in varying proportions (see Chapter 1, Table 1.11). The MINTEQA2 database does not include free energy data for Mn or Ti, and has no mineralogical data for most types of amphibole. “Tremolite” in the MINTEQA database is actually the magnesium end-member of the tremolite series, Ca₂Mg₅Si₈O₂₂(OH)₂. Therefore, the contribution of magnesium into solution is again overestimated, with Na, K, Fe²⁺, Fe³⁺, Mn and Ti dissolution unaccounted for.

3. *Plagioclase represented by mixtures of the end-members 'albite(low)' and anorthite.* the MINTEQA2 database contains information about plagioclase end-members only. The actual composition of plagioclase in rocks was not identified, but assumptions had to be made about plagioclase composition between An₀ (albite) and An₁₀₀ (anorthite), and albite and anorthite values had to be entered separately.
4. *Minerals unaccounted for.* Certain other minerals were not present in the database, and could not be accounted for. For example, glaucophane could not be accounted for in model 2(phreeq), and all the alteration product had to be assumed to be muscovite.

Modelling was carried out on morainic rocks to which both petrological and chemical analysis had been carried out, namely rocks 1, 2, 3, 4, 6 and 8. Two extremes of morainic rock mineralogy are presented here, namely rocks 1 and 2, with the “model” mineralogy input as shown in Table 5.18 (the full input files are presented in Appendix A (PHREEQC Input Files A-6 and A-7)). The mineralogy as identified by petrological observations is presented in the table as a comparison. Due to the results obtained in model PC(phreeq) (Table 5.17), an initial solution O₂(aq) concentration of 2 mg/L was inputted.

*Table 5.11 Input mineralogy of rocks 1 and 2, for PHREEQC equilibrium models 1(phreeq) and 2(phreeq) respectively. *Model 2(phreeq) was rerun with all plagioclase entered as anorthite (see text), and ** with 10 mg/L O₂(aq)*

Actual identified mineral	Model mineral	rock 1 (M)	rock 2 (M)
calcite	calcite	0.026	-
pyrite	pyrite	3.33×10 ⁻⁴	3.33×10 ⁻⁴
haematite/ilmenite/oxidised pyrite	haematite	2.5×10 ⁻⁴	2.5×10 ⁻⁴
muscovite/glaucophane	muscovite	2.62×10 ⁻³	-
quartz	quartz	6.66×10 ⁻⁴	-
K-feldspar	K-feldspar/microcline	7.19×10 ⁻⁵	3.6×10 ⁻⁴
plagioclase (50%)	albite(low)	-	0.031*
plagioclase (50%)	anorthite	-	0.0288*
clinopyroxene	diopside	-	3.2×10 ⁻³
olivine	forsterite	-	2.8×10 ⁻³
amphibole	tremolite	-	8.6×10 ⁻⁴
Dissolved species:	pCO ₂ (g)	5×10 ⁻⁴	5×10 ⁻⁴
	pH	7.4	7.4
	O ₂ (aq)	2 mg/L	2 mg/L**

Model 1(phreeq) achieved the solution chemistry described in Table 5.12.

Table 5.12 PHREEQC-modelled solution chemistry of the dissolution product of rock 1, and comparison with corresponding results for experiment 1(c).

Species	Model 1(phreeq) (neq/mL)	Experiment 1(c) (neq/mL)
Ca ²⁺	240	320
HCO ₃ ⁻	100	390
CO ₃ ²⁻	41	32
K ⁺	48	46
SO ₄ ²⁻	33	1.4
pCO ₂	10 ^{-6.4}	10 ⁻⁵
pH	10.1	9.1

The concentrations of Ca^{2+} and HCO_3^- are underestimated by the model, with Ca^{2+} values closer to the equilibrium values obtained in model C(phreeq). The pH, and hence pCO_2 values, are also an order of magnitude apart.

Model 2(phreeq) achieved the solution chemistry described in Table 5.13, with different results dependent on plagioclase composition and $\text{O}_2(\text{aq})$ concentration.

Table 5.13 PHREEQC-modelled solution chemistry of the dissolution product of rock 2, and comparison with corresponding results for experiment 2(c).

Species (neq/mL)	Model 2(phreeq) (plag=An ₅₀)	Model 2(phreeq) (plag=An ₁₀₀)	Model 2(phreeq) (plag=An ₁₀₀)	Exp. 2(c) (neq/mL) (24h closed sys.)
Initial $\text{O}_2(\text{aq})$	2mg/L	2mg/L	10mg/L	
Ca^{2+}	7	440	846	87
HCO_3^-	20	17	17	-
CO_3^{2-}	2	6	3	-
Na^+	950	-	-	6
K^+	5	360	360	45
Mg^{2+}	403	790	1700	17
SO_4^{2-}	16	15	150	197
pCO_2	$10^{-6.5}$	$10^{-6.9}$	$10^{-6.9}$	-
pH	9.4	9.7	9.7	7.4

The model produced very different results depending on the Na/Ca ratio of the plagioclase phase. It consistently, however, overestimated the concentration of cations in solution other than Ca^{2+} , and underestimated the concentration of sulphate.

Despite the assumptions and approximations required to run the model with the data available, it is clear that experimental results deviate strongly from equilibrium conditions, and that most minerals are governed not by solution equilibria but by grain surface conditions. Controls such as grain size, turbulence and roughness are therefore likely to be dominant. Calcite dissolution behaviour in the laboratory experiments was somewhat closer to results obtained by equilibrium modelling, but still deviated considerably. This is consistent with previous reports of equilibrium model use (Fairchild *et al.*, 1999), which reported overestimates of calcium dissolution flux using the Plummer-Wigley-Parkhurst model of calcite dissolution (Plummer *et al.*, 1978) (see Section 1.4.3), and attributed the discrepancy to a lack of resolution of CO_2 -hydration kinetics.

5.5.3.2 Inverse modelling of dissolution of experimental solutions

Inverse modelling represents the reaction of an initial solution with minerals and gases to produce a second solution. The model calculates the amount of gases and minerals produced or consumed from the difference in concentrations between the two solutions (Parkhurst, 1995) (see Section 2.5.4 for full methodology). Modelling of pyrite/calcite dissolution

experiments between time=60 minutes and later times were possible, so that post-rapid acquisition evolution could be simulated. Attempts at modelling of morainic rock experiments over this time scale were again unsuccessful (see Section 2.5.4).

The evolution of the solution chemistry during open system dissolution of 0.2g/L calcite plus 0.2g/L pyrite was modelled (model PC(inv)), using the 60 minute concentrations of Ca^{2+} , SO_4^{2-} , HCO_3^- and pH as ‘Solution 1’, and the corresponding 1440 minute values as ‘Solution 2’ (see Chapter 4, Table 4.1) The input file is shown in Appendix A (PHREEQC Input File A-8).

Inverse modelling may produce different scenarios that satisfy the evolution of chemistry between the starting and end solutions, depending on the number of solid phases entered as possible solutes or precipitates. With model PC(inv), the following phase transfers were enabled:

1. Calcite was allowed to dissolve and precipitate.
2. Gypsum was added to the model as a possible precipitate, as coprecipitation of Ca^{2+} and SO_4^{2-} is possible.
3. Pyrite was allowed to oxidise but not precipitate, as reducing conditions were not envisaged.
4. $\text{Fe}(\text{OH})_3$ was allowed to precipitate as the likely dissolution product of pyrite oxidation.
5. Oxygen and CO_2 phase transfers between liquid and gas were allowed.

With the above restrictions, two potential scenarios were identified, as shown in Table 5.14. In the first scenario, $10^{-3.6}\text{M}$ CO_2 was consumed to produce protons and alkalinity, and 0.35mg/L ($10^{-5.5}\text{mol}$) pyrite was oxidised to drive the overall mass transfer of 24mg/L ($10^{-3.62}\text{mol}$) calcite. The same mass transfer is calculated by simple stoichiometry.

Table 5.14 Results of PHREEQC inverse modelling of calcite + pyrite dissolution between 60 and 1440 minutes.

Phase	mass transfer (scenario 1), mg/L	mass transfer (scenario 2), mg/L
calcite	+24	+48
gypsum	-	-41
pyrite	+0.35	+15
$\text{Fe}(\text{OH})_3(\text{amorphous})$	-0.32	-13
$\text{O}_2(\text{g})$	+0.36	+15
$\log \text{CO}_2(\text{g}) (\text{M})$	-3.6	-

Scenario 2 involves a much higher amount ($10^{-3.9}\text{mol}$) of sulphide oxidation, which supplies the protons to drive dissolution of $10^{-3.3}\text{mol}$ calcite. In this scenario, no $\text{CO}_2(\text{g})$ is consumed,

but much higher quantities (15mg/L) of O₂(g) are used. The additional SO₄²⁻ produced by the extra pyrite oxidation is coprecipitated with Ca²⁺ as 10^{-3.6}mol gypsum.

Although Scenario 2 is unlikely due to the low SI(gypsum) of the final solution (-3.97), it shows the possibility for this reaction, and that precipitated gypsum may be present in glacial conditions.

5.5.4 Comparison with kinetic models

The ‘Plummer-Wigley-Parkhurst’ (PWP) model of calcite dissolution, developed by Plummer *et al.* (1978), with developments by Busenberg and Plummer (1986) and Chou *et al.* (1989) is discussed in Section 1.4.3. A derivation of the PWP model (see Equation 1.18) for bicarbonate and CO₂, at 0°C, using rate constants as published in Wollast (1990) is described in Equation 5.21.

*Equation 5.21 Derivation of overall experimental rate law for dissolution of calcite (Wollast, 1990), at 0°C. Units for r_d are mol/cm²/s. Rate constants used for derivation were as follows:
 k_1 : 10^{-4.12} (mean rates for calcite powders in Plummer *et al.*, 1978; Chou *et al.*, 1989)
 k_2 : 10^{-7.47} (rate for calcite powder in Plummer *et al.*, 1978)
 k_3 : 10^{-10.06} (mean rates for calcite powders in Plummer *et al.*, 1978; Chou *et al.*, 1989)
 k_4 : 10^{-1.98} (mean rates for calcite powders in Nancollas and Reddy, 1971; Inskeep and Bloom, 1985; Chou *et al.*, 1989)*

$$r_d = 10^{-4.12-\text{pH}} + 10^{-8.59} \text{pCO}_2 + 10^{-10.06} - 10^{\text{pH}-12.6} [\text{Ca}^{2+}] [\text{HCO}_3^-]$$

The rate of calcite dissolution from calcite according to this model was published to vary between 10^{-10.2} and 10^{-11.2}mol/cm²/s in the pH range 7-10 (Chou *et al.*, 1989), and are calculated as 10^{-10.16} for experiment 9(c) after 24h, and 10^{-10.06} for experiment 9(r) after 28h using the same equation. The actual rates of overall Ca²⁺ acquisition in experiments 1/5/9(r), assuming a specific surface area of 0.87m²/g (refer to Section 2.3.1.1), ranged between 10^{-12.2} and 10^{-12.6}mol/cm²/s, an order of magnitude lower than the published rate. (The rate of dissolution of calcite under open system conditions, determined in Section 5.4.1.1 (Table 5.2), after the initial rapid stage of acquisition, was 10^{-8.47}mol/s, with undetermined surface area.)

The discrepancy between the calculated rates according to the PWP model, and observed rates of dissolution in experiments in this study and the studies of Fairchild *et al.* (1999) may be attributed to kinetic controls on dissolution, which cannot be considered in the PWP model (Fairchild *et al.*, 1999). Such potential factors involve the kinetics of CO₂-drawdown, modification of overall and surface properties in multi-minerallic sediments, and effective modifications of reactive surface area depending on discharge levels, proportion of sediment in suspension, channel form (including water surface area/volume ratio, and channel basal

form), flocculation with other mineral grains, and many other factors. In laboratory experiments, these factors would be manifested in terms of vessel shape, stirring mechanism and rate, surface area of the water/air interface. The discrepancies show that caution has to be applied when interpreting calculated rates, even in relatively pure carbonate catchments, and that in dominantly non-carbonate catchments, the PWP model is unlikely to be applicable.

5.6 CONCLUSION

Laboratory experiments simulating chemical weathering in subglacial environments have allowed the isolation of the major controls on solute acquisition from materials encountered beneath *Haut Glacier d'Arolla*. The rate of acquisition of major cations has been shown to be related to numerous factors:

- a) Rock mineralogy and bulk chemistry
- b) $p\text{CO}_2$
- c) Sulphide oxidation, dependent on the reactive surface area of pyrite
- d) Saturation, particularly with respect to calcite
- e) Temperature
- f) Residence times
- g) Rock/water ratios

Mineralogy had a major effect on solute acquisition, with rock Ca^{2+} content determining whether equilibrium processes or reactive surface area are more important controls on Ca^{2+} acquisition, the rock ratio of Ca^{2+} to other metal cations affecting the relationship between Ca^{2+} and $p\text{CO}_2$, and the mutual abundance of the metallic species affecting the acquisition of each other. The ratios between specific metal reaction sites and water volume are strongly influenced by mineralogy. Calcite saturation is approached in experiments dissolving calcite and marble, with acquisition rate closely linked to $p\text{CO}_2$ recovery in open systems. Waters that became supersaturated with respect to calcite in the initial period of rapid acquisition, precipitated calcite, resulting in negative rates of acquisition.

Sulphate concentrations were thought to closely reflect the extent of pyrite oxidation, in the absence of sulphate minerals. The effect of sulphide oxidation on the magnitude of calcium acquisition was shown to be insignificant if concentrations of SO_4^{2-} in excess of approximately 50neq/mL were not achieved. However, in experiments where sulphide oxidation produced around 30neq/mL SO_4^{2-} , $p\text{CO}_2$ levels did not reduce to the same extent as in SO_4^{2-} -absent solutions, suggesting that sulphide oxidation replaced carbonation to some extent, rather than occurring as an additional, independent process.

In experiments with sediment comprising a mixture of calcium-rich morainic rocks and pyrite (experiments 1P/5P/9P(c)/(r)), SO_4^{2-} levels reached up to 190 neq/mL, and the magnitude of calcite dissolution is significantly increased. The experimental results suggest that this effect is rapid, as the only difference in Ca^{2+} acquisition rate occurs in the first hour, at odds with some previous studies (e.g. Fairchild *et al.*, 1994), but consistent with suggestions in Tranter *et al.* (1993) that sulphide oxidation was a relatively rapid process. This suggests that pyrite oxidation relies on the production of freshly-ground, highly reactive ultrafine pyrite material, and that an insoluble oxidised layer may be produced, through which pyrite oxidation is severely restricted.

Residence times show a significant effect on acquisition in direct and indirect ways:

- a) With fast-flowing water, contact times with sediment may be of great importance. This represents the initial period of the experiments presented here.
- b) If residence times are very long, then acquisition rates even in closed system environments may become significant.
- c) With access to pCO_2 , acquisition is largely governed by pCO_2 , but since CO_2 drawdown is the controlling factor in these circumstances, residence times, together with turbulence, will control CO_2 drawdown and ultimately control the rate of Ca^{2+} acquisition in calcitic waters.

The effect of turbulence was not determined in these studies, which were undertaken at approximately constant stirring rates. The effect of turbulence on calcite dissolution is discussed in Morse (1983).

The relationships between solute concentrations and the various controls were quantified where possible, providing equations indicating the relative importance of each control. These equations allow the input of field water quality data, in order that variables that cannot be identified in the field may be input. These variables include the overall rock chemistry likely to have resulted in the observed chemistry, and inferences of mineralogy. This is carried out and discussed in Chapter 6.

PHREEQC speciation modelling revealed important factors influencing the solubility and adsorbability of trace elements, for instance lead and nickel complexed with carbonate, which increased the potential for adsorption onto silicate mineral surfaces. Adsorption was an important factor with many trace elements, with the result that some were more concentrated in experiments involving much lower rock/water ratios. These included zinc, iron and uranium. Ratios between rubidium and potassium, calcium and strontium and certain rare-earth elements may potentially indicate provenance variations. Ca/Sr ratios provided a particularly useful indicator of carbonate provenance and access to pCO_2 .

However, many trace elements showed highly variable dissolution characteristics, demonstrating that caution must be taken when using trace elements as indicators of solute provenance in meltwaters draining *Haut Glacier d'Arolla*.

6. APPLICATION OF EXPERIMENTAL AND GEOCHEMICAL MODELS TO HYDROGEOCHEMICAL DATA

6.1 INTRODUCTION

Laboratory investigations of solute acquisition which simulated subglacial water-rock interactions have identified and quantified the controls of dissolution behaviour of the major species found in solution. The investigations used rocks and sediment characteristic of the catchment containing *Haut Glacier d'Arolla*, and encompassed the chemical conditions encountered.

This chapter compares experimental models of solute acquisition based on laboratory simulation experiments (Section 5.5) with data of bulk meltwater quality draining *Haut Glacier d'Arolla* between 1989 and 1996 (Brown, 1991; Lamb, 1997; Tranter *et al.*, 1997; Seagen, 1999, and Section 4.2). The experimental model of acquisition of major cations presented in Chapter 5 is used to determine the dominant controls on solute acquisition in subglacial environments. The inferred controls are evaluated by comparison with geochemical modelling techniques using PHREEQC and previous studies. Additionally, the potential application of key trace indicators of solute acquisition processes investigated in Section 5.5 are evaluated in the light of a small batch of trace element data from the 1996 meltseason. This gives an initial overview of trace element behaviour in glacial environments and how they compare with laboratory controls.

6.2 APPLICATION OF EXPERIMENTAL MODELS TO GLACIAL GEOCHEMICAL DATA

6.2.1 Introduction

The experimental models of controls on acquisition of major species described in Chapter 5 encompasses dissolution of a wide range of morainic rocks found in the catchment of *Haut Glacier d'Arolla*, and both “open” and “closed” conditions. Table 6.1 summarises the data of major ions, acidity, $O_2(aq)$, pCO_2 and SI(calcite) for experiments and bulk meltwater over the 1989-1996 period. The wide range of experimental conditions envelops the extremes of the parameters for the period of sampling of bulk meltwaters described in Chapter 2.

Experimental data is summarised in two sections, (a) closed experiments 1-9/M(c) involving morainic rock, over the period 60-1440min, and (b) reopened experiments 1/5/9/M(r) for

Table 6.1 Summary of major element data of laboratory experiments and bulk meltwater draining *Haut Glacier d'Arolla* (1989-90 and 1992-96 meltseasons). BMW = bulk meltwater, SD = standard deviation. Concentrations of cations and anions in neq/mL, O₂(aq) is in mg/L. See text for explanation of "Type 2 borehole".

		pH	HCO ₃ ⁻	O ₂	Cl ⁻	NO ₃ ⁻	SO ₄ ²⁻	Na ⁺	K ⁺	Mg ²⁺	Ca ²⁺	pCO ₂	SI(calcite)
Closed system morainic rock experiments (rocks 1-9/M)	Mean	9.4	290	6.4	15	2.9	17.1	13	30	11	270	-5.4	-0.3
	SD	0.8	110	1.4	20	7.4	46.1	11	20	7.6	86	0.5	0.7
	Max Min	10.6 7.1	420 0.0	10.7 4.9	90 0.0	40 0.0	200 0.0	38 1.0	69 1.9	35 0.0	370 49	-4.3 -6.7	0.7 -2.8
Open system morainic rock experiments (rocks 1/2/5/9/M)	Mean	8.0	360	6.2	10	0.9	24	13	29	19	340	-3.9	-1.8
	SD	0.8	250	1.3	13	1.2	59	6.4	23	12	220	0.8	1.2
	Max Min	9.3 6.7	1010 0.0	8.7 4.3	65 0.0	4.5 0.0	190 0.0	31 4.5	67 3.0	55 5.9	920 90	-2.7 -5.5	-0.3 -4.1
BMW 1996 (Seagren, 1999)	Mean	7.5	270	6.8	1.8	12	110	17	13	35	330	-3.37	-2.45
	SD	0.5	45	1.2	0.9	4.3	33	3.5	2.4	6.5	67		
	Max Min	9.1 6.9	390 180	9.2 3.8	9.2 0.7	21 0.1	190 53	26 9.9	18 7.6	53 21	490 210	-4.81 -2.94	-0.52 -3.42
BMW 1995 (this study)	Mean	7.1	220	6.3	3.2	0.05	97	14	10	27	320	-3.06	-2.95
	SD	1.8	58	1.3	2.4	0.27	20	4	4	6	60		
	Max Min	8.3 6.5	180 330	9.3 3.5	21 0.1	2.9 0	340 64	32 12	36 8	67 22	555 256	-4.34 -2.28	-1.60 -3.47
BMW 1994 (Lamb, 1997)	Mean	6.5	280				100	11	10	27	320	-2.35	-3.45
	Max Min	9.1 6.9	400 250				300 58	30 7.6	22 7.6	54 19	540 280	-4.80 -2.80	-0.47 -3.16
	Mean	7	290				120	18	12	27	320	-2.84	-2.93
BMW 1993 (Lamb, 1997)	Max Min	9.1 6.9	580 180				282 61	41 12	37 8.5	54 19	540 280	-4.64 -2.94	-0.31 -3.30
	Max Min	8.9 7	360 220				220 46	55 11	36 8.6	110 26	560 250	-4.64 -2.96	-0.70 -3.16
	Mean	7	250				50	8.6	6.9	23	170	-2.90	-3.27
BMW 1990 (Brown, 1991)	Max Min	9.1 6.5	460 200				340 20	27 5.2	19 3.3	27 5.2	410 140	-4.74 -2.50	-0.53 -3.95
	Mean	8	230				54	11	9	24	230	-3.94	-2.18
	Max Min	8.2 6.8	320 190				240 30	36 5.1	18 5.4	49 15	470 160	-5.00 -2.82	-1.52 -3.62
Mean Type 2 borehole (Lamb <i>et al.</i> , in preparation)	Mean		480		6.3	10	270	18	15	82	650		
	SD		200		5.1	9.0	170	18	8.0	23	310		

sampling periods 1470, 1500, 1560 and 1680min. Both closed and open system experiments are included as both environments are believed to exist in the subglacial environment of *Haut Glacier d'Arolla*. Open system averages are therefore rather skewed towards the dissolution behaviour of carbonate-rich rocks. The maximum and minimum experimental values are, however, beyond the extremes of bulk meltwater quality with the exception of high field concentrations of Mg²⁺ and SO₄²⁻.

The mean values of *in situ* waters collected from boreholes are also included in Table 6.1 (Lamb *et al.*, in preparation). "Type 2" subglacial waters are the most frequently sampled subglacial waters, and are associated with boreholes that have established connections to the

glacier bed. They are believed to be representative of subglacial distributed (delayed flow) meltwaters (Seagren, 1999). These waters therefore represent relatively undiluted subglacial meltwaters that would be expected to have long residence times and to have encountered periods without access to atmospheric gases. Nevertheless, concentrations of individual species other than Mg^{2+} and SO_4^{2-} in these waters are still encompassed by the range encountered in experiments involving morainic rocks.

6.2.2 Inference of geochemical parameters using experimental models of cation acquisition

Experimental modelling isolated the effects on cation acquisition caused by variations in pCO_2 , SI(calcite), pH, temperature, rock chemistry, mineralogy, rock/water ratio and residence times. The individual equations for calcium, magnesium, sodium and potassium contain parameters that cannot be directly measured in the field, namely the nature of rock/sediment in contact with the meltwater and residence times. Therefore, inputting the known variables from field data into the equations can quantify the unknown parameters, gaining some insight into the mean mineralogy of the composite of sediment in contact with bulk meltwater and give an additional means of measuring expected residence times.

This model does not quantify hydrological parameters such as variations in discharge levels, the proportion of sediment in suspension, seasonal evolution of channel forms and so forth, as these factors can not be properly simulated in static laboratory experiments. The model is concerned with determining the provenance of the chemical reactions occurring in the subglacial drainage system. This is the remaining unknown variable that cannot be accounted for with field investigations. Therefore, assumptions of meltwater solute provenance can be verified, and therefore processes of solute acquisition can be inferred with greater confidence.

The following section presents suggestions of solute provenance based on the equations of calcium, sodium, potassium and magnesium acquisition presented in Chapter 5. The applicability and limitations of these suggestions are then discussed.

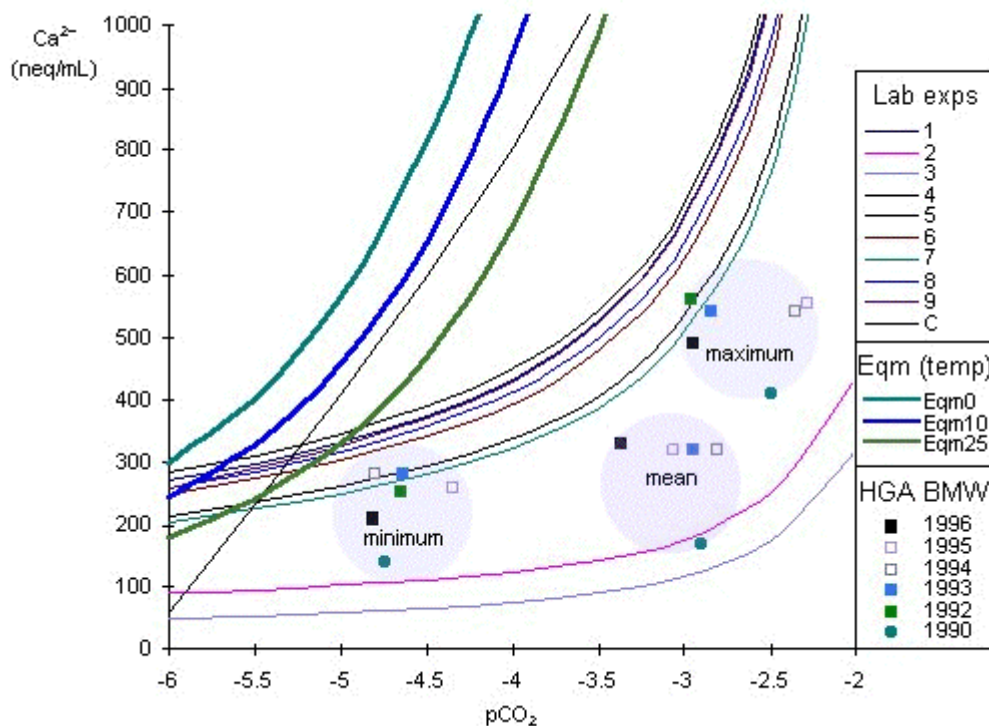
6.2.2.1 Indication of the processes of calcium acquisition

The experimental model of controls on Ca^{2+} acquisition (Equation 5.14) involved parameters for pCO_2 , total cation content of reactive rock, calcium content of reactive rock, SI(calcite), SO_4^{2-} content, temperature and mineralogy. Experimental investigations of dependence on residence time concluded that time is only a significant direct influence on Ca^{2+} concentration until equilibrium is reached, often within one hour of rock-water contact. In

experiments 1/5/9(rd), containing significant calcite mineralogy, but also experiment M(rd), which dissolved sediment of a much lower calcite content, the effect of 50% dilution with deionised water was to drive a further period of rapid dissolution to return Ca^{2+} concentrations to the equivalent of undiluted experiments. Therefore, inferences of calcium provenance can be made regardless of dilution, assuming a residence time of greater than one hour, and a post-mixing environment of greater than approximately 30min.

Plotting Ca^{2+} versus pCO_2 for experimental data clearly showed the variations in Ca^{2+} acquisition between different rock types in contact with the experimental solution (Section 5.6). The range of relationships between Ca^{2+} and pCO_2 in experimental models depending on rock type/mineralogy is demonstrated in Figure 6.1, and compared with the mean relationship between Ca^{2+} and pCO_2 for each field sampling season between 1989 and 1996, and the relationships at extreme Ca^{2+} concentrations for each season. The mean field results were within the boundaries of the relationships encountered by dissolution of sampled morainic rocks, with higher $\text{Ca}^{2+}/\text{CO}_2(\text{g})$ ratios than Rocks 2 and 3, but lower than the remaining rocks.

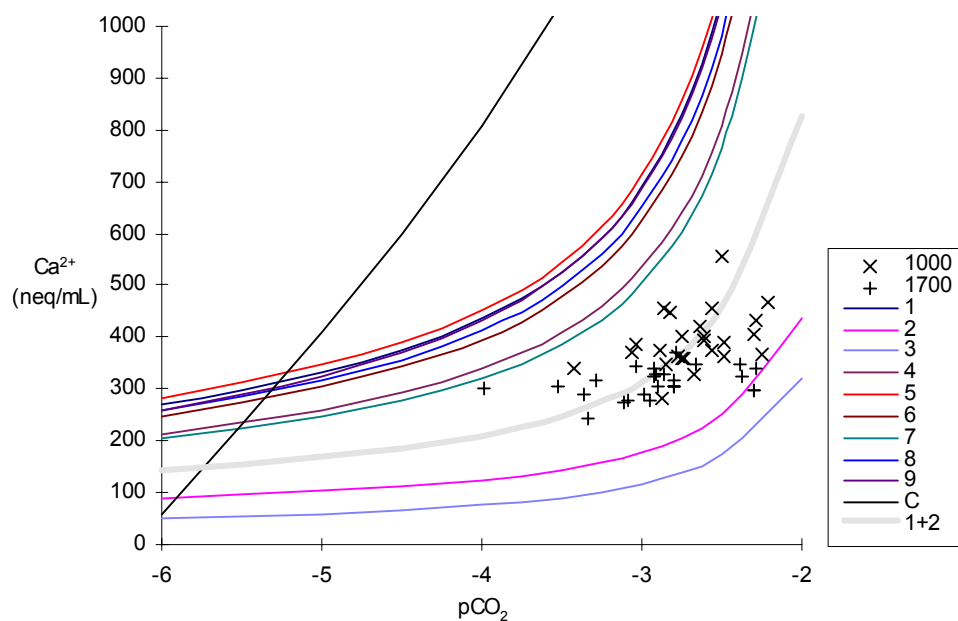
Figure 6.1 Calculated relationships between Ca^{2+} and pCO_2 using Equation 5.13, with the relationship at minimum, mean and maximum Ca^{2+} concentrations for meltseasons 1990-1996.



A better picture of the seasonal range in the relationship between Ca^{2+} and pCO_2 may be gathered using data of minimum and maximum discharge samples of bulk meltwater from

Haur Glacier d’Arolla in the 1995 sampling season (Figure 6.2), collected daily at 10:00 and 17:00 respectively. The ratios for minimum and maximum discharge both plot in a region of the graph between the modelled trends of the experiments with lowest $\text{Ca}^{2+}/\text{pCO}_2$ ratios (experiments 2/3) and the remaining experiments. A single rock type is therefore unlikely to be the sole significant source of cations in the subglacial weathering system. This is unsurprising given the various geological units apparently underlying the glacier (Brown, 1991).

Figure 6.2 Calculated relationships between Ca^{2+} and pCO_2 using Equation 5.13, with 10:00 and 17:00 field data from the 1995 sampling period, and the 1996 diurnal cycle data, superimposed.



The unknown variables in Equation 5.16 are all measurements of rock cation content. Given the assumptions that all sediment that contacted the meltwater as it passed through the subglacial hydrological system was of similar rock type to rocks 1-9, and of a comparable grain size distribution, the limits of the unknown variables are parameterised by the geologic data in Chapter 3 (Table 6.2).

Table 6.2 Parameterised limits of unknown variables in Ca^{2+} acquisition equation

Parameter	Lower limit (ng/mL)	Upper limit (ng/mL)
Ca(s)	830000 (Rock 3)	2.7×10^8 (Rock 9)
Sr(s)	1700 (Rock 3)	3.5×10^6 (Rock 5)
Ca(s)/Sr(s)	42 (Rock 7)	150 (Rock 8)
M(s)	7.1×10^7 (Rock 4)	2.7×10^8 (Rock 9)
M-Ca(s)	7.5×10^6 (Rock 9)	8.7×10^7 (Rock 2)

For the purposes of inferring solute provenance, the above demonstration of multiple sources of calcium in bulk meltwater shall be considered analogous to an experiment containing proportions of sediment of each source. Spatial variations could only be accounted for using meltwater from various sources beneath the glacier, from boreholes or from stream portals.

Inferences of provenance may be made by creating theoretical mixtures of rocks 1-9 in various proportions, and inputting the modelled values of Ca(s), M(s) and Sr(s) into Equation 5.14, together with the measured bulk meltwater quality data (i.e. pCO₂, SI(calcite), SO₄²⁻ and temperature), by trial-and-error until the modelled Ca²⁺ concentration matches the measured concentration. Only realistic combinations were considered; for instance, a system based dominantly on the dissolution of quartz vein material is not realistic.

Table 6.3 shows the modelled Ca²⁺ and SO₄²⁻ concentrations of theoretical mixtures that were closest to the mean and extreme field Ca²⁺ concentrations, using Equation 5.14. It was found that the theoretical dissolution of mixtures of rocks 1 and 2 produced modelled concentrations which closely matched the Ca/pCO₂ relationships found in these samples. The modelled relationship between pCO₂ and Ca²⁺ using a theoretical 32%:68% mixture of rocks 1 and 2 is plotted on Figure 6.2.

Table 6.3 Modelled mean rock Ca content of subglacial sediment, determined by theoretical dissolution of mixtures of rocks 1 and 2 producing calculated concentrations of Ca²⁺ equivalent to those of mean and extreme concentrations in bulk meltwater draining *Haut Glacier d'Arolla* during the latter part of the 1995 meltseason.

bulk meltwater sample (1995)	Field Ca ²⁺ (neq/mL)	rock 1/2 % ratio	Calculated Ca ²⁺ (neq/mL)	Ca(s) (mmol)
volume-weighted mean	320	32:68	320	9.03
17/08 10:00 (Ca high)	550	38:62	550	10.1
05/08 17:00 (Ca low)	240	29:71	240	8.48

6.2.2.2 Indications of provenance of sodium acquisition

The applicability of experimental models may be investigated by the degree of compatibility between models representing the acquisition of each cation. The mean content of sodium in sediment contacting bulk meltwater was modelled using Equation 5.13. Table 6.4 shows the modelled content of sodium produced by dissolution of theoretical sediments of the same composition as those accounting for correct concentrations of calcium (Table 6.3). These values are, however, tentative, given the uneven relationship between sodium acquisition and pCO₂ demonstrated in Section 5.5.2. The calculated values are higher than that of the appropriate mixtures between rocks 1 and 2. This is likely to be due to the influence of sulphide oxidation. The volume weighted mean concentration of SO₄²⁻ in 1995 bulk meltwaters was 97neq/mL, and the mean increase in sodium concentration in experiments

due to sulphide oxidation producing $165 \pm 7 \text{ neq/mL}$ was $59 \pm 31\%$. By simple calculation, the calculated overestimation of sodium rock content may be expected to be between 16 and 53%. The calculated range of sodium content accounting for sulphide oxidation encompasses the sodium content of the theoretical mixtures of rocks 1 & 2 presented in Table 6.4.

Table 6.4 Modelled mean rock Na content of subglacial sediment, produced by theoretical dissolution of mixtures of rocks 1 and 2 producing calculated concentrations of Ca^{2+} equivalent to those of mean and extreme concentrations in bulk meltwater draining *Haut Glacier d'Arolla* during the latter part of the 1995 meltseason.

BMW sample (1995)	Na^+ (neq/mL)	Na(s) without accounting for SO		Na(s) accounting for SO		rocks1/2 % ratio	Na(s) (mmol) rocks 1:2 mix
		1h	24h	1h	24h		
volume-weighted mean	14.5	4.72	4.17	1.32-4.25	1.32-3.75	32:68	2.13
17/08 10:00 (Ca high)	17.8	6.36	5.63	1.78-5.72	1.58-5.07	38:62	2.07
05/08 17:00 (Ca low)	12.1	3.51	3.11	0.98-3.16	0.87-2.80	29:71	2.17

The estimates of sodium content of the rocks and sediment in contact with bulk meltwaters are by necessity only qualitative, but they are consistent with the estimated provenance calculated using Equation 5.16.

6.2.2.3 Indication of potassium provenance using experimental equations

The theoretical mean potassium content of rocks and sediment in contact with bulk meltwaters was inferred using Equation 5.14, by inputting $\text{K}^+(\text{aq})$ values, calculated values of pCO_2 , inferred $\text{Ca}(\text{s})$ values from Section 6.2.3.1, and an increment of time. The volume-weighted mean K^+ values for the 1995 field season produce theoretical $\text{K}(\text{s})$ rock content levels considerably lower than those produced by the proportioned mixtures of rocks 1 and 2 proposed above (Table 6.5).

Table 6.5 Modelled mean rock K content of subglacial sediment, produced by theoretical dissolution of mixtures of rocks 1 and 2 producing calculated concentrations of Ca^{2+} equivalent to those of mean and extreme concentrations in bulk meltwater draining *Haut Glacier d'Arolla* during the latter part of the 1995 meltseason.

BMW sample (1995)	K^+ (neq/mL)	K(s) without accounting for SO		rocks1/2 % ratio	K(s) (mmol) rocks 1:2 mix
		1h	24h		
volume-weighted mean	10.4	0.17	0.16	32:68	1.91
17/08 10:00 (Ca high)	8.7	0.17	0.16	38:62	1.85
05/08 17:00 (Ca low)	17.8	0.21	0.20	29:71	1.94

The relationship between rock content of potassium and K^+ concentration in solution presented in Equation 5.14 is therefore not transferable to interpretation of bulk meltwater quality. Although the influence of sulphide oxidation could not be quantified as part of Equation 5.14, the addition of this parameter would have reduced the inferred concentrations of $\text{K}(\text{s})$ presented in Table 6.5. It is likely that the effects of turbulence (stirring rate in

experiments) (discussed for carbonates in Fairchild *et al.*, 1999), rock-water ratio (e.g. Brown, 1991; Seagren, 1999) and resorption (Drever and Hurcomb, 1986) were significant factors in the dissolution of aluminosilicate minerals. It is of note that only experiments C/P/8/9/M(c) and 9(r)/(rd) produced concentrations of K^+ as low as those found in bulk meltwaters draining *Haut Glacier d'Arolla*, all of which produced concentrations of Na^+ and Mg^{2+} that were much lower than field values. It is possible that resorption processes in channels below a glacier would be more effective than in laboratory experiments due to the greater (reacted) rock/sediment/precipitate surface area in contact with meltwater than experimental waters.

6.2.2.4 Magnesium

The theoretical mean magnesium content of rocks and sediment in contact with bulk meltwaters can be inferred using Equation 5.15, by inputting $Mg^{2+}(aq)$ values, calculated pCO_2 values, and an increment of time (Table 6.6). The volume-weighted mean Mg^{2+} values for the 1995 field season produce theoretical $Mg(s)$ rock content levels considerably higher than those of a theoretical mixture of rocks 1 and 2 in the proportions suggested by calcium provenance calculations (Section 6.2.3.1).

Table 6.6 Modelled mean rock Mg content of subglacial sediment, produced by theoretical dissolution of mixtures of rocks 1 and 2 producing calculated concentrations of Ca^{2+} equivalent to those of mean and extreme concentrations in bulk meltwater draining *Haut Glacier d'Arolla* during the latter part of the 1995 meltseason.

BMW sample (1995)	Mg^{2+} (neq/mL)	Mg(s) without accounting for SO		rocks1/2 % ratio	Mg(s) (mmol) rocks 1:2 mix
		1h	24h		
V.W.M. (1995)	26.9	3.26	2.44	20:80	0.56
17/08/95 10:00	66.6	8.50	6.37	26:74	0.54
05/08/95 17:00	21.5	2.45	1.84	18:82	0.57

The effect of pyrite oxidation on magnesium acquisition was not quantifiable from the experiments undertaken, due to wide variations between experiments, but showed that very large increases in Mg^{2+} concentration could be expected due to protons produced by pyrite oxidation, possibly due to cation exchange with dissolved iron produced by sulphide oxidation being strongly adsorbed onto mineral surfaces. The extent of pyrite oxidation associated with concentrations of SO_4^{2-} experienced in 1995 bulk meltwaters could have increased Mg^{2+} concentrations by anything between 15 and 210% compared to theoretical concentrations in the absence of pyrite oxidation, which would significantly reduce the $Mg(s)/Mg^{2+}(aq)$ ratio and reduce the results of $Mg(s)$ calculations closer to those determined using the rock proportions calculated by calcium provenance determinations. Similarly,

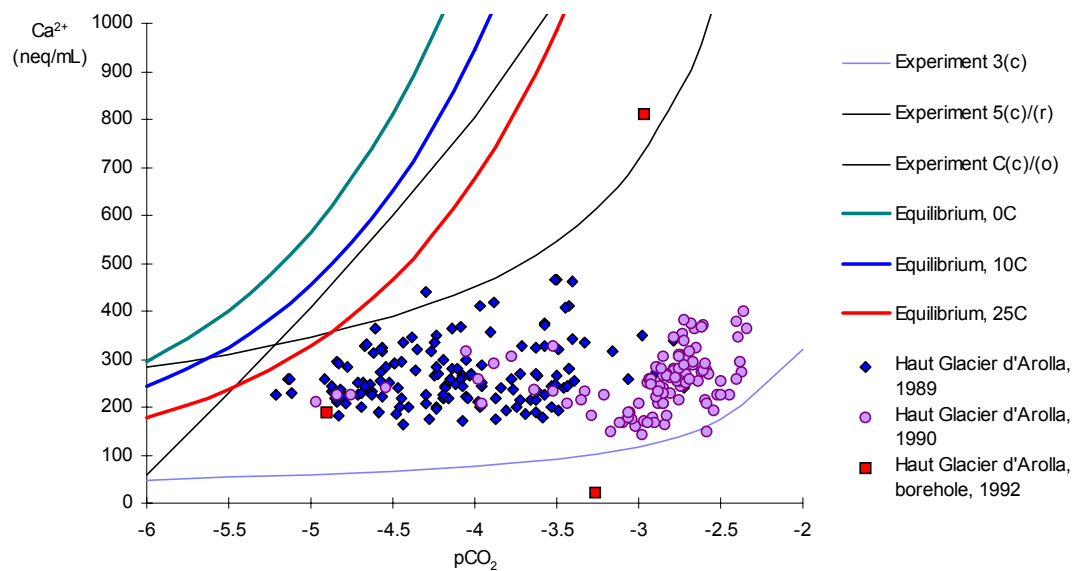
longer periods of open system weathering than was undertaken in laboratory experiments could significantly reduce the $Mg(s)/Mg^{2+}(aq)$ ratio.

6.2.3 Comparison of global bulk meltwater data with laboratory models

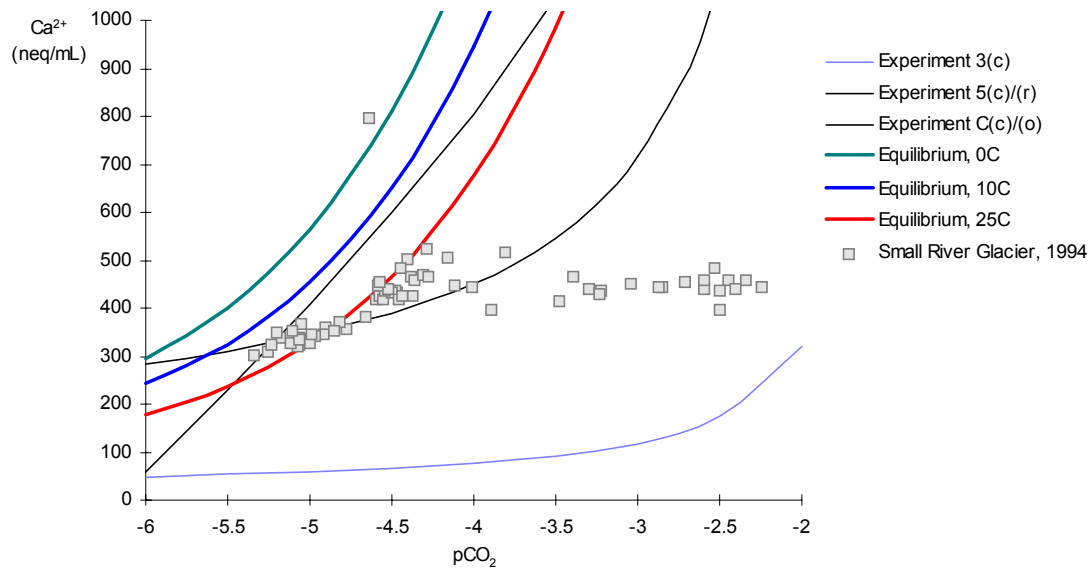
Data of Ca^{2+} concentration and pCO_2 in bulk meltwaters from various catchments are shown in Figure 6.3. On each plot, these data are compared with the modelled relationships of laboratory experiments described in Section 5.5, and the equilibrium relationships at 0, 10 and 25°C (see Section 5.3.1.5).

Figure 6.3 Bulk glacial meltwater from various catchments: the relationship between Ca^{2+} and pCO_2 . Relationships are compared with extreme modelled laboratory experimental relationships, and with equilibrium relationships at 0, 10 and 25°C.

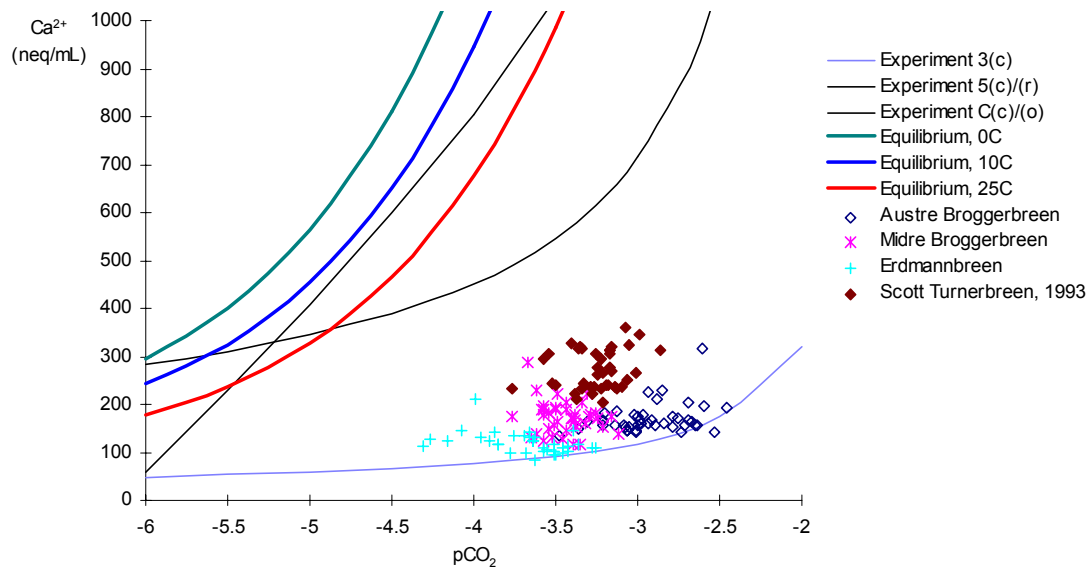
(a) Haut Glacier d'Arolla: bulk meltwater, 1989 and 1990 [Brown, 1991]



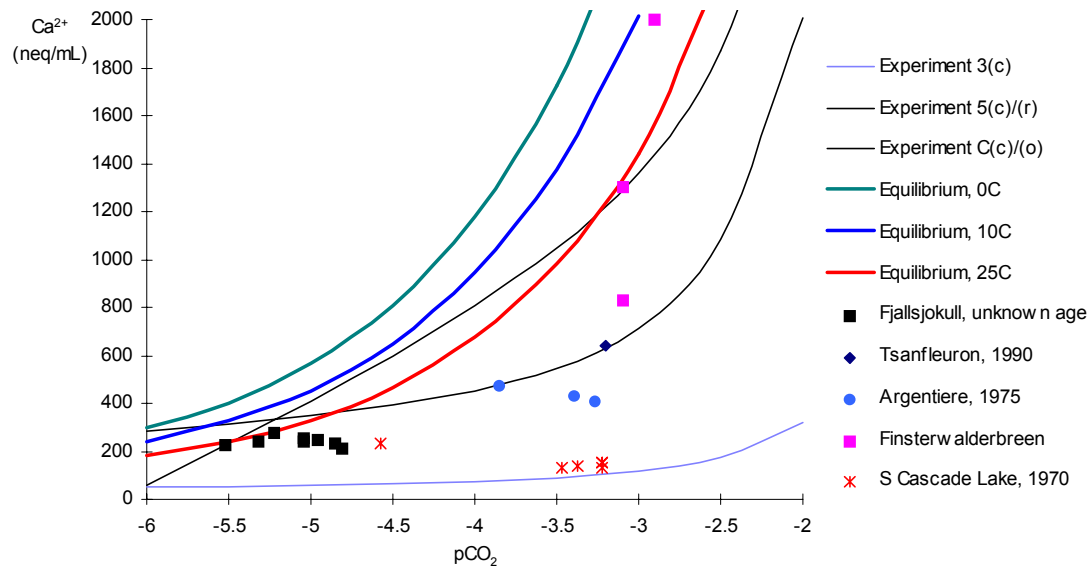
(b) Small River Glacier, B.C., Canada: bulk meltwater, 1994 (Brown, unpublished data)



(c) Svalbard glaciers: bulk meltwater: Austre Broggerbreen, Midre Broggerbreen, Erdmannbreen (Hodson, unpublished data); Scott Turnerbreen, 1993 (Hodgkins, unpublished data)



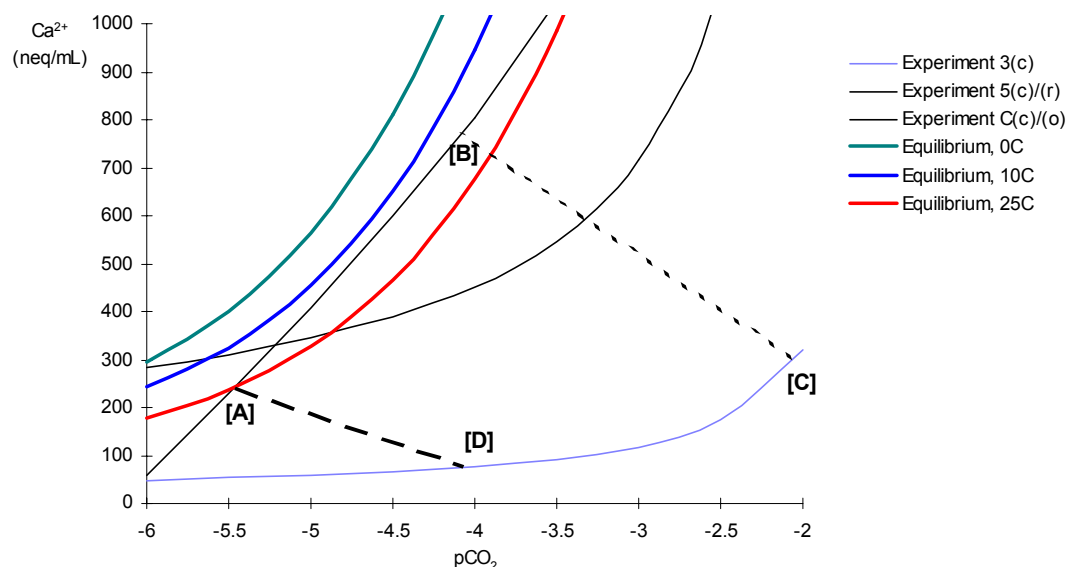
(d) Fjallsjokull, S.E. Iceland: bulk meltwater (unknown age) (Raiswell & Thomas, 1984); Argentière, 1975: (Thomas & Raiswell, 1984); South Cascade Lake, proglacial lake, 1970; Glacier de Tsanfleuron, Switzerland, mean bulk meltwater, 1990 [Fairchild, 1994]; Finsterwalderbreen, spring upwelling meltwaters, 199x [Wadham, 2000]



The relationships between Ca^{2+} and pCO_2 in bulk meltwaters from many glacial regions around the world are shown to plot within a boundary marked out by experimental extremes and equilibrium proportions. These boundaries are drawn on Figure 6.4.

Almost all data fits within the boundaries set by the extreme laboratory experiments, which model dissolution of a virtually calcium-free quartz vein (experiment 3) and of a marble (experiment 5). However, some data from Small River Glacier lies above the $\text{Ca}^{2+}/\text{pCO}_2$ relationship of experiment 5, and is close to the equilibrium relationship for pure calcite dissolution (experiment C). This glacier dominantly overlies limestone [Smart, 1996]. The mean result from Glacier de Tsanfleuron, also overlying carbonates [Fairchild, 1994], lies on the modelled trend of experiment 5.

Figure 6.4 Suggested global boundaries of the Ca^{2+} - pCO_2 relationship in bulk meltwaters draining glaciers



The upper limit of Ca^{2+} acquisition at a given pCO_2 is generally below the equilibrium level at 0°C . At pCO_2 levels of below $10^{-5.5}\text{M}$, Ca^{2+} concentrations in all bulk meltwaters were below 400neq/mL .

There is also a low limit of Ca^{2+} concentration, which decreases with increasing pCO_2 (point [A] on Figure 6.4). This boundary is determined by rock calcium content. High-calcium rocks in glacial conditions have been shown in this study to dissolve rapidly, exhausting existing dissolved CO_2 , and producing an ostensibly closed system due to the limiting factor of CO_2 -drawdown rates from the atmosphere, if accessible [REFS]. This low limit is approximately 300neq/mL Ca^{2+} at $10^{-5.5}\text{M}$ pCO_2 . Below this level of pCO_2 , carbonation-driven calcite dissolution is insignificant [REF].

A low Ca-content rock is generally dominated by silicate minerals, which dissolve at much slower rates than carbonates, due to lower solubilities and the formation of insoluble oxidised layers coating mineral surfaces (see CHAPTER X). Therefore, the overall requirement of CO_2 is less than in carbonate catchments, and in open-system environments the rate of CO_2 -drawdown can keep pace with the rate of CO_2 -removal by carbonation-driven dissolution. The theoretical extreme of this boundary would be zero Ca^{2+} at atmospheric pCO_2 ($10^{-3.5}\text{M}$). However it is unlikely that any catchment would be completely devoid of calcium, and are therefore unlikely to plot below the modelled trend of experiment 3 (point [D] on Figure 6.4). The slope of this lower boundary is effectively set by the the rate of dissolution of Ca^{2+} until dissolved CO_2 is exhausted. This slope was approximately mirrored in laboratory conditions, for example experiment C(o) (see Figure 5.10).

Values of $p\text{CO}_2$ above atmospheric levels in solutions are the result of the moving equilibrium between dissolved carbonate species and increasing $\text{Ca}^{2+}(\text{aq})$ and other dissolved metals. An explanation of this may be found in CHAPTER X. Therefore in open system waters with slow dissolution rates and/or long residence times, the concentration of dissolved CO_2 is dependent on the magnitude of carbonation-driven dissolution of Ca^{2+} and other metals (particularly Mg^{2+} in carbonate catchments). This reflects the modelled relationship between Ca^{2+} and CO_2 in experiment 3, which also appears to form the lower boundary in global meltwaters.

The upper boundary between points [B] and [C] is likely to be an artefactual one, set by the residence times of meltwaters in the catchments studied: most are fairly small glaciers with short residence times during the periods of study. Meltwaters with long residence times, such as those which are contained within the glacier overwinter, may reach much higher concentrations of Ca^{2+} . An example is the borehole sample shown in Figure 6.3a. Additionally, samples of spring upwellings at Finsterwalderbreen, Svalbard, reached Ca^{2+} concentrations as high as 2000neq/mL, with a $p\text{CO}_2$ of $10^{-2.9}\text{M}$ [Wadham, 2000] (see Figure 6.3d). The Ca^{2+} - $p\text{CO}_2$ relationship in these samples is still within the broad boundaries described above.

In summary, the [A]-[B], and [A]-[D]-[C] boundaries on Figure 6.4 are likely to be applicable for all meltwaters due to the physical constraints described above. The [B]-[C] boundary may describe an upper limit for many of the bulk meltwaters of global glaciers, whether cold-based, warm-based, or polythermal, during the main meltseason. This boundary is not applicable to meltwaters retained within glaciers for long periods of time.

6.2.4 Discussion of the limitations and necessary assumptions

a) Limitations of experiments

Table 6.7 shows a summary of the unavoidable differences between laboratory experiments and the subglacial environment. Experiments designed to simulate subglacial environments and the acquisition of solute in meltwaters cannot encompass all characteristics of field processes. The physical nature of the flow environment cannot be simulated whilst retaining the ability to isolate processes, and the effects of short-term temporal variations in parameters such as atmospheric access, turbulence, pooling, flow rate, acid addition, groundwater flow and so on can not be evaluated. These compromises in cross-conformity were necessary in

order to simplify the modelled processes of acquisition in order that individual processes may be isolated and quantified.

b) Assumptions and necessary simplifications

The calculations of bulk meltwater provenance using the experimental models presented in this section relied on assumptions of field conditions and simplifications of the relationships

Table 6.7 Unavoidable differences in physical and chemical conditions between laboratory simulation experiments and the subglacial environment.

Laboratory experiment	Subglacial environment
<ul style="list-style-type: none"> • Single body of water without input or output, except for fixed dilution experiments • Constant flow rate except for unmeasurable variations during sampling and filtration • Constant, but unmeasured, turbulence • Fixed periods of access to and isolation from the atmosphere • Solely lithogenic sources of cations • Limited sources of anions and acidity • No freezing/melting • No stagnation • Residence times limited to 28h • Fixed rock sources • Fixed rock-water ratios • Fixed dilution events (time, extent of dilution and dilution solution water quality) • Initial and dilution water is deionised 	<ul style="list-style-type: none"> • Continual addition of icemelt, snowmelt, groundwater, supraglacial meltwater and valleyside runoff, and loss by percolation into sediment, refreezing and pooling • Continual variation in flow rate • Periodic turbulence variations dependent on flow path • Sporadic periods of atmospheric isolation and access • Other potential sources of cations such as evaporites and aerosol • Various potential sources of anions and acidity such as aerosol, acidic pools, icemelt etc. • Continual potential for ice fractionation • Potential for pooling, allowing for reequilibration with the atmosphere, long residence times, freezing fractionation and precipitation events • Pooling may extend residence times to several days or months • Possible continual variation in type of rock in contact with water • Possible continual variation in rock-water ratios dependent on flow paths and discharge levels • Continual and variable dilution between waters of variable quality • Input meltwaters may contain significant protons, carbonate species and ions from glacier surface processes, fractionation etc.

between rock cation content and corresponding cation concentration in solution. These are summarised below.

1. Residence times are assumed to be greater than the period of rapid acquisition, with calculations based purely on Stage 2 acquisition. This is a reasonable assumption given studies of likely residence times of meltwater draining *Haut Glacier d'Arolla* (Nienow *et al.*, 1996a), but may not be true for all waters draining the glacier portal (dye tracing experiments measured residence times from channels beneath an upstream part of the glacier, but significant amounts of meltwater may be in contact with the glacier bed for much shorter periods, such as supraglacial streams and sidewall runoff that enter the glacier near the snout).
2. The influence of sulphide oxidation was assumed to be an instant phenomenon not affecting acid hydrolysis during Stage 2, based on the experience of dissolution experiments, but this suggestion is at odds with the suggestions of previous studies (e.g. Fairchild *et al.*, 1994)
3. No gypsum is assumed to be present in rocks, or precipitated and redissolved. However, PHREEQC inverse models demonstrated the potential for gypsum precipitation (see Section 5.6.3.2). Also, the possibility of gypsum being present in rock 2, and therefore in the catchment of *Haut Glacier d'Arolla*, could not be categorically disproved in this study (see Section 4.3.4.2).
4. Reasons for variations in the rate of CO₂-drawdown could not be established.
5. The effects of pyrite oxidation were evaluated using dominantly carbonate-rich rocks, and pyrite from an external source.
6. As experiments 3/4/6/7/8 were not carried out under reopened conditions, open system dissolution was inferred from the characteristics of experiments 1/2/5/9(r) and C(o).
7. Determinations of the mineralogical factor, $\Delta\text{Ca}^{2+}_{\text{MIN}}$, of mixtures between rock types were not established experimentally, and were assumed to be weighted averages between $\Delta\text{Ca}^{2+}_{\text{MIN}}$ values for individual experiments, but may in reality be likely to be nearer to 1, as the proportion of rock with the high $\Delta\text{Ca}^{2+}_{\text{MIN}}$ value may exert a greater influence on the overall chemical process.
8. Effects of sulphide oxidation were very varied on Na, K and Mg acquisition, so that a quantified model of acquisition of these elements could not encompass all potential controls

c) *Summary*

The suggestion that dissolution of a 32%:68% mix of rocks 1 and 2 could account for the mean field Ca^{2+} concentrations is corroborated by the calculations of Na and Mg provenance, which gave values close to the content of such a mix. In fact, the chemical similarity of Rocks 1, 5 and 9 mean that a 73%:27% mix of Rocks 2 and 5, or a 71%:29% mix of Rocks 2 and 9, also provide acceptable results.

The mean $\text{K}^+(\text{aq})$ field concentration was lower than those produced by the dissolution of all morainic rocks tested other than Rocks 8, 9 and pure calcite and pyrite. The mixture of these rocks could not provide a realistic explanation for the levels of Ca, Mg and Na encountered in the field, as the rock content of Mg and Na is similarly low in these rocks. It was apparent from Section 5.3.4 that the relationship between $\text{K}^+(\text{aq})$ and $\text{K}(\text{s})$ was complex, and although the proposed relationship fitted the laboratory data, it is possible that this relationship was circumstantial to the conditions of those experiments, and variations in factors not investigated, such as turbulence, adsorption effects of previously reacted sediment, etc, play an important part in the behaviour of K^+ dissolution in glacial environments.

The calculations of $\text{Na}(\text{s})$ and $\text{Mg}(\text{s})$ from mean field data, using Equations 5.10 and 5.12 and assuming 1 hour's dissolution, both showed closer results to the respective contents of a 32%:68% Rock 1&2 mixture. Although the variables involved are more numerous than presented in the Equation, for instance rock-water ratios, this may suggest that mean residence times are in the order of a few hours rather than 24 hours or more. This is supported by numerous other studies at *Haut Glacier d'Arolla*, including dye-tracing experiments (Nienow *et al.*, 1996a; Nienow *et al.*, 1996b).

6.3 METHODS OF SIMULATING SUBGLACIAL WEATHERING USING GEOCHEMICAL MODELLING COMPUTER PACKAGES

Models of the nature of the hydrological network draining *Haut Glacier d'Arolla* have been established using dye-tracing experimentation (Nienow *et al.*, 1996a; Nienow *et al.*, 1996b) and hydrograph/chemograph separation techniques (Brown and Tranter, 1990; Seagren, 1999). However, none of these techniques can establish the provenance of dissolution reactions. Estimations of phase transfer have hitherto relied on assumptions of the likely provenance of major ions in bulk meltwater, corroborated by estimations of geology based on optical petrological investigations of pre-reacted proglacial sediment (Brown *et al.*, 1996b).

The calculations of provenance of geologically parameterised laboratory experiments in Chapter 5 gave more direct evidence of the reactive mineralogy of sediment underlying *Haut*

Glacier d'Arolla. Simulation of solute acquisition in subglacial environments using direct mineralogical data may also be carried out by geochemical modelling (Fairchild *et al.*, 1999). Models such as the PWP (Plummer *et al.*, 1978) and B-D models (Dreybodt *et al.*, 1996) estimate rates of dissolution of carbonates in a H₂O-CO₂-CaCO₃ system (see Section 1.5.3). These have been applied to meltwater quality of glaciers in carbonate catchments (Fairchild *et al.*, 1999), but are less useful in predominantly silicate catchments where the overall dissolution equilibria are significantly altered (Raiswell, 1984). PHREEQC, based on ion-association aqueous models, can predict the effect of mixing of solutions and set mineralogy, and conduct inverse modelling, which finds sets of mineral and gas mole transfers that may account for composition differences between waters (Parkhurst, 1995).

To evaluate different forms of geochemical modelling and compare each method with the experimental models presented above, PHREEQC modelling was carried out by three different modelling approaches:

1. Modelled dissolution to equilibrium of a theoretical mix of sediment types (see Section 5.6.2.2).
2. Modelled proportional mixing of solutions in equilibrium with individual rock types.
3. Inverse modelling using field supraglacial and bulk meltwater as pre- and post-reacted data.

Models 1 and 2 simulate the mixing extremes of a subglacial geochemical system. Model 1 suggests that sediment is homogenised beneath the glacier, without spatial variations in geology, whereas model 2 suggests that rock types are spatially exclusive in the subglacial drainage system, with isolated equilibrium dissolution of individual rock types followed by equilibrium mixing of the two solutions. This should not be confused with mixing of channelised and distributed flow waters. This is examined in model 3, where the phase transfers necessary to accommodate the observed chemical evolution between supraglacial meltwater “input” and bulk meltwater are modelled.

None of these models describe the spatial and temporal variations within the glacier, but rather describe the overall transfers between phases in the glacial hydrological network. Models 1 and 2 rely on the inferences of theoretical mineralogy of rocks beneath the glacier made in Section 6.2, and evaluate the nature of rock-water interactions with respect to equilibrium conditions. Model 3 determines the extent of dissolution of suggested minerals required to evolve the solution chemistry from supraglacial to bulk meltwater, irrespective of equilibrium conditions, serving as a comparison with the experimental models.

a) Model 1: modelled dissolution of mixed sediment

Section 5.6.2 showed that equilibrium modelling of pure pyrite and calcite closely correlated with experimental results, but modelling of mixed sediment dissolution using PHREEQC differs greatly from experimental results due to the greater importance of kinetic factors that can not be taken into account. Similarly, modelling dissolution using the input mineralogy shown in Table 6.8 produced a model solution chemistry distinctly different from that modelled using laboratory rate equations (Table 6.1) and those observed in bulk meltwaters of *Haut Glacier d'Arolla* (Table 6.9).

Table 6.8 Input mineralogy of a theoretical 32%:68% mix of rocks 1 and 2, for PHREEQC equilibrium modelling.

Mineral	Rock 1 (M)	Rock 2 (M)	32:68 mix (M)
calcite	0.026	-	5.2×10^{-3}
pyrite	3.3×10^{-4}	3.3×10^{-4}	3.3×10^{-4}
haematite	2.5×10^{-4}	2.5×10^{-4}	2.5×10^{-4}
muscovite	2.6×10^{-3}	-	5.2×10^{-4}
quartz	6.7×10^{-4}	-	1.3×10^{-4}
K-feldspar/microcline	7.2×10^{-5}	3.6×10^{-4}	3.0×10^{-4}
plagioclase	-	0.031*	0.025
anorthite	-	0.029*	0.023
diopside	-	3.2×10^{-3}	2.6×10^{-3}
forsterite	-	2.8×10^{-3}	2.2×10^{-3}
tremolite	-	8.6×10^{-4}	6.88×10^{-4}
pCO ₂ (g)	5×10^{-4}	5×10^{-4}	5×10^{-4}
pH	7.4	7.4	7.4
O ₂ (aq)	2 mg/L	2 mg/L**	2 mg/L**

It is of note that these results are produced by modelling reaction to equilibrium, and it is clear from the relationships between the rock content and extent of dissolution of Na, K and Mg, that equilibrium is not reached, with the number of surface sites and surface-exchange processes restricting dissolution of these elements. The modelled concentration of Ca²⁺ closely reflects that of field and laboratory concentrations, which were clearly governed by equilibrium processes. The difference between Ca²⁺ acquisition and other cations may be due in part to the relatively rapid dissolution kinetics of calcite, which creates a premium of protons, and retards the acquisition of aluminosilicate minerals. Additionally, Raiswell (1984) suggests that the dissolution of calcite can supply a larger dissolved load than aluminosilicate dissolution, as the latter requires a larger amount of H₂CO₃ derived from CO₂-drawdown.

Table 6.9 PHREEQC-modelled solution chemistry of a theoretical 32%:68% mix of rocks 1 and 2, and comparison with mean 1995 field data.

Species	Rock 1+2 (neq/mL)	Rock 1+2 (neq/mL) (forced pCO ₂)	Volume-weighted mean 1995 field data
Ca ²⁺	69	320	320
HCO ₃ ⁻	64	3300	250
CO ₃ ²⁻	370	94	-
Na ⁺	1200	122	15
K ⁺	-	-	10
Mg ²⁺	0.02	3100	27
SO ₄ ²⁻	122	33	97
pCO ₂	10 ^{-7.5}	10 ^{-3.5}	10 ^{-2.7}
pH	11.0	8.6	7.23

b) Model 2: modelled equilibrium mixing of individual solutions

Solution mixing modelling was carried out using the method described in Section 2.5.2. Chemical data for experiments 1(c) and 2(c) after 24h closed system dissolution were input as separate solutions, and then allowed to mix in 32%:68% proportions to a fixed log pCO₂ of -3.5, emulating evolution under a reopened system. The model was repeated for experiments 1(r) and 2(r) after a further 4h dissolution under open access to the atmosphere. This model emulates conservative mixing between the two solutions, as sediment is not assumed to be in the solution at the time of mixing. The main results are shown in Table 6.10.

The closed system concentrations of Ca²⁺ and HCO₃⁻ were lower than those produced in bulk meltwater draining *Haut Glacier d'Arolla*. However, modelled mixing of open system experiments produced concentrations of major ions, alkalinity and values of pH, pCO₂ and SI(calcite) that were within the parameters of bulk meltwater chemistry.

This model shows that a mixture of solutions dissolving rocks 1 and 2, in the proportions suggested by experimental calculations, could describe the bulk meltwater chemistry observed at *Haut Glacier d'Arolla*, but that a period of open system dissolution both prior to mixing, and subsequent to mixing, was necessary for this to occur. This is not an unreasonable scenario.

Table 6.10 Modelled chemistries of mixed solutions of experiments 1(c) and 2(c) after 24h closed system dissolution, and 1(r) and 2(r) after 4h reopened dissolution, in the proportion 32%:68%.

Element in solution	Model 1(c)+2(c) (neq/mL)	Model 1(r)+2(r) (neq/mL)
HCO ₃ ⁻	122	312
CO ₃ ²⁻	0.2	1.1
Ca ²⁺	161	345
Fe ^{total}	2.3	7.9
K ⁺	45	55
Mg ²⁺	17	45
Na ⁺	6.1	12
SO ₄ ²⁻	132	128
Sr ²⁺	2.3	1.6
DO ₂	5.0mg/L	3.4mg/L
H ₄ SiO ₄	4.3mg/L	4.3mg/L
pH	7.3	7.7
pCO ₂	-4.9	-3.5
SI(calcite)	-2.9	-1.7

c) *Model 3: inverse modelling of field data*

Inverse modelling was carried out using PHREEQC to predict the mineral dissolution required to modify the solution chemistry of a sample of supraglacial meltwater collected at 13:00 on 31 July 1995, to that of a sample of bulk meltwater taken four hours later. The methodology and limitations of inverse modelling are described in Section 2.5.4. The two solutions, and the minerals allowed to dissolve and precipitate are shown in the input file (Appendix A; PHREEQC input file A-4). Given the allowed parameters, three possible models were identified that could satisfy the observed modification of solution chemistry (Table 6.11). All three models predict a similar amount of calcite dissolution (12-14mg/L) and pyrite oxidation (2.5mg/L). The remaining acquisition varies between the models, with varying proportions of biotite, plagioclase, microcline and olivine used to describe the evolution of meltwater chemistry beneath a glacier. Precipitation products included Ca-montmorillonite and amorphous Fe(OH)₃, with precipitated dolomite also predicted in model 1.

The arbitrary selection of plagioclase anorthite content (An_n) and olivine forsterite content (Fo_n) values, given the lack of experimental data, must be emphasised at this point.

The three models are consistent in predicting the domination of calcite dissolution, with abundant plagioclase dissolution and significant pyrite dissolution. These results do not allow for gypsum dissolution or precipitation, so the sulphate source is restricted to pyrite. This is consistent with previous studies, but the results of inverse modelling of laboratory pyrite/calcite dissolution experiments (Section 5.6.2.2) showed that precipitation of gypsum may occur.

Table 6.11 Modelled transfers of minerals into (+) and out of (-) solution during evolution from supraglacial to bulk meltwater at *Haut Glacier d'Arolla* (31 July 1995). Percentages of total transfer into solution are shown for each model.

Phase	Model 1 (mg/L)	%	Model 2 (mg/L)	%	Model 3 (mg/L)	%
calcite	+14	53%	+13	55%	+12	52%
dolomite	-2.8					
Ca-montmorillonite	-6.0		-4.7		-6.0	
biotite	+4.0	15%			+1.9	8%
kaolinite						
plagioclase (An ₃₇)	+5.6	22%	+4.3	18%	+5.6	24%
microcline			+2.1	9%	+1.4	6%
olivine (Fo ₅₀)			+1.8	8%		
diopside						
tremolite						
pyrite	+2.5	10%	+2.5	11%	+2.5	11%
Fe(OH) ₃ (a)	-2.2		-3.3		-2.2	
log CO ₂ (g) (M)	-4.0		-4.1		-4.0	
O ₂ (g)	+2.5		+2.6		+2.5	

The addition of gypsum as a potential mineral source and precipitation product adds eight further possibilities of provenance (Table 6.12). Models 7, 10 and 11 demonstrate significant gypsum precipitation, whereas models 4, 5, 6, 8 and 9 demonstrate gypsum dissolution in place of pyrite dissolution. These models are unlikely, as they either require high precipitation levels (unlikely at low temperatures) or reaction significant amounts of gypsum. It may be possible that small amounts of gypsum may be precipitated under certain circumstances, such as if meltwaters become isolated from the flow network, and become frozen, producing supersaturation with respect to gypsum. These precipitates would then be readily dissolved if they regained contact with subglacial meltwater.

Table 6.12 Additional modelled transfers of minerals into (+) and out of (-) solution during evolution from supraglacial to bulk meltwater at *Haut Glacier d'Arolla* (31 July 1995), involving phase transfer of gypsum. Percentages of total transfer into solution are shown for each model.

Phase	model 4	%	model 5	%	model 6	%	model 7	%	model 8	%	model 9	%	model 10	%	model 11	%
calcite	+9.6	37	+9.6	36	+8.7	36	+22	56	+8.1	34	+8.1	34	+25	57	+22	58
dolomite	-2.8		-2.8										-2.8			
gypsum	+7.0	27	+7.1	27	+7.1	30	-16		+7.1	29	+7.0	29	-19		-15	
Ca-montmorillonite	-6.0		-6.0		-4.7		-6.0		-6.0		-6.0		-6.0		-4.7	
biotite	+4.0	15	+4.0	15			+1.9	5	+1.8	7	+1.9	8	+4.0	9		
kaolinite																
plagioclase An ₃₇	+5.6	21	+5.6	21	+4.3	18	+5.6	14	+5.6	23	+5.6	23	+5.6	13	+4.3	11
microcline					+2.1	9	+1.4	4	+1.4	6	+1.4	6			+2.1	6
olivine (Fo ₅₀)			+0.07	0.3	+1.8	8			+0.07	0.3					+1.8	5
diopside																
tremolite																
pyrite	+0.05	0.2					+8.2	21			+0.05	0.2	+9.1	21	+7.8	21
Fe(OH) ₃ (a)					-1.1		-7.3						-8.1		-8.1	
log CO ₂	-3.8		-3.8		-3.9				-3.9		-3.9					
O ₂ (g)	+0.05		+0.003		+0.09		+8.2		+0.003		+0.05		+9.1		+7.9	

The presence of gypsum in contact with glacial meltwaters therefore provides a sulphate source without the need of an oxidising agent to aid sulphide oxidation, whereas gypsum

precipitation may allow the dissolution of calcite without the need for CO₂-drawdown. Both these effects have important implications for the interpretation of meltwater data.

6.4 APPLICATION OF EXPERIMENTAL INVESTIGATIONS OF KEY INDICATOR SPECIES TO FIELD DATA

Analysis of bulk meltwater chemistry at *Haut Glacier d'Arolla* and elsewhere has generally only been concerned with major elements. The only published trace element data for the catchment (Brown and Fuge, 1998a; Brown and Fuge, 1998b), was collected over a diurnal cycle, with 18 samples collected between 10:00, 17/08/1996 and 10:00 the following day. This dataset cannot therefore be said to be representative of an entire field season. Nonetheless, it is to date the most useful set of parameters by which to judge the applicability of laboratory data in glacial environments. Table 6.13 compares mean diurnal trace element concentrations and mean laboratory experiment concentrations over all time increments and both open- and closed-system conditions. For more detailed experimental trace element data analysis, see Section 4.3.5.

Table 6.13 Comparison of mean diurnal major and trace element concentrations (August 17-18, 1996) and mean laboratory experiment concentrations (all time increments). Data in ng/mL. Comparable datasets are marked with a ✓, incompatible datasets are marked with a ✗. Data forms basis for (Brown and Fuge, 1998a; Brown and Fuge, 1998b).

species	mean concentration (BMW 1996)	mean concentration (mean all lab)	
NO ₃	60 ±18	180 ±240	✓
Cl	640 ±285	610 ±730	✓
SO ₄	910 ±330	1100 ±2600	✓
Mg	350 ±73	120 ±130	✗
Al	130 ±21	77 ±31	✗
Ca	4000 ±1400	4800 ±2700	✓
Ti	5.7 ±1.6	14 ±7	✗
Mn	5.4 ±1.1	6.7 ±5.2	✓
Fe	460 ±81	170 ±76	✗
Co	0.16 ±0.07	1.2 ±3.0	✗
Ni	0.91 ±0.29	2.1 ±1.2	✗
Cu	0.63 ±0.47	1.5 ±0.8	✓
Zn	0.85 ±0.78	5.2 ±7.4	✗
Rb	0.45 ±0.23	3.5 ±2.3	✗
Sr	14 ±3.8	42 ±53	✗
Ba	0.98 ±0.56	0.71 ±0.43	✓
Pb	0.23 ±0.14	3.1 ±3.0	✗
U	0.62 ±0.28	0.03 ±0.06	✗
HCO ₃	14000 ±4500	13000 ±9100	✓
pH	8.6 ±0.3	8.7 ±1.1	✓
Sr/Ca	0.007 ±0.001	0.0087 ±0.0071	✓

Unsurprisingly, differences between concentrations of certain elements in the field and in the laboratory were evident. Whilst concentrations of Mg, Al, Fe and U were significantly higher in bulk meltwaters than in laboratory experiments, Ti, Co, Ni, Cu, Zn, Rb, Sr and Pb were significantly higher in laboratory experiments. A possible reason for the high field Mg, Al, Fe and possibly U concentrations is the relatively high suspended sediment concentrations in bulk meltwater, some of which may have been of a small enough grain size to pass through the filtration process and therefore be included in the ICPMS analysis. Since Mg, Al and Fe are all abundant elements in the solid phase, but of relatively low solubility, this would enhance their apparent concentrations.

6.4.1 Comparison of modelled speciation between experimental simulations, bulk meltwater and average river data

Speciation defines the form in which ions are present in solution, i.e. free ions, complexes, ion pairs, acid molecules and so forth (see Section 1.6.2). Modelling of speciation using PHREEQC was carried out using data of average river water (Henderson, 1976; main source Drever, 1982; additional data Ward, 1995), average bulk meltwater (main source Brown and Fuge, 1998a, additional data: this study), and mean laboratory experiments (this study) (Table 6.14). Excess silica was assumed in all cases, and initial $O_2(aq)$ levels were set as 10mg/L, due to a lack of individual data. For details of methodology, see Section 2.5.1.

Trace element speciation in laboratory experiments appears to follow a similar pattern to both mean bulk meltwater draining the *Haut Glacier d'Arolla*. Although minor variations exist, it appears that the dominant species of all elements is the same in both field and laboratory data, due to the parameterisation of the laboratory experiments using conditions and materials appropriate to the *Haut Glacier d'Arolla* catchment. Therefore, interpretation of comparisons between the two datasets should not be complicated by the influence of complex variation. However, the average river water data showed significant differences in the speciation of a number of elements, such as Zn, V, Fe and Al. The effects of speciation differences were discussed in Sections 1.6 and 5.2, and the differences indicated here illustrate that speciation does need to be considered if the role of trace metals in meltwater chemistry is to be elucidated.

6.4.2 Evaluation of key indicator species by comparison of experimental and bulk meltwater data from *Haut Glacier d'Arolla*.

Potential key indicators of solute provenance were identified in Chapter 5 (Table 4.17). Analysis of bulk meltwaters over the diurnal period 09:00 17/08/96 to 10:00 18/08/96 included analysis of some of these elements (U, Pb, Zn, Ti, Cr, Rb, K, Ca, Sr, SO₄, Co, Na, Cl, Re, NO₃), but data for others were not reported (REE, W, Re, Mo, As, Th, Hg, I) (Brown and Fuge, 1998a). The use of these species as key indicator species is evaluated in this section.

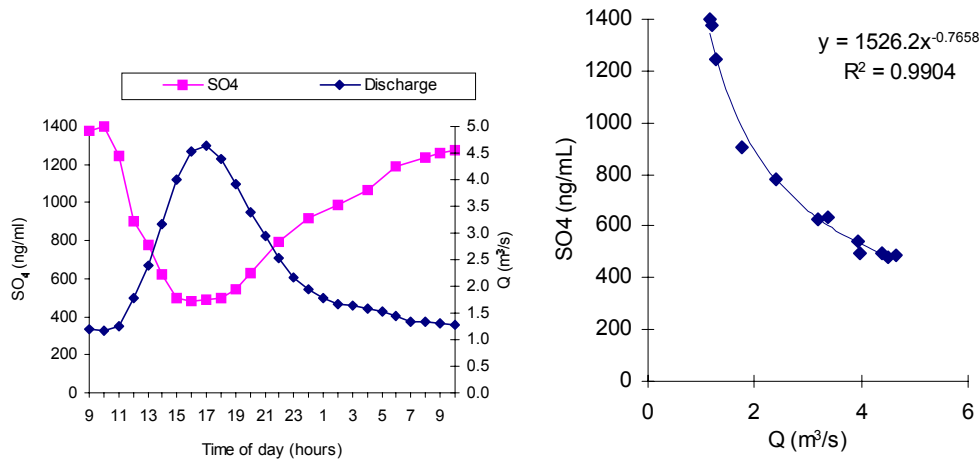
Table 6.14 Dominant speciation of major, minor and trace elements in various waters. Average river water data from Drever (Henderson, 1976; 1982; additional data Ward, 1995). Average bulk meltwater data from Brown (1998a), (additional data: this study). Dashes indicate no data available

	dominant species	average river data		average bulk meltwater		mean laboratory experiments	
		log M	% species	log M	% species	log M	% species
Al	Al(OH) ₄ ⁻	-7	25	-7	4	-6	61
	Al(OH) ₃	-6	74	-6	96	-6	39
Ba	Ba ²⁺	-7	100	-8	100	-9	100
C	HCO ₃ ⁻	-4	98	-4	98	-4	96
Ca	Ca ²⁺	-4	98	-4	100	-4	99
Cl	Cl ⁻	-4	100	-5	100	-5	100
Cu	Cu(OH) ₂	-7	94	-8	100	-9	100
Fe	Fe(OH) ₄	-7	53	-5	77	-6	88
	Fe(OH) ₃	-7	31	-6	19	-7	11
	Fe(OH) ₂ ⁺	-7	16	-7	4	-8	1
K	K ⁺	-5	100	-5	100	-5	100
Mg	Mg ²⁺	-4	98	-5	100	-5	99
Mn	Mn ²⁺	-7	98	-7	100	-7	99
N	NO ₃ ⁻	-5	100	-6	100	-6	100
Na	Na ⁺	-4	100	-5	100	-5	100
Ni	Ni ²⁺	-9	3	-9	8	-10	3
	NiCO ₃	-8	95	-8	92	-8	96
Pb	Pb ²⁺	-11	1	-11	3	-11	1
	PbCO ₃	-9	93	-9	74	-9	79
	Pb(OH) ⁺	-10	4	-10	20	-9	15
Rb	Rb ⁺	-8	100	-8	100	-8	100
S	SO ₄ ²⁻	-4	95	-5	98	-6	97
Si	H ₄ SiO ₄	-5	99	-5	99	-5	96
Sr	Sr ²⁺	-7	100	-7	100	-7	100
U	UO ₂ (CO ₃) ₂ ²⁻	-10	59	-9	67	-11	64
	UO ₂ (CO ₃) ₃ ⁴⁻	-10	39	-9	26	-11	34
Zn	Zn ²⁺	-7	43	-9	31	-9	11
	Zn(OH) ₂	-8	13	-8	57	-8	76
	ZnCO ₃	-7	34	-9	10	-9	9

a) *Sulphate and uranium as indicators of sulphide oxidation*

SO₄²⁻ concentrations in laboratory experiments were shown to be strongly influenced by pyrite content of sediment, with unusually high concentrations resulting from dissolution of Rock 2 (Section 5.5.1). Calculations of provenance using PHREEQC inverse modelling also identified gypsum as a potential source of SO₄²⁻ (Section 6.3c).

Figure 6.5 Concentrations of SO_4^{2-} in bulk meltwater draining *Haut Glacier d'Arolla* between 09:00, 17 August and 10:00, 18 August, 1996. Discharge is also shown.



Sulphate concentration displayed a very close inverse relationship with discharge ($r=1.00$, $n=20$), consistent with data for previous years (see Section 3.5.X) (Figure 6.5). This suggests that sulphide oxidation and/or sulphate dissolution were not important processes in quickflow waters, so that a straightforward dilution effect occurs.

The diurnal pattern of uranium is close to that of both that of SO_4^{2-} ($r=0.93$, $n=18$) and Ca^{2+} ($r=0.87$, $n=18$) (Figure 6.5), but short-term increases in concentration at 18:00, 02:00, 06:00 and 09:00 were concurrent with peaks in Ca^{2+} concentration, suggesting a common provenance or control, which did not affect the concentration of SO_4^{2-} (Figure 6.6).

Figure 6.6 Concentrations of U^{total} , SO_4^{2-} and Ca^{2+} in bulk meltwater draining *Haut Glacier d'Arolla* between 09:00, 17 August and 10:00, 18 August, 1996.

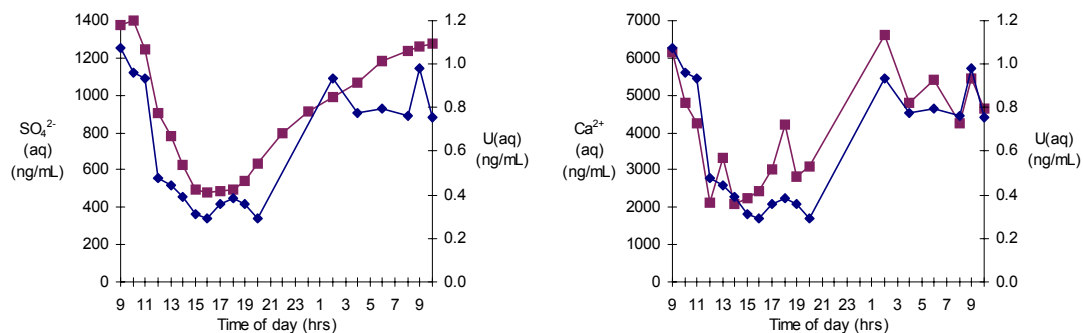
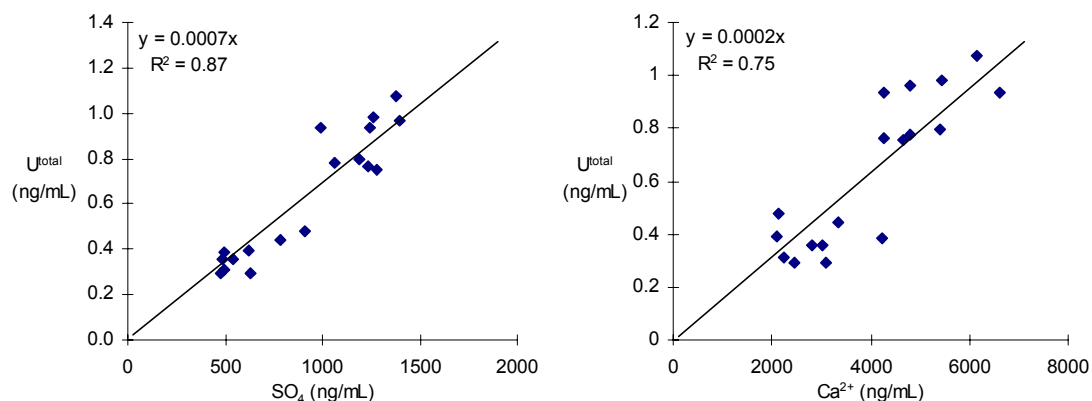


Figure 6.7 Concentrations of U^{total} in bulk meltwater draining *Haut Glacier d'Arolla* between 09:00, 17 August and 10:00, 18 August, 1996, plotted versus SO_4^{2-} and Ca^{2+} .

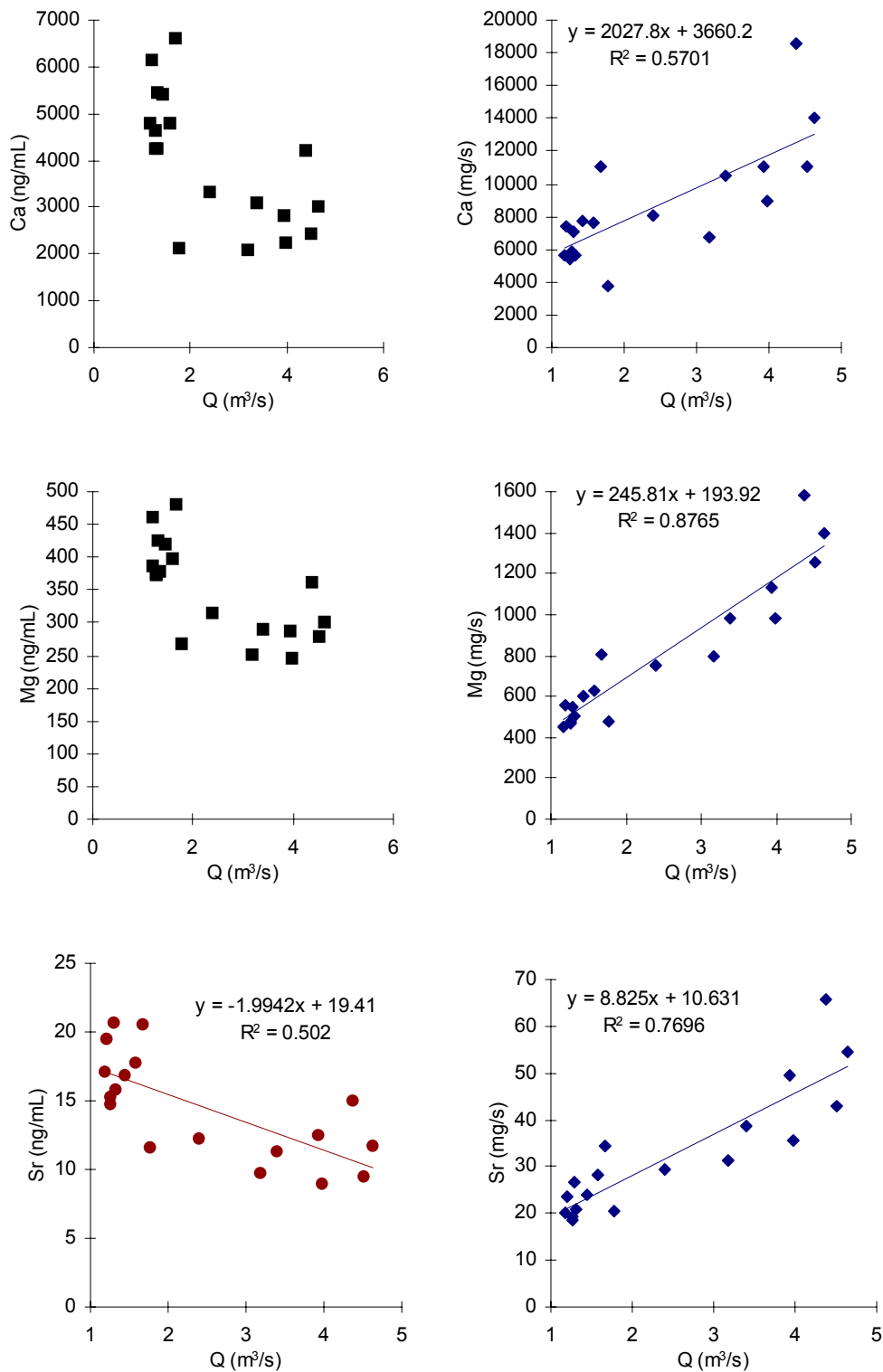


The chemical signature of U in bulk meltwater therefore reflects its behaviour in the laboratory experiments, in which U was only significantly present in solution when both pyrite and calcite were present in the reactive sediment. The peak levels in bulk meltwater are similar to the levels in such laboratory experiments, at around 1.0ng/mL. These investigations suggest that sulphide minerals are the dominant source of SO_4^{2-} , since no morainic rocks could produce equivalent U levels without pyrite being added. This may preclude gypsum being a significant source of SO_4^{2-} in bulk meltwater.

b) Strontium and magnesium as indicators of carbonate dissolution

With the exception of U and SO_4 (discussed above), variations in element concentration linked to discharge were only significant in the data for Ca^{2+} , Mg^{2+} , Ba^{2+} and Sr^{2+} . Strontium, magnesium and calcium have well-documented close inter-relationships in bulk meltwater data from *Haut Glacier d'Arolla* (Brown and Fuge, 1998a). This was thought to show that Mg and Sr share provenance with Ca (Brown and Fuge, 1998a). This study has shown that Sr and Ca have a similar provenance (although not exactly so), but showed a poor relationship between Mg and Ca rock content in analysed morainic rocks (see Chapter 3). The correlation between Ca^{2+} and Mg^{2+} concentrations in experimental solutions was significantly higher than in the rock traces, particularly in open-system conditions, and demonstrated that the relationship between Ca^{2+} and Mg^{2+} is not necessarily an indicator of common provenance, but may demonstrate that magnesium in carbonate minerals is more soluble than from other minerals. The use of (Ca+Mg) as an indicator of carbonate provenance in mass-balance investigations (e.g. Fairchild *et al.*, 1994; Brown *et al.*, 1996a) must therefore be treated with caution when studying non-carbonate catchments.

Figure 6.8 Concentrations and flux of calcium, magnesium and strontium in bulk meltwater draining *Haut Glacier d'Arolla* between 09:00, 17 August and 10:00, 18 August, 1996

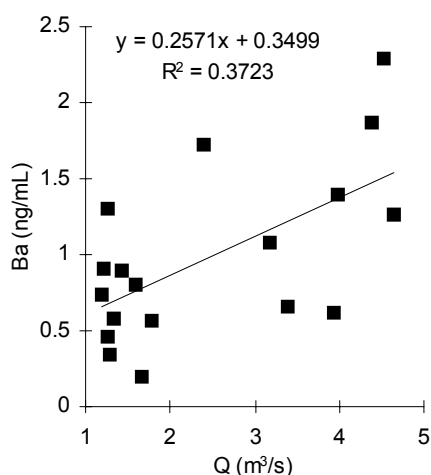


c) Other potential indicators of sulphide oxidation

Barium is the only analysed trace element that was positively correlated with discharge. Figure 6.9 shows that the correlation, although significant, was rather weak, and

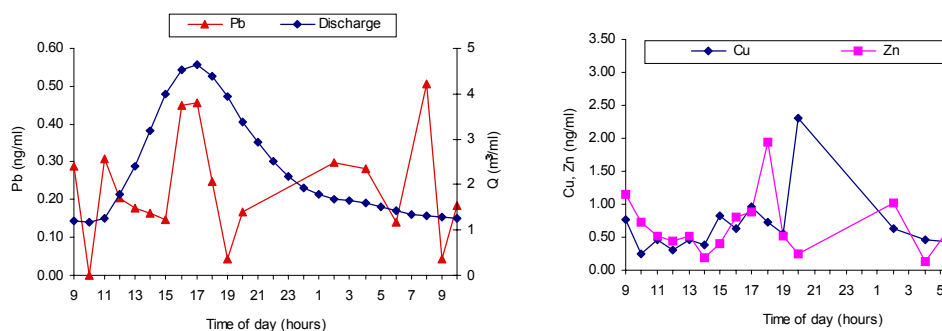
concentrations are very low, reflecting the range of concentrations achieved in laboratory experiments. It is possible with many less soluble elements that analysed solution concentrations may be affected by ionisation of microparticles which passed through the filtration process, during the analytical procedure.

Figure 6.9 Concentrations of Ba^{2+} in bulk meltwater draining *Haut Glacier d'Arolla* between 09:00, X August and 10:00, Y August, 1996.



Lead and zinc concentrations in bulk meltwaters were consistently lower than those of the laboratory experiments, and both these and Cu showed particularly erratic fluctuations over the diurnal period (Figure 6.10). None of the elements showed a discernable diurnal cycle, and it would appear that analytical variation may be too great to gain useful information from the data.

Figure 6.10 Concentrations of Pb^{2+} , Cu^{total} and Zn^{2+} in bulk meltwater draining *Haut Glacier d'Arolla* between 09:00, X August and 10:00, Y August, 1996.



d) *Inter-elemental associations*

There were certain temporal associations between elements in individual samples, as shown by the increases in Cr, Ni and Ti at 02:00 and 09:00 in Figure 6.11. However, each element also showed individual variations, for example Cr at 18:00 and Ti at 16:00. Therefore, ratios

between each element are often quite varied (Figure 6.12). With often no pattern of variation between elements, it is clear that a much larger database of field samples is necessary to be able to discern noise from temporal variation.

Figure 6.11 Concentrations of Ni^{2+} , Cr^{total} and Ti^{total} in bulk meltwater draining *Haut Glacier d'Arolla* between 09:00, X August and 10:00, Y August, 1996.

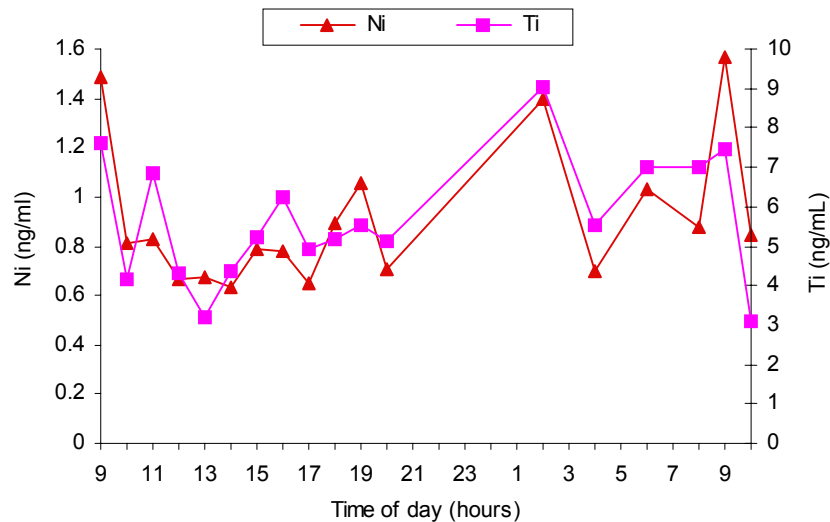
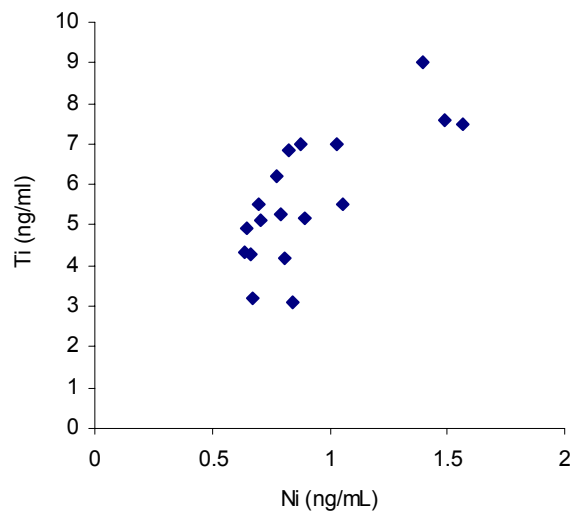


Figure 6.12 Relationship between Ni^{2+} and Ti^{total} in bulk meltwater draining *Haut Glacier d'Arolla* between 09:00, X August and 10:00, Y August, 1996.



6.5 CONCLUSION

The modelled relationships between solute acquisition and various chemical controls, presented in Chapter 5, are compared with the water quality of bulk meltwater draining *Haut Glacier d'Arolla* between 1989 and 1995. The field calcium/pCO₂ relationships consistently

plotted within a range encompassed by the laboratory experiments dissolving morainic rocks, and following a similar trend to the modelled regression.

The experimental model of calcium acquisition was iterated for different combinations of mixtures of morainic rocks until the resultant trend represented a visual “best-fit” through the points representing the maximum and minimum discharge $\text{Ca}^{2+}/\text{pCO}_2$ ratios of the 1995 field sampling period. Further iterations were made to find mixtures that represent the ratio at the seasonal maximum and minimum Ca^{2+} concentrations. Consistently, mixtures of diopside marble (rock 1) and serpentinised olivine gabbro (rock 2) in proportions between approximately 30:70% and 40:60% described the relationships between Ca^{2+} and pCO_2 encountered in the field. Fitting the same ratios into the equations of sodium also provided consistency between laboratory and field determinations. However, magnesium and potassium rock provenance determinations using field data were not consistent with the rock mixture ratios suggested by calcium acquisition modelling. This was because the datasets for Mg^{2+} and K^+ concentrations between laboratory and field conditions were incompatible. It is suggested that adsorption of K^+ may be greater in the field than in laboratory experiments, and that Mg^{2+} may be indirectly affected by sulphide oxidation and longer periods of open system weathering than was undertaken in laboratory experiments.

Caution was expressed as to the qualitative nature of the laboratory models when interpreting weathering within subglacial channels, as conditions of laboratory and field environments are difficult to equate (e.g. Schnoor, 1990; Drever and Clow, 1995). Despite this, the indication of mineralogical phase transfer suggested by the experimental models are consistent with the predictions of inverse modelling using PHREEQC presented in this chapter, although alternative scenarios are also demonstrated.

Variations in trace metal speciation between meltwater draining *Haut Glacier d’Arolla* and river water averages highlighted the need for a knowledge on trace metal speciation if these elements are to become useful indicators of solute provenance and processes of chemical weathering. The necessity for large datasets in field investigations is also highlighted, due to high experimental artifactual error.

7. CONCLUSIONS

7.1 INTRODUCTION

Chemical weathering in glacial environments occurs at an enhanced rate in comparison with global average terrestrial weathering rates. This has important implications for the understanding of the role of the cryosphere in global chemical cycles, particularly those pertaining to storage and release of greenhouse gases involved in chemical weathering, such as carbon dioxide.

This thesis has investigated processes of solute acquisition in subglacial environments. The objective of this research has been to develop the understanding of chemical processes occurring within the hydrological network of an alpine glacier, so that more informed interpretation of field-collected meltwater quality data may be carried out.

Previous studies of bulk meltwater chemistry have suggested numerous controls on the rates of solute acquisition in subglacial environments, including proton availability, access to atmospheric gases, solute provenance, meltwater residence times and drainage dynamics. The limited amount of related laboratory studies carried out previous to this study had begun to isolate the controls on solute acquisition.

The approach of this study has been three-fold. Firstly, a series of investigations was carried out to identify the range of compositions of solid, liquid and gas phases involved in chemical interactions in a glacial environment. Secondly, to isolate and determine processes, rates and controls on solute acquisition in subglacial environments. Thirdly, to elucidate the role of minor and trace elements in subglacial weathering regimes, and investigate their potential use as indicators of solute provenance.

Parameterisation investigations involved collection of morainic rock and meltwater samples from *Haut Glacier d'Arolla*. Morainic rock was analysed petrologically to identify major rock types and mineralogy, and by analysis of rock digestions to determine the range of rock chemistry. Meltwater samples were analysed for major ions and chemical properties to generate detailed time-series data on seasonal and diurnal ranges of solute load. The data of morainic rock and meltwater chemistry was used to design a suite of parameterised laboratory experiments using materials of known composition, in conditions simulating solute acquisition in subglacial environments. The effects of access to atmospheric gas, mineralogical variations and dilution were individually investigated. Results from these experiments enabled the relationships between individual controls on solute acquisition to be

modelled. Application of the models to bulk meltwater quality data enabled the likely reactive chemistry of rocks and sediment to be constrained, based on the rock types investigated, and therefore the relative importance of solute provenance in comparison to atmospheric and hydrological controls, to be identified.

Detailed study of the behaviour of minor and trace elements investigated variations in solubility, mobility, speciation and common-ion relationships with provenance and chemical regime. These investigations identified a number of elements that may be useful in identifying major solute processes in glacial environments, with necessary caution expressed due to the relatively low concentrations of the majority of these species compared to global averages, and the necessity for a detailed understanding of speciation of these species in order to constrain the somewhat unpredictable nature of variability often encountered.

7.2 ESTABLISHMENT OF A SET OF GEOCHEMICAL DATA ALLOWING PARAMETERISATION OF LABORATORY INVESTIGATIONS

The datasets presented in this study represent a large step forward in the range of data available for studies of subglacial solute acquisition. Specifically, this is the first study to provide chemical data of unreacted sediment, meltwater and laboratory experiments, and is also the first study to consider trace elements in detail. The importance of establishing the link between reactive sediment and post-reacted solutions is that it allowed direct observations of solute provenance relationships to be considered.

7.2.1 Rock mineralogy and chemistry

Petrological investigations of freshly-crushed rocks sampled from medial moraines on *Haut Glacier d'Arolla* have revealed that reactive minerals such as calcite, are significantly more concentrated in unweathered rocks from the catchment than from proglacial outwash sediment. The major mineralogy of the rocks at *Haut Glacier d'Arolla* is dominated by quartz and feldspar, with significant amounts of pyroxene, micas, chlorite, carbonates and secondary mineralization. Feldspar, carbonate and pyroxenes are more abundant than had previously been identified (e.g. Brown, 1991).

The chemistry of rocks sampled from *Haut Glacier d'Arolla* moraine material is dominated by silica, with calcium and sodium the dominant metal cations. Three of nine rocks analysed contained in excess of 20% calcium. Potassium, magnesium and iron contribute less than 2% (mean) each to mean rock content. Trace elements contribute less than 0.2% of the total rock

content. Many trace elements were identified that consistently associate with specific major elements and/or rock types.

7.2.2 Bulk meltwater chemistry

The chemistry of sampled bulk meltwater draining *Haut Glacier d'Arolla* over the latter part of the 1995 meltseason showed pronounced diurnal variation, and seasonal evolution of chemical trends. All major dissolved species showed strong, inverse correlation with discharge level, which in turn is inversely proportional to residence time (Nienow *et al.*, 1996). This indicates the difference in solute concentration in delayed flow meltwaters, with relatively long residence times, and quickflow meltwaters, with relatively shorter residence times. Variations in $\text{SO}_4^{2-}/(\text{SO}_4^{2-}+\text{HCO}_3^-)$ with discharge indicate that sulphide oxidation, indicated by SO_4^{2-} concentrations, does not occur to the same magnitude in the post-mixing environment as carbonation-driven acid hydrolysis, indicated by HCO_3^- , and is therefore more confined to the distributed drainage network than other processes of solute acquisition. The relationship between Ca^{2+} and SO_4^{2-} suggests that sulphide oxidation-driven carbonate dissolution accounts for a significant proportion of the calcite dissolved in subglacial environments, but that carbonation-driven dissolution is also an important process. However, a significant positive correlation between pCO_2 values and SO_4^{2-} concentration suggests that protons supplied by SO_4^{2-} may reduce the extent of carbonation reactions, rather than purely provide additional potential reaction.

In addition to supraglacial and bulk meltwater quality over diurnal and seasonal time scales, additional parameters were quantified, specifically water quality variations between portal channels at the glacier snout, and supraglacial meltwater quality. Significant variation in meltwater between the main glacier portals was identified, consistent with cross-glacier variations in the mineralogy of morainic rocks. Samples of supraglacial meltwater with ionic concentrations similar to those of bulk meltwater were also identified, indicating the possibility of pressure-induced movement of small amounts of meltwater from the glacier base to the surface.

7.3 EXPERIMENTAL SIMULATIONS OF SUBGLACIAL SOLUTE ACQUISITION

Increases in cationic concentration with time were shown to be relatively small after a period of rapid acquisition following initial emplacement of the sediment in deionised water (“Stage 1”). This initial period generally lasted less than one hour. Under closed system conditions,

acquisition of major cations was virtually nil in Stage 2. Anions other than NO_3^- also showed this pattern of dissolution.

Calcium and bicarbonate were the dominant dissolved species in most experiments, accounting for a mean 85% of total (analysed) dissolved species by equivalent units. Sulphate concentrations were only significant in experiment 2 (dissolving olivine gabbro), and experiments 1P/5P/9P, where crushed pyrite was artificially added.

Calcium acquisition was one to two magnitudes higher than other cations, and was strongly affected by carbonate equilibrium processes that varied with temperature and carbonate speciation. Provenance and the availability of protons derived from sulphide acquisition and dissolved CO_2 affected initial rapid acquisition. Sulphide oxidation was dramatically curtailed after the initial period, thought to be due to the formation of an impenetrable oxidated cap on pyrite grain surfaces. Therefore, the influence of sulphide oxidation on Ca^{2+} acquisition is thought to be negligible during Stage 2 acquisition.

Stage 2 acquisition of Ca^{2+} was strongly connected with pCO_2 , indicating that CO_2 -drawdown was an important control. Temperature and aluminosilicate mineralogy affected carbonate speciation, which in turn affected the extent of protons produced by CO_2 -drawdown that were used in calcium-mineral dissolution. Supersaturation of calcite occurred in some experiments causing reprecipitation of calcium and thus negative rates of dissolution.

The influence of lithogenic provenance was shown to be important on many elements, and magnesium and sodium showed strong correlation between rock content and solution concentration under closed system conditions. However, the acquisition of these species was also affected by pCO_2 and sulphide oxidation.

7.3.1 Experimental models of solute acquisition in subglacial environments

The isolation of controls on solute acquisition discussed above allowed a degree of quantification of individual controls to be made. Quantification was established by investigating the relationship between individual cations and the specific controls, e.g. Ca^{2+} versus pCO_2 . Therefore all relationships were established on an observational basis and are therefore specific to the laboratory experiments. Their application to bulk meltwater data is discussed later.

Specific controls on the acquisition of major cations in laboratory experiments were identified as follows:

i) Calcium

An equation describing the relationship between calcium, $p\text{CO}_2$, SI(calcite), temperature, metal content of sediment, carbonate equilibria and mineralogy has been established, encompassing experiments under open- and closed-system conditions, and a wide range of rock types and chemistry. Rock-water contact time did not affect the relationship between these factors beyond the initial rapid stage. Difficulty was encountered in establishing a factor that described variations due to mineralogy, but a tentative suggestion that the ratio between calcium and strontium may help identify these variations was made.

ii) Sodium, potassium and magnesium

The relationships between the other major cations and rock-water contact time, $p\text{CO}_2$ and the effect of mineralogy in the suite of dissolution experiments have been established. The relative simplicity of the inferred controls on Na^+ , K^+ and Mg^{2+} was due to the relatively lower concentrations of these ions. However, the effect of sulphide oxidation on the magnitude of acquisition of these species could not be quantified due to unaccountable inter-experimental variations in the magnitude of this effect.

The combination of the equations describing each of these relationships fitted all experimental variation beyond one hour's dissolution. Prior to one hour, separate (log) time-dependent rate equations described the nature of acquisition. Confidence in the model was gained by the fact that wide ranges in experimental conditions could be described by relatively simple relationship equations.

7.3.2 Application of laboratory models to bulk meltwater data

The parameterisation of the laboratory experiments with field data, and using field-sampled material, increases the likelihood of the relationships observed in the experiments also applying to dissolution in the field. The differences between rates in the field and in the laboratory are, however, well documented (eg. Schnoor, 1990; Nordstrom, 1996). Therefore, caution must be given to the quantitative applicability of the model in subglacial conditions. Given this note, useful interpretations were made by inputting field data into the laboratory acquisition equations.

Plotting the differing modelled relationships between Ca^{2+} and $p\text{CO}_2$ according to sediment type, over a wide range of $p\text{CO}_2$, provided a template onto which field data was plotted. The position of field data relative to the experimental relationships gave an overview of possible rock types that could account for the unknown provenance variables. Iterating combined sediment chemistry data into the equations provided a modelled subglacial sediment

composition. This sediment dominantly consists of olivine gabbro and marble in an approximate 68%:32% proportion. The model sediment was also tested for the relationships between other cations and sediment/time. The sediment fitted these equations, and tentatively suggested a residence time of 1-4 hours, rather than 24 hours, in each case.

7.3.3 Studies of trace element behaviour in experimental simulations

In addition to major cation and anion analysis, large numbers of experimental samples were analysed for a suite of 44 standardised and 13 unstandardised minor and trace elements. Unstandardised analysis is of use in determining inter-elemental relationships both in rocks and solution. Dissolution of many trace elements reached similar magnitudes to those encountered in the proglacial stream of *Haut Glacier d'Arolla* (Brown and Fuge, 1998). Many of these were considerably lower than global river or stream averages, and indeed barely above detection limits.

The dissolution behaviour of many elements in laboratory experiments was significantly related to the extent of carbonate dissolution. In many cases this effect masked evidence of provenance. Such elements included: Ag, As, B, Be, Bi, Cd, Cs, Hg, In, K, Li, Mn, Pb, Sc, Sn, Ti, Th and heavy Rare-Earth elements (YEE). Some elements showed closer relationships with provenance, e.g. Mg, Na, W. Potentially useful indicators of pyrite oxidation included Pb, U and Zn, with Cr tending to indicate hydrothermal deposits. Certain inter-rare-earth element ratios had potentials for distinguishing carbonate from silicate provenances. Rb/K ratios had the potential to discern mineralogical differences of reactive sediment of a palaeosedimentary origin from those of igneous origin. Sodium and tungsten provenances were generally mutually exclusive to Ca and Sr provenances. Finally, Ca/Sr ratios were used in the model to distinguish calcite provenance from other Ca-mineral provenance.

The general conclusion of the trace element study of laboratory data is that the dissolution of most elements is influenced more by solution properties than by provenance. Most elements are present in the major rock types at variations of within two magnitudes, and therefore attributing assumptions of provenance or process may be equivocal. Of the potentially useful elements, other than Sr and Rb, concentrations are generally very low in glacial meltwaters, and more stringent sampling, filtration and storage regimes, more sensitive analysis and numerous repeat experiments are necessary to overcome the high variability of analytical results. Additionally, the effects of speciation, complexation and sorption cannot be satisfactorily determined with incomplete species analysis. In particular, anionic and non-

ionic species such as iodide, chloride, silicic acid, ammonia etc, and precipitation of iron/manganese/aluminium oxides may have significant effects on trace element behaviour.

Whilst this study has given an initial evaluation of the range and variation of trace element concentrations, and their common associations, the use of trace elements as indicators of solute provenance and processes of acquisition in meltwaters draining *Haut Glacier d'Arolla* would require large datasets to overcome the high degrees of variability encountered in relatively constant conditions. The applicability of any key indicators of solute processes identified for the *Haut Glacier d'Arolla* catchment to other glacial catchments may also be questionable due to the complex and variable natures of trace element deposits, and would require extensive catchment-specific laboratory investigations, including rock digestion analyses.

7.4 CRITIQUE OF THE EXPERIMENTAL MODELS

The laboratory model provided a geologically realistic estimation of solute provenance variables in the field, bolstered by the fact that no other combination of significant proportions of common morainic rocks could account for the inter-relationships between known variables observed. As a further test, inverse geochemical modelling of meltwater evolution between supraglacial and bulk meltwater draining *Haut Glacier d'Arolla* was carried out using PHREEQC, to independently predict the solute provenance. Whilst this method cannot predict rock type, it does predict mineral proportions of an assumed homogeneous reactive sediment. The mineralogy predicted by PHREEQC modelling was similar to the estimation of provenance using laboratory models.

Experimental variations observed in this study were compared with previous experimental studies. Empirical studies of carbonate dissolution were shown to predict incorrectly high rates of acquisition, due to the lack of account of the additional proton requirement of non-carbonate dissolution. Power rate laws of major cation acquisition from proglacial sediment (Brown *et al.*, 1996) were shown to follow a similar path of $\text{Ca}^{2+}/\text{pCO}_2$ evolution as laboratory experiments in this study, with a slowing down of the process caused by larger grain sizes, prewashing of sediment and low calcium content. This study closely followed investigations of carbonate dissolution in a carbonate-rich glacial catchment (Fairchild *et al.*, 1994), which demonstrated the two-stage process of calcite dissolution beginning with rapid acquisition accompanied by falling pCO_2 , and continuing at a slower rate allowing pCO_2 to recover towards atmospheric values. However, in contrast to the study of Fairchild *et al.*, sulphide oxidation was shown to have its major effect in the initial period of acquisition

rather than the second stage, consistent with interpretations of field variables (Section 3.5) (see also Seagren, 1999) that suggested that sulphide oxidation was not an important process in the post-mixing environment of the subglacial hydrological network.

Limitations

The estimation of meltwater residence time using laboratory models of controls on Na^+ , K^+ and Mg^{2+} dissolution requires caution, and can in no way be considered as either unequivocal or a step forward in the investigation of this parameter. The particular concern of this calculation is the lack of data on the proportion and effect of microfine particles in subglacial meltwater. Nevertheless, the predictions inferred from the laboratory model are realistic, which adds weight to the overall applicability of the model.

Further potential problems with the comparison between physical, hydrological and chemical processes in laboratory experiments and the field include:

Turbulence:

The simulation of an evolving channel hundreds or thousands of metres long is obviously impossible in the laboratory, and the comparison between a body of water continually accessing, passing over and removing fresh (and partially weathered) sediment and reactive rock surfaces, and a stirred bottle in continual contact with a fixed amount of homogeneous sediment is unavoidably tenuous. The variation in velocity and turbulence of flow in the subglacial drainage network is also difficult to recreate in simple laboratory experiments: an investigation of calcite precipitation rates with increased stirring rate noted significant variations (Rickard & Sjöberg, 1983, cited in Morse, 1983).

Dilution:

Although simple dilution was investigated in this study, the reality of mixing between unevolved supraglacial meltwater and subglacial meltwater of varying degrees of chemical evolution could not be satisfactorily investigated due to the countless combinations of mixing that would be necessary. PHREEQC modelling of the dilutions that were carried out did not provide satisfactory comparisons with observed results, and hence could not shorten the process of investigation.

Freeze-thaw:

Another aspect not examined in this study is the effect of concentration of solute species during partial freezing of subglacial meltwater, and whether this fractionation process would significantly alter chemical signatures.

7.5 RECOMMENDATIONS FOR FURTHER WORK

7.5.1 Field parameterisation

The study of solute provenance was greatly improved in this study by a relatively small number of morainic rock analyses. The importance of catchment geology on solute acquisition was also clearly illustrated in this study. A full and detailed geological survey of any glacial catchment being studied would allow more confident estimations of the proportions of reactive minerals available, and give a more representative picture of overall bulk reactive chemistry. Modelled relations between provenance and solution chemical properties could therefore be better accounted for.

Sampling should also include, if possible, sediment collected at the ice/bedrock interface. The ideal location of collection would be from boreholes upglacier, where freshly comminuted sediment not in contact with major channels could be collected. Investigations on grain size distribution, grain roughness (by scanning electron microscopy) and mineralogy (by X-ray diffraction analysis) would enable better parameterisation of laboratory experiments. Obtaining “representative” samples is always a problem with limited-point-of-access collection techniques such as borehole sampling, and therefore this would be a major undertaking.

Finally, the importance of local geology on solute acquisition means that a localised study involving a single glacier is insufficient to produce a model of solute acquisition that would encompass wide ranges of catchment characteristics. The study therefore needs to be broadened to include other glaciated catchments with differing geologies.

7.5.2 Species analysis

A problem with the interpretation of field and laboratory results in this and previous studies was the reliance on pH data and charge balance errors to calculate alkalinity, $p\text{CO}_2$ and $\text{SI}(\text{calcite})$. Alkalinity titrations compared favourably with calculated alkalinity determinations, but pH had no real cross-reference, and therefore any individual errors would be transferred through to $p\text{CO}_2$ and $\text{SI}(\text{calcite})$ calculations. Additionally, these calculations were based on thermodynamic equilibria, but various examples of thermodynamic modelling using PHREEQC throughout this study showed that dissolution did not follow thermodynamic patterns. Whilst kinetic controls are less important in carbonate

equilibration, independent measurement of $p\text{CO}_2$ would certainly be advantageous, considering the importance of $p\text{CO}_2$ in the laboratory model of calcium acquisition.

Additional problems with PHREEQC were encountered due to the lack of $\text{SiO}_2(\text{aq})$ and Al^{3+} data, and fully standardised Fe analyses. These values are required to run inverse models involving silicate and aluminosilicate minerals. In this study, approximate values were entered based on the findings of previous studies (Lamb *et al.*, 1995; Brown and Fuge, 1998), with high uncertainties allowed. This is not ideal, however, as certain parameters have notably changed in magnitude between years, notably $\text{SO}_4^{2-}(\text{aq})$. Additionally, speciation modelling of field samples and laboratory experiments using PHREEQC would have been more comprehensive given $\text{SiO}_2(\text{aq})$, Fe, Al, and $\text{O}_2(\text{aq})$ data, and information on oxidation state. Future studies of speciation of major, and trace element geochemistry in glacial meltwaters would be better served with the aid of these analyses, and other potential anions such as ammonia, fluoride, etc.

Although not investigated here, stable isotope fractionation of H, O, C and S may be of use as indicators of provenance. There are many applications where isotope analysis may be of potential use:

- $^{18}\text{O}/^{16}\text{O}$ ratio is much higher in SiO_2 than $\text{Fe}(\text{OH})_3$. This is due to the high ionic potential of Si and the low ionic potential of Fe. Similar fractionations exist for many compounds involving cations of different ionic potential. $^2\text{D}/^1\text{H}$ ratios follow similar trends.
- $^{18}\text{O}/^{16}\text{O}$ is likely to be different in carbonates of sedimentary and hydrothermal origin.
- $^{18}\text{O}/^{16}\text{O}$ fractionation also occurs in snow and ice formation, and may indicate water source.
- $^{34}\text{S}/^{32}\text{S}$ is generally lower in evaporite sulphate than in igneous and metamorphic rocks, although the range of values in sedimentary and metamorphic rocks is rather high. Studies may reveal a potential use of $^{34}\text{S}/^{32}\text{S}$ analysis in discerning sulphate from pyrite, gypsum and atmospheric sources, which would be extremely useful in the study of sulphide oxidation as a proton source in glacial meltwaters.

It is not anticipated that concentrations of heavy isotopes in meltwaters would be sufficient for use as indicators of solute provenance.

7.5.3 Trace element analytical technique

The study of trace elements was compromised in a number of ways, many of which could be overcome in a more detailed study. The major problems were:

- Standardisation: the study used “all-element” standards containing 100 ng/mL of each included element. Therefore, concentrations of most laboratory standards were closer to blank determinations than standard concentrations, resulting in high errors. A standardisation technique dedicated to the lower concentrations of trace elements encountered in glacial meltwaters and simulation experiments may improve accuracy of analysis.
- In a number of cases, determinations of experimental and field trace elements were below the values of blank determinations, but showed systematic variability with experimental condition or time of day. Improvement of quality of analysis, including vessel cleaning techniques and grade of deionised water and acids used, would be necessary to distinguish low levels of trace metals. Any use of rare-earth elements as indicators of provenance would certainly require these measures.
- The limited number of field analyses for trace elements available for this study were not sufficient to give a representative picture of field concentrations. If the study of trace elements in glacial meltwater is deemed worthy of further investigation, large sample numbers would be required to compensate for the larger variations involved with trace element analysis in comparison with major elements.

7.5.4 Laboratory methods & techniques

Further information could be gathered about the processes of chemical weathering in laboratory experiments by analysing post-experiment filter residue for bulk chemistry and mineralogy using XRD.

The suite of laboratory experiments could be expanded to include additional variants of sediment/water contact regimes. These could include controlled (and varying) stirring rates, individual mineral dissolution investigations, stepwise sediment addition, stepwise deionised water addition and constant sampling techniques.

1. Stirring rate could be varied to investigate the effect on solute acquisition. This would require a more specialised stirring device than was employed in this study.
2. A detailed geological study of mineralogy would enable experimentation regarding the dissolution of each common individual mineral under glacial conditions, and known proportions of each mineral in combination to reflect catchment-wide averages. This would require partial crushing to enable mineral grain separation, microscopic separation of grains into mineral-specific sediment, and subsequent further crushing to powder to homogenize.

3. Continual addition of small amounts of sediment would simulate meltwater constantly accessing unweathered sediment. This may occur in periods of high pressure flow in channels where melt is forced away from channel axes into the surrounding sediment at the ice/bedrock interface. If closed system dissolution using this technique was to be investigated, a sealed sediment chamber with controllable access to the solution, but isolated from the atmosphere, would be necessary (see also point 5).

4. Continual dilution with deionised water into a solution with fixed mass of reactive sediment would simulate the constant input of supraglacial meltwater into basal meltwater, and evaluate “post-mixing” reactions. As with sediment addition, the logistics of adding fresh water into the experiment under closed system conditions is more complicated than the techniques carried out in this study (see also point 5).

5. A better knowledge of the processes occurring in the initial minutes of laboratory experiments could be obtained if constant sampling and pH, DO₂ and alkalinity measurement was carried out over this period. Constant or high frequency sampling proved difficult in this study for a number of reasons:

- i. Existing analysis techniques for ion concentration determination and pH required filtration. Trials using pH meters directly in ongoing, unfiltered experiments revealed significant drift of reading due to contamination through the pH electrode membrane. The reverse diffusion of probe buffer solution (KCl) also had contamination issues for the solution. Electrodes without internal solution were also tested but these hand-held devices were not of sufficient accuracy.
- ii. Removal of sample from a sealed container would create internal pressure on the vessel, unless a syringe-type container of sufficient size could be obtained. Large quantities of sample would be required for external pH measurement, major ion and trace element determination (at least 70mL), with the result that frequent sampling would rapidly use up all solution unless very large containers were used.
- iii. Filtration for pH and ion analysis takes around five minutes to complete, and is not a fixed-time process as it depends on sediment content, so frequent time intervals can only be approximate, would include a filtration delay, and would be difficult for one individual to carry out due to procedural constraints.

The problems of closed system experiments could only be solved by carrying out the entire experiment in a sealed environment, such as a fume cupboard, with a gas-purged ambience and sealed-glove access, so that pH and DO₂ electrodes, filtration equipment and sample bottles could be used within the sealed environment. Additionally, to emulate a closed

system glacial environment, the unit would also have to be refrigerated to glacial temperatures.

In summary, the key to improving the accuracy of quantification of controls on solute acquisition in subglacial environments is to better establish the link between geology and fluid properties. The key is therefore a more detailed study of the geology of the *Haut Glacier d'Arolla* (or other) catchment, particularly with regard to mineralogy. Further experimentation leading from this study based on an extended knowledge of geology and mineralogy could more definitely constrain controls on solute acquisition in meltwater draining *Haut Glacier d'Arolla*, and a repeat of the experiments parameterised at other glacial catchments could eventually establish an overall model applicable to most glacial meltwater streams.

7.6 CONCLUSION

This study has provided a major step forward in the understanding of glacial geochemistry, by identifying the dominant controls on solute acquisition in subglacial meltwater beneath *Haut Glacier d'Arolla*, and establishing a semi-quantitative model of those controls. Trace element studies were not essential to further the understanding of the dominant controls on solute acquisition, but a greater knowledge of the behaviour of trace elements in glacial conditions has been obtained, and potential was identified for certain elemental inter-relationships to describe provenance variations if exhaustive studies were undertaken.

The validity of empirical geochemical models in predicting dissolution behaviour in glacial conditions using geochemical computer models was shown to be compromised because dissolution in laboratory simulation experiments was divergent from equilibrium rates. This indicated that kinetic controls such as variations in rate of drawdown of CO₂ into solution due to channel dynamics, and the “aging” of mineral surfaces due to continued cation exchange and formation of insoluble residues, have significant effects on the rates and inter-relationships between controls on solute acquisition. Inverse modelling was shown as a simple and useful tool that could be used in conjunction with petrological and geochemical investigations.

This thesis has revealed the importance of provenance on solute acquisition, indicating that similar studies in areas of different catchment geology are necessary to widen the scope of this model to represent the majority of glacial catchments.

BIBLIOGRAPHY

- Ahrens, L.H. (1964) Aspects of the geochemistry of the rare earths. In *Progress In The Science And Technology Of The Rare Earths*, Vol. 1 (ed. Eyring, L.), Pergamon Press, Oxford, 1-29.
- Allison, J.D., Brown, D.S. and Novo-Gradac, K.J. (1990) *MINTEQA2/PRODEFA2 - a geochemical assessment model for environmental systems - version 3.0 user's manual*. Environmental Research Laboratory, Office of Research and Development, U.S. Environmental Protection Agency, Athens, Georgia, 106pp.
- Ball, J.W. and Nordstrom, D.K. (1991) WATEQ4F--User's manual with revised thermodynamic database and test cases for calculating speciation of major, trace and redox elements in natural waters. *U.S. Geological Survey Open-File Report 90-129*, 185pp.
- Barrie, L.A. (1991) Snow formation and processes in the atmosphere that influence its chemical composition. In *Seasonal snowpacks: processes of compositional change* (ed. Davies, T. D., Tranter, M. and Jones, H. G.), Springer-Verlag, Berlin, 1-20.
- Bathey, M.H. (1981) *Mineralogy For Students*. Longman Scientific & Technical, Harlow, 355pp.
- Behrens, H., Bergmann, H., Moser, H., Rauert, W., Stichler, W., Ambach, W., Eisner, H. and Pessl, K. (1971) Study of the discharge of alpine glaciers by means of environmental isotopes and dye tracers. *Zeitschrift für Gletscherkunde und Glazialgeologie* **8**, 79-102.
- Berner, R.A. and Morse, J.W. (1974) Dissolution kinetics of calcium carbonate in sea water. IV: Theory of calcite dissolution. *American Journal of Science* **274**, 108-134.
- Berner, R.A. (1995) Chemical weathering and its effect on atmospheric CO₂ and climate. *Reviews in Mineralogy* **31**, 565-583.
- Bierens de Haan, S. (1991) A review of the rate of pyrite oxidation in aqueous systems at low temperatures. *Earth Science Reviews* **31**, 1-10.
- Bierens de Haan, S., Rae, J.E. and Parker, A. (1994) Pyrite oxidation in the Tertiary sands of the London Basin aquifer. *Applied Geochemistry* **9**, 161-173.
- Broecker, W.S. and Oversby, V.M. (1971) *Chemical Equilibria in the Earth*. McGraw-Hill Book Company, New York, 318pp.
- Brown, G.H. and Tranter, M. (1990) Hydrograph and chemograph separation of bulk meltwaters draining the Upper Arolla Glacier, Valais, Switzerland. *Hydrology in Mountainous Regions. 1. Hydrological Measurements; The Water Cycle (Proceedings of the Two Lausanne Symposia)*, 429-437.
- Brown, G.H. (1991) Solute provenience and transport pathways in Alpine glacial environments. *Unpublished Ph.D. Thesis*, University of Southampton.
- Brown, G.H., Sharp, M.J., Tranter, M., Gurnell, A.M. and Nienow, P.W. (1994) Impact of post-mixing chemical reactions on the major ion chemistry of bulk meltwaters draining the Haut Glacier d'Arolla, Valais, Switzerland. *Hydrological Processes* **8**, 465-480.
- Brown, G.H., Tranter, M., Sharp, M.J., Davies, T.D. and Tsiouris, S. (1994) Dissolved oxygen variations in Alpine glacial meltwaters. *Earth Surface Processes and Landforms (short communications)* **19**, 247-253.
- Brown, G.H., Tranter, M. and Sharp, M.J. (1996) Experimental investigations of weathering of suspended sediment by Alpine glacial meltwaters. *Hydrological Processes* **10**, 579-597.

- Brown, G.H., Sharp, M.J. and Tranter, M. (1996) Subglacial chemical erosion - seasonal variations in solute provenance, Haut Glacier d'Arolla, Valais, Switzerland. *Annals of Glaciology* **22**, 25-31.
- Brown, G.H. and Fuge, R. (1998) Minor and trace element chemistry and provenance in Alpine glacial meltwaters. *Ninth International Symposium on Water-Rock Interaction* (Faupo, New Zealand, 30 March-3 April 1998). WRI Series, Balkema, 297-300.
- Brown, G.H. and Fuge, R. (1998) Trace element chemistry of glacial meltwaters in an Alpine headwater catchment. *Headwater Control IV: Hydrology, Water Resources and Ecology in Headwaters*, (Proceedings of the HeadWater '98 Conference held at Meran/Merano, Italy, 20-23 April 1998), IAHS Publication no. 248, 435-442.
- Brownlow, A.H. (1979) *Geochemistry*. Prentice-Hall, Inc., Englewood Cliffs, NJ, USA, 498pp.
- Busenberg, E. and Clemency, C.V. (1976) The dissolution kinetics of feldspars at 25°C and 1atm CO₂ partial pressure. *Geochimica et Cosmochimica Acta* **40**, 41-49.
- Busenberg, E. and Plummer, L.N. (1986) A comparative study of the dissolution and crystal growth kinetics of calcite and aragonite. In *Studies in Diagenesis*, Vol. U.S.G.S. Bulletin 1578 (ed. Mumpton, F. A.), U.S. Government Printing Office, Washington, D.C., 139-168.
- Cadle, S.H. (1991) Dry deposition to snowpacks. In *Seasonal snowpacks: processes of compositional change* (ed. Davies, T. D., Tranter, M. and Jones, H. G.), Springer-Verlag, Berlin, 21-66.
- Carrucio, F.T., Geidel, G. and Pelletier, M. (1981) Occurrence and prediction of acid drainages. *Proceedings of the American Society of Civil Engineering* **107**, 167-179.
- Charlton, S.R., Macklin, C.L. and Parkhurst, D.L. (1997) PhreeqcI - A graphical user interface for the geochemical computer program PHREEQC. U.S. Geological Survey.
- Chillrud, S.N., Pedrozo, F.L., Temporetti, P.F., Planas, H.F. and Froelich, P.N. (1994) Chemical weathering of phosphate and germanium in glacial meltwater streams - effects of subglacial pyrite oxidation. *Limnology and Oceanography* **39**, 1130-1140.
- Chou, L., Garrels, R.M. and Wollast, R. (1989) Comparative study of the dissolution kinetics and mechanisms of carbonates in aqueous solutions. *Chemical Geology* **70**, 77.
- Christie, G.L. (1995) Speciation. In *Environmental Analytical Chemistry* (ed. Fifield, F. W. and Haines, P. J.), Blackie Academic & Professional/Chapman & Hall, Glasgow, 279-290.
- Church, M. (1974) On the quality of some waters on Baffin Island, Northwest Territories. *Canadian Journal of Earth Sciences* **11**, 1676-1688.
- Clark, A. (1979) *Minerals*. Hamlyn, London, 128pp.
- Colbeck, S.C. (1989) Air movement in snow due to wind-pumping. *Journal of Glaciology* **35**, 209-213.
- Collins, D.N. (1977) Hydrology of an Alpine glacier as indicated by the chemical composition of meltwater. *Zeitschrift für Gletscherkunde und Glazialgeologie* **13**(1), 219-239.
- Collins, D.N. (1978) Hydrochemistry of an alpine glacier as indicated by the chemical composition of meltwater. *Zeitschrift für Gletscherkunde und Glazialgeologie* **13**, 219-238.
- Collins, D.N. (1979) Sediment concentration in melt waters as an indicator of erosion processes beneath an Alpine glacier. *Journal of Glaciology* **23**(89), 247-257.
- Collins, D.N. (1979) Hydrochemistry of meltwaters draining from an alpine glacier. *Arctic & Alpine Research* **11**, 307-324.
- Collins, D.N. (1981) Seasonal variation of solute concentration in meltwaters draining from an Alpine glacier. *Annals of Glaciology (IGS)* **2**.

- Collins, D.N. (1983) Solute yield from a glacierized high mountain basin. *Dissolved Loads of Rivers and Surface Water Quantity/Quality Relationships*, 41-49.
- Collins, D.N. (1989) Seasonal development of subglacial drainage and suspended sediment delivery to meltwaters beneath an Alpine glacier. *Annals of Glaciology* **13**, 45-50.
- Collins, D.N. (1990) Seasonal and annual variations of suspended sediment transport in meltwaters draining from an Alpine glacier. *Hydrology in Mountainous Regions. 1 - Hydrological Measurements; the Water Cycle*, 439-446.
- Collins, D.N. (1995) Dissolution kinetics, transit times through subglacial hydrological pathways and diurnal variations of solute content of meltwaters draining from an alpine glacier. *Hydrological Processes* **9**, 897-910.
- DIONEX Corporation. (1992) *Installation instructions and troubleshooting guide for the IonPac(R) AG4A-SC Guard Column/AS4A-SC Analytical Column*, 57pp.
- DIONEX Corporation. (1994) *Installation instructions and troubleshooting guide for the IonPac(R) CG12A Guard Column/CS12A Analytical Column*, 54pp.
- DIONEX Corporation. (1994) *Installation instructions and troubleshooting guide for the Cation Self-Regenerating Suppressor-I (4mm/2mm)*, 44pp.
- Drever, J.I. (1982) *The Geochemistry Of Natural Waters*. Prentice-Hall, New Jersey, 388pp.
- Drever, J.I. and Hurcomb, D.R. (1986) Neutralisation of atmospheric acidity by chemical weathering in an alpine drainage basin in the Noth Cascade Mountains. *Geology* **14**, 221-224.
- Drever, J.I. and Clow, D.W. (1995) Weathering rates in catchments. *Reviews in Mineralogy* **31**, 463-483.
- Drever, J.I. and Stillings, L.L. (1997) The role of organic acids in mineral weathering. In *Colloids and Surfaces A-Physicochemical and Engineering Aspects*, Vol. 120, 167-181.
- Dreybott, W., Lauckner, J., Liu, Z., Svensson, U. and Buhmann, D. (1996) The kinetics of the reaction $\text{CO}_2 + \text{H}_2\text{O} \rightarrow \text{H}^+ + \text{HCO}_3^-$ as one of the rate-limiting steps for the dissolution of calcite in the system $\text{H}_2\text{O}-\text{CO}_2-\text{CaCO}_3$. *Geochimica et Cosmochimica Acta* **60**, 3375-3381.
- Fairchild, I.J., Bradby, L. and Spiro, B. (1993) Reactive carbonate in glacial systems: a preliminary synthesis of its creation, dissolution and reincarnation. In *Earth's Glacial Record* (ed. Deynott, M. *et al.*), Cambridge University Press, Cambridge.
- Fairchild, I.J., Bradby, L., Sharp, M. and Tison, J.-L. (1994) Hydrochemistry of carbonate terrains in Alpine glacial settings. *Earth Surface Processes and Landforms*. **19**(1), 33-54.
- Fairchild, I.J., Killawee, J.A., Hubbard, B.P. and Dreybott, W. (1999) Interactions of calcareous sediment with glacial meltwater: a field test of dissolution behaviour. *Chemical Geology* **155**, 243-263.
- Fenn, C.R. (1987) Electrical conductivity. In *Glacio-fluvial Sediment Transfer - An Alpine Perspective* (ed. Gurnell, A. M. and Clark, M. J.), Wiley, London, 377-414.
- Ferguson, R.I. (1973) Sinuosity of supraglacial streams. *Geological Society of America Bulletin* **84**, 251-256.
- Feth, J.H., Roberson, C.E. and Polzer, W.L. (1964) Sources of mineral constituents in water from granitic rocks, Sierra Nevada, California and Nevada. In *U.S. Geological Survey Water Supply Paper*.
- Fifield, F.W. (1995) Separation techniques. In *Environmental Analytical Chemistry* (ed. Fifield, F. W. and Haines, P. W.), Blackie Academic & Professional/Chapman & Hall, Glasgow, 81-104.
- Fountain, A.G. (1996) Effect of snow and firn hydrology on the physical and chemical characteristics of glacial runoff. *Hydrological Processes* **10**, 509-521.

- Francois, L.M. and Gerard, J.C. (1986) A numerical model of the evolution of ocean sulphate and sedimentary sulfur during the last 800 million years. *Geochimica et Cosmochimica Acta* **50**, 2289-2302.
- Garrels, R.M., Thompson, M.E. and Siever, R. (1960) Stability of some carbonates at 25°C and one atmosphere total pressure. *American Journal of Science* **258**, 402.
- Garrels, R.M. and Christ, C.L. (1965) *Solutions, Minerals, and Equilibria*. Harper & Row, New York, 450pp.
- Gill, R. (1996) *Chemical Fundamentals of Geology*. Chapman & Hall, London, 298pp.
- Goldschmidt, V.M. and Muir, A. (1958) Geochemistry. In *The International Series of Monographs on Physics* (ed. Marshall, W. and Wilkinson, D. H.), Oxford University Press, 730pp.
- Gomez, B. and Small, R. (1985) Medial moraines of the Haut Glacier d'Arolla, Valais, Switzerland: debris supply and implications for moraine formation. *Journal of Glaciology* **31**(109), 303-307.
- Goodman, D. (1971) Ecological investigations of ice worms on Casement Glacier, Southeast Alaska. *Ohio State University Institute of Polar Studies Report* **39**, 1-59.
- Gorham, E. (1961) Factors influencing supply of major ions to inland waters, with special reference to the atmosphere. *Geological Society of America Bulletin* **72**, 795-840.
- Gurnell, A.M. and Fenn, C.R. (1984) Flow separation, sediment source areas and suspended sediment transport in a pro-glacial stream. *Channel Processes: Water, Sediment, Catchment Controls Supplement* **5**, 109-119.
- Hamilton, W.R., Woolley, A.R. and Bishop, A.C. (1974) *Hamlyn Guide to Minerals, Rocks and Fossils*. Hamlyn, London.
- Henderson, E.S. (1976) *Chemistry Today*. Macmillan, London, 447pp.
- Hering, J.G. and Morel, F.M.M. (1990) The kinetics of trace metal complexation: implications for metal reactivity in natural waters. In *Aquatic Chemical Kinetics* (ed. Stumm, W.), Wiley, New York, 145-171.
- Hering, J.G. and Stumm, W. (1990) Oxidative and reductive dissolution of minerals. In *Mineral-Water Interface Geochemistry*, Vol. 23 (ed. Hochella, M. F. and White, A. F.), Mineral Society of America, 427-465.
- Hock, R. and Hooke, R.L. (1993) Evolution of the internal drainage system in the lower part of the ablation area of Storglaciären, Sweden. *Geological Society of America Bulletin* **105**(4), 537-546.
- Holdren and Berner. (1979) Mechanisms of feldspar weathering. 1. Experimental studies. *Geochimica et Cosmochimica Acta* **43**, 1161-1171.
- Holland, H.D. (1978) *The Chemistry of the Atmosphere and Oceans*. John Wiley & Sons, New York, 351pp.
- Hooke, R.L., Wold and Hagen. (1985) Subglacial hydrology and sediment transport at Bondhusbreen, South-West Norway. *Bulletin of the Geological Society of America* **96**(3), 388-397.
- Hooke, R.L. (1989) Englacial and subglacial hydrology: a qualitative review. *Arctic and Alpine Research* **21**(3), 221-233.
- Hubbard, B.P., Sharp, M.J., Willis, I.C., Nielsen, M.K. and Smart, C.C. (1995) Borehole water-level variations and the structure of the subglacial hydrological system of Haut Glacier d'Arolla, Valais, Switzerland. *Journal of Glaciology* **41**, 572-583.

- Humphrey, N., Raymond, C. and Harrison, W. (1986) Discharges of turbid water during mini-surges of Variegated Glacier, Alaska, U.S.A. *Journal of Glaciology* **32**, 195-207.
- Hunter, K.A. and Liss, P.S. (1982) Organic matter and the surface charge of suspended particles in estuarine waters. *Limnology and Oceanography* **27**(2), 322-335.
- Inskip, W.P. and Bloom, P.R. (1985) An evaluation of rate equation for calcite precipitation kinetics at pCO₂ less than 0.01atm and pH greater than 8. *Geochimica et Cosmochimica Acta* **49**, 2165-2180.
- Jarvis, K.E., Gray, A.L. and Houk, R.S. (1992) *Handbook of Inductively Coupled Plasma Mass Spectrometry*. Blackie, Glasgow, 11-57.
- Johannessen, M. and Henriksen, A. (1978) Chemistry of snowmelt water: changes in concentration during melting. *Water Resources Research* **14**, 615-619.
- Keller, W.D. and Reesman, A.L. (1963) Glacial milks and their laboratory-simulated counterparts. *Bulletin of the Geological Society of America* **74**, 61-76.
- Kol, E. (1942) The snow and ice algae of Alaska. *Smithsonian Miscellaneous Collections* **101**(16,1), 36.
- Krauskopf, K.B. (1979) *Introduction to Geochemistry*. McGraw-Hill, New York, 617pp.
- Krauskopf, K.B. and Bird, D.K. (1995) *Introduction to Geochemistry*. McGraw-Hill, New York, 647pp.
- Lamb, H.R., Tranter, M., Brown, G.H., Hubbard, B.P., Sharp, M.J., Gordon, S., Smart, C.C., Willis, I.C. and Nielsen, M.K. (1995) The composition of subglacial meltwaters sampled from boreholes at the Haut Glacier d'Arolla, Switzerland. *Biogeochemistry of Seasonally Snow-Covered Catchments (Proceedings of a Boulder Symposium, July 1995)*, 395-403.
- Lamb, H.R. (1997) Chemical weathering in Alpine subglacial environments. *Unpublished Ph.D. Thesis*, University of Bristol.
- Lamb, H.R., Tranter, M., Sharp, M.J., Brown, G.H., Hubbard, B.P. and Willis, I.C. (in preparation) The geochemistry and hydrology of subglacial meltwaters at Haut Glacier d'Arolla, Switzerland: true and artifact water compositions.
- Langmuir, D. (1978) Uranium solution-mineral equilibria at low temperatures with applications to sedimentary ore genesis. *Geochimica et Cosmochimica Acta* **42**, 547-570.
- Lasaga, A.C. (1984) Chemical kinetics of water-rock interactions. *Journal of Geophysical Research* **89**(NB6), 4009-4025.
- Leece, S.A. (1993) Flow separation and diurnal variability in the hydrology of Conness Glacier, Sierra Nevada, California, U.S.A. *Journal of Glaciology* **39**(132), 216-222.
- Lees, H., Kwok, S.C. and Suzuki, I. (1969) The thermodynamics of iron oxidation by the ferrolaccilli. *Canadian Journal of Microbiology* **15**, 43-46.
- Lowson, R.T. (1982) Aqueous oxidation of pyrite by molecular oxygen. *Chemical Review* **82**, 461-497.
- Lundgren, D.G. and Silver, M. (1980) Ore leaching by bacteria. *Annals of Reviews in Microbiology* **34**, 263-283.
- MacKenzie, W.S. and Adams, A.E. (1993) *A Colour Atlas of Rocks and Minerals in Thin Section*. Manson Publishing, London, 192pp.
- McKibben, M.A. and Barnes, H.L. (1986) Oxidation of pyrite in low temperature acidic solutions: rate laws and surface textures. *Geochimica et Cosmochimica Acta* **50**, 1509-1520.

- McLaren, J.W. (1992) The analysis of natural waters by ICP-MS. In *Handbook of Inductively Coupled Plasma Mass Spectrometry* (ed. Jarvis, K. E., Gray, A. L. and Houk, R. S.), Blackie, Glasgow, 266-337.
- McLennan, S.M. (1989) Rare earth elements in sedimentary rocks: influence of provenance and sedimentary processes. In *Geochemistry and Mineralogy of Rare Earth Elements*, Vol. 21 (ed. Lipin, B. R. and McKay, G. A.), Mineral Society of America, 169-200.
- Morse, J.W. (1983) The kinetics of calcium carbonate dissolution and precipitation. In *Carbonates: Mineralogy and Chemistry*, Vol. 11 (ed. Reeder, R. J.), Mineralogical Society of America, Washington DC, 227-264.
- Moses, C.O., Nordstrom, D.K., Herman, J.S. and Mills, A.L. (1987) Aqueous pyrite oxidation by dissolved oxygen and by ferric iron. *Geochimica et Cosmochimica Acta* **51**, 1561-1571.
- Moses, C.O. and Herman, J.S. (1991) Pyrite oxidation at circumneutral pH. *Geochimica et Cosmochimica Acta* **55**, 471-482.
- Nancollas, G.H. and Reddy, M.M. (1971) The crystallization of calcium carbonate, II. Calcite growth mechanism. *Journal of Colloid Interface Science* **37**, 824-829.
- National Institute of Science and Technology. (web site) The NIST Reference on Constants, Units and Uncertainty. *Web site address*: <http://physics.nist.gov/cuu/Units/index.html>
- Nicholson, R.V., Gillham, R.W. and Reardon, E.J. (1988) Pyrite oxidation in carbonate-buffered solution: 1. Experimental kinetics. *Geochimica et Cosmochimica Acta* **52**, 1077-1085.
- Nienow, P.W., Sharp, M.J. and Willis, I.C. (1996) Velocity-discharge relationships derived from dye-tracer experiments in glacial meltwaters: implications for subglacial flow conditions. *Hydrological Processes*, **10**, 1411-1426.
- Nienow, P.W., Sharp, M.J., Willis, I.C. and Richards, K.S. (1996) Dye tracer investigations of the spatial structure of the subglacial drainage system of the Haut Glacier d'Arolla, Valais, Switzerland. *Journal of Glaciology*.
- Nordstrom, D.K. (1982) Aqueous pyrite oxidation and the consequent formation of secondary iron minerals. *Soil Science Society of America, Special Publication* **10**, 37-56.
- Nordstrom, D.K. and Munoz, J.L. (1985) *Geochemical Thermodynamics*. Benjamin/Cummings Publishing Co., Inc., Menlo Park, Ca., USA, 477pp.
- Nordstrom, D.K. (1996) Trace metal speciation in natural waters: computational vs. analytical. *Water, Air and Soil Pollution* **90**, 257-267.
- Odén, S. and Ahl, T. (1970) Förurningen av skandinaviska vatten. The acidification of Scandinavian lakes and rivers (English summary). *Sartryck Ur Ymer, Årsbok*, 103-122.
- Orion Research Incorporated. (1991) *Oxygen Electrode Instruction Manual (Model 97-08)*, 24pp.
- Orion Research Incorporated. (1991) *Laboratory Products Group Portable pH/ISE Meters Instruction Manual (Models 230A/250A/290A)*, 60pp.
- Oxburgh, R., Drever, J.I. and Sun, Y.-T. (1994) Mechanism of plagioclase dissolution in acid solution at 25°C. *Geochimica et Cosmochimica Acta* **58**, 661-669.
- Parkhurst, D.L., Thorstenson, D.C. and Plummer, L.N. (1980) phreeqc--A computer program for geochemical calculations (Revised and reprinted August, 1990.). *U.S. Geological Survey Water-Resources Investigations Report* **80-96**, 195.
- Parkhurst, D.L. (1995) User's guide to PHREEQC - a computer program for speciation, reaction-path, advective transport, and inverse geochemical calculations. U.S. Geological Survey.

- Peltier, L. (1950) Geographic cycle in periglacial regions as it is related to climatic geomorphology. *Annals of the Association of American Geographers* **40**, 214-236.
- Plummer, L.N., Wigley, T.M.L. and Parkhurst, D.L. (1978) The kinetics of calcite dissolution in CO₂-water systems at 5° and 60°C and 0.0 to 1.0 atm CO₂. *American Journal of Science* **278**, 179-216.
- Post, W.M., Peng, T.-H., Emanuel, W.R., King, A.W., Dale, V.H. and DeAngelis, D.L. (1990) The Global Carbon Cycle. *American Scientist* **78**, 310-326.
- Rainwater, F.H. and Guy, H.P. (1961) Some observations on the hydrochemistry and sedimentation of the Chamberlain Glacier area, Alaska. *U.S. Geological Survey Prof. Paper* **414-C**, 74pp.
- Raiswell, R.W., Brimblecombe, P., Dent, D.L. and Liss, P.S. (1980) *Environmental Chemistry: The Earth-Air-Water Factory*. Edward Arnold, London, 184pp.
- Raiswell, R.W. and Thomas, A.G. (1984) Solute acquisition in glacial meltwaters. 1. Fjalljökull (S.E. Iceland): bulk meltwaters with closed-system characteristics. *Journal of Glaciology* **30**(104), 35-43.
- Raiswell, R. (1984) Chemical models of solute acquisition in glacial meltwaters. *Journal of Glaciology* **30**(104), 49-57.
- Rankama, K. and Sahama, T.G. (1950) *Geochemistry*. The University of Chicago Press, Chicago, 912.
- Reynolds Jr., R.C. and Johnson, N.M. (1972) Chemical weathering in the temperate glacial environment of the Northern Cascade Mountains. *Geochimica et Cosmochimica Acta* **36**, 537-554.
- Röthlisberger, H. (1972) Water pressure in intra- and subglacial channels. *Journal of Glaciology* **11**, 177-204.
- Röthlisberger, H. and Lang, H. (1987) Glacial Hydrology. In *Glacio-Fluvial Sediment Transfer: An Alpine Perspective* (ed. Gurnell, A. M. and Clark, M. J.), John Wiley & Sons, Chichester, 207-284.
- Ruffles, L. (1999) *Unpublished Ph.D. Thesis*, University of Wales, Aberystwyth.
- Schnoor, J. (1990) Kinetics of chemical weathering: a comparison of laboratory and field weathering rates. In *Aquatic Chemical Kinetics*. (ed. Stumm, W.), Wiley, New York, 475-504.
- Seagren, A.G. (1995) Controls on dissolved oxygen variability in alpine supraglacial meltwaters, Haut Glacier d'Arolla, Switzerland. *Unpublished Undergraduate Dissertation*, University of Cambridge.
- Seagren, A.G. (1999) The Nature of Solute Acquisition and Suspended Sediment Dynamics in Channelised Subglacial Weathering Environments, Haut Glacier d'Arolla, Valais, Switzerland. *Unpublished Ph.D. Thesis*, University Of Wales, Aberystwyth.
- Sharp, M.J. (1991) Hydrological inferences from meltwater quality data: the unfulfilled potential. *Proceedings of the British Hydrological Society National Symposium*, 5.1-5.8.
- Sharp, M., Richards, K., Willis, I., Arnold, N. and Nienow, P. (1993) Geometry, bed topography and drainage system structure of the Haut Glacier d'Arolla, Switzerland. *Earth Surface Processes and Landforms* **18**, 557-571.
- Sharp, M.J. (1995) Comments on the use of chemically based mixing models in glacier hydrology. *Journal of Glaciology* **41**, 241-246.
- Shoemaker, E.M. (1986) Subglacial hydrology for an ice sheet resting on a deformable aquifer. *Journal of Glaciology* **34**, 217-227.

- Sjöberg, E.L. (1978) Kinetics and mechanism of calcite dissolution in aqueous solutions at low temperatures. *Acta University of Stockholm, Contributions in Geology* **332**, 1-92.
- Small, R.J. (1987) Englacial and Supraglacial Sediment: Transport and Deposition. In *Glacio-Fluvial Sediment Transfer* (ed. Gurnell, A. M. and Clark, M. J.), John Wiley & Sons, Chichester, 111-145.
- Smith, E.E., Svanks, K. and Shumate, K. (1968) Sulfide to sulfate reaction series. *Second Symposium on Coal Mine Research*, 1-11.
- Stenborg, T. (1973) Some viewpoints on the internal drainage of glaciers. *International Symposium on the Hydrology of Glaciers, 7-13 September, 1969*, 117-131.
- Stollenwerk, K.G. (1994) Geochemical interactions between constituents in acidic groundwater and alluvium in an aquifer near Globe, Arizona. *Applied Geochemistry* **9**, 353-369.
- Stone, A.T. and Morgan, J.J. (1990) Kinetics of chemical transformations in the environment. In *Aquatic Chemical Kinetics* (ed. Stumm, W.), Wiley, New York, 1-41.
- Stone, D.B. and Clarke, G.K.C. (1996) *In situ* measurements of basal water quality and pressure as an indicator of the character of subglacial drainage systems. *Hydrological Processes* **10**, 615-628.
- Stumm, W. and Bilinski, H. (1972) Trace metals in natural waters: difficulties of interpretation arising from our ignorance on their speciation. In *6th International Conference on Water Pollution Research*, Pergamon Press, New York, 39-49.
- Stumm, W. and Morgan, J.J. (1981) *Aquatic Chemistry: An Introduction Emphasizing Chemical Equilibria in Natural Waters*. Wiley Interscience, New York, 780.
- Stumm, W. and Morgan, J.J. (1996) *Aquatic Chemistry: Chemical Equilibria and Rates in Natural Waters*. Wiley Interscience, New York, 1024.
- Sugden, D.E. and John, B.S. (1976) *Glaciers and Landscape*. Edward Arnold, London, 376pp.
- Tamm, O. (1924) Experimental studies on chemical processes in the formation of glacial clay. *Sverig. Geol. Unders. Arsbok* **18(5)**, 1-20.
- Tangborn, W.V. (1966) Glacier mass budget measurements by hydrologic means. *Water Resources Research* **2**, 105-110.
- Taylor, S.R. and McLennan, S.M. (1985) *The Continental Crust: Its Composition and Evolution*. Blackwell, Oxford, 312pp.
- Theakstone, W.H. and Knudsen, N.T. (1996) Isotopic and ionic variations in glacier river water during three contrasting ablation seasons. *Hydrological Processes* **10**, 523-539.
- Thomas, A.G. and Raiswell, R. (1984) Solute acquisition in glacial melt waters. II. Argentière (French Alps): bulk melt waters with open-system characteristics. *Journal of Glaciology* **30(104)**, 1984.
- Toran, L. and Harris, R.F. (1990) Interpretation of sulphur and oxygen isotopes in biological and abiological sulphide oxidation. *Geochimica et Cosmochimica Acta* **53**, 2341-2348.
- Tranter, M., Mills, R. and Raiswell, R. (1989) Chemical weathering reactions in Alpine glacial meltwaters. *6th International Symposium on Water-Rock Interaction*, 687-690.
- Tranter, M. (1991) Controls on the composition of snowmelt. In *Seasonal snowpacks; processes of compositional change.*, Vol. G28 (ed. Davies, T. D., Tranter, M. and Jones, H. G.), NATO ARW Series, 241-271.
- Tranter, M. and Raiswell, R. (1991) The composition of the englacial and subglacial component in bulk meltwaters draining the Gornergletscher. *Journal of Glaciology* **37**, 59-66.

- Tranter, M., Brown, G.H., Raiswell, R., Sharp, M.J. and Gurnell, A. (1993) A conceptual model of solute acquisition by Alpine glacial meltwaters. *Journal of Glaciology* **39**, 573-581.
- Tranter, M., Brown, G.H., Hodson, A., Gurnell, A. and Sharp, M.J. (1994) Variations in the nitrate concentration of glacial runoff in Alpine and sub-Polar environments. *Yokohama Symposia J2 and J5: Snow and Ice Covers - Interactions with the Atmosphere and Ecosystems.*, 299-311.
- Tranter, M., Brown, G.H., Hodson, A.J. and Gurnell, A.M. (1996) Hydrochemistry as an indicator of the nature of subglacial drainage system structure: a comparison of Arctic and Alpine environments. *Hydrological Processes* **10**, 541-556.
- Tranter, M., Sharp, M.J., Brown, G.H., Willis, I.C., Hubbard, B.P., Nielsen, M.K., Smart, C.C., Gordon, S., Tulley, M. and Lamb, H.R. (1997) Variability in the chemical composition of *in situ* subglacial meltwaters. *Hydrological Processes* **11**, 59-77.
- Turekian, K.K. and Wedepohl, K.H. (1961) Distribution of the elements in some major units of the earth's crust. *Geological Society of America Bulletin* **72**, 175-182.
- Underwood, D.N. and Webster, D.E. (1975) *Chemistry*. Edward Arnold, London, 484pp.
- van Breeman, N. (1972) Soil forming processes in acid sulfate soils. In *Acid Sulfate Soils*, Vol. 18 (ed. Dost, H.), International Institute for Land Reclamation and Improvement, Wageningen, Netherlands, 66-130.
- Veizer, J. (1983) Trace elements and isotopes in sedimentary carbonates. In *Carbonates: Mineralogy and Chemistry*, Vol. 11 (ed. Reeder, R. J.), Mineralogical Society of America, Washington DC, 265-299.
- Vlasov, K.A. (1966) Geochemistry of Rare Elements. In *Geochemistry and Mineralogy of Rare Elements and Genetic Types of Their Deposits*, Vol. 1 (ed. Vlasov, K. A.), Israel Program for Scientific Translations, 688pp.
- Volborth, A. (1969) *Elemental Analysis in Geochemistry*. Elsevier, Amsterdam, 373pp.
- Walder, J.S. (1986) Hydraulics of subglacial cavities. *Journal of Glaciology* **32**, 439-445.
- Walder, J.S. and Fowler, A.C. (1994) Channelised subglacial drainage over a deformable bed. *Journal of Glaciology* **40**, 3-15.
- Ward, N.I. (1995) Trace elements. In *Environmental Analytical Chemistry* (ed. Fifield, F. W. and Haines, P. J.), Blackie Academic & Professional/Chapman & Hall, Glasgow, 320-351.
- Weertman, J. (1957) On the sliding of glaciers. *Journal of Glaciology* **3**, 33-38.
- Weertman, J. (1972) General theory of water flow at the base of a glacier or ice sheet. *Review of Geophysics and Space Physics* **10**, 287-333.
- Wentzler, T.H. (1971) A study of the interactions of limestone in acids. *Unpublished M.S. Thesis Thesis*, Pennsylvania State University.
- Wharton, R.A. and Vinyard, W.C. (1983) Distribution of snow and ice algae in Western North America. *Madrono* **30**, 201-209.
- Wiersma, C.L. and Rimstidt, J.D. (1984) Rates of reaction of pyrite and marcasite with ferric iron at pH 2. *Geochimica et Cosmochimica Acta* **48**, 85-92.
- Williamson, M.A. and Rimstidt, J.D. (1994) The kinetics and electrochemical rate-determining step of aqueous pyrite oxidation. *Geochimica et Cosmochimica Acta* **58**(24), 5443-5454.
- Willis, I.C., Sharp, M.J. and Richards, K.S. (1990) Configuration of the drainage system of Midtalsbreen, Norway, as indicated by dye-tracing experiments. *Journal of Glaciology* **36**, 89-101.

- Willis, I.M., Sharp, M.J., Tranter, M., Hubbard, B.P., Nielsen, M., Smart, C., Brown, G.H., Arnold, N., Hodgkins, R., Lamb, H., Gordon, S. and Ketterling, B. (1995) Water storage, drainage evolution and water quality in Alpine glacial environments. NERC Grant GR3/8114.
- Winkler, P. (1980) Observations on acidity in continental and in marine atmospheric aerosols and in precipitation. *Journal of Geophysical Research* **85C**, 4481-4486.
- Wollast, R. (1990) Rate and mechanism of dissolution of carbonates in the system CaCO₃-MgCO₃. In *Aquatic Chemical Kinetics* (ed. Stumm, W.), Wiley, New York, 431-445.
- Zachara, J.M., Cowan, C.E. and Resch, C.T. (1993) Metal cation/anion adsorption on calcium carbonate: implications to metal ion concentrations in groundwater. In *Metals in groundwater* (ed. Allen, H. E., Perdue, E. M. and Brown, D. S.), Lewis Publishers, Chelsea, MI, 37-71.
- Zeman, L.J. and Slaymaker, H.O. (1975) Hydrochemical analysis to discriminate variable runoff source areas in an alpine basin. *Arctic and Alpine Research* **7**(4), 341-351.

APPENDIX A - PHREEQC GEOCHEMICAL MODEL INPUT FILES

PHREEQC Input File Appendix A -1 Example input file for PHREEQC speciation modelling. Values for rock 1 are presented.

```

TITLE Experiment 1(c) (24 hours).
SOLUTION 1 Laboratory experiments concs, 24 hours
temp      10
pH        9.1
pe        8.451
redox     pe
units     mg/kgs
Ca        6489   ppb
Mg        209   ppb
Na        146   ppb
K         1798  ppb
Fe        70   ppb
Mn        19   ppb
Si        4.28
Cl        149   ppb
Alkalinity 23660 ppb   as HCO3
U         0.02  ppb
O(0)     10    ppm   as O2
Al        52   ppb
B         19   ppb
Ba        0.48 ppb
Br        0    ppb
Cd        0.1  ppb
Cu        1    ppb
Li        2.6  ppb
Pb        1.5  ppb
Sr        295  ppb
Zn        4.6  ppb
S         66   ppb   as SO4
N         0    ppb   as NO3
As        3    ppb
Be        1.2  ppb
Cr        0.88 ppb
Hg        0.72 ppb
Ni        0.5  ppb
Rb        4.2  ppb
Sb        0.13 ppb
Tl        0.03 ppb
V         0.66 ppb
EQUILIBRIUM_PHASES 1
CO2(g)   -3.5  10.0
END

```

PHREEQC Input File Appendix A -2 Example input file for Phreeqc speciation modelling.
Values for a theoretical 32%:68% mix between Rock 1 & 2 are presented. Trace element data is omitted here but was included in the actual file.

```

TITLE Rock 1 & Rock 2 mix (1440min)
SOLUTION 1 Experiment 1(c)
  temp      10
  pH        9.1
  pe        8.451
  redox     pe
  Alkalinity 23660          ppb    as HCO3
  Cl        149          ppb
  N         0.00         ppb    as NO3
  S         66          ppb    as SO4
  Na        146          ppb
  K         1798         ppb
  Mg        209          ppb
  Ca        6489         ppb
  O(0)     10          ppm    as O2
  Si        4.28
EQUILIBRIUM_PHASES 1
  CO2(g)   -3.5        10
SOLUTION 2 Experiment 2(c)
  temp      10
  pH        7.4
  pe        8.451
  redox     pe
  units     mg/kgs
  Alkalinity 0.00       ppb    as HCO3
  Cl        449          ppb
  N         677          ppb    as NO3
  S         9442         ppb    as SO4
  Na        139          ppb
  K         1764         ppb
  Mg        212          ppb
  Ca        1743         ppb
  O(0)     10          ppm    as O2
  Si        4.28
EQUILIBRIUM_PHASES 2
  CO2(g)   -3.5        10
MIX 1 Mixing Solutions 1 & 2
  1         0.32
  2         0.68
END

```

PHREEQC Input File Appendix A -3 Input file of Phreeqc modelling of 0.2g/L pyrite + 0.2g/L calcite dissolution

```

SOLUTION 1 Deionised water in equilibrium with atmosphere
  temp      5
  pH        7.4
  pe        4
  redox     O(-2)/O(0)
  units     mg/kgw
  O(0)     10          mg/kgw  as O2
EQUILIBRIUM_PHASES 1 Pyrite and calcite
  Calcite  0.0          2e-3
  Pyrite   0.0          1.666e-3
GAS_PHASE 1
  -pressure 1.0
  -volume   1.0
  -temperature 5
  CO2(g)   5e-4

```

PHREEQC Input File Appendix A -4 Input file of Phreeqc inverse modelling of solute acquisition in subglacial meltwater

```

TITLE Rock 1.--Inverse modeling of field data
SOLUTION 1 Supraglacial meltwater composition, 31/07/95, 1535
temp      0
pH        6.78
pe        8.451
redox     pe
units     Mol/kgw
Ca        2.34e-5
Mg        7.1e-7
Na        1.46e-6
K         1.27e-6
Si        4.28   mg/kgw
S         2.45e-6 as SO4-2
Alkalinity 4.31e-5 as HCO3-
Al        1e-6
Fe        1e-7

SOLUTION 2 Laboratory experiments concs, 24 hours
temp      0
pH        7.61
pe        8.451
redox     pe
units     Mol/kgw
Ca        1.58e-4
Mg        1.43e-5
Na        1.43e-5
K         1.08e-5
Si        4.28   mg/kgw
S         4.38e-5 as SO4-2
Alkalinity 2.64e-4 as HCO3-
Al        1e-6
Fe        5e-7

```

```

INVERSE_MODELING 1
-solutions 1 2
-uncertainty 0.2
-phases
    Kaolinite      precip
    Ca-montmorillonite precip
    CO2(g)
    O2(g)
    Calcite
    Dolomite       precip
    Biotite        dissolve
    Plagioclase(An37) dissolve
    Olivine(Fo50)  dissolve
    Microcline     dissolve
    Diopside       dissolve
    Pyrite         dissolve
    Tremolite      dissolve
    Fe(OH)3(a)    precip
-balance
    Fe      1
    Al      1
-minimal

```

PHASES 1 # Do not change this number it is used by the program!

```

Biotite
    KMg3AlSi3O10(OH)2 + 6H+ + 4H2O = K+ + 3Mg+2 + Al(OH)4- + 3H4SiO4
    log_k 0.0
Plagioclase(An37)
    Na0.62Ca0.37Al1.38Si2.625O8 + 5.5 H+ + 2.5H2O = \
    0.62Na+ + 0.37Ca+2 + 1.38Al+3 + 2.625H4SiO4
    log_k 0.0
Olivine(Fo50)
    FeMgSiO4 + 4H+ = Mg+2 + Fe+2 + H4SiO4
    log_K 0.0
Microcline
    KAlSi3O8 + 4H2O + 4H+ = 3H4SiO4 + Al+3 + K+
    log_k 0.616
Diopside
    CaMgSi2O6 + 2H2O + 4H+ = Ca+2 + Mg+2 + 2H4SiO4
    log_k 19.886
Tremolite
    Ca2Mg5Si8O22(OH)2 + 8H2O + 14H+ = 2Ca+2 + 5Mg+2 + 8H4SiO4
    log_k 56.546

```

END

PHREEQC Input File Appendix A -5 Modifications to this file were made as follows: (1) separate runs for O(0) values of 0, 2, 4, 8, 10 mg/kgw; (2) separate runs for 0.2g/L pyrite ("P(phreeq)"), 0.2g/L calcite ("C(phreeq)"), 0.2g/L pyrite + 0.2g/L calcite ("PC(phreeq)"). (total runs: 15)

```
TITLE Model PC(phreeq): Equilibrium of pyrite and calcite using 2ppm
O2
SOLUTION 1
  temp      5
  pH        7.4
  redox     O(-2)/O(0)
  units     mg/kgw
  O(0)     2      mg/kgw as O2
EQUILIBRIUM_PHASES 1 Pyrite and calcite
  Calcite  0.0      2e-3
  Pyrite 0.0      1.666e-3
GAS_PHASE 1
  -pressure 1.0
  -volume   1.0
  -temperature 5
  CO2(g) 5e-4
```

PHREEQC Input File Appendix A -6 Input file for PHREEQC speciation modelling of solution evolution in contact with pyrite and calcite

```
TITLE Model 1(phreeq): Equilibrium of rock 1 minerals using 2ppm O2
SOLUTION 1
  temp      5
  pH        7.4
  pe        4
  redox     O(-2)/O(0)
  units     mg/kgw
  O(0)     2      mg/kgw as O2
EQUILIBRIUM_PHASES 1 GP1: py, ca, mu, qz, hm, hb, kf
  Calcite  0      0.026
  Pyrite 0      3.33e-4
  K-mica 0.0      2.616e-3
  Quartz 0.0      6.657e-4
  Hematite 0.0      2.5e-4
  K-feldspar 0.0      7.19e-5
GAS_PHASE 1
  -pressure 1.0
  -volume   1.0
  -temperature 5
  CO2(g) 5e-4
```

PHREEQC Input File Appendix A -7 Modifications to this file were made as follows: separate runs for proportions of Albite(low) to Anorthite: (a) 0.030636 to 0.0280754 (to represent An₅₀); (b) 0.015318 to 0.043131 (to represent An₇₅); (c) 0 to 0.005751 (to represent An₁₀₀)

```
TITLE Model 2(phreeq): Equilibrium of rock 2 minerals using 2ppm O2
SOLUTION 1
  temp      5
  pH        7.4
  pe        4
  redox     O(-2)/O(0)
  units     mg/kgw
  O(0)     2      mg/kgw as O2
EQUILIBRIUM_PHASES 1 GP2: di py hm kf pl50 di ol(s)
  Pyrite 0      0.000333
  Hematite 0      0.00025
  Microcline 0      0.0003595
  Albite(low) 0      0.030636
  Anorthite 0      0.028754
  Diopside 0      0.003232
  Talc 0      0.0010546
  Forsterite 0      0.002843
  Tremolite 0.0      8.616e-4
GAS_PHASE 1
  -pressure 1.0
  -volume   1.0
  -temperature 5
  CO2(g) 5e-4
```

PHREEQC Input File Appendix A -8 Input file for inverse PHREEQC modelling of solution evolution in contact with pyrite and calcite

```
TITLE Model PC(inv) --Inverse modeling of 0.2g/L pyrite + 0.2g/L calcite
SOLUTION 1      0.2g/L pyrite + 0.2g/L calcite (1 hour, open)
  -units      mol/l
  pH          9.12
  Ca          9.91e-5
  Alkalinity  1.77e-4      as HCO3-
  S(6)       5.78e-6      as SO4-2

SOLUTION 2      0.2g/L pyrite + 0.2g/L calcite (24 hours, open)
  -units      mol/l
  pH          8.57
  Ca          3.42e-4
  Alkalinity  6.54e-4      as HCO3-
  S(6)       1.17e-5      as SO4-2

INVERSE_MODELING 1
  -solutions 1 2
  -uncertainty 0.5 0.2
  -phases
      CO2(g)
      O2(g)
      Calcite
      Gypsum      precip
      Fe(OH)3(a)  precip
      Pyrite      dissolve

END
```

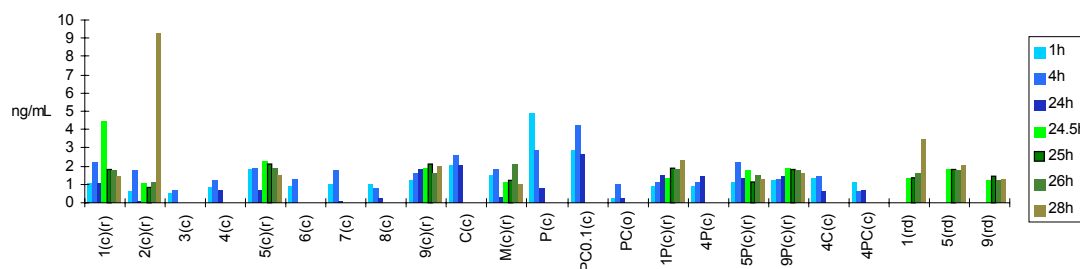
APPENDIX B - RESULTS OF TRACE ELEMENT ANALYSIS: NON-CATEGORIZABLE ELEMENTS

Interpretation of the following trace elements indicated that it was unlikely that these elements would act as indicators of either solute provenance or processes of solute acquisition. They were characterised by uneven progressions in concentration with time, extremely low concentrations, and/or lack of relationship with rock content.

Copper

Cu solute yields were generally very low (Figure 4.2), and concentrations in solution were not strongly rock type-dependent., although levels were generally a little higher in experiments involving calcite-rich and pyrite-rich rocks (experiments 1/2/5/9/C/P/PC_{0.1}/1P/5P/9P(c)) (Figure Appendix B .1). This is reflected in higher solute yields in these experiments. Levels did not increase under open conditions as with Fe and Ag, although the high concentration in experiment 2(r), 28h, if not spurious, may be a feature of the high sulphate concentrations in this solution, producing stable CuSO₄ complexes. This is not indicated by PHREEQC modelling, however, and is not repeated in the experiments involving pyrite and calcium-rich rocks.

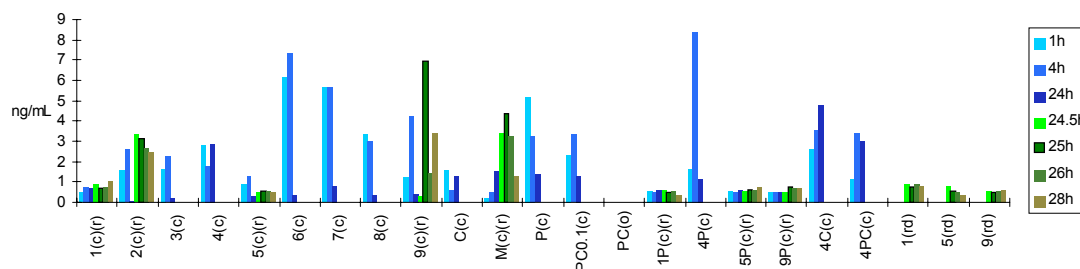
Figure Appendix B .1 Mean concentrations of Cu (ng/mL) in laboratory experiments, at 1, 4, 24, 24.5, 25, 26, 28 hours (where applicable).



Vanadium

Solute yields were particularly low in the case of V, and results are somewhat erratic. However, despite the apparently low V content in pyrite (see Section 3.4.2.2), V is relatively concentrated in some (though not all) solutions reacting with pyrite (Figure Appendix B .2). The overall dissolution behaviour of V would appear to fairly closely match that of Fe, but with lower concentrations in waters reacting with Ca-rich rocks. V generally shows a low solubility in the long-term, with higher concentrations at 1 and 4 hours than at 24 hours.

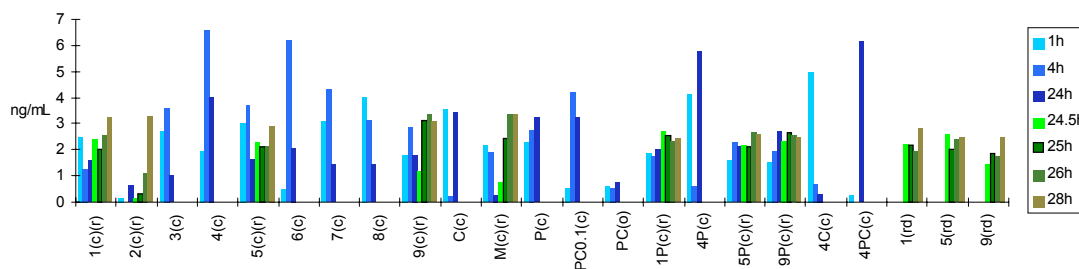
Figure Appendix B .2 Mean concentrations of V (ng/mL) in laboratory experiments, at 1, 4, 24, 24.5, 25, 26, 28 hours (where applicable).



Scandium

High solute yields of scandium were produced from almost all experiments, and over all time scales (Figure 4.2). However, the concentrations were not representative of rock provenance, as similar amounts were produced from calcite, pyrite and various rock types, under open or closed system conditions (Figure Appendix B .3). Furthermore, no speciation modelling data is available for Sc. Little effective interpretation of this data can therefore be made.

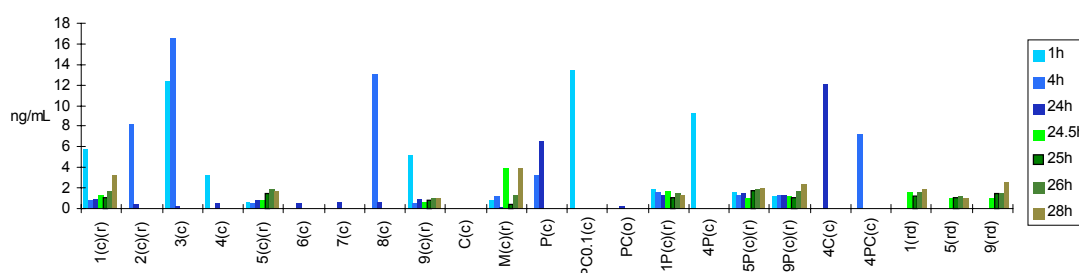
Figure Appendix B .3 Mean concentrations of Sc (ng/mL) in laboratory experiments, at 1, 4, 24, 24.5, 25, 26, 28 hours (where applicable).



Chromium

Cr analysis proved to be rather irregular, with one blank determination showing a level of 6.3ng/mL, with another having a level of 0.42ng/mL. This casts doubt on the other results, which rarely rise above 6.5ng/mL (Figure Appendix B .4). Although there appears to be a link between Cr concentration and pyrite presence, typically only one sample of each experiment reacting pyrite produces a significant Cr concentration, at a random time interval. This is also the case with the quartz veins (rocks 3 and 8). This suggests that in the rocks tested, Cr is mainly found in an uncommon discrete hydrothermal phase such as magnetite or chromite. A certain amount of increased mobility in the presence of calcite dissolution is evident from these experiments, which may be due to an increase in solubility of the common Cr complex, CrO_4^{2-} , in higher ionic strength solutions.

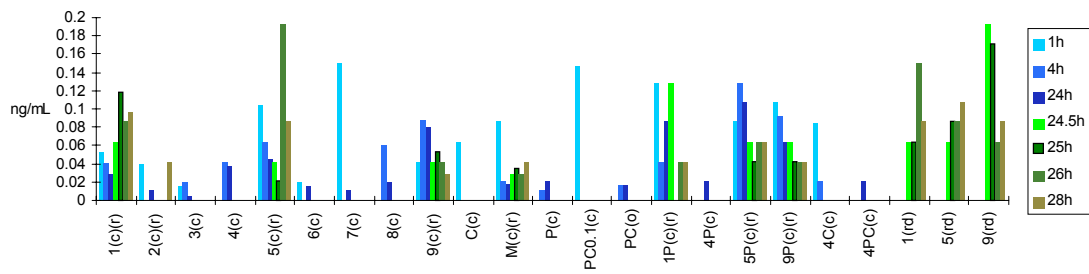
Figure Appendix B .4 Mean concentrations of Cr (ng/mL) in laboratory experiments, at 1, 4, 24, 24.5, 25, 26, 28 hours (where applicable).



Tellurium

Tellurium concentrations were very low in all experiments (Figure Appendix B .5), reflecting the low solubility of Tl in natural waters (Table 1.5). Concentrations are generally below 0.1 ng/mL, with blank determinations showing similar levels. Long term solubility of Tl is also evidently low. Concentrations may be linked to ion exchange reactions associated with carbonate dissolution, but concentrations are very low and uneven.

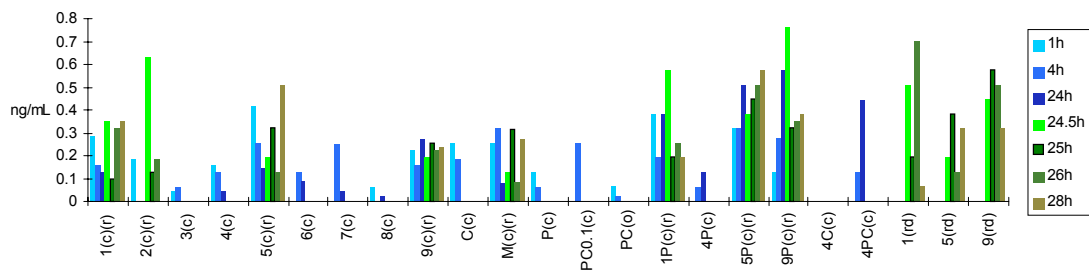
Figure Appendix B.5 Mean concentrations of TI (ng/mL) in laboratory experiments, at 1, 4, 24, 24.5, 25, 26, 28 hours (where applicable).



Antimony

Sb is not present in any rocks at higher than 0.5 ng/mL (Table 3.4.1), and so, although Figure 4.2 indicates that the element displays quite high solubility, concentrations in solution remained below ng/mL level (Figure Appendix B.6). The solute yields suggest that Sb is more soluble in solutions with calcite, but may also be influenced to a small degree by pyrite dissolution.

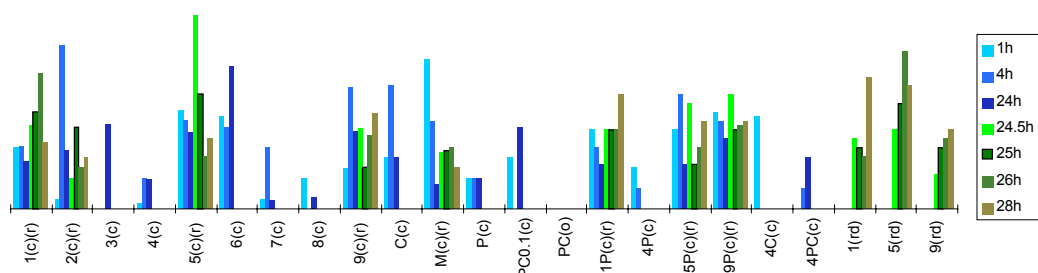
Figure Appendix B.6 Mean concentrations of Sb (ng/mL) in laboratory experiments, at 1, 4, 24, 24.5, 25, 26, 28 hours (where applicable).



Silver

Ag analyses were unstandardised, but appear to show highest concentrations in solutions with Ca-rich rocks 5, 6, 9 and C (experiments 5/6/9/C(c)), and also rocks 2 and 3 after 24 hours (experiments 2/3(c)) (Figure Appendix B.7). Silver concentrations did not appear to be particularly high in the presence of pyrite, and was not significantly enhanced in products of mixtures of Ca-rich rocks (1, 5, 9, C) and pyrite (experiments 1P/5P/9P(c)), relative to those without pyrite added (experiments 1/5/9(c)). Solubility of Ag may be affected by ion exchange with the extent calcite released by calcium carbonate dissolution (Fairchild *et al.*, 1994).

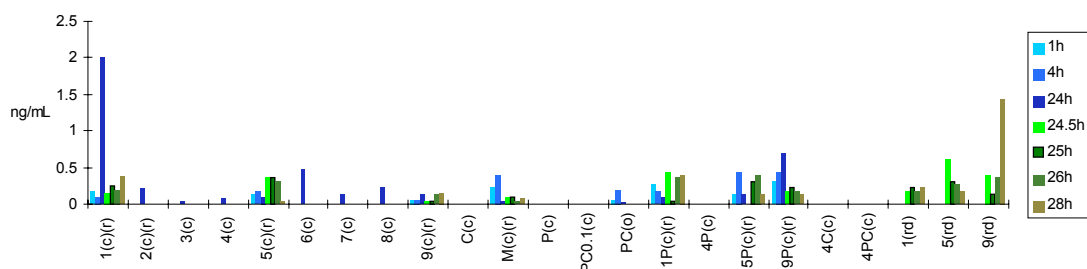
Figure Appendix B.7 Mean concentrations of Ag (ng/mL) in laboratory experiments, at 1, 4, 24, 24.5, 25, 26, 28 hours (where applicable). There are no units, as the analysis was unstandardised.



Tin

Sn concentrations gained from dissolutions were below 1ng/mL in all experiments, except one analysis of solution with rock 1 after 24 hours, which at 4.8ng/mL may be spurious as the other experiments involving the same rock type for the same length of time were both less than 1ng/mL. Solute yields were generally much higher after 24 hours than at 1 hour (Figure Appendix B .1). No acquisition was detected from calcite or pyrite.

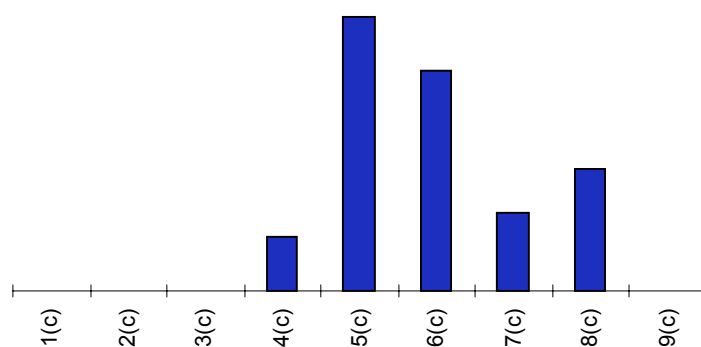
Figure Appendix B .8 Mean concentrations of Sn (ng/mL) in laboratory experiments, at 1, 4, 24, 24.5, 25, 26, 28 hours (where applicable).



Zirconium

Only one, closed system, determination of Zr for each of rocks 1-9 was carried out. It does appear that rock 5 contains a relatively soluble Zr-bearing mineral, however, as the concentration was relatively higher in experiment 5(c) compared to solutions with rocks that are more Zr-rich.

Figure Appendix B .9 Mean concentrations of Zr (ng/mL) in laboratory experiments, at 1, 4, 24, 24.5, 25, 26, 28 hours (where applicable). There are no units, as the analysis was unstandardised.



Cadmium, indium, iodine

Cadmium, indium and iodine display dissolution patterns similar to the REE, and at similarly low concentrations (Figure Appendix B .10, Figure Appendix B .11, Figure Appendix B .12). However, iodine acquisition continued up to 24 hours and in open system, reflecting the high mobility of the anion.

Figure Appendix B .10 Mean concentrations of Cd (ng/mL) in laboratory experiments, at 1, 4, 24, 24.5, 25, 26, 28 hours (where applicable).

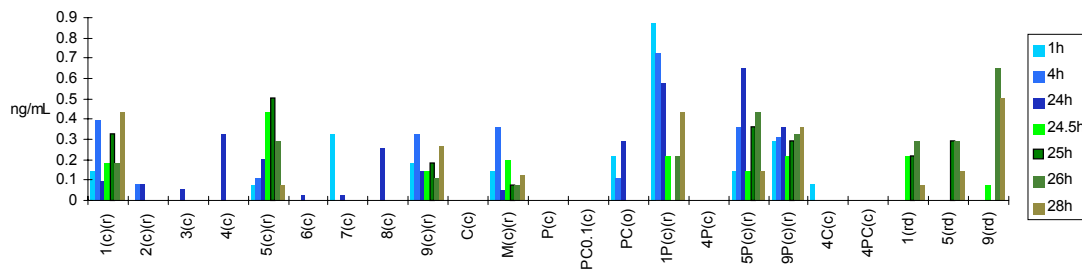


Figure Appendix B .11 Mean concentrations of In (ng/mL) in laboratory experiments, at 1, 4, 24, 24.5, 25, 26, 28 hours (where applicable).

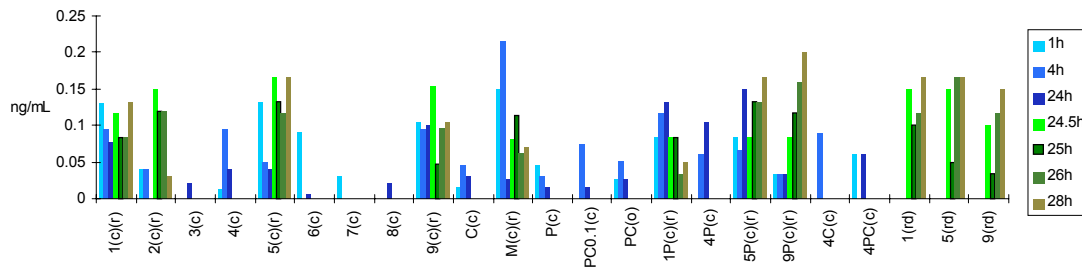
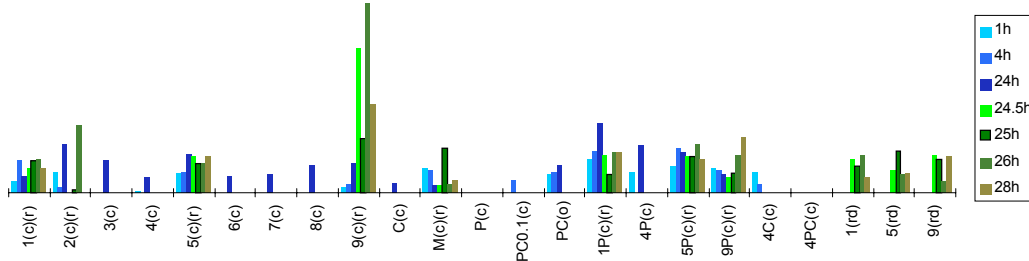


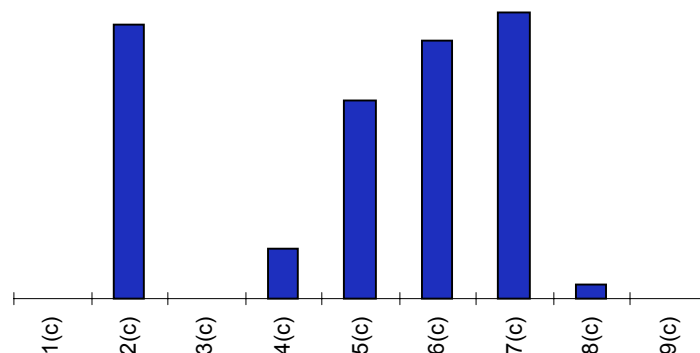
Figure Appendix B .12 Mean concentrations of I (ng/mL) in laboratory experiments, at 1, 4, 24, 24.5, 25, 26, 28 hours (where applicable). There are no units, as the analysis was unstandardised.



Bromine

Bromine determinations were not calibrated with a standard solution, and did not reach concentrations higher than the blank level in any experiment (Figure Appendix B .13).

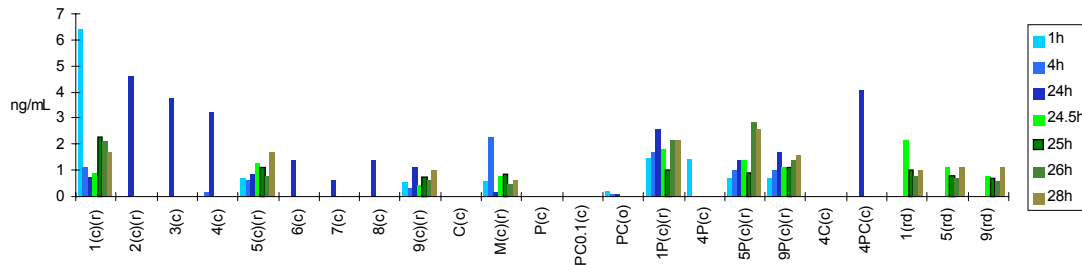
Figure Appendix B .13 Mean concentrations of Br (ng/mL) in laboratory experiments, at 1, 4, 24, 24.5, 25, 26, 28 hours (where applicable).



Mercury

Mercury displayed unusually high levels of acquisition in some experiments, but the high results were rather random, generally one sample per rock type, at no particular time interval, suggesting that these results were either experimental or instrument error. There is a general Hg presence from the dissolution of rocks 1, 5, 9 and M, however (Figure Appendix B .14).

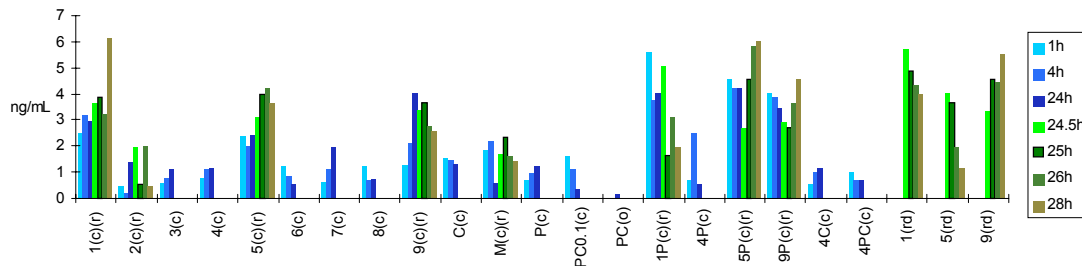
Figure Appendix B .14 Mean concentrations of Hg (ng/mL) in laboratory experiments, at 1, 4, 24, 24.5, 25, 26, 28 hours (where applicable).



Arsenic

Arsenic is evidently a mobile species, remaining in solution at similar or greater levels at 24 hours than at 1 hour. Concentrations of As after 24 hours were highest in rocks 1, 5, 9 and C, however, and show increases in response to pyrite.

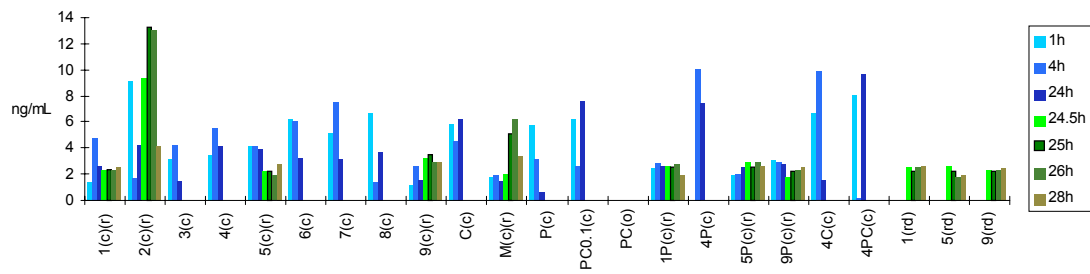
Figure Appendix B .15 Mean concentrations of As (ng/mL) in laboratory experiments, at 1, 4, 24, 24.5, 25, 26, 28 hours (where applicable).



Lithium, Beryllium, Boron

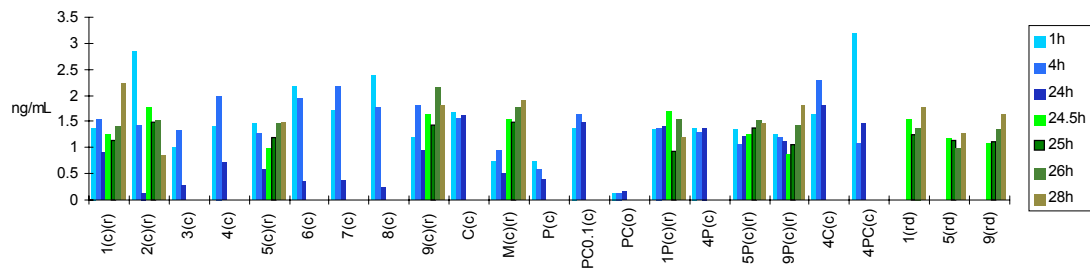
Figure Appendix B .16 shows the results for lithium, beryllium and boron. Details of the rock contents of these elements is not available. Lithium is generally present in mica and other silicate minerals (see Section 1.7.1.1) (Vlasov, 1966), and was released from all morainic rocks in concentrations between 2 and 9ng/mL under closed system conditions. However, similar concentrations were released from both pyrite and calcite. Li is documented as substituting for both Fe and Ca (Vlasov, 1966).

Figure Appendix B .16 Mean concentrations of Li (ng/mL) in laboratory experiments, at 1, 4, 24, 24.5, 25, 26, 28 hours (where applicable).



Beryllium is likely to be associated dominantly with clays, and is uncommon in carbonates and quartzites, but the presence of dissolved Be from experiments P(c) and C(c) is at odds with the theory. Concentrations in all experiments, despite being higher than blank determinations, are in fact very similar, regardless of solute type, access to CO₂ or dilution.

Figure Appendix B .17 Mean concentrations of Be (ng/mL) in laboratory experiments, at 1, 4, 24, 24.5, 25, 26, 28 hours (where applicable).



Boron concentrations are also similar in all experiments, with no significant variations noted between solute type.

Figure Appendix B .18 Mean concentrations of B (ng/mL) in laboratory experiments, at 1, 4, 24, 24.5, 25, 26, 28 hours (where applicable).

